ISSN 0021-9673

VOL. 702 NOS. 1 + 2 19 MAY 1995

COMPLETE IN ONE ISSUE

1994 International Symposium on Preparative Chromatography Washington, DC, 12–15 June 1994

JOURNAL OF CHROMATOGRAPHY A

INCLUDING ELECTROPHORESIS AND OTHER SEPARATION METHODS

EDITORS
U.A.Th. Brinkman (Amsterdam)
R.W. Giese (Boston, MA)
J.K. Haken (Kensington, N.S.W.)
C.F. Poole (London)
L.R. Snyder (Orinda, CA)
S. Terabe (Hyogo)

EDITORS, SYMPOSIUM VOLUMES,
E. Heftmann (Orinda, CA), Z. Deyl (Prague)

EDITORIAL BOARD
D.W. Armstrong (Rolla, MO)
W.A. Aue (Halifax)
P. Boček (Brno)
P.W. Carr (Minneapolis, MN)
J. Crommen (Liège)
V.A. Davankov (Moscow)
G.J. de Jong (Weesp)
Z. Deyl (Prague)
S. Dilli (Kensington, N.S.W.)
Z. El Rassi (Stillwater, OK)
H. Engelhardt (Saarbrücken)
M.B. Evans (Hatfield)
S. Fanali (Rome)
G.A. Guiochon (Knoxville, TN)
P.R. Haddad (Hobart, Tasmania)
I.M. Hais (Hradec Králové)
W.S. Hancock (Palo Alto, CA)
S. Hjertén (Uppsala)
S. Honda (Higashi-Osaka)
Cs. Horváth (New Haven, CT)
J.F.K. Huber (Vienna)
J. Janák (Brno)
P. Jandera (Pardubice)
B.L. Karger (Boston, MA)
J.J. Kirkland (Newport, DE)
E. sz. Kováts (Lausanne)
C.S. Lee (Ames, IA)
K. Macek (Prague)
A.J.P. Martin (Cambridge)
E.D. Morgan (Keele)
H. Poppe (Amsterdam)
P.G. Righetti (Milan)
P. Schoenmakers (Amsterdam)
R. Schwarzenbach (Dübendorf)
R.E. Shoup (West Lafayette, IN)
R.P. Singhal (Wichita, KS)
A.M. Siouffi (Marseille)
D.J. Strydom (Boston, MA)
T. Takagi (Osaka)
N. Tanaka (Kyoto)
K.K. Unger (Mainz)
P. van Zoonen (Bilthoven)
R. Verpoorte (Leiden)
Gy. Vigh (College Station, TX)
J.T. Watson (East Lansing, MI)
B.D. Westerlund (Uppsala)

EDITORS, BIBLIOGRAPHY SECTION
Z. Deyl (Prague), J. Janák (Brno), V. Schwarz (Prague)

ELSEVIER

ATTENTION

Please note that Vol. 701 (Cumulative Indexes Vols. 652–700) will appear in October 1995. Please do not claim; nothing is missing.

JOURNAL OF CHROMATOGRAPHY A

INCLUDING ELECTROPHORESIS AND OTHER SEPARATION METHODS

Scope. The *Journal of Chromatography A* publishes papers on all aspects of **chromatography, electrophoresis** and related methods. Contributions consist mainly of research papers dealing with chromatographic theory, instrumental developments and their applications. In the *Symposium volumes*, which are under separate editorship, proceedings of symposia on chromatography, electrophoresis and related methods are published. *Journal of Chromatography B: Biomedical Applications* —This journal, which is under separate editorship, deals with the following aspects: developments in and applications of chromatographic and electrophoretic techniques related to clinical diagnosis or alterations during medical treatment; screening and profiling of body fluids or tissues related to the analysis of active substances and to metabolic disorders; drug level monitoring and pharmacokinetic studies; clinical toxicology; forensic medicine; veterinary medicine; occupational medicine; results from basic medical research with direct consequences in clinical practice.

Submission of Papers. The preferred medium of submission is on disk with accompanying manuscript (see *Electronic manuscripts* in the Instructions to Authors, which can be obtained from the publisher, Elsevier Science B.V., P.O. Box 330, 1000 AH Amsterdam, Netherlands). Manuscripts (in English; *four* copies are required) should be submitted to: Editorial Office of *Journal of Chromatography A*, P.O. Box 681, 1000 AR Amsterdam, Netherlands, Telefax (+31-20) 485 2304, or to: The Editor of *Journal of Chromatography B: Biomedical Applications*, P.O. Box 681, 1000 AR Amsterdam, Netherlands. Review articles are invited or proposed in writing to the Editors who welcome suggestions for subjects. An outline of the proposed review should first be forwarded to the Editors for preliminary discussion prior to preparation. Submission of an article is understood to imply that the article is original and unpublished and is not being considered for publication elsewhere. For copyright regulations, see below.

Publication information. *Journal of Chromatography A* (ISSN 0021-9673): for 1995 Vols. 683–714 are scheduled for publication. *Journal of Chromatography B: Biomedical Applications* (ISSN 0378-4347): for 1995 Vols. 663–674 are scheduled for publication. Subscription prices for *Journal of Chromatography A*, *Journal of Chromatography B: Biomedical Applications* or a combined subscription are available upon request from the publisher. Subscriptions are accepted on a prepaid basis only and are entered on a calendar year basis. Issues are sent by surface mail except to the following countries where air delivery via SAL is ensured: Argentina, Australia, Brazil, Canada, China, Hong Kong, India, Israel, Japan, Malaysia, Mexico, New Zealand, Pakistan, Singapore, South Africa, South Korea, Taiwan, Thailand, USA. For all other countries airmail rates are available upon request. Claims for missing issues must be made within six months of our publication (mailing) date. Please address all your requests regarding orders and subscription queries to: Elsevier Science B.V., Journal Department, P.O. Box 211, 1000 AE Amsterdam, Netherlands. Tel.: (+31-20) 485 3642; Fax: (+31-20) 485 3598. Customers in the USA and Canada wishing information on this and other Elsevier journals, please contact Journal Information Center, Elsevier Science Inc., 655 Avenue of the Americas, New York, NY 10010, USA, Tel. (+1-212) 633 3750, Telefax (+1-212) 633 3764.

Abstracts/Contents Lists published in Analytical Abstracts, Biochemical Abstracts, Biological Abstracts, Chemical Abstracts, Chemical Titles, Chromatography Abstracts, Current Awareness in Biological Sciences (CABS), Current Contents/Life Sciences, Current Contents/Physical, Chemical & Earth Sciences, Deep-Sea Research/Part B: Oceanographic Literature Review, Excerpta Medica, Index Medicus, Mass Spectrometry Bulletin, PASCAL-CNRS, Referativnyi Zhurnal, Research Alert and Science Citation Index.

US Mailing Notice. *Journal of Chromatography A* (ISSN 0021-9673) is published weekly (total 52 issues) by Elsevier Science B.V., (Sara Burgerhartstraat 25, P.O. Box 211, 1000 AE Amsterdam, Netherlands). Annual subscription price in the USA US$ 5389.00 (US$ price valid in North, Central and South America only) including air speed delivery. Second class postage paid at Jamaica, NY 11431. **USA POSTMASTERS**: Send address changes to *Journal of Chromatography A*, Publications Expediting, Inc., 200 Meacham Avenue, Elmont, NY 11003. Airfreight and mailing in the USA by Publications Expediting.

See inside back cover for Publication Schedule, Information for Authors and information on Advertisements.

© 1995 ELSEVIER SCIENCE B.V. All rights reserved.

0021-9673/95/$09.50

No part of this publication may be reproduced, stored in a retrieval system or transmitted in any form or by any means, electronic, mechanical, photocopying, recording or otherwise, without the prior written permission of the publisher, Elsevier Science B.V., Copyright and Permissions Department, P.O. Box 521, 1000 AM Amsterdam, Netherlands.

Upon acceptance of an article by the journal, the author(s) will be asked to transfer copyright of the article to the publisher. The transfer will ensure the widest possible dissemination of information.

Special regulations for readers in the USA – This journal has been registered with the Copyright Clearance Center, Inc. Consent is given for copying of articles for personal or internal use, or for the personal use of specific clients. This consent is given on the condition that the copier pays through the Center the per-copy fee stated in the code on the first page of each article for copying beyond that permitted by Sections 107 or 108 of the US Copyright Law. The appropriate fee should be forwarded with a copy of the first page of the article to the Copyright Clearance Center, Inc., 222 Rosewood Drive, Danvers, MA 01923, USA. If no code appears in an article, the author has not given broad consent to copy and permission to copy must be obtained directly from the author. The fee indicated on the first page of an article in this issue will apply retroactively to all articles published in the journal, regardless of the year of publication. This consent does not extend to other kinds of copying, such as for general distribution, resale, advertising and promotion purposes, or for creating new collective works. Special written permission must be obtained from the publisher for such copying.

No responsibility is assumed by the Publisher for any injury and/or damage to persons or property as a matter of products liability, negligence or otherwise, or from any use or operation of any methods, products, instructions or ideas contained in the materials herein. Because of rapid advances in the medical sciences, the Publisher recommends that independent verification of diagnoses and drug dosages should be made.

Although all advertising material is expected to conform to ethical (medical) standards, inclusion in this publication does not constitute a guarantee or endorsement of the quality or value of such product or of the claims made of it by its manufacturer.

♾ The paper used in this publication meets the requirements of ANSI/NISO 239.48-1992 (Permanence of Paper).

Printed in the Netherlands

For Contents see p. VII.

JOURNAL OF CHROMATOGRAPHY A

VOL. 702 (1995)

JOURNAL OF CHROMATOGRAPHY A

INCLUDING ELECTROPHORESIS AND OTHER SEPARATION METHODS

EDITORS

U.A.Th. BRINKMAN (Amsterdam), R.W. GIESE (Boston, MA), J.K. HAKEN (Kensington, N.S.W.), C.F. POOLE (London), L.R. SNYDER (Orinda, CA), S. TERABE (Hyogo)

EDITORS, SYMPOSIUM VOLUMES

E. HEFTMANN (Orinda, CA), Z. DEYL (Prague)

EDITORIAL BOARD

D.W. Armstrong (Rolla, MO), W.A. Aue (Halifax), P. Boček (Brno), P.W. Carr (Minneapolis, MN), J. Crommen (Liège), V.A. Davankov (Moscow), G.J. de Jong (Weesp), Z. Deyl (Prague), S. Dilli (Kensington, N.S.W.), Z. El Rassi (Stillwater, OK), H. Engelhardt (Saarbrücken), M.B. Evans (Hatfield), S. Fanali (Rome), G.A. Guiochon (Knoxville, TN), P.R. Haddad (Hobart, Tasmania), I.M. Hais (Hradec Králové), W.S. Hancock (Palo Alto, CA), S. Hjertén (Uppsala), S. Honda (Higashi-Osaka), Cs. Horváth (New Haven, CT), J.F.K. Huber (Vienna), J. Janák (Brno), P. Jandera (Pardubice), B.L. Karger (Boston, MA), J.J. Kirkland (Newport, DE), E. sz. Kováts (Lausanne), C.S. Lee (Ames, IA), K. Macek (Prague), A.J.P. Martin (Cambridge), E.D. Morgan (Keele), H. Poppe (Amsterdam), P.G. Righetti (Milan), P. Schoenmakers (Amsterdam), R. Schwarzenbach (Dübendorf), R.E. Shoup (West Lafayette, IN), R.P. Singhal (Wichita, KS), A.M. Siouffi (Marseille), D.J. Strydom (Boston, MA), T. Takagi (Osaka), N. Tanaka (Kyoto), K.K. Unger (Mainz), P. van Zoonen (Bilthoven), R. Verpoorte (Leiden), Gy. Vigh (College Station, TX), J.T. Watson (East Lansing, MI), B.D. Westerlund (Uppsala)

EDITORS, BIBLIOGRAPHY SECTION

Z. Deyl (Prague), J. Janák (Brno), V. Schwarz (Prague)

ELSEVIER

Amsterdam – Lausanne – New York – Oxford – Shannon – Tokyo

© 1995 ELSEVIER SCIENCE B.V. All rights reserved.

0021-9673/95/$09.50

No part of this publication may be reproduced, stored in a retrieval system or transmitted in any form or by any means, electronic, mechanical, photocopying, recording or otherwise, without the prior written permission of the publisher, Elsevier Science B.V., Copyright and Permissions Department, P.O. Box 521, 1000 AM Amsterdam, Netherlands.

Upon acceptance of an article by the journal, the author(s) will be asked to transfer copyright of the article to the publisher. The transfer will ensure the widest possible dissemination of information.

Special regulations for readers in the USA – This journal has been registered with the Copyright Clearance Center, Inc. Consent is given for copying of articles for personal or internal use, or for the personal use of specific clients. This consent is given on the condition that the copier pays through the Center the per-copy fee stated in the code on the first page of each article for copying beyond that permitted by Sections 107 or 108 of the US Copyright Law. The appropriate fee should be forwarded with a copy of the first page of the article to the Copyright Clearance Center, Inc., 222 Rosewood Drive, Danvers, MA 01923, USA. If no code appears in an article, the author has not given broad consent to copy and permission to copy must be obtained directly from the author. The fee indicated on the first page of an article in this issue will apply retroactively to all articles published in the journal, regardless of the year of publication. This consent does not extend to other kinds of copying, such as for general distribution, resale, advertising and promotion purposes, or for creating new collective works. Special written permission must be obtained from the publisher for such copying.

No responsibility is assumed by the Publisher for any injury and/or damage to persons or property as a matter of products liability, negligence or otherwise, or from any use or operation of any methods, products, instructions or ideas contained in the materials herein. Because of rapid advances in the medical sciences, the Publisher recommends that independent verification of diagnoses and drug dosages should be made.

Although all advertising material is expected to conform to ethical (medical) standards, inclusion in this publication does not constitute a guarantee or endorsement of the quality or value of such product or of the claims made of it by its manufacturer.

(∞) The paper used in this publication meets the requirements of ANSI/NISO 239.48-1992 (Permanence of Paper).

Printed in the Netherlands

SYMPOSIUM VOLUME

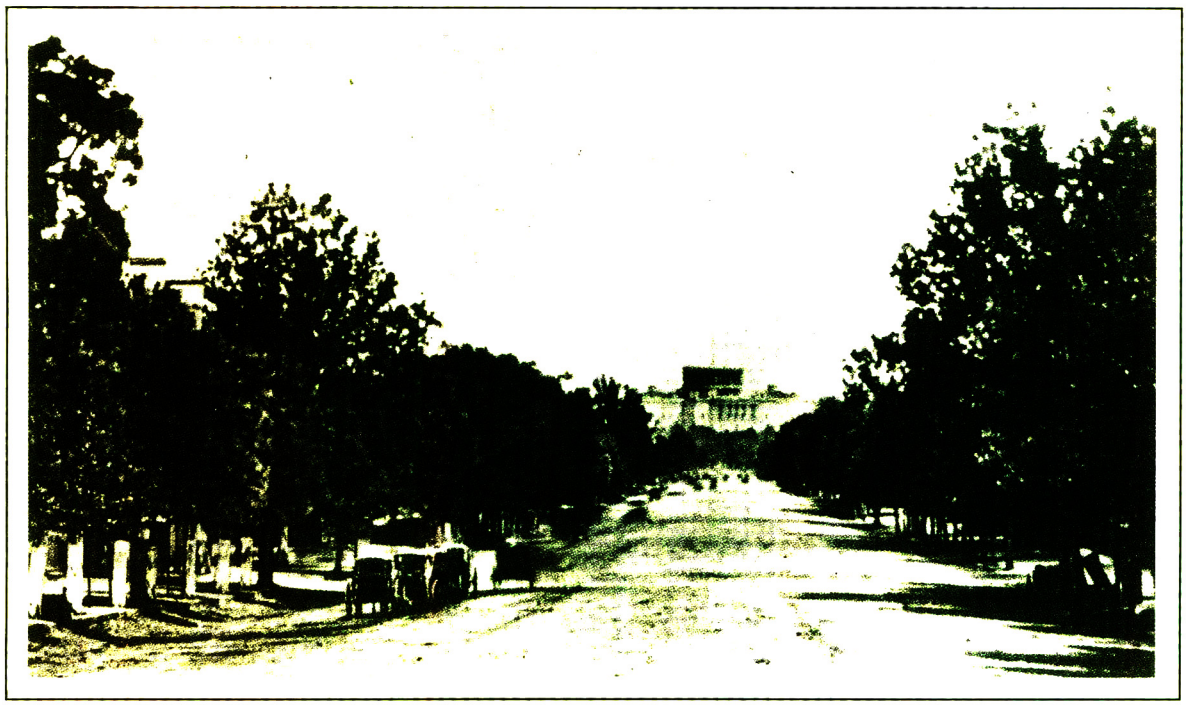

1994 INTERNATIONAL SYMPOSIUM ON PREPARATIVE CHROMATOGRAPHY

Washington, DC (USA), 1–15 June 1994

Guest Editor

G. GUIOCHON

(Knoxville and Oak Ridge, TN, USA)

VOL. 702, NOS. 1 + 2 JOURNAL OF CHROMATOGRAPHY A 19 MAY 1995

CONTENTS

(Abstracts/Contents Lists published in Analytical Abstracts, Biochemical Abstracts, Biological Abstracts, Chemical Abstracts, Chemical Titles, Chromatography Abstracts, Current Awareness in Biological Sciences (CABS), Current Contents/Life Sciences, Current Contents/Physical, Chemical & Earth Sciences, Deep-Sea Research/Part B: Oceanographic Literature Review, Excerpta Medica, Index Medicus, Mass Spectrometry Bulletin, PASCAL-CNRS, Referativnyi Zhurnal, Research Alert and Science Citation Index)

1994 INTERNATIONAL SYMPOSIUM ON PREPARATIVE CHROMATOGRAPHY, WASHINGTON, DC, 12–15 JUNE 1994

LIQUID CHROMATOGRAPHY TECHNIQUES AND THEORY

LARGE-SCALE PROTEIN SEPARATIONS

ห้องสมุดกรมวิทยาศาสตร์บริการ
- 5 ม.ค. 2536

ELSEVIER

Journal of Chromatography A, 702 (1995) 1–2

JOURNAL OF CHROMATOGRAPHY A

Foreword

"PREP '94", the 1994 edition of the well known series of Symposia on Preparative Chromatography, took place in Arlington, VA, June 12–15, 1994, at the Georgetown University Conference Center, in Washington DC, USA. As the previous meetings in this series, it was attended by close to 300 participants. Although the traditional features of a scientific meeting were kept (29 oral communications were presented and 25 poster contributions were exhibited and discussed), important changes were made in the organization of the symposium. An exhibition of the equipment, material, and products used in preparative chromatography offered to the attendant an opportunity to get more familiar with recent developments in this area. Three symposium workshops, three manufacturers' seminars and two round table discussions were organized the Sunday before the opening of the meeting, during the lunches and the afternoon pauses. The format of these workshops, seminars and discussions were conducive to intense exchanges of ideas. The topics selected emphasized practical and concrete considerations, thus complementing the more fundamental aspect of the classical part of the program.

Preparative chromatography is a complex process at all levels, from its principles to method development, implementation, and equipment design. The successful development of a new application requires the understanding of many physicochemical phenomena. A comprehensive knowledge of the state of the art in materials, equipment, and products, especially stationary phases, is necessary. An exhibit with ample opportunity for contact with manufacturers and suppliers complements well a scientific meeting. With process chromatography having been practiced in industry for ten years, many can now successfully use the concepts of tag-along and displacement effect to increase production rate. However, our level of understanding is deepening. The rapid development of fast computers is permitting the use of general programs for the optimization of the experimental conditions of a new separation. The advent of the simulated moving bed unit will make modeling by computer a necessity. Similarly, only a rich scientific program permits the clarification of the issues and variables necessary to utilize a modern technology. The quality of the presentations made at PREP '94 demonstrates the vigor of the research effort undertaken in both academy and industry as well as the importance of the separation problems encountered in various applications.

The help of Dr. John Frenz (Genentech), Dr. Anita Katti (Mallinckrodt Chemical, Inc.), Dr. Joan Newburger (R.W. Johnson Pharmaceutical Research Institute), Dr. Klaus Unger (Johannes Gutenberg-Universität), and Dr. Linda Wang (Purdue University), the members of the scientific committee of PREP '94, in the review of the abstracts submitted, and in the organization of the program was greatly appreciated. The sponsorship of the Washington Chromatography Discussion Group is gratefully acknowledged, as well as the support extended by Prochrom for the organization of the social program. It is a pleasure to thank Mrs. Janet Cunningham, Sym-

SSDI 0021-9673(95)00416-5

posium Manager, whose organizational skills allowed its successful operation. The present volume of the *Journal of Chromatography A* includes the papers submitted during the symposium. These papers represent the nature and intensity of the research carried out in preparative chromatography. We hope that this volume will prove useful to those involved in this field.

We are grateful to the Editor of the Symposium Volumes and to the editorial staff of the *Journal of Chromatography A* for their professionalism and dedication in producing this volume.

Knoxville, TN, USA Georges Guiochon

ELSEVIER

Journal of Chromatography A, 702 (1995) 3–26

JOURNAL OF CHROMATOGRAPHY A

Review

Separation of biomolecules using adsorptive membranes

D. Keith Roper[a,*], Edwin N. Lightfoot[b]

[a]*Merck Research Laboratories, WP16-121P, Sumneytown Pike, P.O. Box 4, West Point, PA 19486, USA*
[b]*Chemical Engineering Department, University of Wisconsin, 1415 Johnson Drive, Madison, WI 53706, USA*

Abstract

The efficient recovery of labile biomolecules requires rapid, reliable separation processes using mild conditions. Adsorptive membranes are available in a range of chemistries and geometries which permit their application as clarification, concentration, fractionation and purification tools in a biorecovery sequence. Available devices exhibit low backpressure, short residence times and high volumetric throughputs relative to conventional chromatographic packed beds. Non-uniform flow, dead volumes and backmixing observed in some adsorptive membrane systems preclude them from achieving substantial improvements in resolution relative to conventional packed beds. Improvements in design and operation of these systems should increase their separation performance tenfold. Adsorptive separations using affinity, ion-exchange and hydrophobic membranes are reviewed.

Contents

* Corresponding author.

0021-9673/95/$29.00 © 1995 Elsevier Science B.V. All rights reserved
SSDI 0021-9673(95)00010-0

1. Introduction

The purpose of this review is to examine applications of microporous polymeric membranes as substrates for the adsorptive liquid chromatography of biological macromolecules. Rapid developments in biotechnology and the pharmaceutical potential of biomolecules are fueling demand for reliable, efficient methods to purify preparative amounts of proteins, peptides and nucleic acids. Recombinant gene products currently approved for drug use by the Food and Drug Administration (FDA) include insulin, growth hormone, interferons, erythropoietin and tissue plasminogen activator [1]. Additional polypeptide therapeutics being examined in human clinical trials number in the hundreds; thousands more are currently being investigated.

Recovery of fragile molecules from a biological host environment requires attention to their unique characteristics. For example, time-consuming recovery processes cause unnecessary degradation of many gene products. Variants of proteins and nucleic acids are generated during downstream processing by deamidation, oxidation, proteolysis, nicking and aggregation. The fraction of degradation products increases with residence time [2], so shorter process times can net higher recoveries and product purity.

Mild processing conditions also help to maintain the native conformation and hence the biological activity of biomolecules. Avoiding extreme pH or temperature values, shear and exposure to air–water interfaces prevents subsequent denaturation of many enzymes. Avoiding non-polar solvents and hydrophotic adsorbents which are commonly used to purify small solutes also reduces destabilization of biological products.

Additional considerations arise as biological molecules are prepared in sufficient amounts for evaluation as drug candidates. Selected purification methods must consistently remove potentially hazardous variants, in addition to host cell proteins, DNA, endotoxins and viral elements, from complex feed streams [3]. High resolution is commonly required to meet stringent purification standards set for recombinant DNA products. Variants differing from an enzymatic product by one amino acid or contaminant levels greater than 1 ppm have not been permitted in previous pharmacological preparations [4].

Large-scale recovery operations must be efficient, as the cost of recovering biomolecules can dominate total product manufacturing costs [5]. Inefficient processes consume inordinate volumes of expensive solvents which must eventually be regenerated or disposed. Costs resulting from solvent tankage and consumption during downstream recovery represent a significant fraction of biological recovery costs [6]. Finally, the reliability of process equipment must be well documented to merit approval from regulatory agencies.

These characteristics of biological products and considerations for their preparative recovery are practical issues which are addressed here as we evaluate reported applications of membrane chromatography. The range of reported investigations of membrane adsorption allow us to

consider: (1) what features of adsorptive membranes permit rapid, non-denaturing recovery of biological products?; (2) what is the performance of adsorptive membranes measured using techniques commonly applied to chromatographic packed beds? (3) how are adsorptive membranes best configured and operated to provide adequate resolution and efficiency for biological preparations?

2. Novel chromatographic membranes

Membrane chromatography systems function as short, wide chromatographic columns in which the adsorptive packing consists of one or more microporous membranes in series, each derivatized with adsorptive moieties. They were derived, by and large, from filtration modules and consequently exist in a similar variety of configurations: flat or spiral-wound sheets, hollow fibers and cast cylindrical plugs.

Adsorptive membrane chromatography reflects technological advances in both membrane filtration and fixed-bed liquid chromatography. Membranes are employed as filters to separate biomolecules whose size differs by roughly an order of magnitude or more. Membrane filtration is used in bioprocess recovery to remove cell debris, colloidal or suspended solids [7] and virus particles [8] from homogenized suspensions of bacterial cells. Membranes may be configured in tangential-flow, hollow fiber, asymmetric or dead-end filtration geometries. A recent variation of membrane filtration, called "membrane filtration affinity purification" [9], is intended to increase the selectivity of size-based membrane separations. Affinity ligands are coupled to nanoparticles in order to bind selectively proteins of interest. The particles are subsequently filtered from the process stream.

By comparison, separation occurs in liquid chromatography as molecules in a mobile stream are preferentially retained by an adjacent stationary phase. Less strongly retained molecules are carried away by the solvent stream, gradually leaving a pure band of the preferentially adsorbed species. To increase the chromatographic capacity, ligands specific to the retained species are bound to the large, intraparticle surface area of porous resins. Mobile phase species access these ligands by Brownian thermal diffusion.

Chemical modification of filtration membranes to adsorb biomolecules in the filtrate originally employed biospecific affinity ligands [10]. Dissolved molecules are carried directly to adsorptive sites in these membranes by bulk flow, eliminating the long diffusion time required by resin-based chromatography. This adaptation increases the throughput of affinity processes. Ligands intended for pseudo-affinity, ion-exchange, hydrophobic interaction and reversed-phased interaction have also been coupled to membrane substrates.

Many adsorptive membrane separations are performed using conventional filtration apparatus to concentrate and recover the product of interest. Other adsorptive membranes are configured for compatibility with existing chromatographic pumps, detectors and associated peripherals. The term "high-performance membrane chromatography" has been applied to separations achieved by selective adsorption or retention on membrane substrates [11,12].

3. Scope of the review

The literature which describes column liquid chromatography or membrane filtration is large and comprehensive. The scope of this review is limited to analyses and applications of adsorptive membrane systems, which are the hybrid synthesis of these two technologies. Adsorptive membranes are being applied to separations in many fields. We review representative applications, paying particular attention to work whose scope indicates features peculiar to adsorptive membranes, or suggests developments in their design and operation. It will become apparent that an understanding of fundamental chromatographic principles is useful in order to take advantage of the unique attributes of membranes as adsorptive substrates. Advances in the sciences of membrane filtration and column chro-

ห้องสมุดกลาง ... บริการ

matography are also likely to improve membrane chromatography.

4. Adsorptive membrane chromatography

Adsorptive membranes consist of a substrate to which an interactive ligand is chemically coupled. These membrane systems are available for use in a number of separation configurations or geometries. We review in Section 4.1 reported substrates and coupling chemistries. We then consider in Section 4.2 a variety of separation configurations and briefly discuss the applications for which they appear best suited. We conclude in Section 4.3 with a summary of available adsorptive membrane systems whose performance has been characterized.

4.1. Membrane substrates and coupling chemistries

Ideally, adsorptive membrane substrates are mechanically resilient and resistant to solvents used to activate coupling [10]. They should not participate in secondary hydrophobic adsorption. Hydrophobic adsorption produces non-specific retention that interferes with product resolution and can also contribute to the denaturation of biopolymers. Polymeric and inorganic materials which constitute membrane substrates in several different geometries are listed in Table 1. Many of these materials are also widely used as membrane filters.

Cellulose is a popular substrate for adsorptive membranes. Native and derivatized cellulose membranes are soluble only in some strong acids [10]. Ion-exchange activity of residual carboxylic and aldehyde side groups can be neutralized with borohydride reduction, and secondary hydrophobic interactions are eliminated by the high level of hydration in these membranes. Rigid, hydrophilic cellulose grafted with gel-type polymers has been linked to spacer arms on which active derivatives for ligand coupling were introduced [13]. Regenerated cellulose is non-rigid and must be adequately supported to prevent deformation or wrinkling.

Several recent investigators have examined adsorptive membranes made of acrylic copolymers. Thin discs of macroporous poly(glycidyl methacrylate–co-ethylene dimethacrylate) (GMA–EDMA) have been synthesized by free-radical polymerization of a mixture of a monovinyl monomer, such as styrene or methacrylate, and a divinyl monomer such as divinylbenzene, in a heated mold [11,14]. Synthesis is initiated by azobisisobutyronitrile in the presence of porogenic solvents between two heated plates. Epoxy groups are modified to furnish functional group sites for hydrophobic interaction chromatography (HIC) or ion-exchange chromatography (IEC). Sulfuric acid hydrolysis destroys residual underivatized groups to prevent secon-

Table 1
Common geometries and materials of chromatographic membranes

Geometry	Material	Ref.
Thin sheet	Cellulose	[13]
	Regenerated cellulose	[31,40]
	Poly(glycidyl methacrylate–co-ethylene dimethacrylate)	[15,14,11]
	Poly(glycidyl methacrylate)	[16]
	Nylon	[39]
	Titanium	[19]
Hollow fiber	Polyethlyene	[22]
	Silicon dioxide glass	[24]
Spiral-wound	Cellulose/GMA–DEAEMA copolymer	[73]
Cross-linked rod	Poly(styrene–co-divinylbenzene)	[17,18]

dary associations between biomolecules and the substrate [15]. A GMA substrate is also commercially available [16].

A reported polymerization similar to that for GMA–EDMA has been used to synthesize a continuous rod of microporous, membrane-like substrate directly within a cylindrical column [17,18]. The poly(styrene–co-divinylbenzene) matrix was used directly for reversed-phase chromatography of model polypeptides and proteins. Polymer rods fill the void volume corresponding to interstitial pore spaces characteristic of granular packed beds with additional porous substrate. The minimum interstitial, non-adsorptive dead volume in a bed packed with cylindrical spheres was estimated to be 26%. Nylon substrates are also used.

In addition to polymers, inorganic substrates have been studied. An ion-exchange membrane has been formed using an oxide of titanium. Polyethyleneimine (PEI) ion-paired with the oxide support and was subsequently cross-linked with glutaraldehyde to form a reactive film to which anion-exchange ligands were coupled [19]. Titania is more alkali stable than silica, and adsorption of PEI on titania is straightforward [20]. Alkaline conditions will not erode the PEI coating.

Unlike flat membrane sheets which are typically supported in conventional filtration apparatus, hollow-fiber membranes must be intrinsically rigid, as well as hydrophic and resistant to solvents. Adsorptive membrane hollow fibers formed from both polymeric and inorganic substrates have been examined.

Radiation-induced graft polymerization of 2-hydroxyethyl methacrylate (HEMA), vinyl acetate (VAc) and glycidyl methacrylate (GMA) on to a polyethylene hollow-fiber microfiltration membrane introduced alchoholic hydroxyl groups that reduced non-selective protein adsorption in proportion to diol density while maintaining pure water flux [21]. Protein binding changed from irreversible to reversible. The hydrophilized membrane served as a microporous support on to which sulfopropyl groups were immobilized for the anion exchange of lysozyme.

Two affinity systems have also been produced by coupling with the epoxide groups of GMA. A hydrophobic amino acid, L-phenylalanine, was coupled to form a pseudo-biospecific ligand for selective immobilization of bovine γ-globulin [22]. Chemical conversion of the expoxide to iminodiacetate and subsequent chelation with copper were used to produce an immobilized metal affinity membrane (IMAM) [23]. As with the thin-sheet disks, sulfuric acid treatment of unconverted epoxide reduced non-specific adsorption by His–Leu and bovine serum albumin (BSA). Glass hollow-fiber microfiltration membranes have also been used as substrates for immobilized metal chelate affinity membranes [24].

Commercially available substrates and coupling chemistries are available in addition to those we have considered. Protein A and IgG were coupled to epoxy-activated polymeric membranes by 16 h of incubation at an optimum pH of about 8 [25]. Remaining reactive groups were blocked by treatment with 2% ethyl glycinate in 0.1 *M* borate bufer. Ligands including plant lectins, carbohydrates and enzyme inhibitors can be attached to monoclonal antibodies using a stable secondary amine linkage which allows little leaching.

We now consider the relative merits of each of the geometries of membrane chromatography.

4.2. Adsorptive membrane geometry

Adsorptive membrane chromatography can be performed using a number of commercially available or laboratory-prepared geometries. In Fig. 1 we illustrate individual thin-sheet and hollow-fiber membranes together with stacked-membrane, spiral-wound and Chromarod membrane columns.

Individual membranes in the form of thin sheets, disks or hollow fibers are convenient inexpensive and versatile. Sheets or disks may be mounted in conventional ultrafiltration units or in specially prepared cartridges. This permits rapid, low-pressure adsorption of limited amounts of sorbate, in either batch or continuous recycle mode. In this way, intended product may be concentrated substantially. Individual

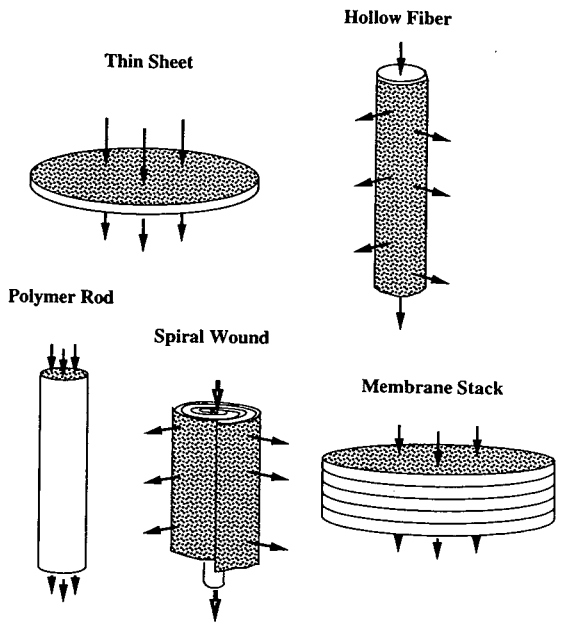

Fig. 1. Schematic comparison of the configurations that have been proposed for membrane-based adsorption. Arrows illustrate the direction(s) of bulk flow. Pattern indicates membrane cross-sectional area which lies roughly perpendicular to bulk flow.

sheets or disks appear best suited for laboratory methods which selectively adsorb the product of interest from a large, dilute sample volume.

Product recovery from complex feed volumes such as homogenized cell paste, animal serum or blood plasma typically fouls dead-end adsorption systems. High-molecular mass antifoams added to fermentation broths also foul membranes and can reduce flux rates by 50% or more [26]. Cross-flow operation utilizing either sheets or hollow fibers has been used to treat such feeds at small scale [27]. Hollow fibers are usually available bundled within a shell using potting material that may swell if exposed to organic solvents.

The capacity of single adsorptive membranes for preparative recovery may be limited. To achieve the adsorptive capacities necessary for preparative biological recovery, multiple thin-sheet disk membranes are stacked in series and housed in a rigid cylindrical shell. Alternatively, a single thin sheet wound around a permeable, cylindrical core can be similarly packaged. Stacked-membrane and spiral-wound geometries allow local variations in porosity and membrane thickness which may compromise the separation performance of single sheets [28] to be averaged out in the direction of flow.

Adsorptive spiral-wound and stacked membrane columns are compatible with conventional high-performance liquid chromatography (HPLC) systems. They have a number of advantages relative to packed-bed chromatography. The cross-sectional dimension of membrane columns which lies perpendicular to the flow direction is considerably longer than the flow path. In contrast, granular adsorptive beds are commonly packed with a length-to-diameter ratio of 2.5 or greater. The large packed-column aspect ratio is necessary to maintain frictional support to resins from the column wall, in order to resist settling and cracking [29]. Consequently, membrane-column residence times are short and backpressures are small, whereas the volumetric capacity is large with respect to large-scale chromatography [30]. These features increase throughput and decrease processing times, as discussed in Section 6, reducing the requirement for expensive or hazardous solvents and tankage. They also yield shorter residence times, which in turn reduces protein degradation by proteolysis and denaturation. Fig. 2 contrasts stacked-membrane and resin-packed columns.

Despite their abbreviated flow path, adsorptive membrane columns achieve resolutions comparable to those with packed chromatographic beds [31]. Separation performance of membrane chromatography is considered further in Section 5. On the other hand, it has been reported that the shallow flow path of spiral-wound adsorptive beds precludes high-resolution separations [13]. In spiral-wound membranes the flow direction does not coincide with gravity. Small defects are not self-stabilized by radial flow through the bed. This potentially biases spiral-wound beds toward channeling.

Membrane rod chromatography by Svec [17,18] produces a column with attributes of both membrane adsorbers and packed resin beds. Like an adsorptive membrane, the polymeric

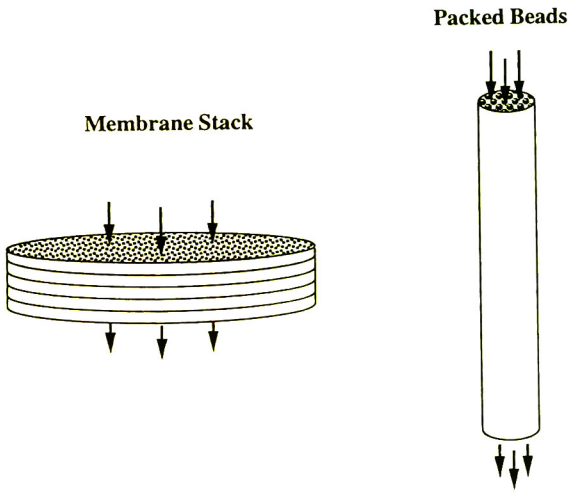

Fig. 2. Comparison of membrane stack with packed bed for adsorptive chromatography. Hold-up volumes of both systems are similar. Length-to-width aspect ratio of packed bed often corresponds to width-to-length dimensions of stacked membrane. This results in lower backpressures and larger volumetric throughput for stacked membranes.

matrix of the cylindrical plug cast within a column is a macroporous structure (0.1–10.0 μm I.D.) producing relatively low backpressure. Linear decreases in efficiency due to intraparticle diffusion at increasing flow-rates are not observed. Channeling or settling is unexpected in the matrix. At the same time, the matrix is resistant to deformation, like a packed resin bed, and column length-to-width aspect ratios are well above 2.5.

4.3. Membrane chromatographic columns

A number of commercially available adsorptive membrane devices have been considered in the literature. Many of these are summarized with their respective manufacturers and categorized by type of interactive chemistry or activity in Table 2.

Ion-exchange membranes and their manufacturers include Millipore MemSep, LKB Zeta Prep and FMC ActiDisc and Acti-Mod cartridge, Amicon MAC capsules, Sartorius Sartobind Q and S and Pall Lowprodyne membranes. Apparently the earliest commercially available ion-exchange membrane was a cation-exchange disk, SP-Zetaprep from LKB, (Bromma Sweden) [72]. Affinity systems consisting of protein A and protein G ligated to cellulose are available (Millipore MemSep; Memtek MAC disks, Genex AbSorbent G and Cuno Zetaffinity).

Table 2
Commercially available adsorptive membranes whose performance has been previously examined

Tradename	Type	Manufacturer	Ref.
MAC	Anion exchange	Amicon Division (Memtek), W.R. Grace, Beverly, MA, USA	[59]
Zetaffinity 10	Affinity	Cuno, Life Sciences, CT, USA	[13]
ActiDisc, Acti-Mod	DEAE	FMC Bioproducts, Rockland, ME, USA	[14,59]
Quick Disk	Q, C-4	Säulentechnik Knauer, Berlin, Germany	[16]
AbSorbent	Protein G	Genex	[38]
MemSep	DEAE, QMA, SP, protein A and G	Millipore, Bedford, MA, USA	[31,47,60]
Loprodyne	Protein A	Pall Bio Support, Portsmouth, UK	[30,39]
Sartobind	Q, S Epoxy	Sartorius	[25,42,53]
Zetaprep	SP	LKB, Bromma, Sweden	[54,72]

Morphologies different than conventional stacked beds include radial flow through spiral-wound cartridges, such as the ion-exchange ZetaPrep cartridges and affinity Zetaffinity 10 cartridges.

5. Adsorptive membrane chromatographic performance

The separation effectiveness in adsorptive membrane chromatography increases with the number of available adsorptive sites and their relative affinity for the biological molecule of interest. Separation efficiency decreases owing to backmixing, dispersion, molecular diffusion and finite ligand–ligate association rates.

5.1. Characterizing membrane columns

The separation performance and physical attributes of adsorptive membrane units are characterized in much the same fashion as chromatographic packed beds. Most commonly, the effluent response to a sharp input pulse or step change in concentration of a single model adsorbate is detected using UV–Vis absorption. Features of the curve, notably its temporal moments, indirectly indicate mass transport rate effects such as dispersion, backmixing and ligand–ligate interactions. They are also used to measure equilibrium adsorption attributes which include column capacity and non-linear interaction at high adsorbate concentration.

Recently, environmental scanning electron microscopy [32] and nuclear magnetic resonance microscopy [33] have been used to characterize membrane separchim units in order to avoid the ambiguities associated with effluent analysis. Both are high-resolution techniques. Magnetic resonance has the advantage of allowing non-destructive and non-invasive visualization of static and operating units using one of a number of contrast sensitivities [34,35].

A magnetic resonance image of a representative adsorptive stacked membrane, the MemSep 1000 cartridge (Millipore, Bedford, MA USA) is reproduced in Fig. 3 [36]. The dimensions of the stacked-membrane bed are 5 mm × 17.17 mm I.D., which constitutes a 1.4-ml nominal bed volume. The length-to-width aspect ratio of the cartridge which appears in the image (1.2:1) is six times larger than the actual ratio (1:5) in order to enlarge physical features of the adsorptive bed. Forty microporous membranes approximately 120 μm thick with a nominal pore diameter of 1.2 μm comprise the stack. The membrane substrate is pure regenerated cellulose. A uniform matrix porosity of 0.827 has been reported [37].

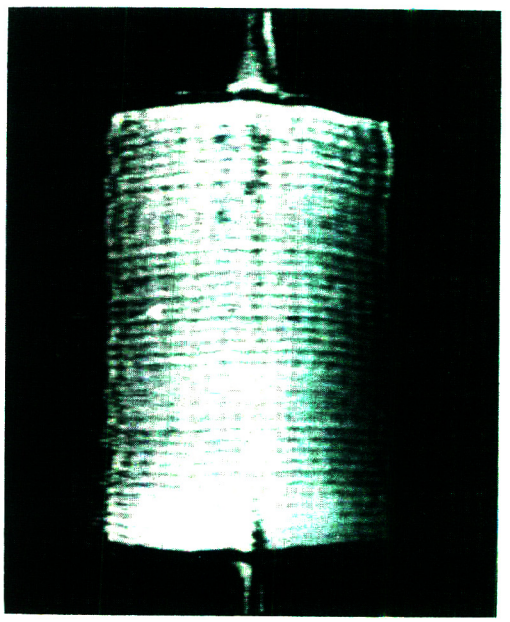

Fig. 3. Spin-echo magnetic resonance image of an adsorptive stacked membrane. A 1.8-mm sagittal slice parallel to the axis and through the centerline of a MemSep 1000 is shown. The cartridge is connected to inlet and outlet tubing and filled with non-flowing water. A long spin–lattice relaxation delay (1 s) and short spin–spin relaxation delay (0.4 ms) make signal intensity or brightness proportional to proton density. The length-to-width aspect ratio of the membrane bed in the image, 1.2:1, is six times larger than the physical ratio of 1:5 to enlarge physical features of the adsorptive bed.

The spin-echo image in Fig. 3 illustrates water distributed in a 1-mm slice of a MemSep 1000 stacked membrane parallel to its axis and through its centerline. Signal intensity (white-

ness) is proportional to proton density or water concentration. Incoming mobile solvent (white) enters the column by passing through an upstream Luer-lock adaptor (top). Porous frits (black) at upstream and downstream ends of the membrane bed (grayish to white) distribute incoming fluid across the membrane cross-sectional area. (The frits appear bowed owing, in part, to the contracted horizontal aspect of the image.) Nine donut-shaped gaskets (black), which appear as rectangles on either side of the bed, encircle the stack, separating every four membranes. They are intended to exclude solvent from the bed periphery and prevent incoming fluid from bypassing membrane stack. Outgoing solvent (white) leaves the column through a thin Luer-lock adaptor.

5.2. Mass transport effectiveness

Dissolved solute molecules are transported through an adsorptive membrane by bulk flow of the mobile solvent (convection). Within the membrane, solutes experience three consecutive transport rate resistances to ideal, equilibrium separation: dispersion, Brownian thermal diffusion and kinetic sorbate–sorbent interaction. We briefly consider each of these processes in succession. A pictorial representation of convection and dispersion at the microscopic level is suggested in Fig. 4.

5.2.1. Convection

At a pseudo-continuum scale large with respect to membrane porosity, but small relative to membrane dimensions, bulk flow through porous membranes has been characterized by Darcy's law with a membrane permeability given by the Blake–Kozeny equation [11]. In this description, local velocity is proportional to local pressure drop, as has been demonstrated [30]. GMA–EDMA copolymer membranes exhibited a linear increase in permeability with increasing pressure drop [38]. Nominal pore sizes reported for two nylon membranes, 0.45 and 3 μm, are representative of the range of pore diameters found in adsorptive membranes [39]. Measured permeability of the 3-μm membrane was ten times

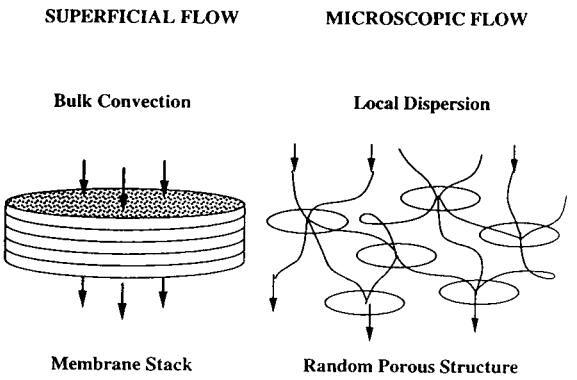

Fig. 4. Idealized diagram showing bulk flow of solvent through a membrane stack and microscopic dispersion of solvent within membranes pores. Characteristic mass transport effects differ at different scales. The random porous structure in adsorptive membranes, whose nominal dimension is of the order of microns, exhibits local mixing. Stacked-membrane beds, whose dimensions are of the order of millimeters, exhibit pressure-dependent flow.

that of the 0.45-μm sheet. Polymer-rod columns have an average pore size of 19.5 μm [18].

Ideally, bulk flow of solvent carries adsorbate molecules toward the column outlet at the same rate in each volume of the column. Accordingly, physical and mathematical descriptions of packed-bed chromatography generally assume a constant, uniform interstitial velocity. In adsorptive membranes, however, it has been shown that the axially directed velocity of a mobile solvent can be much faster in the center of the separation unit than near the edges of the adsorptive bed. Direct, *in situ* measurements of local velocity in operating membrane separation units obtained by magnetic resonance flow imaging reveal non-uniform radial and axial variations in interstitial velocity [40]. The decrease in apparent porosity from the center of the bed to the gasket area evident in Fig. 3 may account for the decrease in velocity observed adjacent to the gaskets. Velocity in ideal porous media increases non-linearly with void fraction [41]. Jetting occurs around the center of another membrane stack at flow-rates exceeding 5 ml/min, resulting in little or no adsorption near the periphery [42].

Bypassing and uneven fluid distribution are additional sources of non-uniform flow. Incom-

ing fluid which bypasses the membrane stack or distributes unevenly across the adsorptive membrane cross-section has been indirectly observed by dye injection [14]. Other stacked-membrane systems, however, have demonstrated an absence of bypassing or channeling [43]. A fluid distributor consisting of semicircular channels radiating out from the fluid inlet which were connected by annular grooves gave the most even fluid distribution in a group of laboratory-scale stacked-membrane columns [14].

Where they are present, local variations in the rate of bulk flow within a column degrade a separation by backmixing previously separated solutes. The result is asymmetric elution peaks and breakthrough curves with unexpected width. The most pervasive indication of non-uniform flow in membrane systems is peak tailing. Tailing is pronounced in peaks from step-gradient elution of model proteins from adsorptive membranes [11,42,43]. Illustrated effluent profiles from a variety of commercially available stacked-membrane columns exhibit notable tailing [16,25,44]. Secondary solute–matrix interactions could also contribute to tailing of eluting peaks.

The most direct evidence linking tailing and non-uniform flow combines magnetic resonance flow imaging, effluent analysis and a novel reversed-flow experiment to descriminate between tailing due to extra-column dispersion and tailing due to non-uniform flow using a non-adsorptive tracer [40]. Quantitative decreases in separation efficiency corresponding to asymmetry and especially peak tailing in effluent responses from non-adsorbing pulse injections have been linked directly to non-uniform flow.

5.2.2. Dispersion

During convection in bulk flow, individual adsorbate molecules are dispersed owing to micro-scale fluid-phase phenomena [45]: mixing by solid obstructions to flow, incomplete connectivity, eddies and recirculation from regional pressure gradients. An analytical description of Fickian convective dispersion also includes the dispersive effect of random Brownian diffusion in the direction of flow [46].

In the absence of backmixing and intraparticle diffusion, convective dispersion remains as the primary contributor to band broadening or separation inefficiency in adsorptive membranes. Broadening due to dispersion can be estimated by analogy with packed chromatographic beds [47]. Widths of effluent profiles from adsorptive membranes broadened by dispersion alone are expected to decrease with increasing velocity, giving plate heights on the order of 1 μm.

5.2.3. Diffusion

The primary mass transport advantage of adsorptive membranes relative to conventional packed beds is their lack of intraparticle diffusion. To access most of the adsorptive capacity in a packed bed, adsorbates must diffuse from the flowing, interstitial fluid through tortuous, porous particles. Hence the effective path length for intraparticle diffusion in conventional chromatography corresponds to the particle diameter, which typically exceeds 5–10 μm on the preparative scale owing to backpressure limitations. In derivatized membranes, adsorptive sites are directly adjacent to the bulk fluid, so the effective diffusion path length is less than the substrate pore size, which, in turn, is commonly less than 1 μm. Increasing the membrane pore size from 0.45 to 3 μm had no measurable effect on the adsorption rate [39], suggesting solutes were quickly convected to adsorption sites on membrane surfaces.

Reducing the diffusional path length allows volumetric throughputs to be increased substantially, while maintaining membrane capacity. A reduction in intraparticle diffusion noted for macroporous, pellicular resins affords a similar advantage [48]. Adsorption efficiency is increased dramatically for biological macromolecules such as proteins and plasmid DNA, since the diffusion rate is proportional to solute diffusivity.

Nonetheless, diffusion of adsorbates into other dead volumes which are permeated by the mobile phase but inaccessible to flow could affect the separation efficiency and prolong regeneration. For example, the presence of a signal between adjacent exclusion gaskets in Fig. 3 (about 0.25 mm apart) implies that these vol-

umes are accessible to buffers and dissolved solutes by Fickian diffusion. An order-of-magnitude estimate of the diffusive solute permeation distance into the gap between gaskets is $L = (2DT_\nu)^{1/2}$, where T_ν is the permeation time-scale and D and ν are solute diffusivity and interstitial velocity, respectively.

For slow (1 ml/min), narrow-pulse protein separations typical of chromatographic analysis, the appropriate permeation time-scale is $0.25/\nu$, which equals the 0.25 mm separating the gaskets divided by the solute velocity past the gap. This shows that the corresponding distance is negligible (about 1 μm). However, for adsorptive membrane concentration in preparative bioseparations using frontal or recirculating operating modes, the time available for permeation may be 1 h or more. The corresponding permeation distance approaches 100 μm. Complete recovery of product that diffused between gaskets will take at least as long as the initial loading. It has been observed experimentally that about 2 h are necessary to exchange buffers completely and achieve a steady UV absorbance baseline in a MemSep 1000 [40]. This equilibration time corresponds to the time required for a salt to diffuse from the stacked-membrane periphery, through the intergasket gap to the moving fluid phase.

5.2.4. Adsorption

The rate of adsorption on to conventional ion-exchange and hydrophobic interaction media is typically unappreciable with respect to dispersive and diffusional resistances to mass transport. Sorbate–sorbent interaction is often considered instantaneous [39]. On the other hand, the formation of an affinity complex is often so slow as to become the rate-limiting mass transport process [49]. It remains to be shown that convective dispersion is negligible with respect to reaction kinetics in existing affinity membrane systems. Affinity association kinetics must be considered in determining the operating velocity of a membrane which optimizes dynamic capacity.

5.2.5. Extra-column backmixing

The separation performance of adsorptive membranes can be severely degraded by backmixing in volumes outside the adsorptive membrane bed: distributors, tubing, adaptors, valves, mixers and pumps. Excessive peak broadening and dilution have been attributed to significant dead volumes in fluid distributors [14], filter holders [50] and Luer slip outlets [42]. The last appeared to act as a continuous mixer. A 1-ml extra-column void volume, monitored by UV adsorption of effluent BSA in a non-adsorbing mobile phase, produced a broad, asymmetric breakthrough curve under adsorbing conditions [51]. This broadened transitions between plateaus of emerging eluents which have differing binding affinities.

Extra-column band broadening is more significant in adsorptive membrane systems than in chromatographic columns owing to the large ratio of throughput to bed volume in the former. Experimental evidence suggests that extra-column band broadening changes little with velocity [52]. Its effect is significant relative to other mass transport resistances, and has been observed to predominate [51].

A simple experimental protocol has been suggested to discriminate between peak broadening and tailing arising from extra-column backmixing, convective dispersion or non-uniform flow [47]. This should allow users to select a membrane stack with the highest separation potential, and allow manufacturers to design more efficient membrane adsorption systems.

5.3. Thermodynamics of adsorptive membranes

Having accounted for the possible degradation of separation efficiency of backmixing and resistance to mass transport, we now consider the intrinsic separation potential of membranes determined by the available number of adsorptive sites and their relative affinity for the molecule of interest. We discuss measured capacities of adsorptive membranes and measurements and models of their equilibrium behavior.

5.3.1. Capacity

Reported capacities for several adsorptive membranes are summarized in Table 3. Static capacities increased from 3.3 to just over 50 mg

Table 3
Reported capacity values of adsorptive membranes for several biological macromolecules: monoclonal antibody (MAb), malate dehydrogenase (Md), human serum albumin (HSA), ribonuclease (Rib), lysozyme (Lys), ovalbumin (Ova), bovine serum albumin (BSA), γ-globulin (G-G), immunglobulin G (IgG) and a mixture of IgG and IgA (BGG)

Membrane	Capacity (g/m^2)	Static capacity (mg/ml)	Dynamic capacity (mg/ml)	Ref.
C-4		200–400	50	[38]
Cation exchange			50 (MAb)	[55]
Dye affinity	10.7 (Md)	50.8 (Md)	45.7 (Md)	[53]
Anion exchange			5.8 (HSA)	[31]
Copolymer		20 (Rib), 26 (Lys), 47 (Ova)	5 (Rib), 0 (Lys), 5 (Ova)	[38]
Copolymer		40 (Ova)		[15]
L-Phe affinity hollow fiber			50 mg BGG/g fiber	[22]
Anion exchange			30–40 g BSA/g membrane	[16]
Anion exchange	1.29	20		[19]
Dye affinity		8.6 (Lys), 5.6 (BSA)	7.8 (Lys), 7.6 (BSA)	[57]
Protein A/ IgG affinity		4.74 (IgG–rabbit), 0.51 (protein A)		[25]
Protein A affinity		3.3 (G-G)	2.9 (G-G)	[39]
Ion exchange			8 IgG per cartridge	[54]

macromolecule per ml of membrane. These are typically lower than for comparable porous chromatographic resins, with occasional exceptions [30]. It has been reported that the volumetric capacity is large with respect to large-scale chromatography [30].

Static capacity values are obtained by equilibrating a known amount of membrane with a concentrated volume of dissolved solute and measuring the solute uptake relative to the membrane volume. Mass, volume and surface-area measurements which are equivalent are unique to each membrane and allow capacity to be expressed in alternative units. For example, 1 cm^2 of Sartobind Blue 2 membrane corresponds to 0.021 ml or 8.2 mg of the membrane [53].

Dynamic capacity values are obtained by flowing concentrated solute through a membrane and measuring the mass adsorbed per unit volume of membrane bed at a breakthrough concentration 10% of the inlet concentration [50]. Some adsorbent volumes remain unused owing to back-mixing, non-uniform flow and resistance from mass transport rate processes. As a result, dynamic capacities are smaller than corresponding static values. Solute capacity varies with adsorptive conditions including solvent composition, buffer concentration, pH and flow-rate [54]. Increasing the flow-rate lowered membrane capacities in the ion exchange of selected model proteins, while slightly raising the hydrophobic interaction capacity in other systems [11,42]. A dynamic capacity of 50 mg/ml for MAb on a strongly acidic S cation exchanger was obtained

while loading of flow-rates exceeding 800 ml/min (0.57 cm/min) on a pleated 1400 cm^2 membrane [55].

The dynamic capacity of one dye-affinity membrane remained within 95% of its static value, whereas that of a corresponding dye-affinity packed bed decreased by 50% when linear velocity was increased over tenfold [54]. The column however, retained more of its original capacity as the percentage of *Escherichia coli* extract added to the feed was increased to 10%, while the membrane became blocked at 5%. Dynamic capacities were also maintained after more than ten-fold flow-rate increases for HSA adsorption on a DEAE anion exchanger [31].

The capacity of a protein A membrane decreased by 30% after about 30 use and regeneration cycles, suggesting that its long-term stability may be suspect [25]. In general, affinity matrices containing proteins cannot be cleaned with NaOH or used with high protein concentrations or crude solutions. In contrast, binding capacities in ion-exchange membranes are routinely maintained after 25–100 cycles of use and high-salt regeneration [42,56].

Membrane geometry and coupling chemistry also influence capacity. The measured capacity of Ultipor microfiltration membranes was highest when PEI was used as a spacer arm to couple Cibacron Blue F3G-A to the nylon-66 membrane substrate [57]. In nylon membranes with 0.45- and 3-μm pores, the static and dynamic capacities were 3.3 and 2.9 mg/ml, respectively, for membranes [39].

This suggests using the membrane with the larger pore size to decrease the backpressure at higher flow-rates.

5.3.2. Equilibrium

Measured adsorption equilibrium isotherms of protein A, IgG [25] and BSA [30] on pseudo-affinity membranes appear to be of the Langmuir type. This suggests that an adsorption monolayer exists and that non-linear effects on separation performance at high surface concentrations of adsorbate are significant. Values of Z (the number of interaction sites for a solute–adsorbent pair) and log K (parameter including equilibrium formation constant, phase ratio and bound solute concentration) obtained experimentally for ion-exchange adsorptive membranes are smaller than under comparable packed-bed conditions [11]. Local equilibrium behavior of multi-component adsorption has been observed on ion exchangers [58]. The sum of the natural logarithms of the retention and capacity factors on reversed-phase polymer rods decreased in proportion to the organic volume fraction [18]. This is comparable to reported reversed-phase packed-bed behavior.

Single and binary solute adsorption on affinity membranes has been theoretically analyzed using a local-equilibrium model [59]. Computer simulations indicated that solutes with identical equilibrium sorption isotherms whose sorption kinetics differ can be separated on affinity membranes. Simulated axial diffusion and slow adsorption degrade separation owing to differences in local equilibrium, particularly on membrane stacks less than 3 cm. Local equilibrium behavior is not reached on commercially available units at typical operating flow-rates.

Adsorption-rate models of membranes which fail to account for the effects of non-uniform flow, convective dispersion and extra-column broadening which dominate adsorptive membrane mass transport (see Section 5.2) cannot be expected to predict reliably effluent shape or describe separation performance.

5.4. Plate height estimates of membrane efficiency

A popular, scale-independent measure of adsorptive separation efficiency is the plate height, H, or column height equivalent to a theoretical plate. For systems with a linear adsorption isotherm, constant equilibrium distribution coefficient, concentration-independent transport properties and uniform flow, the plate height is defined as the ratio of effluent peak variance to the length of the column. The plate height decreases with increasing column efficiency.

A description of separation efficiency in adsorptive membranes based on fundamental mass transport processes suggests that plate heights should decrease from about 10 μm at 0.05 cm/

min to less than 1 μm at about 5 cm/min [33]. Corresponding plate height measurements in two membrane columns in the absence of non-uniform flow and extra-column backmixing agreed with this description. Reported plate height and corresponding velocity ranges for membrane adsorbers are summarized in Table 4.

Reported plate height estimates vary over three orders of magnitude in the same range of velocity. Other than for a single, 200-μm membrane supported in an ultrafiltration cell [25], the remaining plate heights were estimated for stacked-membrane cartridges. Varying plate height estimation methods, unaccounted for backmixing and variations in stacked-membrane structure and operation contributed to the range of reported values.

Investigators in four studies observed significant increases in effluent band broadening (and therefore plate height) due to dispersion in extra-column dead volumes [57,25,52,47]. However, in only two cases were extra-column effects removed from plate height estimates. Extra-column broadening is probably the reason for the unexpectedly large reported plate heights and their relatively small increase with velocity.

The theoretically large efficiencies of membrane adsorbers are not realized in most reported separations. Measured plate heights, for the most part, have been comparable to fixed-bed efficiencies [60]. At the same time, few mixtures of model proteins require more than a handful of theoretical plates to achieve a product purity in excess of 98% [61].

6. Operation of membrane adsorption

Building on experimental results which illustrate their unique mass transport, thermodynamic and geometrical aspects, we summarize the appropriate operation of adsorptive membranes.

In Section 6.1 we review the location within a biological recovery sequence appropriate for membrane adsorption. We then consider in Section 6.2 operating modes of membrane adsorption. In Section 6.3 the reported throughput of membrane adsorption is compared with that of conventional packed-bed chromatography.

6.1. Membrane adsorption in biological recovery

Recovery of labile genetic templates or gene products for their biological host environment typically involves several consecutive isolation processes which distinguish the product from one or more contaminants based their differing physico-chemical structures. It is useful to organize the individual processes of a non-denaturing, protein recovery sequence into four categories as suggested by Scopes [62] and Lightfoot and Cockrem [63]. A cellular extract, harvested from the fermentation, which contains unexcreted product is first homegenized and clarified to render the product accessible. Lysis of whole cells by enzymatic degradation, ultrasonication, Gaulin-press homogenization or milling releases

Table 4
Experimental adsorptive membrane plate heights (H)

H range (μm)	Velocity range (cm/min)	Estimation method	Extra-column mixing included	Ref.
3.3–0.59	0.52–3.8	Reversed-flow	No	[47]
3–7	0.07–0.22	Unreported	Yes	[25]
25	0.1–2	Unreported		[31]
50–110	4–1.5	EMG fit	Yes	[44]
80–160	1–45	Unreported		[18]
400	0.04–1	Unreported	Yes	[11]
250–800	0.035–6.5	Moments	No	[52]

and solubilizes intracellular enzymes. Subsequent precipitation of cell debris, nucleic acids and insoluble proteins by centrifugation decreases fouling in later process steps. Selective precipitation is effected by adding salt, organic solvent, detergent or polymers such as polyethyleneimine and poly(ethylene glycol) to the buffered cell lysate [64].

Size-selective membrane microfiltration removes cell debris, colloidal or suspended solids or virus particles [8] from the clarified lysate. Subsequent diafiltration into an appropriate buffer prepares the solution for a concentrating adsorptive process in an economical fashion [26]. Microfiltration and concentration have been performed simultaneously using a spiral-wound membrane adsorber [54]. Incompletely clarified lysate has been shown to foul dead-end stacked-membrane adsorbers, at concentrations as low as 5% [53]. Membrane adsorption has also been applied simultaneously to filter and concentrate recombinant product secreted into a complex fermentation medium. Elution of the bioproduct and contaminants with similar physical properties is discussed in Section 6.2.

Additional complementary separation processes are usually required to fractionate the product from similar contaminants based on differences in size, mass, isoelectric point, charge density and hydrophobicity. Examples of affinity, ion-exchange, hydrophobic interaction and reversed-phase membrane adsorbers used to fractionate product mixtures are discussed in Section 7.

Finally, the concentrated product is purified from closely related variants by a high-resolution technique (prior to final formulation and packaging of pharmaceutical bioproducts). Purification often requires differential adsorption in an adsorptive column with a large number of theoretical plates to attain the required purity. Overall recovery yields which had hovered at about 30% are becoming as high as 60–70% in recent reports [65].

In Fig. 5 the consecutive isolation processes are shown. Adsorptive membranes have been inserted in the clarification, concentration, fractionation and purification steps. In these processes, literature reports have indicated their successful application in a similar recovery train.

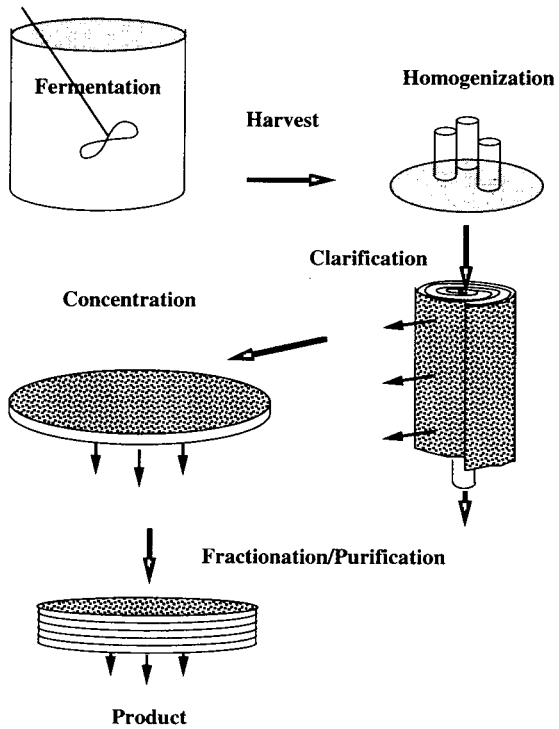

Fig. 5. Schematic illustration showing a typical sequence of processes to recover non-secreted protein from bacterial host. Adsorptive membranes are reported to have been used to clarify, concentrate, fractionate and purify homogenized cell extract. Clarification has also been performed using hollow fibers and stacked membranes. Polymer rods have also been used for concentration, fractionation and purification.

6.2. Selective elution vs. differential migration

Membrane adsorbers can be operated in two distinct ways to separate and purify a designated biomolecule from similar contaminants. Often buffer conditions can be manipulated to instantaneously desorb, in series, a number of adsorbates. This procedure is referred to as selective elution. Considerations and advantages of selective elution are examined first. In other cases the desired product is gradually separated from contaminants due to its preferential affinity for

the stationary solid phase as the buffer conditions are kept constant, or gradually changed. This procedure, commonly called differential migration, will also be discussed.

Selective elution and differential migration represent the two extremes in operating adsorptive separations. Gradient elution of small molecules from granular columns often first results in differential migration, and then subsequently in selective elution as the concentration of the desorber increases. This "mixed-mode" scenario is less likely to occur in adsorptive-membrane separation of biomolecules, for reasons which we now address.

6.2.1. Selective elution

To date the most common application of adsorptive-membrane separation has been to concentrate product from dilute, clarified lysate or fermentation broth by pumping multiple bed volumes of feed through the membrane at buffered conditions which favor the adsorption of the desired product. After washing the bed to remove weakly-adsorbed contaminants, the product of interest and similar contaminants are eluted consecutively by changing the pH, ionic strength or organic composition of the mobile phase. Selective elution by isocratic, stepwise or gradient changes in mobile phase composition is commonly employed to purify the product. The membrane is regenerated and subsequently re-equilibrated in the adsorptive buffer in order to repeat the process.

Regeneration of adsorptive membranes, which are easily backflushed to remove residual protein contaminant, is determined by their chemistry. A strongly-basic QAE-ZetaPrep anion exchanger required only 1 *M* NaCl [54] for regeneration. Ion-exchange membranes can be completely regenerated by successively applying strong NaOH and HCl, or by in-line steam sterilization. Affinity columns, however, cannot be regenerated in this manner due to the labile nature of their ligands. By comparison, silica-based adsorbents dissolve within 30 min in boiling 1 *M* KOH (pH 14), as do analogues derived from magnesia and controlled-pore-glass [20].

As an example of concentration and purification by selective elution, immunoglobulin G (IgG) was adsorped from hybridoma culture supernatant onto a radial-flow membrane with an anion-exchange matrix in a running buffer of 50 m*M* Tris–HCl, pH 8.0 [54]. Weakly-bound contaminant proteins were seletively eluted by first increasing the NaCl concentration from 0 to 50 m*M* in the buffer. Another step increase of NaCl to 150 m*M* selectively eluted the IgG at a concentration ten times greater than that in the feed. Seventy percent of the original IgG was removed in the targeted fraction, while 30% of contaminating proteins were eliminated. The cartridge was regenerated with 1 *M* NaCl and re-equilibrated in the running buffer.

Elution by gradient or step-change in mobile phase composition often completely desorbs concentrated solutes. Such completely-desorbed solutes are convected toward the outlet of the adsorptive bed in the mobile-phase buffer at a velocity equal to that of the mobile phase. We noted in Section 5.3 that experimentally-obtained values of Z and log K for stacked-membrane adsorption have been found to be smaller than those for granular chromatographic beds operated under comparable conditions. This fact implies that relatively small changes in mobile phase composition can cause complete desorption of solutes from membrane matrices. It is therefore likely that separation by selective elution from adsorptive membranes is common, whether intended or not.

The thickness of the membrane bed in which separation takes place is relatively narrow. On the other hand, the entire length of the bed following desorption participates in mass transport processes explained in Section 5.2. During elution from adsorptive membranes, adjacent bands of solute broaden due to non-uniform flow, convective dispersion, and extracolumn backmixing. Completely-desorped solute bands broaden without further purification and can eventually overlap, producing a decrease in product purity relative to their initially desorbed state [66]. While non-uniform flow and extracolumn backmixing can severely increase peak broadening in membrane chromatography after desorption, these effects are not commonly predominant in granular packed beds. So packed-column length has less reported effect on res-

olution. Broadening during elution in granular columns is predominantly due to intraparticle diffusion. Provided flow non-uniformity and extracolumn mixing is limited, short membrane adsorbers are expected to degrade the purity of adjacent eluting bands less than longer granular columns.

As an example of lessened post-desorption broadening in membrane adsorbers, consider results from a separation by Tennikova and coworkers [38]. A negligible concentration gradient across one membrane was observed, resulting in instantaneous desorption throughout the adsorptive membrane bed. Resolution of model proteins on a GMA–EDMA 1-mm long membrane achieved by gradient elution were slightly better than those obtained using a packed, GMA–EDMA 140-mm long microcolumn [15]. It appears likely that this separation was achieved by selective elution. At a constant gradient slope in time, resolution in another membrane system was reported to be independent of flow-rate [14,42]. Resolution in this case was likely achieved by complete, selective elution of the solutes. Of course, performance of differing membrane adsorbers varies. Thicker beds have demonstrated relatively greater resolution by eliminating bypassing, improving flow uniformity [14].

6.2.2. *Differential migration*

Elution by gradient or step-change in mobile phase composition may also produce differential migration of concentrated solutes, in which the average velocity of each desorbed solute is proportional to its fractional equilibrium fluid-phase concentration. Resolution of adjacent bands in differential migration increases in proportion to the number of theoretical plates in a membrane. Differential migration further purifies a product from closely-related contaminants or a subtle variant.

Gradient elution is normally used to remove adsorbed components from membranes. Gradient elution is convenient since it is difficult to determine a priori the modifier concentration required to selectively elute just the desired species. In one example, a NaCl gradient removed human tumor necrosis factor, an unglycosylated polypeptide consisting of 157 amino acids, from an ion-exchange membrane [16]. Decreasing the gradient slope (or increasing the gradient volume) has been reported to improve resolution in stacked-membrane protein separations [11]. This feature can indicate separation by differential migration is taking place.

The additional effort required to determine appropriate step changes in mobile phase composition becomes more important at production scale, where efficient use of solvent and desorbent improves process economics. Stepwise elution typically produces more efficient membrane separations than linear gradients [14]. For example, stepwise NaCl increases eluted two plasma membrane glycoproteins from heparin and collagen stacked-membrane columns more successfully than a linear gradient [67]. In separate studies, stepwise salt increases eluted three model proteins from the respective membrane successively with less peak overlap and less solvent usage than a gradient [11,31]. High purity in consecutive step elutions, particularly at high protein loading, suggests binding sites available to biomolecules on adsorptive membranes are homogeneous.

Forethought in organizing a series of purification processes can also improve separation efficiency. A single elution step was used in each of a series of membrane adsorptions —cation-exchange, dye-affinity, and anion-exchange— to rapidly recover formate dehydrogenase [50]. The series was organized so that the elution buffer from one membrane served as the adsorption buffer for the next, avoiding buffer exchange, pH modification or dead time between successive steps.

The efficiency of selective elution using step changes in desorbent suggests this operating mode of membrane chromatography is preferable to differential migration, when conditions to effect selective elution can be determined.

6.3. *Throughput of adsorptive membrane separations*

The reported resolution, recovery and capacity of many adsorptive membranes are comparable to those of fixed-bed systems [16,56]. Pore size

apparently has little effect on resolution [30]. Relative concentration factors (about tenfold) and bed capacities of adsorptive membranes are smaller than those of packed-bed analogs [50,56].

The primary advantage of adsorptive membranes which compensates for these marginal characteristics is their substantially higher throughput. In one reported comparison, the total separation time using membranes was half that of corresponding fixed beds [16]. Another comparison reported that throughputs of cation- and anion-exchange membranes, 0.60 g/h of recombinant antithromin III and 2.1 g/h of MAb, respectively, were than four and thirteen times larger than with corresponding fixed-bed gel matrices [56]. Reported cycle times for membrane recovery were ten times faster than for columns [30]. The lack of mass transfer resistance by intraparticle diffusion permits greater interstitial velocities in membranes than in particulate beds while maintaining capacity [23]. This advantage has been referred to as "fast reaction kinetics" [14].

The speed at which membranes separations are performed decreases solvent usage and product degradation, which improves process economics and recovery yields. In mAb purification, for example, product losses by proteolytic cleavage or cleavage of disulfide bonds increase with processing time [54]. Radial membrane adsorption used to isolate mAb purified 10 l of supernatant within 3 h [54]. The recovery of β-1,4-D-xylanase with an SP-ZetaPrep 250 ion-exchange membrane yielded a higher product activity at less cost when compared with competitive ultrafiltration and precipitation processes [68]. The processing rate by ultrafiltration in this case was less than one third that of ion-exchange adsorption. Precipitation required uneconomical amounts of salts and solvents, while the costs of pumps and pumping were higher for ultrafiltration than for adsorption.

Neraly all reported analyses concur that backpressures in adsorptive membranes are low, even at high flow-rates [11,14,69]. Membrane backpressures are as much as 100 times lower than for comparable packed beds at the same flow-rate [15,38] (polymer rods are the single exception [18]). Owing to these limited backpressures, flow-rates of 200–500 ml/min are accessible without the use of high-pressure pumps or equipment [56,70]. Reduced backpressures become a greater advantage as the mobile phase viscosity and the scale of separation increase.

The porous nature and hydrophilicity of some membrane beds may account for additional reported advantages. Clogging by insoluble precipitates produced during adsorption or regeneration was reduced relative to packed beds [43]. Clogging could be prevented by prefiltering prior to adsorption. The use of detergents allows the separation of hydrophobic proteins and does not present difficulties [14]. The interstitial void volume due to empty spaces between spherical beads in a packed bed is avoided in membranes. This reduces the non-adsorptive dead volume by 26% [38]. Nominal values reported for bulk membrane bed porosity ranged from 50 to 82.7% [37,38]. Minimal shearing has also been noted [43].

6.4. Scale-up

Reports of scale-up of membrane chromatography to larger throughputs are favorable. A stacked-membrane column, scaled up by maintaining the bed length while increasing the bed diameter from 10 to 50 mm, produced a resolution equivalent to its laboratory-scale counterpart [14]. In another stacked-membrane scale-up resolution of monoclonal antibodies (mAb) was reproducible at 30 times the laboratory-scale flow-rate and sample volume [54]. The dynamic capacities of ion-exchange and dye-affinity membrane stacks for formate dehydrogenase remained constant after a 40-fold increase in cross-section [50].

A radial-flow membrane chromatographic column was scaled up by increasing both the diameter and height [13]. The flow-rate was increased in proportion to the cartridge volume in order to maintain the real-time behavior of the cartridge. The apparent specific capacity decreased slightly as the adsorptive bed volume increased to 12.8 times its original value.

There is, however, a dearth of commercially available production-scale devices whose characterization has been reported.

7. Applications of adsorptive membrane chromatography

In this section, reported applications of the adsorptive recovery of biomolecules using membrane substrates are reviewed. The applications are categorized according to the ligand chemistry of adsorption. We first consider affinity separations in Section 7.1. Examples of biospecific, dye ligand, immobilized metal, and pseudo-affinity adsorption have been reported. Ion-exchange membrane adsorption is summarized next in Section 7.2. Both weak and strong cation- and anion-exchange ligands are commercially available and have been examined. Section 6.3, considers membrane adsorption by Van der Waals or hydrophobic interaction. Membranes categorized as analogs of hydrophobic interaction and of reversed-phase chromatographic chemistries have had limited application. While indicating the range of applications of membrane adsorption in this section, we focus on applications to actual (rather than model) separations which suggest insights into the use of adsorptive membranes which could be extended by other members of the chromatographic community.

7.1. Affinity chromatography

Membranes were first widely used as substrates for affinity adsorption [11]. Development of an affinity system requires concerted effort focussed on achieving one-step purification of 1000-fold with nearly complete recovery in good scenarios. Membrane substrates offered a workable alternative to particulate affinity adsorbents whose low flow-rates were dictated by gel compressibility, pore diffusion and backpressure limitations [13]. Table 5 lists the ligand, ligate, elution conditions and geometry of several affinity membrane adsorptions. Some additional affinity separations are given in Table 3. A brief review of affinity applications can be found in Ref. [25]. We examine diffusional response, capacity, elution, and ligand choice in affinity membrane separations.

Table 5
Examples of affinity membrane adsorption

Ligand	Ligate	[22,69]
Protein A	γ Globulin	[39]
Ligand	Trypsin, trypsin-like proteases	[13]
Ligand	Glycoproteins	[67]
Heparin, collagen	Hydrophobic proteins	[14]
Dye	Bovine serum albumin (BSA)	[30]
Dye	Formate dehydrogenase, pyruvate decarboxylase	[30]
mAb	BSA	[71]
Protein A	IgG	[71]
Phe, Tyr	IgG, IgA	[22,69]
Copper	Amino acids	[23]

A brief order-of-magnitude anlysis illustrates the diffusional advantage of affinity membranes. The characteristic time for association between a ligand and an immobilized antigen is about 1 s, while the time for protein diffusion ($6 \cdot 10^{-7}$ cm^2/s for BSA) to the center of a 50-μm porous bead is greater than 40 s. So eliminating intraparticle diffusion increases the dynamic capacity and throughput efficiency of affinity adsorption (see Sections 5.2, 6.3) [39]. Improved throughputs were demonstrated using IgG adsorped to a Protein A hollow-fiber membrane [71] and amino acids separated by a metal affinity membrane (IMAM) [23].

Capacity of affinity membranes for biomolecules are in general lower than those observed in ion exchange or reversed-phase systems. An estimated one to two percent of potential affinity sites actually bind the ligate. Observed multipoint attachment of ligand and ligate also limits binding capacity [25]. Consequently, a capacity value of 1–2 mg/ml is acceptable. So demonstrated capacities listed in Table 3 for dye and pseudo-biospecific ligands which increase from 2.9 to 50.8 mg/ml are considered good. The open-pore structure of membrane matrices is reported to increase accessibility to affinity ligands and reduce steric hindrance relative to small-pore adsorbents.

Elution conditions required to remove ligates from affinity systems are determined by the interaction(s) involved. Ionic strength is increased to minimize non-specific electrostatic interactions and decreased to reduce hydrophic effects. Hydrophobic and Van der Waals interactions can also be absolved by reducing surface tension using a non-ionic detergent such as Triton X-100, ethylene glycol, or ethanol. High concentration of a chaotropic salt such as thiocyanate can eliminate both non-specific electrostatic and hydrophobic interactions. Elution from affinity membrane beds predominantly employs gradient or step changes in eluant composition to selectively elute products. Effluent curves measuring the adsorption, wash, and elution of a mixture of IgG and IgA on Phe and Tyr pseudo-affinity membranes have been reported [69].

Pseudo-biospecific ligands have been widely used in reported affinity-membrane adsorption. Examples include protein A, protein G, heparin, collagen, and two amino acids: arginine (Arg), and L-phenylalanine (Phe) coupled with an epoxide group. Josic and co-workers [14,67] reported pseudo-specific adsorption was preferable for preparative recovery since the mild elution conditions employed maintained the native conformation of glycoproteins. Antigen–antibody complexes created during indirect immunoaffinity adsorption were only disrupted by acid (pH 2.4) which resulted in a loss of enzymatic activity. Indirect immunoaffinity consists of a matrix coupled to protein A or G which non-covalently binds antibody. The antibody then, in turn, associates with the antigen. It was also observed that monoclonal antibodies (mAb) raised against membrane glycoproteins lost almost 90% of their binding activity upon covalent immobilization [67].

Dye adsorbents which demonstrate affinity for nucleotide binding sites on enzymes have also been employed. Monoclonal antibodies were the most common immunoaffinity ligand used. An immobilized metal affinity membrane (IMAM) was developed by chemical conversion of the membrane epoxide to iminodiacetate and subsequent chelation with copper [23]. Affinity ligands are covalently attached to membrane matrices using coupling chemistries briefly reviewed in Section 4.2. Stable linkages are necessary to prohibit leaching of the ligand into the effluent stream. The length of spacer armed used is critical in the observed performance of affinity membrane systems.

7.2. Ion-exchange separations

Ion-exchange separations take advantage of electrostatic interaction between surface charges on biomolecules such as amino acids or proteins and clusters of charged groups on membrane. An adsorbing biomolecule displaces counterions associated with the surface, discharging a complementary buffer salt in the process. Adequate buffering is required to shield native protein structures from changes in pH adjacent to exchange surfaces (Donnan effect) and pH effects induced by sorption. Selection of an appropriate buffer is critical to the success of membrane ion-exchange. Large molecules ($M_r > 1\,000\,000$) such as plasmid DNA, are able to access charged groups which envelope large pores of membrane adsorbers, though they would commonly be excluded from cellulose-based ion exchangers. Mobile phases and buffers employed in ion-exchange bioseparations are non-denaturing to hydrophilic proteins. Elution and recovery of biologicals using ion exchange are considered, as well as effects of additivese and flowrate on performance.

Table 6 lists reported ion-exchange membrane adsorption of a number of proteins, polypeptides and nucleic acids. A brief summary of ion-exchange membrane applications may also be found in [25]. Purification factors achieved by ion exchange are typically an order of magnitude lower than immunoaffinity or dye affinity adsorption. On the other hand, lack of leaching from the adsorbent, less inactivation during adsorption and reduced expense for ligand favor ion exchange.

Ion-exchange membrane separations are most often accomplished by selectively eluting (see Section 6.2) the desired product using an increase in salt to reduce the retention factor. Separation by differential migration is less com-

Table 6
Examples of ion-exchange membrane adsorption

Ligand	Ligate	Geometry	Ref.
Q	Polypeptide TNF	Membrane stack	[16]
PEI	BSA, Lys, Ova	Formed in place	[19]
SP	TPA	Zetaprep	[72]
S.Q	Formate dehydrogenase	Stack	[50]
	Membrane proteins		[14]
QAE	mAb	Zetaprep	[54]
SP	β-1,4-D--Xylanase	Zetaprep	[68]
	Nucleic acid		[43]
Q, S	Antithrombin III, mAb	Stack	[55,56]

mon. Thermodynamic functions of ionic strength in membranes such as capacity, equilibrium, selectivity, and retention were considered in Section 5.3. Alternatively, elution by adjusting pH can permit consecutive ion-exchange adsorptions without intervening buffer exchange. One novel ion-exchange application produced sequential elution of denatured proteins, (oligo)ribonucleotides, DNA and DNA complexes using organic eluants at high ionic strength [43].

The hydrophilicity of adsorptive membrane matrices and the biofavorable eluting conditions possible in ion-exchange desorption result in high reported recoveries. Separation of rat-serum and kidney-plasma membrane proteins by anion exchange gave recoveries exceeding 85% [14]. BSA recovery from an S cation-exchange membrane was better than 80% [42]. Recovery of monoclonal antibodies from cell culture supernatant using anion exchange were 96% [55].

Ion exchange is often used as the first concentrating step following clarification of a cell extract (See Section 6.1). Effects of components which remain in the clarified cell supernatant from typical lysis buffers such as detergents have been examined. Non-ionic and zwitterionic detergents had no adverse effect on membrane anion-exchange separations at concentrations up to 1% [14], even though clouding in high-salt solutions above critical micelle concentration interfered with optical detection. Anionic SDS prohibited separation by binding to proteins, coating them with negative charges. Reported scale-up to preparative throughputs is most commonly performed using ion-exchange systems (See Section 6.3) since concentration by ion exchange is widely employed. For example, isolation of mAb with p*I* values between 5.4 and 6.1 from hybridoma culture supernatant employed anion-exchange QAE cartridges at laboratory, preparative and pilot scales [54].

Of course, operating conditions significantly influence outcomes of membrane ion exchange, as discussed in Sections 5 and 6. Peak-shapes resulting from ion exchange have been improved by modifying commercially available membrane adsorbers to reduce extracolumn volume [42]. Gradient changes in salt concentration were replaced by steps to desorb proteins, improving resolution. However flow-rate had an undetectable effect on peak shape, indicating the on–off nature typical of membrane ion-exchange separation of proteins.

7.3. Hydrophobic and reversed-phase separations

Separations of biomolecules on hydrophobic and reversed-phase stationary phases rely on Van der Waals interactions between uncharged patches on the molecules and water-heating surfaces of the adsorbent. Selection of an appropriate buffer and elution conditions is critical to ensure useful isoforms of the product can be obtained from the separation. The tendency of hydrophobic interactions is to denature proteins. For example, only 20% of original tumor necrosis factor was recovered in biologically-active form from a C-4 membrane adsorber [16], due to partial dissociation of active trimer into inactive monomers. Acetic acid rinsing was necessary to remove remaining inactivated monomer from the matrix.

Reported hydrophobic separations listed in Table 7 are useful for comparison with packed-column results. They may also indicate poten-

Table 7
Examples of hydrophobic membrane adsorption

Ligand	Ligate	Geometry	Ref.
C_4	Human tumor necrosis factor	Membrane stack	[16]
C_4, C_8	Myo, Lys, Ova, Chy	Membrane stack	[38]
STDVB	[D-Phe]-bradykinin, egg albumin, HSA	Polymer rod	[11,18]
GMA–EDMA	Myo, Lys, Rib, Chy	Membrane disk	[11]

tially useful assays with which to monitor protein-purification sequences.

Protein capacities available on hydrophobic membrane adsorbers shown in Table 3 are typical of packed-bed values: 10–100 mg/ml stationary phase. Adsorption in these systems occurs at high salt. So hydrophobic interaction may be performed immediately after ion-exchange concentration without an intermediate buffer exchange. The membrane both desalts the feed and discriminates between molecules of differing hydrophobicity.

Elution from hydrophobic adsorbents can be effected by lowering temperature, changing pH, or adding polyol such as ethylene glycol or nonionic detergent to the carrying buffer. Most commonly, composition of an organic modifier is increased in quantity sufficient to desorb the product of interest without precipitating it within the system. In reported examples, retention factor decreased rapidly with small changes in mobile-phase acetonitrile composition [18]. This allowed peptide separation on hydrophobic membranes to occur ten times as fast as on beaded styrenic resin. The sum of natural logs of the retention and capacity factors on reversed-phase polymer rods were observed to decrease in proportion to the organic volume fraction [18]. This performance is comparable to reported reversed-phase packed-bed behavior.

Relatively few hydrophobic or reversed-phase membrane adsorptions of biomolecules have been performed, due to the hydrophilic nature of the most labile proteins and polypeptides. Hydrophobic membrane adsorbers are commercially available in more limited varieties than their ion-exchange or affinity counterparts.

8. Conclusions

Adsorptive membranes are available in a variety of chemistries which are largely hydrophilic with minimal secondary interactions. Owing to the small bed heights, large cross-sectional surface areas and neglible intraparticle diffusion common to most adsorptive membranes, they exhibit low backpressures, short residence times and high volumetric throughputs. These features increase throughput and decrease processing times, relative to conventional fixed beds, reducing the requirement for expensive or hazardous solvents and tankage. Their shorter residence times reduce protein degradation by proteolysis and denaturation.

The range of geometries available for membrane adsorption allow incorporation of these systems into early-stage product concentration and recovery from cell lysate. Different models with more theoretical plates are available to fractionate and purify the desire product from closely related contaminants.

The separation performance of existing adsorptive membranes is reported to rival that of packed chromatographic beds in many cases. However, a number of anomalous mass transport effects have been observed: non-uniform flow, dead spaces and extra-column dispersion. These effects are not observed in all membrane systems and appear to be eliminated by proper design. Their combined effect where present is to reduce adsorptive membrane efficiency on the laboratory scale, as measured by the plate height, to the level of packed beds. Theory indicates that adsorptive membrane efficiencies should exceed those of granular beds by a factor

of ten or more. Although acceptable for small-scale analysis, adsorptive membranes appear to be capable of substantial improvement.

Future applications of adsorptive membranes will take advantage of their demonstrated strengths. Speed and resolution make membrane chromatography a likely candidate for on-line process monitoring and sidestream analysis. Low backpressure and low volumetric capacity relative to packed beds suggest that adsorptive membranes may be useful as subunits in simulated moving beds. Cross-flow adsorptive membrane geometries would allow product recovery from crude homogenates and unclarified cell culture supernatants without fouling of the membrane.

References

[1] W.H. Hancock, S. Wu and J. Frenz, *LC · GC*, 10 (1992) 96–104.

[2] X. Zhang, R.D. Whitley and N.-H.L. Wang, presented at *the AIChE Annual Meeting, Los Angeles, CA, November 17–22, 1991.*

[3] V.R. Anicetti, B.A. Keyt and W.S. Hancock, *Tibtech*, 7 (1989) 342–349.

[4] R.C. Dean, presented at *the Am. Soc. Mech. Eng. Seminar on Process Equipment Technology for the Manufacture of Biopharmaceuticals, 1988.*

[5] K.L. Carson, *GEN*, 14, No. 6 (1994) 12.

[6] J.A. Asenjo, J. Parrado and B.A. Andrews, *Ann. N.Y. Acad. Sci.*, 646 (1991) 334–356.

[7] M.D. Weiss, *GEN*, 14, No. 7 (1994) 8.

[8] A. Sadana, *BioPharm.* 7, No. 3 (1994) 34.

[9] T.G.I. Ling and B. Mattiasson, *Biotechnol. Bioeng.*, 34 (1989) 1321–1325.

[10] E. Klein, *Affinity Membranes, J. Wiley, New York*, 1991, p. 14.

[11] T.B. Tennikova and F. Svec, *J. Chromatogr.*, 646 (1993) 279–288.

[12] J.G. Dorsey, W.T. Cooper, J.F. Wheeler, H.G. Barth and J.P. Foley, *Anal. Chem.*, 66 (1994) 500R–546R.

[13] S.H. Huang, S. Roy, K.C. Hou and G.T. Tsao, *Biotechnol. Prog.*, 4 (1988) 159–165.

[14] D. Josic, J. Reusch, K. Loster, O. Baum and W. Reutter, *J. Chromatogr.*, 590 (1992) 59–76.

[15] T.B. Tennikova, B.G. Belenkii and F. Svec, *J. Liq. Chromatogr.*, 13 (1990) 63–70.

[16] J. Luksa, V. Menart, S. Milicic, B. Kus, V. Gaberc-Porekar and D. Josic, *J. Chromatogr. A* 661 (1994) 161–168.

[17] Q.C. Wang, F. Svec and J.M.J. Frechet, *Anal. Chem.*, 65 (1993) 2243–2248.

[18] Q.C. Wang, F. Svec and J.M.J. Frechet, *J. Chromatogr. A*, 669 (1994) 230–235.

[19] Y. Li and H.G. Spencer, *J. Biotechnol.*, 26 (1992) 203–211.

[20] R.M. Chicz, Z. Shi and F.E. Regnier, *J. Chromatogr.*, 359 (1986) 121–130.

[21] M. Kim, J. Kojima, K. Saito and S. Furusaki, *Biotechnol. Prog.*, 10 (1994) 114–120.

[22] M. Kim, K. Saito, S. Furusaki, T. Sugo and I. Ishigaki, *J. Chromatogr.*, 586 (1991) 27–33.

[23] H. Iwata, K. Saito and S. Furasaki, *Biotechnol. Prog.*, 17 (1991) 412–418.

[24] G.C. Serafica, J. Pimbley and G. Belfort, *Biotechnol. Bioeng.*, 43 (1994) 21–36.

[25] P. Langlotz and K.H. Kroner, *J. Chromatogr.*, 591 (1992) 107–113.

[26] R.S. Tutunjian, *Bio/Technol.*, 3 (1985) 1985 615–626.

[27] R. Molinari, J.L. Torres, A.S. Michaels, P.K. Kilpatrick and R.G. Carbonell, *Biotechnol. Bioeng.*, 36 (1990) 572–580.

[28] S.-Y. Suen and M.R. Etzel, *Chem. Eng. Sci.*, 47 (1992) 1355–1364.

[29] G.B. Cox, *LC · GC*, 8 (1990) 690–694.

[30] K.-G. Briefs and M.-R. Kula, *Chem. Eng. Sci.*, 47 (1992) 141–149.

[31] J.A. Gerstner, R. Hamilton and S.J. Cramer, *J. Chromatogr.*, 596 (1992) 173–180.

[32] R. Hamiltonian, presented at *the AIChE Annual Meeting, Los Angeles, CA, November 17–22, 1991.*

[33] D.K. Roper and E.N. Lightfoot, presented at *the AIChE Annual Meeting, St. Louis, MO, November 7–12, 1993.*

[34] G. Guillot, in E. Guyen, J.P. Nadal and Y. Pomeau (Editors), *Disorder and Mixing*, Kluwer, New York, 1988.

[35] S. Saini and J.T. Ferrucci, in D.P. Swanson, H.M. Chilton and J.H. Thrall (Editors), *Pharmaceuticals in Medical Imaging*, Macmillan, New York, 1990.

[36] D.K. Roper, M.E. Anderson and E.N. Lightfoot, in preparation.

[37] M.S. Le and J.L. Sanderson, US Pat., 4 895 806 (1990).

[38] T.B. Tennikova, M. Bleha, F. Svec, T.V. Almazova and B.G. Belenkii, *J. Chromatogr.*, 555 (1991) 9–107.

[39] M. Unarska, P.A. Davies, M.P. Esnouf and B.J. Bellhouse, *J. Chromatogr.*, 519 (1991) 53–67.

[40] D.K. Roper, *Ph.D. Thesis*, University of Wisconsin–Madison, Madison, WI, 1994.

[41] R.B. Bird, W.E. Stewart and E.N. Lightfoot, *Transport Phenomena*, Wiley, New York, 1960.

[42] O.W. Reif and R. Freitag, *J. Chromatogr. A*, 654 (1993) 29–41.

[43] N. van Huynh, J.C. Motte, J.F. Pilette, M. Decleire and C. Colson, *Anal. Biochem.*, 211 (1993) 61–65.

[44] K.K. Raths, *M.S. Thesis*, University of Wisconsin–Madison, Madison, WI, 1992.

[45] M.A. Northrup, T.J. Kulp, S.M. Angel and G.F. Pinder, *Chem. Eng. Sci.*, 48 (1993) 13–23.
[46] D.L. Koch and J.F. Brady, *J. Fluid Mech.*, 154 (1985) 399–427.
[47] D.K. Roper and E.N. Lightfoot, *J. Chromatogr.*, in press.
[48] N.B. Afeyan, N.F. Gordon, L. Mazsaroff, L. Varady, S.P. Fulton, Y.B. Yang and F.E. Regnier, *J. Chromatogr.*, 519 (1990) 1–29.
[49] F.H. Arnold, H.W. Blanch and C.R. Wilke, *Chem. Eng. J.*, 30 (1985) B9–B23.
[50] B. Champluvier and M.-R. Kula, *Bioseparation*, 2 (1992) 343–351.
[51] S.-Y. Suen, *Ph.D. Thesis*, University of Wisconsin-Madison, Madison, WI, 1994.
[52] D.D. Frey, R. Van de Water and B. Zhang, *J. Chromatogr.*, 597 (1992) 173–179.
[53] S. Krause, K.H. Kroner and W.-D. Deckwer, *Biotechnol. Techn.*, 5 (1991) 199–204.
[54] A. Jungbauer, F. Unterluggauer, K. Uhl, A. Buchacher, F. Steindl, D. Pettauer and E. Wenisch., *Biotechnol. Bioeng.*, 32 (1988) 326–333.
[55] D. Lutkemeyer, S. Siwiora, H. Buntemeyer and J. Lehmann, presented at *the 10th DECHEMA Annual Biotechnology Meeting, Karlsruhe, 1–3 June, 1992.*
[56] D. Lutkemeyer, M. Bretschneider, H. Buntemeyer and J. Lehmann, *J. Chromatogr.*, 639 (1993) 57–66.
[57] B. Champluvier and M.-R. Kula, *J. Chromatogr.*, 539 (1991) 315–325.
[58] W.F. Weinbrenner and M.R. Etzel, *J. Chromatogr. A*, 662 (1994) 414–419.
[59] S.-Y. Suen, M. Caracotsios and M.R. Etzel, *Chem. Eng. Sci.*, 48 (1993) 1801–1812.
[60] S. Yamamoto and Y. Sano, *J. Chromatogr.*, 597 (1992) 173–179.
[61] J.L. Coffman, D.K. Roper and E.N. Lightfoot, *Bioseparation*, 4 (1994) 183–200.
[62] R. Scopes, *Protein Purification*, Springer, New York, 1987.
[63] E.N. Lightfoot and M.C.M. Cockrem, *Sep. Sci. Technol.*, 22 (1987) 165–189.
[64] S. Englard and S. Seifter, in M.P. Deutscher (Editor), *Methods in Enzymology* Vol. 182, Academic Press, San Diego, 1990.
[65] P. Schadle, presented at *PrepTech94, Industrial Separations Technology Conference Secaucus, NJ, March 22–24, 1994.*
[66] B.G. Belinki, A.M. Podkladenko, O.I. Kurenbin, V.G. Mal'tsev, D.G. Nasledov and S.A. Trushin, *J. Chromatogr.*, 645 (1993) 10–15.
[67] D. Josic, K. Zeilinger, Y.-P. Lim, M. Raps, W. Hofmann and W. Reutter, *J. Chromatogr.*, 484 (1989) 327–335.
[68] L.U.L. Tan, E.K.C. Yu, G.W. Louis-Seize and J.N. Saddler, *Biotechnol. Bioeng.*, 30 (1987) 96–100.
[69] M. Kim, K. Saito, S. Furusaki, T. Sato, T. Sugo and I. Ishigaki., *J. Chromatogr.*, 585 (1991) 45–51.
[70] K.C. Hou and T.-P.D. Liao, *US Pat.*, 4 663 163 (1987).
[71] S. Brandt, R.A. Goffe, S.B. Kessler, J.L. O'Connor and S.E. Zale, *Bio-Technol.*, 6 (1988) 779–782.
[72] A. Upshall, A.A. Kumar, M.C. Bailey, M.D. Parker, M.A. Favreau, K.P. Lewison, M.L. Joseph, J.M. Maraganore and G.L. McKnight, *Bio/Technol.*, 5 (1987) 1301–1304.
[73] K.C. Hou and G. Cogswell, *US Pat.*, 4 639 513 (1987).

ELSEVIER

Journal of Chromatography A, 702 (1995) 27–44

JOURNAL OF CHROMATOGRAPHY A

Study of the packing behavior of axial compression columns for preparative chromatography

Matilal Sarker[a,b], Georges Guiochon[a,b,*]

[a]*Department of Chemistry, University of Tennessee, Knoxville, TN, 37996-1600, USA*
[b]*Analytical Chemistry Division, Oak Ridge National Laboratory, Oak Ridge, TN 37831, USA*

Abstract

The behavior of the packing of axial compression columns (5 cm I.D.) has been studied using IMPAQ C_{18} silica (average particle size 17 μm) as the stationary phase and water–methanol solutions as the eluent. Provided the frits used at both column ends are properly cleaned, columns of the same efficiency as analytical columns are easily and reproducibly obtained. The efficiencies of several columns for acetone (poorly retained), phenol (moderately retained) and cresol (strongly retained) were found to remain unchanged over periods of 100 to 200 h.

The column length was monitored during operations. It was found to decrease slowly over time, and to change when the packing solvent is replaced by the experimental eluent, and during gradient elution. It is smaller when the eluent contains more water. The total porosity and the permeability of the axial compression columns were lower than those of analytical columns.

1. Introduction

Preparative high-performance liquid chromatography has become a method of choice for the extraction, the separation and the purification of fine chemicals and biochemicals from complex mixtures in the laboratory and at the production-scale level [1]. In the pharmaceutical industry, it is the only general-purpose method available for the production of pure enantiomers. It permits the purification of antibiotics, peptides and proteins to extremely high levels of purity. Its main inconvenience is the large cost of this process. Considerable effort has been devoted recently to its improvement, especially in the areas of application selection [1–3], and of the choice of the proper chromatographic system [1–4], as well as in the fundamental theory of the process [5–7], its modes of application [7,8] and in the optimization of the experimental conditions for maximum production rate or minimum cost [7,9–11]. Surprisingly, however, the properties of the column itself have been largely ignored. Few studies have been devoted to packing technologies, the structure and the homogeneity of the bed, and its main properties, i.e., its porosity and permeability.

The packing should be optimized for stability, efficiency and low hydraulic resistance. Operators have long complained that after a certain period of satisfactory operation, the performance of a conventional packed column

* Corresponding author. Address for correspondence: Department of Chemistry, University of Tennessee, Knoxville, TN 37996-1600, USA.

0021-9673/95/$09.50 © 1995 Elsevier Science B.V. All rights reserved
SSDI 0021-9673(95)00130-1

and particularly its efficiency decrease rapidly. If the column is open, large voids appear at the top of the bed. Turbulences develop easily in these voids and are deleterious for the separation. This phenomenon does not appear in dynamic compression columns because voids cannot form when the bed settles. This explains their popularity among practitioners. It has even been shown that restoring dynamic compression after some interruption can mend the effects of voids or cracks formed inside the column bed during this interruption and restores the initial efficiency [12].

Three different compression technologies have been developed, annular [13], axial [14–16] and radial [17,18] compression. Although each of these approaches could be used either in the static or in the dynamic mode, instrumentation is available only for axial and radial dynamic compression. The former has been used with columns 2.5 to 80 cm in diameter, the latter for analytical columns and for preparative columns up to 20 cm in diameter. In a separate paper, we have reported on the behavior of radial compression columns [12]. The goal of the present work is a study of the packing performance of dynamic axial compression columns.

The original design of the axial compression column is due to Godbille and Devaux [14,15]. No systematic investigation of the properties and performance of these columns has been published to the best of our knowledge. However, Kroeff et al. [19] have demonstrated their usefulness in the purification of recombinant proteins, and more specifically, of human insulin. This type of column is widely used in industry. A number of reports mentioning their preparation [20] and systematic use can be found [21]. However, evidence regarding the superiority of dynamic compression columns over conventional ones is still mainly circumstantial. In this work we report on studies made with a dynamic axial compression column (5.0 cm I.D.). The work involves the packing of these columns, the determination of their efficiency and the study of their stability.

2. Experimental

2.1. Dynamic axial compression column

The unit used consists of an LC.50.VE.500.100 Column Skid, obtained from Prochrom (Champigneulles, France). The column is made of a stainless-steel cylinder (59.0 cm × 5.0 cm), with outer grooves at 15° angles and an inside cone at 10° angles at both ends. The grooves assist in fitting the top flange with a metallic clamp and the base with metallic braces. The inside cone at each end assists the entry of the piston chevron seals. The maximum working pressure of this column is 100 bar.

The compression unit consists of a Haskel (Burbank, CA, USA) pump, a pump oil reservoir, a three-way hydraulic valve and a hydraulic jack, all components being housed in a four legged stand. The Haskel pump drives the hydraulic jack and is assisted by compressed air from a cylinder. The upward or downward movement of the hydraulic jack is controlled by the three-way distribution valve which directs the oil flow. The piston is connected with the jack. The piston head contains a sample distributor and the inlet frit. It is connected to a tubing for the incoming mobile phase. The outer layer of the piston head contains chevron V-seals for proper sealing. The top flange contains a sample distributor, the outlet frit and an O-ring for proper sealing of the frit against the column wall.

2.2. Solvent-delivery system

A Kiloprep 100 HPLC pump was obtained from Biotage (Charlottesville, VA, USA). The pump is designed to deliver solvents up to 500 ml/min at a maximum pressure of 138 bar. The flow-rate is set manually. The system includes also two solvent ports and an injection valve with an injection loop.

2.3. Stationary phase

The column was packed with IMPAQ RG1020C18 a reversed-phase C_{18} bonded silica

(BTR Separations, Wilmington, DE, formerly The PQ Corporation). The product specifications provide for irregular particles having an average size of 16.7 μm and an average pore size of 100 Å.

A 10 × 0.46 cm analytical column was packed in this laboratory using the same stationary phase, and a conventional slurry packing method at 345 bar. The characteristics of these columns are summarized in Table 1.

2.4. Chemicals

Acetone, *m*-cresol, phenol, methyl benzoate, toluene, acetonitrile, nitric acid, ammonium hydrogenfluoride, 2-propanol and methanol were purchased from Baxter (Atlanta, GA, USA) and were 99.9% pure. L-Isoleucine, L-phenylalanine and L-tryptophan were purchased from Sigma (St. Louis, MO, USA). Distilled water from the chemistry department plant was filtered on a 1.2-μm membrane before use.

2.5. Detector

A UV–visible detector (Model 204; Linear Scientific, Reno, NV, USA) equipped with a variable-pathlength preparative cell was used to collect chromatograms. With a short cell pathlength the detector response remains linear up to much higher concentrations than with conventional HPLC detectors. The cell can be operated up to 138 bar at 500 ml/min flow-rate. For height equivalent to a theoretical plate (HETP) measurements the cell path length was kept to its maximum so that reasonable response could be obtained with analytical size injections. For overloading experiments the cell path length was set to its minimum.

Careful detector calibration was done with solutions of known concentrations of phenol in methanol–water solutions (40:60, v/v). The column was disconnected from the solvent line, the whole delivery line was then purged with each new solution of phenol, and the detector response recorded while flowing the solution at 50 ml/min. A calibration curve was constructed by plotting the known concentration (C) versus the detector response (R, volt). A fourth-degree polynomial ($C = 2\,054\,441R^4 - 405\,263R^3 + 28\,252R^2 - 737.2R + 5.295$) gives a good fit to these data.

2.6. Pressure sensor

The column inlet pressure was measured with an Omega pressure transducer Model PX603-2KG5V (Omega, Stamford, CT, USA). This transducer gives a 1–5 V d.c. linear output at 0 to 138 bar. Its response time is 1 ms. The output was adjusted to read 0.402 V d.c. for 0 bar and 2.022 V d.c. for 138 bar, for compatibility with the data acquisition system. Calibration shows

Table 1
Characteristics of axial compression columns

Column properties	Column 8	Column 9	Column 10	Column 0[a]
Dimensions (cm)	15.6 × 5.0	16.2 × 5.0	20.0 × 5.0	10 × 0.46
Hold-up volume (ml)	181.0	212.0	258.4	1.13
Total porosity (solvent A)	0.60	0.67	0.66	0.68
Phase ratio (solvent A)	0.69	0.50	0.52	0.47
Total porosity (solvent B)	0.57	0.63	0.62	0.71
Phase ratio (solvent B)	0.77	0.63	0.62	0.41
k'(acetone)	0.37	0.38	0.40	0.26
k'(phenol)	2.72	2.90	3.17	2.50
k'(cresol)	6.10	6.59	7.41	6.29

Solvent A = pure methanol; solvent B = methanol–water (40:60, v/v).
[a] Analytical column.

that the inlet pressure (P, bar) and the voltage output (V, volt) are related by $P = (V - 0.402)/(1.1745 \cdot 10^{-2})$.

2.7. Displacement sensor

Dynamic changes of the column length were measured with an Electro-Mike displacement sensor Model PAA1555 (Reagan Controls, Charlotte, NC, USA) which includes a displacement transducer and a transmitter with analog output of 2 to 9 V d.c. at 2.0 mm–9.0 mm range. The output voltage was attenuated to 2.2 V d.c. for our data system. Calibration of the sensor output with known targets shows the response to be linear in the 2–9 mm range, d (distance between target and sensor, mm) and V (output, V) being related by $d = (0.20 \pm 0.01)V + (0.18 \pm 0.06)$.

The sensor was fixed to the four-legged stand holding the column and the steel target to the compression piston. Thus, an increase in target distance meant a decrease in column length. Depending on the movement of the piston the distance between the sensor and the target increases or decreases. The resolution of the sensor is approximately 0.01 mm. Its drift (when recording the length of a metal bar) is less than 0.01 mm/day. However, the actual column length, which is measured directly, is known within only 2 mm.

2.8. Data acquisition system

The data system consists of a Waters system interface module (SIM) with two A/D convertors (Milford, MA, USA). This SIM is capable of simultaneous monitoring four sensors and/or detectors and can control three HPLC pumps. The digitized data from the SIM was collected by a Waters Maxima 820 version 3.3 loaded in a NEC computer. All the data files were translated to ASCII format for further use and uploaded to the computer network of the University of Tennessee. For treatment of these data, several DOS- and VMS-based software programs were developed in our laboratory.

2.9. Methods

In the experiments reported here, several solvents were used as eluent. The primary mobile phases were methanol (solvent A) and a mixture of methanol–water (40:60, v/v; solvent B). Other solvents used were water and acetonitrile–water (70:30). The primary test samples were low-concentration solutions of acetone, phenol and *m*-cresol in the eluent. Other test samples contained low concentration solutions of isoleucine, phenylalanine, uracil, methyl benzoate and toluene in appropriate solvents. Sample volumes for HETP measurements were 1.5 ml, injected by filling an appropriate loop. The sample concentrations for overloaded experiments were 200 g/l phenol or higher. Typical sample volumes for these experiments were 10 ml injected from a loop. For obvious economic and waste management reasons, the solvents were pumped in closed circuit, with a 15–20-l buffer reservoir on the solvent line. The solvent was replaced when the baseline absorbance became significantly higher than that of fresh solvent.

Three outputs were recorded in most of the experiments. These were: the UV detector, the displacement and the pressure sensors. The chromatographic data were used to calculate column efficiencies, from the width at peak half-height, and retention factors. The reduced velocities and reduced plate heights were fitted to the Van Deemter equation [22], using a non-linear least-squares fit. The classical Wilke–Chang [23] equation was used to estimate the diffusion coefficients of the compounds used. The adsorption isotherm of phenol was derived using the ECP method [7].

The data from the pressure transducer were converted to pressure units, and the output from the displacement sensor to changes in the column length.

2.10. Procedure for packing an axial compression column

The procedure described below is recommended by the manufacturer. It has been fol-

lowed carefully for all the columns whose performance are discussed in this report. It involves the following steps:

(1) The flow distributors and the frits are positioned inside the top flange and the piston head. If frits are already in place and were used for a previous column, *they must be cleaned carefully before being used again* (see next section).

(2) The column is fixed to its base. Then, the piston is pushed inside, and all the way up through, until it protrudes at the column exit. The seal bolts are checked. They should be snug and are adjusted if necessary. Too much tightening can break the seals and too little tightening cause leaks.

(3) The tubing between the pump and the piston head is disconnected and closed with a sealing nut. A small stainless tubing is fixed to the top flange to drain out the excess solvent while packing the column.

(4) The desired amount of silica (usually ca. 200 g) is measured in a 2-l beaker, with about 800 ml acetone. The slurry is stirred and left settle for about 15 min. The supernatant is decanted, or drained with a large syringe, to remove the fine particles still suspended. This procedure for removing fines is repeated two or three times (optional). Finally the slurry volume is adjusted to 800–900 ml with acetone.

(5) The piston is positioned at a certain distance from the top of the column. The distance is calculated so that the space above the piston can hold all the slurry.

(6) The air pressure in the Haskel pump is adjusted to give the desired oil pressure (100 bar) in the hydraulic manometer. The equivalent piston pressure inside the column is 41 bar.

(7) The slurry is poured into the column and the height of liquid adjusted to the top of the column by moving the piston. The top flange is placed and secured with the metallic clamp.

(8) The piston is moved upward by the pump, compressing the slurry and expelling the excess solvent which is collected in an empty beaker. When the air pump stops resetting, or the piston stops moving, the packing is done.

Unfortunately, columns packed with acetone are not as good as columns packed with 2-propanol, while use of the former solvent is recommended to eliminate the fine particles. Steps 5–8 are the most practical procedure to eliminate acetone. The column is then unpacked immediately, the extruded stationary phase suspended in 2-propanol, and the column repacked following steps 5–8.

Wu and Lohse [20] recommend a simpler procedure which applies when the packing material does not contain fines. They also recommend the use of a higher packing pressure, 60 to 80 atm (1 atm = 101 325 Pa), and the closing of the inlet valve to prevent the mobile phase from flowing from the column at both ends during compression of the slurry. There is a close compromise to adopt between an insufficient compression pressure which does not give a good, stable column, and too large a compression pressure which causes excessive particle breakage. The optimum pressure depends on the packing material.

A convenient variant of the packing procedure consists in removing the fine particles with 2-propanol, by suspending the stationary phase in 1 l of this solvent, waiting ca. 30 min, decanting the supernatant from the top of beaker, adding an equivalent amount of 2-propanol to the slurry, and repeating the procedure two or three times. Finally, the volume of slurry is adjusted to 800 ml and the column is packed following steps 5–8. Then, it is no longer necessary to repack the column.

2.11. Cleaning and installing frits

Frits are held in position in a machined groove. At room temperature the frit has a diameter slightly larger than the cavity where it is housed. To be installed, the frit must be shrunk by cooling it in liquid nitrogen; cooling in dry ice is insufficient. Once cold, the frit is pushed inside the flange or the piston head. Top flange frits are wider than piston frits and cannot be exchanged.

Before replacing a frit, it is necessary to remove the old one. Prochrom supplied us with an adapter that permits cooling the frit alone

while it is inside the piston head or the top flange. After cooling for about 15 min, the frit is removed with a pusher device. The process of removing old frits is more difficult than the process of putting new frits in.

There are two types of frits available, a sintered stainless-steel plate, or a fine mesh grid. In both cases, it is important to use only new frits, or to clean old ones very carefully. The grid frits are more difficult to foul and easier to clean than the sintered metal plates. Cleaning the frits can be done quite effectively by following a very simple procedure. The top flange and the piston head are removed from the column assembly. The top flange and then the piston head is connected to an erlenmeyer flask through a rubber cork and a tubing, while the side arm of the flask is connected to a water suction pump. The cooling adaptor is connected to the flange or the piston head. Liquids poured into the adaptor are sucked into the flask. The following solutions were used in this order: (1) filtered distilled water (200 ml), (2) methanol (200 ml), (3) filtered distilled water (200 ml), (4) 20% ammonium hydrogenfluoride in water (400 to 500 ml), (5) 0.5 *M* nitric acid (200 ml), (6) filtered distilled water (200 ml) and (7) methanol (200 ml).

This cleaning procedure is more complicated but less hazardous than the washing with hot concentrated sodium hydroxyde. Its efficiency seems comparable. As shown below, it gives excellent results.

2.12. Unpacking an axial compression column

Axial compression columns can be achieved, following a simple, easy procedure.

(1) The column must be flushed first with an organic solvent. Otherwise, the pressure necessary to unpack the column may be very high.

(2) The control valve is set on neutral, and the pressure set to zero by switching off the air pressure in the Haskel pump. This results in a drop of the hydraulic pressure only after the hydraulic valve is brought to the downward position. When the oil pressure reads zero, the valve is returned to neutral.

(3) The system is left for 10 to 15 min to achieve hydraulic equilibrium, and the tubing is disconnected from the top flange, which is unfastened and open up slowly to avoid that residual pressure pushes it out to some extent.

(4) The piston pressure is set to ca. 41 bar and it starts pushing the bed out of the column. If necessary, the piston pressure is increased gradually.

(5) Usually, the stationary phase comes out as one piece, but it may break very easily.

3. Results and discussion

3.1. The learning curve

Learning to install, pack, operate and use a dynamic axial compression column was most simple. The only noteworthy difficulty that we encountered is in understanding how much care should be devoted to the process of cleaning the frits. Different criteria could be used as a measure of the learning process. A standardized procedure was used to test all the columns made. The column efficiency turns out of be the most difficult characteristic to reproduce and does not vary much from one compound to another one. The retention factors tend to be related only to the nature of the stationary phase and to its amount, i.e., to the packing density. The separation factors, loadability and production rate are too specific of the compounds selected. Thus, the column efficiency, or rather its HETP, was selected for this study.

The reduced HETP obtained for acetone with the first ten columns packed are shown in Fig. 1. In our opinion, the learning process should be much faster, as our early failures had nothing to do with the learning process itself. The first two columns were tested using water as the mobile phase, and isoleucine, phenylalanine and tryptophan dissolved in water as samples. The efficiencies of these columns were poor, but the efficiencies of analytical columns are as poor under such experimental conditions. Water was abandoned and replaced by methanol, with acetone as the sample (column 3). The next three columns (4–

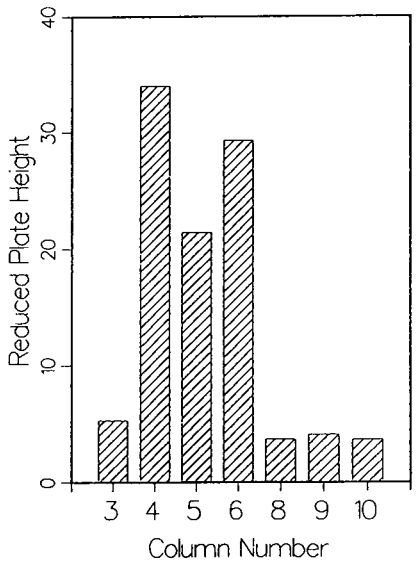

Fig. 1. Learning curve. Plot of the minimum reduced plate height achieved versus the rank of the column packed in the laboratory.

6) were packed with a laboratory-made top flange in which a thermocouple (0.16 mm O.D.) was inserted through a hole, to measure possible thermal effects in the column. Clearly, this affected the column efficiency much more than expected. Probably channeling develops along the thermocouple. Also during the packing of these three columns, cracking noises were heard coming from inside the column.

The next column (7) was never tested. While packing it crushing noises were heard again, the packing process was interrupted, and the column was opened. Similar crushing sounds were also heard while unpacking this column. However, the core obtained looked homogeneous, dense and no harm seemed to have occurred to the packing material. So, that same packing material was redispersed as a slurry and used to pack column 8, which was a good column (Fig. 1). The frit cleaning procedure described above was developed after this column 7 was aborted. The crushing noises were not heard again, but other investigators have reported similar experience.

3.2. Effect of the extra-column volumes

The apparent column efficiency is derived from the recorded chromatograms. The band widths of the peak obtained result from a combination of all the sources of band broadening, including axial dispersion and mass transfer resistances inside the column, which we are interested to know, and a number of possible extra-column contributions, which we must eliminate or correct for in order to determine the separate contributions of axial dispersion and mass transfer resistances. The theory of signals shows that, if the effect of several parts of the instrument combine following a shift-invariant convolution, which is the case in linear chromatography [24], the contributions of the extra-column volumes could be corrected by calculating separately the moments of the concentration distributions given by the detector with and without columns. The moments are given by the following equations

$$\mu_0 = \int_0^\infty y(t)\mathrm{d}t$$

$$\mu_n = \frac{1}{\mu_0} \cdot \int_0^\infty t^n y(t)\mathrm{d}t$$

$$\mu_1 = \frac{1}{\mu_0} \cdot \int_0^\infty t y(t)\mathrm{d}t$$

$$\sigma^2 = \frac{1}{\mu_0} \cdot \int_0^\infty (t-\mu_1)^2 y(t)\mathrm{d}t$$

where t is the time, $y(t)$ is the detector response, μ_n is the nth moment, and σ^2 is the variance of the peak. The zeroth moment is the peak area, the first moment the retention time of the mass center of the distribution, and the second moment is the variance of this distribution [25]. In linear chromatography, the first two moments are additive. The measured values of the retention time and the band variance are the sums of the contributions of the column and the instrument. This allows the calculation of the true retention time and the column efficiency, by subtracting the contributions of the extra-column volumes

$$\sigma^2_{\text{measured}} = \sigma^2_{\text{column}} + \sigma^2_{\text{extra-column}}$$

$$t_{\text{R,measured}} = t_{\text{R,column}} + t_{\text{R,extra-column}}$$

It is easy to estimate the contribution of the extra-column volumes to the measured efficiency by replacing the column with a short length of narrow empty tube having a comparable hydraulic resistance and injecting the same samples, provided the detector response time is sufficiently fast [26]. Chromatograms were recorded with acetone (non-retained) as sample, and pure methanol as the eluent, with and without the column. The variances of all the peaks obtained were derived from their second moment. The results are shown in Fig. 2. The instrument contributions to the apparent column efficiency are entirely negligible, which was expected since the total volume of the sampling valve, detector cell, and tubing is small compared to the column hold-up volume (ca. 210 ml). Accordingly, the results reported below are not corrected for the extra-column volumes.

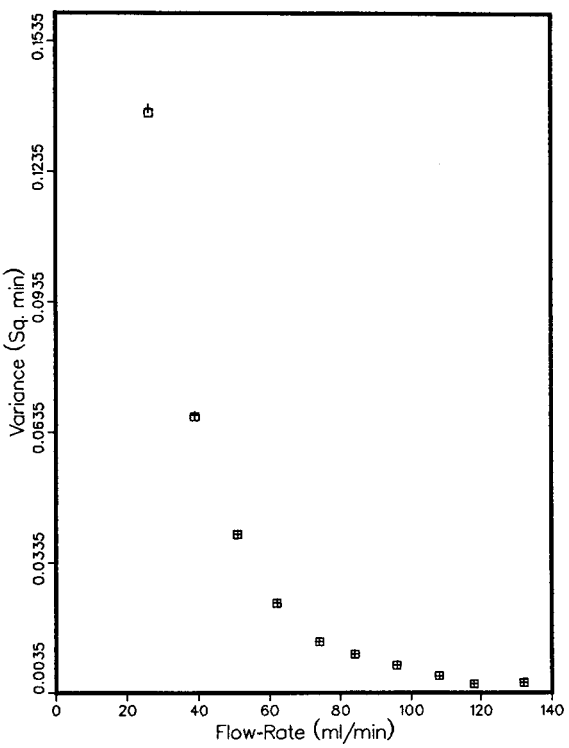

Fig. 2. Plot of the corrected column variance and the apparent column variance (sum of the variance contributions of the column and the extra-column parts of the equipment) versus the mobile phase (methanol) flow-rate for acetone. The variances were calculated from the second moment. □ = Column variance; + = measured variance.

3.3. Column test results

Columns 8–10 were tested immediately after packing, by measuring their efficiency for unretained acetone with methanol as the eluent. Then the column was subjected to aging under different conditions, for extended periods of 100 to 200 h, and the efficiency measured periodically. A selection of the results obtained is given in Table 2 which contains the best parameters a and c of the Van Deemter equation obtained by fitting the experimental data to this equation with $b = 1.80$. The last column of Table 2 gives the approximate time during which the individual column had been used prior to the measurement.

3.4. Column performance with pure methanol

In this series of experiments, pure methanol was used as the eluent and a 1.5% solution of acetone in methanol as the sample. The characteristics of the columns studied are reported in Table 1. The column lengths were determined with methanol as the eluent. Acetone is not retained in pure methanol, and its retention time was used to measure the column void volume. The total porosity of the columns, derived from the hold-up volumes of the negative water peaks with water–methanol solutions as the eluent, are also reported. There are some differences between the values of the total porosity and the phase ratio[1] measured with these two different solvents, but these differences are the same on the three preparative columns and on the analytical column. They are related to the excess isotherm and the dependence of the (small) amount of organic solvent adsorbed from the

[1] Phase ratio, $F = (1 - \epsilon)/\epsilon$, with ϵ = total column porosity.

Table 2
Van Deemter parameters for representative axial compression columns

Col	Solvent	Sample	a	c	h_{min}	ν_{opt}	Hours used
8	A	Acetone	2.94	0.134	3.92	3.67	18
8	A	Acetone	2.61	0.185	3.76	3.12	26
8	B	Acetone	3.85	0.093	4.67	4.40	37
		Phenol	4.31	0.099	5.15	4.27	
		Cresol	4.08	0.076	4.82	4.87	
8	B	Acetone	3.97	0.093	4.79	4.40	46
		Phenol	4.63	0.091	5.44	4.45	
		Cresol	4.61	0.064	5.29	5.30	
8	B	Acetone	3.46	0.116	4.37	3.94	109
		Phenol	3.87	0.096	4.70	4.33	
		Cresol	3.57	0.114	4.48	3.97	
9	A	Acetone	3.30	0.083	4.07	4.66	10
9	B	Acetone	5.02	0.080	5.78	4.74	68
		Phenol	6.12	0.044	6.68	6.40	
		Cresol	6.68	0.073	7.40	4.97	
9	B	Acetone	5.40	0.073	6.12	4.97	183
		Phenol	6.81	0.072	7.53	5.00	
		Cresol	6.42	0.063	7.09	5.35	
10	A	Acetone	3.13	0.133	4.11	3.68	10
10	A	Acetone	2.87	0.165	3.96	3.30	39
10	B	Acetone	4.48	0.104	5.35	4.16	111
		Phenol	7.69	0.087	8.48	4.55	
		Cresol	11.11	0.054	11.73	5.77	
10	B	Acetone	4.58	0.100	5.43	4.24	132
		Phenol	6.67	0.101	7.52	4.22	
		Cresol	7.03	0.068	7.73	5.14	
0	A	Acetone	2.71	0.118	3.63	3.91	NA
0	A	Acetone	2.76	0.120	3.69	3.87	NA
0	A	Acetone	2.38	0.174	3.50	3.22	NA

aqueous solution on the composition of this solution [27,28].

The optimum values of the reduced plate heights obtained with the three preparative columns and with the analytical column are very close, within the margin of error. A plot of the reduced plate height versus the reduced velocity for column 10 and for the analytical column is shown in Fig. 3. These plots are very similar.

The range of variations of the values obtained with acetone for the parameter a (2.38 to 3.30, average 2.84, relative standard deviation 10%) is

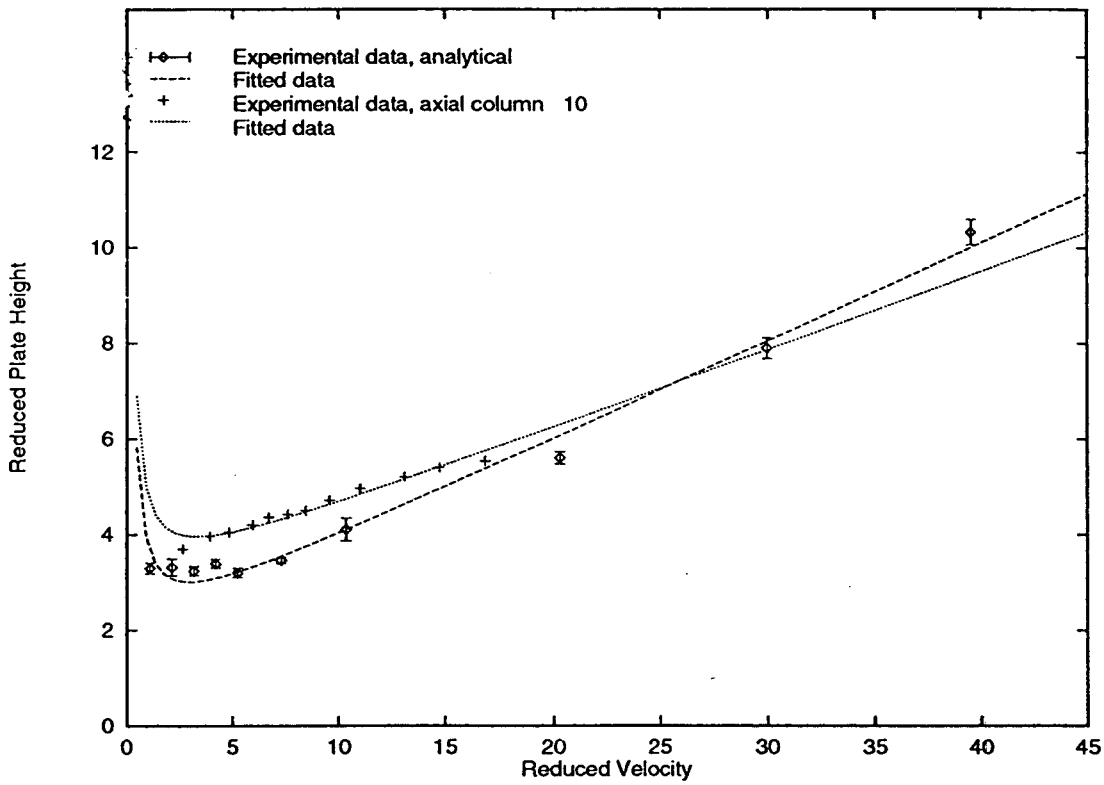

Fig. 3. Plot of the reduced plate height for acetone versus the reduced velocity of the mobile phase (methanol). Axial compression column number 10 (19.80 cm × 5.00 cm) after 39 h of column use. The analytical column (10.0 cm × 0.46 cm) was packed in the laboratory with the same stationary phase.

much narrower than that of the parameter c (0.083 to 0.185, average 0.139, relative standard deviation 24%), probably reflecting the fact that the range of mobile phase velocities within which the HETP data were acquired is too narrow to afford a good reproducibility of this parameter [29].

3.5. Column performance with methanol–water (40:60)

In all further series of experiments, a methanol–water (40:60) solution (solvent B) was used as the eluent instead of pure methanol. A 1.5-ml portion of a low-concentration solution of acetone (15 ml/l), phenol (4.3 g/l) and *m*-cresol (2.5 ml/l) dissolved in the eluent was injected as the sample. The sample also contained excess water, whose negative peak was used to determine the hold-up time. A representative chromatogram of this sample is shown in Fig. 4, with the experimental conditions described in the caption.

The column efficiency was measured and the data fitted to the van Deemter equation. The results are compiled in Table 2. Because almost no data points were acquired at flow velocities below the optimum for maximum efficiency, the precision on the parameter b would be very poor. Accordingly, a constant value of 1.80 was assumed for b in the regression of the experimental data to the Van Deemter equation. The values of the other two parameters of the reduced plate height equations are practically unaffected by the use of the columns for 100 to 200 h. The results obtained with column 9 are

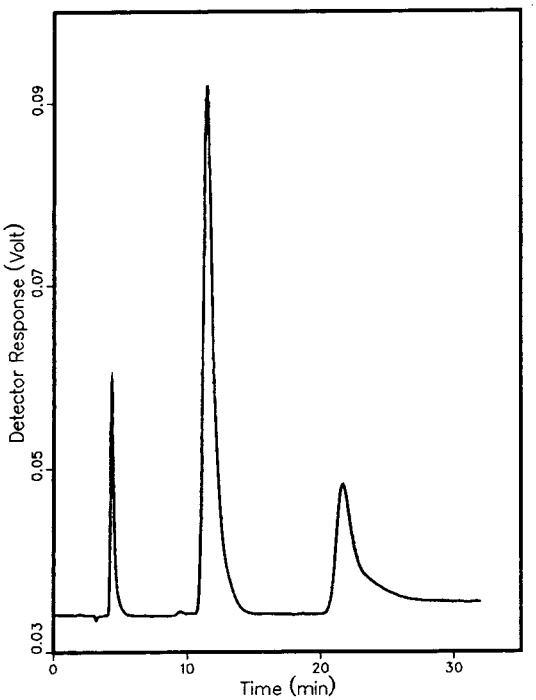

Fig. 4. A representative chromatogram obtained with axial compression column 10 (19.75 cm × 5.0 cm). Experimental conditions: 1.5 ml sample containing acetone (15 ml/l), phenol (4.3 g/l) and *m*-cresol (2.5 ml/l) dissolved in methanol–water (40:60, v/v) with a slight excess of water. The small negative peak is due to the excess water in the sample.

discussed separately in a further section. The values obtained for the parameter *a* for the three compounds on any given column are not constant but exhibit a significant dependence on the retention. On the other hand, the values obtained for the parameter *c* for a given compound on the different columns but with the same stationary phase are different. These apparent inconsistencies with the prediction of a simple model probably reflect, at least in a large part, the empirical character of the Van Deemter equation [7, p. 200].

3.6. Effect of replacing 2-propanol by methanol after completion of the column packing

As we are interested in the bed structure and the parameters which may affect it, it was interesting to follow the change in column length, at constant compression pressure and flow-rate, associated with the replacement of the packing solvent, 2-propanol (surface tension, 21.7 dyn/cm at 20°C; 1 dyn = 10^{-5} N), by the standard eluent, methanol (surface tension, 22.6 dyn/cm at 20°C). The experiment was done on column 8, just after completion of its packing. The signals of the three detectors, the UV detector set at 254 nm, the pressure and the position sensors, were monitored simultaneously during 90 min. The mobile phase flow-rate was set at 66 ml/min, and isopropanol was abruptly replaced by methanol 0.15 min after data acquisition began. The eluent was wasted for the first 15 min, then recycled. The initial column length was 16.0 cm and the initial target distance of the displacement sensor was 1.14 mm.

The variations of the column length, inlet pressure, and UV-detector signal are reported in Fig. 5. The UV-detector signal originates from impurities in the solvents which are not HPLC grade and do not have the low UV-cutoff wavelength of the highly pure solvents. The trace of the detector signal shows that all the isopropanol is washed out of the column within less than ca. 7 min. A steady baseline is then obtained, corresponding to the elution of pure methanol. The total volume of methanol passed during that time corresponds approximately to 2 column volumes (V_0 = 181 ml, Table 1; F_v = 66 ml/min), which is not surprising as it includes the amount of mobile phase needed to wash the pump and all the connecting tubings. The replacement of 2-propanol by methanol is accompanied by a rapid oscillation of the inlet pressure, which increases from 0.2 bar (pump restarts) to above 11 bar (column still almost completely filled with 2-propanol), then decreases to 4 bar in about 5 min (column fully washed with methanol), and finally stabilizes at 4.5 bar, after about 15 min. The viscosities of 2-propanol and methanol are 1.77 and 0.510 cP at 30°C, respectively.

The variation of the column length is more complex. It remains stable during the first few minutes, then increases slightly when the 2-propanol is nearly gone, to fall very rapidly, by 2 mm, while the 2-propanol finishes to be washed away. After a short pause, the column length

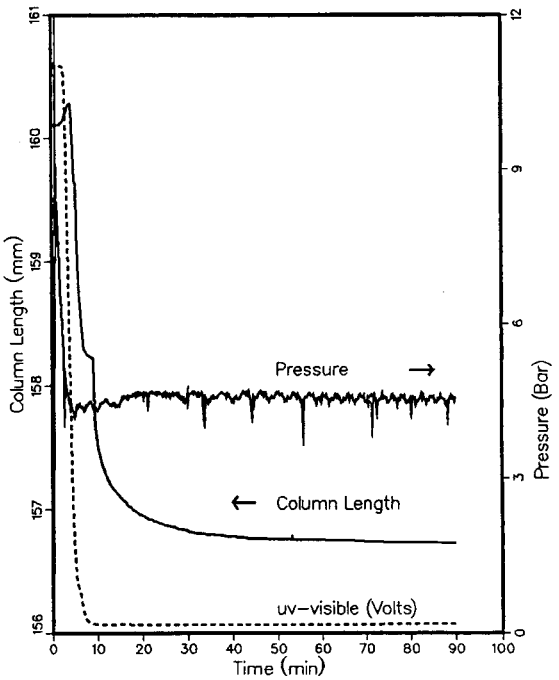

Fig. 5. Plot of the dynamic changes in column length, inlet pressure and UV–visible absorption (UV range 0–1.6 V) versus time when the packing solvent (isopropanol) is replaced by the mobile phase used (methanol). Flow-rate, 66 ml/min. The newly packed axial compression column 8 (16.0 cm × 5.0 cm) was used and the solvent change was a step gradient. The resolution of the position sensor is approximately 0.01 mm and its drift less than 0.01 mm/day.

begins to decrease again, and is not completely stabilized after 90 min. The total reduction in column length is approximately 3.5 mm, or 2%. The column length record is in agreement with the behavior of the dynamic compression unit. The Haskel pump resets at the 4th, the 5th and the 9th minutes, confirming that the column shrinks rapidly during a minute or so, about 4 min after the beginning of the operation, then reaches another equilibrium. It is difficult to explain the details of the column length record, but the trends is clear. Whether because of the increase in surface tension of the mobile phase, or for another reason, the packing density increases when 2-propanol is replaced by methanol, and it takes time for the particles to settle in the bed.

3.7. Variation of the column length during a concentration gradient

After 2-propanol was replaced by methanol, the efficiency of column 8 was measured with pure methanol as the eluent and acetone as the sample (Section 3.4). Three successive sets of experiments were done to acquire all the data needed. After approximately 26 h, the column length was stable at 15.54 cm. In order to carry out the next series of experiments, pure methanol (A) has to be replaced by a methanol–water (40:60) (B) solution. This was done using an exponential concentration gradient, generated by siphoning 4 l of solution B into a 0.5-l flask of A (connected to the pump), at a constant flow-rate equal to the set flow-rate of the pump (40 ml/min). The column length was recorded during that time.

This experiment took over 100 min. After 67 min the solvent in the bottle of A was replaced by fresh solution B. This set-up provided a slow gradient. The signals of the three detectors were acquired and the results are shown in Fig. 6. The pressure rises progressively, corresponding to the increase in viscosity (0.60 cP for methanol, 1.7 cP for B at 20°C, non-linear variation). The column length decreases by about 0.13 mm. The irregular aspect of the curve corresponds to the definition of the sensor, ca. 0.01 mm. This change is parallel to the concentration gradient. It is of a much lesser magnitude than the one observed in the previous case (replacement of 2-propanol by methanol). Note that, from the end of the experiment described in the previous section (Fig. 4) to the beginning of the one discussed here, the column length has been reduced by 1.3 mm (in ca. 26 h). There must be a limit to the packing density which can be reached without breaking particles but it is unclear whether this limit has been reached in any of our columns.

3.8. Relationship between flow-rate and inlet pressure

Measuring the column inlet pressure as a function of the flow-rate serves two main pur-

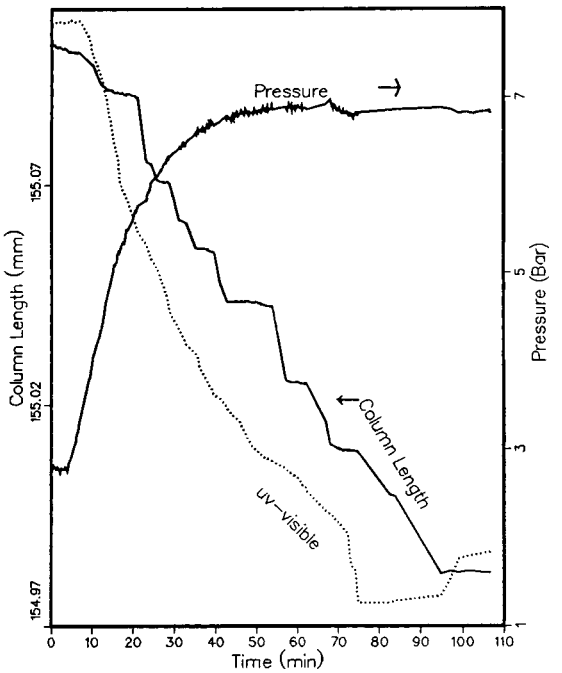

Fig. 6. Plot of the dynamic changes in column length, inlet pressure and UV–visible absorption at 290 nm (detector output in V; UV range 0.018–0.065 V) versus time during a methanol–water gradient (100% to 40% methanol). Axial compression column 8 after 26 h of use with and stabilized length (15.54 cm × 5.00 cm). See text for further details. The resolution of the position sensor is approximately 0.01 mm and its drift less than 0.01 mm/day.

poses in liquid chromatography. First, by reference to previous values obtained with the same column, it permits the detection of blockages occurring anywhere in the system. Secondly, it permits the calculation of the column permeability which, in turn, gives an estimate of the hydrodynamic particle size. The first determinations lead to an estimated particle size which was much lower than the expected value of 16.7 μm given by the supplier and confirmed by previous determinations [12].

Since there was no evidence of particle breakage to the significant extent which could explain this low value of the column permeability (see later), we measured the permeability of the instrument itself, including the tubings, the valves and the frits used in the axial compression column (nominal average pore size, 3 μm). An empty column was obtained by placing the two frits 14 cm apart, with no slurry in the column, and setting the hydraulic valve to neutral. The inlet pressure was measured at different flow-rates for solvent B, and a calibration curve constructed with these data. An excellent fit was obtained a third-degree polynomial with a forced y intercept at zero, giving $P = 0.0715F_v + 1.367 \cdot 10^{-4}F_v^2 - 1.19 \cdot 10^{-7}F_v^3$, with P = inlet pressure (bar) and F_v = flow-rate (ml/min). This calibration curve is used to correct the pressure readings for all columns. We have not observed any significant variation when an old frit is replaced by a new one. As an illustration, Fig. 7 shows the raw data obtained on column 10 after different periods of time, and the data obtained with the empty column.

Obviously, the contribution of the equipment is not negligible. This is not surprising as the diameter of the tubing connecting the pump and the column is relatively small (1 mm). With this diameter, it is possible to achieve a short residence time in the tubings and a rapid radial mass

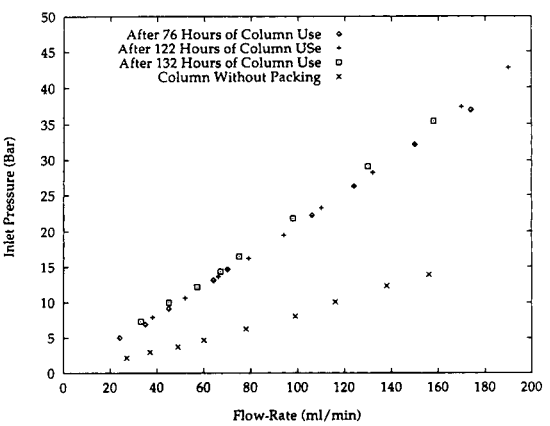

Fig. 7. Relationship between mobile phase flow-rate and column pressure drop. Plot of the column inlet pressure versus the mobile phase flow-rate. See symbols in figure. Top line, uncorrected data without correction for axial compression column 10 after 76, 122 and 132 h of column use. Lower line, same plot for a column without packing (i.e., the flow resistance is due only to the connecting tubings and frits). The relative standard deviations on the measurements of the inlet pressure and the flow-rate are 1.1 and 1%, respectively.

transfer because of secondary (i.e., radial) flow arising at the flow-rates typically used with the column (around 50 ml/min or larger). Turbulent flow takes place in the connecting tubings for a flow-rate[2] of the order of 120 ml/min. Turbulent flow minimizes the dispersion of the front and rear boundaries of the injection at high flow-rates. As a consequence of the narrow diameter, however, the pressure drop in the connecting tubes is not negligible and the data should be corrected to obtain the actual column permeability.

When the measured column permeability is corrected for the equipment contribution, and a value of 1000 is used for the specific permeability, estimates of 19.5 ± 0.4 μm, 19.1 ± 0.2 μm and 18.5 ± 0.4 μm were obtained for the average particle size, after the column has been used for 76, 122 and 132 h; respectively. The apparent decrease in particle size is a consequence of the progressive compaction of the packing reported above. The whole three sets of data are shown in Fig. 8. The data points in this figure appear slightly scattered, but the systematic variation corresponding to the progressive decrease in apparent average particle size indicated above is included in these fluctuations. Nevertheless, we see that the inlet pressure does not change much over the duration of the experiment. The solid line in this figure is the linear least-square fit of the data, with a slope of 0.124 ± 0.002 and an intercept of 0.326 ± 0.154. The particle sizes obtained from these experiments are in good agreement with previous results [12].

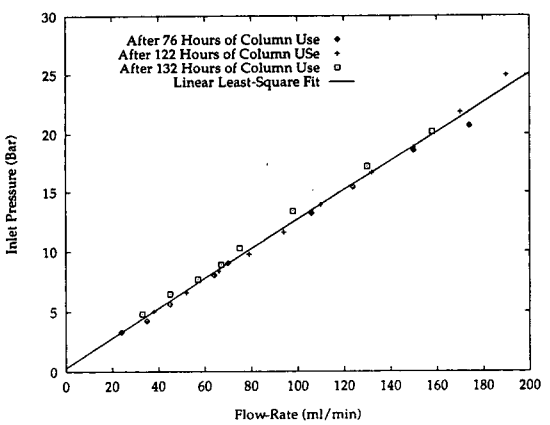

Fig. 8. Relationship between mobile phase flow-rate and column pressure drop. Plot of the column inlet pressure versus the mobile phase flow-rate. Same data as in Fig. 7, after correction for the pressure drop inside connecting tubes and column frits.

[2] $Re = (ud\rho)/\eta = (4F_v\rho)/\pi d\eta)$. For $F_v = 120$ ml/min, $\rho = 0.8$ g/ml, $\eta = 1$ cP, and $Re = 2000$, $d \approx 0.10$ cm.

3.9. Variation of the total column porosity with time

The total porosity of axial compression columns is smaller than that of analytical columns or radial compression columns [12]. With IMPAQ as a stationary phase and solvent B as the mobile phase, typical values are 0.69 to 0.71 for analytical columns, and 0.68 to 0.70 for radial compression columns, while the values obtained for axial compression columns range between 0.57 and 0.67. Careful measurements were performed to study the variation of the total porosity of one column during a change of the mobile phase. This column was packed with the IMPAQ material recovered from a radial compression cartridge (column 2 in our previous work, Ref. [12]) after it was open to take samples for particle size analysis. As the results of this analysis had showed that no particle fragmentation had taken place [12], and an analytical column packed with the material had exhibited the same efficiency as columns packed with fresh packing, the material was used to pack axial compression columns.

A plot of the total porosity of this column as a function of time is shown in Fig. 9. The inset of this figure shows a plot of the column length versus time. The first four data points were derived from the retention time of the non-retained acetone peaks in pure methanol as eluent. The last five data points were derived from the retention time of the negative peak of water in a methanol–water (40:60, v/v) solution. The total porosity decreased rapidly during two periods. First, during the first 20 h of column use, then when the eluent was changed from pure methanol to a more polar (aqueous) solution (same effect as illustrated for column 8 in Fig. 6). This effect is certainly in relation with

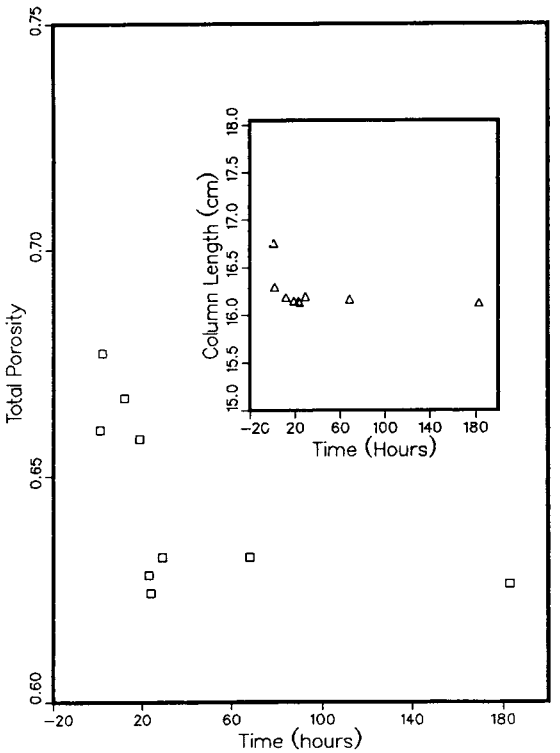

Fig. 9. Plot of the total porosity of the column versus the time of column use for axial compression column 9. Inset: plot of the column length versus the time of column operation. The resolution of the position sensor is approximately 0.01 mm and its drift less than 0.01 mm/day.

the surface tension of the eluent, but its exact origin is unknown, and further work is necessary to understand it. Because methanol is only very weakly adsorbed by the stationary phase (the retention factor of methanol in pure water is lower than 1), the change in measurement procedure should not affect the value of t_0 significantly. Furthermore, the porosity drop at 21 h is in agreement with the decrease of the column length observed during the replacement of pure methanol by a methanol–water (40:60) solution, previously documented for column 8 (Fig. 6).

3.10. Evolution of the particle size distribution

The particle size distribution were measured by Miller [30] using a Coulter Multisizer using 5% LiCl in methanol as the electrolyte, as in a previous report [12]. The experimental data obtained are reported in Table 3 and illustrated in Fig. 10. The relative standard deviation of the determinations of the average particle sizes is between 1 and 2%. The repeatability in a series of measurement is better by nearly an order of magnitude (Table 3). Most of the samples (2–7, included) were from column 8 (Table 2), open after 160 h of operation. They were taken from the entrance, exit and middle, along the wall and in the center. Sample 1 was scrapped from the piston frit of column 8, samples 8 and 9 were from the center of column 9 and sample 10 was a reference. Column 8 was packed with the material previously used to pack column 7. Column 8 was first used for various conventional determinations and operated for approximately 150 h; then a study of the effect of the axial compression pressure on the column performance was undertaken. These experiments were done in the pressure range of 20 to 65 bar. During the study, the column bed was compressed several times for several hours under pressures exceeding the value recommended by the manufacturer for irregular-shaped particles (41 bar). Column 9

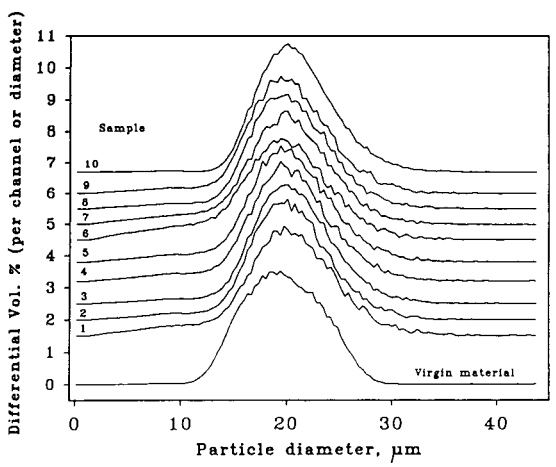

Fig. 10. Particle size distribution of samples of the stationary phase. Differential volume distributions obtained with a Coulter Multisizer counter. Samples: 1 = scraped from the piston frit of column 8; 2 = column 8, outlet, center; 3 = column 8, outlet, wall; 4 = column 8, middle, wall; 5 = column 8, middle, center; 6 = column 8, inlet, wall; 7 = column 8, inlet, center; 8 = column 9, middle, wall; 9 = column 9, middle, center; 10 = virgin material.

was packed with material recycled from the content of the cartridge 2 previously studied in the radial compression equipment [12]. In both cases, the stress applied to the packing was higher than what should be expected under standard operation.

The distributions based on the particle volume is shown in Fig. 10. They are all nearly identical and do not show a significant increase in the volume fraction of small particles. The only differences are a slight ramp from 0 to 12 μm for the samples 1 (scrapped from the piston frit, i.e., at the column entrance) and 6 (column entrance, along the wall), instead of the baseline. Except for these two samples 1 and 6, there is almost no difference between the values of D_v10/D_v90[3] for the virgin material and the samples. By contrast, however, the distributions based on the number of particles (not shown) exhibit an increase in the number of fine particles which is significantly larger than observed with the radial compression column [12], as expected since the packing material used with the axial compression column was recycled from a radial compression cartridge. Given this origin of the samples, explained above, this result indicates that the packing material is reasonably resistant to abrasion and crushing but suggests also that a given batch of stationary phase can be used only a limited number of times. We note also that the ratio D_v50/D_p50, which is the ratio of the medians of the distributions of the particle volumes and numbers, is about the same for all our samples, except for the virgin material and for the packing material on the piston side of the column or at the entrance (samples 1 and 6), regions which seem to have suffered more than the rest. Since the column entrance is the location where the mechanical stress applied by the piston to the packing is concentrated, this result was expected. Our results do not agree with those of Marme et al. [31] who had reported an enrichment in fine particles towards the exit of an axial compression column after 30 h of operation. In our experiments, the fine particles do not seem to migrate significantly but are slightly more abundant in the region where the mechanical stress is higher.

The extent of particle fragmentation during the various operations carried out is somewhat more important with axial compression than it has been observed with radial compression [12]. The difference is not very large, however. No decrease in column performance has been observed, either by us or by others, which could be related to the increase in the proportion of small particles. As a matter of fact, excellent column efficiencies are reproducibly observed. Nevertheless, attention should be paid to this phenomenon, especially when studying the suitability of new column packing materials.

4. Conclusions

As often reported by others at scientific meetings [1], we have found that it is simple and easy to obtain axial compression columns with a reproducibly high efficiency. The learning procedure is fast. If the packing material needed is available, an experienced operator can pack a new column, make a few simple tests and be ready to operate it for the separation required in about an hour. This, however, requires that the stationary phases used need no elutriation, or have been so treated in advance. The most critical issue is the cleanliness of the frits which must be extreme. Fortunately, a simple procedure which gives good results is available. As with all other packing methods, there is no other way to find out whether a newly packed column is good but to test it, although if sounds (e.g., crushing sounds) are heard coming from inside the column while packing it, it is usually poor.

Once packed, the columns remain stable and efficient for as long as we could operate them, 200 h at most, as safety regulations prevented us to operate the instrument unattended overnight or during week-ends. Columns could be packed with stationary phase reused from previous columns, either radial compression cartridges or other radial compression columns. The station-

[3] D_v10 and D_v90 are the particle sizes above which are found 10% and 90%, respectively, of the volume of packing material.

ary phase did not seem to suffer any serious degradation due to its packing, unpacking, and repacking operations. The efficiency of columns obtained with recycled stationary phase is the same as the one achieved with axial compression columns obtained from fresh packing. The slight increase observed in the number of fine particles (Fig. 10) is insufficient to affect the performance.

Because the length of all columns decreases slowly over an extended period of time, so do their total porosity and their permeability. Thus the apparent particle size decreases. The effect is not due to the fragmentation of the packing particles. It is caused by the slow increase in bed consolidation. Thus, it is not surprising that the total porosity and permeability of axial compression columns is lower than that of analytical and of radial compression columns packed with the same phase. The effect is masked in part by the low permeability of the frits used on the instrument. The consequences of this effect remain reasonably easy to manage, as the axial compression pressure required for optimum column performance is moderate. The dependence of the flow-rate on the compression pressure is uncertain at this stage. The phenomenon appears complex, as the column length is also related to the composition of the eluent. Further investigation are in progress.

Acknowledgements

This work has been supported in part by Grant CHE-9201662 of the National Science Foundation and by the cooperative agreement between the University of Tennessee and the Oak Ridge National Laboratory. We acknowledge the long-term free loan by Prochrom (Champigneulles, France) of a LC.50.VE.500.100 Column Skid with a 5 cm I.D. dynamic axial compression column. We thank Biotage (Charlottesville, VA, USA) for the long-term free loan of a Kiloprep 100 solvent-delivery system and a Linear Scientific Model 204 UV detector equipped with a preparative-scale cell. We thank BTR Separations (Wilmington, DE, formerly The PQ Corporation) for the generous gift of 5 kg of IMPAQ RG1020C18 and a semi-preparative Linear Scientific detector. We appreciate the measurements made by Neil Miller of the particle size distribution of samples taken from an axial compression column.

We are grateful to Henri Colin (Prochrom), A.M. Katti (Mallinckrodt Specialty Chemicals, St. Louis, MO, USA), Jack Kirkland (Rockland Technologies, Newport, DE, USA), Klaus Lohse (BTR Separations) and Neil Miller (The PQ Corporation) for insightful discussions.

References

[1] *J. Chromatogr.*, Vol. 484 (1988), Vol. 556 (1991), Vol. 557 (1991), Vol. 590, No. 1 (1992); *J. Chromatogr. A*, Vol. 658, No. 2 (1994).
[2] E. Francotte and A. Junker-Buchkeit, *J. Chromatogr.*, 576 (1992) 576.
[3] W.S. Hancock (Editor), *HPLC in Biotechnology*, Academic Press, New York, 1992.
[4] E. Boschetti, *J. Chromatogr. A*, 658 (1994) 207.
[5] J.H. Knox and H.M. Pyper *J. Chromatogr.*, 363 (1986) 1.
[6] L.R. Snyder, J.W. Dolan and G.B. Cox, *J. Chromatogr.*, 484 (1989) 437.
[7] G. Guiochon, S. Golshan-Shirazi and A.M. Katti, *Fundamentals of Preparative and Non-Linear Chromatography*, Academic Press, Boston, MA, 1994.
[8] G. Ganetsos and P.E. Barker (Editors), *Preparative and Production Scale Chromatography*, Marcel Dekker, New York, 1939.
[9] S. Golshan-Shirazi and G. Guiochon, *Anal. Chem.*, 61 (1989) 1368.
[10] S. Golshan-Shirazi and G. Guiochon, *J. Chromatogr.*, 517 (1990) 229.
[11] A. Felinger and G. Guiochon, *Biotechnol. Bioeng.*, 41 (1993) 134.
[12] M. Sarker and G. Guiochon, *J. Chromatogr. A*, 683 (1994) 293.
[13] Separations Technology, Wakefield, RI, *US Pat.*, 4 737 292 (April 12, 1988).
[14] Roussel-Uclaf, Romainville, *US Pat.*, 3 966 609, 4 (June 17, 1976).
[15] E. Godbille and P. Devaux, *J. Chromatogr.*, 122 (1976) 317.
[16] H. Colin, P. Hilaireau and J. de Tournemire, *LC·GC*, 8 (1990) 302.
[17] Waters Assoc., *US Pat.*, 4 211 658 (1980); *US Pat.*, 4 228 007 (1980); *US Pat.*, 4 250 035 (1981).
[18] J.N. Little, R.L. Cotter, J.A. Prendergast and P.D. McDonald, *J. Chromatogr.*, 126 (1976) 439.

[19] E.P. Kroeff, R.A. Owens, E.L. Campbell, R.D. Johnson and H. Marks, *J. Chromatogr.*, 461 (1989) 45.
[20] D.-R. Wu and K. Lohse, *J. Chromatogr. A*, 658 (1994) 381.
[21] J. Dingenen, I. Somers, F. Pauwels and A. van Loon, in M. Perrut (Editor), *PREP'92*, Société Française de Chimie, Paris, 1992, p. 359.
[22] J.J. van Deemter, F.J. Zuiderweg, and A. Klinkenberg, *Chem. Eng. Sci.*, 5 (1956) 271.
[23] C.R. Wilke and P. Chang, *AIChE J.*, 1 (1955) 264.
[24] E.V. Dose and G. Guiochon, *Anal. Chem.*, 61 (1990) 1723.
[25] E. Kucera, *J. Chromatogr.*, 19 (1965) 237.
[26] M. Martin, H. Colin and G. Guiochon, in H. Engelhardt (Editor), *Handbook of Liquid Chromatography*, Springer, Berlin, 1986.
[27] J.H. Knox and R. Kaliszan, *J. Chromatogr.*, 349 (1985) 211.
[28] F. Riedo and E. sz. Kovats, *J. Chromatogr.*, 239 (1982) 91.
[29] H. Colin, J.C. Diez-Masa, T. Czaychowska, I. Miedziak and G. Guiochon, *J. Chromatogr.*, 167 (1978) 41.
[30] N. Miller, Conshohocken, PA, personal communication, 1994.
[31] S. Marme, M. Hallmann, K.K. Unger, E. Baumeister, K. Albert and E. Bayer, in M. Perrut (Editor), *PREP'92*, Société Française de Chimie, Paris, 1992, p. 135.

ELSEVIER

Journal of Chromatography A, 702 (1995) 45–57

JOURNAL OF CHROMATOGRAPHY A

"Perfusion chromatography". The effects of intra-particle convective velocity and microsphere size on column performance

A.I. Liapis*, Y. Xu, O.K. Crosser, A. Tongta

Department of Chemical Engineering and Biochemical Processing Institute, University of Missouri–Rolla, Rolla, MO 65401-0249, USA

Abstract

A mathematical model describing the dynamic adsorption in columns with spherical bidisperse perfusive or spherical bidisperse purely diffusive adsorbent particles is presented and its solution is obtained numerically. The adsorption of bovine serum albumin on spherical anion-exchange porous particles was studied for different values of the intraparticle Peclet number, Pe_{intra}, and of the microsphere diameter, d_m. The results show a departure from spherical symmetry of the isoconcentration profiles of the adsorbate in the porous adsorbent particle as Pe_{intra} increases. This spherical asymmetry increases the adsorbate availability in the pore fluid of the macroporous region and also increases the concentration of the adsorbate in the adsorbed phase in the upstream half of the spherical adsorbent particle. If, for example, the concentration profiles of the adsorbate in the adsorbed phase of the porous adsorbent particles could be determined experimentally and if these profiles show a departure from spherical symmetry, then this result could suggest that the porous adsorbent particles may have exhibited perfusion behavior under the conditions of operation of the column. The dynamic percentage utilization of the adsorptive capacity of the column increases as Pe_{intra} increases and d_m decreases. The percentage breakthrough to be selected for column switching is influenced by the magnitude of Pe_{intra} because of its effect on the dynamic percentage utilization of the adsorptive capacity of the column.

1. Introduction

The separation process that involves the flow of a liquid phase through the through-pores of porous chromatographic particles packed in a column [1–5] has been called by Afeyan et al. [1] "perfusion chromatography". This term "perfusion chromatography" is often not defined with precision. In this work, as in previous publications [2–5], we define "perfusion chromatography" as referring to any chromatographic system in which the intraparticle convective velocity, v_p, is non-zero [1–5].

Liapis and McCoy [4] considered that the perfusive adsorbent particles with a bidisperse [4] porous structure have a macroporous region made by the through-pores [1,2,4,5] in which intraparticle convection and pore diffusion occur, and a microporous [4] region made by spherical microparticles (microspheres [1]) that

* Corresponding author.

0021-9673/95/$09.50 © 1995 Elsevier Science B.V. All rights reserved
SSDI 0021-9673(94)01022-6

are taken to be purely diffusive. In this work, a mathematical model that could describe adsorption in columns having spherical perfusive adsorbent particles with a bidisperse porous structure is presented. The model is then solved and used to study the dynamic behavior of a column system involving the adsorption of bovine serum albumin (BSA) on spherical anion-exchange porous particles.

2. Mathematical model

Adsorption is considered to take place from a flowing liquid stream in a fixed bed of spherical perfusive adsorbent particles of bidisperse porous structure under isothermal conditions. The differential mass balance for the adsorbate in the flowing fluid stream gives [2–4]

$$\frac{\partial C_d}{\partial t} - D_L \cdot \frac{\partial^2 C_d}{\partial x^2} + \frac{V_f}{\varepsilon} \cdot \frac{\partial C_d}{\partial x} = -\frac{(1-\varepsilon)}{\varepsilon} \frac{\partial \bar{C}_{ps}}{\partial t} \tag{1}$$

The initial and boundary conditions of Eq. (1) are as follows:

$$\text{at } t = 0: \quad C_d = 0, \quad 0 \leq x \leq L \tag{2}$$

$$\text{at } x = 0: \quad \frac{V_f}{\varepsilon} \cdot C_d \Big|_{x=0} - D_L \cdot \frac{\partial C_d}{\partial x}\Big|_{x=0} = \frac{V_f}{\varepsilon} \cdot C_{d,in}, \quad t > 0 \tag{3}$$

$$\text{at } x = L: \quad \frac{\partial C_d}{\partial x}\Big|_{x=L} = 0, \quad t > 0 \tag{4}$$

The value of $C_{d,in}$ may be constant or it may vary with time. An expression for estimating D_L was presented by Arnold et al. [6], but in certain systems the axial dispersion is so low that by setting its value equal to zero the error introduced in the prediction of the behavior of an affinity adsorption system is not significant [6,7]. When the axial dispersion coefficient is set equal to zero, Eq. 3 (with $D_L = 0$) becomes as follows:

$$\text{at } x = 0: \quad C_d = C_{d,in}, \quad t > 0 \tag{5}$$

The spherical perfusive adsorbent particles with a bidisperse [4] porous structure are considered to have a microporous [4] region made by spherical microparticles (microspheres [1]) that are taken to be purely diffusive, and a macroporous [4] region made by the through-pores [1,2,4,5] in which intraparticle convention and pore diffusion occur. Liapis and McCoy [4] were first in proposing the above representation for the bidisperse perfusive adsorbent particles and in modeling the mass transfer mechanisms in the macroporous and microporous regions of the bidisperse perfusive adsorbent particles. The mass transfer mechanisms in the macroporous and microporous regions are presented on p. 86 of Ref. [4]. In Fig. 1, a diagram of a spherical perfusive adsorbent particle with a bidisperse porous structure is shown; x_1 represents the axial coordinate for the spherical perfusive adsorbent particle and is parallel to the axial coordinate x of the column.

The differential mass balance for the adsorbate in the macroporous region of a perfusive adsorbent particle of spherical geometry is given by

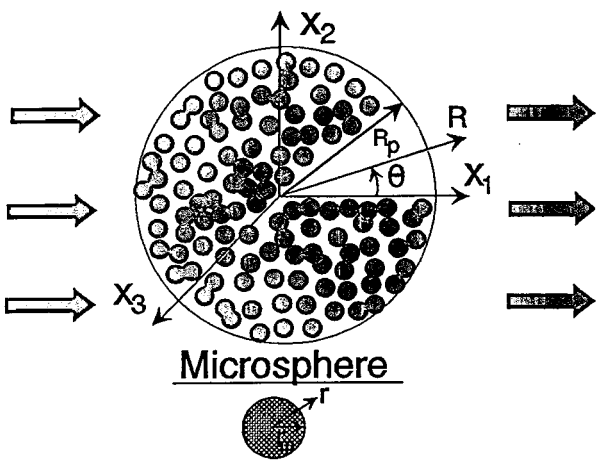

Fig. 1. Spherical perfusive adsorbent particle with a bidisperse porous structure (the arrows indicate the direction of fluid flow). R_p = Radius of perfusive particle; r_m = radius of microsphere.

$$\varepsilon_p \cdot \frac{\partial C_p}{\partial t} + \varepsilon_p v_{pR} \cdot \frac{\partial C_p}{\partial R} + \varepsilon_p v_{p\theta}\left(\frac{1}{R}\right)\frac{\partial C_p}{\partial \theta} + (1-\varepsilon_p)\frac{\partial \bar{C}_s}{\partial t} = \varepsilon_p D_p\left[\left(\frac{1}{R^2}\right)\frac{\partial}{\partial R}\left(R^2 \cdot \frac{\partial C_p}{\partial R}\right) + \left(\frac{1}{R^2 \sin\theta}\right)\frac{\partial}{\partial \theta}\left(\sin\theta \cdot \frac{\partial C_p}{\partial \theta}\right)\right] \quad (6)$$

The variables v_{pR} and $v_{p\theta}$ represent the intraparticle velocity components along the R and θ directions, respectively. Neale et al. [8] obtained analytical expressions for the stream functions outside and inside the permeable spheres. By using the expression of Neale et al. [8] for the stream function inside the particle, the following equations for v_{pR} and $v_{p\theta}$ are obtained:

$$v_{pR} = V_f \cos\theta\left[F - \left(\frac{H}{\xi^2}\right)\left(\frac{\sinh\xi}{\xi} - \cosh\xi\right)\right] \quad (7)$$

$$v_{p\theta} = -V_f \sin\theta\left\{F - \left(\frac{H}{2\xi}\right)\left[\left(\frac{\xi\cosh\xi - \sinh\xi}{\xi^2}\right) - \sinh\xi\right]\right\} \quad (8)$$

Neale et al. [8] reported the expressions for ξ, F and H, which are as follows:

$$\xi = \frac{R}{\sqrt{K_p}} \quad (9)$$

$$F = \frac{B}{\beta^3} + 10D \quad (10)$$

$$H = \frac{1}{J}\left[6\beta^2(\operatorname{sech}\beta)(1-\eta^5)\right] \quad (11)$$

where

$$\beta = \frac{R_p}{\sqrt{K_p}} \quad (12)$$

$$\eta = (1-\varepsilon)^{1/3} \quad (13)$$

$$J = 2\beta^2 - 3\beta^2\eta + 3\beta^2\eta^5 - 2\beta^2\eta^6 + 90\beta^{-2}\eta^5 + 42\eta^5 - 30\eta^6 + 3 - \frac{\tanh\beta}{\beta}(-3\beta^2\eta + 15\beta^2\eta^5 - 12\beta^2\eta^6 + 90\beta^{-2}\eta^5 + 72\eta^5 - 30\eta^6 + 3) \quad (14)$$

$$B = \frac{1}{J}\left[3\beta^3 + 2\beta^3\eta^5 + 30\beta\eta^5 - \frac{\tanh\beta}{\beta}(3\beta^3 + 12\beta^3\eta^5 + 30\beta\eta^5)\right] \quad (15)$$

$$D = -\frac{\eta^5 A}{\beta^5} \quad (16)$$

$$A = \frac{1}{J}\left[\beta^5 + 6\beta^3 - \frac{\tanh\beta}{\beta}(3\beta^5 + 6\beta^3)\right] \quad (17)$$

The value of the particle permeability, K_p, in Eqs. 9 and 12 depends on the diameter of the microspheres, d_m, the porosity of the macroporous region, ε_p, and on the pore-size distribution of the macroporous region. The pore-size distribution of the macroporous region depends on the process employed to aggregate the microspheres to construct the spherical perfusive particle. As a first approximation, the value of K_p could be estimated from the expressions for K_p reported in Refs. [9–11]. The axial component of the intraparticle velocity, v_{px_1}, which is parallel to the flowing fluid stream along the axis of the column, is given by

$$v_{px_1} = v_{pR}\cos\theta - v_{p\theta}\sin\theta \quad (18)$$

The initial and boundary conditions of Eq. 6 are as follows:

at $t = 0$: $C_p = 0$, $0 \le R \le R_p$ (19)

at $R = R_p$: $C_p = C_d$, $t > 0$, $0 \le \theta \le \pi$ (20)

at $R = 0$: $C_p =$ finite, $t > 0$, $0 \le \theta \le \pi$ (21)

at $\theta = 0$: $\left.\frac{\partial C_p}{\partial \theta}\right|_{\theta=0} = 0$, $0 \le R \le R_p$ (22)

at $\theta = \pi$: $\left.\frac{\partial C_p}{\partial \theta}\right|_{\theta=\pi} = 0$, $0 \le R \le R_p$ (23)

The differential mass balance for the adsor-

bate in a purely diffusive spherical microparticle (microsphere) is given by [4]

$$\varepsilon_{pm}\cdot\frac{\partial C_{pm}}{\partial t}+\left(\frac{1}{1-\varepsilon_p}\right)\frac{\partial C_{sm}}{\partial t}$$

$$=\varepsilon_{pm}D_{pm}\left(\frac{\partial^2 C_{pm}}{\partial r^2}+\frac{2}{r}\cdot\frac{\partial C_{pm}}{\partial r}\right) \quad (24)$$

The accumulation term, $\partial C_{sm}/\partial t$, of the adsorbed species can be quantified if a thermodynamically consistent mathematical model could be constructed that could describe the mechanism of adsorption for the adsorbate. For isothermal adsorption systems, the term $\partial C_{sm}/\partial t$ could be of the form

$$\frac{\partial C_{sm}}{\partial t}=f(C_{pm}, C_{sm}, \boldsymbol{k}) \quad (25)$$

where f represents the functional form of the dynamic adsorption mechanism for the adsorbate, and $\boldsymbol{k}$ represents the vector of the rate constants that characterize the interaction kinetics between the adsorbate molecules and the active sites. One well known form of Eq. 25 for single-component adsorption ($A+S\underset{k_2}{\overset{k_1}{\rightleftharpoons}}AS$) is as follows [2,4,12]:

$$\frac{\partial C_{sm}}{\partial t}=k_1 C_{pm}(C_T-C_{sm})-k_2 C_{sm} \quad (26)$$

The term $\partial C_{sm}/\partial t$ in Eq. 24 could now be replaced by the right-hand side of Eq. 26. The initial and boundary conditions of Eqs. 24 and 25 (and also of Eq. 26) are considered to be as follows:

$$\text{at } t=0: \quad C_{pm}=0, \quad 0\leq r\leq r_m \quad (27)$$

$$\text{at } t=0: \quad C_{sm}=0, \quad 0\leq r\leq r_m \quad (28)$$

$$\text{at } r=r_m: \quad C_{pm}=C_p(t,R,\theta), \quad t>0 \quad (29)$$

$$\text{at } r=0: \quad \left.\frac{\partial C_{pm}}{\partial r}\right|_{r=0}=0, \quad t>0 \quad (30)$$

The variable $\bar{C}_s$ in Eq. 6 could be calculated from the following expression:

$$\bar{C}_s=\frac{3}{r_m^3}\left[\int_0^{r_m}\varepsilon_{pm}C_{pm}r^2\,dr+\int_0^{r_m}\left(\frac{1}{1-\varepsilon_p}\right)C_{sm}r^2\,dr\right] \quad (31)$$

The accumulation term $\partial\bar{C}_s/\partial t$ in Eq. 6 is obtained by differentiating Eq. 31 with respect to time, and hence

$$\frac{\partial\bar{C}_s}{\partial t}=\frac{3}{r_m^3}\left\{\frac{\partial}{\partial t}\left(\int_0^{r_m}\varepsilon_{pm}C_{pm}r^2\,dr\right)+\frac{\partial}{\partial t}\left[\int_0^{r_m}\left(\frac{1}{1-\varepsilon_p}\right)C_{sm}r^2\,dr\right]\right\} \quad (32)$$

For a given pair of values of R and θ, the average concentration of the adsorbate in the adsorbed phase, $\bar{C}_{sa}$, is obtained from the following expression:

$$\bar{C}_{sa}=(1-\varepsilon_p)\frac{3}{r_m^3}\left[\int_0^{r_m}\left(\frac{1}{1-\varepsilon_p}\right)C_{sm}r^2\,dr\right] \quad (33)$$

Finally, the term $\partial\bar{C}_{ps}/\partial t$ in Eq. 1 is given by

$$\frac{\partial\bar{C}_{ps}}{\partial t}=\frac{3}{2R_p^3}\left\{\frac{\partial}{\partial t}\left(\int_0^{\pi}\int_0^{R_p}\varepsilon_p C_p R^2\sin\theta\,dR\,d\theta\right)+\frac{\partial}{\partial t}\left[\int_0^{\pi}\int_0^{R_p}(1-\varepsilon_p)\bar{C}_s R^2\sin\theta\,dR\,d\theta\right]\right\} \quad (34)$$

since

$$\bar{C}_{ps}=\frac{3}{2R_p^3}\left\{\int_0^{\pi}\int_0^{R_p}[\varepsilon_p C_p+(1-\varepsilon_p)\bar{C}_s]R^2\sin\theta\,dR\,d\theta\right\} \quad (35)$$

The dynamic behavior of a column adsorption system involving spherical perfusive adsorbent particles with a bidisperse porous structure could be obtained by solving simultaneously Eqs. 1, 6, 24 and 25. It should be noted that Eq. 26 could be used for Eq. 25 with the understanding that Eq. 26 represents only one possible form of Eq. 25.

It should be mentioned that if the intraparticle velocity is zero ($v_{pR}=v_{p\theta}=0$), then the spherical adsorbent particles are considered to be purely

diffusive. In this case, the concentration C_p is considered to be independent of θ, and thus the term $\partial C_p/\partial\theta$ in Eq. 6 is taken to be equal to zero. Further, the boundary conditions given by Eqs. 22 and 23 are not needed, and the boundary condition at $R=0$ becomes $(\partial C_p/\partial R)|_{R=0} = 0$.

2.1. Numerical solution

The solution of the equations of the mathematical model presented in this work was obtained by employing (a) the method of orthogonal collocation [4,9,13,14] on the space variable r of the continuity equation of the adsorbate in the microparticle, (b) the double collocation [13,15] method on the space variables R and θ of the continuity equation of the adsorbate in the macroporous region (through-pores) and (c) the method of orthogonal collocation on finite elements [4,9,13] on the space variable x of the continuity equation of the adsorbate in the flowing fluid stream in the column; the resulting non-linear ordinary differential equations were integrated by using Gear's method [14], which is employed in the LSODES component of the ODEPACK [16] software package.

3. Results and discussion

In this work, the dynamic behavior of a column system involving the adsorption of bovine serum albumin (BSA) into spherical anion-exchange porous particles was studied, for different values of the intraparticle Peclet number, Pe_{intra}, and of the microparticle (microsphere) diameter, d_m. The diameter of the adsorbent particles, d_p, was taken to be $1.5\cdot10^{-5}$ m, and three different values for the diameter of the microparticles, d_m, were employed: $7.13\cdot10^{-8}$, $7.13\cdot10^{-7}$ and $7.13\cdot10^{-6}$ m. If the intraparticle Peclet number, Pe_{intra}, could be defined as

$$Pe_{intra} = \frac{v_{px_1} d_p}{D_p} \tag{36}$$

then, from Eqs. 7, 8 and 18, it is apparent that the value of v_{px_1}, and hence the value of Pe_{intra}, depends on the values of R and θ considered in the evaluation of v_{px_1}. The value of v_{px_1} becomes independent of the values of R and θ when $H=0$ in Eqs. 7 and 8. For purely diffusive adsorbent particles $Pe_{intra}=0$, whereas for adsorbent particles with non-zero intraparticle fluid flow $Pe_{intra}>0$. In Table 1, the values of the parameters used for the dynamic simulations of the adsorption system studied in this work are presented. The values of other parameters are reported in the captions of the figures. It should be mentioned that the value of C_T in Table 1 represents the largest (maximum) amount of BSA that could be adsorbed per unit volume of the adsorbent particle. Further, the value of $C_{d,in} = 0.1$ kg/m^3 in Table 1 indicates that the value of the inlet concentration of the adsorbate in the flowing fluid stream remains constant for all times of the adsorption stage (that is, the value of $C_{d,in}$ in the boundary condition given by Eq. 5 remains constant and equal to 0.1 kg/m^3 for all times), and this indicates that the simulation studies of this work examine systems of frontal analysis.

The values of the parameters of the system studied are such that the value of H in Eqs. 7 and 8 is essentially equal to zero. Thus, the values of v_{pR}, $v_{p\theta}$ and v_{px_1}, for the adsorption system studied, are obtained from the following expressions:

$$v_{pR} \approx FV_f \cos\theta \tag{37}$$

$$v_{p\theta} \approx -FV_f \sin\theta \tag{38}$$

$$v_{px_1} = FV_f \tag{39}$$

In this case, the expression for the intraparticle Peclet number when using Eq. 36 is

Table 1
Values of the parameters of the column system involving the adsorption of BSA on spherical anion-exchange porous adsorbent particles

$C_{d,in} = 0.1$ kg/m^3; $C_T = 78.3$ kg/m^3; $d_p = 1.5\cdot10^{-5}$ m;
$\varepsilon = 0.35$; $\varepsilon_p = 0.13$; $\varepsilon_{pm} = 0.48$; $T = 296$ K;
$D_p = 3.835\cdot10^{-12}$ m^2/s, $D_{pm} = 7.08\cdot10^{-12}$ m^2/s, $D_L = 0$;
$K = k_1/k_2 = 8.026$ m^3/kg; $k_1 = 1.05$ m^3/kg·s;
$k_2 = 0.131$ s^{-1}; $L = 0.1$ m, $V_f = 2.778\cdot10^{-3}$ m/s

$$Pe_{\text{intra}} = \frac{v_{px_1} d_p}{D_p} = \frac{(FV_f)d_p}{D_p} \quad (40)$$

In this work, the Pe_{intra} given by Eq. 40 was varied between 0 and 150.

The numerical solution of the mathematical model presented in the previous section allows the determination of intraparticle concentration profiles of the adsorbate in the pore fluid and in the adsorbed phase, and also the determination of transport rates and the dynamic performance of the adsorption system for a variety of adsorbent particle characteristics and operating conditions of the column. Some sample calculations of the adsorption of BSA into spherical anion-exchange porous particles are presented for the purpose of illustrating certain important features of the adsorption system in the presence of intraparticle fluid flow.

In Figs. 2a–7a, the dimensionless isoconcentration profiles of the adsorbate in the pore fluid of the pores of the macroporous region of the adsorbent particle are presented, and in Figs. 2b–7b the dimensionless isoconcentration profiles of the adsorbate in the adsorbed phase of the absorbent particle are shown. In Figs. 2–7 the outermost contours represent the isoconcentrations at the surface ($R = R_p$) of the particle, and the data in Figs. 2–7 were obtained for the position in the column located at $x = 0.125L$ and at time $t = 60$ min.

The effect of increasing Pe_{intra} is clearly shown through the change in the symmetry of the concentration profiles of the adsorbate in the adsorbent particle. Examination of the concentration contours of Figs. 2 and 5, for $Pe_{\text{intra}} = 0$ and 5, respectively, shows that there is a departure from spherical symmetry of the concentration profiles of the adsorbate as Pe_{intra} increases. As Pe_{intra} increases, the smallest concentration moves downstream, and hence there is higher adsorbate availability in the pore fluid of the macroporous region and a higher concentration of adsorbate in the adsorbed phase in the upstream half of the sphere than the downstream half. This is due to the intraparticle fluid flow mechanism operating in the same direction as pore diffusion in the upstream part of the absorbent particle but opposite to the pore diffusion mechanism downstream. Further, the fluid moving by intraparticle convection to the downstream part of the adsorbent particle has limited adsorbate content as most of the adsorbate was already adsorbed upstream. The results in Figs. 2–7 also show that the magnitude of the departure from spherical symmetry of the con-

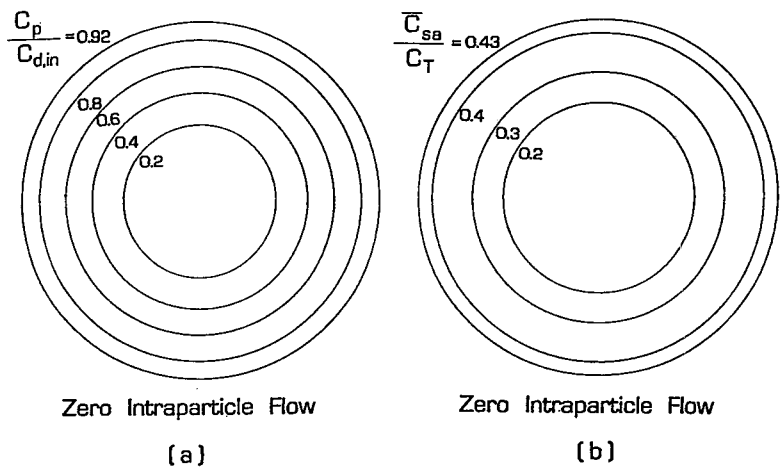

Fig. 2. Isoconcentration contours of the concentration of the adsorbate in the pore fluid of the macroporous region and in the adsorbed phase of the porous adsorbent particle when $d_m = 7.13 \cdot 10^{-8}$ m and $Pe_{\text{intra}} = 0$, at $x = 0.125L$ and $t = 60$ min. (a) $C_p/C_{d,in}$; (b) $\bar{C}_{sa}/C_T$.

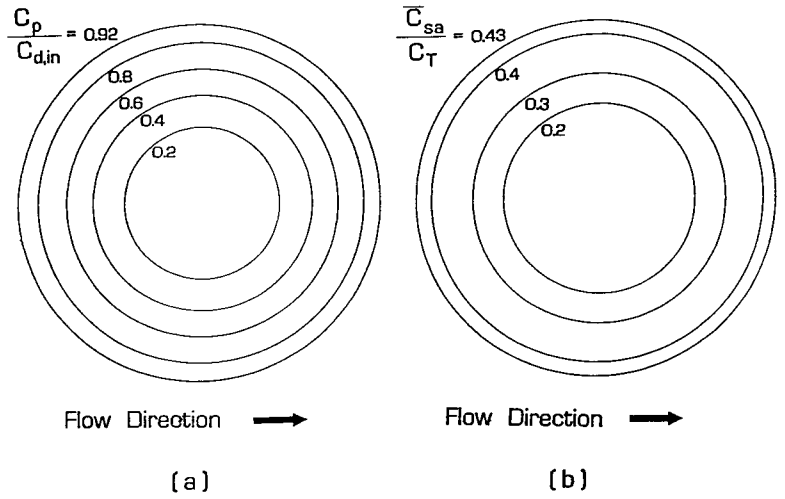

Fig. 3. Isoconcentration contours of the concentration of the adsorbate in the pore fluid of the macroporous region and in the adsorbed phase of the porous adsorbent particle when $d_m = 7.13 \cdot 10^{-8}$ m and $Pe_{intra} = 1$, at $x = 0.125L$ and $t = 60$ min. (a) $C_p/C_{d,in}$; (b) $\bar{C}_{sa}/C_T$.

centration profiles of the adsorbate increases as the magnitude of Pe_{intra} increases. Also, by comparing the results in Figs. 2 and 3 it can be observed that the differences in the concentration profiles are insignificant, whereas by comparing the results in Figs. 2 and 4 it becomes apparent that there are some slight differences between the concentration profiles. The data in Figs. 2–7 indicate that the beginning of an observable departure from spherical symmetry of the concentration profiles of the adsorbate occurs, for the adsorption system studied, for

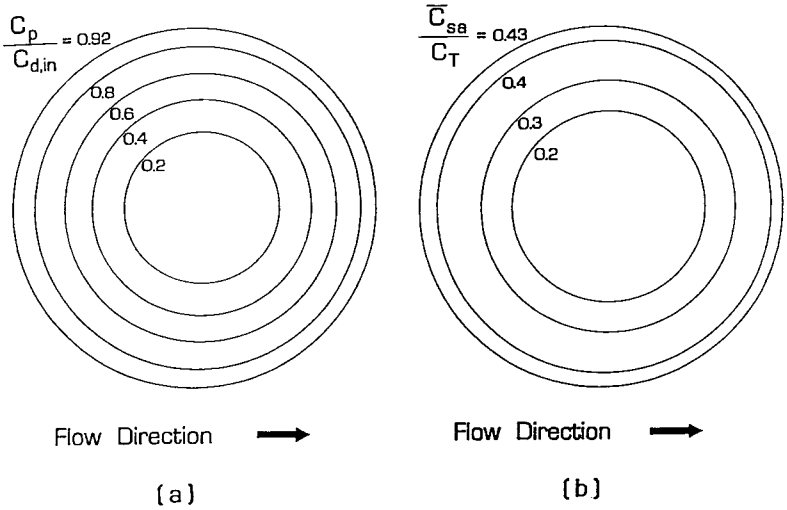

Fig. 4. Isoconcentration contours of the concentration of the adsorbate in the pore fluid of the macroporous region and in the adsorbed phase of the porous adsorbent particle when $d_m = 7.13 \cdot 10^{-8}$ m and $Pe_{intra} = 2$, at $x = 0.125L$ and $t = 60$ min. (a) $C_p/C_{d,in}$; (b) $\bar{C}_{sa}/C_T$.

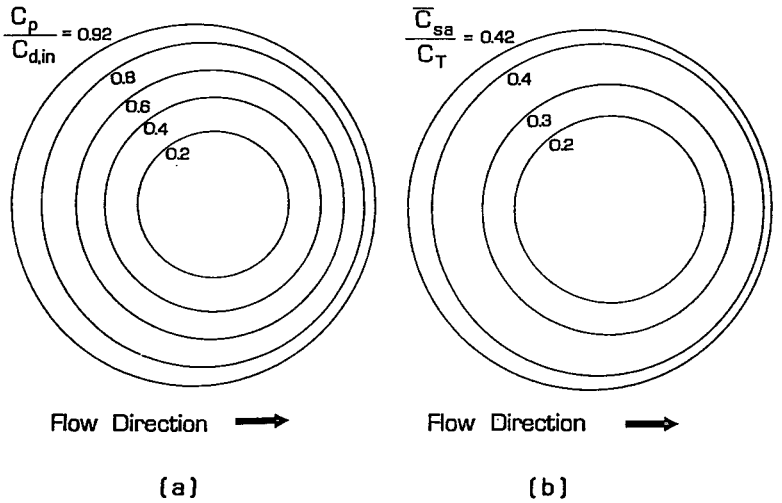

Fig. 5. Isoconcentration contours of the concentration of the adsorbate in the pore fluid of the macroporous region and in the adsorbed phase of the porous adsorbent particle when $d_m = 7.13 \cdot 10^{-8}$ m and $Pe_{intra} = 5$, at $x = 0.125L$ and $t = 60$ min. (a) $C_p/C_{d,in}$; (b) $\bar{C}_{sa}/C_T$.

values of $Pe_{intra} \geq 2$. It should also be mentioned that as Pe_{intra} increases and the adsorbate concentration minimum moves downstream, the overall adsorbate content of the spherical adsorbent particle increases; this was also the case when the porous adsorbent particle had slab [2,4] geometry. It is also worth mentioning that model simulations using the values of the parameters in Table 1, the values of the intraparticle Peclet numbers reported in the captions of Figs. 2–7 and considering the size of the microspheres to be either $d_m = 7.13 \cdot 10^{-7}$ or $7.13 \cdot 10^{-6}$ m, provided isoconcentration profiles whose behavior was similar to the behavior of the iso-

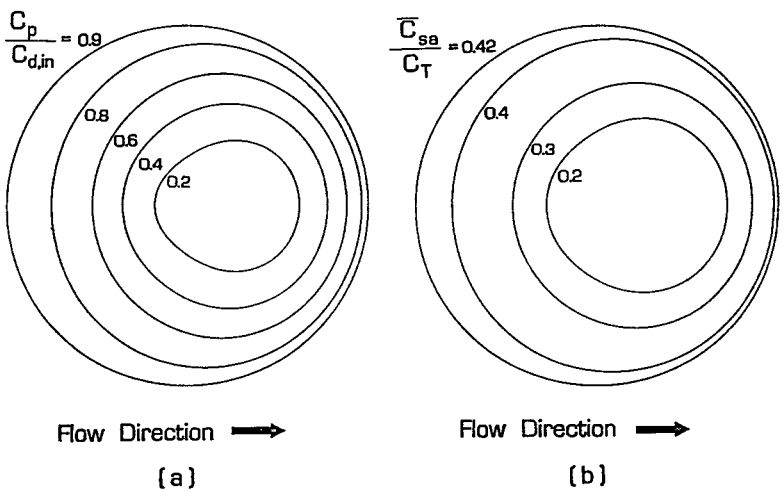

Fig. 6. Isoconcentration contours of the concentration of the adsorbate in the pore fluid of the macroporous region and in the adsorbed phase of the porous adsorbent particle when $d_m = 7.13 \cdot 10^{-8}$ m and $Pe_{intra} = 10$, at $x = 0.125L$ and $t = 60$ min. (a) $C_p/C_{d,in}$; (b) $\bar{C}_{sa}/C_T$.

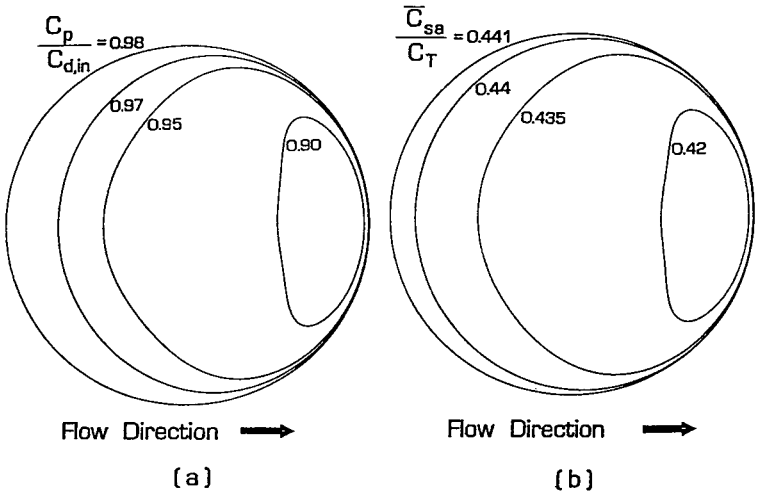

Fig. 7. Isoconcentration contours of the concentration of the adsorbate in the pore fluid of the macroporous region and in the adsorbed phase of the porous adsorbent particle when $d_m = 7.13 \cdot 10^{-8}$ m and $Pe_{intra} = 50$, at $x = 0.125L$ and $t = 60$ min. (a) $C_p/C_{d,in}$; (b) $\bar{C}_{sa}/C_T$.

concentration profiles presented in Figs. 2–7, as the value of the intraparticle Peclet number was being increased.

At this point, it may be useful to suggest that if the intraparticle convective velocity could not be measured experimentally for a given kind of chromatographic porous adsorbent particles, then the behavior of the results in Figs. 2–7 could be considered to provide an indirect test for determining if a given kind of chromatographic porous adsorbent particles could exhibit perfusion behavior when the column in which these particles are packed is operated under conditions of interest to the user. For instance, if it had been determined experimentally that the immobilized adsorption sites on the surface of the pores of the porous adsorbent particles were distributed evenly throughout the interior of the particles, then it might be possible to label the adsorbate molecules of the flowing fluid stream and determine experimentally the concentration profiles of the adsorbate molecules in the adsorbed phase of the chromatographic porous adsorbent particles taken from different axial positions of the bed, after the column was operated under conditions of interest to the user. If the experimentally determined concentration profiles of the adsorbate molecules in the adsorbed phase of the porous adsorbent particles show a departure from spherical symmetry, then this result could suggest that the chromatographic porous absorbent particles of the column may have exhibited perfusion behavior under the conditions of operation of the column.

In Table 2, the dynamic percentage utilization of the adsorptive capacity of the column at 1% and 10% breakthrough is presented. The total adsorptive capacity of the column is defined as the total amount of adsorbate in the adsorbed phase (in the column) at equilibrium (evaluated with respect to the value of $C_{d,in}$). The dynamic utilization of the adsorptive capacity of the column is defined as the ratio of the total amount of adsorbate in the adsorbed phase of the column when the desired breakthrough occurs to the total adsorptive capacity of the column. The dynamic percentage utilization of the adsorptive capacity of the column is obtained by multiplying the dynamic utilization of the adsorptive capacity of the column (defined above) by 100. The results in Table 2 show that for a given value of d_m, the dynamic percentage utilization of the adsorptive capacity of the column increases as the value of Pe_{intra} increases. Further, for a given value of Pe_{intra} the dynamic percentage utilization of the adsorptive capacity of the column

Table 2
Dynamic percentage utilization of the adsorptive capacity of the column at 1% [$(C_d(t, L)/C_{d,in}) \cdot 100 = 1\%$]) and 10% [$(C_d(t, L)/C_{d,in}) \cdot 100 = 10\%$)] breakthrough

d_p (m)	d_m (m)	Pe_{intra} (see Eq. 40)	Time at which 1% breakthrough occurs (min)	Time at which 10% breakthrough occurs (min)	Percentage utilization at 1% breakthrough	Percentage utilization at 10% breakthrough
$1.5 \cdot 10^{-5}$	$7.13 \cdot 10^{-8}$	0.0	25.2	48.0	18.440	34.380
		0.035	25.2	48.0	18.440	34.380
		0.1	25.2	48.0	18.440	34.380
		1.0	25.2	48.3	18.440	34.579
		2.0	25.2	48.3	18.440	34.581
		5.0	25.2	48.6	18.441	34.793
		10.0	25.5	50.1	18.661	35.835
		20.0	26.4	56.7	19.322	40.439
		30.0	27.9	71.1	20.425	50.514
		40.0	30.6	80.4	22.407	57.344
		50.0	36.9	87.3	27.011	62.471
		100.0	69.0	106.2	50.546	76.727
		109.0	72.3	108.3	52.966	78.305
		150.0	84.9	114.6	62.224	83.153
$1.5 \cdot 10^{-5}$	$7.13 \cdot 10^{-7}$	0.0	25.2	48.0	18.439	34.376
		0.035	25.2	48.0	18.439	34.376
		0.1	25.2	48.0	18.439	34.376
		1.0	25.2	48.0	18.439	34.377
		2.0	25.2	48.3	18.440	34.577
		5.0	25.2	48.6	18.440	34.789
		10.0	25.5	49.8	18.660	35.633
		20.0	26.1	56.7	19.103	40.437
		30.0	27.9	71.1	20.425	50.511
		40.0	30.6	80.4	22.406	57.340
		50.0	36.6	87.3	26.791	62.467
		100.0	68.4	106.2	50.104	76.719
		109.0	72.0	108.3	52.747	78.300
		150.0	84.9	114.6	62.223	83.148
$1.5 \cdot 10^{-5}$	$7.13 \cdot 10^{-6}$	0.0	18.6	45.3	13.591	32.368
		0.035	18.6	45.3	13.591	32.268
		0.1	18.6	45.3	13.591	32.268
		1.0	18.6	45.3	13.591	32.269
		2.0	18.6	45.6	13.592	32.470
		5.0	18.6	45.9	13.592	32.685
		10.0	18.9	47.4	13.812	33.739
		20.0	20.1	54.9	14.692	38.984
		30.0	22.5	67.2	16.451	47.668
		40.0	26.4	76.5	19.309	54.442
		50.0	33.0	83.1	24.139	59.340
		100.0	60.6	101.1	44.378	72.873
		109.0	63.6	102.9	46.582	74.240
		150.0	75.0	109.2	54.955	79.029

increases as the value of d_m decreases; a significant change occurs as d_m increases from $7.13 \cdot 10^{-8}$ to $7.13 \cdot 10^{-6}$ m. However, it should also be noted by examining the data in Table 2 that the ratios of the dynamic percentage utilizations obtained from increasing values of d_m decrease as Pe_{intra} increases. Consideration of the above observations suggests that the decreases in the dynamic percentage utilization with increasing values of d_m could be reduced by increasing the value of Pe_{intra}. In Fig. 8, the dynamic percentage utilization of the adsorptive capacity of the column at 1% and 10% breakthrough for values of Pe_{intra} from 0 to 150 are presented for $d_m = 7.13 \cdot 10^{-8}$ and $7.13 \cdot 10^{-6}$ m. The results in Fig. 8 indicate that at 1% breakthrough the

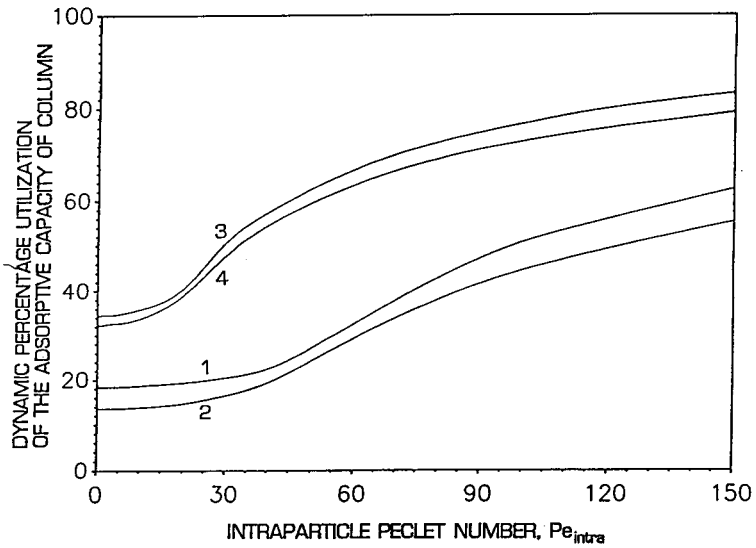

Fig. 8. Dynamic percentage utilization of the adsorptive capacity of column at 1% and 10% breakthrough as a function of intraparticle Peclet number, Pe_{intra}, for $d_m = 7.13 \cdot 10^{-8}$ and $7.13 \cdot 10^{-6}$ m. (1) 1% breakthrough when $d_m = 7.13 \cdot 10^{-8}$ m; (2) 1% breakthrough when $d_m = 7.13 \cdot 10^{-6}$ m; (3) 10% breakthrough when $d_m = 7.13 \cdot 10^{-8}$ m; (4) 10% breakthrough when $d_m = 7.13 \cdot 10^{-6}$ m.

dynamic percentage utilization, for a given d_m value, is similar for Pe_{intra} from 0 to about 20, whereas at 10% breakthrough the dynamic percentage utilization, for a given d_m value, is similar for Pe_{intra} from 0 to about 10. These results suggest that if one plans to switch the column at 1% breakthrough, then a higher dynamic percentage utilization of the adsorptive capacity than that obtained with purely diffusive particles requires that the value of Pe_{intra} of the adsorbent particles should be ≥ 20, and if one plans to switch the column at 10% breakthrough, then the value of Pe_{intra} of the adsorbent particles should be ≥ 10.

4. Conclusions

A mathematical model that could be used to describe adsorption in columns with spherical bidisperse perfusive or spherical bidisperse purely diffusive adsorbent particles was constructed and presented. A numerical solution procedure was also developed and used to solve the unsteady-state spatially multi-dimensional nonlinear partial differential equations of the model. The numerical solution of the mathematical model allows the determination of intraparticle concentration profiles of the adsorbate in the pore fluid and in the adsorbed phase of the spherical bidisperse porous adsorbent particles, the transport rates for a variety of adsorbent particle characteristics and operating conditions of the column and the determination of the concentration of the adsorbate in the flowing fluid stream everywhere in the column including its exit, for intraparticle Peclet numbers ≥ 0.

The dynamic adsorption of BSA on spherical anion-exchange porous particles packed in a column was studied for different values of the intraparticle Peclet number, Pe_{intra}, and of the microparticle diameter, d_m. It was found that the spherical symmetry of the isoconcentration profiles during adsorption inside a porous adsorbent particle, characteristic of purely diffusive porous adsorbent particles, is significantly altered as the magnitude of Pe_{intra} is increased above 2 for the system studied. As Pe_{intra} increases, the smallest concentration of the adsorbate moves downstream, and hence there is higher adsorbate availability in the pore fluid of the macroporous

region and a higher concentration of adsorbate in the adsorbed phase in the upstream than the downstream half of the sphere. Further, as Pe_{intra} increases and the adsorbate concentration minimum moves downstream, the overall adsorbate content of the spherical adsorbent particle increases, and this increases the driving force for mass transfer into the microspheres (microparticles).

It was suggested that if the intraparticle convective velocity could not be measured experimentally for a given kind of chromatographic porous adsorbent particles, then the behavior of the results in Figs. 2–7 could be considered to provide an indirect test for determining if a given kind of chromatographic adsorbent particles could exhibit perfusion behavior when the column is operated under conditions of interest to the user. If, for example, the concentration profiles of the adsorbate molecules in the adsorbed phase of the porous adsorbent particles could be determined experimentally, and if the experimentally determined concentration profiles show a departure from spherical symmetry, then this result could suggest that (considering that the adsorption sites on the surface of the pores were distributed evenly throughout the interior of the adsorbent particles) the porous adsorbent particles of the column may have exhibited perfusion behavior under the conditions of operation of the column.

The dynamic percentage utilization of the adsorptive capacity of the column, for a given value of d_m, increases as Pe_{intra} increases. Further, for a given value of Pe_{intra} the dynamic percentage utilization of the adsorptive capacity of the column increases as the value of d_m decreases. The dynamic percentage utilizations of the adsorptive capacity of the column at 1% and 10% breakthrough, for the system studied here, are increased above that obtained from purely diffusive porous adsorbent particles by increasing Pe_{intra} above 20 and 10, respectively.

Finally, the percentage breakthrough to be selected for column switching is influenced by the value of Pe_{intra} because of its effect on the dynamic percentage utilization of the adsorptive capacity of the column.

Symbols

A	molecule of adsorbate
AS	adsorbate–active site complex
C_d	concentration of adsorbate in the flowing fluid stream of the column (kg/m^3 of bulk fluid)
$C_{d,in}$	concentration of adsorbate at $x<0$ when $D_L \neq 0$, or at $x=0$ when $D_L=0$ (kg/m^3 of bulk fluid)
C_p	concentration of adsorbate in the fluid of the macropores (through-pores) (kg/m^3 of macropore volume)
C_{pm}	concentration of adsorbate in the fluid of the micropores (kg/m^3 of micropore volume)
$\bar{C}_{ps}$	average concentration of adsorbate defined in Eq. 35 (kg/m^3 of perfusive particle)
$\bar{C}_s$	average concentration of adsorbate defined in Eq. 31 (kg/m^3 of microparticle)
$\bar{C}_{sa}$	average concentration of adsorbate in the adsorbed phase defined in Eq. 33 (kg/m^3 of perfusive particle)
C_{sm}	concentration of adsorbate in the adsorbed phase of the microparticle (kg/m^3 of perfusive particle)
C_T	maximum equilibrium concentration of adsorbate in the adsorbed phase of the microparticle (kg/m^3 of perfusive particle)
d_p	diameter of spherical porous adsorbent particle, ($d_p=2R_p$) (m)
D_L	axial dispersion coefficient of adsorbate (m^2/s)
d_m	diameter of spherical microparticle ($d_m=2r_m$) (m)
D_p	effective pore diffusion coefficient of adsorbate in the macropores (through-pores) (m^2/s)
D_{pm}	effective pore diffusion coefficient of adsorbate in the micropores (m^2/s)

$f(C_{pm}, C_{sm}, \boldsymbol{k})$	functional form defined after Eq. 25
F	parameter given by Eq. 10
H	parameter given by Eq. 11
$\boldsymbol{k}$	vector of adsorption rate constants defined after Eq. 25
k_1	adsorption rate constant in $A + S \underset{k_2}{\overset{k_1}{\rightleftharpoons}} AS$ (m^3 of micropore volume/kg · s)
k_2	adsorption rate constant in $A + S \underset{k_2}{\overset{k_1}{\rightleftharpoons}} AS$ (s^{-1})
K	equilibrium adsorption constant of adsorbate, $K = k_1/k_2$ (m^3/kg)
K_p	particle permeability (m^2)
L	column length (m)
Pe_{intra}	intraparticle Peclet number $[Pe_{intra} = (v_{px_1} d_p)/D_p]$ (dimensionless)
r	radial distance in microparticle (m)
r_m	radius of microparticle (m)
R	radial distance in perfusive particle (m)
R_p	radius of perfusive particle (m)
S	active site
T	temperature (K)
t	time (s)
$\boldsymbol{v}_p$	intraparticle velocity vector (m/s)
v_{pR}	intraparticle velocity component along the R direction (m/s)
$v_{p\theta}$	intraparticle velocity component along the θ direction (m/s)
v_{px_1}	axial component of the intraparticle velocity given by Eq. 18 (m/s)
V_f	column fluid superficial velocity (m/s)
x	axial distance in column (m)
x_1, x_2, x_3	space coordinates of perfusive particle as shown in Fig. 1 (m)

Greek letters

β	parameter defined in Eq. 12
ε	void fraction in column
ε_p	macropore (through-pore) void fraction
ε_{pm}	micropore void fraction
η	parameter defined in Eq. 13
θ	polar coordinate angle (rad)
ξ	variable defined in Eq. 9

Acknowledgements

A.I.L. gratefully acknowledges partial support of this work by Monsanto and the NATO Scientific Affairs Division under Grant No. 880770.

References

[1] N.B. Afeyan, N.F. Gordon, I. Mazsaroff, L. Varady, S.P. Fulton, Y.B. Yang and F.E. Regnier, *J. Chromatogr.*, 519 (1990) 1.
[2] A.I. Liapis and M.A. McCoy, *J. Chromatogr.*, 599 (1992) 87.
[3] M.A. McCoy, A.I. Liapis and K.K. Unger, *J. Chromatogr.*, 644 (1993) 1.
[4] A.I. Liapis and M.A. McCoy, *J. Chromatogr. A*, 660 (1994) 85.
[5] A.I. Liapis, *Math. Modelling Sci. Comput.*, 1 (1993) 397.
[6] F.H. Arnold, H.W. Blanch and C.R. Wilke, *Chem. Eng. J.*, 30 (1985) B25.
[7] F.H. Arnold, H.W. Blanch and C.R. Wilke, *Chem. Eng. J.*, 30 (1985) B9.
[8] G. Neale, N. Epstein and W. Nader, *Chem. Eng. Sci.*, 28 (1973) 1865.
[9] M.A. McCoy, *Ph.D. Dissertation*, Department of Chemical Engineering, University of Missouri–Rolla, Rolla, MO, 1992.
[10] A.I. Liapis and K.K. Unger, in G. Street (Editor), *Highly Selective Separations in Biotechnology*, Blackie, Glasgow, 1994.
[11] A.E. Rodrigues, J.C. Lopes, Z.P. Lu, J.M. Loureiro and M.M. Dias, *J. Chromatogr.*, 590 (1992) 93.
[12] B.H. Arve and A.I. Liapis, *AIChE J.*, 33 (1987) 179.
[13] J. Villadsen and M.L. Michelsen, *Solution of Differential Equation Models by Polynomial Approximation*, Prentice-Hall, Englewood Cliffs, NJ, 1978.
[14] C.D. Holland and A.I. Liapis, *Computer Methods for Solving Dynamic Separation Problems*, McGraw-Hill, New York, 1983.
[15] J. Villadsen and J.P. Sorensen, *Chem. Eng. Sci.*, 24 (1969) 1337.
[16] T. Wicks, *Scientific Computing and Analysis Library Report, SCA-LR-52*, Boeing Computer Services, Seattle, 1988.

ELSEVIER

Journal of Chromatography A, 702 (1995) 59–68

JOURNAL OF CHROMATOGRAPHY A

Validation studies in the regeneration of ion-exchange celluloses

Peter R. Levison*, Stephen E. Badger, Russell M.H. Jones, David W. Toome, Michael Streater, Navin D. Pathirana, Simon Wheeler

Whatman International Ltd., Springfield Mill, Maidstone, Kent ME14 2LE, UK

Abstract

The effectiveness of a clean-in-place procedure involving treatment with 0.5 *M* NaOH for 16 h at room temperature has been examined following process-scale chromatography of 1.85 kg hen egg-white proteins on the DEAE-cellulose, Whatman Express-Ion Exchanger D and the QA-cellulose, Whatman Express-Ion Exchanger Q in 251 columns operating at flow-rates of 150 cm/h. Treatment of the media with 0.5 *M* NaOH did not affect the performance of the media after re-equilibration. The NaOH treatment was effective for sanitization and depyrogenation of columns of Express-Ion D and Express-Ion Q following gross microbial contamination. Furthermore, hydrolysis of the DEAE functional groups from Express-Ion D during treatment with 0.5 *M* NaOH was beyond the limits of detection, i.e. $<0.01\%$ of the total DEAE content of the exchanger.

1. Introduction

Ion-exchange chromatography is a widely used technique in the downstream processing of commercially important biopolymers. For low-pressure chromatography, ion exchangers are traditionally based on polysaccharide supports including cellulose, agarose and dextran [1,2]. In industrial applications, particularly in the manufacture of biopharmaceuticals, regulatory aspects of the chromatographic process are an important consideration in process development. Process validation is a complex subject and the key issues have been adequately reviewed elsewhere [3]. In the present study we are interested only in the validation of a specific anion-exchange chromatography process, using cellulose-based adsorbents, with emphasis on aspects of sanitization and leachables. Large-scale ion-exchange processes can be carried out using either batch stirred tank or column techniques [4] although the latter technique may be more desirable where validation is important since it is a closed system and consequently much easier to manage and control compared with an open batch stirred tank unit operation.

During the chromatographic step it is necessary, in the validated process, to demonstrate that the product eluted during the process is of the desired quality with regard to sterility, endotoxin content and contaminants arising from the chromatographic medium itself (leachables). The medium would typically undergo a clean-in-place protocol (CIP) periodically during use, and this CIP protocol is an opportune step to effect sanitization, but may adversely affect the process if it were to result in chemical attrition of the medium, i.e. generation of leachables. We have

* Corresponding author.

SSDI 0021-9673(94)00991-0

previously reported that storage of the anion-exchange celluloses DE52 [5], QA52 [6], DE92 [7] and DEAE-cellulose/D856 [8] in 0.5 *M* NaOH for a period of 12–16 h represents typical conditions for an effective CIP. Furthermore we have shown that these conditions effect simultaneous sterilization and depyrogenation of heavily contaminated columns of DE52 and QA52 following challenge with ca. $1 \cdot 10^9$ *Escherichia coli* per ml [6,9,10]. It has been reported that agarose-based ion exchangers for example can be cleaned using dilute NaOH [11] and these conditions have been investigated for use in sanitization. Storage of various chromatographic media in dilute NaOH at concentrations of up to 1 *M* and the use of dilute ethanol have been shown to be effective for sanitization using a range of microorganisms [3,11–13].

The question of leachables is a key issue in validation [3] and if leachables derived from the chromatographic medium were to coelute with the product then the consequences could be quite severe. It could be argued that if leachables were generated during column regeneration (CIP) then provided they were washed out prior to product elution they would not pose a problem. While this argument may be justified, the effects on chromatographic performance including capacity and resolution would likely be significant, thereby rendering the process irreproducible. There is little published information on leachables although the subject has received some attention in the field of affinity chromatography where it is referred to a ligand leakage [14–16]. A study was recently reported [17] on leachables arising from the anion-exchange agarose, DEAE-Sepharose Fast Flow, where extended storage in 1 *M* NaOH gave rise to limited hydrolysis of the functional groups from the matrix.

In the present study we examine validation aspects of a CIP procedure used in conjunction with the process-scale chromatography of hen egg-white proteins on two fast flowing anion-exchange celluloses derivatised with either DEAE or QA functional groups. The CIP procedure which is effective in column regeneration has been examined for chromatographic performance, sanitization and also for media stability in terms of leachables.

2. Experimental

2.1. Materials

Cell debris remover (CDR), Express-Ion D (formerly named DEAE-cellulose/D856) and Express-Ion Q (formerly named QA-cellulose/D856) were obtained from Whatman International (Maidstone, UK). A G450 × 500 glass chromatography column fitted with 30-μm polypropylene bed supports was obtained from Amicon (Stonehouse, UK). N,N-Diethylethanolamine was obtained from Aldrich (Gillingham, UK). 2,3-Dihydroxypropyltrimethylammonium chloride was a generous gift from Degussa (Hanau, Germany). Tris(hydroxymethyl)aminomethane (Tris) was obtained from Merck (Poole, UK). All other chemicals were of analytical-reagent grade. Fresh size 2 hen eggs were obtained from Barradale Farms (Headcorn, UK).

2.2. Feedstock preparation

Egg whites were separated from 600 fresh hen eggs and diluted to 14% (v/v) with 0.025 *M* Tris–HCl buffer (pH 7.5). The egg-white suspension was clarified using a total of 22 kg of pre-equilibrated CDR in a batch mode. Spent CDR was removed by centrifugation through a 1.6 × 0.6 mm slotted screen (EHR 500 basket centrifuge; Robatel and Mulatier, Lyons, France) and the sample was clarified through a Grade 541 filter paper (Whatman International). The clear solution (200 l) containing 9.24 mg/ml of total protein was used for chromatography on Express-Ion Q.

2.3. Process-scale chromatography

Express-Ion Q (15.9 kg) was equilibrated with 0.025 *M* Tris–HCl buffer (pH 7.5) to give a final slurry concentration of ca 30% (w/v). The slurry was transferred to the 50 cm × 45 cm I.D.

column barrel section and the bed consolidated at a pressure of ca. 10 p.s.i. (1 p.s.i. = 6894.76 Pa) according to the column manufacturer's guidelines. The packed column (16 cm × 45 cm I.D.) had a volume of ca. 25 l and a packing density of 0.214 kg/l. The ion exchanger was used with the egg-white feedstock accordingly: (i) analytical loading, (ii) preparative loading, (iii) clean-in-place, (iv) analytical loading. A pressure–flow-rate test was carried out after column packing and after the CIP procedure. All procedures were carried out at room temperature (15–20°C).

(i) Analytical loading

Egg-white feedstock (10 l) was loaded on to the column and non-bound material removed by washing with 0.025 *M* Tris–HCl buffer (pH 7.5) (50 l). Bound material was eluted using a linear gradient of 0–0.5 *M* NaCl in 0.025 *M* Tris–HCl buffer (pH 7.5) (200 l). A flow-rate of 4 l/min was maintained throughout.

(ii) Preparative loading

Egg-white feedstock (200 l) was loaded on to the column and non-bound material removed by washing with 0.025 *M* Tris–HCl buffer (pH 7.5) (100 l). Bound material was eluted using a linear gradient of 0–0.5 *M* NaCl in 0.025 *M* Tris–HCl buffer (pH 7.5) (200 l). A flow-rate of 4 l/min was maintained throughout.

(iii) Clean-in-place procedure

The column of Express-Ion Q was washed in 0.5 *M* NaOH (50 l), depressurized and allowed to stand at room temperature for 16 h. The column was repressurized and washed successively with water (50 l), 0.1 *M* Tris–HCl buffer (pH 7.5) (50 l) and 0.025 *M* Tris–HCl buffer (pH 7.5) (200 l). A flow-rate of 4 l/min was maintained throughout.

(iv) Analytical loading

Egg-white feedstock (10 l) was chromatographed on Express-Ion Q as described in (i).

2.4. Assays

Pooled fractions at various stages of chromatography were assayed for protein content by measuring the absorbance at 280 nm against standard solutions of ovalbumin. Throughout the column procedures the effluent was monitored for absorbance at 280 nm and by conductivity.

2.5. Sanitization testing

Studies on sanitization of Express-Ion D and Express-Ion Q were carried out as an external contract with Safepharm Labs., Derby, UK, using their standard operating procedures. For the microbial challenge, cultures of *E. coli* NCIMB 8545, *Staphylococcus aureus* NCIMB 9518, *Pseudomonas aeruginosa* NCIMB 8626, *Aspergillus niger* IMI 149007, *Candida albicans* NCPF 3179 and *Bacillus subtilis* NCIMB 3054 were grown, and mixed to give a suspension of microorganisms containing ca. $1 \cdot 10^7$ colony forming units (cfu)/ml.

(i) Column studies

Express-Ion D and Express-Ion Q were equilibrated with 0.025 *M* sodium phosphate buffer (pH 7.4) and packed into 15-ml columns (19 cm × 1 cm I.D.). The suspension of microorganisms (45 ml) was loaded onto each column and the final 15-ml fractions collected as the pre-CIP samples. The beds were washed with 0.5 *M* NaOH (45 ml) and stood at room temperature for 12–24 h. The columns were washed successively with sterile endotoxin-free water (45 ml) sterile endotoxin-free 0.1 *M* sodium phosphate buffer (pH 7.4) (45 ml) and sterile endotoxin-free 0.025 *M* sodium phosphate buffer (pH 7.4) (90 ml). The final 15-ml fractions were collected under aseptic conditions as the post-CIP samples. Flow-rate was maintained at 1 ml/min throughout.

The pre-CIP samples were tested for total viable counts (TVCs), sterility and endotoxin, using the Limulus Amoebocyte Lysate test (LAL). The post-CIP samples were tested for TVCs, sterility, LAL and pyrogens using the rabbit pyrogen test.

(ii) Batch studies

Express-Ion D and Express-Ion Q were equilibrated with 0.025 *M* sodium phosphate buffer (pH 7.4). Equilibrated Express-Ion D and Express-Ion Q (10 g) were each mixed with the suspension of microorganisms (10 ml) and a solution of NaOH (45 ml) added to give a final concentration of 0.5 *M*. The suspension was incubated at room temperature for 12–24 h. A sample of each suspension (5 ml) was withdrawn, adjusted to pH 7.4 using 1 *M* HCl, and tested for TVCs.

2.6. Leachables testing

Express-Ion D and Express-Ion Q were equilibrated with 0.025 *M* sodium phosphate buffer (pH 7.4) and packed into 15 ml columns (19 cm × 1 cm I.D.). 0.025 *M* sodium phosphate buffer (pH 7.4) (45 ml) was passed through each column and the final 15-ml fractions collected as sample 1. Each bed was washed with 0.5 *M* NaOH (45 ml) and stood in 0.5 *M* NaOH at room temperature for 16 h. Each column was washed with 0.5 *M* NaOH (45 ml) and the first 30-ml fractions collected as sample 2. Each column was washed successively with water (45 ml), 0.1 *M* sodium phosphate buffer (pH 7.4) (45 ml) and 0.025 *M* sodium phosphate buffer (pH 7.4) (90 ml). The final 15-ml fractions were collected as sample 3. Flow-rate was maintained at 1 ml/min throughout.

For Express-Ion D, samples 1, 2 and 3 were analysed for N,N-diethylethanolamine by GC–MS. Samples 1, 2 and 3 (10 ml) were extracted with dichloromethane (2 ml). The dichloromethane samples were analysed using a Hewlett-Packard Model 5890 gas chromatograph coupled to a Model 5972 mass-selective detector. The column used was a Hewlett-Packard HP5-MS capillary 30 m × 0.25 mm I.D. with a 0.25-μm film thickness. Injection volume was 1 μl, via a splitless injector, at a temperature of 180°C, using helium carrier gas at a constant flow-rate of 1 ml/min. The oven temperature programme was 35°C for 2 min, then 10°C/min to 100°C, then 30°C/min to 250°C then 250°C for 0.5 min. The interface temperature to the MS system was 280°C and masses scanned were 86, 58 and 117 with a dwell time of 50 ms/mass. The instrument was calibrated using standard aqueous solutions containing 1, 10 and 50 mg/l N,N-diethylethanolamine and extracted as described above. The abundance of the 86 ion was used for quantification and masses 58 and 117 used as qualifier ions.

For Express-Ion Q, samples 1, 2 and 3 were analysed for 2,3-dihydroxypropyltrimethylammonium chloride by ion chromatography. The samples were analysed using a Dionex Model DX100 ion chromatograph equipped with a Dionex CS12 column. The mobile phase was 20 m*M* methanesulphonic acid at a flow-rate of 0.8 ml/min. Peaks were detected by suppressed conductivity. The system was calibrated using standard solutions of 2,3-dihydroxypropyltrimethylammonium chloride in either 0.025 *M* sodium phosphate buffer, pH 7.4 or 0.5 *M* NaOH.

3. Results and discussion

We have previously reported that Express-Ion D exhibits rapid binding kinetics facilitating its operation at high flow-rates for process-scale chromatography [8]. In our earlier work, we reported that Express-Ion D had a dynamic binding capacity of 84 mg protein/ml column volume following a saturation loading of 9.26 mg/ml hen egg-white proteins at a flow-rate of 140 cm/h [8]. Under similar conditions the capacity of Express-Ion Q was found to be 80 mg protein/ml column volume [18]. For the preparative loading of hen egg-white proteins on Express-Ion Q a total of 1.848 kg of protein was loaded onto the column which represents a submaximum loading of ca. 73 mg protein/ml packed column volume. The absorbance profile of the column eluate during the process run is represented in Fig. 1. The protein mass balance data for this study are summarised in Table 1. In order to assess the capture efficiency of the adsorptive process during a single pass through the column a binding efficiency is calculated according to:

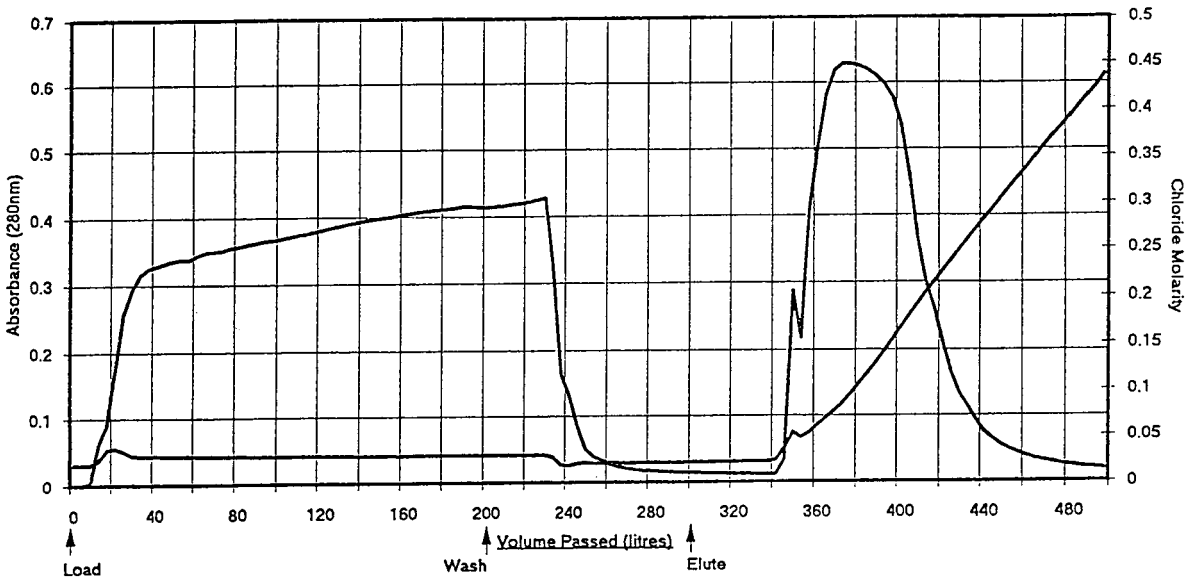

Fig. 1. Absorbance profile of column eluate during preparative chromatography of 9.24 mg/ml hen egg-white proteins on Express-Ion Q on a process scale (16 cm × 45 cm I.D.) using 0.025 *M* Tris–HCl buffer (pH 7.5), at a flow-rate of 150 cm/h at 15–20°C.

$$\text{binding efficiency (\%)} = \frac{\text{mass of protein adsorbed}}{\text{mass of protein loaded}} \cdot 100 \quad (1)$$

The data in Table 1 demonstrate that 1.593 kg of protein bound to Express-Ion Q during the loading stage which is equivalent a protein capacity of 62.7 mg protein/ml column volume. This reflects utilisation of ca. 86% of the maximum theoretical capacity of the Express-Ion Q and compares well with the data reported for Express-Ion D [8]. In this study we appeared to recover 100% of the adsorbed protein (Table 1) whereas for Express-Ion D recovery was ca 93% [8]. We have previously reported that a CIP using 0.5 *M* NaOH for 12–16 h (overnight) is effective at restoring column performance for DE52 [5], QA52 [6], DE92 [7] and Express-Ion D [8] in each case following preparative loadings. The analytical loading of egg-white on the Express-Ion Q after CIP is represented by the chromatogram in Fig. 2b. The elution profile is similar, if not slightly improved, over that seen after column packing (Fig. 2a), indicating that the NaOH treatment has no detrimental effect on the chromatographic performance of the medium. This is in keeping with our previous studies on Express-Ion D [8]. The pressure–flow-

Table 1
Protein mass balance during preparative chromatography of hen egg-white proteins on Express-Ion Q

Stage of chromatography	Feedstock total protein (g)	Total protein (g)		Binding efficiency (%)
		In mobile phase	Adsorbed on Express-Ion Q	
Loading	1848	236	1612	
Wash		19	1593	86.2
Elution		1640	0	

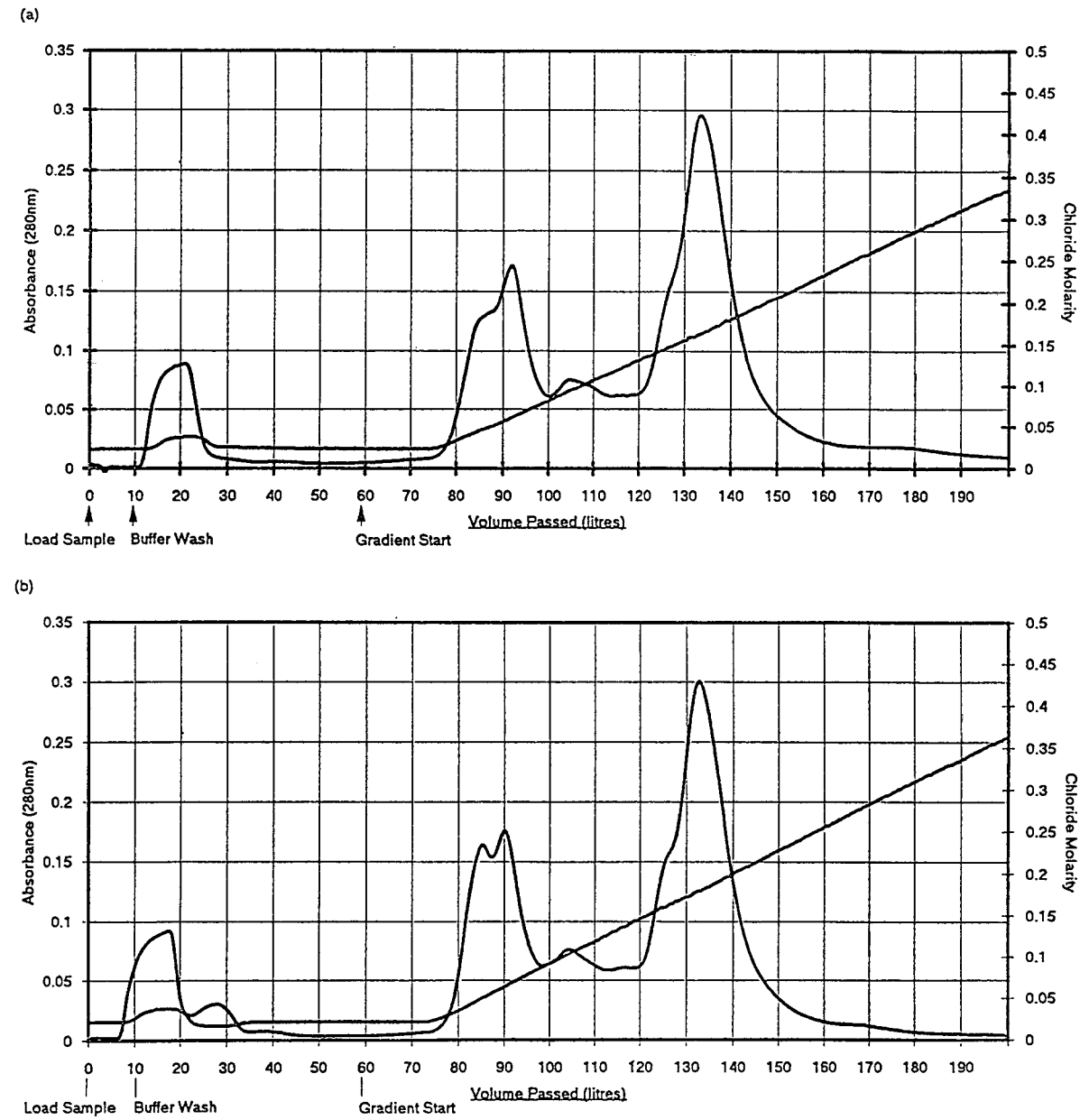

Fig. 2. Column chromatography of hen egg-white proteins on Express-Ion Q on a process scale (16 cm × 45 cm I.D.) using 0.025 *M* Tris–HCl buffer (pH 7.5). (a) Analytical loading (100 g) before preparative run, (b) analytical loading (100 g) after CIP; flow-rate 150 cm/h at 15–20°C.

rate data obtained before and after the CIP procedure are summarised in Table 2 and there was no significant effect on flow performance of the Express-Ion Q following overnight storage in 0.5 *M* NaOH.

Having demonstrated that storage of columns

Table 2
Pressure–flow-rate relationship during process-scale chromatography of hen egg-white proteins on Express-Ion Q

Pressure (p.s.i.)	Flow-rate (cm/h)	
	After column packing	Post-CIP
5.0	134.7	131.7
7.5	173.6	173.6
10.0	212.4	217.0

of Express-Ion D and Express-Ion Q in 0.5 *M* NaOH for 12–16 h is an effective bed regeneration following preparative chromatography of hen egg-white proteins, the effectiveness of such a treatment for bed sanitization was investigated. In this study a similar CIP was carried out using sodium phosphate buffer as the mobile phase as this was considered to be more suitable for sustaining the viability of microorganisms than a Tris buffer. Following a challenge with a mixed suspension of *E. coli*, *S. aureus*, *P. aeruginosa*, *A. niger*, *C. albicans* and *B. subtilis* the column effluents had a high bioburden with a significant endotoxin content (Table 3). Following the CIP and subsequent bed re-equilibration using sterile endotoxin-free buffers, the column effluents gave negative responses in the total viable count test, were sterile and contained very low levels of endotoxin giving a negative response in the rabbit pyrogen test (Table 3). The data presented in this study demonstrate that overnight treatment with 0.5 *M* NaOH is an effective regime for sanitization of packed columns of Express-Ion D and Express-Ion Q following a very heavy microbial challenge using a mixed suspension of microorganisms which are recommended for use in validation studies [3]. In this study a total of 15 bed volumes of various mobile phases were passed through the columns following the microbial challenge. It is therefore possible that sanitization has been effected purely by displacement of the microorganisms rather than as a result of their physiological incompatibility with 0.5 *M* NaOH. Consequently the mixed suspension of microorganisms was incubated with 0.5 *M* NaOH, in the presence of Express-Ion D and Express-Ion Q. The results of these batch studies are summarised in Table 4. The data show that following storage in 0.5 *M* NaOH no total viable counts were recorded. These data reinforce the effectiveness of our CIP protocol for simultaneous sanitization of a packed column of Express-Ion D and Express-Ion Q.

The final validation aspect of this study concerns leachables, and specifically hydrolysis of the functional group from the ion exchangers during the CIP procedure. Whatman Internation-

Table 3
Sanitization testing of columns of Express-Ion D and Express-Ion Q

Stage of investigation	TVC (cfu/ml)	Sterility test	Endotoxin (EU/ml)	Rabbit pyrogen test
Express-Ion D				
Challenge	$5.5 \cdot 10^6$	nd[a]	nd	nd
Pre-CIP	$7.7 \cdot 10^4$	Fail	>60	nd
Post-CIP	<1	Pass	<0.06	Pass
Express-Ion Q				
Challenge	$4.6 \cdot 10^6$	nd	nd	nd
Pre-CIP	$7.6 \cdot 10^3$	Fail	>60	nd
Post-CIP	<1	Pass	<0.06	Pass

[a] nd = Not determined.

Table 4
Influence of 0.5 *M* NaOH on viability of microorganisms during batch storage with Express-Ion D and Express-Ion Q

Stage of investigation	TVC (cfu/ml)	
	Express-Ion D	Express-Ion Q
Pre-CIP	$1.1 \cdot 10^7$	$4.2 \cdot 10^6$
Post-CIP	<1	<1

Table 5
Leachables testing during CIP of Express-Ion D

Sample	[N,N-Diethylethanolamine] (mg/l)
1, Pre-CIP	<1[a]
2, Post-CIP	<1[a]
3, Re-equilibration	<1[a]

[a] Limits of detection.

al derivatises the microgranular cellulose matrix with the diethylamineothyl (DEAE) group:

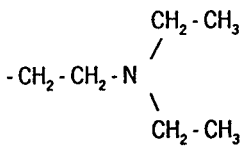

and the 2-hydroxypropyltrimethylammonium (QA) group:

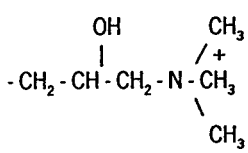

In each case the functional group is covalently attached to the cellulose via ether linkages to the distal carbon atoms [19]. If hydrolysis of the functional groups were to take place then it is reasonable to expect that the groups would be liberated as the alcohols N,N-diethylethanolamine and a 2,3-dihydroxypropyltrimethylammonium salt from Express-Ion D and Express-Ion Q, respectively. If hydrolysis of the functional group were to occur as a result of exposure to NaOH then the liberated amines would be present in the displaced NaOH fraction following the CIP procedure. The first two displaced column volumes of effluent during the post-CIP wash from the Express-Ion D column (sample 2) were collected and analysed for N,N-diethylethanolamine by GC–MS. These data are summarised in Table 5 and the chromatograms represented in Fig. 3. The data demonstrate that no detectable hydrolysis of the functional group had occurred during the CIP and the NaOH fraction (sample 2) and the re-equilibrated media (sample 3) contained no detectable volatile organics under conditions where the alcohol derivative of the functional group can be identified by GC–MS (Fig. 3b). In this investigation the column of Express-Ion D contained 3.05 dry g of media. This is equivalent to 3.0 mmol of DEAE groups. The detection limits for GC–MS were determined to be 1 mg/l for N,N-diethylethanolamine. On the basis of a 30-ml volume of displaced NaOH this corresponds to detection limits of 0.256 μmol of DEAE groups and it may therefore be deduced that hydrolysis of the functional groups represents $<0.01\%$ of those present within the packed column of Express-Ion D under the CIP conditions used in this study.

While we obtained a sample of the anticipated hydrolysis product of Express-Ion Q, namely, 2,3-dihydroxypropyltrimethylammonium chloride we were unable to separate or identify the material by GC–MS under similar conditions to those used for N,N-diethylethanolamine. Attempts to derivatise the material by either methylation or benzoylation were unsuccessful.

We were able to detect 2,3-dihydroxypropyltrimethylammonium chloride by ion chromatography and the analysis of samples 1, 2 and 3 obtained from the Express-Ion Q study are reported in Table 6. The limits of detection of 2,3-dihydroxypropyltrimethylammonium chloride were 5 mg/l for 0.025 *M* sodium phosphate buffer, pH 7.4 and 25 mg/l for 0.5 *M* NaOH. The data demonstrate that no detectable hydrolysis of the QA groups had occurred during the CIP and both the NaOH fraction (sample 2)

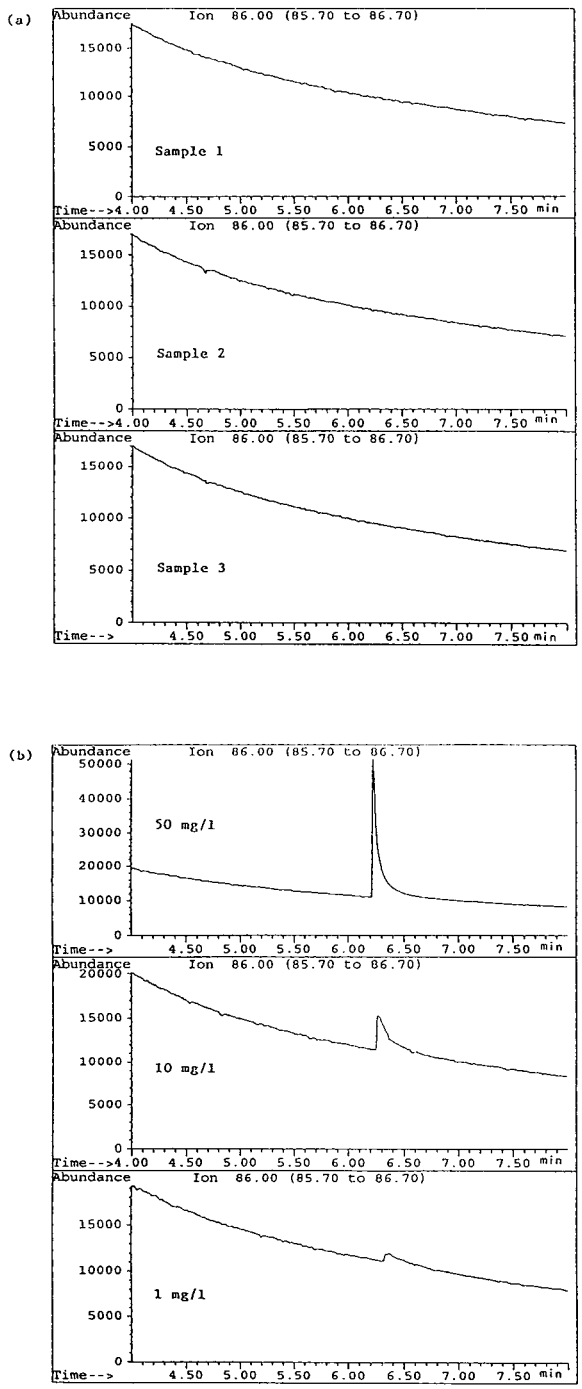

Fig. 3. Analysis of (a) sample 1, sample 2 and sample 3 obtained from the leachables study and (b) standards containing 50, 10 and 1 mg/l N,N-diethylethanolamine. Full analytical details are described in the text.

Table 6
Leachables testing during CIP of Express-Ion Q

Sample	[2,3-Dihydroxypropyltrimenthylamine] (mg/l)
1, Pre-CIP	$<5^a$
2, Post-CIP	$<25^a$
3, Re-equilibration	$<5^a$

[a] Limits of detection.

and the re-equilibrated media (sample 3) contained no ionic species under conditions where the alcohol derivative of the functional group is identifiable by ion chromatography. For the post-CIP sample (30 ml) a detection limit of 25 mg/l corresponds to 4.44 μmol of QA groups (as a chloride salt) within this volume. The 15-ml column of Express-Ion Q contained 3.07 μmol QA groups (3.3 dry g media) and it may therefore be deduced that hydrolysis of the functional groups represents $<0.15\%$ of those present within the packed column of Express-Ion Q under the CIP conditions used in this study.

In this study we have demonstrated that following process-scale column chromatography of hen egg-white proteins on Express-Ion Q a CIP treatment involving storage in 0.5 *M* NaOH for 16 h, had no significant detrimental effect on the chromatographic performance of the bed. This data supports our previous findings for Express-Ion D [8]. The CIP procedure was found to be an effective sanitization protocol for both media following a gross microbial contamination with a mixed culture of six microorganisms. During the CIP, hydrolysis of the functional groups from Express-Ion D and Express-Ion Q was found to be insignificant. Studies of this type are guidelines towards validation of these media in regulated processes and form the basis for extended, process-specific validation studies.

Acknowledgements

We wish to thank Dr. B. Ghandi of Degussa Ltd., Wilmslow, UK and his colleagues in Degussa AG, Hanau, Germany for the preparation

and gift of a research material 2,3-dihydroxypropyltrimethylammonium chloride.

References

[1] D. Friefelder, *Physical Biochemistry*, Freeman, San Francisco, CA, 2nd ed., 1982, p. 249.
[2] E.F. Rossomando, *Methods Enzymol.*, 182 (1990) 309.
[3] G.K. Sofer and L.-E. Nyström, *Process Chromatography: A Guide to Validation*, Academic Press, London, 1991, Ch. 2, p. 5.
[4] P.R. Levison, in G. Ganetsos and P.E. Barker (Editors), *Preparative and Production Scale Chromatography*, Marcel Dekker, New York, 1993, p. 617.
[5] P.R. Levison, S.E. Badger, D.W. Toome, D. Carcary and E.T. Butts, in R. de Bruyne and A. Huyghebaert (Editors), *Downstream Processing in Biotechnology II*, Royal Flemish Society of Engineers, Antwerp, 1989, p. 2.11.
[6] P.R. Levison, M.L. Koscielny and E.T. Butts, *Bioseparation*, 1 (1990) 59.
[7] P.R. Levison, S.E. Badger, D.W. Toome, M.L. Koscielny, L. Lane and E.T. Butts, *J. Chromatogr.*, 590 (1992) 49.
[8] P.R. Levison, S.E. Badger, D.W. Toome, M. Streater and J.A. Cox, *J. Chromatogr. A*, 658 (1994) 419.
[9] P.R. Levison and F.M. Clark, presented at the *Pittsburgh Conference, Atlanta, 1989*, abstracts, p. 754.
[10] P.R. Levison, in G. Subramanian (Editor), *Preparative and Process-Scale Liquid Chromatography*, Ellis Horwood, Chichester, 1991, p. 146.
[11] G.K. Sofer and L.-E. Nyström, *Process Chromatography: A Practical Guide*, Academic Press, London, 1989, Ch. 9, p. 93.
[12] C. Nguyen, X. Pouradier Duteil, Y. Moroux and E. Boschetti, in Y. Briand, C. Doienel and A. Faure (Editors), *Proteins Purification Technologies*, Vol. 4, GRBP, Clermont-Ferrand, 1990, p. 233.
[13] R.F. Burgoyne, M.C. Priest, K.L. Roche and G. Vella, *J. Pharm. Biomed. Anal.*, 11 (1993) 1317.
[14] M. Goldberg, K.L. Knudsen, D. Platt, F. Kohen, E.A. Bayer and M. Wilchek, *Bioconjugate Chem.*, 2 (1991) 275.
[15] P. Füglistaller, *J. Immunol. Methods*, 124 (1989) 171.
[16] M. Baeseler, H.-F. Boeden, R. Koelsch and J. Lasch, *J. Chromatogr.*, 589 (1992) 93.
[17] M. Andersson, I. Drevin and B.-L. Johansson, *Process Biochem.*, 28 (1993) 223.
[18] R.M.H. Jones and D.W. Toome, personal communication.
[19] P.R. Levison in J.F. Kennedy, G.O. Phillips and P.A. Williams (Editors), *Cellulosics: Materials for Selective Separations and Other Technologies*, Ellis Horwood, Chichester, 1993, p. 25.

ELSEVIER

Journal of Chromatography A, 702 (1995) 69–80

JOURNAL OF CHROMATOGRAPHY A

Estimating plate heights in stacked-membrane chromatography by flow reversal

D. Keith Roper[a,*], Edwin N. Lightfoot[b]

[a]*Merck Research Laboratories, P.O. Box 4 WP16-121P, Sumneytown Pike, West Point, PA 19486, USA*
[b]*Chemical Engineering Department, University of Wisconsin, 1415 Johnson Drive, Madison, WI 53706, USA*

Abstract

A novel method to quantitatively evaluate chromatographic separation performance is presented. Distortion of effluent profiles by non-uniform flow is eliminated by reversing flow direction during the experiment. A semiempirical approach accounts for extracolumn effects on peak shape. Effluent profiles are fitted to a closed-form mathematical description of the experiment to estimate plate height values. Plate heights obtained from two stacked-membrane columns decrease from 3.3 μm at 0.52 cm/min to 0.59 μm at 3.8 cm/min, in agreement with dispersive theory. Performance estimates based on moments or bandwidth measurement are less reliable than this method when non-uniform flow or extracolumn effects are significant.

1. Introduction

The purpose of this work has been to measure the separation capability of stacked-membrane chromatography. Reliance upon chromatography as a preparative tool is growing rapidly, particularly in biotechnology [1,2] and in the pharmaceutical [3,4] industry. This has motivated several recent chromatographic developments: efficient perfusive [5,6] and hyperdiffusive [7] column packings, novel polymeric stacked-membrane [8] and chromarod [9] adsorptive geometries, and improved counterflow [10,11] and recycle [12] operating modes.

Stacked-membrane chromatography seems well suited to the demands of preparative biochromatography. Stacked-membrane column residence times are short and bed volumes are small [13]. This counteracts protein degradation by proteolysis and denaturation which increases with processing time [14]. It also increases throughput, reducing the requirement for expensive solvents and tankage common to large-scale chromatography [15].

Stacking multiple membranes in series averages variations in porosity and membrane thickness which may compromise separation performance of single sheets [16]. Stacking also increases bed capacity. Consequently, the performance of existing devices is sufficient to resolve many proteins by informed selection of differential migration and differential elution or "on–off" strategies [17]. Stacked membrane separations of model protein systems are comparable to similar high-pressure liquid chromatographs [18] without requiring high-pressure columns, peripherals or pumps. Preparative stacked-membrane separations maintain laboratory-scale protein purity at high throughput when scaled up with respect to flow-rate and mass loading [19].

* Corresponding author.

0021-9673/95/$09.50 © 1995 Elsevier Science B.V. All rights reserved
SSDI 0021-9673(94)01068-4

On the other hand, reported measurements of stacked-membrane efficiency vary over nearly two orders of magnitude. Plate height values are compared in the Van Deemter plot [20] in Fig. 1. Plate height [21], which measures effluent bandwidth, increases as resistances to mass transfer from convective dispersion, intraparticle diffusion, boundary layer phenomena, and adsorption in conventional columns become large.

One possible explanation for the variation in Fig. 1. is that plate height completely characterizes band broadening of *symmetric* Gaussian line shapes [22]. Chromatographic systems with a linear adsorption isotherm, constant equilibrium distribution coefficient and concentration-independent transport properties exhibit Gaussian effluent curves whose plate heights equal the ratio of effluent-peak variance to the column length [23,24]. In contrast, stacked-membrane effluent profiles obtained by Raths and by Gerstner were visibly skewed.

It is also likely that different estimation methods contributed to the range of estimated plate heights. Accurate plate height estimates are obtained by fitting time-domain effluent profiles to an appropriate description [25]. This avoids errors from extracolumn effects, noise, baseline drift, tail truncation and peak skewness which undermine methods relying on tangents, moments, or isolated points on a curve.

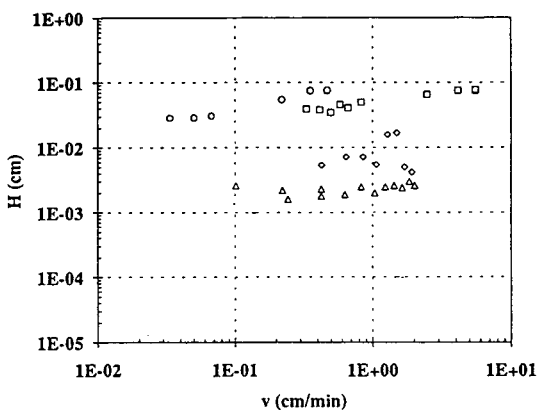

Fig. 1. Plate heights estimated from stacked-membrane effluents. Frey et al. [27] used the experimental method of moments to analyze two stacks of 600 μm poly(vinyl chloride) membranes: 10 mm $L \times 25$ mm I.D. (○) and 50 mm $L \times 25$ mm I.D. (□). Raths [42] fitted effluent profiles from 120-μm regenerated cellulose membranes to an exponentially modified Gaussian: 5 mm $L \times 17$ mm I.D. (◇). Gerstner [19] used an unreported method to analyze stacks of 120-μm regenerated cellulose membranes: 10 mm $L \times 28$ mm I.D. (△).

Finally, reported plate heights, H, are at least ten times greater than values anticipated by an order-of-magnitude analysis of microscopic transport rate processes: intraparticle diffusion is eliminated in ideal stacked membranes by derivatizing adsorptive sites on surfaces of membranes permeated by interconnecting flow-through pores. Boundary-layer fluid-phase mass transfer is negligible as Nusselt numbers in these systems are well above the lower limiting value of 4 [26]. These approximations suggest H in linear, non-adsorbing systems reduces to $H = 2\epsilon/v$ where ϵ represents Fickian convective dispersion. Stacked-membrane chromatography is typically operated such that $H \approx 2D_f/v$ (see Section 2) where D_f is the effective solute diffusivity in unbounded solution. For proteins in stacked membranes, $D_f \approx 5 \cdot 10^{-7}$ cm^2/s and $v \approx 1$ cm/min so that $H \approx 1$ μm.

Three practical questions arise from our observations: (1) How is stacked-membrane plate height accurately measured? (2) What are plate heights of existing stacked-membrane devices? (3) Can commercially available stacked membranes achieve theoretically anticipated efficiencies? We address these issues, beginning with a conceptual description of fundamental mass transport in stacked membranes. Using this description we propose a novel, unambiguous method for determining stacked-membrane efficiencies. We derive analytic expressions, apparently new, which describe the proposed experiment. These expressions allow prediction of separation performance in the presence of significant extracolumn broadening and non-uniform flow.

2. Theory

Two principal, contrasting hypotheses of chromatographic transport in stacked-membrane beds have been examined by previous inves-

tigators: one-dimensional plug flow on the one hand, and two-dimensional unit-cell potential flow on the other. Each proposes a fundamentally different velocity distribution in the porous bed. As a result, broadening in stacked-membrane effluent curves has been attributed to substantially different sources.

After comparing the attributes of these descriptions, we originate a straightforward experimental approach to distinguish between them. Description of this experiment in simple, analytical terms allows separation efficiency in stacked membranes to be characterized.

2.1. Dispersed plug flow in stacked membranes

Consider first a constant, uniform velocity distribution, v, which results from one-dimensional, plug flow parallel to the stacked-membrane axis [13,16,27–29]. A mean particle diameter, $D_p = 3/2d_p(1-\epsilon_b)/\epsilon_b$ in the membrane bed is estimated from its average pore size, d_p, and bulk porosity, ϵ_b [30]. Consequently, a stacked-membrane analogue of the familiar one-dimensional equations of chromatography [31,32] may be derived. Analytic solutions to this equation set are available for numerous special cases [33] including non-linear adsorption [34] and gradient elution [35]; computational solutions are required for more general evaluation of non-linear effects [36] including sample overloading [37].

To determine whether assuming uniform velocity adequately characterizes stacked membranes, a lumped-parameter, asymptotic solution to pseudocontinuum chromatographic equations [38] simplified for non-adsorbing conditions is sufficient. This dispersed plug flow solution anticipates fluid-phase solute concentration distribution c_f from a sharp-pulse input of solute mass m_0 will be a Gaussian function of axial coordinate z when time t is treated as a parameter:

$$c_f(z,t) = \frac{m_0 u}{A\epsilon_b\sqrt{2\pi H z_0}} \cdot \exp\left[\frac{-(z-z_0)^2}{2Hz_0}\right] \qquad (1)$$

The mean solute position, $z_0 \equiv uvt$, is proportional to both the interstitial fluid velocity, v, and the fraction of solute in the moving fluid phase at long times, $u \equiv \alpha\epsilon_b/[\alpha\epsilon_b + (1-\epsilon_b)]$. The column cross-sectional area is A. Subscripts f and b refer to the moving fluid and stationary bulk phases, respectively. The bulk phase consists of derivatized membrane of ideally zero porosity.

The plate height relation for one-dimensional dispersed plug flow in stacked membranes reduces to $H = 2\epsilon/v$, neglecting intraparticle diffusion and fluid-phase mass transfer (see Section 1). This indicates band broadening is due solely to micro-scale fluid-phase mixing phenomena which constitute convective dispersion. These include mixing by solid obstructions to flow, incomplete connectivity, eddies, recirculation from regional pressure gradients, and diffusion [39]. Broadening which results from micro-scale mixing processes is entirely *irreversible*.

The Fickian convective dispersion coefficient is available from Koch and Brady's [40] analysis of ambient, creeping flow in random configurations of fixed spheres which constitute a low fraction of total volume. For a diffusion Peclet number, $Re \cdot Sc \equiv D_p v\epsilon_b/D_f$, greater than unity, they proposed

$$Pe_\epsilon^{-1} = \frac{3}{8}\cdot\epsilon_b + \frac{\pi^2}{12}\cdot\epsilon_b(1-\epsilon_b)\ln\left(\frac{Re\cdot Sc}{2}\right) + \frac{\epsilon_b}{Re\cdot Sc} \qquad (2)$$

$$Pe_\epsilon \equiv \frac{vD_p}{\epsilon}$$

It is evident that broadening in dispersed plug flow *changes with velocity*.

The effluent profile indicated by Eq. 1 approaches Gaussian form in time when evaluated at the column exit as the number of column plates, N, becomes large. This distribution is characterized entirely by its first two temporal moments. Consequently, broadening attributed to dispersed plug flow is *distributed symmetrically* around a mean residence time, $\bar{t} = NH/uv$ with a variance of $s^2 \equiv \bar{t}H/uv$. Scaling the variance by the residence time gives the plate number, $N = \bar{t}^2/s^2$.

These natural outcomes from a constant uniform velocity distribution in stacked-membrane chromatography are summarized in Table 1.

Table 1
Dispersed plug flow vs. non-uniform potential flow in stacked membranes

	One-dimensional plug flow	Two-dimensional potential flow
Plate height	$2\epsilon/v$	$c^2/3b$[a]
Plate height value	ca. 1 μm	ca. 1 mm
Broadening	Dispersive	Mechanical
Broadening reversible	No	Yes
Flowrate-independent plate height	No	Yes
Peak shape	Symmetric about $\bar{t}$	Asymmetric

[a] Plate height for single unit cell.

2.2. Planar potential flow in stacked membranes

Now consider a non-uniform, velocity, $v(\Phi,\Psi)$ distributed along potential function, Φ, and stream function, Ψ, coordinates corresponding to two-dimensional potential flow [30] in *unit cells* of a stacked membrane, as sketched in Fig. 2. Balzereit [41] and Raths [42] postulated that distributor channels introduce fluid into such planar flow cells which parallel the column axis. Two ratios of characteristic lengths describe the unit-cell geometry: b/c, where b is the bed height and c is the distance between adjacent distribution channels; and d/c, where d is the channel width.

Numerical solution by discretization along a scaled Φ coordinate and quadrature in a scaled Ψ coordinate yielded unit-cell effluent profiles which were skewed at low flow-rates. Effects of convection as well as radial and axial diffusion were assessed in these computation. Numerical instability precluded calculation of effluent profiles at flow-rates typical of stacked-membrane operation. But numerical estimates of the effective number of theoretical plates in a unit cell $N_{\text{eff}} = \bar{t}^2/s^2$ (the ratio of first to second central temporal moment) reached an asymptotic value at operational flow-rates for each unit cell geometry. Broadening in effluent from non-uniform, planar unit-cell flow in stacked membranes is *independent of flow-rate*.

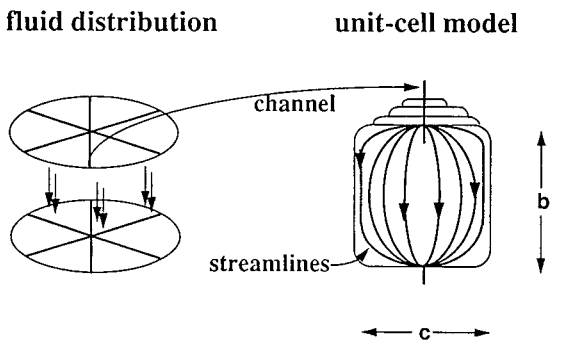

Fig. 2. Two-dimensional potential flow in unit cells of a stacked membrane. Distributor channels etched into distributor endcaps of a stacked-membrane column may introduce fluid into planar flow cells of width c and height b which lie parallel to the axis of the bed [41]. Streamlines are lines of constant velocity.

Flow-rate-independent broadening implies diffusive effects are small relative to convection in non-uniform, unit-cell flow. In other words, band broadening arises entirely from the distribution of residence times corresponding to flow at differing rates along different streamlines, which are lines of constant velocity (see Fig. 2). The geometry of each unit cell —determined by the mechanical structure of the distributors and membrane cross-section— governs its distribution of streamlines. Hence, a potential-flow description of stacked membranes suggests bandwidths have a purely *mechanical* origin.

Broadening dominated by convective residence time differences in stacked membranes is *reversible*, in the sense that a narrow band of tracer particles initially perpendicular to the flow direction will reconverge if the direction of flow is suddenly reversed a short time later.

Negligible diffusion also justifies approximating potential flow in each unit cell by an analytic complex potential [43]. This provides a continuous analytical function for velocity, $v(\Phi,\Psi)$ from which estimates of the first, $\langle t\rangle Q/c^2 \approx b/2c$, and second, $\langle t\rangle^2 Q^2/c^4 \approx (b/2c)^2$, scaled temporal moments can be made [44]. The unit-cell scaled efficiency, $N_{\text{eff}} \approx 3(b/c)^2$ is determined by its geometry.

Stacked-membrane effluent profiles have been calculated by superposing residence time densities of successive unit cells of different geometry, each weighted by the volume fraction of total flow which travels through it [45]. In the MemSep 1000, for example, radial channels distribute flow into successive unit cells whose d/c and b/c decrease to about 0.02 and 0.50 at the periphery of the membrane stack, respectively. Such profiles are *skewed*: tailing in the line shape is similar to measured effluent profiles although the peak is relatively sharp. Plate heights from these profiles by moments analysis are on the order of a millimeter.

Outcomes from non-uniform, two-dimensional potential flow in stacked-membrane chromatography are listed for comparison with dispersed plug flow in Table 1.

2.3. Extracolumn dispersion

Extracolumn contributions to broadening in stacked-membrane effluent profiles are also significant. As stacked-membrane column volume decreases to the same order of magnitude as the volume of injection valves, tubing, adaptors and other peripheral plumbing, it confounds discrimination between dispersed plug flow and planar potential flow by effluent analysis more severely.

Numerical analysis is necessary to rigorously determine extracolumn dispersion at Peclet numbers (ca. 10^6) and times (ca. 0.01 s) typical of stacked-membrane operation, even in short straight [46] or curved [47] cylindrical tubes. And the apparent complexity of peripheral plumbing produces effluent profiles unlike those from simple tubes [48,49].

We adopt, instead, a semiempirical approach to estimate extracolumn effects in stacked-membrane systems. Effluent profiles from peripherals at each experimental condition are fit to an exponentially modified Gaussian (EMG) form [50] which represents the convolution of plug flow and continuous stirred-tank reactors. Results are illustrated in Fig. 3 for precolumn peripherals. Fitted parameters are the mean residence time, $\bar{t}$ and variance σ^2 of the underlying Gaussian and the stirred-tank time constants, τ.

2.4. Reversed-flow analysis of stacked membranes

Fundamental distinctions between dispersion in plug flow and residence-time distribution in planar potential flow preclude attributing broadening caused by either source to the other. In order to distinguish their relative contributions, consider reversing the flow direction at half the mean residence time after a injecting a sharp pulse of tracer at the column inlet. Detect

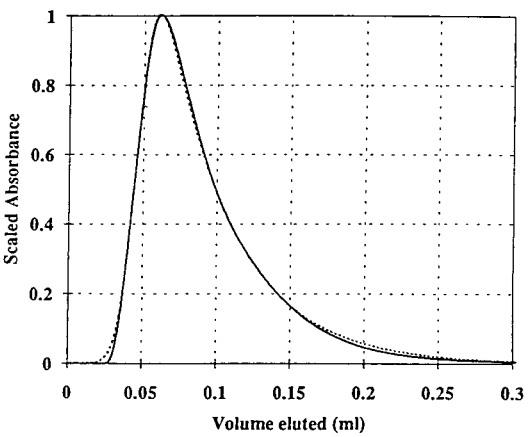

Fig. 3. Effluent from precolumn tubing, fittings and injection valves (solid line) for a MemSep 1000 compared with an exponentially modified Gaussian fit (dashed line). A 20-μl sample of 2.5 mg/ml cytochrome c was eluted at 2 ml/min; absorbance was measured at 280 nm in a 10-mm flow cell. Fitted parameters are the mean residence time, $\bar{t}_r = 0.047$ min and standard deviation $\sigma_r = 0.0097$ min of the underlying Gaussian and the stirred-tank space time, $\tau_r = 0.047$ min.

the cup-mixed effluent profile at the column inlet as it emerges.

Particles convected by different velocities along different streamlines will reconverge following flow reversal. At the detection point, broadening produced by all macroscopically non-uniform flow, including planar potential flow, will disappear. Meanwhile, particles dispersed axially along a streamline by irreversible mixing processes will continue dispersing after flow reversal. The net dispersion of particles traveling at the mean velocity is identical, whether detected at the inlet after flow reversal or detected at the outlet after traversing the entire length of a column symmetric about its midplane.

Aside from large flow non-uniformities, a ratio of operational membrane velocity to macromolecular diffusion coefficient, $(1\ \mathrm{cm/min})/(5\cdot 10^{-7}\ \mathrm{cm^2/s}) \approx 0.3\ \mu\mathrm{m}$, suggests broadening arising from dispersion across streamlines will generally be small. Dispersion coefficients of streamlines with velocities above about 1 cm/min will be comparable, as Eq. 2 suggests (see also Fig. 8).

Qualitative evidence of non-uniform flow is indicated by broadening in forward effluent bands which is more severe than comparable reversed-flow results, provided upstream and downstream peripherals in each experiment are identical. Estimating the variance of a reversed-flow effluent profile promises an unambiguous, quantitative measure of stacked-membrane separation potential after accounting for extracolumn effects.

A symbolic representation of the components which describe a general stacked-membrane system in the absence of non-uniform flow is given in Fig. 4. Since the response of each component to a unit impulse is well known, convolution of successive linear elements using a Green's function approach [51] is an appropriate method to obtain scaled analytical expressions h_F and h_R which describe forward and reverse-flow experiments, respectively.

In forward flow, convolution of the two extracolumn CSTRs yields $c(t) = [\exp(-t/\tau_r) - \exp(-t/\tau_f)]/(\tau_r - \tau_f)$. The response of the complete system is independent of the order in which its elements are analyzed. It is:

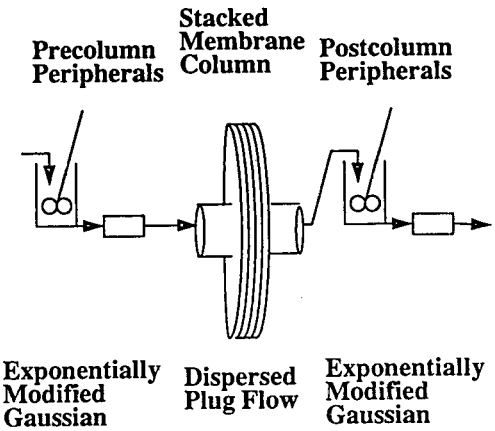

Fig. 4. Conceptual representation of a stacked-membrane column system. Exponentially modified Gaussians (EMGs) account for extracolumn contributions to effluent broadening. EMGs consist of a continuously stirred tank reactor in series with a dispersed plug flow column. The stacked membrane is described by dispersed plug flow in the absence of non-uniform flow.

$$h_F(t) = \frac{1}{2(\tau_r - \tau_f)} \cdot \left\{ \exp\left[\frac{-\sigma_c}{\tau_r} \cdot \left(z_r + \frac{\sigma_c}{2\tau_r} \right) \right] \cdot \left[1 + \mathrm{erf}\left(\frac{z_r}{\sqrt{2}} \right) \right] \right\} - \frac{1}{2(\tau_r - \tau_f)} \cdot \left\{ \exp\left[\frac{-\sigma_c}{\tau_f} \cdot \left(z_f + \frac{\sigma_c}{2\tau_f} \right) \right] \cdot \left[1 + \mathrm{erf}\left(\frac{z_f}{\sqrt{2}} \right) \right] \right\} \quad (3)$$

where subscripts r and f denote the precolumn and postcolumn peripherals. Dimensionless times z_r and z_f are analogues: $z_r \equiv (t - \bar{t}_c)/\sigma_c - \sigma_c/\tau_f$. The composite residence time $\bar{t}_c$ and variance σ_c are sums of the respective moments of the three plug flow reactors: $\bar{t}_c \equiv \bar{t} + \bar{t}_r + \bar{t}_f$ and $\sigma_c^2 = \sigma^2 + \sigma_r^2 + \sigma_f^2$.

The reversed-flow result is obtained in an analogous fashion after reversing the precolumn

peripherals [45]. It is:

$$h_R(t) = \frac{1}{2(\tau_r + \tau_f)} \cdot \left\{ \exp\left[\frac{\sigma_c}{\tau_r} \cdot \left(T + \frac{\sigma_c}{2\tau_r} \right) \right] \cdot \left[\operatorname{erf}\left(\frac{T + \frac{\sigma_c}{\tau_r} + \frac{5\tau_r}{\sigma_c}}{\sqrt{2}} \right) - \operatorname{erf}\left(\frac{T + \frac{\sigma_c}{\tau_r}}{\sqrt{2}} \right) \right] \right\} + \frac{1}{2(\tau_r + \tau_f)} \cdot \left\{ \exp\left[\frac{-\sigma_c}{\tau_f} \cdot \left(T - \frac{\sigma_c}{2\tau_f} \right) \right] \cdot \left[1 + \operatorname{erf}\left(\frac{T - \frac{\sigma_c}{\tau_f}}{\sqrt{2}} \right) \right] \right\} \quad (4)$$

where scaled time $T \equiv (t - \bar{t}_c)/\sigma_c$ and composite residence time and variance are defined as before.

We now summarize our characterization of stacked-membrane performance using the reversed-flow experiment and its analytical description.

3. Experimental

3.1. Materials

All chemicals used were reagent grade except as noted. Two proteins, beef heart cytochrome *c* (Sigma, Type V-A, No. C-2037) and horse heart cytochrome *c* (Sigma, Type II-S, No. C-8266, practical grade) were dissolved at 2.5 mg/ml in 0.02 *M* sodium citrate (Sigma) and 0.5 *M* sodium chloride (Johnson Matthey) at pH 8.0 or buffered to pH 6.0 with hydrochloric acid (Fisher). Solutions were prepared with 18 MΩ distilled, deionized water. Buffers were filtered (0.2 μm) and degassed by vacuum prior to each experimental period.

3.2. Apparatus

Two stacked-membrane columns were analyzed: a 5 mm $L \times 17.17$ mm I.D. Millipore MemSep 1000 DEAE (Bedford, MA, USA) with 1.4 ml nominal bed volume and a 5 mm $L \times 12.7$ mm I.D. Millipore MemSep HP500 DEAE with 0.64 ml nominal bed volume. Forty microporous ($d_p = 1.2$ μm) membranes made from pure regenerated cellulose are stacked in each column for which a uniform matrix porosity ϵ_b 0.827 has been reported [8]. The MemSep 1000 cartridge is rigid polypropylene rated to 7 bar backpressure with recommended volumetric flow-rates between 1.5 and 6 ml/min. The MemSep HP500 cartridge is rigid polyphenylenesulfate rated to 1000 p.s.i. (1 p.s.i. = 6894.76 Pa) and flow-rates between 0.5 and 5 ml/min.

The MemSep 1000 has channels etched into the upper endcap and lower base of the cartridge to distribute and collect the fluid, respectively. There are six evenly spaced channels with semicircular cross-section radiating outward from the fluid inlet. At flow-rates ≤20 ml/min, the channel Reynolds number based on its hydraulic radius, R_h, is <600, suggesting laminar flow. Polypropylene mesh distributors separate the distributors from the membrane stack. Polyethylene seals prevent fluid from pooling near the corners of the bed volume. Bypassing is discouraged by nine exclusion gaskets inserted between every four membranes. Construction of the MemSep HP500 is similar except eight radial distributor arms are connected by about ten concentric grooves of increasing diameter. An antijetting disc is centered beneath the inlet.

Experiments were performed with a Millipore ConSep LC100. From upstream to downstream this system included proportioning valve, gear pump, pressure transducer, UV detector used at 280 nm, and keypad programmer. The ConSep septum injector was replaced by a syringe loading sample injector, Rheodyne Model 7125 (Cotati, CA, USA) equipped with a 20-μl sample loop. The stacked membrane was connected to a Rheodyne Model 7010 injection valve in order to reverse the flow direction. The valves

and column were configured so that precolumn and postcolumn peripherals would have identical lengths and volumes in either forward or reversed flow. A buffer bypass line inserted via a tee between the injection valves and the pressure transducer via a tee dissipated backpressure spikes observed during injection and flow reversal.

Precolumn peripherals included the 20-μl sample loop, 23 cm of 0.02 in. I.D. polyether ether ketone (PEEK) tubing (1 in. = 2.54 cm), luer-lock adaptors for the MemSep 1000, and four ports (two sections) of an injection valve (> 67 μl total). Postcolumn peripherals included 13 cm of 0.02 in. and 6 cm of 0.01 in. I.D. PEEK tubing, two ports (one section) of an injection valve, and the detector volume (> 29 μl total).

3.3. Procedures

Each column was equilibrated at approximately 1 ml/min in high-ionic-strength buffer before proceeding. Two hours of equilibration were required to regain a stable baseline if buffers were changed. This time corresponds to the time necessary for a small solute to diffuse from the periphery of the column through the intergasket space to the membrane bed to be washed out.

Effluent profiles from precolumn and postcolumn tubing at each flow-rate was measured by plumbing the respective sections between the sample loop and the detector. A 20-μl volume of either 2.5 or 1.25 mg/ml protein was injected to obtain three repetitions. Three repetitions of each column effluent profile were obtained similarly with the column inserted between upstream and downstream peripherals. Flow direction in the reversed-flow runs was changed instantaneously at one-half the peak run time of the corresponding forward-flow experiment.

3.4. Data analysis

Data were acquired on an IBM PS/2 Model 70 386 with Gilson 712 software (Middleton, WI, USA). Data analysis on an IBM PS/ValuePoint 466DX2/D used Microsoft Excel Version 4.0 and an equation solver, EES (Middleton, WI, USA); analysis on a Digital Vaxstation 3100 used Fortran 77 programs.

Extracolumn effluents were fitted to an EMG function using the method of Jeansonne and Foley [50] on the Vaxstation to obtain values of τ and σ for each condition. EES was used to solve implicitly for a corresponding t at the point where the EMG peak intersects its underlying Gaussian. Reversed-flow effluents from the MemSep 1000 and MemSep HP500 were fitted iteratively with Excel to Eq. 3 using averaged extracolumn τ values to obtain $\bar{t}_c$ and σ_c for dispersion in the stack. Peak values larger than half-height were weighted heavier to avoid noise from the tails.

Plate heights were calculated as $L\sigma^2/\bar{t}_c^2$, neglecting residence times of the underlying Gaussian in the peripherals. Reported plate heights are averages of four replicates except for a value at 2 ml/min for the MemSep 1000 (three replicates) and a value at 1 ml/min for the MemSep HP500 (two replicates). Standard deviations of MemSep 1000 plate heights were $<4\%$ of the respective values. Higher deviations for MemSep HP500 occurred as estimated σ_c values were not much larger than σ_r and σ_f: 29% at 0.5 ml/min; 28% at 1 ml/min; 61% at 2 ml/min; and 49% at 4 ml/min.

4. Results and discussion

We begin this discussion by evaluating qualitative effects of extracolumn volumes and nonuniform flow on reversed-flow and forward-flow effluent profiles, respectively. We quantitatively compare reversed-flow analysis of stacked-membrane plate heights with methods based on moments and measured curve widths. And we examine the implications of measured plate heights in MemSep stacked membranes on our one-dimensional dispersive description.

A sample reversed-flow effluent profile obtained as noted above from a MemSep 1000 is compared in Fig. 5 with a fit of Eq. 3. Asymmetry and tailing along the leading edge of the data are greater than those along its trailing edge. This corresponds to larger stirred-tank

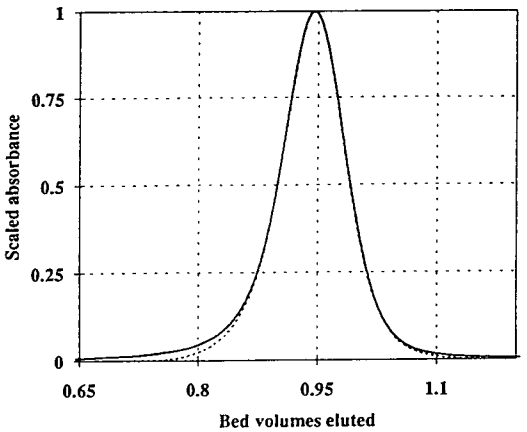

Fig. 5. Comparison of a reversed-flow stacked-membrane effluent shape (solid line) with a fit (dashed line) based on Eq. 3. A 20-μl sample of 2.5 mg/ml cytochrome c was injected into a MemSep 1000 at 2 ml/min for 0.34 min after which the flow direction was reversed. Absorbance at 280 nm was measured across a 10-mm pathlength. Parameter values estimated were the composite mean residence time, $\bar{t}_c$ = 0.664 min and standard deviation σ_c = 0.0175 min.

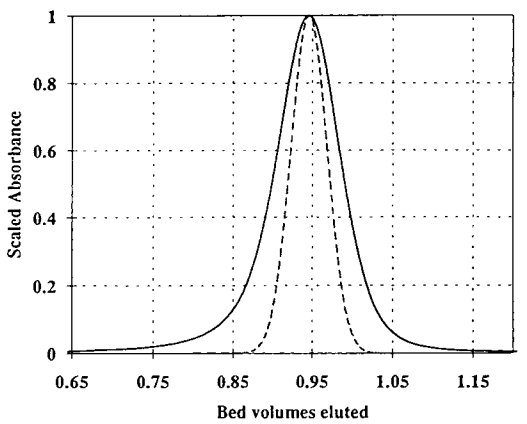

Fig. 6. Comparison of the reversed-flow stacked-membrane effluent profile (solid line) described in Fig. 5 with the Gaussian profile (dashed line) attributed to convective dispersion in the stacked membrane. The Gaussian width at 60.6% of peak maximum, 0.0317 min, was obtained by subtracting variances of precolumn ($\sigma_r^2 = 3.21 \cdot 10^{-5}$ min^2) and postcolumn ($\sigma_f^2 = 2.34 \cdot 10^{-5}$ min^2) peripherals from the composite fitted variance. The data bandwidth at 60.6% of peak maximum was 1.7 × larger than this.

(τ_r = 0.0228 min) and dispersion (σ_r = 0.00566 min) constants in the precolumn peripherals compared with those (τ_f = 0.0185 min, σ_f = 0.00484 min) in postcolumn tubing. Both leading and trailing edges are well matched by the description. (Note that stirred-tank time constants for precolumn and postcolumn peripherals were similar to corresponding space times, V/Q, calculated from peripheral volumes described in Section 3.)

The magnitude of extracolumn contributions to effluent broadening of a stacked-membrane system is illustrated in Fig. 6. The effluent width is 1.7 times that of the convective-dispersion broadening in the stacked membrane. A stacked-membrane plate height estimated from the width at 60.6% peak maximum would have been three times too large. Mistaking this profile for a Gaussian, and neglecting the influence of extracolumn broadening would substantially overestimate stacked-membrane plate heights.

Parameters obtained from extracolumn and reversed-flow experiments allow a priori prediction of forward-flow profiles in the absence of non-uniform flow with Eq. 3. Fig. 7 contrasts the

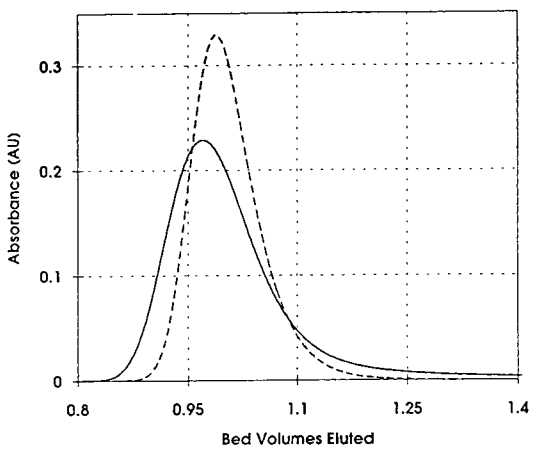

Fig. 7. Comparison of a forward-flow stacked-membrane effluent shape (solid line) with an a priori prediction from Eq. 3 (dashed line) based on parameters obtained from separate experiments. The effluent resulted from a 20-μl sample of 2.5 mg/ml cytochrome c eluted from a MemSep 1000 at 2 ml/min; absorbance at 280 nm was measured across a 10-mm pathlength. Extracolumn stirred-tank time constants, τ_r = 0.0228 min and τ_f = 0.0185 min, were obtained by fitting the respective peripheral effluent profiles to an EMG. Composite residence time, $\bar{t}_c$ = 0.664 min, and standard deviation, σ_c = 0.0175 min, were obtained from a 2 ml/min reverse-flow effluent.

expected peak with the experimentally observed data. Additional broadening in the data arises from non-uniform flow. The most notable consequences of non-uniform flow are (1) severe tailing to 1.94 min and (2) 30% decrease in peak amplitude. Note that the forward-flow prediction in Fig. 7 tails more than its reversed-flow complement in Fig. 6.

Ignoring the effects of non-uniform flow and extracolumn volumes on effluent profiles causes overestimation of stacked-membrane plate heights. The variance of the forward-flow data in Fig. 7 obtained by the experimental method of moments —0.0152 min^2— is 61 times larger than the variance attributable to dispersion in the stacked membrane. Using moments analysis of forward-flow data to estimate plate height as $H \approx L(\langle t^2 \rangle - \langle t \rangle^2)/\langle t \rangle^2$ overestimates stacked-membrane values by orders of magnitude. A "plate height" calculated from the peak width of the forward-flow data in Fig. 7 —0.079 min— is 6.2 times the reversed-flow estimate.

Plate heights estimated for MemSep stacked membranes from reversed-flow experiments are summarized together with predictions from dispersive theory in Fig. 8. These values, ca. 10 times lower than previous reports, are within a factor of three of the theory and tend to decrease with increasing velocity.

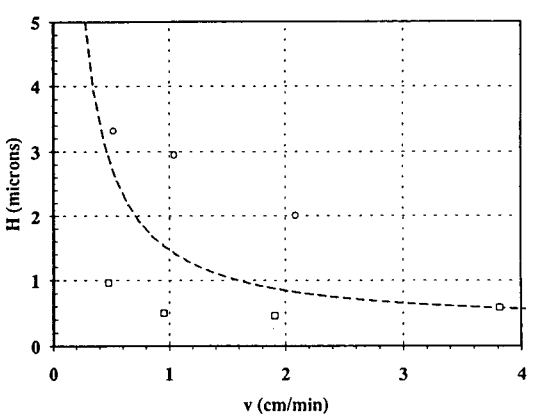

Fig. 8. Plate heigths estimated for a MemSep 1000 (○) at 1, 2 and 4 ml/min and for a MemSep HP500 (□) at 0.5, 1, 2 and 4 ml/min. Respective reversed-flow effluents from a 20-μl injection of 2.5 mg/ml cytochrome *c* were fitted to Eq. 3. Corresponding theoretical plate heights due to convective dispersion, $H = 2\epsilon/v$ (dashed line) were calculated from ϵ in Eq. 2 using $D_f = 11.4 \cdot 10^{-7}$ cm^2/s [52], $D_p = 1.883 \cdot 10^{-4}$ cm, and $\epsilon_b = 0.827$.

In a 5-mm column, the corresponding number of theoretical plates ranges from about 1500 at 0.5 cm/min to a maximum of 10 900 at 2 cm/min. This justifies using a long-column approximation in Eqs. 3 and 4 to describe the stacked membrane. Dispersion along streamlines whose velocities vary from the mean will not differ appreciably in forward or reversed flow because (1) the range of operational stacked-membrane velocities gives approximately the same dispersion (the Van Deemter slope is flat) and (2) the number of stages is high. Profiles from differing streamlines are nearly superimposable in the absence of non-uniform flow, and may be efficiently treated by a one-dimensional description.

Our examination of transport in stacked-membrane systems suggests: (1) reversed-flow analysis measures stacked-membrane plate height more accurately than methods based on moments or peak width, particularly when effects of extracolumn volumes and non-uniform flow on effluent profiles are large; (2) dispersive stacked-membrane plate heights are on the order of a micrometer; (3) both the magnitude and trend of stacked-membrane plate heights estimated by reversing the flow are consistent with intuitive and theoretical estimates of convective dispersion in porous beds.

We have been careful to distinguish between dispersive broadening, and mechanical broadening due to a distribution of residence times. While these processes are physically and mathematically distinct, their common effect, where present, is to diminish the ability to separate efficiently. In spite of apparent flow non-uniformity, commercially available stacked membranes are suitable for analytical separations in which a small percentage of severe tailing is manageable. Careful selection of peripherals to minimize extracolumn broadening (especially downstream of the column) will enhance their performance. For preparative separations in which rapid regeneration, cleanability, and high purity are required, non-uniform flow may hinder the applicability of stacked membranes.

Comparing forward- and reversed-flow results to select an aspect ratio, distributor, or exclusion device to minimize flow non-uniformity in large-scale devices appears useful.

The intrinsic separation potential of stacked membranes which we have measured appears large enough to justify efforts to improve their design. They are, for example, interesting candidates for subunits in Sorbex-type simulated-moving-bed separations. The extremely low solid-phase requirement in moving beds, relative to fixed-bed chromatography, would not demand large membrane capacities. In such a system, low pressure drop, rapid "particle" response times, and low volumetric holdups characteristic of membranes would allow a broader selection of operating conditions while decreasing the demand for high pressure peripherals.

Symbols

Alphanumeric symbols

- A column cross-sectional area (cm^2)
- b length of unit cell (cm)
- c width of unit cell (cm)
- c_f solute concentration in moving fluid phase in chromatography (g/cm^3)
- d width of unit-cell inlet (cm)
- d_p pore diameter in membrane (cm)
- D_f effective solute diffusivity in free solution (cm^2/s)
- D_p effective particle diameter in packed bed (cm)
- h system response to a unit impulse
- H height equivalent to a theoretical chromatographic plate (cm)
- L length of chromatographic column ($=HN$) (cm)
- m_0 total solute mass which enters chromatography column in a pulse (g)
- N number of stages or column plates
- Pe dispersion Peclet number ($\equiv vD_p/\epsilon$)
- Q flow-rate (cm^3/min)
- Re Reynolds number ($\equiv D_p v\epsilon_b/\nu$)
- s standard deviation
- Sc Schmidt number ($\equiv \nu/D_f$)
- t time (s)
- $\bar{t}$ mean residence time in chromatography (s)
- u equilibrium fraction of a species in the fluid phase
- v interstitial velocity in chromatography, velocity in a unit cell (cm/s)
- V volume (cm^3)
- z axial coordinate (cm)
- z_0 mean position of a solute peak at a given time, defined as uvt (cm)

Greek letters

- α_i partition coefficient of a solute between fluid and solid phase
- ϵ convective axial dispersion coefficient (cm^2/s)
- ϵ_b interparticle or column void volume
- ν kinematic viscosity ($\equiv\mu/\rho$) (cm^2/s)
- Φ velocity potential function (cm^2/s)
- Ψ stream function (cm^2/s)
- σ standard deviation (s)
- τ characteristic time (s)

Subscripts and superscripts

- b bulk (stationary) phase in chromatography
- c composite
- f postcolumn peripherals
- F forward flow
- p phase identification subscript
- r precolumn peripherals
- R reversed flow

References

[1] C. Horvath, *GEN*, 14, No. 9 (1994) 4.
[2] R.E. Majors, *LC·GC*, 12 (1994) 278.
[3] E.L. Paul and C.B. Rosas, *Chem. Eng. Progr.*, 12 (1990) 17–25.
[4] V.B. Lawlis and H. Heinsohn, *LC·GC*, 11 (1993) 720–729.
[5] N.B. Afeyan, N.F. Gordon, L. Mazsaroff, L. Varady, S.P. Fulton, Y.B. Yang and F.E. Regnier, *J. Chromatogr.*, 519 (1990) 1–29.
[6] S. Fulton et al., *Biotechn.*, 12 (1992) 742–747.
[7] A. Depalma, *GEN*, 13, No. 1 (1993) 15.
[8] M.S. Le and J.L. Sanderson, *US Pat.*, 4 895 806 (1990).

[9] F. Svec, presented at the *PrepTech94 Industrial Separations Technology Conference, Secaucus, NJ, 22–24 March 1994.*
[10] D.M. Ruthven and C.B. Ching, *Chem. Eng. Sci.*, 44 (1989) 1011–1038.
[11] D.K. Roper and E.N. Lightfoot, *J. Chromatogr. A*, 654 (1993) 1–16.
[12] A. Seidel-Morgenstern and G. Guiochon, *AIChE J.*, 39 (1993) 809–819.
[13] K.-G. Briefs and M.-R. Kula, *Chem. Eng. Sci.*, 47 (1992) 141–149.
[14] X. Zhang, R.D. Whitley and N.-H.L. Wang, presented at the *AIChE Annual Meeting, Los Angeles, CA, 17–22 November 1991.*
[15] P. Schadle, presented at *PrepTech94, Industrial Separations Technology Conference, Secaucus, NJ, 22–24 March 1994.*
[16] S.-Y. Suen and M.R. Etzel, *Chem. Eng. Sci.*, 47 (1992) 1355–1364.
[17] J.L. Coffman, D.K. Roper and E.N. Lightfoot, *Bioseparation*, 4 (1994) 183–200.
[18] D. Josić, J. Reusch, K. Löster, O. Baum and W. Reutter, *J. Chromatogr.*, 590 (1992) 59–76.
[19] J.A. Gerstner, R. Hamilton and S.J. Cramer, *J. Chromatogr.*, 596 (1992) 173–180.
[20] J.J. van Deemter, F.H. Zuiderweg and A. Klinkenberg, *Chem. Eng. Sci.*, 5 (1956) 271–289.
[21] E. Glueckauf, *Trans. Farad. Soc.*, 51 (1955) 34–44.
[22] A. Klinkenberg and F. Sjenitzer, *Chem. Eng. Sci.*, 5 (1956) 258–270.
[23] L.R. Snyder, in Cs. Horváth (Editor), *High-Performance Liquid Chromatography —Advances and Perspectives*, Vol. 1, Academic Press, New York, 1980, pp. 207–316.
[24] J.C. Giddings, *Unified Separation Science*, Wiley, New York, 1991.
[25] A.M. Lenhoff, *J. Chromatogr.*, 384 (1987) 285–299.
[26] A.M. Athalye, S.J. Gibbs and E.N. Lightfoot, *J. Chromatogr.*, 589 (1992) 71–85.
[27] D.D. Frey, R. Van de Water and B. Zhang, *J. Chromatogr.*, 603 (1992) 43–47.
[28] S. Yamamoto and Y. Sano, *J. Chromatogr.*, 597 (1992) 173–179.
[29] H.C. Liu and J.R. Fried, *AIChE J.*, 40 (1994) 40–49.
[30] R.B. Bird, W.E. Stewart and E.N. Lightfoot, *Transport Phenomena*, Wiley, New York, 1960.
[31] R. Aris and N.R. Amundson, *Mathematical Methods in Chemical Engineering*, Prentice Hall, Englewood Cliffs, NJ, 1973.
[32] E.N. Lightfoot, S.J. Gibbs, A.M. Athalye and T.H. Scholten, *Isr. J. Chem.*, 30 (1990) 229–237.
[33] D.M. Ruthven, *Principles of Adsorption and Adsorption Processes*, Wiley-Interscience, New York, 1984.
[34] H.C. Thomas, *J. Am. Chem. Soc.*, 66 (1944) 1664–1666.
[35] S.J. Gibbs and E.N. Lightfoot, *Ind. Eng. Chem. Fundam.*, 25 (1986) 490–498.
[36] F.D. Antia and Cs. Horváth, *J. Chromatogr.*, 484 (1989) 1–27.
[37] A.M. Athalye, *Ph.D. Thesis*, University of Wisconsin, Madison, WI, 1994.
[38] J.F.G. Reis et al., *Sep. Sci. Technol.*, 14 (1979) 367–394.
[39] M.A. Northrup et al., *Chem. Eng. Sci.*, 48 (1993) 13–23.
[40] D.L. Koch and J.F. Brady, *J. Fluid Mech.*, 154 (1985) 399–427.
[41] F. Balzereit, *M.S. Thesis*, University of Wisconsin, Madison, WI, 1991.
[42] K.R. Raths, *M.S. Thesis*, University of Wisconsin, Madison, WI, 1992.
[43] L.M. Milne-Thompson, *Theoretical Hydrodynamics*, Macmillan, London, 5th ed., 1967.
[44] D.K. Roper and E.N. Lightfoot, presented at the *AIChE Annual Meeting, St. Louis, MO, 7–12 November 1993.*
[45] D.K. Roper and E.N. Lightfoot, *Chem. Eng. Sci.*, 49 (1994) 1621–1630.
[46] J.S. Vrentas and C.M. Vrentas, *AIChE J.*, 34 (1988) 1423–1430.
[47] Ph. Daskopolous and A.M. Lenhoff, *AIChE J.*, 34 (1988) 1423–1430.
[48] K.P. Mayock, J.M. Tarbell and J.L. Duda, *Sep. Sci. Technol.*, 15 (1980) 1285–1296.
[49] T. Korenaga, F. Shen and T. Takahashi, *AIChE J.*, 35 (1989) 1395–1398.
[50] M.S. Jeansonne and J.P. Foley, *J. Chromatogr.*, 594 (1992) 1–8.
[51] I. Stakgold, *Greens Functions and Boundary Value Problems*, Wiley, New York, 1979.
[52] M.T. Tyn and T.W. Gusek, *Biotechnol. Bioeng.*, 35 (1990) 327–338.

ELSEVIER

Journal of Chromatography A, 702 (1995) 81–87

JOURNAL OF CHROMATOGRAPHY A

Computer aided desk-top scale-up and optimisation of chromatographic processes

D.J. Wiblin[a,*], Simon D. Roe[a], Richard G. Myhill[b]

[a]*BIOSEP, AEA Technology, 353, Harwell, Oxon OX11 0RA, UK*

[b]*Computational Fluid Dynamics Services, AEA Technology, 8.19, Harwell, Oxon OX11 0RA, UK*

Abstract

Further experimental validation of an existing set of computer programs, called Simulus, will be presented. This validation includes predicting the performance of the recovery of immunoglobulin G from a crude, unclarified tissue culture using a Prosep-G fluidised bed and the recovery of amylase from a crude feedstock using a Streamline DEAE expanded bed. The mathematical theory for these programs will be highlighted. It is not possible to obtain analytical solutions to these sets of equations defining the mass transfer processes within a column and its media. In the prediction of column breakthrough, a well established coarse numerical solution is sufficient to achieve good results, however, when attempting to predict sharp elution profiles, the model fails. A unique discretisation of the same equations will be presented, giving dramatically improved modelling capabilities. The experimental validation, using an amylase/Sephacryl gel filtration chromatography system, gave convincing results.

1. Introduction

The use of adsorption and chromatographic techniques throughout the chemical and pharmaceutical industry is extensive. However, a full process optimisation of high-value products, which are often proteinaceous, is often restricted by the value of the products involved. Furthermore, the commercial environment necessitating "first-to-the-market" competitiveness, often restricts research programmes to process validation and not to the level of efficiency in the full-scale purification facility.

Previous work [1–11] has shown that mathematical equations which model the diffusion, adsorption and convection of target and contaminant molecules within a process can be solved to give accurate predictions of the purity and yield of the final product.

In the past we have shown that a set of programs could be used strategically to assess the effect of operational parameters, such as flow-rate or column aspect ratio, on the performance of a process [3,6,10]. Moreover, it has been shown that complex equilibria existing in ion-exchange and other chromatographic columns could be modelled using simple equations.

Although the theoretical credibility of computer-aided design packages is unquestioned [2], its use will not be widespread until numerous criterion are met: (i) generic programs are written with diverse capabilities, (ii) extensive experimental validation work is undertaken, and (iii) simple, user-friendly packages are compiled.

To this end a design package was developed by BIOSEP [12] and tested on real biological

* Corresponding author.

0021-9673/95/$09.50 © 1995 Elsevier Science B.V. All rights reserved
SSDI 0021-9673(94)01093-5

systems. This design package is incorporated into a proprietary design report available to members of BIOSEP. This paper, however, will seek to address some of the criteria highlighted.

The two sets of equations which we have used model the dynamic equilibrium between molecules in the adsorbed and desorbed states and the rates of diffusion across particle surface boundary layers and through the pores. These equations using a simple discretisation will be used to predict the performance of fluidised and expanded bed chromatography.

One major limitation to modelling elution chromatography is the ability to characterise the sharp peak which often results. With existing models, the column is normally broken down into a number of discrete cells divided equally down the column, however, to model the movement of a sharp peak as it moves down the column requires a highly concentrated discretisation. For the entire column to be discretised in such a fashion would be immensely computer intensive and therefore inviable. This study therefore seeks to address these problems.

In the latest stage of the work, to develop the programs into a useful tool for the chromatographer, we have produced a Windows-compatible version of their suite of adsorption programs, which is called Simulus. Validation will be given in several new key areas of purification.

2. Theory

2.1. Existing models

The basic models and equations which Simulus uses were transferred directly from the original suite of BIOSEP programs. This suite of programs, and their equations, is well documented [12,13] and their worthiness for modelling a number of systems is now well established. The equations for these models are given by Cowan et al. [11], so will not be given again here. The validation of the use of these equations, however, is ongoing and, since several new purification techniques are now commercially available, further validation of their capability to model such new adsorption processes is sought.

2.2. Moving grid strategy

The importance of the model's capability to characterise sharp elution peaks, is paramount for a detailed and accurate estimation of a process's efficiency [14]. The original models, in their simplicity, were proficient at modelling these types of experimental data, but required an immense discretised grid (often over a 200 cells per cm of column). Furthermore, the computational processing power required made the feasibility of using such models impractical. To approach this problem a new model was included into Simulus, called the "moving grid" [15]. This program enables a highly localised discretisation to be positioned around the peak and to subsequently track the theoretical peak as it moves down the column.

In order to validate the application of this moving grid technique, the simplest form of elution chromatography was selected. In size-exclusion chromatography, or gel filtration, a sample is loaded onto the top of a column, and the mixture is separated by diffusion effects only. Here the need for modelling adsorption can be removed which simplifies the initial validation of the program.

The resulting equations which model the process are given below.

When considering a gel filtration column the convection of adsorbate along the length of the column can be described by Eq. 1.

$$\frac{\partial c_b}{\partial t} = D_a \cdot \frac{\partial^2 c_b}{\partial z^2} - \nu \cdot \frac{\partial c_b}{\partial z} - \frac{3k_f V_S}{RV_L} \cdot \left(c_b - c_j|_{r=R}\right) \quad (1)$$

Here the last term represents the quantity of the species under consideration which diffuses across the particle boundary layer. The adsorbate concentration at the surface of the particle is given by Eq. 2:

$$\frac{\partial c_j}{\partial r}|_{r=R} = \frac{k_f}{D_e \epsilon_i} \cdot \left(c_i - c_j|_{r=R}\right) \quad (2)$$

The diffusion of adsorbate into the pores of the particle is described by Eq. 3:

$$\frac{\partial c_j}{\partial t} = D_e \cdot \left(\frac{\partial^2 c_j}{\partial z^2} + \frac{2}{r} \cdot \frac{\partial c_j}{\partial r}\right) \quad (3)$$

assuming the boundary condition holds that the rate of mass transfer at the centre of the particle is zero (Eq. 4).

$$\frac{\partial c_j}{\partial r}\Big|_{r=0} = 0 \tag{4}$$

The simultaneous solution to these differential equations cannot be undertaken analytically, but instead relies upon numerical solution techniques. In past modelling programs, the numerical solution involves dividing the column into identical "cells". Eq. 1 can be solved using the "method of lines" [16] to convert the partial differential equation into a set of ordinary differential equations. This is carried out using a "finite volume discretisation" [16] to integrate over each cell volume, which then gives the required ordinary differential equations. In the moving grid model, each cell is set up as in Fig. 1.

The grid is set up in a similar way to past numerical solutions except that the entire grid is localised to one tenth of the loading length, with the first cell boundary at the inlet to the column. Typically a tenth of the loading length is around 2% of the column length. As the integration proceeds, however, the bulk fluid concentration, c_b, reaches the last cell at which point the outer grid boundary begins to move. As loading finishes, the inner boundary similarly moves as in Fig. 2.

These boundaries are then fixed to ensure that there is no mass flux across each external boundary, i.e. z_0 and z_n, where n is the number of cells, such that there is 98% mass containment. The solution for cases where D_a is negligible (as it is in most cases) is:

$$\frac{dc_i}{dt} = \frac{3k_f V_s}{RV_L} \cdot (c_i^{surface} - c_i) + \frac{1}{h_i} \cdot [(\dot{z}_{i+1} - v) \cdot c|_{z^{i+1}} - (\dot{z}_i - v) \cdot c|_{z^i} - (\dot{z}_{i+1} - \dot{z}_i) \cdot c_i] \tag{5}$$

The program employs instantaneous re-gridding which is carried out at each time step along the integration to maintain 98% of the loaded mass within the confines of the gridded volume (Fig. 2). Increasing this "captured" percentage only results in elongation of the grid and a corresponding reduction in resolution. The remaining grid is divided evenly between the inner and outer boundaries such that for all i, h_i is constant, as in Fig. 3. This movable, expanding grid allows maximum resolution of the peak with a minimum of processing power. The corresponding scenario with the fixed grid (also shown) cannot adequately characterise the diffusive mass transfer due to the prohibitive nature of the discretisation.

The homogeneity of the media within a gel filtration column, allows it to be modelled as a

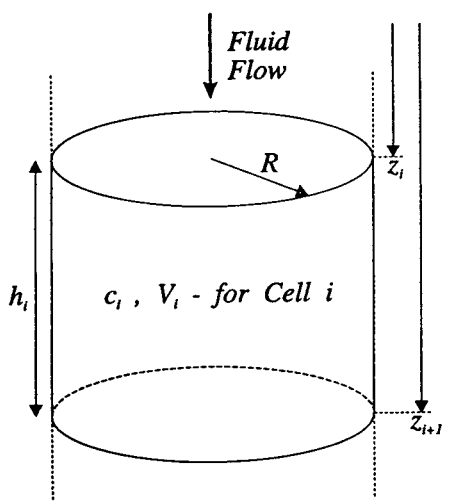

Fig. 1. The cell divisions in the moving-grid discretisation.

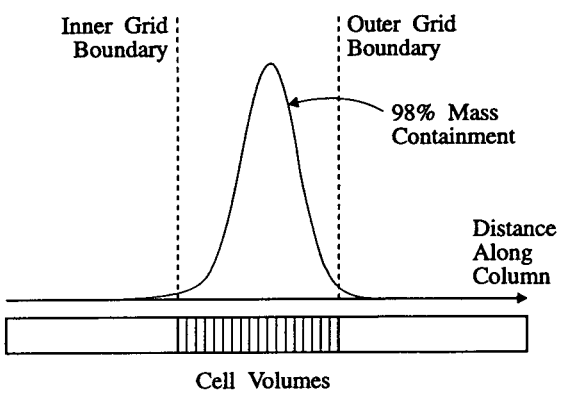

Fig. 2. Grid boundaries tracking the peak movement.

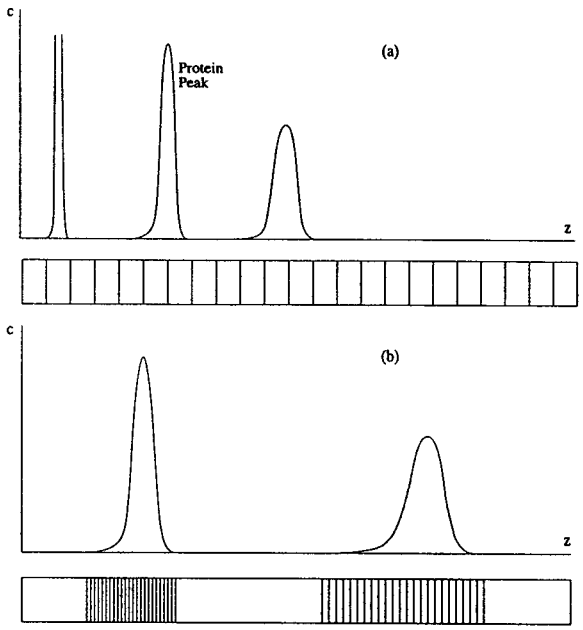

Fig. 3. A comparison of (a) standard grid and (b) moving grid discretisations.

continuous medium. In this case it can modelled as one single particle of radius R split into a number of shells (Fig. 4).

The solution to this problem for a fixed grid system is well documented [14], however, to allow for the movement of the cell grid boundaries, an expansion term (or a shrinking term) must be added to allow for the transfer of particulate phase concentration within the media, from one cell to another. The solution is slightly more complicated though nevertheless

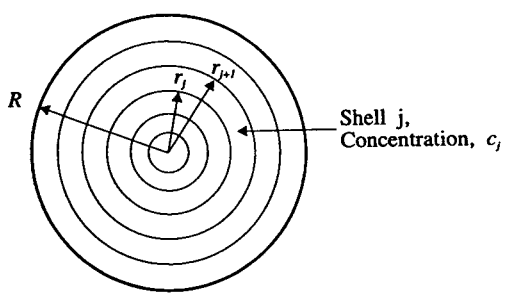

Fig. 4. The particle discretisation.

time consuming to browse through and will hence be excluded from this paper.

In initial studies the difference in processing time, and accuracy, heavily favoured the use of the moving grid (Fig. 5).

In these predictions, 25 cells where used for the moving grid, and 800 cells for the fixed grid giving comparative run times of 1.2 min and 1 h and 49 min respectively (on a 486 DX33 computer with 8 MB of RAM). The predicted peak for the fixed grid could be improved by increasing still further the number cells is the column, however, due to memory limitations of the computer this could not be carried out.

3. Materials and methods

Amongst many others, previous validation work included the purification of aspartic acid using Duolite A162 [11], the adsorption of an intracellular enzyme leucine dehydrogenase onto DEAE-Spherodex [17] and the uptake of α-amylase by QMA-Spherosil [17]. The three processes modelled in this paper have been selected to reinforce the validation of Simulus.

The method employed throughout the modelling of the data was first elucidated by Noble et al. [10]. In short, the strategy adopted was to use experimental results from a small-scale run, which would typically be obtained when assessing the process at laboratory scale, and use characteristic parameters to then predict scale-up and contactor configuration. In many cases it is possible to obtain parameters from, say, a packed bed experiment, and then to predict the outcome of an expanded or fluidised bed process. For the initial validation of the moving grid model results were simply taken from a small column, and used to predict what would happen at a much larger scale.

In each case given below, the analysis using Simulus gives the parameters which best characterise the adsorption process. Simulus also calculates confidence limits [18] to assess the simulation dependency on the parameter in question.

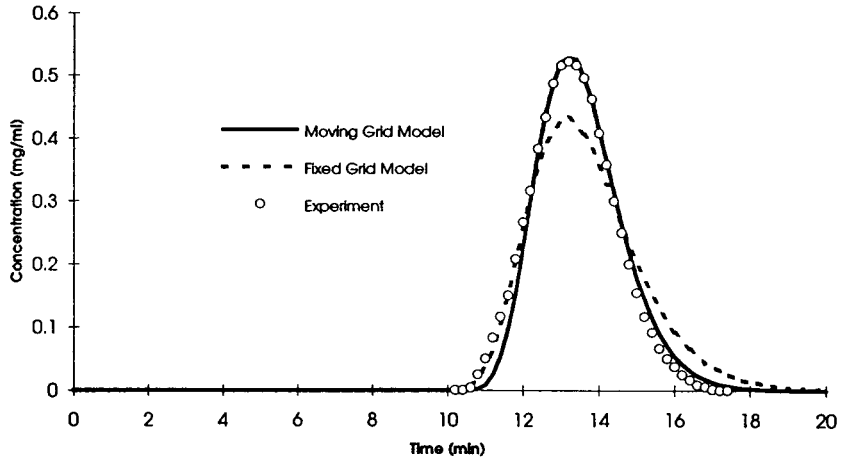

Fig. 5. A comparison between the fixed grid model and the moving grid model using approximate parameters to obtain a close comparison to real experimental results.

3.1. Expanded bed adsorption

The first process is the purification of α-amylase using expanded bed adsorption (or EBA, Pharmacia Biotechnology, Uppsala, Sweden). The unclarified mixture was prepared by dissolving 2 mg ml^{-1} of a crude, bacterial source α-amylase (Sigma, UK) into Tris·HCl buffer at pH 9. Dried yeast (5 g l^{-1})was added to simulate a fermentation broth. The clarified solution was loaded at 10 ml min^{-1} onto a 10 × 1.6 cm column packed with Streamline DEAE media (Pharmacia Biotechnology). The unclarified "broth" was loaded at 100 ml min^{-1} onto a 55 × 5 cm expanded bed (also using Streamline DEAE).

The results from the packed bed study were analysed using Simulus to obtain the parameters which characterise the adsorption process (Fig. 6a). These parameters were then taken and used to predict the outcome of the expanded bed study. The comparison between the real and the predicted results are given in Fig. 6b. This prediction represents approximately a 20-fold scale-up in capacity.

3.2. Affinity fluidised bed adsorption

The second of the two processes is the purification of a monoclonal antibody using affinity

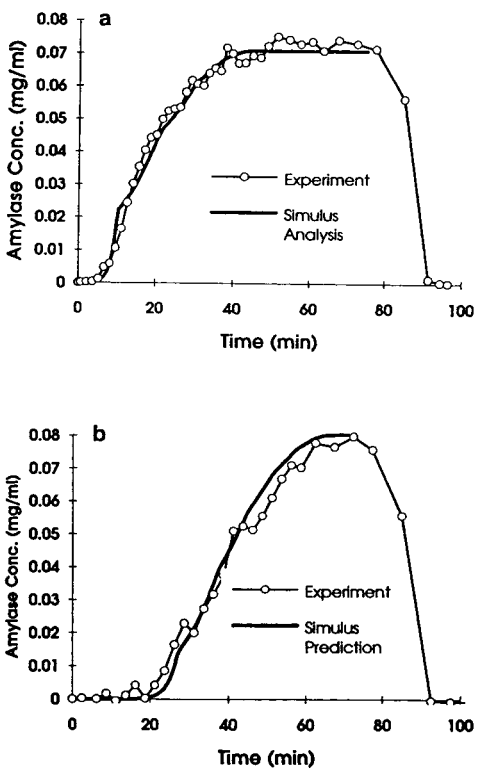

Fig. 6. (a) Comparison between the adsorption of α-amylase onto Streamline DEAE and the results fitted by Simulus. (b) Comparison of adsorption of α-amylase onto Streamline DEAE using EBA technology and the prediction given by Simulus.

fluidised bed adsorption. The approach for this modelling study was the same as for the expanded bed analysis. In the initial packed bed experiments an ideal system was selected. A solution of 20 m*M* trisodium phosphate containing 0.27 mg ml^{-1} of the antibody (cultured at AEA Technology) was loaded onto a 5×0.5 cm Prosep-G packed bed at 0.49 ml min^{-1}. The resulting frontal curve was analysed to obtain parameters which characterise the adsorption kinetics. The comparison of the experimental and the fitted curve is shown below (Fig. 7a).

A similar solution, at 0.275 mg ml^{-1} was then applied to a fluidised bed process with the same type of media, Prosep-G. The bed was fluidised to 16.2×1.0 cm at a constant flow-rate of 1.95 ml min^{-1}. Due to the particle size variation, the bed was observed to be relatively stable with little axial motion. The results from the experiment were compared to predictions given by Simulus (Fig. 7b).

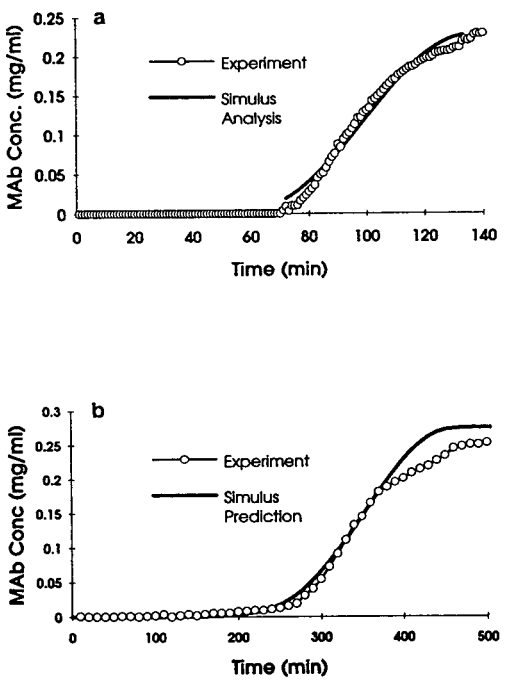

Fig. 7. (a) Comparison between the adsorption of IgG onto Prosep-G and the results fitted by Simulus. (b) Comparison of adsorption of IgG onto Prosep-G using an affinity fluidised bed and the prediction given by Simulus. MAb = Monoclonal antibody.

3.3. Gel filtration

The final model system seeks to validate the use of the moving grid strategy for gel filtration. In the initial studies the selected system was pure α-amylase dissolved into Tris · HCl buffer at pH 7.2. This solution was loaded onto various size columns packed with Sephacryl S100HR. The packing followed the instructions given by the manufacturers [19]. To alleviate non-specific binding, 50 m*M* sodium chloride was also added to the loading and elution buffers. The analysis of the mass transfer processes was undertaken using results from the smallest column used which was 11.2×1.6 cm where the linear flow-rate was 30 cm h^{-1} (Fig. 8a).

The elution profiles of the remaining experiments were then compared to the predictions by Simulus. Accurate correlations were found between the simulation and reality. One such comparison is given in Fig. 8b. In this experiment the amylase solution was loaded onto a 87.7×2.6 cm column (465.2 ml) at 60 cm h^{-1}, corresponding to an increase in throughput of 4000%.

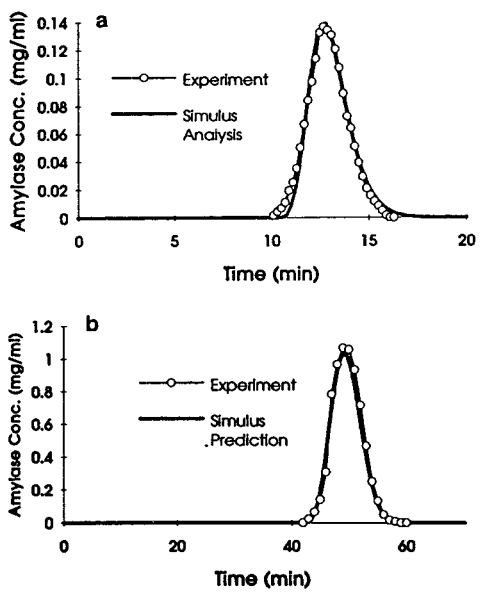

Fig. 8. (a) Comparison between the elution profiles for α-amylase and the results fitted by Simulus for a 22.5-ml column. (b) Comparison between the elution profiles for α-amylase and the prediction given by Simulus for a 465.2-ml column.

In further validation work an industrial gel filtration process was modelled which gave equally convincing results.

4. Conclusions

It is apparent that the inclusion of the moving grid strategy into Simulus will be of great benefit in the modelling of separation processes. The accuracy of the validation with gel filtration, the simplest form of elution chromatography, strengthens this claim.

With the incorporation of new modelling techniques into the current programs, Simulus's overall performance was significantly enhanced and will revolutionise chromatographic modelling techniques.

Symbols

c_b	Bulk phase concentration (kg m^{-3})
c_i	Bulk cell concentration (kg m^{-3})
c_j	Particle shell concentration (kg m^{-3})
$c\|_{z^i}$	Estimated concentration at the z_ith boundary calculated by upwind (or upstream) differencing
D_a	Axial dispersion coefficient (m^2 s^{-1})
D_e	Pore diffusion coefficient (m^2 s^{-1})
ε_i	Effective intraparticle porosity
h_i	Height of the ith cell
k_f	Liquid film diffusion coefficient (m s^{-1})
r	Radial distance (m)
R	Particle radius (m)
t	Time (s)
v	Calculated interstitial velocity of the loading fluid
v	Superficial bulk fluid velocity (m s^{-1})
V_L	Liquid phase volume (m^3)
V_S	Solid phase volume (m^3)
z	Axial distance (m)
$\dot{z}_i$	Velocity of the ith boundary

Acknowledgements

Acknowledgement is made to BIOSEP, AEA Technology, both for permission to publish the work presented in this paper and for their support in doing so. Acknowledgement is also made to Yvonne Gunn for supporting AEA Technology's numerical solver, Facsimile.

Windows is a trademark of Microsoft Corp.

References

[1] A.C. Liapis and D.W.T. Rippin, *Chem. Eng. Sci.*, 32 (1978) 619–627.
[2] H.A. Chase, *J. Chromatogr.*, 297 (1984) 179.
[3] G.H. Cowan, I.S. Gosling, J.F. Laws and W.P. Sweetenham, *J. Chromatogr.*, 363 (1986) 37.
[4] J. Jacobsen, N. Frenz and Cs. Horváth, *J. Chromatogr.*, 316 (1984) 53.
[5] N.F. Kriby, N.K.H. Slater, K.H. Weisenburger, F. Addo-Yobo and D. Duola, *Chem. Eng. Sci.*, 41 (1986) 2005.
[6] G.H. Cowan, I.S. Gosling and W.P. Sweetenham, in M.S. Verrall and M.J. Hudson (Editors), *Separations for Biotechnology*, Ellis Horwood, Chichester, 1987, p. 152.
[7] G.H. Cowan, in A.E. Rodrigues, M.D. LeVan and D. Tondeur (Editors), *Adsorption: Science and Technology (NATO ASI Series E: Applied Sciences*, Vol. 158), Kluwer, Dordrecht, 1989.
[8] H.A. Chase and B. Horstmann, in M.S. Verrall and M.J. Hudson (Editors), *Separations for Biotechnology*, Ellis Horwood, Chichester, 1987.
[9] B.J. Horstmann and H.A. Chase, *Chem. Eng. Res. Des.*, 67 (1989) 243.
[10] J.B. Noble, G.H. Cowan, W.P. Sweetenham and H.A. Chase, in M.J. Slater (Editor), *Ion Exchange Advances*, Elsevier Applied Science, London, 1992, p. 214.
[11] G.H. Cowan, I.S. Gosling and W.P. Sweetenham, *J. Chromatogr.*, 484 (1989) 187.
[12] J.B. Noble, G.H. Cowan, W.P. Sweetenham with contributions from H.A. Chase and B.J. Horstmann, *Prediction of the Performance of Batch Tank Adsorbers and Fixed Bed Adsorption Columns*, BIOSEP, Harwell, August 1988.
[13] D.J. Wiblin, *Simulus Theoretical and Technical Reference*, BIOSEP, Harwell, January 1994.
[14] R.S. Hodges, J.M.R. Parker, C.T. Mant and R.R. Parker, *J. Chromatogr.*, 458 (1988) 147.
[15] J.H. Ferziger, *Numerical Methods for Engineering Applications*, Wiley, New York, 1981.
[16] R.G. Myhill, personal communication, 1992.
[17] J.B. Noble, *Ph.D. Thesis*, Imperial College, London, 1991.
[18] *Packing Instructions, Sephacryl S-100 High Resolution*, Pharmacia LKB Technology, Uppsala, 1987.
[19] A.R. Curtis, W.P. Sweetenham and Y. Gunn, *FACSIMILE User's Guide*, AEA Technology, Harwell, 1993.

ELSEVIER

Journal of Chromatography A, 702 (1995) 89–95

JOURNAL OF CHROMATOGRAPHY A

Modified poly(glycidyl methacrylate–co-ethylene dimethacrylate) continuous rod columns for preparative-scale ion-exchange chromatography of proteins

Frantisek Svec*, Jean M.J. Fréchet

Cornell University, Department of Chemistry, Baker Laboratory, Ithaca, NY 14853-1301, USA

Abstract

A continuous rod of porous poly(glycidyl methacrylate–co-ethylene dimethacrylate) has been prepared by a free radical polymerization within the confines of a 300 × 8 mm I.D. chromatographic column. The epoxide groups of the rod have been modified by a reaction with diethylamine that affords ionizable functionalities required for the ion-exchange chromatographic mode. The properties of this rod column have been characterized and the column has been used successfully for the chromatographic separation of proteins. The column exhibits a dynamic capacity that exceeds 300 mg at a flow velocity of 200 cm/min. An excellent selectivity allows the separation of up to 300 mg of a protein mixture in a single run.

1. Introduction

The inherent problem of all of particulate separation media is the inability to completely fill the space within the chromatographic column. Generally, interparticular porosity contributes to peak broadening and decreases column efficiency. The limited utilization of column space also affects the capital investment costs particularly in preparative-scale separations because the column volume must be much larger than the volume of the separation medium itself.

The column void volume can be decreased or even eliminated when media with a higher degree of continuity are used. Polymerized porous discs [1] or stacked cellulose membranes [2] placed in a cartridge that simulates the function of a chromatographic column exhibit almost no interstitial porosity. However, their efficiency is reduced as a result of non-uniform flow velocity across the membranes due to the cartridge geometry. Rolled cellulose sheets [3] or woven matrices [4] placed in the tube of a chromatographic column can be used successfully for the separations of proteins that can be fractionated using an on–off mode but they have only limited efficiencies. The open-pore silica or polyurethane foams formed directly within a column did not prove to provide sufficient chromatographic properties for normal-phase separations [5,6]. Swollen polyacrylamide gels were compressed in the shape of a column and used successfully for the HPLC separation of proteins and peptides [7–9].

We have introduced HPLC separation media with no discontinuity that consist of a continuous "molded" rod of rigid, highly porous polymer. These rods, that are essentially the equivalent of

* Corresponding author.

0021-9673/95/$09.50 © 1995 Elsevier Science B.V. All rights reserved
SSDI 0021-9673(94)01021-8

a very large single cylindrical particle, are prepared in a single step by a free-radical polymerization directly within the confines of a chromatographic column acting as a mold [10–13]. The concept of molded separation media was verified with relatively short, 50–100 mm long columns that contained modified poly(glycidyl methacrylate–co-ethylene dimethacrylate) [11] or poly(styrene–co-divinylbenzene) rods [12,13]. These proved to be very efficient for the extremely fast reversed-phase HPLC separation of proteins [12] and for the separation of small and mid-size molecules [13].

Subsequently, Matsui et al. [14] used our approach for the preparation of continuous rods of molecularly imprinted polymers and showed their capabilities for molecular recognition in a series of separations of positional isomers and enantiomers. Most recently, Sellergren [15] imitated this approach.

The most important feature of the continuous media is the absence of interparticular volume. Therefore, *all* of the mobile phase is forced to flow *through* the large pores of the separation medium that substitute the column porosity and allow the mobile phase to flow through. According to theory [16–18], mass transport is enhanced by such a convection and has a positive effect on the chromatographic separation [19–21].

The separations achieved with the short columns as well as the low pressure drops along the column and ease of the preparation of the rods led us to prepare a longer rod column for use in the preparative-scale separation of larger amounts of proteins. This communication reports preliminary results obtained with this continuous rod column.

2. Experimental

2.1. Materials

The glycidyl methacrylate and ethylene dimethacrylate (Sartomer, Exton, PA, USA) were distilled under vacuum. Azobisisobutyronitrile (AIBN) was obtained from Kodak, cyclohexanol and dodecyl alcohol from Aldrich. The proteins were purchased from Sigma. All solvents were HPLC grade.

2.2. Preparation of the continuous column

The continuous column was prepared by an in situ polymerization within the confines of the stainless-steel tube of a 300 × 8 mm I.D. chromatographic column. The 40:60 (v/v) mixture of monomers (glycidyl methacrylate and ethylene dimethacrylate, 60:40, v/v) and porogenic diluents (cyclohexanol and dodecanol, 90:10, v/v) in which AIBN (1%, w/v, with respect to monomers) was dissolved, was purged with nitrogen for 15 min. The stainless-steel tube was filled with the above mixture and then sealed at both ends with pieces of polyethylene foil covering rubber septa. The polymerization was allowed to proceed at 55°C for 12 h. The seals were removed, the column was provided with fittings, attached to the HPLC system and heated to 45°C. Tetrahydrofuran (THF) (100 ml) was pumped through the column at a flow-rate of 0.5 ml/min to remove the alcohols and other soluble compounds present in the polymer rod after the polymerization was completed.

2.3. Preparation of amino-functionalized porous rod

The epoxide groups of the polymerized glycidyl methacrylate were allowed to react with diethylamine according to the reaction:

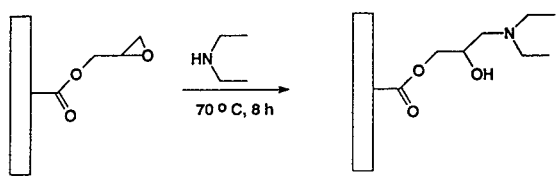

Diethylamine (20 ml) was pumped through the column for 1 h at a flow-rate of 0.33 ml/min. The column was then removed from the chromatographic system, sealed at both ends with plugs and heated in a bath to 70°C for 8 h. The modified column was then reattached to the chromatograph and washed at a flow-rate of 0.5 ml/min first with water for 14 h and then with a

0.01 *M* Tris–HCl buffer solution at pH 7.6 for another 3 h. The content of diethylamino groups determined by elemental analysis was 3.24 mmol/g.

2.4. Characterization of pore properties.

After all of the chromatographic experiments has been completed, the rod was washed with water (2 h at 0.5 ml/min), the bottom column fitting was removed and the polymer rod was pushed out of the tube using pressure of the mobile phase. About 5 cm of the 30 cm long cylinder was cut into small pieces and dried at 70°C. The specific surface area of the macroporous polymer rod was calculated from the BET isotherm of nitrogen; the pore size distribution in the dry state was determined by mercury porosimetry using an automated custom-made combined BET-Sorptometer and mercury porosimeter from Porous Materials, Ithaca, NY, USA.

2.5. Chromatography

A Waters HPLC system consisting of two 501 HPLC pumps, a 707 plus autosampler, and a 486 UV detector, was used to carry out all the chromatography. The data were acquired and processed with Millenium 2010 software (Waters). A solution of chicken egg albumin in 0.01 *M* Tris–HCl buffer (15 mg/ml) was used for frontal analysis and dynamic capacity determination.

3. Results and discussion

The ion-exchange chromatographic mode is often used in large-scale processes for the initial and intermediate purification of proteins. Glycidyl methacrylate-based polymers can be easily functionalized to afford separation media with ionizable groups that are well suited for ion-exchange chromatography. Though the chemistry itself is very important, it is not the only feature required for a successful separation. There are many other requirements that must also be met when designing a separation medium, particularly for large-scale chromatography. These are related to both the material, including porosity, pore size distribution, rigidity and resistance to alkaline solutions, and the chromatographic properties, including dynamic capacity, selectivity, equilibration rate, etc.

3.1. Porous properties of the continuous rod column

Based on an extensive study of the polymerization mechanism of monomer–porogen mixtures in closed molds that will be published elsewhere, we have chosen polymerization conditions that afford a rod with a bimodal pore size distribution typical for the short molded columns. Fig. 1 shows the pore size distribution profile for the rod prepared by a polymerization at 55°C. The total pore volume of the porous polymer is 1.0 ml/g and translates to a porosity of about 55%. According to the mercury porosimetry, the pores in the range of from 50 to 500 nm and those smaller than 50 nm represent 12 and 13% of the total pore volume, respectively. More than 75% of all of the pores have a diameter in the range of 500–2200 nm. These pores are the channels through which the mobile phase flows. Their volume and size are sufficiently large to ensure a modest flow resistance

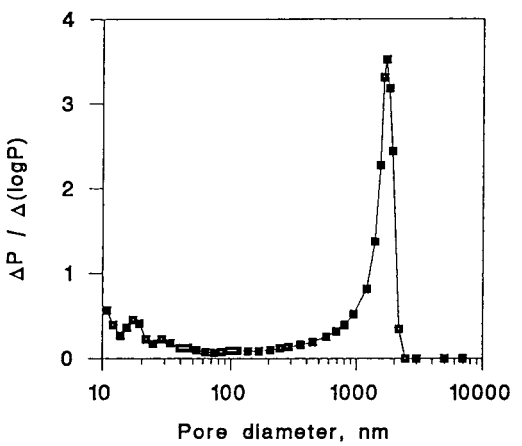

Fig. 1. Differential pore size distribution curve of the modified poly(glycidyl methacrylate–co-ethylene dimethacrylate) rod measured by mercury intrusion porosimetry.

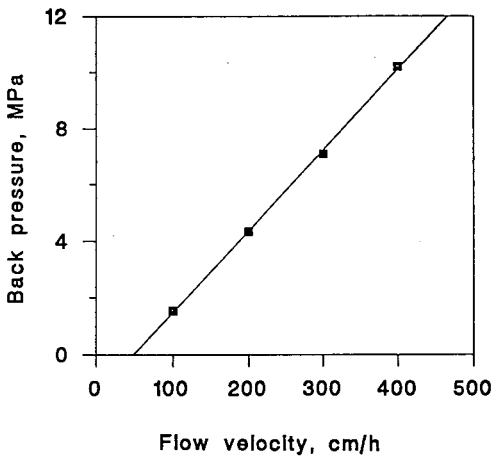

Fig. 2. Effect of flow velocity on back pressure in the continuous poly(glycidyl methacrylate–co-ethylene dimethacrylate) column. Conditions: column 300 × 8 mm I.D.; mobile phase 0.01 *M* Tris–HCl buffer.

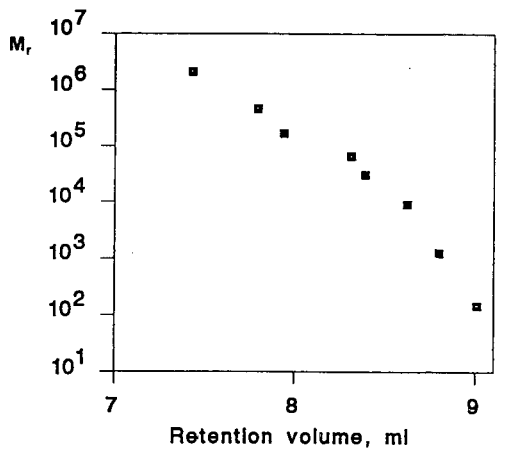

Fig. 3. Size-exclusion chromatography calibration curve of the continuous poly(glycidyl methacrylate–co-ethylene dimethacrylate) 300 × 8 mm I.D. rod column. Conditions: flow-rate 0.5 ml/min; mobile phase tetrahydrofuran; UV detection at 254 nm.

for the 300 mm long column. For example, a back pressure of only 10.2 MPa is obtained at a linear flow velocity of 400 cm/h (Fig. 2). The linearity of the back pressure vs. flow velocity dependency as measured using a buffer solution as the mobile phase clearly documents the rigidity of the long rod that easily withstands pressures higher than 10 MPa.

The size-exclusion calibration curve for the rod as measured with amylbenzene and polystyrene standards in THF shown in Fig. 3 is another tool used for the description of the porous structure in the range of smaller pores. It has a shape similar to that typically found for porous separation media. The mercury porosimetry data measured in the dry state indicate that the volume of pores with a diameter of 10–300 nm represents only about 0.2 ml/g of the polymer or about 1.2 ml for the entire 300 mm long column. This correlates well with the column effective pore volume of 1.6 ml in which the molecules of standards with molecular masses from 140 (amylbenzene with an equivalent sphere diameter of about 1 nm) to 2 100 000 (polystyrene with the diameter of about 300 nm) have been separated. The somewhat larger pore volume determined from the calibration curve includes also pores smaller than 10 nm that are not accessible during measurements by mercury porosimetry.

The specific surface area measured by nitrogen adsorption was found to be 295 m^2/g. This surface area is mainly due to the smallest pores of the rod.

3.2. Chromatographic properties

Breakthrough curve and dynamic capacity

The frontal analysis, which provides the breakthrough curve, serves as a tool for the evaluation of mass transport kinetics. In an ideal case, the breakthrough curve, that shows the solute concentration at the column outlet vs. the total volume passed through the column, is almost vertical. If the saturation rate of the separation medium with the solute of interest is slower than the flow-rate, the curve is less steep. The short rod columns have proved to have excellent mass transfer characteristics [12] with sharp breakthrough profiles independent of the flow velocity within a very broad range. The 300 mm long modified poly(glycidyl methacrylate–co-ethylene dimethacrylate) column also has a breakthrough curve with a sharp front that confirms the fast mass transport kinetics of the rod (Fig. 4). The dynamic capacity of the column for ovalbumin at

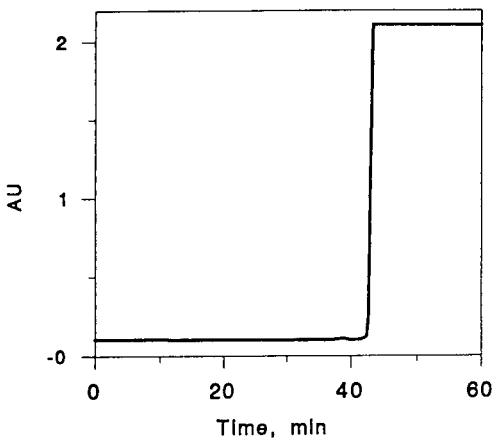

Fig. 4. Breakthrough curve for chicken egg albumin. Conditions: column 300 × 8 mm I.D.; mobile phase 0.01 *M* Tris–HCl buffer pH 7.6; flow-rate 0.5 ml/min; albumine concentration 15 mg/ml, UV detection at 280 nm.

1% breakthrough is 324 mg. Since the column contains 8.1 g of a polymer, the specific capacity is 40.0 mg/g of separation medium or 21.6 mg/ml of column volume.

Effect of loading

In an ideal case, the chromatographic properties of a column are supposed to be independent of the loading within the limits of the total column capacity. Fig. 5 shows peaks for three different injections of chicken egg albumin eluted by a salt gradient. The loadings cover more than two orders of magnitude from 0.33 mg, to 3.75 mg to 62.5 mg. Despite the breadth of this loading range, the retention times for the three peaks are 14.4, 14.6 and 14.5 min, respectively. These almost identical retention times document the invariability of the retention characteristics of the rod column with loadings that span a very broad range of protein concentrations.

It should also be emphasized that the peak asymmetry at 10% height is very good for all of the elutions and does not exceed a value of 1.1. This is well demonstrated with the middle peak of Fig. 5 corresponding to 3.75 mg loading. Obviously, the peak for the highest loading is not shown in its entirety because it exceeds the

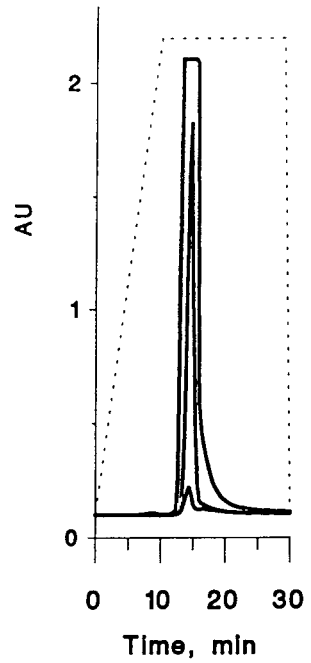

Fig. 5. Effect of column loading on the gradient elution of albumin. Conditions: column 300 × 8 mm I.D.; mobile phase gradient from 0.01 *M* Tris–HCl buffer pH 7.6 to 1 *M* NaCl in the buffer in 10 min; flow-rate 0.5 ml/min; albumin injections 0.3, 3.75 and 62.5 mg, UV detection at 280 nm.

set limits of the UV detector. Therefore, the major part of the tailing, that appears extensive at first glance, is actually in an acceptable range well below the 10% height.

Chemical stability

One of the major perceived limitations of methacrylate-based separation media is the alleged limited stability of their ester bonds to the alkaline conditions that are typically used for the cleaning of columns between operation cycles. It was shown elsewhere [22] that the ester groups can only be hydrolyzed using highly concentrated alkali metal hydroxide solutions at elevated temperatures. However, the column cleaning conditions are relatively mild when compared to those required for the hydrolysis. Therefore, column cleaning with dilute hydroxide is not expected to cause any change in the chemical structure of the modified rods or in their chromatographic properties. This was confirmed by a

series of experiments during which the column was washed four times with 0.1 *M* NaOH at room temperature for 12 h every other night while ovalbumin was used as a probe of column properties. During this period of time, no changes in retention time of ovalbumin were observed.

Chromatographic separations

The ultimate goal in the development of a separation medium is its use for separations. Fig. 6 shows the gradient elution of a protein mixture consisting of lysozyme, soybean trypsin inhibitor and conalbumin (2.5 mg of each). All of the proteins are baseline separated within less than 18 min and the symmetry of the peaks is again excellent. For example, the calculated peak asymmetry for trypsin inhibitor at 10% height is 1.04.

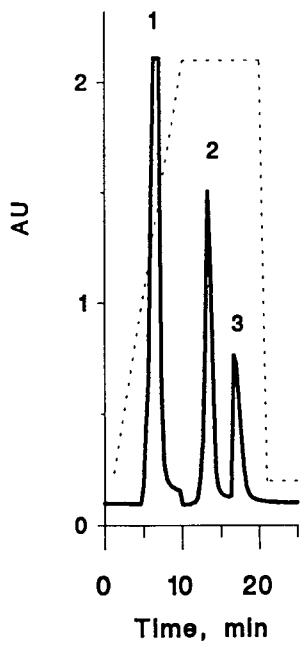

Fig. 6. Separation of lysozyme (1), soybean trypsin inhibitor (2) and conalbumin (3) by ion-exchange chromatography on modified continuous poly(glycidyl methacrylate–co-ethylene dimethacrylate) rod column. Conditions: column 300 × 8 mm I.D.; mobile phase gradient from 0.01 *M* Tris–HCl buffer pH 7.6 to 1 *M* NaCl in the buffer in 10 min; flow-rate 0.5 ml/min; total protein injection 7.5 mg, UV detection at 280 nm.

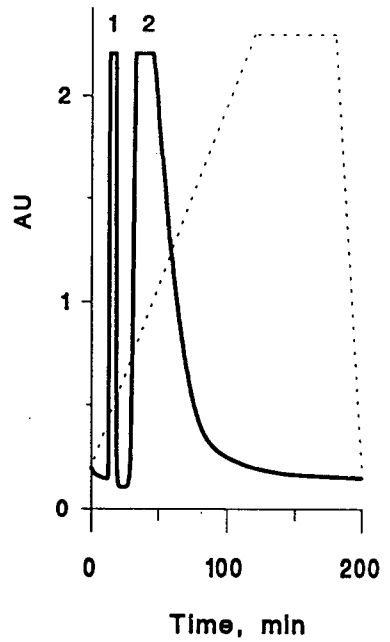

Fig. 7. Separation of bovine serum albumin (1) and chicken egg albumin (2) by ion-exchange chromatography on modified continuous poly(glycidyl methacrylate–co-ethylene dimethacrylate) rod column. Conditions: column 300 × 8 mm I.D.; mobile phase gradient from 0.01 *M* Tris–HCl buffer pH 7.6 to 1 *M* NaCl in the buffer in 120 min; flow-rate 0.5 ml/min; total protein injection 300 mg, UV detection at 280 nm.

High throughputs of the products are generally required for preparative separations. The use of high loadings is one of the options that leads to an increase in the productivity of the separation process. Fig. 7 shows the separation of a protein mixture that contains 66% chicken egg albumin and 33% bovine serum albumin. The total amount of proteins injected (300 mg) is close to the total capacity of the column as determined earlier with ovalbumin. However, baseline separation of both albumins is still achieved within 60 min using a shallow salt gradient (120 min from 100% buffer A to 100% buffer B).

4. Conclusions

We have demonstrated that "molded" columns can be used in a preparative mode for the

separation of larger quantities of proteins. Thus, rod columns with extended dimensions provide a viable alternative to the packed preparative columns. In addition to their ease of preparation, the major advantages of the continuous media are their better exploitation of the space within the column, their good efficiency even at high flow velocities, and their low pressure drop.

Although much remains to be done in the development of larger continuous rod columns, this early work shows their promising chromatographic properties and their great potential for large-scale separations. Further development of the molded rod columns is aimed at the introduction of new chemistries. Since the polymerization mixture involves only one phase, several limitations that restrict the use of some monomers for classical suspension polymerization do not apply for the preparation of the rods and numerous chemistries can be accessed directly by a polymerization. These will complement and expand significantly the chemistries currently available through the polymerization-and-modification process.

5. Acknowledgement

Support of this research by a grant of the National Institute of Health (GM 48364-02) is gratefully acknowledged. This work also made use of MRL Central Facilities supported by the National Science Foundation under Award No. DMR-9121654.

6. References

[1] T.B. Tennikova and F. Svec, *J. Chromatogr.*, 646 (1993) 279.
[2] J.A. Gerstner, R. Hamilton and S.M. Kramer, *J. Chromatogr.*, 596 (1992) 173.
[3] J.F. Kennedy and M. Paterson, *Polymer Int.*, 32 (1993) 71.
[4] Y. Yang, A. Velayudhan, C.M. Ladish and M.R. Ladisch *J. Chromatogr.*, 598 (1992) 169.
[5] L.C. Hansen and R.E. Sievers, *J. Chromatogr.*, 99 (1974) 123.
[6] V. Pretorius, J.C. Davidtz and D.H. Desty, *J. High Resolut. Chromatogr. Chromatogr. Commun.* 2 (1979) 583.
[7] S. Hjertén, J.-L. Liao and R. Zhang, *J. Chromatogr.*, 473 (1989) 273.
[8] J.-L. Liao, R. Zhang and S. Hjertén, *J. Chromatogr.*, 586 (1991) 21.
[9] S. Hjertén, K. Nakazato, J. Mohammad and D. Eaker, *Chromatographia*, 37 (1993) 287.
[10] J.M.J. Fréchet, *Makromol. Chem., Makromol. Symp.*, 70/71 (1993) 289.
[11] F. Svec and J.M.J. Fréchet, *Anal. Chem.*, 64 (1992) 820.
[12] Q.C. Wang, F. Svec and J.M.J. Fréchet, *Anal. Chem.*, 65 (1993) 2243.
[13] Q.C. Wang, F. Svec and J.M.J. Fréchet, *J. Chromatogr. A*, 669 (1994) 230.
[14] J. Matsui, T. Kato, T. Takeuchi, M. Suzuki, K. Yokoyama, E. Tamiya and I. Karube, *Anal. Chem.* 65 (1993) 2223.
[15] B. Sellergren, *Anal. Chem.*, 66 (1994) 1578.
[16] A.I. Liapis, *Math. Modelling Sci. Comput.*, 1 (1993) 397.
[17] A.E. Rodrigues, Z.P. Lu, J.M. Loureiro and G. Carta, *J. Chromatogr. A*, 653 (1993) 189.
[18] A.I. Liapis and M.A. McCoy, *J. Chromatogr. A*, 660 (1994) 85.
[19] N.B. Afeyan, N.F. Gordon, I. Mazsaroff, L. Varady, S.P. Fulton, Y.B. Yang and F.E. Regnier, *J. Chromatogr.*, 519 (1990) 1.
[20] N.B. Afeyan, S.P. Fulton and F.E. Regnier, *J. Chromatogr.*, 544 (1991) 267.
[21] S.P. Fulton, N.B. Afeyan and F.E. Regnier, *J. Chromatogr.*, 547 (1991) 452.
[22] J. Hradil and F. Svec, *React. Polym.*, 3 (1985) 91.

ELSEVIER

Journal of Chromatography A, 702 (1995) 97–112

JOURNAL OF CHROMATOGRAPHY A

Complete design of a simulated moving bed

Frédéric Charton, Roger-Marc Nicoud*

Séparex, B.P. 9, F-54250 Champigneulles, France

Abstract

The operating conditions of a simulated moving bed working under conditions of non-linear chromatography are difficult to find experimentally. A design procedure based on the modelling of multi-component chromatography is described. This rigorous and general procedure can be applied provided that basic data characterizing the experimental system are available. Even if the main parameters to be set are the flow-rates (one internal flow-rate and three out of four inlet/outlet flow-rates), it is explained how other free working parameters can be chosen. Special attention is paid to the column length, mobile phase velocity and particle size. It is shown how strongly they can influence the performance of a simulated moving bed.

1. Introduction

There is considerable interest in the preparative applications of liquid chromatography. In order to make the chromatographic process more attractive, attention is focused on the choice of the operating mode. Among the alternatives to the classical process (elution chromatography), much attention is currently being paid to the simulated moving bed (SMB) [1].

SMB technology was introduced in the late 1950s [2] and has mainly been applied to very large-scale production in the petrochemical and sugar industries [3]. However, separations of pharmaceutical compounds have recently been performed using an SMB [4,5] and other application areas are now opened up such as the fine chemistry, cosmetics and perfumes industries [6].

Different configurations of counter-current adsorption processes have been described [7]. However, the four-zone cascade of the Sorbex type [2] has been demonstrated to be the most efficient [8]. Fig. 1 shows a true moving bed (TMB) made of four zones; "true" refers to an actual circulation of solid and a zone is a coun-

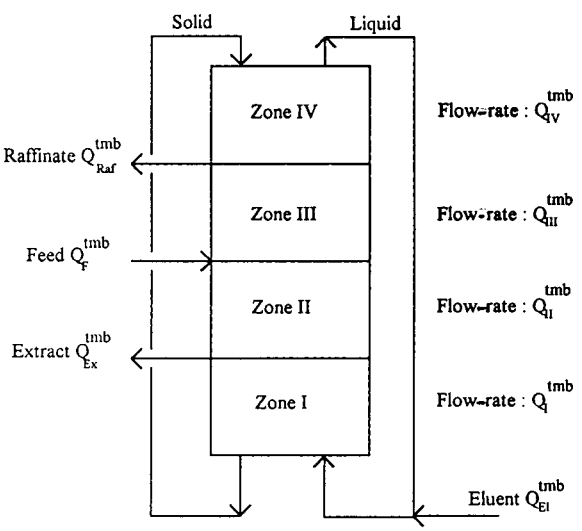

Fig. 1. Schematic representation of a four-zone TMB.

* Corresponding author.

0021-9673/95/$09.50 © 1995 Elsevier Science B.V. All rights reserved
SSDI 0021-9673(94)01026-9

ter-current absorber where the fluid flow-rate is constant and, as explained below, is bordered by an injection point and a collection point. A TMB allows one to perform continuous chromatographic fractionations of binary mixtures (or pseudo-binary mixtures) into two streams of pure components (or pseudo-components). Two inlet lines allow one to inject continuously the solution to be separated (feed) and the eluent. Two outlet lines (extract, raffinate) allow one to withdraw continuously the pure products. The liquid flowing out of zone IV is recycled to zone I, whereas the solid coming out of zone I is recycled to zone IV.

In fact, it is extremely difficult to operate a TMB because it involves the circulation of a solid adsorbent [7], which is why a simulated moving bed [2] is suitable. Most of the benefit of a true counter-current operation can be achieved by using several fixed-bed columns in series and an appropriate shift of the injection and collection points [7]. Fig. 2 shows a schematic representation of an SMB: each zone is divided into identical subsections (in practice, a subsection is a fixed-bed column) and, in order to simulate a counter-current flow, the feed, eluent, extract and raffinate lines are all moved one column forward in the fluid flow direction at fixed time intervals (period). The greater the number of subsections (or columns) per zone the closer is an SMB to a TMB. In fact, an SMB with a small number of columns per zone (usually 2–4) shows almost the same performances as a TMB [7].

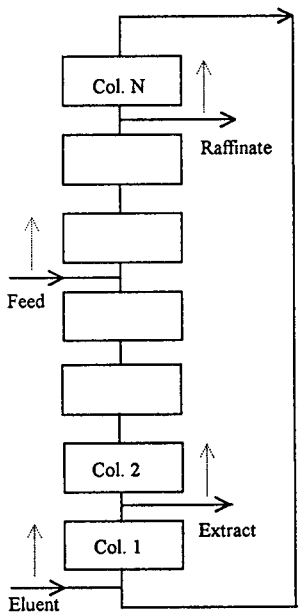

Fig. 2. Schematic representation of a four-zone SMB.

In this paper, we give the steps to be followed when designing an SMB which would allow one to process a given amount of feed per month. The procedure described is based on the modeling of non-linear chromatography, an experimental procedure being likely to fail unless the adsorption isotherms are linear (which is very uncommon in fact or means working at very low concentrations). It is a rigorous, versatile and general procedure. It mainly requires the determination of competitive adsorption isotherms, which is not so tedious and does not require as much work as is sometimes claimed. A few competitive adsorption data, measured using the mixture to be separated (the pure components are not necessary), are usually sufficient to find the operating conditions of an SMB [5].

The parameters we want to evaluate are the following: feed concentrations; number of columns per zone; column length, column diameter; particle size; and recycling (i.e., flow-rate occurring in zone I according to an arbitrary definition chosen in this paper) and inlet/outlet flow-rates. We assume that the following data are available, determined from a laboratory-scale study: equilibrium adsorption isotherms; relationship giving the height equivalent to a theoretical plate versus the mobile phase interstitial velocity u (Van Deemter equation); and relationship giving the pressure drop in the column (per unit length) $\Delta P/L$ versus the mobile phase velocity u (Kozeny–Carman equation).

2. Theory

2.1. TMB and SMB: two equivalent processes

The TMB and SMB concepts are similar. In fact, it has been shown that an SMB and hypothetical TMB whose operating conditions are

Table 1
Relationship between an SMB and its corresponding TMB

TMB	SMB
Steady state	Periodic steady state
Solid flow-rate	Periodic shift of the injection/collection lines
$\dot{M}$	$\Delta T = \frac{(1-\varepsilon)V_c}{\dot{M}}$
Internal flow-rates	Internal flow-rates
Q_k^{tmb} k = I, II, III or IV	$Q_k^{smb} = Q_k^{tmb} + \frac{\varepsilon}{1-\varepsilon} \cdot \dot{M}$
Eluent, extract, feed, raffinate flow-rates	Eluent, extract, feed, raffinate flow-rates
$Q_{El}^{tmb}/Q_{Ex}^{tmb}/Q_F^{tmb}/Q_{Raf}^{tmb}$	$Q_{El}^{smb}/Q_{Ex}^{smb}/Q_F^{smb}/Q_{Raf}^{smb}$

related through the rules in Table 1 [7] have very close performances [9]. Knowing that optimum operating conditions can be found directly for a TMB and that to simulate this kind of process leads to much shorter computation times, it is in our interest to take advantage of this similitude when designing an SMB. Consequently, the design of an SMB should as far as possible resort to the study of its corresponding hypothetical TMB.

The rules in Table 1 just mean that the velocity of the liquid relative to the solid is kept constant. V_c is the volume of one SMB column. The inlet/outlet flow-rates of an SMB and its corresponding TMB are identical. An SMB does not exactly work in a steady state but in a periodic steady state: during a given period, the internal concentration profiles vary, but the internal profiles examined at the same time for two successive periods are identical (except for a one-column translation).

It must be pointed out that a TMB internal concentration profile and consequently some of its performance (the extract and raffinate concentrations and the eluent consumption), depends on only four dimensionless internal flow-rates defined as $q_k^{tmb} = Q_k^{tmb}/\dot{M}$ (k = I, II, III or IV) and no longer on the solid flow-rate.

The average SMB and TMB internal flow-rates Q_m^{smb} and Q_m^{tmb} are related through

$$Q_m^{smb} = Q_m^{tmb} + \frac{\varepsilon}{1-\varepsilon} \cdot \dot{M} = \left(q_m^{tmb} + \frac{\varepsilon}{1-\varepsilon}\right) \dot{M} \quad (1)$$

where

$$Q_m^{tmb} = \frac{\sum_{k=1}^{4} Q_k^{tmb}}{4} = \frac{\dot{M} \sum_{k=1}^{4} q_k^{tmb}}{4} \quad (2)$$

The SMB average interstitial mobile phase velocity is defined relative to Q_m^{smb} as

$$Q_m^{smb} = \varepsilon u_m \Omega \quad (3)$$

where ε is the bed external porosity and Ω the column cross-section.

2.2. Adsorption isotherms

In the case of a single-component system, the adsorption isotherm gives the concentration in the stationary phase $\bar{C}$ versus the mobile phase concentration C when equilibrium is reached, at a given temperature. Even if it can sometimes be linear in a wide concentration range, the $\bar{C}$ vs. C relationship is usually not linear.

In the case of a multi-component mixture, there is usually a competition between the various compounds to access to the adsorption sites. Consequently, $\bar{C}_i$ does not only depend on C_i

but on all liquid-phase concentrations. Each component adsorption isotherm is a relationship of the type $\bar{C}_i = \bar{C}_i(C_1, C_2, \ldots)$.

Many different isotherm equations have been described [10]. Even though it has been challenged because it does not agree with the Gibbs' adsorption isotherm unless all saturation capacities are identical [11], the competitive Langmuir isotherm is often used:

$$\bar{C}_i = \frac{\bar{N}\tilde{K}_i C_i}{1 + \sum_j \tilde{K}_j C_j} \tag{4}$$

where $\bar{N}$ is the saturation capacity, assumed here to be equal for all components, and $\tilde{K}_i$ is a numerical coefficient quantifying the affinity of the solute towards the solid.

In fact, the Langmuir isotherm often fails to fit experimental data and more complex isotherms, such as the modified competitive Langmuir [4] or bi-Langmuir isotherm [12], are suitable. This is especially true with systems exhibiting concentration-dependent apparent selectivities $(\bar{C}_j/C_j)/(\bar{C}_i/C_i)$.

2.3. Equilibrium stage model

Many different models have been applied to the modelling of chromatographic processes [1]. The equilibrium stage model has been shown to be suitable under the usual conditions of high-performance preparative chromatography [13].

The column is considered as an association of cells in series. The adsorption equilibrium is assumed to be reached in each cell, called the equilibrium stage or plate. The broadening effects, linked to the mass transfer kinetics and to the hydrodynamics, are lumped together and are quantified by the number of theoretical plates N which can be derived from an "analytical" pulse injection.

In the case of fixed-bed operations (elution chromatography, SMB, etc.), the mass balance equation for a component i over a plate k is

$$C_{i,k-1} = C_{i,k} + \tau \cdot \frac{dC_{i,k}}{dt} + \tau \cdot \frac{1-\varepsilon}{\varepsilon} \cdot \frac{d\bar{C}_{i,k}}{dt} \tag{5}$$

where τ is the mean residence time of the mobile phase in a plate and ε the external porosity, which is usually in the range 0.35–0.45.

The equilibrium stage concept can also be applied to true moving bed adsorbers [14]. The mass balance equation of a component i over a plate k is

$$C_{i,k-1} + \frac{\dot{M}}{Q} \cdot \bar{C}_{i,k+1} = C_{i,k} + \frac{\dot{M}}{Q} \cdot \bar{C}_{i,k} + \tau \cdot \frac{dC_{i,k}}{dt} + \frac{(1-\varepsilon)}{\varepsilon} \cdot \tau \cdot \frac{d\bar{C}_{i,k}}{dt} \tag{6}$$

where Q and $\dot{M}$ are the fluid and solid flow-rates.

Various numerical methods are available to solve first-order differential equations such as Eqs. 5 and 6 when associated with a set of boundary and initial conditions [15]. We use the Gear's algorithm [16] implemented in the software LSODI belonging to the ODEPACK package [17], which is suitable here because it can handle "stiff" variations of the concentrations.

The steady state of a TMB can be calculated directly without solving Eqs. 6, which leads to much shorter computation times. Assuming the TMB steady state, Eqs. 6 can be simplified into Eqs. 7 when cancelling the accumulation terms:

$$QC_{i,k-1} + \dot{M}\bar{C}_{i,k+1} = QC_{i,k} + \dot{M}\bar{C}_{i,k} \tag{7}$$

where $\bar{C}_{i,k}$ and $C_{i,k}$ are related through the isotherm equations. Eqs. 7 are coupled non-linear algebraic equations and can be solved using a Newton–Raphson method [18].

2.4. Height equivalent to a theoretical plate

The height equivalent to a theoretical plate, H, is defined as

$$H = \frac{L}{N} \tag{8}$$

where L is the column length. It can be related to the experimental system parameters through the Van Deemter [19] or Knox [20] equations, which especially give H as a function of the interstitial mobile phase velocity u. In the case of preparative chromatography, where relatively

high velocities are used, these equations can often be simplified into a linear relationship [21–23]:

$$H = a + bu \tag{9}$$

The parameters a and b are related to the diffusion coefficient, porosity, mass transfer parameters, etc. If internal diffusion is the main resistance to mass transfer, their dependence on the particle diameter d_p is given by [24]:

$$a = Ad_p \tag{10}$$

$$b = Bd_p^2 \tag{11}$$

2.5. Pressure drop

The Kozeny–Carman equation is suitable for the laminar flows met with in chromatography:

$$\frac{\Delta P}{L} = h_k \cdot \frac{36}{d_p^2}\left(\frac{1-\varepsilon}{\varepsilon}\right)^2 \mu u = \frac{\varphi}{d_p^2} u = \Phi u \tag{12}$$

where h_k is the Kozeny coefficient (close to 4.5) and μ the eluent viscosity.

3. Results and discussion

The general procedure we use to design an SMB is described in Fig. 3. It mainly resorts to the equivalence between an SMB and its hypothetical corresponding TMB, as explained previously.

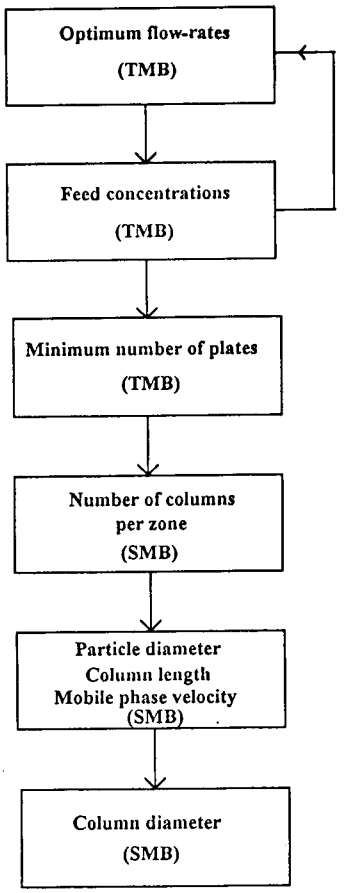

Fig. 3. Design of a simulated moving bed: procedure.

3.1. TMB optimum flow-rates

For a given feed composition, optimum flow-rates, i.e., giving the highest productivity and the lowest eluent composition, are estimated first for an "ideal system", which mainly means that kinetic and hydrodynamic dispersive effects are assumed to be negligible.

The conditions to be applied to TMB internal flow-rates have been broadly described [7]. In preparative chromatography, high feed concentrations are suitable and lead to non-linear adsorption behaviour. The non-linear (and related competitive) effects must be taken into account when evaluating the flow-rates. This issue has been barely addressed in the literature [25,26]. It is outside the scope of this paper to describe exactly the calculation procedure.

As an example, Fig. 4 gives the feed and eluent flow-rates versus the feed concentrations for the following competitive Langmuir isotherms: $\bar{N} = 100\,\mathrm{g/l}$, $\tilde{K}_1 = 0.030$, $\tilde{K}_2 = 0.036$ ($\alpha = \tilde{K}_2/\tilde{K}_1 = 1.2$), when a total separation is sought. It shows how strongly the choice of the flow-rates is influenced by the feed concentrations.

At this point, for any given feed concentrations, the following flow-rates are available: q_k^{tmb}, q_F^{tmb}, q_{El}^{tmb}, q_{Ex}^{tmb}, q_{Raf}^{tmb}.

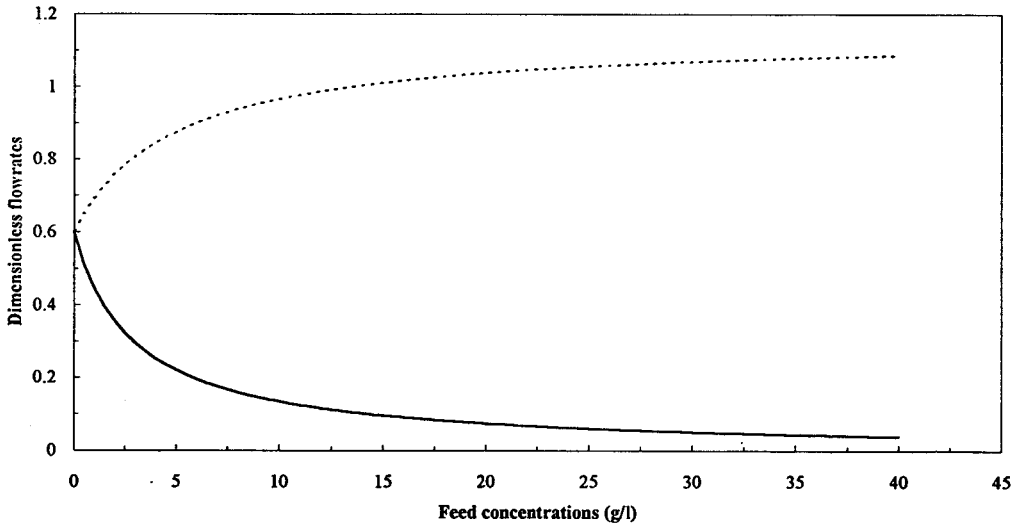

Fig. 4. Influence of the feed concentrations on an "ideal" TMB dimensionless feed (q_F^{tmb}) and eluent (q_{El}^{tmb}) flow-rates. Case of a 1:1 binary mixture with competitive Langmuir isotherms ($\tilde{N} = 100$ g/l, $\tilde{K}_1 = 0.030$ l/g, $\tilde{K}_2 = 0.036$ l/g). The continuous and dotted lines correspond to the feed and eluent flow-rates, respectively.

3.2. Feed concentrations

The feed concentrations have a strong influence on the SMB performances and must be well chosen. The productivity and the eluent composition are two main economic criteria involved in chromatographic processes [27]. Their variations versus the feed concentrations can be checked in order to choose an appropriate feed composition.

This study can be quickly carried out for an "ideal" TMB as mentioned in the previous section. For instance, Fig. 5 shows the variations of the productivity, written as $Q_F^{tmb} C_i^F$ assuming $\dot{M} = 1$ l/h, and of the eluent consumption in the case of the binary system of Fig. 4. The eluent

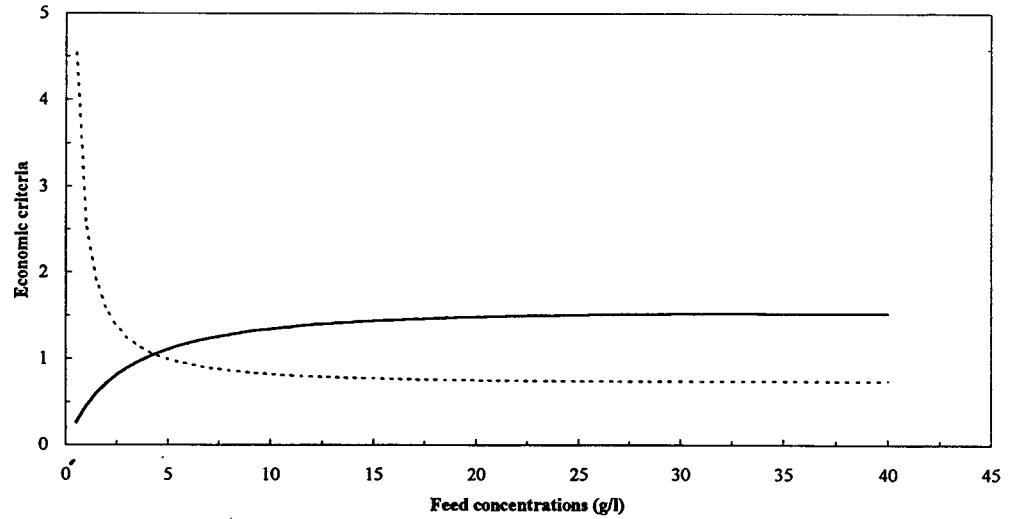

Fig. 5. Influence of the feed concentrations on an "ideal" TMB performance: dotted line, eluent consumption; continuous line, productivity for $\dot{M} = 1$ l/h. Experimental system as in Fig. 1.

consumption is the volume of eluent used to recover a unit mass of pure product and can be evaluated as $(Q_{El}^{tmb} + Q_F^{tmb})/Q_F^{tmb}C_i^F$. The productivity and eluent consumption have been derived from the flow-rates given in Fig. 4.

The productivity increases and the eluent consumption decreases when C_i^F increases; the variations are usually rather steep in the low concentration range and very smooth otherwise. As a consequence, low injection concentrations will have to be avoided. However, even if achievable, very high concentrations will not be suitable because as soon as concentrations are high enough the performances of the TMB (or SMB) are almost constant and very high concentrations can lead to a very low feed flow-rate, which might be difficult to control.

3.3. Number of plates requirement

The flow-rates given in Fig. 4 lead to 100% purities in the case of an "ideal" TMB. The approach used here is to keep these flow-rates and to seek the minimum number of plates N_m required to reach purities as high as 99%.

This procedure is sensible because it has been demonstrated that the performances of a TMB or SMB are only slightly sensitive to the number of plates [9]. In most instances, the number of plates required can easily be achieved and optimum flow-rates are then available.

The steady state of a TMB is calculated, as explained in the Theory section, for different numbers of theoretical plates, an identical number of plates in each zone being assumed. The extract and raffinate purities are derived from each numerical simulation.

Fig. 6 shows the evolution of the extract and raffinate purities versus the TMB total number of plates in the case of the system studied in Fig. 4 for a total feed concentration of 40 g/l; in the present instance, a TMB made of 400 plates (100 per zone) would give purities as high as 99%.

Fig. 7, which was constructed from numerical simulations, gives N_m as a function of the selectivity α and of the feed concentration, written as a dimensionless number $\tilde{K}_1 C_1^F$, in the case of competitive Langmuir isotherms and of a 1:1 binary mixture. Fig. 7 confirms that a very small number of plates is sufficient to obtain the purities expected, provided that conditions of linear chromatography do not prevail, i.e., when $\tilde{K}_1 C_1^F$ does not tend towards zero.

It must be understood that Fig. 7 can be used for all binary Langmuir isotherms provided that the saturation capacity is identical for the two

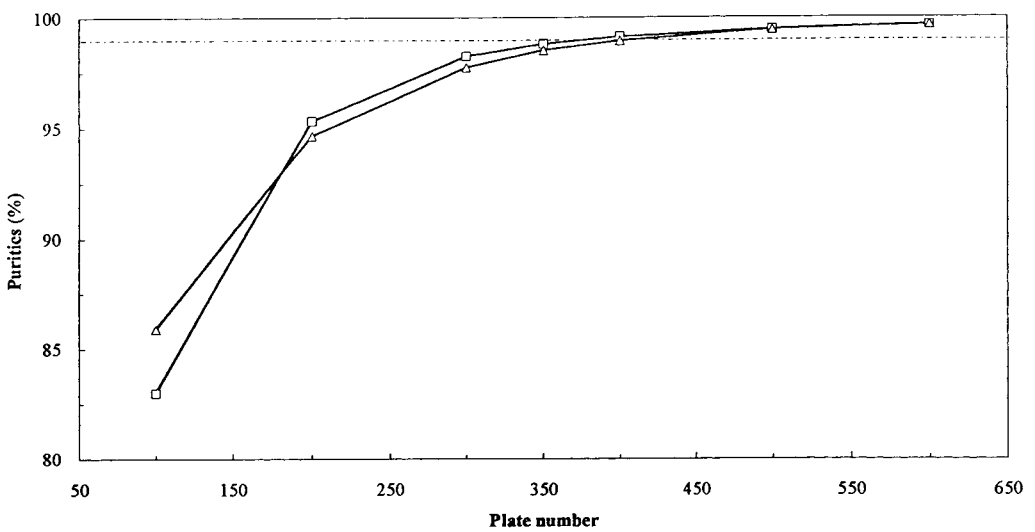

Fig. 6. Evolution of a TMB (□) extract and (△) raffinate purities as functions of the total number of plates. A TMB made of four identical zones (same number of plates per zone) is assumed. Case studied in Fig. 2 with $C_1^F = C_2^F = 20$ g/l.

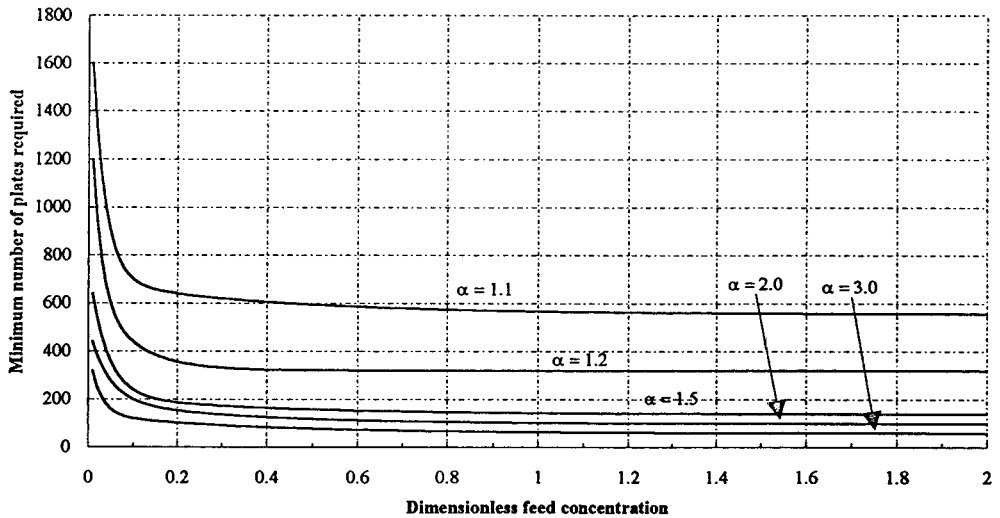

Fig. 7. Minimum number of plates required to reach purities higher than 99% as a function of the selectivity α and of the dimensionless feed concentration $\tilde{K}_1 C_1^F$. Case of 1:1 binary mixtures and competitive Langmuir isotherms with equal saturation capacities.

components. Actually, when introducing dimensionless concentrations $X_{i,k} = \tilde{K}_{i,k} C_{i,k}$ and $Y_{i,k} = \bar{C}_{i,k}/\bar{N}$ into Eqs. 6 in the steady state, it can be proved that N_m depends only on α, $\tilde{K}_1 C_1^F$ and the composition.

3.4. Number of columns per zone

The only way to estimate the number of columns per zone, N_c, is to perform numerical simulations of an SMB including the shift of the injection and collection points at regular time intervals. This kind of calculation can be performed using dummy values of the column volume and TMB solid flow-rate (to estimate the period ΔT). The SMB flow-rates are derived from the TMB flow-rates according to the rules summarized in Table 1.

For the system examined here, it was found out that an eight-column configuration (two columns per zone) was suitable. Fig. 8 compares the SMB (at the half-time period when the periodic steady state is reached) and TMB internal concentration profiles, confirming that the two processes have very close performances.

3.5. Column length and mobile phase velocity for a given particle size

We show here that there is an optimum choice of the column length L and of the average mobile phase velocity u_m which must fulfil plate number and pressure drop constraints.

In a previous section, a minimum number of plates requirement was derived in the case of a TMB made of four identical zones. In the case of an SMB, the internal flow-rate is different from one zone to another. Consequently, assuming identical columns, the number of plates for each column depends on its position (in zone I, II, III or IV). The plate number requirement should be applied to zone I where the internal flow-rate is the highest. However, in practice and for the sake of understanding, the plate number requirement can be applied relatively to the average number of plates per column (estimated with u_m). According to Eqs. 8 and 9, the plate number condition is fulfilled provided that

$$\frac{L}{a + bu_m} \geqslant \frac{N_m}{4N_c} \tag{13}$$

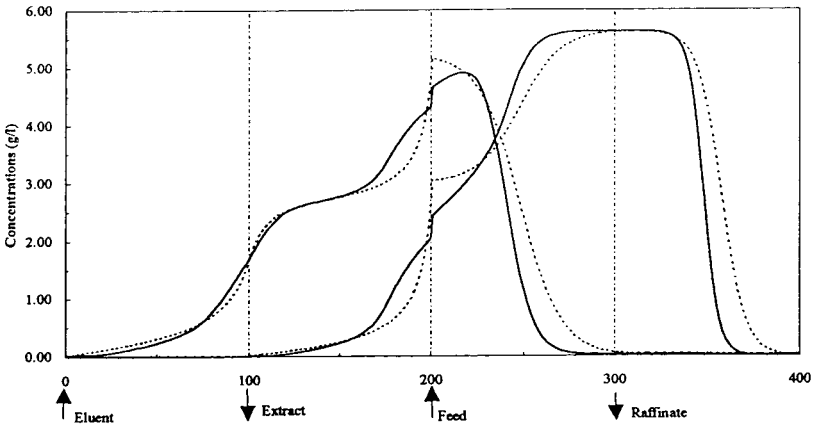

Fig. 8. Comparison between the internal concentration profiles of an SMB (at half-time period in steady state, continuous lines) and of its corresponding TMB (dotted lines). Case studied in Fig. 2 with $C_1^F = C_2^F = 20$ g/l. Total number of plates = 400, i.e., 100 plates per zone for the TMB and eight columns with 50 plates for the SMB.

which is equivalent to

$$\frac{L}{u_m} \geqslant \frac{N_m}{4N_c} \cdot \left(\frac{a}{u_m} + b\right) \tag{14}$$

The pressure drop condition leads to the following equation, which compares the pressure drop in the system (given according to Eq. 12) to the maximum pressure acceptable, P_{max}:

$$\frac{L}{u_m} \leqslant \frac{P_{max}}{4N_c} \cdot \frac{1}{\Phi u_m^2} \tag{15}$$

The hatched area of Fig. 9 gives all the

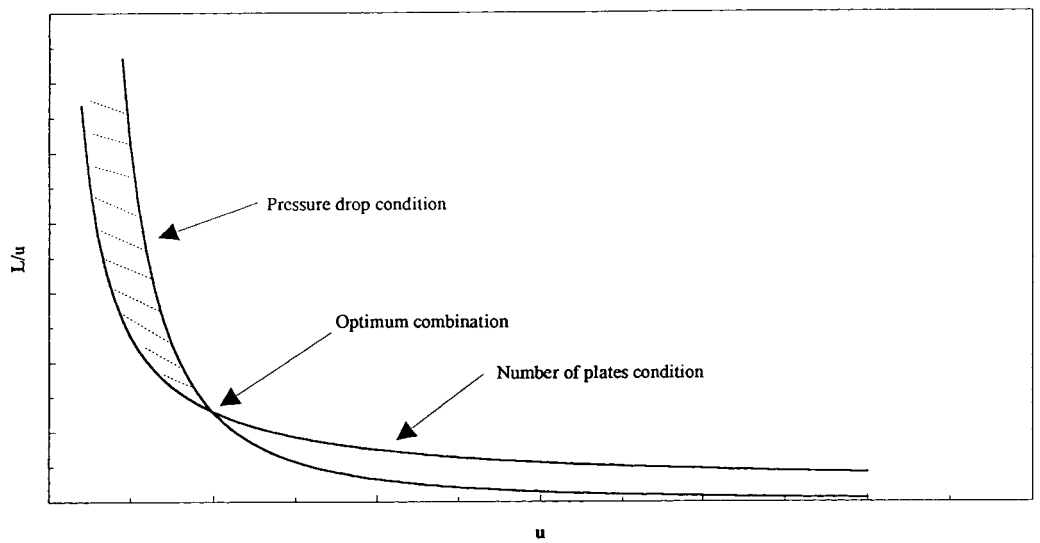

Fig. 9. Schematic representation of the possible values of the ratio L/u_m as a function of u_m. Definition of the optimum combination (L, u_m).

possible values of L/u_m fulfilling simultaneously Eqs. 14 and 15. Every point of this hatched area corresponds to a combination (L, u_m).

The choice of the optimum combination is related to the economic criteria. The eluent consumption can be written as

$$V_i = \frac{Q_{El}^{smb} + Q_F^{smb}}{Q_F^{smb} C_i^F} = \frac{Q_{El}^{tmb} + Q_F^{tmb}}{Q_F^{tmb} C_i^F} = \frac{q_{El}^{tmb} + q_F^{tmb}}{q_F^{tmb} C_i^F} \quad (16)$$

It depends only on the TMB dimensionless internal flow-rates, which themselves depend only on the adsorption isotherms and on the feed concentrations.

The productivity can be estimated from

$$Pr_i = \frac{Q_F^{smb} C_i^F}{4N_c \varepsilon V_c} \quad (17)$$

and can also be written as Eq. 18 on replacing $\dot{M}$ by u_m according to Eqs. 1 and 3 and keeping in mind that $Q_F^{smb} = Q_F^{tmb}$:

$$Pr_i = \frac{q_F^{tmb} \dot{M} C_i^F}{4N_c \varepsilon V_c} = \frac{q_F^{tmb} C_i^F}{4N_c \left(q_m^{tmb} + \frac{\varepsilon}{1-\varepsilon} \right)} \cdot \frac{1}{\frac{L}{u_m}} \quad (18)$$

where q_F^{tmb} and q_m^{tmb} depend only on the isotherms and on the feed concentrations.

Eq. 18 proves that the highest productivity is reached for the smallest value of L/u_m compatible with the pressure drop and plate number conditions. As shown in Fig. 9, the optimum value of L/u_m is met when the two inequalities corresponding to Eqs. 14 and 15 are just fulfilled.

The optimum average mobile phase velocity is the positive root of a quadratic equation and is given by

$$u_m = \frac{1}{2} \left[-\frac{a}{b} + \sqrt{\left(\frac{a}{b}\right)^2 + \frac{4P_{max}}{b\Phi N_m}} \right] \quad (19)$$

The optimum column length and ratio L/u_m can be derived from

$$L = \frac{1}{2} \cdot \frac{N_m}{4N_c} \left[a + b\sqrt{\left(\frac{a}{b}\right)^2 + \frac{4P_{max}}{b\Phi N_m}} \right] \quad (20)$$

$$\frac{L}{u_m} = \frac{N_m}{4N_c} \left[\frac{2a}{-\frac{a}{b} + \sqrt{\left(\frac{a}{b}\right)^2 + \frac{4P_{max}}{b\Phi N_m}}} + b \right] \quad (21)$$

Eq. 21 justifies the procedure followed here to design an SMB and especially the choice of the "minimum number of plates required". Actually, if the plate number is higher than N_m, L/u_m will be higher and the productivity lower. If the plate number is lower than N_m, the flow-rates of an "ideal" TMB no longer allow one to reach the purities expected. Other flow-rates have to be found. In any case, the feed flow-rate will be lower whereas the eluent flow-rate will be higher, leading to an increase in eluent consumption and possibly to a decrease in productivity.

The productivity refers here to the amount of purified product recovered per unit time and unit value of stationary phase immobilized. Another definition of the productivity has also been used in the literature [28]. It refers to the amount of purified product collected per unit time and per unit section column. It can easily be shown, following the same idea, that the two definitions of the productivity lead to the same optimum combination (L, u_m).

As examples, Table 2 shows various ways to reach the 400 plates required for the separation studied in this paper. The results are given for two different stationary phases: high efficiency means 2500 plates for an analytical column (25 cm × 0.46 cm I.D.) with an eluent flow-rate of 1 ml/min and a 10-μm particle size; low efficiency

Table 2
Optimum combination (L, u_m): influence of the stationary phase efficiency

Parameter	High-efficiency phase		Low-efficiency phase	
d_p (μm)	10	40	10	40
u_m (cm/s)	1.1	1.1	0.35	0.36
L (cm)	1.9	29.2	5.9	93.0
L/u_m (s)	1.7	25.8	16.7	258.3

$H(\text{cm}) = 2d_p$ (cm) + 31 870 (or 318 700)$d_p^2 u$ (cm/s). ΔP (bar) = $[3.65 \cdot 10^{-6}/d_p^2\,(\text{cm}^2)] \cdot L(\text{cm}) \cdot u(\text{cm/s})$, i.e., $h_k = 4.5$, $\varepsilon = 0.4$, $\mu = 10^{-3}$ Pa s, $P_{max} = 60$ bar.

means 250 plates for the same experimental conditions. In fact, high efficiency refers to stationary phases such as silica (bonded or not), whereas low efficiency refers to some solid phases used to separate enantiomers (microcrystalline cellulose triacetate). The parameters used in Eqs. 9 and 12 to generate these results are given in Table 2 and are typical experimental values.

As mentioned above, the SMB number of plates requirement is very often weak, and the optimum combination can sometimes lead to unrealistic column lengths, as shown in Table 2. This is especially true in the case of industrial-sized columns with large diameters; as an example, a minimum column length of 5–10 cm would be required for a 20 cm I.D.

3.6. Particle size

In this section, the choice of the particle size is studied. To justify our way of arguing, it is necessary to note that similar stationary phases with different particle sizes usually have the same properties (e.g., specific pore volume, specific interfacial area, ligand concentrations). The adsorption isotherms should be independent of the bead diameter [28].

Again, the economic criterion to be optimized is the productivity as written according to Eqs. 17 and 18, keeping in mind that for each bead diameter the optimum combination (L, u_m) is given by Eqs. 19–21.

Substituting a by Ad_p and b by Bd_p^2 in Eq. 21, it is possible to study the influence of the particle size on the optimum value of L/u_m:

$$\frac{L}{u_m} = \frac{N_m}{4N_c} \cdot \left[\frac{2Ad_p}{-\frac{A}{Bd_p} + \sqrt{\left(\frac{A}{Bd_p}\right)^2 + \frac{4P_{max}}{B\varphi N_m}}} + Bd_p^2 \right] \quad (22)$$

It can be proved that L/u_m tends toward a minimum value $\varphi(AN_m)^2/4N_cP_{max}$ when d_p tends towards zero, whereas it tends towards ∞ when d_p tends towards ∞. These are two mathematical limits and it must be kept in mind that Eq. 11 is certainly no longer valid when d_p is too small. Eq. 22 shows that there is interest in using particles that are as small as possible.

However, it has been mentioned previously that unrealistic column lengths can be reached when applying Eqs. 19–21 in the case of high-efficiency stationary phases. A minimum column length condition often has to be taken into account. The choice of an optimum particle size is related to this latter condition. The equation $L = L_{min}$, where L depends on d_p according to Eq. 20 and L_{min} is the minimum column length acceptable, has to be solved.

As examples, Table 3 gives the optimum values of the particle diameter for the high-efficiency stationary phase in Table 2 for different minimum lengths acceptable. It also compares the values of the ratio L/u_m found for other particle diameters. For a given column length, if the beads are too small, the mobile phase velocity is limited by the pressure drop. If the particles are too large, the velocity must be kept small because of the number of plates

Table 3
Choice of the optimum particle size according to the minimum column length acceptable

Parameter	L_{min} = 10 cm			L_{min} = 20 cm		
d_p (μm)	10	23 (optimum)	40	20	33 (optimum)	60
u_m (cm/s)	0.21	1.12	0.37	0.41	1.13	0.33
L/u_m (s)	48.8	8.9	26.6	48.8	17.7	59.2

condition. Table 3, which gives realistic figures, show how critical the choice of the particle diameter can be. Of course, all bead diameters are not commercially available and the choice should be made as close to the optimum as possible.

Endele et al. [22] studied the influence of the particle size of spherical silica on column efficiencies. They found $b = Bd_p^{1.5}$ instead of $b = Bd_p^2$ as assumed here. In fact, Eq. 11 is valid when internal diffusion is the main limitation to mass transfer. However, this difference does not alter the qualitative results found, even if it could change Eq. 22.

The conclusions of this section do not take into account the influence of the particle size on the price of the stationary phase. To do so, another definition of the productivity including this effect, i.e., amount of pure compound recovered per unit time and unit price of stationary phase immobilized, could be used and the same study could be undertaken.

3.7. Column diameter

Let us assume a column of 1 cm^2 section. The average mobile phase velocity u_m being set at its optimum value, the solid flow-rate is derived from Eqs. 1 and 3. The corresponding feed flow-rate is derived from the relationship $Q_F^{smb} = Q_F^{tmb} = q_F^{tmb}\dot{M}$.

The solid and feed flow-rates are proportional to the column section. Consequently, the minimum column section required to process m_F g of feed per hour is derived from

$$\Omega = \frac{m_F}{Q_F^{smb}(C_1^F + C_2^F)} \tag{23}$$

where Ω is in cm^2, Q_F^{smb} in l/h, C_i^F in g/l and Q_F^{smb} is the feed flow-rate injected in a column of 1 cm^2 section.

Finally, a new value of the solid flow-rate can be calculated and the SMB operating flow-rates can be deduced from the "equivalence" rules summarized in Table 1.

3.8. Experimental applications

The procedure described in this paper has been demonstrated to be effective for many different separations performed using an SMB [4,5]. In this section, we focus on the resolution of the EMD 53986 enantiomers (a synthesis chiral intermediate from Merck, Darmstadt, Germany [29]).

The separation is performed at 25°C on 20–45-μm Cellulspher, a chiral stationary phase prepared from cellulose tri(*p*-methylbenzoate) according to a Ciba-Geigy patent [30], using pure methanol as the mobile phase. It is achieved on a Licosep 12–26, an SMB made of up to twelve Superformance columns (Merck) of 26 mm I.D. and manufactured by Separex (Champigneulles, France). The objective of the separation is to recover each of the enantiomer with a very high purity (close to 99%).

Determination of isotherms

Binary competitive adsorption data are measured using an analytical column (150 × 4.6 mm I.D.) at 25°C, according to the "adsorption–desorption" procedure [10]. The following parameters are found:

$$\bar{C}_1 = 3.96C_1 + \frac{7.07C_1}{1 + 0.140C_1 + 0.317C_2}$$

(less retained enantiomer) (24)

$$\bar{C}_2 = 3.96C_2 + \frac{15.96C_2}{1 + 0.140C_1 + 0.317C_2}$$

(more retained enantiomer) (25)

The agreement between the experimental and calculated values of the solid-phase concentrations is shown in Fig. 10.

Choice of feed concentrations

In the present case, the solubility of the racemic mixture is limited to 8 g/l. The feed concentrations $C_1^F = C_2^F = 3.75$ g/l are chosen.

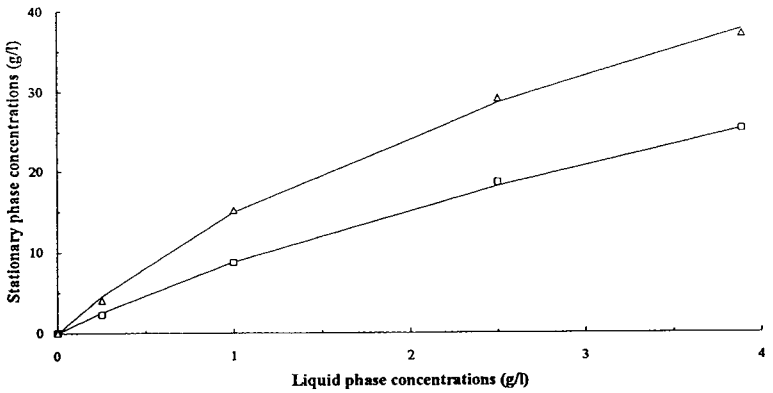

Fig. 10. Separation of EMD 53986 enantiomers. Comparison between experimental and calculated binary competitive adsorption data. Experimental data: △ = More retained enantiomer; □ = less retained enantiomer. Lines = data calculated.

TMB optimum flow-rates

Optimum dimensionless flow-rates are calculated for a hypothetical "ideal" TMB made of an infinite number of plates and a feed composition $C_1^F = C_2^F = 3.75$ g/l. The following operating flow-rates are found: $q_I^{tmb} = 19.92$, $q_{II}^{tmb} = 8.76$, $q_{III}^{tmb} = 11.16$, $q_{IV}^{tmb} = 8.66$. They can also be written as $q_I^{tmb} = 19.92$, $q_{Ex}^{tmb} = 11.16$, $q_F^{tmb} = 2.40$, $q_{Raf}^{tmb} = 2.50$.

Minimum number of plates required

Using the previous flow-rates, the steady state of a "real" TMB is calculated for increasing numbers of plates until the extract and raffinate purities are high enough. In the present case, 200 plates (50 per zone) lead to purities higher than 99%.

Number of columns per zone

An SMB with a total number of plates of 200 is assumed. The influence of the number of columns per zone is checked through numerical simulations (of an SMB) with dummy values of the column volume and solid flow-rate. The columns are assumed to be identical, equivalent to the same number of theoretical plates (i.e., $200/4N_c$ here). The flow-rates applied to the SMB are derived from the rules in Table 1 and using the "TMB optimum flow-rates". Table 4 gives the extract and raffinate purities calculated for various configurations of the process. As can be seen, an eight-column configuration is suitable. It must be pointed out that different numbers of columns could be implemented in each zone, but this possibility is not checked here.

Particle diameter, column length, mobile phase velocity

The particle size is not a free parameter. The optimum mobile phase velocity and column length, allowing one to reach 200 plates for eight columns in series and a maximum acceptable pressure of 40 bar, are sought. They are derived

Table 4
Influence of the number of columns per zone on the SMB performance

No. of columns per zone	Extract purity (%)	Raffinate purity (%)
1	96.4	99.2
2	99.6	99.8
3	99.7	99.9

from the following experimental equations and from Eqs. 19–22:

$$H\,(\mathrm{cm}) = 1.35u\,(\mathrm{cm/s}) + 0.01 \quad (26)$$

$$\Delta P = 2.41u\,(\mathrm{cm/s}) \quad (27)$$

In the case studied, an average velocity u_m = 0.244 cm/s and an 8.5 cm column length are suitable.

The solid flow-rate is then estimated from Eqs. 1 and 3. With a porosity of 0.358, the solid flow-rate is $\dot{M} = 2.20$ ml/min. The SMB operating conditions are calculated using Table 1: ΔT = 13.2 min, $Q_I^{smb} = 44.9$ ml/min, $Q_{Ex}^{smb} = 24.4$ ml/min, $Q_F^{smb} = 5.4$ ml/min, $Q_{Raf}^{smb} = 5.5$ ml/min.

Fig. 11 compares the SMB internal profiles, measured experimentally and calculated at the half-time period when the periodic steady state is reached. Fairly good agreement is obtained; the purities are slightly lower than expected (close to 97%). The purities can be increased, however, by slight adjustment of the flow-rates around the values evaluated first through the procedure described in this paper.

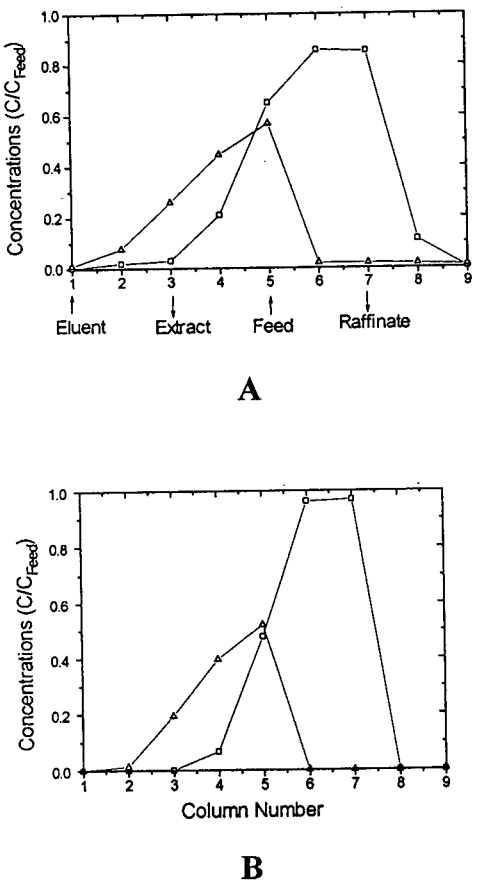

Fig. 11. Separation of EMD 53986 enantiomers. Comparison between the SMB (A) experimental (obtained on a Licosep 12–26) and (B) calculated internal concentration profiles. △ = More retained enantiomer; □ = less retained enantiomer.

4. Conclusions

A procedure allowing the design of an SMB has been described and the different steps to be followed have been briefly explained. The procedure can be used provided that data that can be determined according to classical experimental methods characterizing the system studied are available. It is general and can be applied to almost any kind of isotherm. It is a fast design procedure because it is not based on numerical empiricism, i.e. on a numerical "trial and error" method, but on an a priori guess of the flow-rates.

It has been shown that not only do the flow-rates have to be chosen carefully, but also other parameters such as the column length, the mobile phase velocity and the particle size. For a given bead diameter, the optimum column length and mobile phase velocity have been derived. Because an SMB does not require a high number of theoretical plates to work efficiently, the small particles used in classical preparative HPLC (i.e., in the 10–20-μm range) can lead to an unrealistic optimum column length. In this case, it has been proved that larger particles should be used. In fact, there is an optimum particle size related to the minimum column length condition.

The procedure described here is not only theoretical, it has been applied (at least partly) routinely to pilot-scale separations (i.e., with 2.5 cm I.D. columns) for a few years and we have begun to use it experimentally for industrial-scale separations (i.e., with 20 cm I.D. columns).

Symbols

a, b, A, B	coefficients relating the height equivalent to a theoretical plate to the mobile phase velocity (cm, s^{-1}, dimensionless, $cm^{-2}s^{-1}$, respectively)
C, C_i	mobile phase concentrations (g/l)
C, C_i	solid-phase concentrations (g/l)
$C_{i,k}, \bar{C}_{i,k}$	Concentrations of component i in plate k (g/l)
C_i^F	feed concentrations (g/l)
d_p	particle diameter (cm)
h_k	Kozeny coefficient
H	height equivalent to a theoretical plate (cm)
$\tilde{K}_i, \bar{N}$	isotherm parameters (1/g and g/l, respectively)
L	column length (cm)
L_{min}	minimum column length acceptable (min)
$\dot{M}$	solid flow-rate (ml/min)
m_F	amount of feed processed per unit time (g/h)
N_c	number of columns per zone
N	number of theoretical plates
N_m	minimum number of plates required
P_{max}	maximum pressure acceptable (bar)
Q	fluid flow-rate (ml/min)
Q_k^{tmb}, Q_k^{smb}	TMB and SMB internal flow-rates in zone k (ml/min)
Q_F	feed flow-rate (ml/min)
Q_{Ex}	extract flow-rate (ml/min)
Q_{Raf}	raffinate flow-rate (ml/min)
Q_{El}	internal flow-rate in zone k (ml/min)
$q_k^{tmb}, q_F^{tmb}, \ldots$	dimensionless TMB flow-rates
t	time (min)
u	interstitial mobile phase velocity (cm/s)
u_m	SMB average mobile phase velocity (cm/s)
V_c	SMB column volume (ml)
X, Y	dimensionless concentrations
ΔP	pressure drop (bar)
ΔT	period (min)

Greek letters

α	selectivity
φ, Φ	parameter relating the pressure drop to the mobile phase velocity (Pa s and Pa s/cm^2, respectively)
ε	external porosity
μ	mobile phase viscosity (Pa s)
τ	mobile phase residence time in a cell (min)
Ω	column cross-section (cm^2)

References

[1] G. Ganetsos and P.E. Barker (Editors), *Preparative and Production Scale Chromatography*, Marcel Dekker, New York, 1993.

[2] D.B. Broughton, *US Pat.*, 2 985 589 (1961).

[3] R.M. Nicoud, *LC · GC Int.*, 5 (1992) 43.

[4] R.M. Nicoud, G. Fuchs, P. Adam, M. Bailly, E. Küsters, F.D. Antia, R. Reuille and E. Schmid, *Chirality*, 5 (1993) 267.

[5] R.M. Nicoud, M. Bailly, J.N. Kinkel, R. Devant, T. Hampe and E. Küsters, in R.M. Nicoud (Editor), *Simulated Moving Bed: Basics and Applications*, INPL, Nancy, 1993, pp. 65–88.

[6] G. Hotier, in *Proceedings of the 9th Symposium on Preparative and Industrial Chromatography "Prep 92"*, INPL, Nancy, 1992, pp. 235–240.

[7] D.M. Ruthven and C.B. Ching, *Chem. Eng. Sci.*, 44 (1989) 1011.

[8] C.B. Ching, K.H. Chu, K. Hidajat and M.S. Uddin, *AIChEJ.*, 38 (1992) 1744.

[9] D. Tondeur and M. Bailly, in R.M. Nicoud (Editor), *Simulated Moving Bed: Basics and Applications*, INPL, Nancy, 1993, pp. 95–117.

[10] R.M. Nicoud and A. Seidel-Morgenstern, in R.M. Nicoud (Editor), *Simulated Moving Bed: Basics and Applications*, INPL, Nancy, 1993, pp. 4–34.

[11] M.D. Levan and T. Vermeulen, *J. Phys. Chem.*, 85 (1981) 3247.

[12] S. Jacobson, S. Golshan-Shirazi and G. Guiochon, *J. Am. Chem. Soc.*, 112 (1990) 6492.

[13] S. Golshan-Shirazi and G. Guiochon, *J. Chromatogr. A*, 658 (1994) 149.

[14] U.P. Ernst and J.T. Hsu, *Ind. Eng. Chem. Res.*, 28 (1989) 1211.

[15] B.A. Finlayson, *Non-Linear Analysis in Chemical Engineering*, McGraw-Hill, New York, 1980.

[16] W.H. Press, B.P. Flannery, S.A. Teukolsky and W.T. Vetterling, *Numerical Recipes in Pascal*, Cambridge University Press, New York, 1989, Ch. 15.

[17] A. Hindmarsh, in R.S. Stepleman, M. Carver, R. Psekin, W.F. Ames and R. Vichnevetsky (Editors), *Scientific Computing*, North-Holland, Amsterdam, 1983.
[18] W.H. Press, B.P. Flannery, S.A. Teukolsky and W.T. Vetterlin, *Numerical Recipes in Pascal*, Cambridge University Press, New York, 1989, Ch. 9.
[19] J.J. Van Deemter, F.J. Zuiderweg and A. Klinkenberg, *Chem. Eng. Sci.*, 5 (1956) 271.
[20] J.H. Knox, *J. Chromatogr. Sci.*, 15 (1977) 352.
[21] Cs. Horváth and H.J. Lin, *J. Chromatogr.*, 149 (1978) 43.
[22] R. Endele, I. Halasz and K. Unger, *J. Chromatogr.*, 99 (1974) 377.
[23] D.M. Ruthven and C.B. Ching, in G. Ganetsos and P.E. Barker (Editors), *Preparative and Production Scale Chromatography*, Marcel Dekker, New York, 1993.
[24] J. Villermaux, in A.E. Rodrigues and D. Tondeur (Editors), *Percolation Processes: Theory and Applications*, Sijthoff & Noordhoff, Alphen aan de Rijn, 1981.
[25] H. Rhee, R. Aris and N.R. Amundson, *Philos. Trans. R. Soc. London*, 269 (1971) 187.
[26] C.B. Ching, C. Ho and D.M. Ruthven, *Chem. Eng. Sci.*, 43 (1988) 703.
[27] R.M. Nicoud and M. Bailly, in *Proceedings of the 9th Symposium on Preparative and Industrial Chromatography "Prep 92"*, INPL, Nancy, 1992, pp. 205–220.
[28] A. Felinger and G. Guiochon, *J. Chromatogr.*, 591 (1992) 31.
[29] K. Brandt and J. Nagel, *Eur. Pat.*, 0 450 504 (1990).
[30] E. Francotte and G. Baisch, *Eur. Pat.*, 0 136 270 (1988).

ELSEVIER

Journal of Chromatography A, 702 (1995) 113–123

JOURNAL OF CHROMATOGRAPHY A

Model for ion-exchange equilibria of macromolecules in preparative chromatography

Yonglong Li, Neville G. Pinto*

Department of Chemical Engineering, University of Cincinnati, Cincinnati, OH 45221-0171, USA

Abstract

An adsorption model based on the stoichiometric displacement principle was developed for the non-linear ion-exchange of macromolecules. In this model, the adsorbed phase is a non-ideal surface solution in equilibrium with a non-ideal bulk liquid, and non-idealities in both phases are quantified in terms of activity coefficient corrections. The equilibrium model accounts for the shape and charge of the adsorbates, lateral interactions on the surface and the effects of modulating salts. Practical methods were developed for evaluating model coefficients, and the model was applied to overloaded elution chromatography of bovine serum albumin. It is shown that non-idealities in the liquid phase and lateral interactions on the surface strongly influence elution profiles.

1. Introduction

HPLC has been widely employed for protein separations on both the analytical and preparative scales [1]. Overload elution and displacement modes of operation are often used to increase productivity in preparative processes [2–6]. In contrast to analytical operations, in which the linear equilibrium description is adequate, the non-linear isotherm region is invariably important for overloaded chromatography, owing to the larger column loads. The lack of an appropriate model to describe adequately non-linear equilibria has significantly impeded the design and optimization of preparative processes.

The Langmuir isotherm is a frequently invoked equilibrium model, despite its inadequacy and thermodynamic inconsistency [7,8]. In ion-exchange chromatography of proteins, a modulator, often a salt, is frequently added to the mobile phase in fairly high concentrations (up to 1 M) to modulate the protein retention [9]. As a result, induced salt gradient phenomena are observed [10,11]. Protein molecules have complex three-dimensional structures, relatively high molecular masses and pH-dependent surface charge characteristics. Enthalpy changes accompanying the adsorption process can be endothermic or exothermic, and may be dependent on the coverage [12,13]. In the light of the complexity of the protein ion-exchange process, the traditional Langmuir model cannot adequately describe the equilibrium behavior. Many researchers have been striving to propose more appropriate theoretical frameworks to incorporate factors such as the presence of modulators, lateral interactions, effective charge and size exclusion [14–18]. These efforts have been summarized in a previous paper [19].

In this paper, we present recent developments in our continuing efforts to develop the non-ideal

* Corresponding author.

0021-9673/95/$09.50 © 1995 Elsevier Science B.V. All rights reserved
SSDI 0021-9673(94)01281-4

surface solution (NISS) model for protein ion exchange. Borrowing on concepts developed in solution thermodynamics and the adsorption of gases on solids, this model attempts to incorporate, in a thermodynamically rigorous manner, the major features of protein ion exchange. The emphasis of the current contribution is non-idealities in the mobile phase, the importance of lateral interactions and the evaluation of model parameters. Both equilibrium and column behavior of BSA have been investigated.

2. Theory

2.1. Brief description of the NISS model

In a previous paper [19] we provided a detailed description of the NISS model. In the following description, we summarize the main features and describe the modifications incorporated.

In the NISS model, the adsorption $n-1$ macromolecules, N_1, N_2, ..., N_{n-1}, is considered in the presence of a small counterion (salt) N_n, called the modulator. As per the stoichiometric displacement model (SDM) [16], the mechanism of adsorption is stoichiometric ion exchange with complete co-ion exclusion. The equilibrium distribution for the system is described by

$$\begin{aligned} z_1 N_n^s &+ N_1 \rightleftharpoons z_1 N_n + N_1^s \\ z_2 N_n^s &+ N_2 \rightleftharpoons z_2 N_n + N_2^s \\ &\vdots \\ z_{n-1} N_n^s &+ N_{n-1} \rightleftharpoons z_{n-1} N_n + N_{n-1}^s \end{aligned}$$

For each of these ion-exchange "reactions", the equilibrium constants are related to the species activities by

$$K_i = \frac{(a_n)^{z_i} a_i^s}{(a_n^s)^{z_i} a_i} \quad i = 1, 2, \ldots, n-1 \tag{1}$$

In the adsorbed phase,

$$a_i^s = \gamma_i^s n_i^s \quad i = 1, 2, \ldots, n \tag{2}$$

In the mobile phase,

$$a_i = \gamma_i c_i \quad i = 1, 2, \ldots, n \tag{3}$$

The activity coefficient of the protein in the mobile phase is assumed to be unity since, in most cases, protein solutions are dilute. For what is usually considered a fairly "high" mobile phase protein concentration, say 100 mg/ml, the molar concentration is still low, owing to the high molecular mass of the protein. In contrast, the modulator molar concentration can be orders of magnitude higher. As a result, liquid-phase non-idealities originating from the modulator cannot in general be neglected. With these considerations, Eq. 1 becomes

$$K_i = \frac{(c_n \gamma_n)^{z_i} \gamma_i^s n_i^s}{(\gamma_n^s n_n^s)^{z_i} c_i} \quad i = 1, 2, \ldots, n-1 \tag{4}$$

By definition,

$$\sum_i^n n_i^s = n^s \tag{5}$$

where n^s is the total ion-exchange capacity of the adsorbent. Eqs. 4 and 5, in conjunction with appropriate equations for the activity coefficients in the surface phase and for the modulator in the liquid phase, constitute the equilibrium model.

2.2. Modulator activity coefficients

A variety of methods are available to estimate activity coefficients in electrolyte solutions [20–25]. Among these, the method developed by Bromley [21] has been found to be effective for strong electrolytes up to an ionic strength of about 6. In terms of the ionic strength of the liquid, the Bromley equation is expressed as

$$\log \gamma_{\pm} = \frac{-0.511 I^{1/2}}{1 + I^{1/2}} + \frac{(0.06 + 0.6B)|z_+ z_-| I}{\left(1 + \frac{1.5}{|z_+ z_-|} I\right)^2} + BI \tag{6}$$

This equation contains a single coefficient B, which is readily available for all salts commonly used as modulators in protein ion-exchange chromatography.

2.3. Surface activity coefficients

As before [19], Talu and Zwiebel's [26] equation is employed for the calculation of the activity coefficients in the surface phase:

$$\ln \gamma_i^s = -s_i \ln\left(\sum_{j=1}^{n} \omega_j \alpha_{ij}\right) + s_i - s_i \sum_{j=1}^{n} \frac{\omega_j \alpha_{ij}}{\sum_{k=1}^{n} \omega_k \alpha_{kj}} \qquad i = 1, 2, \ldots, n \quad (7)$$

where s_i is the adsorbate shape factor and ω_j is the surface fraction, defined as

$$\omega_j = \frac{s_j x_j^s}{\sum_{k=1}^{n} s_k x_k^s} \quad (8)$$

α_{ij} is the Boltzmann weighting factor for local compositions. It is calculated using Wilson's method [27] for incorporating differences in intermolecular forces between components of the adsorbed phase; α_{ij} is related to the average lateral interaction energy between segments of nearest-neighbor molecules (e_{ij} or e_{jj}) by

$$\alpha_{ij} = \exp\left[-\frac{\sigma}{2}(e_{ij} - e_{jj})/kT\right] \quad (9)$$

where σ is the coordination number for the adsorbed segments. The energy of interaction parameters e_{jj} and e_{ij} are functions of the spreading pressure. Talu and Zwiebel [26] showed that at low temperatures e_{jj} can be calculated from pure component isosteric heat of adsorption data:

$$e_{jj} = \frac{q_{j\pi}^{st} - q_{j0}^{st}}{\frac{\sigma}{2} \cdot MS_j} \quad (10)$$

where $q_{j\pi}^{st}$ is the isosteric heat of adsorption of pure j at the same spreading pressure as the mixture and q_{j0}^{st} is the isosteric heat of adsorption at zero spreading pressure. The cross-energy parameters are calculated from

$$e_{ij} = (e_{ii}e_{jj})^{1/2}(1 - \beta_{ij}) \quad (11)$$

where β_{ij} is an empirical factor that accounts for differences in size and adsorptive properties of the molecules.

2.4. Model for chromatographic column

The NISS equilibrium model was combined with a kinetic model for a column packed with a porous adsorbent to provide a mathematical description of the chromatographic process. The kinetic description was adapted from Phillips et al. [28], and neglects the effects of axial dispersion. For a species i, the column equations are

$$\frac{\partial c_i}{\partial \tau} + \frac{\partial c_i}{\partial X} + \phi \cdot \frac{\partial \bar{n}_i}{\partial \tau} = 0 \qquad i = 1, 2, \ldots, n \quad (12)$$

$$\frac{\partial \bar{n}_i}{\partial \tau} = St_i(n_i^s - \bar{n}_i) \qquad i = 1, 2, \ldots, n \quad (13)$$

where

$$\tau = \frac{u_0 t}{L}; \quad X = \frac{1}{L}; \quad St_i = \frac{f_i L}{u_0}$$

For a spherical adsorbent, with the liquid-phase mass-transfer resistance assumed to be negligible and using Glueckauf's [29] linear driving force approximation, f_i is related to the protein diffusivity in the particle, $\bar{D}_i$, by

$$f_i = \frac{15\bar{D}_i}{R_p^2} \quad (14)$$

For the isocratic elution mode, the initial and boundary conditions are

$$c_i = \bar{n}_i = 0 \qquad \text{at } \tau = 0, 0 \le X \le 1 \quad i = 1, 2, \ldots, n-1 \quad (15)$$

$$c_n = c_{nF} \text{ and } \bar{n}_n = n^s \quad \text{at } \tau = 0, 0 \le X \le 1 \quad (16)$$

$$c_i = c_{iF} \qquad \text{at } X = 0, 0 \le \tau \le \tau_{feed} \quad i = 1, 2, \ldots, n \quad (17)$$

$$c_i = 0 \qquad \text{at } X = 0, \tau \ge \tau_{feed} \quad i = 1, 2, \ldots, n-1 \quad (18)$$

$$c_n = c_{nF} \qquad \text{at } X = 0, \tau \ge \tau_{feed} \quad (19)$$

$$\left.\frac{\partial c_i}{\partial X}\right|_{X=1} = 0 \qquad \text{at } X = 1, \tau \ge \tau_{feed} \quad i = 1, 2, \ldots, n \quad (20)$$

The coupled partial differential equations were solved numerically using a finite difference scheme. The set of non-linear isotherm equations were solved with a commercial non-linear equation solver package using the Powell hybrid method [30].

3. Experimental

3.1. Materials and apparatus

BSA was obtained from Sigma (St. Louis, MO, USA). Matrex PAE-1000 (a weak anion exchanger, 10 μm diameter, 1000 Å average pore size) was purchased from Amicon (Danvers, MA, USA), and was slurry packed into 0.46 cm I.D. columns at a maximum pressure of 4000 p.s.i. with a Haskel air-driven pump (Alltech, Deerfield, IL, USA). Sodium chloride, silver nitrate, sodium azide and imidazole were obtained from Aldrich (Milwaukee, WI, USA) and hydrochloric acid and methanol from Fisher Scientific (Fair Lawn, NJ, USA). All reagents were used as received.

The chromatographic system for the frontal and elution experiments included an SP8800 gradient HPLC pump (Spectra-Physics, San Jose, CA, USA), a Model 2550 UV–Vis detector (Varian, Sunnyvale, CA, USA) and an HP 3396A integrator (Hewlett-Packard, Palo Alto, CA, USA). The protein concentration was measured with a UV-160/CL-750 spectrophotometer (Shimadzu, Kyoto, Japan).

3.2. Effective protein charge and equilibrium constant

The effective charge (z_i) and equilibrium constant (K_i) of BSA were as measured by linear isocratic elution on a 25 cm × 0.46 cm I.D. column. Details for these experiments have been reported earlier [19]. The salt (NaCl) range used was 0.15–0.4 *M* and experiments were performed at a number of temperatures in the range 6.1–35.5°C.

3.3. Isotherm measurements and equilibrium constant

BSA adsorption isotherms were measured at different sodium chloride concentrations at room temperature by the batch method. PAE-1000 was first weighed into test-tubes, then a known volume of protein solution at known salt and protein concentrations and pH 7 was added to the test-tubes with a syringe. The test-tubes were sealed with Parafilm and placed in a shaker for 24 h. Preliminary experiments had established that equilibrium can be reached in 8–10 h. Special attention was paid to the low protein concentration region because the equilibrium constant K_i was calculated from the data in this region. After equilibration, the slurry solution was centrifuged at 5000 rpm, and the clear solution was analyzed with a UV spectrophotometer at 280 or 310 nm. The equilibrium distribution was calculated from a mass balance.

3.4. Resin capacity

The capacity of the anion exchanger was measured by a procedure similar to that employed by Bentrop and Engelhardt [31], in which the column was first equilibrated with buffer solutions containing Cl^- at pH 7. Subsequent to rinsing the column with deionized water, sodium nitrate solution of known concentration was introduced; a low flow-rate, selected after preliminary experiments, was used to minimize mass-transfer effects. The column effluent was collected, and silver nitrate was used to titrate the Cl^- ions. The total capacity was then back-calculated from an equivalency balance.

3.5. Stanton number

The Stanton number for the column was determined from isocratic elution experiments with BSA on a 25 cm × 0.46 cm I.D. column. The experiments were performed at room temperature using a salt concentration of 0.35 *M*. A 20-μl volume of 5 mg/ml BSA solution was injected into the column and the response was

monitored at 280 nm. A flow-rate range of 0.5–2.5 ml/min was used.

4. Results and discussion

4.1. NISS parameter estimation

For each protein species being considered, the NISS model requires that three coefficients be evaluated: K_i, z_i and S_i. In addition, the isosteric heat of adsorption must be known as a function of surface coverage, and the total capacity of the support n^s must also be available. Previously [19], we described methods for evaluating these coefficients and reported experimental values for BSA on PAE-1000, with NaCl as the modulator. Here we investigated how removing the assumption of solution ideality will affect parameter estimation.

The equilibrium constant K_i and the effective charge z_i can be evaluated from linear isocratic elution data. From Eq. 4, it can be shown that for this mode of chromatography

$$\ln k_i' = \ln[\phi(n^s)^{z_i} K_i] - z_i \ln(c_n \gamma_n) \quad (23)$$

Fig. 1 shows a typical plot of Eq. 23 for BSA. Two lines are shown, both obtained from the same experimental data. In one case the liquid solution was assumed to be ideal, whereas for the other the Bromley equation (Eq. 6) was used to correct for liquid non-ideality. Since the slope of these lines gives z_i and the intercept gives K_i, it appears that whereas z_i is essentially unaffected by liquid non-ideality, K_i is severely influenced. Fig. 2 shows the value of z_i obtained in experiments at other temperatures, with and without the activity coefficient correction. In all cases a z_i value of 4.8 was obtained. These data confirm that z_i is independent of the liquid activity coefficient correction. It is also interesting that, within the temperature range studied, z_i is essentially independent of temperature, indicating that temperature has a secondary influence when compared with pH and modulator [32].

Fig. 3 shows the values of K_i obtained from the elution experiments, with and without the correction for liquid-phase non-ideality. Also plotted are values obtained from independent batch experiments at various modulator concentrations. The match between the two sets indicates that the elution method is reliable for obtaining K_i. It should be noted that the modulator concentration axis (abscissa) only applies to the batch data; for the elution data the points have been separated for clarity only.

The results in Fig. 3 clearly demonstrate that liquid-phase non-ideality can have a strong effect on K_i. Neglecting its influence would, in this

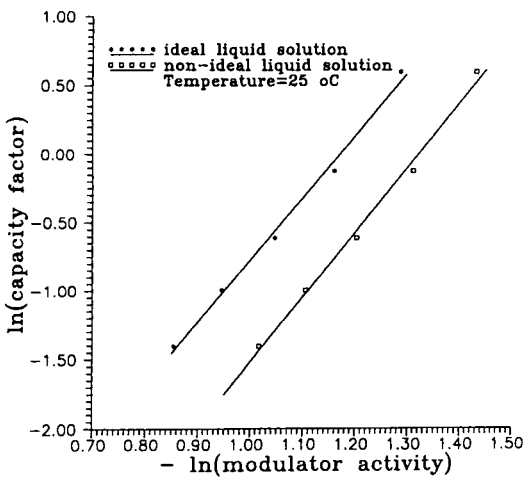

Fig. 1. Effective charge of BSA for ideal liquid solution and non-ideal liquid solution.

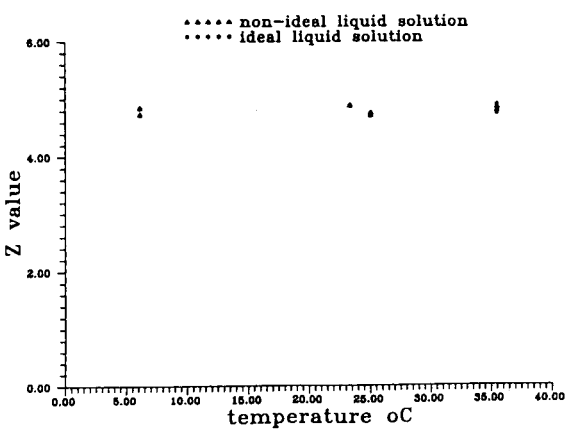

Fig. 2. Effective charge of BSA at different temperatures.

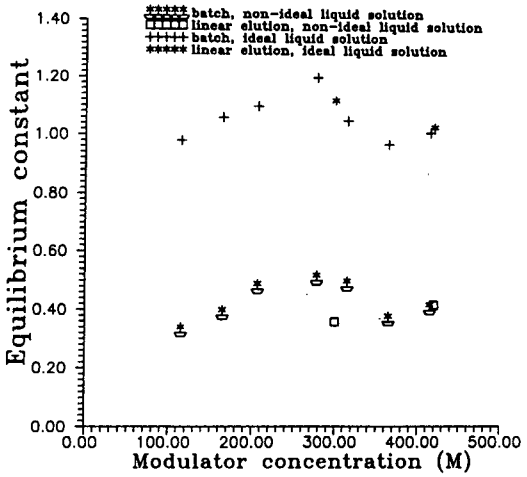

Fig. 3. Equilibrium constant of BSA at different modulator concentrations.

case, lead to an over-estimate of K_i of well over 200%.

The influence of liquid-phase non-ideality can be expected to be even stronger if modulator ions of higher valency are used. Fig. 4 shows the influence of modulator charge on liquid activity coefficient; values in this figure were calculated keeping B (Eq. 6) constant at the value for NaCl and changing the z_i for the counter ion. It should be noted that the further the value of the activity

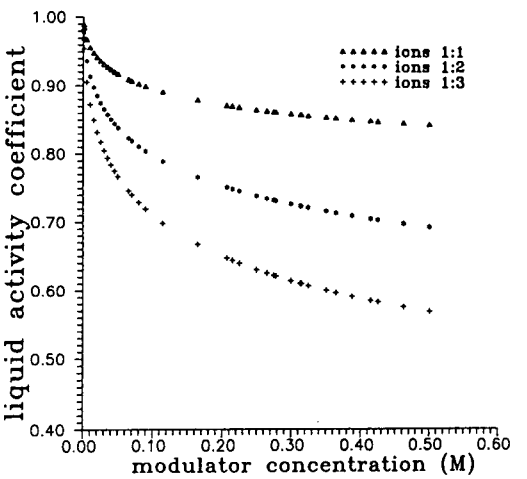

Fig. 4. Effect of type of counter ions on liquid activity coefficient.

coefficient is from 1, the stronger the influence of the liquid phase on K_i.

Fig. 4 also provides an explanation for the observed independence of z_i from the liquid activity coefficient. The modulator concentrations used for the evaluation of z_i (Fig. 1) were always higher than 0.2 M. In this range, the liquid activity coefficient is essentially constant for NaCl (Fig. 4, 1:1). Hence, this coefficient shifts the points in Fig. 1 from their ideal solution value by approximately the same amount at every modulator concentration in the experimental range. It should be noted, however, that at lower concentrations the liquid activity coefficient is a strong function of the concentration. Hence it is to be expected that z_i will not be constant at lower concentrations, which is consistent with experimental observations reported in the literature [32].

The shape factor in Eq. 7 is defined as

$$S_p = \frac{L_p}{L_s} \tag{24}$$

where L_p is the outer free perimeter of the protein and L_s the outer free perimeter of a standard molecule [33]. Selecting the modulator ion as the standard ion, and assuming all adsorbates to have a square imprint,

$$L_s = 4\left(\frac{A_s}{n^s}\right)^{1/2} \tag{25}$$

$$L_p = 4\left(\frac{A_s}{n^p}\right)^{1/2} \tag{26}$$

where A_s is the specific area of the adsorbent and n^s and n^p are the saturation capacities of the adsorbent for the modulator and protein, respectively. The capacity for the modulator is the same as the ion-exchange capacity of the adsorbent, because all the ion-exchange sites are accessible to the small modulator ions [31]. For the proteins, in contrast, only a small fraction of the total ion-exchange sites are accessible. For example, for BSA on PAE-1000, at pH 7 and room temperature, the saturation capacity was found to be 150 mg/g. Using the effective charge of 4.8, this translates into a utilized capacity of approximately 3% of the total capacity.

Substituting Eqs. 25 and 26 into Eq. 24, and using the experimentally obtained ion-exchange capacity of the adsorbent of 360 μequiv./g and the protein saturation capacity at pH 7, a shape factor of 5.5 was calculated. This value is remarkably close to the best-fit value of 5.6 obtained by us earlier [19] from room-temperature isotherm data.

Previously [19], we had measured the dependence of the isosteric heat of adsorption of BSA on PAE-1000 at a very low modulator concentration. This was done by obtaining the adsorption isotherms at a number of temperatures and then calculating the isosteric heat through a Clausius–Clapeyron type equation. With this approach, it was shown that the isosteric heat of adsorption is a linear function of the surface mole fraction of BSA. Although this approach works well, it is experimentally tedious.

For this work, we chose an alternative approach. Based on our earlier results [19], we assume the linear dependence of isosteric heat on protein coverage holds at other modulator concentrations, i.e.,

$$q_{i\pi}^{st} - q_{i0}^{st} = mx_i^s \tag{27}$$

where the coefficient m will change with modulator concentration. This coefficient can be obtained at a given modulator concentration from the best fit of the NISS model to an experimentally measured adsorption isotherm at this concentration. Fig. 5 are the experimental isotherms, the best-fit simulations and the corresponding m values for modulator concentrations of 0.21 and 0.39 M. The advantage of this method is that isotherms have to be measured only at one temperature, instead of a series of temperatures, as was done earlier [19].

4.2. Column behavior

Experimental isocratic elution peaks of BSA were compared with predictions of column simu-

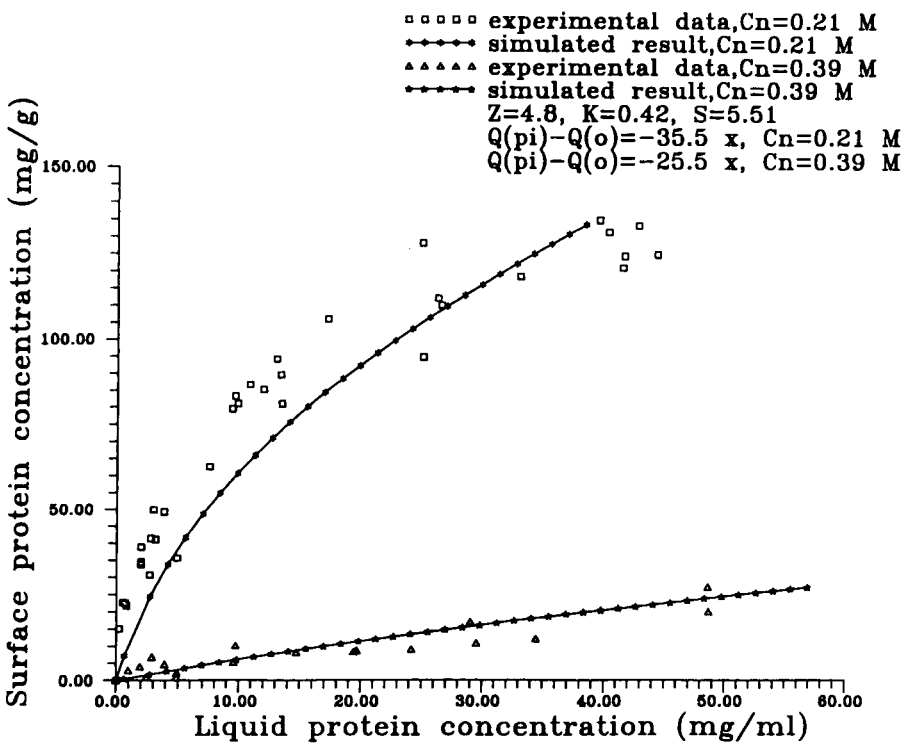

Fig. 5. BSA equilibrium isotherms at 0.21 and 0.39 M NaCl concentrations.

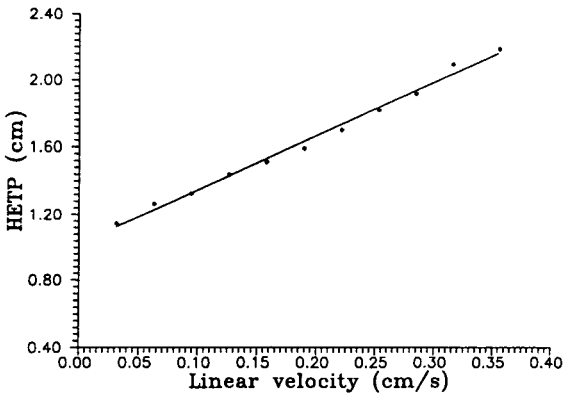

Fig. 6. Relationship between HETP and fluid linear velocity.

lations to establish the validity of the NISS equilibrium description. The mass transfer resistance in the particle phase (Stanton number) was estimated from the elution experiments described earlier, using the moment method of Ma and Lin [34]. According to this method, a plot of HETP vs. fluid velocity should give a straight line. Fig. 6 shows the plot for BSA. From the slope of this line, the BSA diffusivity in the particle was calculated and substituted in Eq. 14 to obtain a Stanton number of 20.

Using the measured equilibrium and kinetic parameters (Table 1), isocratic elution peaks of BSA were simulated at two salt concentrations, 0.21 and 0.39 *M*. Figs. 7–9 are comparisons of these predictions with experimental results. Fig. 7 is the comparison for a column loading of 100 μl of 61.37 mg/ml BSA at 0.39 *M* NaCl. In general, the model predicts the experimental response reasonably well. The peak retention

Table 1
Model parameters for column simulations

Parameter	Value
K_i	0.42
z_i	4.8
S_i	5.51
n^s	360 μequiv./g
St_i	20
$q_\pi^{st} - q_0^{st}$	$-25.5x$ at 0.39 *M* NaCl
	$-35.5x$ at 0.21 *M* NaCl

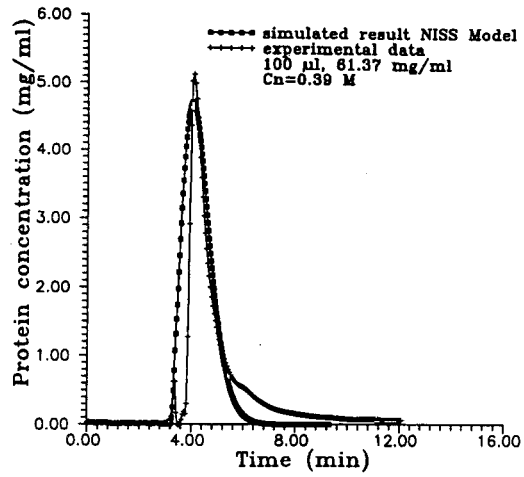

Fig. 7. Comparison of experimental and NISS simulation peaks (100 μl, $C_n = 0.39$ *M*).

times of the two peaks correspond, and peak shapes are characterized by a sharpening front and tailing rear. Also, at a higher column loading (Fig. 8) and lower salt concentration (Fig. 9) the correspondence between the simulated and experimental peaks is maintained.

The differences observed between experimental and simulated peaks are primarily attributed to poor estimation of the kinetic effects and the presence of an impurity or variant of BSA. In

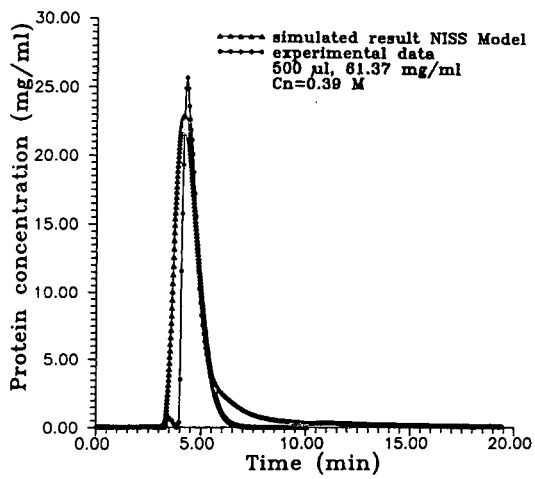

Fig. 8. Comparison of experimental and NISS simulation peaks (500 μl, $C_n = 0.39$ *M*).

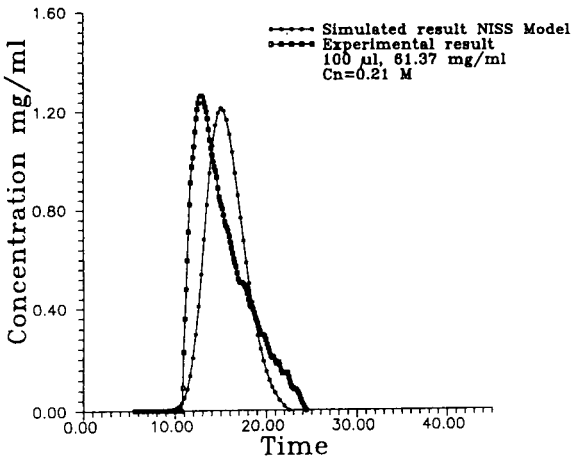

Fig. 9. Comparison of experimental and NISS simulation peaks (100 μl, $C_n = 0.21$ M).

Figs. 7–9 the experimental peaks are all higher than the simulated peaks, and their fronts are sharper. This can be accounted for by small changes in the Stanton number. For example, Fig. 10 illustrates the sensitivity of the peak shape to the Stanton number; a relatively small change from 15 to 20 results in a significant sharpening of the peak and, consequently, a greater peak height. To match the experimental and simulated peak heights in Figs. 7–9 would require only a small change in the Stanton number, one that is within the limit of precision of the estimation method (Fig. 6). Therefore, we believe that this discrepancy is not rooted in problems with the NISS model, but stems from an underestimate of the Stanton number by the moment method [34].

An underestimate of the Stanton number should, however, also result in a simulated peak that has a more diffuse rear than is obtained experimentally . From Figs. 7–9, it is clear that the opposite is observed. This is explained by the presence of an impurity or variant of BSA in the mixture. Fig. 11 shows an isocratic chromatogram of BSA at 0.29 M NaCl. At this modulator concentration, the peak for the impurity (or variant) is clearly indicated. In Figs. 7–9, the region of greatest discrepancy between the rears of the simulated and experimental peaks is at the lower concentrations where the impurity appears.

The importance of accounting for lateral interactions and solution non-ideality for BSA is best illustrated by showing predictions in the absence of these factors. Fig. 12 shows a comparison of the experimental and predicted peaks when lateral interactions are not considered (ideal surface phase). Neglect of the surface repulsive forces between adsorbed BSA molecules results

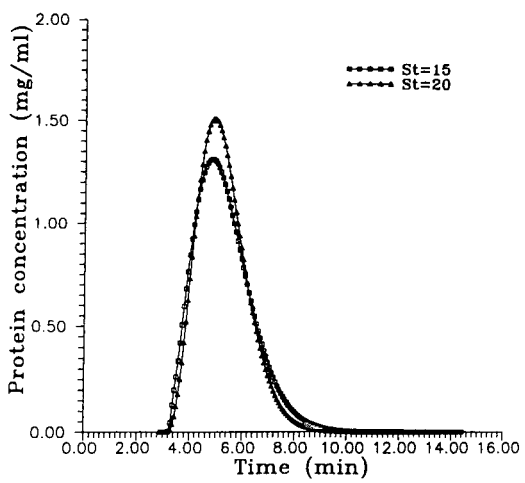

Fig. 10. Effect of Stanton number on column profiles.

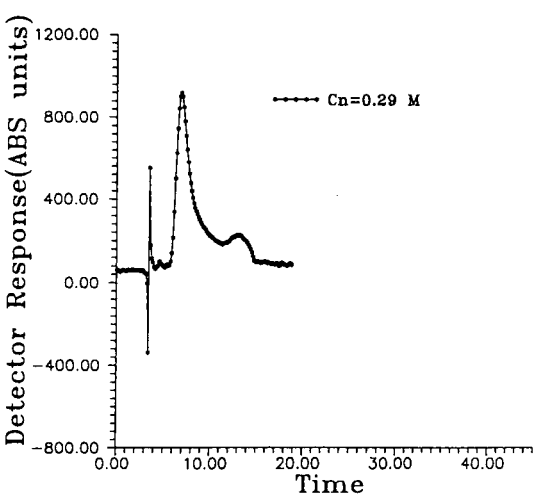

Fig. 11. Isocratic elution of BSA at 0.3 M NaCl.

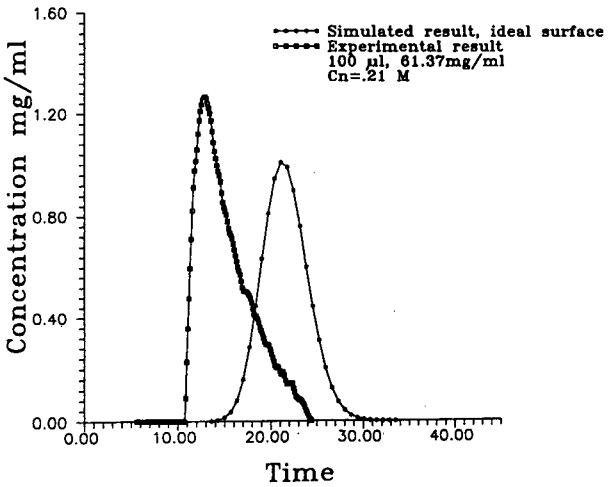

Fig. 12. Predicted BSA elution peak with lateral interactions neglected.

in the prediction of a higher than actual adsorption capacity and, therefore, a significantly longer than observed retention time. Equally poor predictions are obtained if the liquid phase is assumed to be ideal. In this case, as was discussed earlier (Fig. 3), the equilibrium constant is over-estimated. Consequently as illustrated in Fig. 13, peak retention times much higher than observed are obtained.

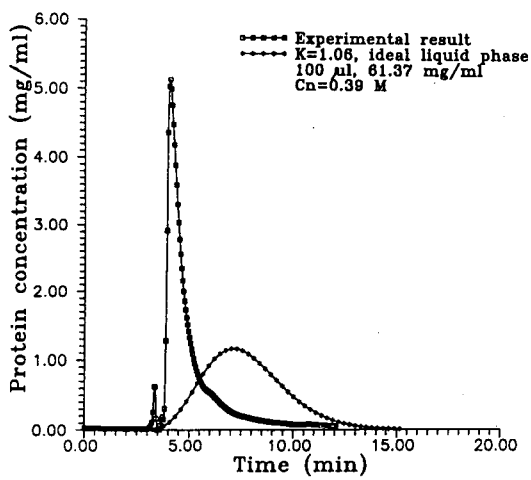

Fig. 13. Predicted BSA elution peak assuming ideal liquid solution.

5. Conclusions

The NISS model provides an effective and thermodynamically consistent approach to modeling protein adsorption for overloaded ion-exchange chromatography. The equilibrium coefficients of this model are conveniently calculated through a combination of elution and batch isotherm experiments. Using BSA as the probe molecule, it has been shown that the prediction of column behavior requires the incorporation of liquid-phase non-idealities; the relatively high modulator concentrations typically encountered in ion-exchange chromatography result in highly non-ideal liquid phases that influence binding strength. Also, lateral interactions on the surface cannot be ignored, and these are a function of surface coverage and modulator concentration.

Symbols

A	specific area of the resin
a_i	activity
B	Bromley constant
c_i	mobile phase concentration
c_{iF}	mobile phase concentration in the feed
$\bar{D}_i$	effective diffusion coefficient
e_{ij}	lateral interaction potential between segment of molecules i and j
f	effective mass transfer coefficient
I	ionic strength
k	Boltzmann constant
k'_i	column capacity factor for species i
K_i	equilibrium constant
l	column length
L	characteristic column length
L_p	protein outer free perimeter
L_s	salt outer free perimeter
m	slope coefficient in Eq. 27
M	Avogadro's number
n	number of species
$\bar{n}_i$	average concentration of species i on surface
n^s	total ion-exchange capacity
n^p	maximum protein capacity
n_i^s	concentration of species i on surface
N_i	adsorbate i

$q_{j\pi}^{st}$ isosteric heat at spreading pressure π
q_{j0}^{st} isosteric heat at spreading pressure zero
R_p radius of particle
S_i shape factor
Sk_i Stanton number for component i
t time
T absolute temperature
u_0 linear velocity
x coverage in mole fraction
X dimensionless length
z_i effective charge

Greek symbols

α_{ij} Boltzmann weighting factors for local segment compositions
β_{ij} empirical factor
ϕ column phase ratio
ω_j surface fraction
γ activity coefficient
σ coordination number
τ dimensionless time

Subscripts

i index for component i
j index for component j
k index for component k
F feed
n modulator
p protein
s salt or specific

Superscripts

s surface phase
st isosteric

Acknowledgement

This work was supported in part by Grant No. CTS-9207631 from the National Science Foundation. This support is gratefully acknowledged.

References

[1] F.E. Regnier, *Chromatographia*, 24 (1987) 241.
[2] Cs. Horváth, J. Frenz and Z. El Rassi, *J. Chromatogr.*, 255 (1983) 273.
[3] A.M. Katti, and G. Guiochon, *J. Chromatogr.*, 499 (1990) 21.
[4] J.H. Knox and H.M. Pyper, *J. Chromatogr.*, 363 (1986) 1.
[5] A. Jungbauer, *J. Chromatogr.* 639 (1993) 3.
[6] G. Subramanian and S.M. Cramer, *Biotechnol. Prog.*, 5 (1989) 92.
[7] P.K. de Bokx, P.C. Baarslag and H.P. Urbach, *J. Chromatogr.*, 594 (1992) 9.
[8] D.M. Ruthven, *Principles of Adsorption and Adsorption Processes*, Wiley, New York, 1984.
[9] A. Velayudhan and M.R. Ladisch, *Anal. Chem.*, 63 (1991) 2028.
[10] E.A. Peterson, *Anal. Chem.*, 90 (1978) 767.
[11] J.A. Gerstner and S.M. Cramer, *Biotechnol. Prog.*, 8 (1992) 540.
[12] W. Norde, *J. Dispers. Sci. Technol.*, 13 (1992) 363.
[13] P.G. Koutsoukos, W. Norde and J. Lyklema, *J. Colloid Interface Sic.*, 95 (1983) 385.
[14] S. Yamamoto, K. Nakanishi and R. Matsuno, *Ion-Exchange Chromatography of Proteins*, Marcel Dekker, New York, 1988.
[15] C.A. Brooks and S.M. Cramer, *AIChE J.*, 38 (1992) 1969.
[16] W. Kopaciewicz, M.A. Rounds, J. Fausnaugh and F.E. Regnier, *J. Chromatogr.*, 266 (1983) 3.
[17] P. Cysewski and G. Jilge, *J. Chromatogr.*, 548 (1991) 61.
[18] F.E. Regnier and I. Mazsaroff, *Biotechnol. Prog.*, 3 (1987) 22.
[19] Y. Li and N.G. Pinto, *J. Chromatogr. A*, 658 (1994) 445.
[20] C.C. Chen and H.I. Britt, *AIChE J.*, 28 (1982) 588.
[21] L.A. Bromley, *AIChE J.*, 19 (1973) 313.
[22] X.H. Lu and G. Maurer, *AIChE J.*, 39 (1993) 1527.
[23] C.C. Chen and L.B. Evans, *AIChE J.*, 32 (1986) 444.
[24] C. Christensen, B. Sander, A. Fredenslund and P. Rasmussen, *Fluid Phase Equilibria*, 13 (1983) 297.
[25] K.S. Pitzer, *J. Phys. Chem.*, 77 (1973) 268.
[26] O. Talu and I. Zwiebel, *AIChE J.*, 32 (1986) 1263.
[27] G.M. Wilson, *J. Am. Chem. Soc.*, 86 (1964) 127.
[28] M.W. Phillips, G. Subramanian and S.M. Cramer, *J. Chromatogr.*, 454 (1988) 1.
[29] E. Glueckauf, *Trans. Faraday Soc.*, 51 (1955) 1540.
[30] D. Kahaner, C. Moler and S. Nash, *Numerical Methods and Software*, Prentice-Hall, Englewood Cliffs, NJ, 1989.
[31] D. Bentrop and H. Engelhardt, *J. Chromatogr.*, 556 (1991) 363.
[32] M.A. Rounds and F.E. Regnier, *J. Chromatogr.*, 283 (1984) 37.
[33] O. Talu, *Ph.D. Dissertation*, Arizona State University, Tempe, AZ, 1984.
[34] Y.H. Ma and Y.S. Lin, *AIChE Symp. Ser.*, No. 242, 81 (1985) 39.

ELSEVIER

Journal of Chromatography A, 702 (1995) 125–142

JOURNAL OF CHROMATOGRAPHY A

Modeling non-linear elution of proteins in ion-exchange chromatography

Stuart R. Gallant, Amitava Kundu, Steven M. Cramer*

Howard P. Isermann Department of Chemical Engineering, Rensselaer Polytechnic Institute, Troy, NY 12180, USA

Abstract

The problem of non-linear elution of a band of protein in isocratic ion-exchange chromatography leads to a pair of coupled non-linear partial differential equations. The equilibrium may be modeled using the Steric Mass Action (SMA) model of ion exchange, which treats both the salt dependence of protein adsorption and the steric shielding present under non-linear conditions. Neglecting axial dispersion, a model of ideal chromatography is formulated that may be solved by the method of characteristics. The predictions of this relatively simple model are shown to agree with experimental results concerning the non-linear elution of cytochrome *c* in a strong cation-exchange column. Of particular interest is the existence of two plateaus in the solution of this problem for large injection volumes. While this result cannot be understood or predicted on the basis of the traditional Langmuir isotherm or other currently available descriptions of adsorption, the chromatographic model presented in this work makes this otherwise anomalous result clear. Further, the use of such a model during parameter estimation is discussed.

1. Introduction

Multi-component isotherms play a crucial role in determining the behavior of non-linear chromatographic systems [1]. When combined with an appropriate description of the transport through the column, a reliable multi-component isotherm makes it possible to predict the chromatographic elution times and band shapes of components in the chromatographic system. Two important effects dictated by isotherm shape are the formation self-sharpening fronts or "shocks" and the formation of rarefaction waves or "tails."

Because of the central importance of multi-component isotherms to the understanding of chromatographic behavior, the last decade has been a renaissance in the study of multi-component isotherms in liquid chromatography [2]. Researchers have investigated and attempted to describe equilibrium adsorption behavior on a wide variety of stationary phase surface chemistries. In this paper, the focus of concern will be the representation of the equilibrium adsorption of a single protein and a counter ion on an ion-exchange surface.

The problem which is investigated, the injection of a chromatographic band of finite width and concentration, has been discussed previously for the Langmuir isotherm [3,4]. Some readers might feel that this is a relatively well understood problem; however, careful examination of the experiments and simulations presented below demonstrates some novel observations about this problem. In particular, the existence of a two-plateau band shape that has not previously been

* Corresponding author.

0021-9673/95/$09.50 © 1995 Elsevier Science B.V. All rights reserved
SSDI 0021-9673(94)00992-9

presented in the literature is predicted by the theoretical treatment and documented by experiment. Further, it is our purpose in this paper to conduct a test of two models of ion-exchange adsorption: The Steric Mass Action (SMA) and Stoichiometric Displacement/Electroneutrality (SDM/Electroneutrality) models. The ability of SMA, SDM/Electroneutrality and a modifier-dependent Langmuir isotherm to represent protein isotherms is evaluated in the Appendix.

Although the model presented here would not apply to cases in which more than one protein was present, it should be clear that implementation of the Steric Mass Action isotherm in a more sophisticated model of mass transport would have wide application for multi-component separations in isocratic, gradient and displacement modes. Our research group has employed this isotherm extensively in the study of displacement chromatography, and new work will be published in the near future on modeling non-linear gradient chromatography.

2. Theory

2.1. Background

A number of researchers have suggested techniques for modeling protein adsorption in ion-exchange chromatography under conditions of varying salt concentration. Boardman and Partridge [5] observed that the retention of proteins in cation-exchange chromatography under dilute conditions could be described using a relatively simple exponential expression. Using the notation employed below, that relationship may be stated as

$$k'_i = \beta \cdot \left(\frac{Q_i}{C_i}\right) = \beta K_{1i} \cdot \left(\frac{\Lambda}{C_1}\right)^{\nu_i} \quad (1)$$

where k'_i is the capacity factor, β is the phase ratio, Q_i is the concentration of bound protein, C_i is the mobile phase protein concentration, K_{1i} is the equilibrium constant of the exchange reaction, Λ is the bed capacity, C_1 is the salt concentration and ν_i is the protein's characteristic charge. Regnier and co-workers [6,7] have employed this model, the Stoichiometric Displacement Model or SDM, in order to predict protein retention in analytical chromatography.

This exchange reaction-based approach has been extended to modeling the adsorption from concentrated protein solutions [8,9]. In preparative chromatography, the concentration of protein adsorbed on the stationary phase will often represent a large fraction of the total bed capacity Λ. In order to represent the limited capacity of the stationary phase, the electroneutrality condition is invoked:

$$\Lambda = Q_1 + \sum_{i=2}^{NC} \nu_i Q_i \quad (2)$$

where Q_1 represents the concentration of salt counter ions bound to the stationary phase, Q_i represents the concentration of the ith component bound to the stationary phase and NC is the number of components in the mobile phase. Utilizing Eq. 2 to represent the finite capacity of the stationary phase, a group of non-linear equations which define the bound concentration of each adsorbed component as a function of the mobile phase concentrations is formulated [10]:

$$Q_i = F_i(C_1, C_2, \ldots, C_{NC}) \quad i = 1, \ldots, NC \quad (3)$$

where the system of non-linear equations F_i may be solved using a Newton–Raphson technique. Combination of these functions with the appropriate mass balances on the adsorbed species in the mobile and stationary phases allows the calculation of simulated chromatograms [8,11]. This type of model will be referred to as the SDM/electroneutrality model below.

As pointed out by Velayudhan [12], the use of the electroneutrality condition may be too loose a restriction on the binding capacity of a chromatographic column for proteins and large polyelectrolytes. Large molecules such as proteins can sterically block substantially more ion-exchange sites than they interact with. Fortunately, as will be shown below, this steric effect may be accounted for by replacing Eq. 2 with a more restrictive condition. The resulting model has been designated the Steric Mass Action (SMA) ion-exchange formalism [13].

2.2. Steric mass action formalism

The Steric Mass Action (SMA) formalism is a three-parameter model of ion exchange designed specifically for representation of multi-component protein–salt equilibrium in ion-exchange chromatography. In the case of a solution dilute in protein, it reduces to the model originally proposed by Boardman and Partridge [5]. However, as the concentration of protein bound to the stationary phase rises, the model takes into account the effect of steric shielding on the capacity of the stationary phase. As a result, it is capable of predicting the multi-component adsorption of protein under dilute and concentrated conditions.

Fig. 1 depicts the equilibrium adsorption of a protein from an aqueous salt solution on to an ion-exchange surface. The protein is bound to the stationary phase at a number of exchange sites given by its characteristic charge, ν_i. As can be seen, a number of sites are not occupied by the protein. In order to maintain of electroneutrality, counter ions will be bound to these sites, some of which may be sterically shielded by the protein. As a result, the sterically shielded sites will be unavailable for exchange as long as this protein remains bound to the surface. The SMA formalism represents this adsorption process as a stoichiometric exchange of mobile phase protein and bound counter ions [13]:

$$C_i + \nu_i \bar{Q}_l \Leftrightarrow Q_i + \nu_i C_l \quad i = 2, \ldots, NC \tag{4}$$

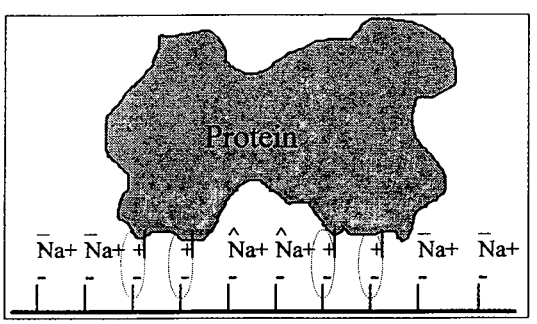

Fig. 1. Schematic diagram of protein binding on a cation-exchange surface (Brooks 1992). Na^+ represents the counter ions, in this case sodium ions. $\hat{N}a^+$ represents the counter ions sterically shielded by the protein.

where C_i and Q_i refer to the concentration of protein in the mobile phase and on the stationary phase, C_1 refers to the concentration of salt in the mobile phase and $\bar{Q}_1$ refers to the concentration of bound salt available for exchange. The equilibrium constant of the reaction may be written as

$$K_{1i} = \left(\frac{Q_i}{C_i}\right)\left(\frac{C_1}{\bar{Q}_1}\right)^{\nu_i} \quad i = 2, \ldots, NC \tag{5}$$

The term "salt" is used generically throughout what follows; however, the reader should bear in mind that what is being discussed are monovalent cations (in cation-exchange chromatography) or anions (in anion-exchange chromatography). For example, in the experiments and simulations below, the protein employed, cytochrome *c*, has a positive characteristic charge, as does the monovalent cation with which it exchanges, sodium.

Each protein molecule may sterically shield some salt counter ions on the adsorptive surface. The amount of salt counter ions blocked by a particular protein will be proportional to the concentration of that protein on the surface:

$$\hat{Q}_{1i} = \sigma_i Q_i \quad i = 2, \ldots, NC \tag{6}$$

Electroneutrality requires that

$$\Lambda = \bar{Q}_1 + \sum_{i=2}^{NC} (\nu_i + \sigma_i) Q_i \tag{7}$$

Having introduced the SMA equations, a word about the meaning of the steric factor is necessary. In ion-exchange chromatography, non-idealities will be present in the mobile and stationary phases. Of course, these non-idealities may be accounted for by the use of activity coefficients. However, as one of the dominant sources of non-ideality is the differences in relative size of the adsorbed components, as suggested originally by Velayudhan [12], it is reasonable to modify the model to include this effect explicitly. Myers [14] has discussed explicit inclusion of nonideal effects in order to avoid the need for activity coefficients in adsorption on activated carbon. Thus, the steric factor may be looked upon as a lumped parameter which

includes a number of non-idealities of the mobile and stationary phase of which the dominant non-ideality is expected to be steric shielding.

Three major features of the SMA single-component isotherm should be noted. First, in dilute protein solutions, the partition ratio of each protein reduces to the following simple relationship:

$$\frac{Q_i}{C_i} = K_{1i}\left(\frac{\Lambda}{C_1}\right)^{\nu_i} \quad i = 2, \ldots, NC \tag{8}$$

Second, the maximum binding capacity of the stationary phase for a particular protein will be

$$Q_{i,\max} = \frac{\Lambda}{\nu_i + \sigma_i} \quad i = 2, \ldots, NC \tag{9}$$

Third, over the entire range of protein concentration, protein adsorption is enhanced by lowering the salt concentration in the mobile phase. These observations agree with experimental observations of the adsorption of both proteins and long-chain polyelectrolytes [15–18].

This model has previously been tested in a number of ways. SMA has been shown to represent single-component isotherms of proteins at varying salt concentrations [15] (see Appendix). The SMA formalism has been used in conjunction with an ideal model of chromatography to predict isotachic displacement chromatograms [16–18]. Further, it has been used in conjunction with a numerical model of chromatography to predict displacement development, confirming its ability to predict multi-component equilibrium [19]. The values of the SMA parameters employed in this study are shown in Table 1.

Table 1
Parameters employed in simulation

Solute	Characteristic charge (ν_i)	Equilibrium constant (K_{1i})	Steric factor (σ_i)
Sodium	1.00	1.00	0.0
Cytochrome *c*	6.15	$6.37 \cdot 10^{-3}$	53.4

Column capacity (Λ) = 590 mM; void fraction (ε) = 0.70.

2.3. Field equations and boundary conditions

In ideal chromatography, transport within the chromatographic column is described by the following system of partial differential equations [20,21]:

$$\frac{\partial C_i}{\partial z} + \frac{\partial C_i}{\partial \tau} + \beta \frac{\partial Q_i}{\partial \tau} = 0 \quad i = 1, \ldots, NC \tag{10}$$

where β is a phase ratio, z is a non-dimensional measure of the axial position ($z = Z/L_{col}$) and τ is a dimensionless time unit ($\tau = t/t_0$). In these non-dimensional coordinates, the velocity of an unretained component in the mobile phase is unity. Non-dimensional time and distance units will be employed in the discussion that follows. Table 2 includes the actual experimental conditions in dimensional units.

In isocratic chromatography, the salt concentration is held constant at the column inlet:

$$C_1(\tau, 0) = C_{1,f} \tag{11}$$

where the subscript 1 refers to the counter ion. During operation, three sequential procedures are carried out on the column, equilibration, loading, and elution:

$$C_2(\tau < 0, 0) = 0 \quad \text{(equilibration)} \tag{12a}$$

$$C_2(0 < \tau < \tau_f, 0) = C_{2,f} \quad \text{(loading)} \tag{12b}$$

$$C_2(\tau > \tau_f, 0) = 0 \quad \text{(elution)} \tag{12c}$$

where the subscript 2 refers to the protein and τ_f represents the duration of the feed pulse in dimensionless units.

The total concentration of components 1 and 2 (counter ion and protein) given in equivalents constitutes a third variable, C_T:

$$C_T(\tau < 0, 0) = C_{1,f} \tag{13a}$$

$$C_T(0 < \tau < \tau_f, 0) = C_{1,f} + \nu_2 C_{2,f} \tag{13b}$$

$$C_T(\tau > \tau_f, 0) = C_{1,f} \tag{13c}$$

Because adsorption of protein displaces a number of counter ions equivalent to the characteristic charge of the protein, ν_2, the disturbance of C_T due to the feed propagates through the column at the mobile phase velocity:

$$C_T(\tau, z) = C_T(\tau - z, 0) \tag{14}$$

Table 2
Non-linear elution cation-exchange chromatography: experimental conditions

Fig.	Feed volume (ml)	Flow-rate (ml/min)	Cytochrome *c* concentration (m*M*)	Sodium concentration (m*M*)
6	0.20	0.2	0.54	150
7	0.20	0.5	0.57	125
8	3.17	0.5	0.29	150

Mobile phase, sodium phosphate buffer (pH 6.0); column, 50 × 5 mm I.D.; column dead volume, 0.69 ml.

A plot of the behavior of C_T is shown in Fig. 2. Within zones 1, 2 and 3, C_T assumes the values $C_{1,f}$, $C_{1,f} + \nu_2 C_{2,f}$ and $C_{1,f}$, respectively. The line that separates zones 1 and 2 intersects the time axis at the moment that the feed pulse enters the inlet of the column. The line that separates zones 2 and 3 intersects the time axis at the moment the feed pulse ends ($\tau_f = 0.29$).

2.4. Solution of the model

The preceding field equations (Eq. 10), isotherm (Eqs. 5 and 7) and boundary conditions (Eqs. 11 and 12) may be solved to produce an ideal chromatogram. Rhee et al. [3] discussed a similar problem when equilibrium is governed by the Langmuir isotherm and only one component is present in the mobile phase. Realization that C_1 and C_2 are not independent (they are linked by C_T) and that the value of C_T at any point in the column is known through Eqs. 13 and 14 allows the approach of Rhee et al. to be applied to the solution of the problem at hand.

The behavior of the variable C_T has been presented in Fig. 2. The solution of the entire ideal model will be superimposed on this development graph. The goal of this process is to calculate the path of the shock that forms at the beginning of the protein peak and the pattern of the rarefaction wave that forms the tail. The shock is divided into three segments, which will be designated A, B and C. The solution will proceed in six steps as described below. On the basis of this description, this model may be implemented in a computer program or, more conveniently, in a computer spreadsheet.

Calculation of the initial frontal protein and salt concentrations

During injection of a feed pulse of finite width, the protein enters the column under conditions of frontal development. The mobile phase concentrations of protein ($C_{2,f}$) and salt ($C_{1,f}$) are the feed concentrations given in Eqs. 11 and 12. Solution of the isotherm, eqs. 5 and 7, allows the stationary phase concentrations of protein and salt to be calculated. As the mobile phase and stationary phase concentrations of protein and salt are uniform everywhere behind this front during the injection, this is called a zone of constant concentration, and the concentrations within the zone will be designated $C_{1,A}$, $C_{2,A}$, $Q_{1,A}$ and $Q_{2,A}$, where $C_{1,A} = C_{1,f}$ and $C_{2,A} = C_{2,f}$.

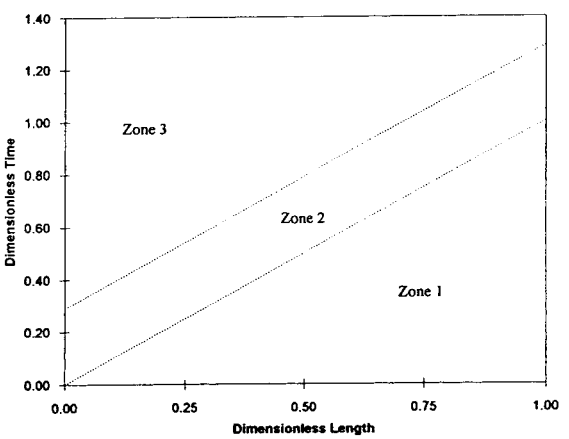

Fig. 2. Development of C_T for the case of isocratic protein elution. In zone 1, $C_T = C_{1,f}$, in zone 2, $C_T = C_{1,f} + \nu_2 C_{2,f}$; and in zone 3, $C_T = C_{1,f}$. For Figs. 2–4, elution of the protein cytochrome *c* in a mobile phase of 150 m*M* sodium at pH 6.0; the feed pulse was injected at a concentration of 0.54 m*M* over 0.29 dimensionless time units.

Calculation of shock segment A

The velocity of this initial front or "shock" may now be calculated. Because the zones in front of and behind the shock are zones of constant mobile and stationary phase concentration, the resulting shock moves along a straight line, given by the equation

$$\tau = \left(1 + \beta \cdot \frac{\Delta Q_{i,A}}{\Delta C_{i,A}}\right) z \quad i = 1 \text{ and } 2 \tag{15}$$

where $\Delta Q_{i,A}$ and $\Delta C_{i,B}$ represent the change in concentration across the shock. Because the protein concentration in front of the shock is zero, it is possible simply to write

$$\tau = \left(1 + \beta \cdot \frac{Q_{2,A}}{C_{2,A}}\right) z \tag{16}$$

where $C_{2,A}$ and $Q_{2,A}$ are the mobile and stationary phase concentrations of protein behind shock segment A.

Shock segment A originates at the point (0, 0) at which the feed is introduced into the column. Examining Fig. 3, it can be seen that the shock travels slower than the changes in total equivalents (C_T) which are plotted in both Figs. 2 and 3. The point at which the second change in total equivalents catches up with shock segment A is labeled K in Fig. 3. Point K is the end of shock segment A.

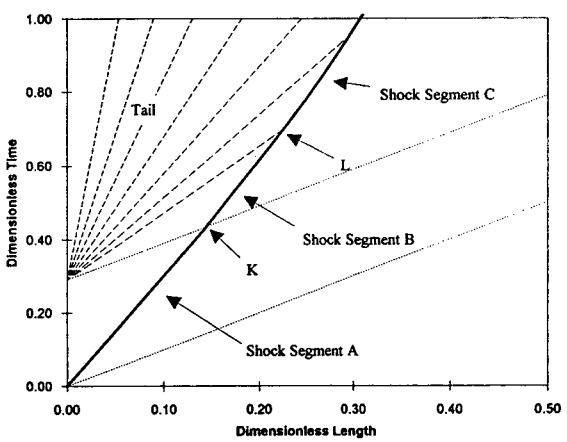

Fig. 3. Development plot for isocratic protein elution. Plot includes changes in the value of C_T (dotted lines), the protein front or "shock" (solid line) and characteristics of the tail or "rarefaction wave" (dashed lines). This figure represents an expanded view of one region of Fig. 4; the calculation was carried out with 50 characteristics in the rarefaction wave. Simulation conditions as in Fig. 2.

Calculation of second plateau concentration

On the basis of Eqs. 13 and 14, it can be seen that the second change in total ion concentration (C_T) passes through the column as a discontinuity traveling at the mobile phase velocity ($u_T = 1$). Of particular interest is the portion of the development plot (Fig. 3) from the end of the feed pulse at $\tau = 0.29$ to the point designated K. Along this dotted line, the change in C_T is made up of changes in the mobile phase concentrations of protein (C_2) and salt (C_1). Below this dotted line, the mobile and stationary phase concentrations have already been calculated. Above this dotted line, they are unknown.

Since the values of C_1 and C_2 change across this line, the line represents a discontinuity in the value of both these quantities. The velocity of any discontinuity within the column is given by the expression

$$u_{sh} = \frac{1}{1 + \beta \cdot \dfrac{\Delta Q_i}{\Delta C_i}} \quad i = 1 \text{ and } 2 \tag{17}$$

As this discontinuity moves through the column with a velocity of unity ($u_{sh} = u_T = 1$), it can be seen that $\Delta Q_i / \Delta C_i = 0$. Hence the bound concentrations of protein and salt do not change across the discontinuity caused by the change in C_T, and are know to be $Q_{2,B} = Q_{2,A}$ and $Q_{1,B} = Q_{1,A}$. However, the mobile phase concentrations do change and must be calculated. Since the total ion concentration above the dotted line (after the discontinuity) is known ($C_T = C_{1,f}$) and since $Q_{2,B}$ and $Q_{1,B}$ have already been established, the individual mobile phase concentrations $C_{1,B}$ and $C_{2,B}$ may be calculated using the SMA isotherm (Eqs. 5 and 7).

It should be noted that, if one attempted to describe the protein's equilibrium using the Langmuir isotherm, such a two-plateau solution would not exist. However, when the SMA for-

malism is employed, the existence of two plateaus in the simulation of the development of a pulse of finite width is a necessity. Experimental results that include such two-plateau development will be presented below.

Calculation of the tail

In order to calculate the boundaries of this second region of constant concentration on the development plot, it is necessary to examine the rarefaction wave or tail of the protein band. The tail exists entirely within zone 3 of Fig. 2, where the total concentration of protein and salt given in equivalents is known ($C_T = C_{1,f}$).

The behavior of the tail may be calculated using the method of characteristics. An infinite number of "characteristics" (lines of constant protein and salt concentration) fan out from the end of the feed pulse at the point (τ_f, 0). The equation of the characteristics is

$$\tau = \tau_f + \left(1 + \beta \cdot \frac{\partial Q_2}{\partial C_2}\right) z \tag{18}$$

where the partial derivative $\partial Q_2/\partial C_2$ is evaluated over the range $0 \leq C_2 \leq C_{2,B}$. Because C_1 and C_2 remain constant along any characteristic, the partial derivative $\partial Q_2/\partial C_2$ remains constant along that characteristic, and the resulting characteristic is a straight line.

In the limiting case of $C_2 = 0$ (i.e., the case of infinite dilution with respect to protein), the partial derivative will be given by

$$\frac{\partial Q_2}{\partial C_2} = K_{12}\left(\frac{\Lambda}{C_T}\right)^{\nu_2} \tag{19}$$

Use of Eq. 19 in the characteristic equation will result in calculation of the slowest characteristic within the tail. The point at which this characteristic reaches the end of the column is labeled M in Fig. 4.

For higher concentrations of protein, the expression for the differential is more complex. Recalling that C_T is constant and known through Eq. 13c and that Eq. 7 describes the stationary phase capacity, differentiation of Eq. 5 leads to the expression

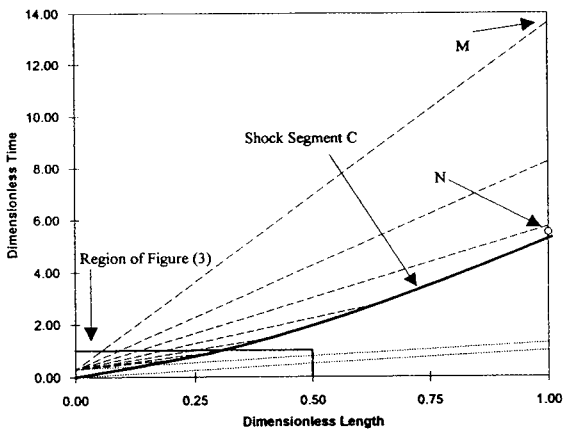

Fig. 4. Development plot for isocratic protein elution. Plot includes changes in the value of C_T (dotted lines), the protein front or "shock" (solid line), characteristics of the tail or "rarefaction wave" (dashed lines) and the estimate of the breakthrough obtained by quadrature applied to Eq. 30 (open circle). The calculation was carried out with 50 characteristics in the rarefaction wave. Simulation conditions as in Fig. 2.

$$\frac{\partial Q_2}{\partial C_2} = \frac{\dfrac{Q_2}{C_2} + \nu_2^2 \cdot \dfrac{Q_2}{C_1}}{1 - \nu_2 + \nu_2 \cdot \dfrac{\Lambda}{\bar{Q}_1}} \tag{20}$$

which is valid throughout the tail and which simplifies to Eq. 19 under conditions of infinite dilution with respect to the protein. Given an arbitrary value of C_2 and using the isotherm in conjunction with the known value of C_T, the quantities C_1, Q_2 and $\bar{Q}_1$ may be calculated. Subsequently, the corresponding characteristic may be calculated using Eqs. 18 and 20. Discretization of C_2 over the range $0 \leq C_2 \leq C_{2,B}$ leads to a fan of the type depicted by the dashed lines in Fig. 4. Below, these characteristics will be used to generate simulated chromatograms.

However, discretization over C_2 is not the method of choice. Because Q_2 and $\bar{Q}_1$ are implicit functions of C_2 and C_1, discretization over C_2 requires a numerical calculation using a Newton–Raphson method for each characteristic. In contrast, when C_T is known, C_2, C_1, Q_2 and $\bar{Q}_1$ are explicit functions of $\bar{Q}_1/C_1$. Thus, the appropriate discretization is obtained using

the variable $\bar{Q}_1/C_1$ over the range $\Lambda/C_T \leq \bar{Q}_1/C_1 \leq \bar{Q}_{1,B}/C_{1,B}$. No matter how many characteristics are employed, the resulting method for generating chromatograms requires only two applications of a Newton–Raphson method.

It should be noted that the ratio $\bar{Q}_1/C_1$ constitutes a fundamental variable of non-linear chromatography when equilibrium is described by the SMA formalism. The separation factor under concentrated conditions is given by the expression

$$\alpha_{ij} = \frac{Q_i}{C_i} \cdot \frac{C_i}{Q_j} = \left(\frac{K_{1j}}{K_{1j}}\right)\left(\frac{\bar{Q}_1}{C_1}\right)^{(\nu_i - \nu_j)} \tag{21}$$

For displacement chromatography, using the dynamic affinity theory of Brooks and Cramer, [22], the affinity parameter λ_i is defined by the following expression:

$$\lambda_i = \left(\frac{K_{1i}}{\Delta}\right)^{1/\nu_i} = \left(\frac{C_1}{\bar{Q}_1}\right)_i \tag{22}$$

where Δ is the partition coefficient of the displacer (Q_d/C_d) and $(\bar{Q}_1/C_1)_i$ is the ratio $\bar{Q}_1/C_1$ defined by the protein microenvironment. It is no coincidence that the ratio $\bar{Q}_1/C_1$ appears in the separation factor and is related to the affinity parameter. In fact, the ratio of the sites on the ion-exchange surface available for exchange to the mobile phase salt concentration is a fundamental variable of nonlinear ion-exchange chromatography. Rearrangement of Eq. 5 make it clear that this ratio

$$Q_i = K_{1i}\left(\frac{\bar{Q}_1}{C_1}\right)^{\nu_i} C_i \quad i = 2, \ldots, NC \tag{23}$$

is directly related to the partition coefficient under linear and non-linear, single-component and multi-component conditions.

Calculation of the development boundaries of the second plateau

Having calculated the concentrations of protein and salt present in the mobile and stationary phases immediately after the second C_T discontinuity, what are the boundaries of this region in the development plot? One boundary will be the characteristic of the tail (rarefaction wave) calculated by solving Eqs. 18 and 20 for the value $C_{2,B}$ (i.e. the value $\bar{Q}_{1,B}/C_{1,B}$). This characteristic is depicted in Fig. 3 as the dashed line with the shallowest slope (highest velocity).

The second boundary of this constant concentration zone will begin at the point labeled K on the development plot Fig. 3. At this point, shock segment A ends and shock segment B begins. Shock segment B represents the path of a front of constant concentration and follows the straight line given by

$$\tau = \left(1 + \beta \cdot \frac{Q_{2,B}}{C_{2,B}}\right) z \tag{24}$$

Having calculated the two previously unknown boundaries of the second zone of constant concentration, the intersection of these two boundaries may also be calculated. This is the point at which the rarefaction wave (tail) reaches the front of the protein pulse, and it is the end of shock segment B. This point is labeled L in Fig. 3.

Calculation of shock segment C

After the rarefaction wave has reached the front of the protein pulse, the concentration of protein on the left side of the shock begins to decline. As a result, the last segment of the shock is not a straight line and a process of integration will be required in order to establish this segment of the shock path. In the discussion of the development of a peak of finite width by Rhee et al. [3], the Langmuir isotherm was employed. As a result, the integration could be carried out analytically. Because the SMA formalism has a more complex form than the Langmuir isotherm, no simple analytical method could be developed. However, two separate methods of numerical integration will be presented below. The first method calculates the path of the shock through the region of curvature and the second determines the breakthrough of the protein front without calculating the shock path. The second method serves as an independent check of the accuracy of the first method.

The goal of this calculation is to extend the shock path from the point L in Fig. 3 to the coordinate $z = 1$ (when the shock emerges from the column). Examination of Figs. 3 and 4 reveals that the characteristics of the tail meet the protein shock after point L in the region of curvature. The velocity of the shock along each characteristic is known exactly and is given by the following version of Eq. 17:

$$u_{sh} = \frac{1}{1 + \beta \cdot \frac{Q_2}{C_2}} \tag{25}$$

The velocity of the characteristics themselves may also be calculated. Consideration of Eq. 18 gives the velocity of any characteristic:

$$u_{char} = \frac{1}{1 + \beta \cdot \frac{\partial Q_2}{\partial C_2}} \tag{26}$$

where the partial derivative can be calculated using Eq. 20. Since the velocity of the characteristics (u_{char}) and the velocity of the shock along each characteristic (u_{sh}) are both known exactly, a numerical technique may be developed to calculate the path of the shock.

The numerical integration begins at point L in Fig. 3. This point corresponds to the intersection of the protein shock and the fastest characteristic of the tail and will be designated (τ_0, z_0). To calculate each new point (τ_{i+1}, z_{i+1}) along the protein shock, the velocity of the shock will be estimated to be the velocity at the current point ($u_{sh,i}$). The intersection of this linear approximation of the shock and the next characteristic (numbered $i + 1$) will then be calculated. The non-dimensional coordinates of this intersection are

$$z_{i+1} = \frac{\tau_f - \tau_i + \frac{z_i}{u_{sh,i}}}{\frac{1}{u_{sh,i}} - \frac{1}{u_{char,i+1}}} \tag{27}$$

$$\tau_{i+1} = \frac{z_{i+1}}{u_{char,i+1}} + \tau_f \tag{28}$$

The results of such a numerical integration are shown in Fig. 4. For clarity, only a fraction of the characteristics employed in the integration are shown in Fig. 4. As the number of characteristics employed in the calculation is increased, the numerical approximation of the shock path will converge to the actual path (the rate of convergence is discussed below). Having calculated the shock path and the rarefaction wave, it is possible to generate simulated chromatograms.

Before these simulated chromatograms are presented, a second independent method to calculate of the breakthrough time of the protein band, but not the shock path, will be presented. The mass of protein injected into the column may be calculated:

$$M_{inj} = C_{2,f} \tau_f V_0 \tag{29}$$

where V_0 is the dead volume of the column. Within the ideal theory of chromatography, a peak resulting from an injection of arbitrary concentration ($C_{2,f}$) and width (τ_f) will always finish eluting from the column at a time dictated by the protein's velocity at infinite dilution and the width of the injection volume. This point (τ_{id}, 1) is labeled M in Fig. 4. If an integration of the mass eluting from the column is carried out, it is expected that the following equation will be satisfied:

$$M_{inj} = V_0 \int_{\tau_{bt}}^{\tau_{id}} C_2(\tau, 1)\, d\tau = -V_0 \int_{\tau_{id}}^{\tau_{bt}} C_2(\tau, 1)\, d\tau \tag{30}$$

where $C_2(\tau, 1)$ is the concentration of protein eluting from the end of the column at non-dimensional time τ and τ_{bt} and τ_{id} are the non-dimensional times at which the protein peak breaks through at the end of the column and at which the protein peak finishes eluting from the column, respectively.

The integral Eq. 30 may be evaluated numerically for the purpose of calculating τ_{bt}. By starting at the tail of the protein band at $\tau = \tau_{id}$ and $C_2 = 0$, it is possible to integrate backwards in time using a method of quadrature such as the trapezoid rule. The process of summation which approximates the integral Eq. 30 will continue as

long as the summation is less than the actual mass injected given by Eq. 29.

If a method of quadrature that overestimates the area within the tail of the chromatogram is employed (e.g., the trapezoid rule), the resulting estimate of τ_{bt} will be slightly later than the true value. In contrast, the numerical method for estimating the shock path described by Eqs. 27 and 28 will result in estimates of τ_{bt} that are slightly early. Thus, if the estimates of τ_{bt} obtained by the two methods agree within a prespecified tolerance, the accuracy of the shock path calculation can be considered confirmed.

The point (τ_{bt}, 1) estimated by quadrature applied to Eq. 30 is represented by an open circle labeled N in Fig. 4. Comparison of the arrival time of the shock with this open circle reveals a small disagreement of the two methods for a calculation using 50 characteristics. By increasing the number of characteristics employed in the calculation, an arbitrary degree of accuracy may be obtained.

Table 3 presents data on the convergence of the numerical integration scheme of Eqs. 27 and 28. The first column of the table presents the number of characteristics employed in calculation of τ_{bt}. The second column presents the value of τ_{bt} obtained by numerical integration along the shock path using Eqs. 27 and 28. The third column presents the change in τ_{bt} with each increase in the number of characteristics employed. Examination of the third column reveals that the numerical scheme converges linearly with the number of characteristics employed. By extrapolating this linear trend to an infinite number of characteristics, it is possible to estimate the true value of τ_{bt}. The result of that extrapolation is contained within the bottom row of the table. The final column of the table presents the percentage error of each of the estimates with respect to the extrapolated value of τ_{bt}.

Table 3
Convergence of numerical approximation of shock segment C

No. of characteristics	τ_{bt} (method 1)	$\Delta\tau_{bt}$	Error (%)
25	5.155		−4.9
50	5.283	0.128	−2.5
100	5.351	0.068	−1.2
200	5.384	0.033	−0.6
400	5.401	0.017	−0.3
∞[a]	5.418	0.017	0.0

[a] The value of τ_{bt} for an infinite number of characteristics was calculated by extrapolation.

During the process of integrating Eq. 30, if the edge of a trapezoid closely coincides with the true value of τ_{bt}, an extremely accurate estimate of τ_{bt} will be obtained. Thus, the values of $\Delta\tau_{bt}$ would not be expected to converge smoothly in the second method. However, its maximum possible error would be bounded and is expected to converge in a manner similar to the first method.

Because only two Newton–Raphson calculations are required in order to solve the model, a calculation involving 400 characteristics is only slightly slower than one involving 25. All calculations were carried out using the Microsoft Excel program on a computer equipped with an Intel 80486 CPU, and the longest required less than 5 s.

Three types of chromatograms that may result

Three broad categories of chromatograms may result from the preceding calculation. If the peak elutes from the column after the points K and L in Fig. 3 have been reached within the column, a non-linear peak without any regions of constant concentration will emerge from the column. Such a peak is shown in Fig. 5a. If point K has been reached inside the column but not point L, then a peak with a single plateau will emerge from the column (Fig. 5b). If neither point K nor point L is reached inside the column, a peak with a double plateau will emerge from the column (Fig. 5c). Assuming that all the operating conditions have been held constant except feed volume, Fig. 5b represents a larger feed volume than Fig. 5a, and Fig. 5c represents a larger feed volume than Fig. 5b.

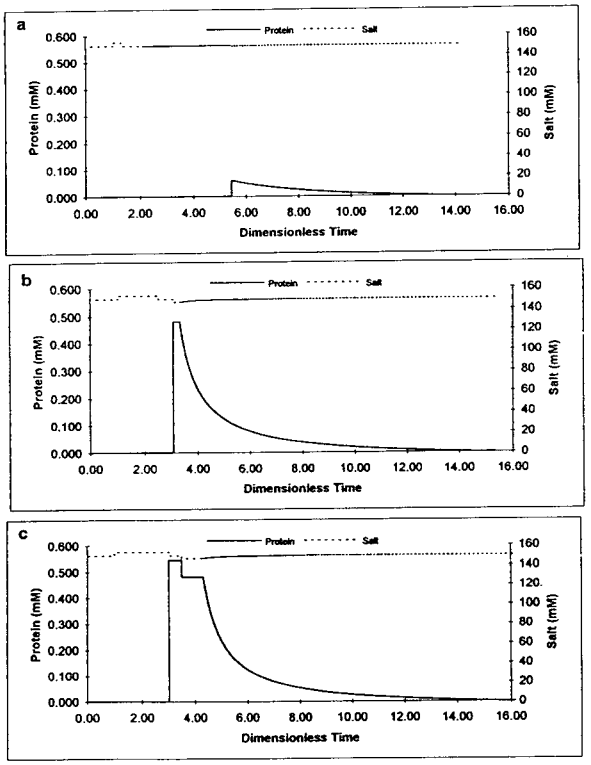

Fig. 5. The three categories of non-linear peaks observed in simulated chromatograms. (a) Feed volume of 0.29 dimensionless time units; simulation conditions as in Fig. 2. (b) Feed volume increased to 1.5 dimensionless time units. (c) Feed volume increased to 2.5 dimensionless time units. The calculations were carried out with 400 characteristics in the rarefaction wave.

3. Experimental

3.1. Materials

Sodium monobasic phosphate, sodium dibasic phosphate, and cytochrome *c* were purchased from Sigma (St. Louis, MO, USA). Sodium chloride was purchased from Aldrich (Milwaukee, WI, USA). Orthophosphoric acid was purchased from Fisher (Rochester, NY, USA). The strong cation-exchange column employed (sulfopropyl, 8 μm, 50 × 5 mm I.D.) was a gift from Waters Chromatography Division of Millipore (Milford, MA, USA).

The carrier was buffered using a solution of sodium monobasic phosphate and sodium dibasic phosphate, the ratio being chosen to give the appropriate pH range. The desired concentration of sodium ions was obtained subsequently by addition of sodium chloride. Finally, the pH was adjusted using phosphoric acid.

3.2. Apparatus

The chromatograph consisted of an LC 2150 pump (Pharmacia–LKB Biotechnology, Piscataway, NJ, USA) connected to the column via a C10W ten-port injector (Valco, Houston, TX, USA). The column effluent was monitored using a Model 757 Spectroflow UV–Vis detector (Applied Biosystems, Ramsey, NJ, USA). The detector signal was recorded using a Powermate 2 personal computer (NEC, Tokyo, Japan) which was running Maxima 820 data collection software (Waters Chromatography Division, Millipore). Data generated in this study were exported to the Microsoft Excel spreadsheet program for analysis.

3.3. Parameter estimation

The estimation of the SMA equilibrium parameters which appear in Table 1 has been discussed in detail previously [15]. In order to determine the column capacity Λ, the column was equilibrated with a carrier of 100 m*M* sodium (pH 6.0). Subsequently, a front of 1 *M* ammonium sulfate was passed through the column, and the column effluent was collected for analysis. The bed capacity was determined by measuring the amount of sodium displaced by the ammonium front.

In order to estimate the characteristic charge ν_i and equilibrium constant K_{1i} of the protein, linear elution experiments were conducted at various mobile phase salt concentrations. The resulting data was fitted to the linearized form of Eq. 1:

$$\log (k_i') = \log (\beta K_{1i} \Lambda^{\nu_i}) - \nu_i \log C_1 \qquad (31)$$

This fitting procedure resulted in an estimate of the characteristic charge ν_i of 6.15 with an uncertainty of ±0.25 and an estimate of the intercept log $(\beta K_{1i}\Lambda^{\nu_i})$ of 14.46 with an uncertainty of ±0.57 (95% confidence interval based on the Student t-distribution).

The concentration of protein bound in frontal operation $(Q_{2,f})$ may be determined using the expression

$$Q_{2,\mathrm{exp}} = \left(\frac{V_B}{V_0} - 1\right) \cdot \frac{C_{2,f}}{\beta} \tag{32}$$

where $C_{2,f}$ is the protein concentration of the front, V_B is the breakthrough volume of the front, V_0 is the dead volume of the column and β is the phase ratio. Using Eq. 32, pairs of known values of $C_{2,f}$ and $Q_{2,f}$ may be established in order to represent the single component isotherm at various salt concentrations.

Having established the isotherm experimentally, an estimate of the steric factor σ_i may now be obtained. Only a single point in the non-linear region of the isotherm, represented by a pair of values of $C_{2,f}$ and $Q_{2,f}$, is required. Of course, the protein concentration $C_{2,f}$ should be relatively high in order to insure that the non-linear region of the isotherm has been reached. Greater accuracy can be expected by conducting frontal experiments at more than one protein concentration and at more than one salt concentration.

Because SMA is an implicit isotherm, calculation of the concentration of bound protein $(Q_{2,\mathrm{SMA}})$ on the basis of known values of mobile phase protein and salt concentrations $(C_{2,f}$ and $C_{1,f})$ requires use of a Newton–Raphson technique. (The designation SMA after $Q_{2,\mathrm{SMA}}$ indicates that this is an estimate made by the SMA formalism.) However, the mobile phase concentration of protein $(C_{2,\mathrm{SMA}})$ may be calculated analytically based on known values of mobile phase salt concentration and stationary phase protein concentration $(C_{1f}$ and $Q_{2,f})$:

$$C_{2,\mathrm{SMA}} = \left[\frac{C_{1,f}}{\Lambda - (\nu_2 + \sigma_2)Q_{2,f}}\right]^{\nu_i} \frac{Q_{2,f}}{K_{12}} \tag{33}$$

Eq. 33 may be used in conjunction with the experimental protein isotherm in order to estimate the steric factor σ_i. The residuals between the experimental protein concentration $(C_{2,f})$ used in Eq. 32 and the estimate of the protein concentration $(C_{2,\mathrm{SMA}})$ obtained from Eq. 33 may be calculated as a function of the steric factor. Minimization of the sum of squares of the residuals using a Newton–Raphson technique will establish the estimated steric factor.

The use of Eq. 33 will be designated the "frontal method" of determination of the steric factor. In this work, multiple non-linear frontal experiments were employed to estimate a steric factor of 53.4. These points are shown in conjunction with the corresponding SMA isotherms in the Appendix.

3.4. Conversion of detector response

In order to compare the predictions obtained from the ideal model presented above with chromatographic experiments, non-linear elution experiments were conducted at 150 and 125 mM salt concentrations. The chromatograms were collected using Maxima 820 data collection software and saved for later analysis. The original data were obtained in units of μV (detector response) versus minutes. During data reduction, the time axis was converted into dimensionless time units. (An unretained tracer capable of exploring all of the pores would emerge from the column at one dimensionless time unit. No measurable pore exclusion of cytochrome c was observed). The detector response was converted from μV to mM cytochrome c using appropriate conversion factors obtained from linear plots of concentration versus detector response.

4. Results and discussion

Having presented the theoretical model of isocratic elution of a pulse of finite width and height, the focus of the discussion will be on a small number of carefully selected experiments to document both the ability of the model to predict this phenomenon and the limitations of the model. Two relatively important constraints

on the model should be understood at the outset. First, ideal chromatography ignores the effect of Taylor dispersion during convective transport within the column and the effects of finite rates of mass transport across the film surrounding the stationary phase particles and within the pores of the particles [1]. As a result, the predictions of an ideal model do not have the rounded contours of experimental chromatograms. Nevertheless, under non-linear conditions, it is expected that an ideal model will provide reasonable predictions of experimental results since thermodynamic spreading of the tail predominates over mass transfer effects. Second, this model only attempts to account for the elution of a single protein. In order to model multi-component separations, interaction of multiple shocks and rarefaction waves must be considered. Typically, such problems are solved by resort to numerical techniques such as finite difference or finite element methods.

Fig. 6 shows the non-linear elution of cytochrome *c* at 150 m*M* salt. As can be seen, the infinite dilution retention of the protein is well predicted at 13.6 dimensionless time units. Slight experimental tailing beyond this point is attributable to the dispersion observed in the column which is not included in the ideal model. The degree of tailing observed in the experimental chromatogram is well matched by the simulation. The front of the experimental cytochrome *c* band is more disperse, but examination of the breakthrough time of the front measured at half-height yields a value of τ_{bt} almost identical with the simulated value (5.4 dimensionless time units).

Fig. 7 shows the non-linear elution of cytochrome *c* at 125 m*M* salt. The decrease in salt concentration has sharply increased the retention of the protein. The infinite dilution retention of the protein is now in the neighborhood of 39 dimensionless time units. And, the maximum concentration of the experimental chromatogram has decreased to approximately 0.015 m*M*. Again, the experimentally observed tailing is well simulated by this model.

Recalling the discussion of Figs. 3 and 4, all peaks go through a period of development in which they are characterized by two plateaus (as depicted in Fig. 5c). Subsequently, the chromatographic band may develop into a band of one plateau (Fig. 5b) or no plateaus (Fig. 5a) if the column is long enough. Having observed two highly tailed peaks of the type depicted in Fig. 5a, it is worth examining the earlier development of a peak of finite width. For this purpose, the feed pulse was increased to a width of 4.6 dimensionless time units and a concentration of 0.29 m*M* cytochrome *c*. Fig. 8 depicts the re-

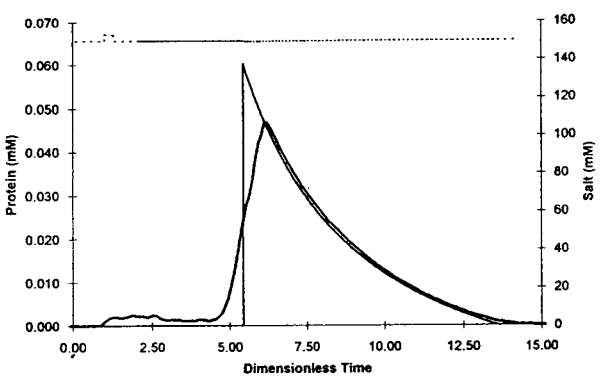

Fig. 6. Elution chromatogram (thick solid line) and simulation (thin solid line) of the protein cytochrome *c* in a mobile phase of 150 m*M* sodium at pH 6.0. The simulated salt profile is depicted as a dotted line. The feed pulse was injected at a concentration of 0.54 m*M* over 0.29 dimensionless time units. The calculation was carried out with 400 characteristics in the rarefaction wave.

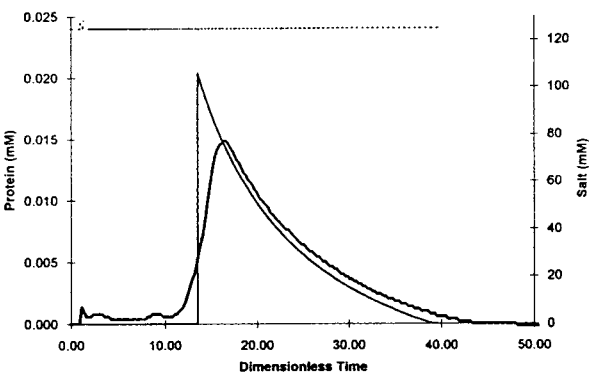

Fig. 7. Elution chromatogram (thick solid line) and simulation (thin solid line) of the protein cytochrome *c* in a mobile phase of 125 m*M* sodium at pH 6.0. The simulated salt profile is depicted as a dotted line. The feed pulse was injected at a concentration of 0.57 m*M* over 0.29 dimensionless time units. The calculation was carried out with 400 characteristics in the rarefaction wave.

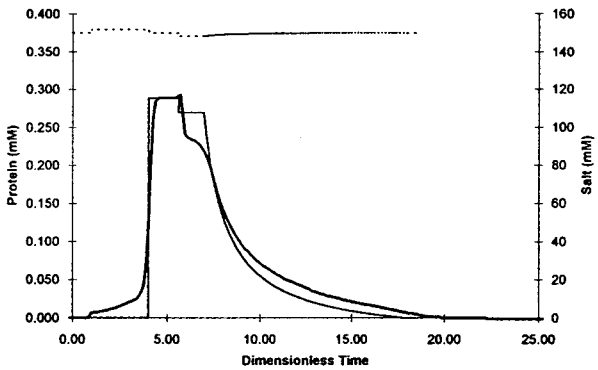

Fig. 8. Elution chromatogram (thick solid line) and simulation (thin solid line) of the protein cytochrome *c* in a mobile phase of 150 m*M* sodium at pH 6.0. The simulated salt profile is depicted as a dotted line. The feed pulse was injected at a concentration of 0.29 m*M* over 4.6 dimensionless time units. The calculation was carried out with 400 characteristics in the rarefaction wave.

sulting two-plateau protein band. The infinite dilution retention is correctly predicted at 17.9 dimensionless time units. (Slight dispersion is observed past that point.) The tail is characterized by the correct degree of tailing. Before the tail, two regions of constant concentration are observed. Remarkable points about these two plateaus are that (1) to the authors' knowledge, no similar peak shape has been reported for isocratic chromatography and (2) no existing model of protein adsorption, other than SMA, would allow this result to be understood. While there is a slight disagreement in the exact concentration (0.23 m*M* experimental compared with 0.27 m*M* simulated), this result nevertheless demonstrates that SMA is uniquely well suited to describe the equilibrium in non-linear ion-exchange chromatography. (See the Appendix for a further discussion of the representation of protein isotherms in ion-exchange chromatography.)

Also included in Figs. 6–8 are the predicted salt concentrations of the model Examination of these salt profiles reveals that the salt concentration changes in isocratic chromatography are small. In Fig. 6, a pulse increase of salt is observed at 1 dimensionless time unit; this pulse was caused by injection of cytochrome *c* during the feed cycle. Subsequently, a slight decrease in salt occurs at the time that the protein peak elutes; this decrease allows C_T to remain constant, satisfying Eqs. 13 and 14. In Fig. 8, the effect of varying C_T and the effect of the elution of the protein peak depressing the salt concentration interact with each other. In fact, these effects are so subtle that most analyses would ignore them completely. However, they must be included if the two-plateau shape of Fig. 8 is to be understood.

Reflection on these simulated salt profiles reveals why the model did not predict more precisely the concentration of the second plateau. In Fig. 8, the carrier sodium concentration is 150 m*M*, the maximum deviation in the simulated salt profile is 151.18 m*M* and the minimum is 148.3 m*M*. Since these changes in salt concentration have such small magnitude, it is relatively easy for the various transport non-idealities to smooth out these changes, leading to a less pronounced two-plateau pattern. However, without the understanding offered by this model, it is likely that observation of such a double plateau would lead to the unwarranted conclusion that the product was not pure.

In Fig. 9, four non-linear peaks are shown. The bold solid line is the experimental peak already seen in Fig. 6. The lighter solid line is

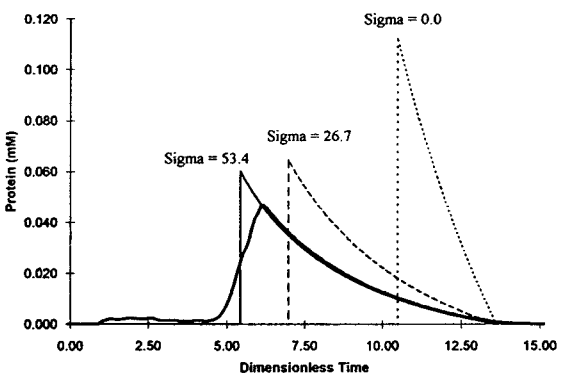

Fig. 9. Elution chromatogram (thick solid line) of the protein cytochrome *c* in a mobile phase of 150 m*M* sodium at pH 6.0. The feed pulse was injected at a concentration of 0.54 m*M* in 0.29 column volumes. Simulations were conducted for these conditions using a steric factor σ_2 of 53.4 (thin solid line), 26.7 (dashed line) and 0.0 (dotted line). The calculations were carried out with 400 characteristics in the rarefaction wave.

the model prediction shown in Fig. 6 for which the steric factor σ_2 is 53.4 (estimated using the frontal method). The dashed line utilizes the same simulation conditions as the solid line except that the steric factor is 26.7, half of the correct value. The dotted line was simulated using a steric factor of 0.0. Examination of Fig. 9 reveals clearly that use of a steric factor of 0.0 will result in significantly incorrect predictions of the non-linear band shape. A number of recent models of ion-exchange equilibrium fail to account for steric effects [8,9]. It is expected that chromatographic models based on such equilibrium will have difficulty accounting for non-linear adsorption. Examination of the peaks generated using steric factors of 53.4 and 26.7 leads to a preference for the 53.4 value. In particular, the tailing is modeled substantially better by the larger σ_2 value, and the breakthrough is estimated more accurately.

Having shown that the model can predict the elution of proteins and that the proper selection of the steric factor is important to accurate modeling of non-linear elution, a method of estimating the steric factor using a non-linear peak will now be discussed. A number of workers have discussed the use of chromatographic models in estimating Langmuir isotherm parameters [23,24]. Although the SMA model is different from the Langmuir isotherm, certain similarities exist between this earlier work and the technique presented below. In particular, the goal of all these methods is to decrease the number of frontal experiments required in parameter estimation, saving time and protein. Also, they take advantage of the fact that, in non-linear chromatography, the solute velocity depends on the mobile phase concentration of the solute.

The "non-linear peak method" of estimating the steric factor of a protein operates by minimizing the residuals between the experimental peak and the simulated chromatogram. Examination of Fig. 9 suggests that focusing on the residuals calculated in the tail (rather than residuals taken in the neighborhood of the breakthrough) would be the most effective strategy. In order to test this method of σ_2 estimation, twelve data points (concentration–elution time pairs) were selected from the experimental chromatogram depicted in Fig. 9. These points were equally spaced between 7.1 and 12.4 dimensionless time units. Using Eqs. 18 and 20, the characteristics corresponding to the selected concentrations were calculated. The residuals between the experimental elution times of these concentrations and the times dictated by the characteristics were then calculated. The value of σ_2 which minimized the sum of squares of the residuals was 50.3. From this calculation, it can be seen that reasonable estimates of the steric factor σ_2 may be obtained by this method.

5. Conclusions

The traditional view of adsorption based on the Langmuir isotherm is inadequate for many of the chromatographic systems employed today. In particular, methods development in the preparative ion-exchange chromatography of proteins demand a rigorous yet convenient description of the salt dependence of binding and of non-linear adsorption. The steric mass action (SMA) model of ion exchange offers such a formalism.

Whether used in a simple, ideal model as presented here or in conjunction with an elaborate multi-component numerical model, the SMA formalism offers the ability to predict elution at various salt concentrations and also non-linear absorption and displacement effects. Because the SMA model builds on existing work that originated with the seminal paper by Boardman and Partridge [5], its use should be easily understood by both academics and process development professionals.

As another step in the adoption of such a model to process development, this paper has focused on two important effects in preparative chromatography: the salt dependence of protein binding and non-linear adsorption. The model that was presented can be easily implemented using one of the spreadsheets widely available for the personal computer. Having such a model available during parameter estimation or process

design can assist the separation scientist in methods development and optimization.

Acknowledgements

The authors acknowledge Millipore for providing the data collection system and the stationary phase employed. This research was supported by a Presidential Young Investigator Award to S.M.C. from the National Science Foundation.

Symbols

C	mobile phase concentration (mM)
$C_{i,\mathrm{A}}$	mobile phase concentration behind shock segment A (mM)
$C_{i,\mathrm{B}}$	mobile phase concentration behind shock segment B (mM)
$C_{i,\mathrm{f}}$	feed concentration at column inlet (mM)
F_i	function which returns Q_i when given $C_1, \ldots, C_{NC}$ (mM)
K_{1i}	equilibrium constant
k'	capacity factor
K	point of transition from shock segment A to shock segment B
L	point of transition from shock segment B to shock segment C
L_{col}	column length (cm)
M	point at which the tail of the chromatographic band elutes from the column
M_{inj}	mass of protein injected (μmol)
NC	number of components present in mobile phase
Q_i	stationary phase concentration (mM)
$Q_{i,\mathrm{A}}$	stationary phase concentration behind shock segment A (mM)
$Q_{i,\mathrm{B}}$	stationary phase concentration behind shock segment B (mM)
$Q_{i,\max}$	maximum possible single-component bound protein concentration (mM)
$\bar{Q}_1$	bound salt which is not sterically shielded (mM)
$\hat{Q}_1$	bound salt which is sterically shielded (mM)
$\bar{Q}_{1,\mathrm{B}}/C_{1,\mathrm{B}}$	ratio $\bar{Q}_1/C_1$ in constant concentration zone behind shock segment B
t	time dimension (s)
u_{char}	characteristic velocity (cm/s)
u_{sh}	shock velocity (cm/s)
u_0	chromatographic velocity, $u_0 = u_s/\varepsilon$ (cm/s)
V_0	dead volume of the column determined by a small tracer molecule (ml)
Z	axial position in column (cm)
z	dimensional axial position (Z/L)
z_i	ith position in the numerical integration of shock segment C

Greek letters

β	phase ratio $[(1-\varepsilon)/\varepsilon]$
Δ	change in a variable across a discontinuity
ε	void fraction
Λ	column capacity (mM)
ν_i	characteristic charge
σ_i	steric factor
τ	dimensionless time or column dead volumes ($\tau = t/t_0 = V/V_0$)
τ_{f}	dimensionless feed pulse time
τ_i	ith time in the numerical integration of shocked segment C

Subscripts

i	mobile/stationary phase component number ($i = 1$ designates salt)

Appendix

An important goal of this paper is to suggest that the SMA formalism is a superior method of depicting ion-exchange adsorption of proteins in chromatography. While the main body of this paper focuses on chromatographic development in nonlinear chromatography, this Appendix will be devoted to the depiction of isotherms. The parameter estimation process was described briefly in the main body of this paper. Within this Appendix, three isotherms will be compared for their efficacy at depicting protein adsorption

data. The first is the SMA formalism [13]. The second is the SDM/electroneutrality model [8,9]. The third formalism is the modifier-dependent Langmuir isotherm of Antia and Horváth [25]:

$$Q_i = \frac{a_i C_s^{-Z} C_i}{1 + \sum_{j=1}^{NC} \frac{a_j}{\lambda_j} C_s^{-Z} C_j} \quad \text{(A1)}$$

where C_s is the mobile phase salt concentration, C_i and Q_i are the mobile phase and stationary phase protein concentrations and Z_i, a_i and λ_i are parameters of the model. The modifier-dependent Langmuir was not employed in the main text because it would have been incapable of predicting the two-plateau peak shape.

In parameter estimation, the most reasonable approach in fitting a three-parameter model to experimental data is to use two parameters to fit the region of infinite dilution and to use the third parameter to fit the non-linear region of the isotherm. That is the approach described in the section of this paper devoted to parameter estimation for the SMA formalism. The benefit of this method is that, is that, by devoting two parameters to the infinite dilution data, chromatograms simulated at low concentrations should be fairly accurate. Any deviations between the model and the experiment will appear in the high-concentration regime.

Adopting this philosophy of fitting, all three of the models mentioned above should be able to predict low concentration [log(k') versus log(salt concentration) data] well. The data set employed to test the non-linear predictive capacity of these models consisted of cytochrome *c* data taken using frontal chromatography at 90, 125 and 150 m*M* sodium. The SMA formalism treated these data with little difficulty, as seen in Fig. A1a. The steric factor employed to obtain this fit was 53.4.

The SDM/electroneutrality model had difficulty in the non-linear regime because it is a two-parameter model. The predictions made by this model are obtained by using the SMA equilibrium equations while setting the SMA steric factor σ_i to zero. As the degree of non-linearity increases, the SDM/electroneutrality predictions diverge dramatically from the experimental data in Fig. A1b.

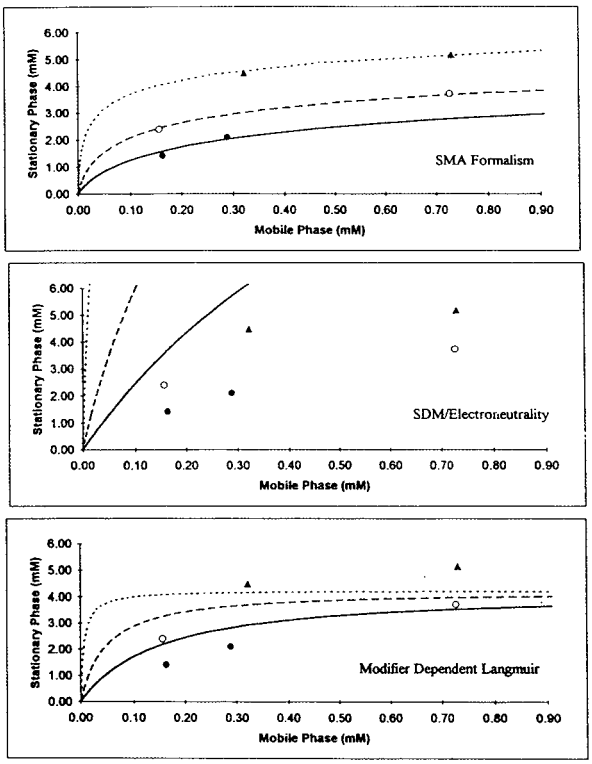

Fig. A1. Isotherms of cytochrome *c* on a strong cation-exchange column at pH 6.0. The experimental data was collected at (▲) 90, (○) 125 and (●) 150 m*M* sodium. The predictions of the three isotherms are depicted at 90 m*M* (dotted line), 125 m*M* (dashed line) and 150 m*M* (solid line) sodium.

In order to fit the model of Antia and Horváth, using two parameters to fit the infinite dilution data (as Antia and Horváth suggest), Z_i is chosen equal to the characteristic charge within the SMA formalism and a_i is set equal to the group of SMA parameters: $K_{1i}\Lambda^{Pi}$. Finally, λ_i is estimated by minimizing the sum of squares error between the values Q_i obtained in non-linear frontal experiments and the model's estimates of those values. In preparing Fig. A1c, λ_i was selected to be 4.3. Examining the figure, while substantially better than SDM/electroneutrality, this model is inferior to SMA in its ability to predict non-linear protein adsorption. This formalism has the additional disadvantage of

being unable to account for induced salt gradients in displacement chromatography. Hence it is wholly inadequate to account for the behavior of proteins in displacement chromatography [13].

More extensive tests of the ability of SMA to predict isotherms of proteins and polyelectrolytes across a range of salt have already been conducted [15–19].

References

[1] F.G. Helfferich and P.W. Carr, *J. Chromatogr.*, 629 (1993) 97.

[2] J.C. Bellot and J.S. Condoret, *Process Biochem.*, 28 (1993) 365.

[3] H. Rhee, R. Aris and N.R. Amundson, *First-Order Partial Differential Equations: Vol. I, Theory and Application of Single Equations*, Prentice-Hall, Englewood Cliffs, NJ, 1986.

[4] H. Rhee, R. Aris, and N.R. Amundson, *First-Order Partial Differential Equations: Vol. II, Theory and Application of Hyperbolic Systems of Quasilinear Equations*, Prentice-Hall, Englewood Cliffs, NJ, 1989.

[5] N.K. Boardman and S.M. Partridge, *Biochem. J.*, 59 (1955) 543.

[6] W. Kopaciewicz, M.A. Rounds, J. Fausnaugh and F.E. Regnier, *J. Chromatogr.*, 266 (1983) 3.

[7] R.R. Drager and F.E. Regnier, *J. Chromatogr.*, 359 (1986) 147.

[8] A. Velayudhan and C. Horváth, *J. Chromatogr.*, 443 (1988) 13.

[9] P. Cysewski, A. Jaulmes, R. Lemque, B. Sebille, C. Vidal-Madjar and G. Jilge, *J. Chromatogr.*, 548 (1991) 61.

[10] A. Velayudhan and C. Horváth, *J. Chromatogr. A*, 663 (1994) 1.

[11] J.C. Bellot and J.S. Condoret, *J. Chromatogr.*, 484 (1993) 1.

[12] A. Velayudhan, *Doctoral Dissertation*, Yale University, New Haven, CT, 1990.

[13] C.A. Brooks and S.M. Cramer, *AIChE J.*, 38 (1992) 1969.

[14] A.L. Myers, *AIChE J.*, 29 (1983) 691.

[15] S.D. Gadam, G. Jayaraman and S.M. Cramer, *J. Chromatogr.*, 630 (1993) 37.

[16] J.A. Gerstner and S.M. Cramer, *Biotechnol. Prog.* 8 (1992) 540.

[17] J.A. Gerstner and S.M. Cramer, *BioPharm* 5 (1992) 42.

[18] G. Jayaraman, S.D. Gadam and S.M. Cramer, *J. Chromatogr.*, 630 (1993) 53.

[19] S.D. Gadam, S.R. Gallant and S.M. Cramer, *AIChE J.*, in press.

[20] P.C. Wankat, *Rate-Controlled Separations*, Elsevier, London, 1990.

[21] P.K. de Bokx, P.C. Baarslag and H.P. Urbach, *J. Chromatogr.*, 594 (1992) 9.

[22] C.A. Brooks and S.M. Cramer, *Chem. Eng. Sci.*, in press.

[23] J.A. Jonsson and P. Lovkvist, *Chemometrics*, 5 (1989) 303.

[24] E.V. Dose, S. Jacobson and G. Guiochon, *Anal. Chem.*, 63 (1991) 833.

[25] F. D. Antia and C. Horváth, *J. Chromatogr.*, 484 (1989) 1.

ELSEVIER

Journal of Chromatography A, 702 (1995) 143–155

JOURNAL OF CHROMATOGRAPHY A

Ion-exchange displacement chromatography of proteins Dendritic polymers as novel displacers

Guhan Jayaraman[a], Yu-Fei Li[b], J.A. Moore[b], Steven M. Cramer[a,*]

[a]*Howard P. Isermann Department of Chemical Engineering, Rensselaer Polytechnic Institute, Troy, NY 12180-3590, USA*
[b]*Department of Chemistry, Rensselaer Polytechnic Institute, Troy, NY 12180, USA*

Abstract

While the ability to carry out simultaneous concentration and purification in a single displacement step has significant advantages for downstream processing of biopharmaceuticals, a major obstacle to the implementation of displacement chromatography has been the lack of appropriate displacer compounds. All protein displacement separations reported to date have employed relatively high-molecular-mass (>2000) polyelectrolyte displacers. In this paper, results are presented on the discovery that low-molecular-mass dendritic polymers can be successfully employed as efficient displacers for protein purification in ion-exchange systems. Pentaerythritol-based dendritic polyelectrolytes ranging in molecular mass from 480 to 5100 were investigated as potential displacers for the purification of proteins in cation-exchange systems. The adsorption properties of these dendrimers were investigated using the steric mass action (SMA) model of non-linear ion-exchange chromatography. An analysis of the resulting SMA parameters using a dynamic affinity plot indicated that these dendrimers should have sufficient affinity to act as protein displacers. Displacement separations of protein mixtures in cation-exchange systems were carried out using zero-, first- and second-generation dendrimers. These experiments demonstrate that this new class of dendritic polyelectrolytes can indeed act as efficient protein displacers. The ability of a low-molecular-mass compound such as the "zero'-generation dendrimer (M_r 480) to displace proteins is very significant in that it represents a major departure from the conventional wisdom that large polyelectrolyte polymers are required to displace proteins in ion-exchange systems. In addition to the fundamental interest generated by low-molecular-mass displacers, it is likely that these displacers will have significant operational advantages as compared to large polyelectrolyte displacers.

1. Introduction

The design of efficient and cost-effective downstream processes for the large-scale purification of biomolecules from complex biological mixtures continues to be one of the major challenges facing the biotechnology industry [1]. In recent years, displacement chromatography has attracted considerable attention as a promising preparative technique for protein separations [2–5]. Displacement chromatography can be carried out using existing chromatographic systems with minor modifications to enable the sequential perfusion of the column with the carrier, feed, displacer and regenerant solutions [6]. The key operational feature which distinguishes displacement from step-elution chromatography is the use of a high-affinity displacer compound. In displacement chromatography, the column is first equilibrated with a carrier

* Corresponding author.

0021-9673/95/$09.50 © 1995 Elsevier Science B.V. All rights reserved
SSDI 0021-9673(94)01007-2

under conditions wherein the components to be separated have a relatively high affinity for the stationary phase. A large volume of the feed mixture is then loaded onto the column, followed by a constant infusion of the displacer solution. The displacer is selected such that it has a higher affinity for the stationary phase than any of the feed components. (Note: a more detailed discussion of affinity in displacement systems is given below). Under appropriate conditions, the product components exit from the column as adjacent "square wave" zones of highly concentrated pure material, in the order of increasing affinity of adsorption. Finally, after the breakthrough of the displacer from the column outlet, the high-affinity displacer must be desorbed from the stationary phase by employing an appropriate regeneration protocol, followed by re-equilibration with the carrier.

The displacement mode of chromatographic operation offers tremendous potential for simultaneous concentration and purification of biomolecules. The peak tailing observed in overloaded elution chromatography is greatly reduced in the displacement mode due to self-sharpening boundaries formed in the process. Since the process takes advantage of the non-linearity of the adsorption isotherms, a chromatographic column operated in the displacement mode can process higher feed loads, enabling the purification of large amounts of material with relatively small chromatographic columns [6–8].

Displacement chromatography is fundamentally different from desorption chromatography (e.g., affinity chromatography, step-gradient chromatography). The displacer, having an affinity higher than any of the feed components, competes effectively for the adsorption sites on the stationary phase. An important distinction between displacement and desorption is that the displacer front always remains behind the adjacent feed zones in the displacement train, while desorbents (e.g., salt, organic modifiers) move through the feed zones. The implications of this distinction are quite significant in that displacement chromatography can potentially concentrate and purify components from mixtures having low separation factors while in the case of desorption chromatography, relatively large separation factors are generally required to give satisfactory resolution.

Anion-exchange displacement chromatography has been studied by several investigators. Carboxymethyl-dextrans have been used in carrier displacement chromatography by Peterson and co-workers [8–10] to separate protein mixtures with anion-exchange columns. They have also reported the purification of monoclonal antibodies by "complex-displacement chromatography" on a cation-exchange column: CM-cellulose [11]. Torres and Peterson [12] have recently reported on the purification of guinea pig serum proteins and mouse liver cytosol proteins by anion-exchange displacement chromatography using a heterogeneous mixture of carboxymethyl dextrans as spacer displacers. In these carrier displacement systems the feed components co-elute with the heterogeneous displacer compounds.

Horváth and co-workers have employed chondroitin sulfate to displace β-galactosidase [13] and β-lactoglobulins [14]. They have also employed displacement chromatography in concert with frontal chromatography and an intermittent column flush to separate relatively large quantities of the proteins β-lactoglobulin A and B [15]. Ghose and Mattiasson [16] have examined the purification of lactate dehydrogenase using a carboxymethyl-starch displacer. Jen and Pinto have employed the smallest polyelectrolyte displacers to date, using a 2000 molecular mass sodium salt of polyvinyl sulfonate [17] and dextran sulfate [18] as displacers in anion-exchange systems.

Cramer and co-workers [19–23] have identified a variety of efficient polyelectrolyte displacers for protein purification including DEAE-dextran, dextran sulfate, protamine, heparin and pentosan polysulfate. Patrickios et al. [23] have employed block methacrylic polyampholytes as protein displacers in anion-exchange systems. To date, all reports in the literature on protein purification by ion-exchange displacement chro-

matography have employed relatively large polyelectrolytes ($M_r > 2000$) as the displacers.

The displacement mode of chromatography, while receiving attention from the academic community has not been widely employed in the biopharmaceutical industry to date. This inertia in industry with respect to displacement chromatography has been attributed to: a dearth of efficient displacers for protein purification, the lack of an appropriate theoretical framework for the rational design of displacement separations, and a paucity of case studies which demonstrate the utility of displacement chromatography for difficult bioseparation problems. A particular problem with the implementation of this technology for biotherapeutics has been the reluctance to employ high-molecular-mass displacers due to regulatory constraints and cost requirements.

As described above, all studies on ion-exchange protein displacement chromatography reported in the literature to date, have employed relatively high-molecular-mass polyelectrolytes as displacers. In this paper, a novel class of displacers, low-molecular-mass pentaerythritol-based dendrimers, are investigated for their relative efficacy in displacement purification of proteins in cation-exchange systems. These molecules have a distinctly different conformation as compared to "linear-chain molecules". Dendritic polymers (also known as starburst polymers) are three-dimensional, highly ordered oligomeric and polymeric compounds formed by reiterative reaction sequences starting from smaller molecules —"initiator cores" such as ammonia or pentaerythritol [24]. The syntheses proceed via discrete stages referred to as generations. The syntheses and structural characterization of the zero- (PE–TMA4), first- (PE–TMA12) and second- (PE–TMA36) generation pentaerythritol-based dendrimers are described elsewhere [25]. The architectural features of the cationic dendrimers employed in this study are presented in Fig. 1. In this manuscript the nonlinear adsorption behavior of these dendrimers are examined and their efficacy as displacers for ion-exchange displacement chromatography of proteins is investigated.

2. Theory

2.1. Dynamic affinity in ion-exchange displacement chromatography

The steric mass action (SMA) ion-exchange model developed by Brooks and Cramer [26] explicitly accounts for *steric effects* in multicomponent protein equilibria and is able to predict complex behavior in ion-exchange displacement systems. In order to present the dynamic affinity plot [27] (described below) for displacement chromatography it is first useful to briefly review the SMA model. Consider an ion-exchange resin with a total capacity, Λ, equilibrated with a carrier buffer solution containing salt counterions. Upon adsorption, the protein interacts with ν_i stationary phase sites (characteristic charge), displacing an equal number (ν_i) of monovalent salt counterions. In addition, the adsorption of the protein also results in the steric hindrance of σ_i salt counterions (steric factor). These *sterically* hindered salt counterions are *unavailable* for exchange with the protein in free solution. For a system of n proteins and a single mobile phase modifying salt, n equilibrium expressions can be written to represent the stoichiometric exchange of each individual protein with the salt.

$$C_i + \nu_i \bar{Q}_1 Q_i + \nu_i C_1 \quad i = 2, 3, \ldots, n+1 \qquad (1)$$

where C and Q are the mobile and stationary phase concentrations, and the subscripts i and 1 refer to the protein and salt, respectively. The overbar, $\bar{}$, denotes bound salt counterions *available* for exchange with the protein. The equilibrium constants, K_{1i}, for the ion-exchange process is defined as:

$$K_{1i} \equiv \left(\frac{Q_i}{C_i}\right) \cdot \left(\frac{C_1}{\bar{Q}_1}\right)^{\nu_i} \quad i = 2, 3, \ldots, n+1 \qquad (2)$$

Electroneutrality on the stationary phase requires:

$$\Lambda \equiv \bar{Q}_1 + \sum_{i=2}^{n+1} (\nu_i + \sigma_i) Q_i \qquad (3)$$

For a single protein, substituting Eq. 3 into

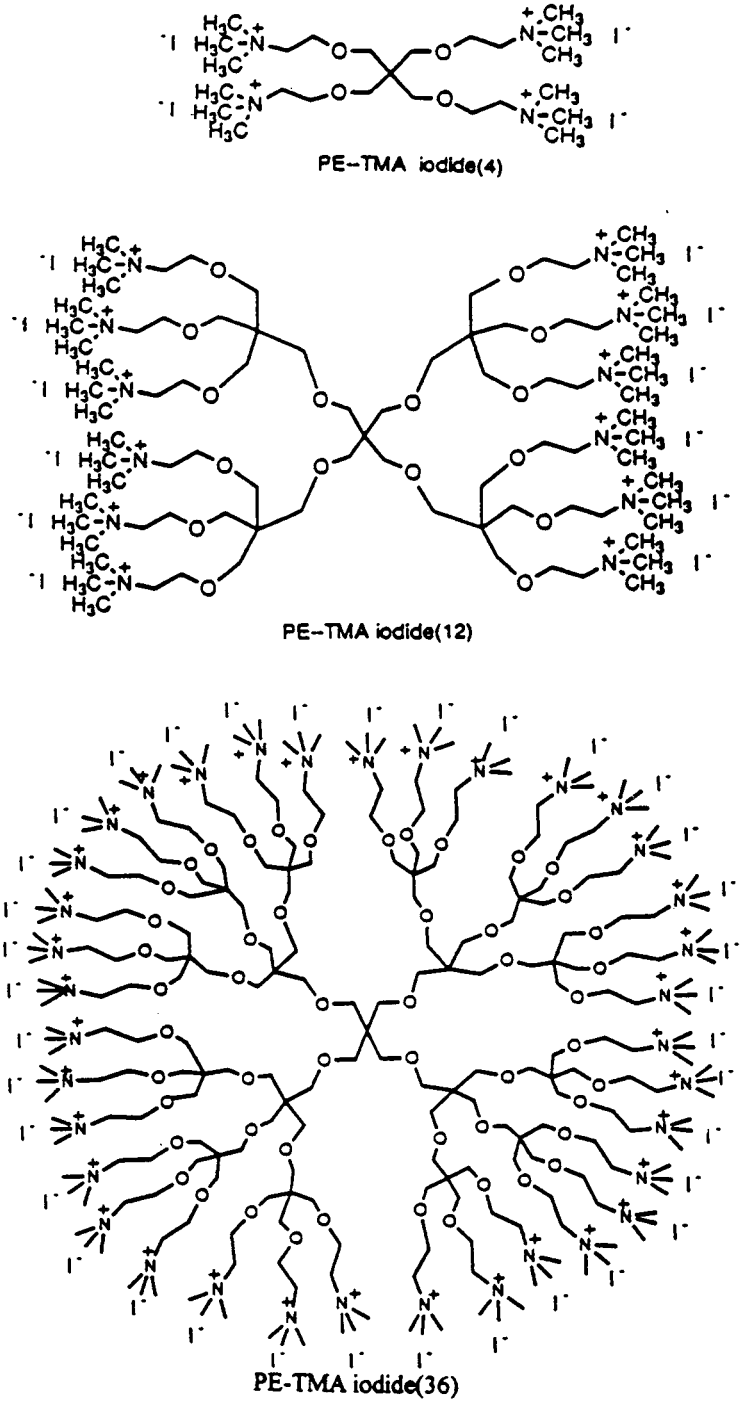

Fig. 1. Architectural features of dendrimer displacers.

Eq. 2 and rearranging yields the following implicit isotherm.

$$Q_i = K_i C_i \cdot \left(\frac{\Lambda - (\nu_i + \sigma_i) Q_i}{C_1} \right)^{\nu_i} \quad (4)$$

The equilibrium stationary phase concentration of the protein, Q_i, is implicitly defined in terms of its mobile phase concentration and the concentration of the salt. Thus, once the SMA equilibrium parameters of the protein are determined [28], the isotherm of the protein can be constructed at any mobile phase salt condition.

The velocity of the displacer as well as the feed components in the isotachic displacement train is determined from a solute movement analysis to be:

$$u_d = \frac{u_0}{1 + \beta \cdot \frac{Q_d}{C_d}} \quad (5)$$

The slope of the displacer operating line, Δ, is calculated using the displacer's implicit single component isotherm.

$$\Delta = \frac{Q_d}{C_d} = K_{1d} \cdot \left(\frac{\Lambda - (\nu_d + \sigma_d) Q_d}{(C_1)_d} \right)^{\nu_d} \quad (6)$$

Consider the displacement separation of a feed solution containing two proteins: a and i. The separation results in the formation of an isotachic displacement train with the two feed components traveling at a velocity u_d characterized by Δ. We have shown through a stability analysis [26] that the order of elution of feed components in isotachic displacement train can be determined from the following expression:

$$\sqrt[\nu_a]{\frac{K_{1a}}{\Delta}} < \sqrt[\nu_i]{\frac{K_{1i}}{\Delta}} \quad (7)$$

The elution order of the feed components in the isotachic displacement train will be a followed by i when Eq. 7 is satisfied. In general, we wish to determine the set of all species i with characteristic charge ν_i and equilibrium constant K_{1i}, that will displace feed component a in an isotachic displacement train traveling at a velocity defined by Δ. The left side of Eq. 7 can be written as the parameter λ_a (Eq. 8), which characterizes the dynamic affinity of species a traveling with a velocity characterized by Δ.

$$\lambda = \sqrt[\nu_i]{\frac{K_{1i}}{\Delta}} \quad (8)$$

After some rearrangement and taking the logarithm of both sides, the following relation can be written:

$$\log K_{1i} > \log \Delta + \log (\lambda_a) \nu_i \quad (9)$$

Thus, on a plot of $\log K_{1i}$ versus ν_i (Brooks dynamic affinity plot), Eq. 9 defines two regions demarcated by a line with slope $\log \lambda_a$ and intercept $\log \Delta$. As seen in Fig. 2 [27], the line originates at the point Δ on the ordinate axis and passes through the point defined by the linear equilibrium properties, K_{1a} and ν_a, of species a. The region above the *affinity line* includes all solutes which will displace solute a when traveling at a velocity characterized by Δ. Conversely, solutes in the region below the *affinity line* will be displaced by solute a under these conditions.

The Brooks dynamic affinity plot provides a simple method for determining the elution order of feed components in isotachic displacement separations. In addition to providing insight into the dynamic affinity of displacement systems, the Brooks dynamic affinity plot also indicates that low-molecular-mass molecules with sufficiently high equilibrium constants and relatively small characteristic charges may have utility as displacers for protein purification systems. In this paper we will explore the utility of low-molecular-mass

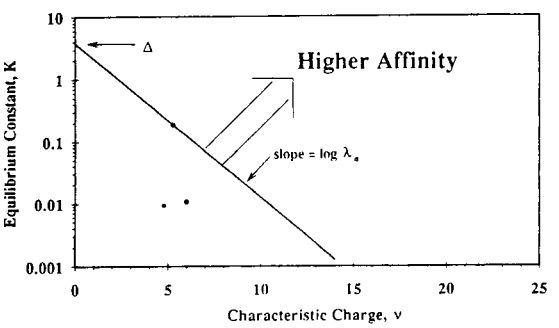

Fig. 2. Brooks dynamic affinity plot [27].

dendrimers as displacers for ion-exchange displacement chromatography of proteins.

3. Experimental

3.1. Materials

Strong cation-exchange "SCX" (sulfopropyl, 8 μm, 50 × 5 mm I.D.) columns were donated by Millipore (Waters Chromatography Division, Millipore, Milford, MA, USA). Sodium chloride, sodium monobasic and dibasic phosphate and all proteins were purchased from Sigma (St. Louis, MO, USA). All the pentaerythritol-based dendrimers were synthesized according to the procedures described elsewhere [25]. M_r 500 cut-off cellulose ester disc membranes were obtained from Spectrum (Houston, TX, USA). Reagent-grade cesium chloride (99.999%) was obtained from Aldrich (Milwaukee, WI, USA). Polyvinylsulfuric acid potassium salt (PVSK) and *o*-toluidine blue indicator were obtained from Nalco (Naperville, IL, USA).

3.2. Apparatus

Diafiltration of the first- and second-generation dendrimers was carried out using an Amicon 8050 stirred cell (Amicon, Danvers, MA, USA). Lyophilization of the diafiltered compounds was carried out using a Model Lyph Lock 4.5 Freeze Dry System (Labconco, Kansas City, MO, USA). All frontal and elution chromatographic experiments were carried out with a modular chromatographic system consisting of a Model LC 2150 pump (LKB Produkter, Bromma, Sweden) and a Spectroflow 757 UV–Vis detector (Applied Biosystems, Foster City, CA, USA) connected to a Waters Maxima 820 chromatographic workstation. Fractions of the column effluent were collected using an LKB 2212 Helirac fraction collector (LKB Produkter). Sodium ion analysis was performed using a Perkin-Elmer Model 3030 (Norwalk, CT, USA) atomic absorption spectrophotometer. A 10-port valve Model C10W injector (Valco, Houston, TX, USA) with multiple loops was used to conduct all the frontal experiments.

3.3. Procedures

Purification of polyelectrolytes

All the dendritic polymers employed in this study were subjected to elemental analysis and linear chromatographic characterization to examine the purity and the linear retention behavior of each compound. The zero-generation dendrimer, PE–TMA-(4) iodide, had a very high degree of purity after synthesis as deemed from the elemental analysis of the compound [25] and therefore was not subjected to further purification. The first- and second-generation dendritic polyelectrolytes, on the other hand contained some impurities and were subjected to diafiltration with a M_r 500 cut-off cellulose ester membrane (Spectrum) in an Amicon ultrafiltration cell to remove the low-molecular-mass impurities. The purified compounds were then lyophilized.

Estimation of SMA equilibrium parameters

The SMA parameters [i.e. characteristic charge (ν), steric factor (σ) and equilibrium constant (K)] for proteins and the zero-, first- and second-generation dendritic displacers were determined using the protocols developed by Gadam et al. [28]. Briefly, the characteristic charge and the equilibrium constant for the proteins were determined using linear elution techniques, while the steric factor of the proteins was determined using a single non-linear frontal chromatographic experiment. The SMA parameters of the dendrimers were determined using the method of induced salt gradient and sequential frontal chromatographic techniques.

Operation of the displacement chromatograph

In all displacement experiments, the columns were initially equilibrated with the carrier buffer and then sequentially perfused with feed, displacer and regenerant solutions (see figure legends for details). The feed and displacer solutions were prepared in the same carrier buffer. Fractions were collected directly from the

column effluent to avoid extra-column dispersion of the purified components.

Regeneration

The cation-exchange column was regenerated after each displacement experiment by passing 10–15 column volumes of 1 *M* NaCl in 100 m*M* phosphate buffer, pH 11.0, to assure complete regeneration of the column.

Protein analysis by HPLC

Protein analyses of the fractions collected during the displacement experiments were performed by ion-exchange HPLC under isocratic elution conditions. 150 m*M* NaCl in 50 m*M* sodium phosphate buffer at pH 6.0 was employed as mobile phase. Displacement fractions were diluted 10–100-fold with the mobile phase and 20-μl samples were injected into a 100×5 mm I.D. SCX column at a flow-rate of 0.5 ml/min. The column effluent was monitored at 280 nm. The protein compositions of the fractions were then used to construct a histogram of the displacement profiles.

Dendrimer analysis

All dendrimers were analyzed using a colloidal titration assay provided by Nalco. A known amount of sample was dissolved in 100 ml of deionized water and the solution was titrated against 0.001 *M* PVSK in presence of the *o*-toluidine blue indicator. Linear calibrations for amount of sample with titrant volume were obtained for these titrations.

Analyses for sodium counterions

Sodium was analyzed using atomic absorption spectrometry. Effluent fractions were diluted 2000–3000-fold in tubes containing 5 g/l cesium chloride solution (to minimize background noise) and their amounts calculated against known Na^+ ion standards (10–50 μM). The sodium compositions of the fractions were then used to construct a histogram of the salt profiles during the displacement experiments.

4. Results and discussion

4.1. SMA parameters of dendritic displacers

Zero-, first- and second-generation dendrimers were synthesized as described elsewhere [25]. The molecular masses and net charges of the zero-, first- and second-generation dendrimers were 480, 1620 and 5128; and 4, 12 and 36, respectively. The characteristic charge (ν), steric factor (σ), σ/ν ratio and equilibrium constant (K) of the dendrimers were determined by frontal chromatography and are presented in Table 1. The SMA parameters were found to be insensitive to both salt and solute concentration for these dendrimers. As seen in the table, the characteristic charges were 1.7, 4.2 and 11 for the zero-, first- and second-generation dendrimers. Thus, only 30–40% of the charged groups on the dendrimers are bound to the surface. This is in contrast to polyelectrolytes such as dextran-based displacers, where 60–80% of the charged moieties are bound to the surface of the SCX

Table 1
SMA parameters for proteins and dendrimers

Protein/ displacer	Characteristic charge (ν)	Steric factor (σ)	σ/ν ratio	Saturation capacity (mM)	Equilibrium constant (K_i)
α-Chymotrypsinogen A	4.8	49.2	10.3	10.4	$9.2 \cdot 10^{-3}$
Cytochrome *c*	6.0	53.6	8.9	9.4	$1.1 \cdot 10^{-2}$
PE–TMA 4^+	1.7	1.5	0.88	185	11
PE–TMA 12^+	4.2	6.5	1.55	55.3	22
PE–TMA 36^+	11	16.7	1.52	20.9	2.5

Chromatographic conditions: SCX column (bed capacity, $\Lambda = 580$ mM); sodium phosphate buffer, pH 6.0.

resin [28]. The lower percentage of surface-bound groups for the dendrimers is a reflection of the inflexible nature of these molecules relative to "linear-chain" polyelectrolytes such as dextrans.

Surprisingly, even the relatively small zero- and first-generation dendrimers exhibited a measurable steric factor. It is important to note that the steric factor is a measure of steric hindrance effects which can occur both "underneath" as well as "around" the adsorbed molecule. It is possible that the steric factor for these dendrimers is determined to a large extent by charge repulsive forces between the adsorbed highly charged dendrimers. As seen in the table, the σ/ν values are considerably different for the proteins and dendrimers. While the σ/ν ratios are on the order of 7–10 for proteins, they are almost an order of magnitude lower for the dendrimers. The first-and second-generation dendrimers exhibited similar σ/ν values (approximately 1.5), while the lower-molecular-mass zero-generation dendrimer exhibited a σ/ν value of 0.88. These data suggest that the lower-molecular-mass zero-generation dendrimer exhibits a relatively higher surface coverage under nonlinear conditions. It turns out that the σ/ν ratio is an important parameter for displacer design since it determines the level of induced salt gradient produced upon the adsorption of the displacer [29]. A higher value of σ/ν for a displacer molecule corresponds to lower levels of induced salt-gradient in ion-exchange displacement systems for a given breakthrough volume. The results presented here indicate that the zero-generation dendritic displacer will produce a correspondingly higher induced salt gradient as compared to the higher-generation dendrimers.

Table 1 also presents the equilibrium constants for the proteins and dendrimers. While the characteristic charges of the proteins and the dendrimers are comparable, the equilibrium constants for the dendrimers are two to three orders of magnitude higher than the proteins. These results are very important with respect to the ability of these dendrimers to act as protein displacers. In addition, it is interesting to note that the equilibrium constant of the second-generation material is an order of magnitude lower than the zero- and first-generation dendrimers. One possible explanation for this difference is that the larger second-generation dendrimer is unable to get as close to the chromatographic surface as the smaller dendrimers. The relationship between the physico-chemical properties of the displacers and the SMA parameters is the subject of active research in our laboratory.

According to the conventional wisdom, based on results observed with derivatized polysaccharide displacers, a high-molecular-mass compound with a relatively high characteristic charge is required for protein displacement chromatography. However, as described in the Theory section, the dynamic affinity plot of Brooks and Cramer [27] indicates that the ability of a given compound to act as a displacer is determined by its dynamic affinity parameter (Eq. 8) which is a function of the equilibrium constant, characteristic charge, and slope of the displacer operating line.

A dynamic affinity plot was constructed for the zero-, first- and second-generation dendrimers and the feed proteins α-chymotrypsinogen A, cytochrome c. According to this analysis (Fig. 3), it can be predicted that both the zero-, first- and second-generation dendrimers should act as effective displacers for these proteins. Although the zero-generation dendrimers has a lower characteristic charge than either of the two proteins, its higher "affinity" can be attributed to the equilibrium constant which is 3 orders of magnitude higher than those of the proteins. The ability of these dendritic molecules to displace proteins would provide a good test case for the dynamic affinity plot as well as a significant departure from the conventional wisdom that high-molecular-mass polyelectrolytes are required for protein displacements.

4.2. Displacement chromatography of proteins by dendritic displacers

Displacement chromatography of a binary protein mixture of α-chymotrypsinogen A and cytochrome c was carried out with each generation of the dendritic displacers. In order to

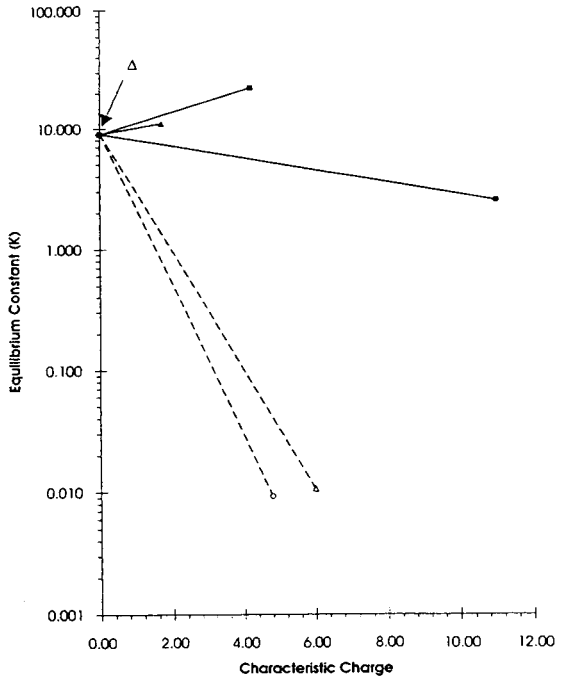

Fig. 3. Dynamic affinity plot for dendrimers and feed proteins. ○ = α-Chymotrypsinogen A; △ = cytochrome *c*; ▲ = PE–TMA 4; ■ = PE–TMA 12; ● = PE–TMA 36.

compare the relative efficacies of the various generations of displacers, the inlet concentration of each displacer on a mass basis was kept the same. In addition, the initial salt concentration in the carrier solution was reduced for the zero-generation experiment in order to maintain comparable salt microenvironments in the displacement zones. (Note: this is due to the elevated induced salt gradient produced by the zero-generation dendrimer). The displacement experiment with the second-generation dendrimer displacer is shown in Fig. 4. As expected, the second-generation dendrimer (M_r 5280) with a characteristic charge of 11 was readily able to displace the proteins. The displacement experiment with the first-generation dendrimer was then carried out. As seen in Fig. 5, this relatively low-molecular-mass dendrimer was able to produce an efficient displacement of the model proteins. This separation was characterized by very sharp displacement boundaries and the separation of trace impurities associated with the α-chymotrypsinogen A [19]. The zero-generation dendrimer was then investigated for its ability to act as a displacer for protein separation. The results of this experiment are presented in Fig. 6. As seen in the figure, this low-molecular-mass dendrimer (M_r 480) with a characteristic charge of 1.7 was indeed able to displace the proteins. This result is quite significant in that it is in contrast to the conventional wisdom that large polyelectrolytes are required for protein displacement. Furthermore, it confirms the predictions of the dynamic affinity plot (Fig. 3) that low-molecular-mass displacers with small characteristic charges and sufficiently high equilibrium constants can indeed function as protein displacers.

These displacements clearly demonstrate that increasing the molecular mass and number of charged groups on these dendrimers has little effect on their efficacy as displacers. Furthermore, the ratio of steric factor to characteristic charge for the first- and second-generation dendrimers (about 1.5) is comparable to that of the higher-molecular-mass dextran polyelectrolytes [19,28]. Therefore, for the same breakthrough volumes, these dendritic displacers induce the same level of induced salt gradient as the dextran displacers. In other words, the first- and second-generation dendrimers have the same efficacy as high-molecular-mass "linear-chain" polyelectrolytes for protein displacement separations in ion-exchange systems.

The level of induced salt gradient obtained with the zero-generation displacer was significantly higher than those obtained with the first- and second-generation dendrimers. Again, this is due to the relatively low σ/ν ratio (0.88) of the zero-generation dendrimer. Nevertheless, it is more advantageous to employ a low-molecular-mass displacer due to several distinct operational advantages which are discussed below.

5. Conclusions

This research has resulted in the discovery that low-molecular-mass dendritic polymers can in-

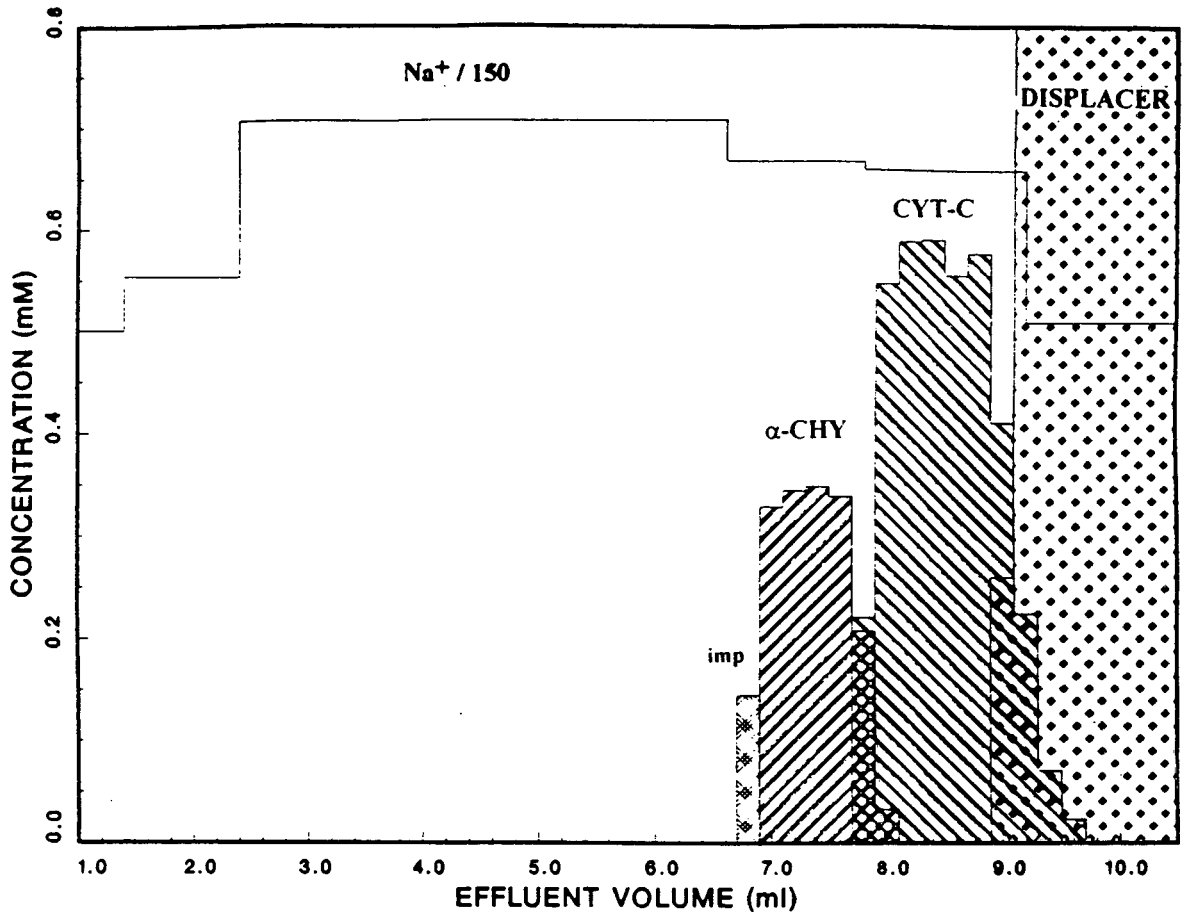

Fig. 4. Displacement separation of a two component protein mixture using second generation (PE–TMA 36) dendritic polyelectrolyte as displacer. Column: 100 × 5 mm I.D. strong cation exchanger (8 μm); Carrier: 75 m*M* sodium phosphate buffer, pH 6.0; Feed: 1.0 ml of 0.35 m*M* α-chymotrypsinogen A (α-CHY) and 0.7 m*M* cytochrome *c* (CYT-C) in carrier. Displacer concentration, 1.96 m*M*; flow-rate 0.1 ml/min; 200-ml fractions. imp = Impurity.

deed be employed as efficient displacers for protein purification. The ability of a low-molecular-mass compound such as the zero-generation dendrimer (M_r 480) to displace proteins is very significant in that it represents a major departure from the conventional wisdom that large polyelectrolyte polymers are required to displace proteins in ion-exchange systems. In addition to the fundamental interest generated by low-molecular-mass displacers, it is likely that these displacers will have significant operational advantages as compared to large polyelectrolyte displacers. First and foremost, if there is any overlap between the displacer and the protein of interest, these low-molecular-mass materials can be readily separated from the purified protein during post-displacement downstream processing involving size-based purification methods. (e.g. size-exclusion chromatography, ultrafiltration) Furthermore, the relatively low cost of synthesizing low-molecular-mass displacers, can be expected to significantly improve the economics of displacement chromatography. It is also likely that column regeneration with these materials will require less extreme conditions and reduced regenerant volumes. Additional potential advantages include: the ability to precisely control molecular design parameters such as size, shape,

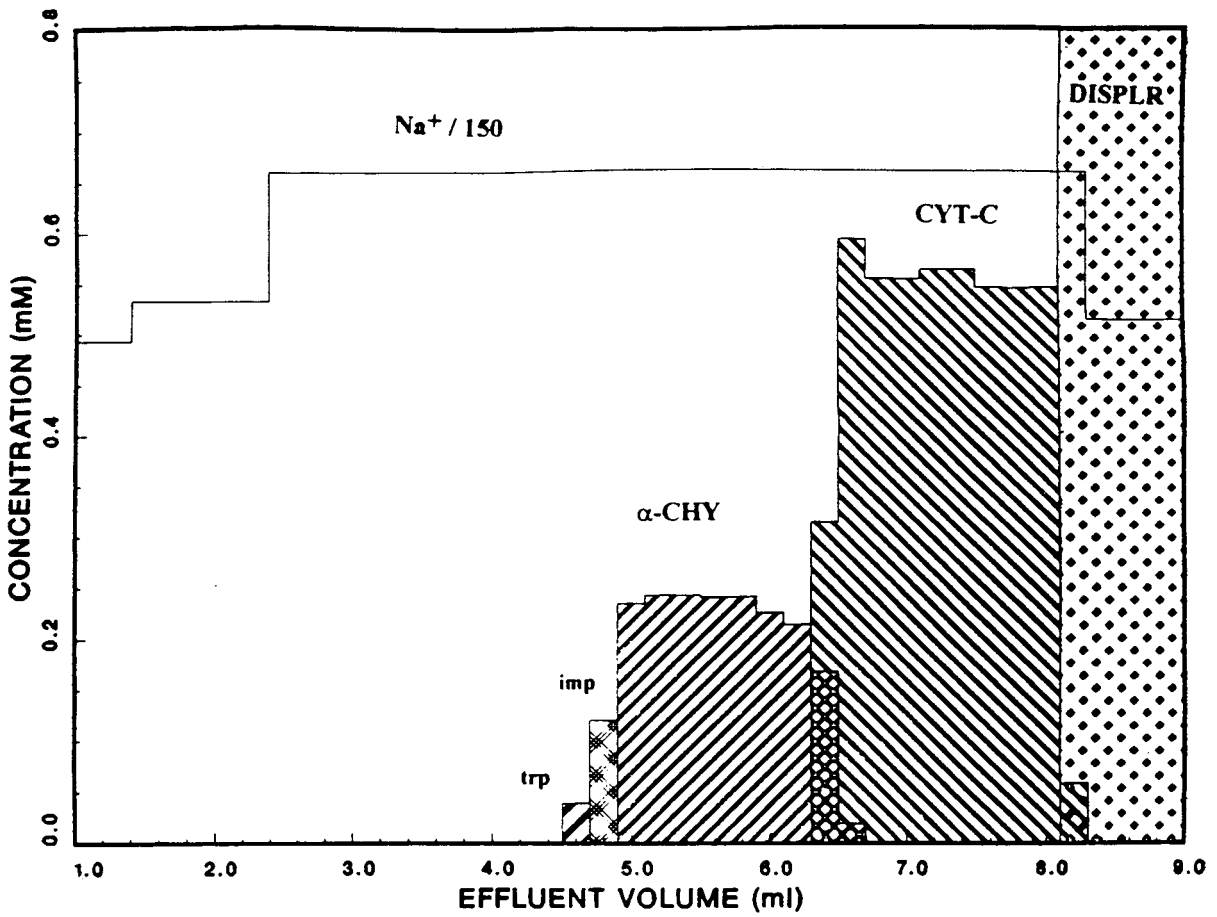

Fig. 5. Displacement separation of a two-component protein mixture using first generation (PE–TMA 12) dendritic polyelectrolyte as displacer. All conditions as in Fig. 4 except feed: 1.0 ml of 0.4 m*M* α-chymotrypsinogen A and 0.8 m*M* cytochrome *c* in carrier; and displacer (DISPLR) concentration, 6.17 m*M*. trp = Trypsin.

topology, flexibility and degree of functionalization for the dendritic molecules; the rapid mass transport and relatively low viscosities of these small high affinity displacers will facilitate the use of these displacers in high throughput, fast flow chromatographic systems. Clearly, it is very important to consider what other low-molecular-mass compounds could also be employed as displacers for protein purification. We are carrying out a detailed investigation into the design of efficient low-molecular-mass displacers for protein purification. Research on how systematic changes in the displacer chemistry and structure affect important displacer chromatographic properties such as dynamic affinity, induced gradients, and effective operating regimes will be the subject of a future report.

6. Symbols and abbreviations

6.1. Symbols

C	mobile phase concentration (mM)
K	non-dimensionalized equilibrium constant (dimensionless)

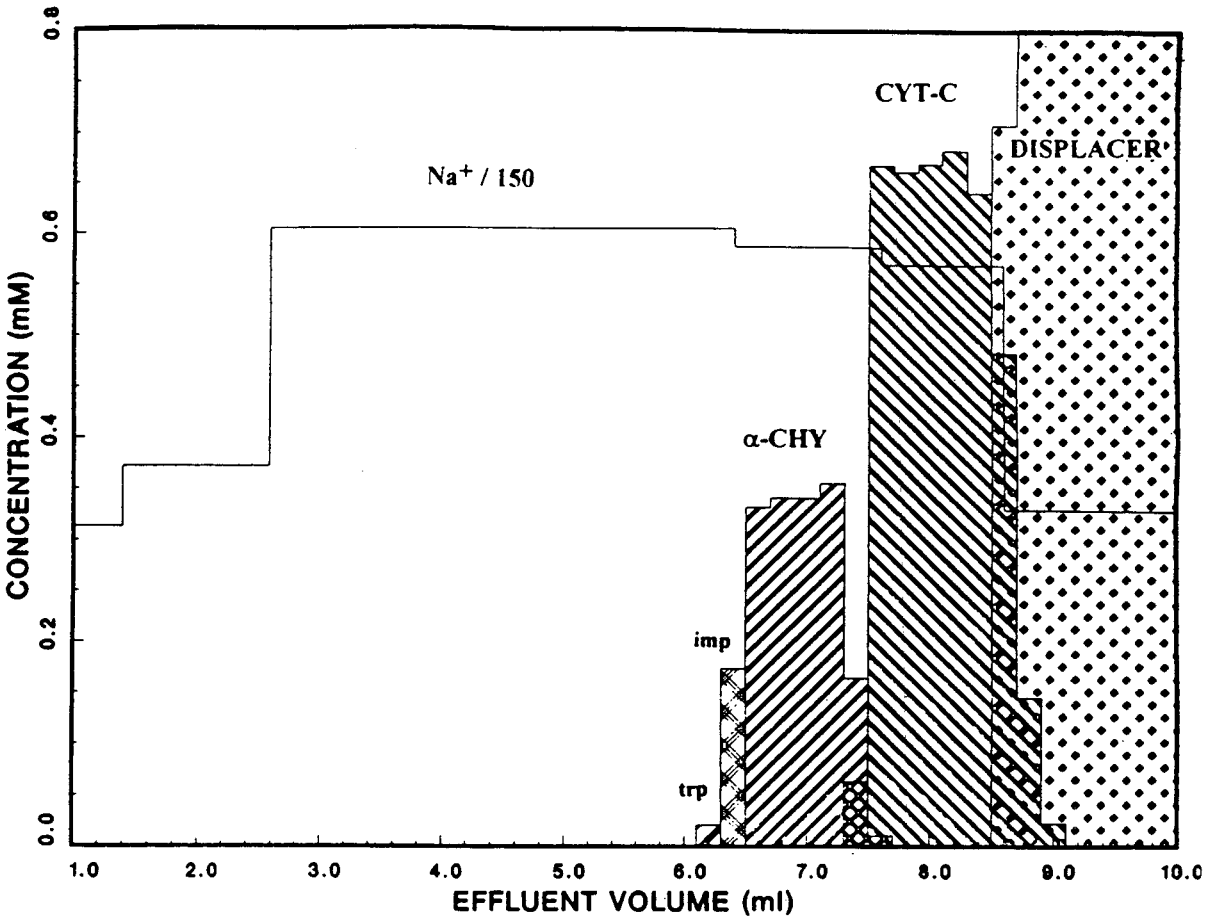

Fig. 6. Displacement separation of a two-component protein mixture using zero generation (PE–TMA 4) dendritic polyelectrolyte as displacer. All conditions as in Fig. 4 except carrier: 50 m*M* sodium phosphate buffer, pH 6.0; feed: 1.2 ml of 0.35 m*M* α-chymotrypsinogen A and 0.7 m*M* cytochrome *c* in carrier; displacer concentration, 21 m*M*.

Q	stationary phase concentration (m*M*)
u	velocity (cm/s)

Greek letters

β	column phase ratio, $(1-\varepsilon)/\varepsilon$
Δ	slope of displacer operating line
ϵ	total porosity
Λ	stationary phase capacity (monovalent salt counterion)
ν	characteristic charge
σ	steric factor

Subscripts and superscripts

–	sterically non-hindered
0	unretained solute
d, D	displacer
i	solute
1	salt

6.2. Abbreviations

SMA	steric mass action model
CM	carboxymethyl
DEAE	diethylaminoethyl
PE–TMA	pentaerythritol–trimethylamine

SCX strong cation exchanger
PVSK polyvinylsulfuric acid potassium salt

References

[1] B.J. Spalding, *Bio/Technology*, 9 (1991) 225.
[2] J. Frenz and Cs. Horváth, in Cs. Horváth (Editor), *High-Performance Liquid Chromatography —Advances and Perspectives*, Vol. 8, Academic Press, Orlando, FL, 1988, p. 211.
[3] S.M. Cramer and G. Subramanian, *Sep. Purif. Methods*, 91 (1990) 31.
[4] S.M. Cramer and C.A. Brooks, in Cs. Horváth and L.S. Ettre (Editors), *Chromatography in Biotechnology (ACS Symposium Series*, No. 529), American Chemical Society, Washington, DC, 1993, p. 29.
[5] J. Frenz, *LC·GC*, 10 (1992) 668.
[6] Cs. Horvath, in F. Bruner (Editor), *The Science of Chromatography*, Elsevier, Amsterdam, 1985, p. 179.
[7] J. Frenz, Ph. Van Der Schrieck and Cs. Horváth, *J. Chromatogr.*, 330 (1985) 1.
[8] E.A. Peterson, *Anal. Biochem*, 90 (1978) 767.
[9] E.A. Peterson and A.R. Torres, *Anal. Biochem.*, 130 (1983) 271.
[10] A.R. Torres, S.C. Edberg and E.A. Peterson, *J. Chromatogr.*, 389 (1987) 177.
[11] A.R. Torres and E.A. Peterson, *J. Chromatogr.*, 499 (1990) 47.
[12] A.R. Torres and E.A. Peterson, *J. Chromatogr.*, 604 (1992) 39.
[13] A.W. Liao and Cs. Horváth, *Ann. N.Y. Acad. Sci.*, 589 (1990) 182.
[14] A.W. Liao, Z. El Rassi, D.M. LeMaster and Cs. Horváth, *Chromatographia*, 24 (1987) 881.
[15] A.L. Lee, A.W. Liao and Cs. Horváth, *J. Chromatogr.*, 443 (1988) 31.
[16] S. Ghose and B.J. Mattiasson, *J. Chromatogr.*, 547 (1991) 145.
[17] S.-C.D. Jen and N.G. Pinto, *J. Chromatogr*, 519 (1990) 87.
[18] S.-C.D. Jen and N.G. Pinto, *J. Chromatogr. Sci.*, 29 (1991) 478.
[19] G. Jayaraman, S.D. Gadam and S.M. Cramer, *J. Chromatogr.*, 630 (1993) 53.
[20] J.A. Gerstner and S.M. Cramer, *Biotech. Progr.*, 8 (1992) 540.
[21] J.A. Gerstner and S.M. Cramer, *BioPharm*, 5, No. 9 (1992) 42.
[22] S. Gadam and S.M. Cramer, *Chromatographia*, in press.
[23] C.S. Patrickios, S.D. Gadam, S.M. Cramer, W.R. Hertler and T.A. Hatton, *Biotechnology Progr.*, in press.
[24] D.A. Tomalia, A.M. Naylor and W.A. Goodard III, *Angew. Chem., Int. Ed. Engl.*, 29 (1990) 138.
[25] Y.J. Li, J. Moore, G. Jayaraman and S.M. Cramer, *Chem. Materials*, submitted for publication.
[26] C.A. Brooks and S.M. Cramer, *AIChE J.*, 38 (1992) 1969.
[27] C.A. Brooks and S.M. Cramer, *Chem. Eng. Sci.*, in press.
[28] S.D. Gadam, G. Jayaraman and S.M. Cramer, *J. Chromatogr.*, 630 (1993) 37.
[29] C.A. Brooks and S.M. Cramer, *J. Chromatogr.*, 683 (1995) 187.

ELSEVIER

Journal of Chromatography A, 702 (1995) 157–162

JOURNAL OF CHROMATOGRAPHY A

Effect of stationary phase on preparative protein separation in reversed-phase chromatography

Dauh-Rurng Wu*, Hellen C. Greenblatt

BTR Separations, Concord Plaza, Quillen Building, 3521 Silverside Road, Wilmington, DE 19810, USA

Abstract

A matrix of Zorbax Pro-10 (10 μm) packing materials with differing alkyl chain lengths (C_3, C_8, C_{18}) and pore sizes (60 Å, 150 Å, 300 Å) was utilized to determine the influence of chain length and pore size on chromatographic performance (i.e., resolution) and column capacity. Proteins ranging in size from M_r 5700 to 68 000 were used as model compounds. For each category of packing material, retention times of the proteins decrease and peak widths increase with increasing sample loading. Among the matrix materials, C_3/300 Å and C_8/300 Å provide the highest resolution of a mixture of proteins with total protein loading from 60 μg to 6 mg on analytical columns (25 × 0.46 cm).

The influence of alkyl chain length and pore size on column capacity was investigated by frontal chromatography. For a fixed chain length, materials with larger pore size provide greater column capacity of the model proteins. In addition, for materials of the same pore size, the longer the alkyl chain, the greater the column capacity. Column capacity for a given alkyl chain length and pore size is indirectly correlated to protein size; the greater column capacity is found for the smaller tested proteins.

1. Introduction

Reversed-phase high-performance liquid chromatography (HPLC) has become an important and powerful technique in the isolation and purification of large biomolecules [1–3]. The selection of packing material with appropriate characteristics for reversed-phase HPLC is critical. The importance of the surface (i.e., pore size and surface area) properties of the stationary phase in ion-exchange [4,5] and reversed-phase [6–9] HPLC has been identified. In general, material with larger pores is suitable for separation of large biomolecules. However, there is little comprehensive data on the influence of pore size and alkyl chain length on resolution and loading capacity of large biomolecules in a reversed-phase mode.

In this paper, we examine the influence of pore size and alkyl chain length on resolution and loading capacity of proteins. This information will provide a better understanding of the effect of these two parameters on resolution and

* Corresponding author.

0021-9673/95/$09.50 © 1995 Elsevier Science B.V. All rights reserved
SSDI 0021-9673(94)01139-7

loading capacity. Additionally, the effect of protein size on capacity is also explored.

2. Experimental

2.1. Material

Bonded Zorbax 10 μm silica-based materials were obtained from BTR Separations (Wilmington, DE, USA). Bovine serum albumin (BSA, M_r 68 000), lysozyme (M_r 14 400), ribonuclease A (M_r 13 700), insulin (M_r 5700) and trifluoroacetic acid (TFA) were from Sigma (St. Louis, MO, USA). Acetonitrile was purchased from Fisher Scientific (Malvern, PA, USA). Series 410 LC pump, LC-95 UV–Vis detector and Nelson 2700 chromatography software were obtained from Perkin-Elmer (Cupertino, CA, USA).

2.2. Methods

Separation of ribonuclease A, lysozyme and BSA was conducted in 25 × 0.46 cm columns packed with a variety of bonded Zorbax phases with pore sizes of 60 and 300 Å. The separation conditions were 10 to 70% acetonitrile with 0.1% TFA in 20 min at a flow-rate of 2 ml/min, a wavelength of 280 nm, and room temperature. The total sample loading was from 60 μg to 6 mg for each packing material. Resolution was calculated by:

$$R_s = 2(t_{R2} - t_{R1})/(W_2 + W_1)$$

where t_{R2} and t_{R1} are retention times of two adjacent peaks; W_2 and W_1 are peak widths at the baseline.

Columns of 5 × 0.46 cm were packed with a variety of bonded Zorbax phases in pore sizes of 60, 150 and 300 Å to study the effect of pore size and alkyl chain length on protein capacity using frontal chromatography. BSA, lysozyme and insulin were employed as model proteins in this capacity study. Protein solutions of 1 mg/ml in 0.1% aqueous TFA were continuously passed through columns at 1 ml/min until breakthrough occurred and absorbance became constant. The time at the half heights of breakthrough was measured and utilized to calculate protein column capacities.

3. Results and discussion

3.1. Effect of sample loading on retention time and resolution

Fig. 1 shows the result of separation of ribonuclease A, lysozyme and BSA at different sample loadings (from 20 μg to 2 mg of each protein) on Zorbax Pro-10 C_3/300 Å material. The retention

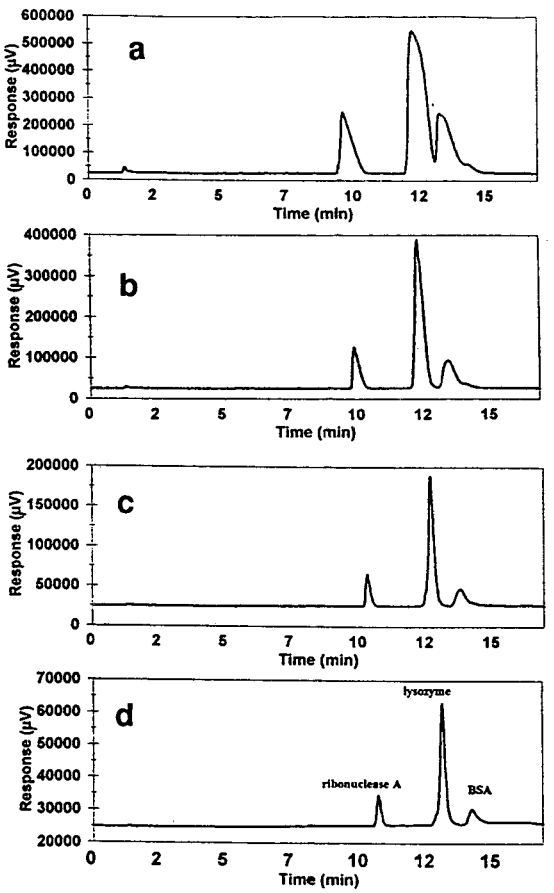

Fig. 1. Separation of ribonuclease A, lysozyme and BSA at sample loadings of total protein from 60 μg to 6 mg on Zorbax Pro-10 C_3/300 Å material (individual protein loading from 20 μg to 2 mg). (a) 6 mg; (b) 1.2 mg; (c) 0.3 mg; (d) 0.06 mg.

time of each protein decreases, and peak width increases, with increasing sample loading. This indicates that these proteins have Langmuir-like isotherms (concave down). Resolution decreases with increasing sample loading due to decreasing retention time and increasing peak width. A similar trend of retention time and resolution is observed for other Zorbax packing materials with different pore sizes and alkyl chain lengths.

3.2. Effect of pore size on retention time and resolution

Fig. 2 presents separations of ribonuclease A, lysozyme and BSA on Zorbax C_8/60 Å and C_8/300 Å at a total sample loading of 0.3 mg. The retention time of each protein decreases as the pore size decreases from 300 to 60 Å. Although 60 Å material has a higher surface area than 300 Å material, this phenomenon may be due to a size-exclusion effect with the 60 Å material. Due to size exclusion, the majority of large molecules may not be able to penetrate into the pores, resulting in less accessible surface area for the large molecules. The influence of pore size on retention time of BSA in C_8 and C_{18} at different sample loading is presented in Fig. 3a and b, respectively. Within the range of sample loading, 300 Å materials provide higher retention times than 60 Å ones. However, the difference in retention time is reduced with increasing protein loading.

The effect of C_8 pore size on the resolution of BSA and lysozyme is shown in Fig. 4a at different sample loadings from 20 μg to 2 mg. The 300 Å material offers higher resolution than the 60 Å material. The lower resolution of the 60 Å material is primarily due to the lower selectivity, shorter retention times (size-exclusion effect) and lower saturation capacity of the material. However, differences in resolution are reduced with increasing sample loading. The results presented on Fig. 4b indicate that C_{18}/60 Å material provides a higher resolution than C_{18}/300 Å. [C_8 results were reversed, i.e., C_8/300 Å resulted in

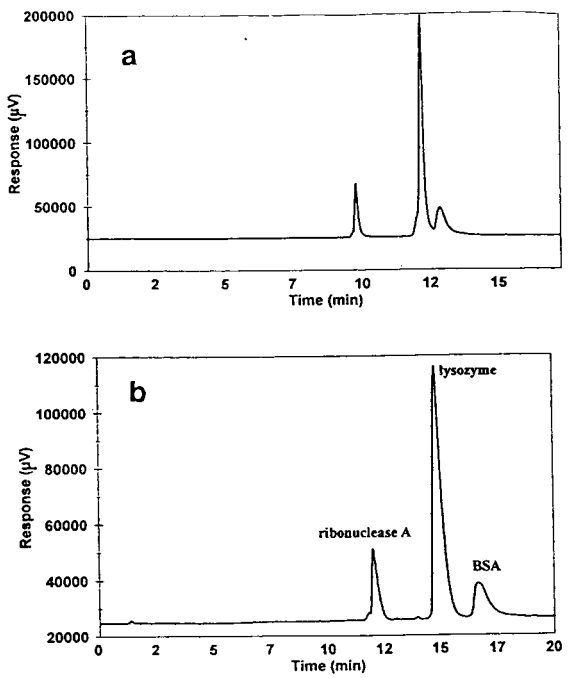

Fig. 2. Separation of ribonuclease A, lysozyme and BSA on Zorbax C_8/60 Å (a) and C_8/300 Å (b) materials at a total protein loading of 0.3 mg.

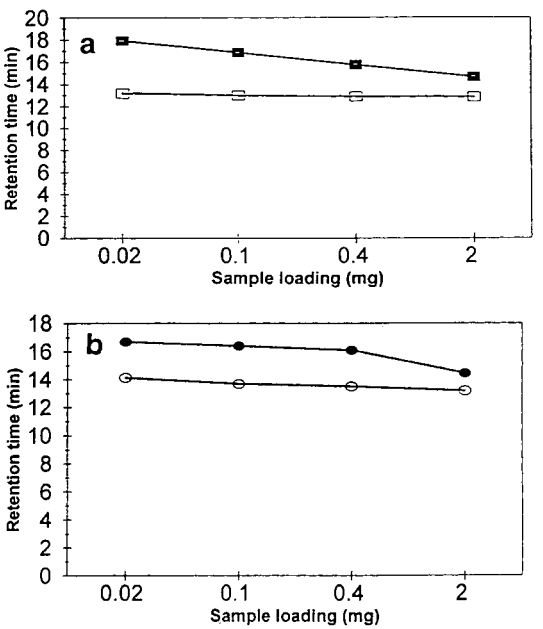

Fig. 3. Effect of pore size on retention time of BSA at different sample loadings on (a) Zorbax C_8/60 Å (□) and C_8/300 Å (■) and (b) Zorbax C_{18}/60 Å (○) and C_{18}/300 Å (●).

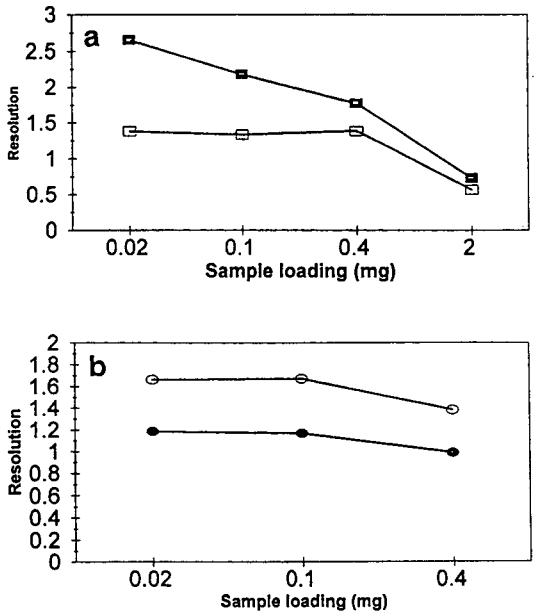

Fig. 4. Effect of pore size on resolution of BSA and lysozyme at different sample loadings on (a) Zorbax C_8/60 Å (□) and C_8/300 Å (■) and (b) Zorbax C_{18}/60 Å (○) and C_{18}/300 Å (●).

better resolution than C_8/60 Å (Fig. 4a)]. The lesser resolution of C_{18}/300 Å is due to peak tailing, which may be controlled by slow kinetic desorption and/or intra-particle mass transfer. Since the majority of the larger molecules are restricted to the exterior of the 60 Å particle, diffusion distance is significantly reduced and therefore the intra-particle mass transfer effect on resolution may not be significant.

3.3. Effect of alkyl chain length on retention time and resolution

Fig. 5 represents the separation of ribonuclease A, lysozyme and BSA on 300 Å material with differing alkyl chain lengths (C_3, C_8 and C_{18}) at a total sample loading of 1.2 mg. Both C_8 and C_{18} have greater retention than C_3 resulting from the stronger interaction between these two stationary phases and the model compounds. The influence of alkyl chain length on retention

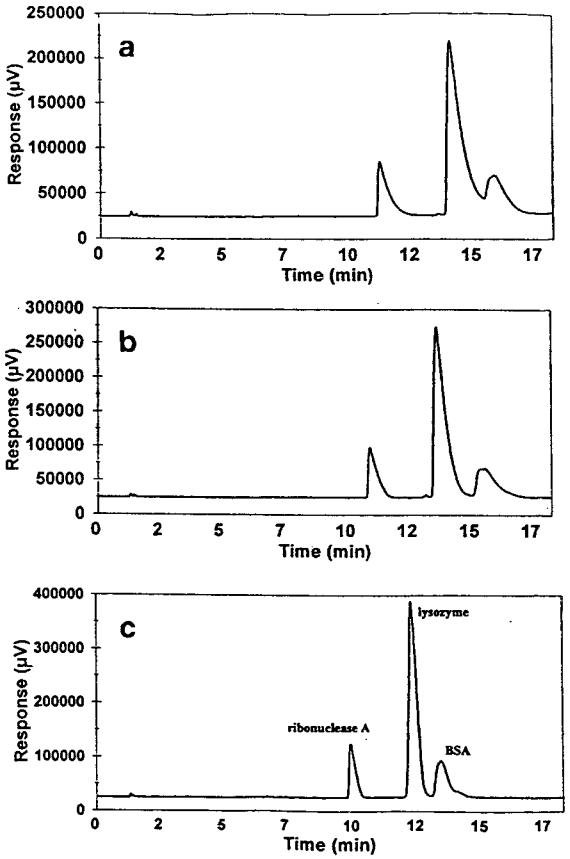

Fig. 5. Separation of ribonuclease A, lysozyme and BSA on Zorbax 300 Å material with differing alkyl chain lengths [C_3 (c), C_8 (b)and C_{18} (a)] at a total sample loading of 1.2 mg.

time specifically of BSA at different sample loadings is presented in Fig. 6.

Columns of three different alkyl chain lengths

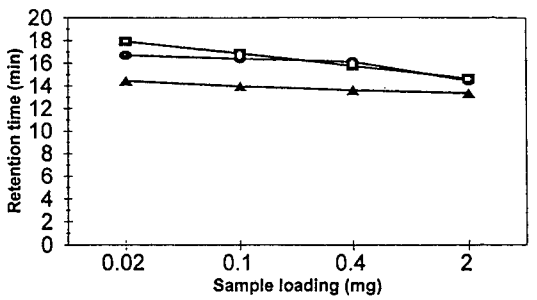

Fig. 6. Effect of alkyl chain length on retention time of BSA at different protein loadings on Zorbax C_3/300 Å (▲), C_8/300 Å (■) and C_{18}/300 Å (●).

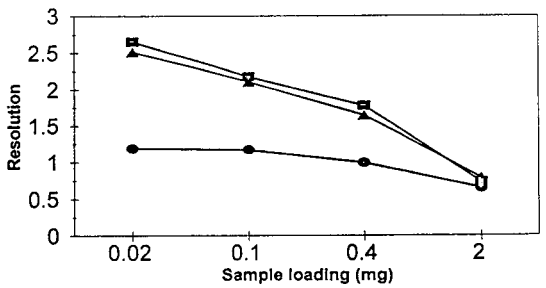

Fig. 7. Effect of alkyl chain length on resolution of BSA and lysozyme at different protein loadings on Zorbax C_3/300 Å (▲), C_8/300 Å (■) and C_{18}/300 Å (●).

(C_3, C_8 and C_{18}) bonded to 300 Å Zorbax were individually tested using 20 μg to 2 mg of each protein. C_3/300 Å and C_8/300 Å were best able to resolve BSA from lysozyme (Fig. 7). The lower resolution of C_{18} is due to peak tailing. Since C_8 and C_{18} have surface coverage values of 3.44 μmol/m^2 and 3.14 μmol/m^2, respectively and both are end-capped, the more severe peak tailing in C_{18} is mainly caused by slower kinetic desorption between the stationary phase and the proteins. C_3, due to its polymeric bonding (i.e., trifunctional silanes), has a higher surface coverage than C_8 and C_{18}. Therefore, the sharper peak shapes in C_3 than in C_8 and C_{18} are likely due to the combination of higher surface coverage and faster kinetic desorption.

3.4. Effect of pore size, alkyl chain length and protein size on column capacity

Table 1 compares the column capacities for BSA (M_r 68 000) of packing materials with different pore sizes and alkyl chain lengths. The data indicates that for the same alkyl chain length, it is the larger pore size which provides the greatest column capacity. Additionally, there is a greater difference in column capacity when comparing the 150 Å to 300 Å pore size, than comparing the 150 Å to the smallest pore size. This phenomenon may be due to a size-exclusion effect. For the same pore size, a longer alkyl chain length also results in a higher column capacity possibly due to stronger interactions between the stationary phases and BSA. Column capacity for lysozyme with different pore size and alkyl chain length show a similar trend (Table 2).

Table 1
Effect of pore size and alkyl chain length on BSA column capacity

Chain length	Column capacity (mg)		
	300 Å	150 Å	60 Å
C_3	2.3	N/A[a]	N/A
C_8	7.0	1.0	0.7
C_{18}	9.0	2.8	1.41

[a] Not available.

Table 2
Effect of pore size and alkyl chain length on lysozyme column capacity

Chain length	Column capacity (mg)		
	300 Å	150 Å	60 Å
C_3	15.7	N/A	N/A
C_8	23.0	5.5	0.6
C_{18}	29.0	23.3	10.0

The effect of protein size on column capacity for BSA, lysozyme and insulin using C_8 materials with different pore sizes are shown in Fig. 8. For a given pore size and ligand length, proteins with larger molecular masses bind with lower column capacity (possibly due to steric hindrance). The pore size effect becomes less pronounced with decreasing protein size.

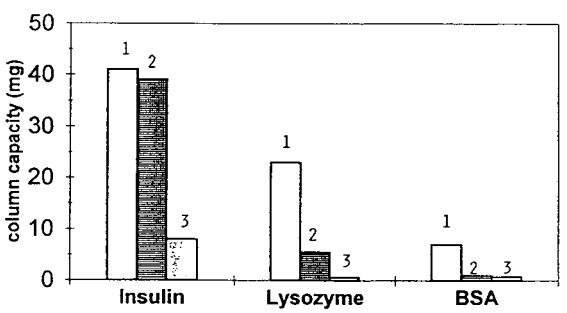

Fig. 8. Effect of protein size on column capacity on Zorbax C_8/300 Å (1), C_8/150 Å (2) and C_8/60 Å (3).

4. Conclusions

When testing a matrix of various packing materials, C_3/300 Å and C_8/300 Å provide the highest resolution of a mixture of model proteins with a total protein loading of 60 μg to 6 mg [onto analytical columns (25×0.46 cm)]. For any fixed chain length, material with a larger pore size provides greater column capacity. In addition, for materials with the same pore size, the longer the alkyl chain, the greater the column capacity. Column capacity for a given alkyl chain length and pore size is indirectly correlated to protein size. In this study, the higher column capacity is found for the smaller proteins.

References

[1] E.P. Kroeff, R.A. Owens, E.L. Campbell, R.D. Johnson and H.I. Marks, *J. Chromatogr.*, 461 (1989) 45.

[2] S. Linde and B.S.Welinder, in C.T. Mant and R.S. Hodges (Editors), *High-Performance Liquid Chromatography of Peptides and Proteins*, CRC Press, Boca Raton, FL, 1991, p. 351.

[3] P.H. Corran, in R.W.A. Oliver (Editor), *HPLC of Macromolecules: a Practical Approach*, IRL Press, Oxford, 1989, p. 127.

[4] M.P. Nowlan and K.M. Gooding, in C.T. Mant and R.S. Hodges (Editors), *High-Performance Liquid Chromatography of Peptides and Proteins*, CRC Press, Boca Raton, FL, 1991, p. 203.

[5] W. Kopaciewicz, M.A. Rounds and F.E. Regnier, *J. Chromatogr.*, 318 (1985) 157.

[6] Y.S. Kim, B.W. Sands and J.L. Bass, *J. Liq. Chromatogr.* 10 (1987) 839.

[7] B.W. Sands, Y.S. Kim and J.L. Bass, *J. Chromatogr.*, 360 (1986) 353.

[8] G.B. Cox, L.R. Snyder and J.W. Dolan, *J. Chromatogr.*, 484 (1989) 409.

[9] W. Kopaciewicz and F.E. Regnier, *J. Chromatogr.*, 358 (1986) 119.

ELSEVIER

Journal of Chromatography A, 702 (1995) 163–172

JOURNAL OF CHROMATOGRAPHY A

High performance liquid chromatography of *Bacillus circulans* peptidoglutaminase for laboratory and industrial uses

Jamel S. Hamada

US Department of Agriculture, ARS, Southern Regional Research Center, New Orleans, LA 70179, USA

Abstract

Gel permeation and anion-exchange chromatography were used to develop methodology for large-scale production of peptidoglutaminase (PGase) from *Bacillus circulans* cell extract. Sample load, flow-rate and elution profiles were optimized to obtain a highly active DNA-free PGase preparation in high yield. PGase was fractionated into I and II and purified up to 1430-fold for enzymatic determination of glutamine, molecular cloning and protein deamidation research. PGases were also separated directly from *B. circulans* extract (20–30 mg) in one peak with an 8-fold purification on a 43-ml anion-exchange column at 2 cm/min in 35–40 min. More than 65% of the cell extract proteins were eluted after the PGase peak and contained all the nucleic acids. This method appears to meet the requirements of purity, yield, speed and other economic aspects for successful production of PGase for potential modification of food proteins in industrial reactors.

1. Introduction

Deamidation of proteins is the hydrolysis of amide groups to acidic groups and is carried out to increase the net negative charges on proteins. This lowers the isoelectric point of the protein and increases solubility, emulsifying capacity and other important functional properties in mildly acidic food systems [1]. An enzymatic approach to protein deamidation is preferred over chemical approaches because of the mild conditions, safety, speed and selectivity of enzymatic reactions. Transglutaminase, protease and peptidoglutaminase (PGase) are the only enzymes reported in the literature for protein deamidation. PGase seems to be the most feasible for industrial application because of the prohibitive cost and other potentially severe problems for the food processor that may be associated with the other two enzymes [2]. PGase hydrolyzes the γ-amides of L-glutamine (Gln) residues in peptides and proteins and is used to modify their structures. PGase can be separated into two fractions (I and II) by multiple steps of conventional chromatography [3]. Fraction I hydrolyzes the amide groups on C-terminal Gln residues and II hydrolyzes the amide groups on the other Gln residues.

It is crucial for the successful use of PGase for protein modification in industry to develop large-scale methodology for producing food-grade PGase. Processes for the production and/or use of PGase must be cost-effective, and amounts of DNA and other extraneous materials must be less than that specified by the US Food and Drug Administration. Bioreactor methods were developed in this laboratory for the recovery and multiple use of PGase in industrial settings [2]. However, large-scale purification methods such as precipitation, gel adsorption and ultrafiltration

SSDI 0021-9673(94)01267-9

could not fractionate PGases into I and II and were ineffective in increasing PGase specific activity by more than 2-fold [2,4]. Therefore, there is a need for a better preparative method to obtain large quantities of PGase from *Bacillus circulans* cell extract in high yields that are free of all the nucleic acids. Most enzymes manufactured for industrial use need to be stable and inexpensive but do not need to be highly purified [5]. Cost, desired purity, speed, practicality, stability and yield are among the main issues that should be addressed in method development for preparative chromatography. This work reports (1) the successful application of HPLC methods to isolation and fractionation of PGase on a laboratory scale for use in research and (2) the suitable values of variables for fast, practical, efficient large-scale HPLC method of PGase for industrial uses.

2. Experimental[1]

2.1. Preparation and assay of PGase

B. circulans (ATCC 21590) cells were grown, harvested and extracted with 0.01 *M* phosphate buffer, pH 8.0, as previously reported [4]. Cell extracts and eluates were evaluated for PGase I and II activities in 0.05 *M* phosphate buffer, pH 7.0 at 30°C, using the synthetic substrates carbobenzoxy (CBZ)-L-glutamine and *tert.*-butoxycarbonyl (Boc)-L-glutaminyl-L-proline (Peptides International, Louisville, KY, USA), respectively. The specific activities of PGase I and PGase II in cell extract were 9–14 and 11–15 μmol mg^{-1} h^{-1}, respectively.

2.2. The HPLC system

The preparative chromatography system Delta Prep 3000 from Waters Assoc. (Milford, MA, USA) was used for analytical and preparative HPLC separation of *B. circulans* cell extracts. Aliquots of PGase in 0.02 or 0.05 *M* sodium phosphate buffer, pH 8.0. were filtered through a 0.45-μm Millex-HV Filter (Millipore, Bedford, MA, USA) before their injection. Elution was monitored at 280 nm by a Model 481 Lambda-Max spectrophotometer detector connected to a Waters 745B data module for the integration of the proportions of various eluted peaks. Fractions were collected using a Foxy fractionator (ISCO, Lincoln, NE, USA). HPLC-grade reagents and solvents were used throughout this investigation.

2.3. Analytical quaternary methylamine (QM) anion-exchange HPLC

Preliminary ion-exchange separation of PGase was performed on an analytical column Accell QMA, 15 cm × 3.9 mm I.D. (Waters). The protein load was 1.0 mg protein in 20 μl 0.02 *M* phosphate buffer, pH 8.0. Eluent used in gradient separation was 0.05 *M* sodium phosphate buffer (pH 8.0) and 0.1–0.8 *M* KCl at a flow-rate of 0.5 ml/min.

2.4. Semipreparative QM and DEAE anion-exchange separation

Ion-exchange separation of PGase was performed on a steel column (15 cm × 19 mm I.D.) packed with Accell Plus QMA medium from Waters and a 15 cm × 21.5 mm I.D. prepacked column Protein-PAK DEAE 5 PW (Waters). The protein load was 2–30 mg in 1–3 ml 0.02 *M* phosphate buffer, pH 8.0. The gradient separation eluent was 0.05 *M* sodium phosphate buffer (pH 8.0) and 0.1–0.8 *M* KCl. The flow-rate was 1.5–10.0 ml/min.

2.5. Semipreparative gel permeation

A prepacked column of cross-linked methacrylate gel (Ultrahydrogel Linear, 30 cm × 7.8 mm I.D. from Waters) with an effective fractionation range from M_r 2000 to $7 \cdot 10^6$ was used. Aliquots of PGase sample (20 μl) in 0.05 *M* sodium phosphate buffer (pH 8.0) were injected

[1] Commercial firms are mentioned in this publication solely to provide specific information. Mention of a company does not constitute a guarantee or warranty of its products by the US Department of Agriculture nor an endorsement by the Department over products of other companies not mentioned.

then eluted with 0.05 *M* sodium phosphate buffer (pH 8.0). The flow-rate was 0.3 ml/min and protein load was 2–30 mg. The high protein load run was repeated 12 times and the corresponding fractions from each run that contained PGases were pooled, dialyzed and then lyophilized, after excluding the fractions eluted in the first and last 6 min. This protein (0.1 mg) was reinjected and separated again under same conditions used with the other gel permeation separations. Ferritin, catalase, aldolase, bovine albumin, hen albumin and chymotrypsinogen A were used for column calibration. Their apparent molecular masses were 540, 240, 158, 67, 45 and $25 \cdot 10^3$, respectively, according to the manufacturer, Sigma (St. Louis, MO, USA).

2.6. Purification and fractionation of PGase

The pooled PGase peak from the multiple injection to the Ultrahydrogel Linear column was injected into the Accell Plus QMA column (2 mg), then eluted with 0.05 *M* sodium phosphate buffer (pH 8.0) and KCl gradient at 1.5 ml/min to fractionate PGase into I and II. Fractions containing either PGases I or PGase II activities were dialyzed, freeze-dried and stored at −20°C until used.

2.7. PGase deamidation of protein hydrolysates

The protein hydrolysates were previously prepared [6] by hydrolyzing soy protein, casein and gluten to 5, 10, 15 and 20% peptide bond hydrolysis with Alcalase (Novo Lab., Wilton, CT, USA). The extent of deamidation, using PGases I and II was calculated as the ratio of ammonia released enzymatically to the total amide content of the protein hydrolysate, multiplied by 100.

2.8. Analyses of DNA and protein fractions

Protein contents of PGase preparations and eluates were measured by the BCA method of Smith et al. [7]. The nucleic acid concentration in PGase preparations and eluates was measured by the spectrophotometric method of Schleif and Wensink [8]. Sodium dodecyl sulfate–polyacrylamide gel electrophoresis (SDS-PAGE) was performed on 8–25% polyacrylamide gels using the PhastSystem (Pharmacia/LKB, Uppsala, Sweden) and a pH 8.9, 0.125 *M* Tris–borate buffer containing 0.1% SDS, as originally described by Koenig et al. [9].

2.9. Statistical analysis of variance

Multi-factor analysis of variance [10] of variables was performed using the software package and the procedures of Statgraphics (Rockville, MD, USA).

3. Results and discussion

3.1. Analytical separation and scale-up of anion-exchange chromatography

In earlier work, PGase separation into I and II was achieved by sequential precipitation with streptomycin sulfate (to remove nucleic acids) and ammonium sulfate followed by chromatography on Sephadex G-200, DEAE-Sephadex and hydroxyapatite [3]. In developing the separation method here, newly introduced, advanced HPLC tools were taken advantage of so that the PGase separation is carried out directly from the cell extract without any sample preparation or other fractionation techniques. Therefore, key interdependent experimental parameters such as mobile phase composition, pH, and ionic strength were investigated to fractionate PGase into I and II and obtain a fast, high-recovery separation. The method development for anion-exchange chromatography was first initiated by using an analytical column (15 cm × 3.5 mm I.D.) to assess the chromatographic performance of the anion exchanger Accell QMA. The separation was carried out at pH 8.0 using the KCl gradient program and other initial conditions based on the conventional separation on DEAE-Sephadex [3]. The proteins were separated into six major peaks (each contained more than 2% of the total protein) with the last three peaks, grouped to one main peak, containing 65% of the total protein (Fig. 1A). PGases were not separated into I and II as the preceding peak had 89% of

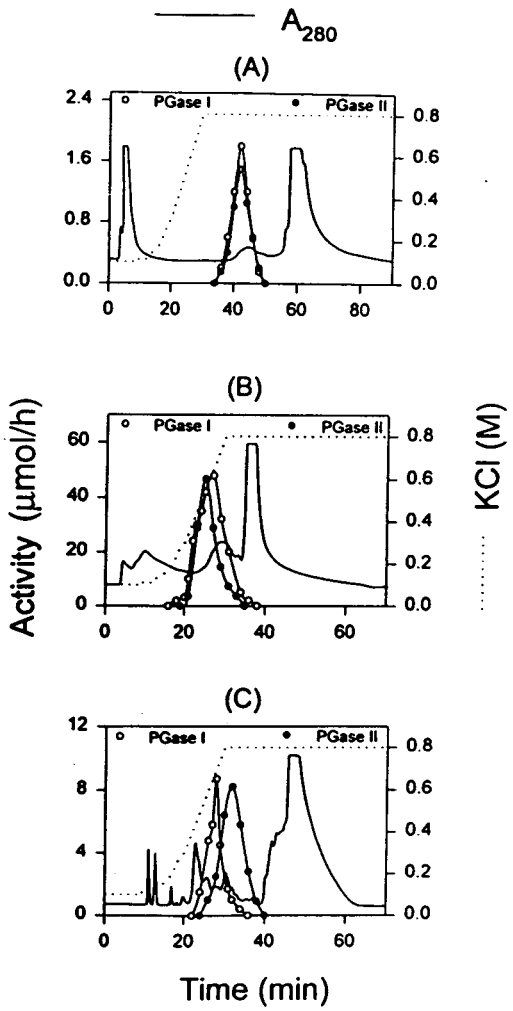

Fig. 1. Anion-exchange separation of *B. circulans* proteins using (A) QM anion-exchange (15 cm × 3.9 mm I.D.) column at 1.0 mg load and 0.5 ml/min, (B) 15 cm × 19 mm I.D. QM anion-exchange column (30 mg load) at 5.0 ml/min and (C) DEAE anion-exchange (15 cm × 21.5 mm I.D.) column at 5 mg load and 5 ml/min.

the activity units of both PGase I and II with 9-fold increase in their specific activities.

This separation was scaled-up to a semipreparative scale using a 15 cm × 19 mm I.D. column with the same bed length but about 30 times the volume of the analytical column. Scale-up of ion-exchange process is usually achieved by increasing the column diameter while maintaining the column bed height and linear flow-rate constant [11]. Chromatographic separation loads are usually scaled up a number of times equal to the ratio of their cross sectional areas. Here, the protein load was increased from 1 to 30 mg, a scale-up factor of 30 based on the volumes of the two columns. Ideally, runs are carried out at the same linear velocity (flow-rate in ml divided by the cross-section area of the column) to maintain an equivalent time frame for the small- and large-scale separations [12]. During scale-up, the flow-rate was changed from 0.5 ml/min (5.2 cm/min) to 5 ml/min (1.8 cm/min). The reduction of scale factor for the linear flow-rate was chosen to improve PGase resolution in an attempt to affect the separation of PGases I and II. To gain some increase in resolution, many chromatographic separations are scaled up at much lower flow-rates than those based on maintaining linear velocity [13]. The Accell QMA chromatography on the semipreparative column using 0.05 *M* phosphate buffer (pH 8.0) and a scaled-up KCl gradient (Fig. 1B) also gave six peaks of which the last one accounted for 69% of the total protein. PGases I and II were still eluted in one peak with 86% recovery and a 9-fold purification

Reducing the protein load gradually from 30 to 5 mg increased fold purification from 7 to 12 but was ineffective in fractionating PGase into I and II. A typical anion separation of the proteins from the extract of *B. circulans* cells is presented in Fig. 1C in which another column (15 cm × 21.5 I.D.) containing DEAE anion exchanger was used at a flow-rate of 5 ml/min and 5 mg load, with the optimal gradient profile developed for the QM anion-exchange runs. The PGase yield was 89% and the ion exchange gave 16 peaks, of which the last peak contained all the nucleic acids and accounted for 72% of the total protein. This peak was preceded by the peaks of the of PGase I and II. PGases were fractionated into I and II but there was still overlapping. The PGases were purified 13.6- and 11.4-fold, respectively, for PGases I and II with an average of 12.5-fold. In all the runs, separation efficiencies of the DEAE and Accell columns were comparable. In spite of that, the Accell column is preferred because it can be easily self-packed

and the support medium can be effectively regenerated for continuous use.

3.2. Effect of flow-rate and protein load on anion-exchange separation

Flow-rates and protein loads were varied to study their effects on the QM anion separation (Table 1). Analysis of variance indicated that both flow-rate and protein load significantly affected the purity of the PGase. The last peak of the chromatographs contained a large portion of the injected protein ranging from 65–80%. Protein content of this peak as a percentage of the total injected proteins was independent of the protein load but it declined significantly by increasing the flow-rate. Regardless of its protein content, this peak contained all the nucleic acids of the injected cell extract and thus they can be easily separated from the PGase peaks. Fig. 2 shows the anion separation using the QM column (A) and the DEAE column (B) at 3 ml/min and 10 mg protein load. Reducing protein load from 30 to 10 mg and flow-rate from 5 to 3 ml/min was still ineffective in ending overlapping in the fractionation of PGase into I and II. However, reducing the protein load injected into the anion column from 10 to 5 mg or less and the flow-rate from 3 to 1.5 ml/min resulted in separation of I and II after retention times of 74 and 93 min, respectively, with complete resolution of the two peaks (Fig. 2C). The PGases were purified 14.2- and 14.7-fold, respectively, and followed by the last peak that contained 78% of the protein. The separation of *B. circulans* cell extract with protein load of 20 mg and a flow-rate of 6 ml/min is shown in Fig. 2D. PGases I and II were not separated, but rather they eluted in one peak. The yield and the degree of purification of PGase were more than 85% and 8-fold, respectively and the separation was complete in 35–40 min. More than 65% of the protein was eluted last after the PGase peak, which contained all the nucleic acids that were in the injected sample. The conditions of this separation were the most suitable for scale-up applications since increasing flow-rates to more than 6 ml/min or loading to more than 30 mg led to the deterioration of the separations, particularly the fold purification of PGase peak.

Sample load is a key parameter influencing throughput since it has a dramatic effect on separation efficiency (α), column efficiency, retention time and even peak shape [13]. Sample load is directly proportional to α and hence the easiness or difficulty of separation. Also, as sample load is increased, the effective plate count decreases until the efficiency reaches a point that the column is no longer useful for practical separation. Both the flow-rate and protein load were reduced to effect the fractionation of PGases into I and II and were also maximized to develop a large-scale method (Fig. 2). Flow-rate is the operational variable which most influences time. High flow-rates are possible with separation efficiencies, α, of more than 2.0, while working within the constraints of acceptable back pressure and practical solvent handling capabilities. As α becomes smaller, the flow-rates may have to be decreased to maintain

Table 1
Fold purification of the PGase peaks separated on QM anion exchanger at various protein loads and flow-rates

Flow-rate (ml/min)	Protein load (mg)			Multiple range analysis[a]	
	5	10	20	Mean ± standard error	Homogenous groups
1.5	14.2	12.2	10.0	12.1 ± 0.2	I
3.0	11.9	9.9	9.2	10.3 ± 0.2	II
6.0	11.5	9.5	8.3	9.8 ± 0.2	III

[a] For fold purification by flow-rate. Group I is significantly different from group II and from group III, but groups II and III do not differ significantly from each other.

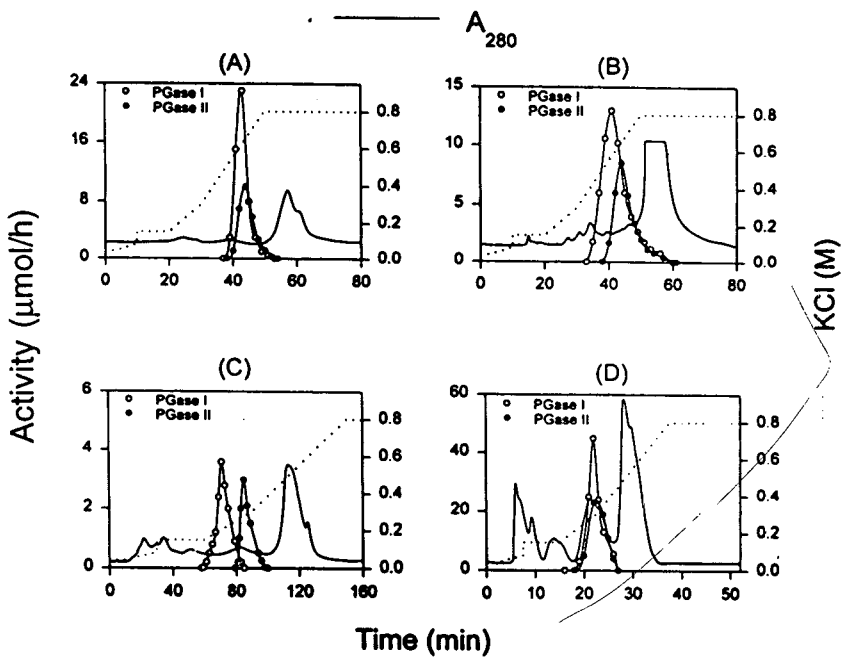

Fig. 2. Anion-exchange chromatography of *B. circulans* proteins on (A) QM column, (B) DEAE column (10 mg load at 3.0 ml/min for both runs), (C) QM anion exchanger at 1.5 ml/min with protein load of 5 mg, and (D) QM ion exchanger at 6.0 ml/min and 20 mg load of cell extract proteins.

the desired degree of resolution and solute recovery [13].

3.3. Gel permeation HPLC

The separation of the proteins from *B. circulans* (2 mg loads) on the Ultrahydrogel column is presented in Fig. 3A. Gel permeation gave 9 peaks, of which the first three were non-PGase proteins and accounted for 91% of the total protein with all the nucleic acids present in the third peak. The 4th peak had PGase I and II activities and only 0.4–0.6% of the protein. This resulted in a 250-fold increase of the specific activity of both PGases with 90% yield. The PGases were slightly separated into two overlapping peaks (Fig. 3A) allowing the estimation of their molecular masses. Estimated M_r values were $180 \cdot 10^3$ and $220 \cdot 10^3$ for PGases I and II, respectively. Runs of 20–30 mg loads (Fig. 3B) gave only six overlapping peaks. Although the yield was basically as high as that of the runs of lower loads, the separation efficiency was inferior: the specific activity of the PGase peak increased only 60–100-fold and this peak contained about 20–35% of the nucleic acids. At these high protein loads, each of the PGases had a small tailing peak containing 13.5% of the total activity with an estimated M_r of $90 \cdot 10^3$ and $110 \cdot 10^3$ for PGases I and II, respectively (Fig. 3B). These lower-M_r species of PGases were evidently dissociated forms of the $180 \cdot 10^3$ or $220 \cdot 10^3$ PGases. Kikuchi and Sakaguchi [14] reported the M_r of the non-dissociated PGases to be $200 \cdot 10^3$ and the PGase I and II to be $90 \cdot 10^3$ and $125 \cdot 10^3$, respectively, in dissociating conditions of 0.1 *M* KCl and pH 10.9. The pooled PGases of the 20–30 mg loads were reinjected into the gel permeation column. PGases were separated into two overlapping peaks (Fig. 3C) with retention times corresponding to estimated M_r of $180 \cdot 10^3$ and $220 \cdot 10^3$ for PGases I and II, respectively. More than half of the injected proteins were removed during this run, doubling

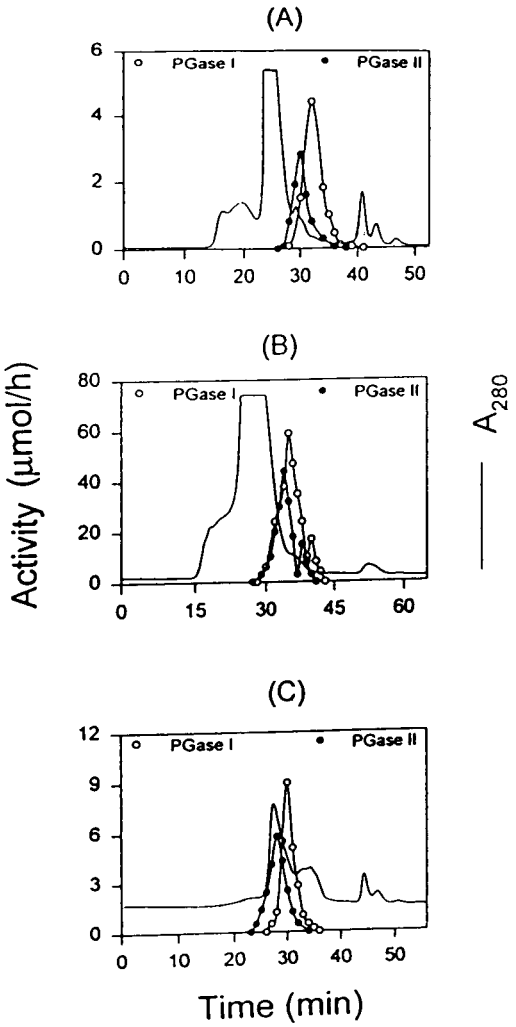

Fig. 3. Gel permeation of *B. circulans* proteins on acrylate gel (30 cm × 7.8 mm I.D.) at a flow-rate of 0.5 ml using 2 mg (A) and 20 mg (B) of cell extract proteins. Pooled active peaks (0.1 mg) from (B) were reinjected (C).

the fold purification of the PGase (I and II) preparation.

3.4. Role of the PGases in protein deamidation

PGase I and PGase II obtained by anion-exchange HPLC were used to hydrolyze the amide groups of the glutamine residues in three proteins with diverse structures. The deamidation of the hydrolysates of soy protein, casein and gluten using PGase I and PGase II is presented in Fig. 4. The total PGase deamidation of protein hydrolysates, the sum of % deamidation by PGases I and II, was equal to the percent deamidation previously obtained [2] using partially purified preparations of *B. circulans* cell extract, which were mixtures of PGases I and II. Here, over 52, 37 and 39% total protein deamidation was achieved for soy protein, casein and gluten, respectively, that had 20% peptide bond hydrolysis (20 DH). PGase I alone was responsible for 17, 21 and 42% of the deamidation of soy, casein and gluten at a DH range of 5–15 but dropped to 16, 17 and 31% at 20 DH. PGase II was responsible for the remainder of the deamidation. Gill et al. [15] found no deamidating activity of PGase I toward whey and casein proteins or their 4 DH hydrolysates. Here both enzymes (PGase I and II) were needed for the completion of the deamidation of proteins. Therefore, PGase preparations must contain both enzymes. Separation of PGase I from PGase II is not needed, providing that sufficient PGase I activity is present in the PGase I and II mixture.

3.5. Purification of PGases to homogeneity by gel permeation and anion HPLC

Proteins of *B. circulans* cell extracts were first subjected to gel permeation chromatography to obtain a PGase peak with a 60–100-fold increase in specific activity (20–30 mg loads). PGase was further fractionated on an Accell preparative column (2 mg loads) into I and II (Table 2). The average yield of PGase activity units was 80%. Specific activity of the PGase peak increased 1310- and 1540-fold for PGases I and II, respectively, as compared to the original cell extract (average 1425-fold). Kikuchi et al. [3] used conventional chromatography to obtain 13 and 21% of total activity of PGases I and II from *B. circulans* cell extract with 400- and 420-fold purification, respectively. The SDS-PAGE patterns of the PGase I and PGase II contained one band each with M_r of $45 \cdot 10^3$ and $55 \cdot 10^3$, respectively, as estimated using protein markers (Fig. 5). It appears from these data and the gel

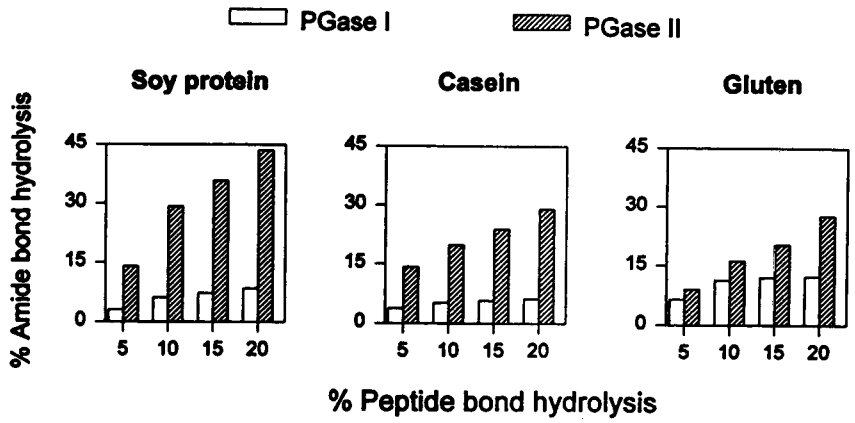

Fig. 4. Percent deamidation of protein hydrolysates effected by PGase I and PGase II, both purified from cell extract by anion chromatography.

permeation data that *B. circulans* PGases have M_r of $180 \cdot 10^3$ and $220 \cdot 10^3$ that can be dissociated into $90 \cdot 10^3$ and $110 \cdot 10^3$ units, respectively. Also, dissociated PGases may have one intermolecular disulfide bond linking two subunits of $45 \cdot 10^3$ for PGase I and $55 \cdot 10^3$ for PGase II.

It appears that the purity of both PGases is sufficient to make them suitable for use in probing for cloning these enzyme. Re-engineering the PGases is necessary to increase their production during fermentation and the relative concentration of PGase II, responsible for the majority of protein deamidation (60–80%). Additionally, cloning would allow the production of these enzymes in a food grade microorganism such as *Bacillus subtilis* or *Saccharomyces cervisiae*. Further, using these purification methods on a laboratory scale are helpful in obtaining PGases for use in the determination of glutamine in proteins or peptides. The individual content of asparagine and glutamine, making up the total amide content in protein or protein hydrolysate can be determined by amino acid and amide analysis, liquid chromatography or by enzymatic methods [1]. Enzymatic methods, however, may be more reliable because of their selectivity and the liable nature of the amide group even at very mild experimental conditions. Purified PGases can be used in the determination of glutamine in peptides and proteins according to the method of Kikuchi [16].

Table 2
Deamidating activity and yield of *B. circulans* extract after HPLC purification

Enzyme or HPLC method	PGase I					PGase II				
	Protein (mg)	Total units[a]	Recovery (%)	Specific activity[b]	Fold purification	Protein (mg)	Total units[a]	Recovery (%)	Specific activity[b]	Fold purification
Cell extract	344	3234	100	9.4	–	344	4919	100	14.3	–
Gel permeation	4.1	3007	93	734	78	3.7	4526	92	1257	88
Ion exchange	0.2	2587	80	12 317	17	0.16	3539	78	22 025	18

[a] One unit releases 1.0 μmol NH_3 per h.
[b] Units per mg protein.

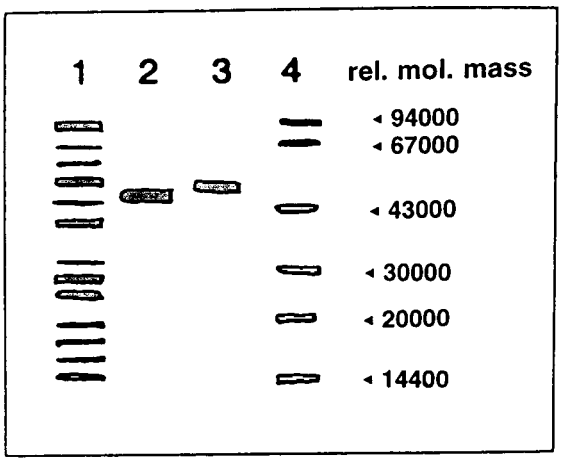

Fig. 5. SDS-PAGE of *B. circulans* cell extract (lane 1) and PGase I (lane 2) and PGase II (lane 3) both purified from cell extract by gel permeation and anion-exchange chromatography. Samples in lane 4 are the molecular mass markers.

3.6. Preparative separation method of PGase for industrial use

Ion-exchange chromatography is widely used for downstream processing of significant proteins [11] but gel permeation fractionation of proteins is also considered a standard technique that can be scaled up to process level. The relatively high purity and the excellent resolution achieved with gel permeation were offset by the enzyme contamination with nucleic acids and the lack of speed for this method of separation. Protein overloading resulted in contamination of PGase preparations with DNA due to overlapping of the PGase peak with preceding peak that contained all the DNA. Because nucleic acids are heterogenous and contain molecules with widely different sizes, they can be eluted into more than one peak on gel permeation with late elution of the peak containing low molecular masses [17].

On the other hand, ion exchange can be of more practicable value in large-scale production of proteins. Since both PGases are needed for protein deamidation and their fractionation is not required, the conditions of PGase separation on the QM column using 20–30 mg protein at 6 ml/min were the most suitable for the scale-up process. In this method, PGase could be separated directly from *B. circulans* extract in one chromatographic run in less than 1 h with high purity and high yield. More than two-third of the injected protein was found in the last peak, which contained all the nucleic acids of the injected cell extract. Due to the high negative charges in DNA phosphate groups, anion-exchange separation can be the most effective technique for the removal of DNA contaminant from protein preparations [17,18]. Therefore, this purification program would have an impact on the economy of this large-scale technique since expensive chromatographic separations, chemical or enzymatic treatments for the removal of nucleic acids from *B. circulans* extracts are not needed. Furthermore, this anion separation method meets the requirements of purity, yield, speed, and the practical and economical aspects for successful large-scale production of the enzyme. Therefore, this suitable separation developed on this preparative unit is ready to be scaled-up directly using appropriate equipment.

4. Conclusions

(1) PGase can be isolated from *B. circulans* cell extract by preparative scale HPLC using either anion-exchange or gel permeation, but only the former yields an enzyme entirely free of nucleic acids. In gel permeation the nucleic acids elute before the PGase, resulting in some tailing, whereas in anion exchange the nucleic acids elute after the PGase.

(2) PGase can be separated cleanly into its component fractions, PGase I and PGase II, by anion-exchange HPLC if the protein load and flow-rate are both reduced. The SDS-PAGE patterns of the two PGases show subunits of $45 \cdot 10^3$ and $55 \cdot 10^3$, compared to M_r of $180 \cdot 10^3$ and $220 \cdot 10^3$ for the undissociated enzymes.

(3) Both PGase I and PGase II are needed to match the extent of deamidation of typical protein hydrolysates achieved with the whole PGase, contrary to a literature report. For this application, the separation of the two PGases is probably unnecessary.

(4) Anion-exchange separation on preparative

HPLC unit was optimized to develope methodology for the potential production of kilogram quantities of PGase from *B. circulans* cell extract.

References

[1] J.S. Hamada, *Crit. Rev. Food Sci. Nutri.*, 34 (1994) 283.
[2] J.S. Hamada, in B.J.F. Hudson (Editor), *Biochemistry of Food Proteins*, Elsevier Applied Science Publ., London, 1992, p. 249.
[3] M. Kikuchi, H. Hayashida, E. Nakano and K. Sakaguchi, *Biochemistry*. 10 (1971) 1222.
[4] J.S. Hamada, F.F. Shih, A.W. Frank and W.E. Marshall, *J. Food Sci.* 53 (1988) 671.
[5] P.S.J. Cheetham, in A. Wiseman (Editor), *Handbook of Enzyme Biotechnology, Part B, Industrial Utilization of Enzymes and Cells*. Ellis Horwood, Chichester, 1986, p 274.
[6] J.S. Hamada, *J. Agr. Food Chem.*, 40 (1992) 719.
[7] P.K. Smith, R.I. Krohn, G.T. Hermanson, A.K. Mallia, F.H. Gartner, M.D. Provenzano, E.K. Fujimoto, N.M. Goeke, B.J. Olson and D.C. Klenk, *Anal. Biochem.*, 150 (1985) 76.
[8] R.F. Schleif and P.C. Wensink (Editors), *Practical Methods in Molecular Biology*, Springer, New York, 1981, p. 90.
[9] R. Koenig, H. Stegemann, H. Francksen and H.L. Paul, *Biochim. Biophys. Acta*, 207 (1970) 184.
[10] R.W. Walpole and R.H. Myers, *Probability and Statistics for Engineers and Scientists*, Macmillan, New York, 1989, p. 486.
[11] P.R. Levison, in G. Ganttsos and P.E. Barker (Editors), *Preparative and Production Scale Chromatography*, Marcel Dekker, New York, 1993, p. 617.
[12] N.J. Little, R.I. Cotter, J.A. Prendergast and P.D. McDonald, *J. Chromatogr.*, 126 (1976) 439.
[13] P.D. McDonald and B.A. Bidlingmeyer, in B.A. Bidlingmeyer (Editor), *Preparative liquid Chromatography (Journal of Chromatography Library*, Vol. 38), Elsevier, Amsterdam, 1987, p. 1.
[14] M. Kikuchi and K. Sakaguchi, *Agr. Biol. Chem.*, 37 (1973) 827.
[15] B.P. Gill, A.J. O'Shaughnessey, P. Henderson and D.R. Headon, *Irish J. Food Sci. Technol.*, 9 (1985) 33.
[16] M. Kikuchi, *Anal. Biochem.*, 59 (1974) 83.
[17] P. Ng and G. Mitra, *J. Chromatogr A.*, 658 (1994) 459.
[18] W. Jiscot, J.J.C.C. Van Hertrooij, J.W.T.M.K. Gebbinck, T.V. Velden-de Groot, D.J.A. Crommelin and E.C. Beuvery, *J. Immunol. Methods*, 124 (1989) 143.

ELSEVIER

Journal of Chromatography A, 702 (1995) 173–189

JOURNAL OF CHROMATOGRAPHY A

Separation of biotin labeled proteins from their unlabeled counterparts using immobilized platinum affinity chromatography

Dale Miles[a], Antonio A. Garcia[b,*]

[a]*Pharmacyclics, Inc., 995 Arques Avenue, Sunnyvale, CA 94086, USA*

[b]*Department of Chemical, Bio and Materials Engineering, Arizona State University, Tempe, AZ 85287-6006, USA*

Abstract

A stationary phase selective for biotin labeled proteins has been developed by immobilizing platinum(II) ions to a polyacrylamide gel. Bovine serum albumin (BSA) and biotin labeled BSA (BSA-Biotin) have been applied individually to a packed column containing the modified gel. At pH 4.8 using column superficial velocities of 1.0 and 0.25 cm/min respectively, 40% and 73% of the applied BSA-Biotin were bound to the activated gel while no unconjugated BSA was bound. A 1.0 *M* imidazole–HCl solution at pH 7 was successfully used to elute bound BSA-Biotin, indicating that binding to immobilized Pt(II) is reversible.

1. Introduction

Avidin (M_r 16 000) and streptavidin (M_r 14 000) are small proteins which form extremely strong non-covalent bonds with biotin (dissociation constant 10^{-15} *M*) [1]. Avidin is a glycoprotein derived from egg white with an isoelectric point of 10, whereas streptavidin, which is obtained from Streptomyces avidinni, is carbohydrate-free and has an isoelectric point of about 5.5 [1]. (Strept)avidin has been shown to contain biotin binding sites deeply recessed within the protein, and four tryptophanyl residues per binding site have been implicated in hydrophobic interaction with biotin [1]. The (strept)avidin-biotin system is appealing because the binding of biotin to (strept)avidin is complete and rapid, and does not require special reaction conditions. Furthermore, the biological activity of most proteins is preserved after biotinylation, and the ability of each (strept)avidin moiety to bind four biotin molecules amplifies the desired result [1].

Since 1980, an explosion in the number of applications utilizing avidin-biotin technology has occurred. Some applications are listed by Wilchek and Bayer [1] in a recent review. An extensive literature is available on avidin-biotin technology, and several excellent reviews have been published [1–6]. The high affinity of avidin for biotin is advantageous for initial capture of biotinylated species from solution, but a disadvantage for elution and recovery [1]. Even under harsh elution conditions, such as 6.0 *M* guanidine chloride at pH 1.5, poor recovery of the biotinylated molecules is sometimes observed. When elution is successful, the activity of the biotinylated species is often irreversibly reduced. Biotin itself can sometimes be used to

* Corresponding author.

0021-9673/95/$09.50 © 1995 Elsevier Science B.V. All rights reserved
SSDI 0021-9673(94)00882-5

release biotinylated compounds from an avidin affinity column, although poor recoveries are generally noted, even when extremes of pH and long equilibration times are used.

Several researchers have used modified forms of avidin in order to improve recoveries. Avidin immobilized to a sepharose column can be converted to a monomeric form by denaturing the avidin tetramer with guanidinium chloride, leaving a single subunit immobilized to the sepharose. The dissociation constant for immobilized monomer-biotin is about 10^{-7} M. However, there are still some high affinity binding sites which must be blocked with biotin before using the column for affinity chromatography [1]. In general, elution of the retained product is accomplished by removing the target from the binder, or cleaving the biotin–binder bond, with the (strept)avidin–biotin bond left intact. This has led to low recoveries or protein denaturation [1].

It would be desirable to develop a universal affinity chromatography column based on the (strept)avidin-biotin system which could be recharged with a different biotinylated binder depending on the target protein desired. Such a system has been studied by Hofmann et al. [7] who attached 2-iminobiotin instead of biotin to each binder. The advantage of this system is that 2-iminobiotin binding to avidin is a strong function of pH, and varies from $3 \cdot 10^{-8}$ at pH 9 to $1.2 \cdot 10^{-6}$ at pH 6. Therefore, when the column is operated at pH 9 or above, the 2-iminobiotinylated binder is more firmly attached to the column [1]. The column can be charged with a new iminobiotinylated binder after first washing off the original binder using a buffer with $pH < 6$. Although this system appears very attractive, it has several drawbacks. First, many proteins are irreversibly denatured at high pH, therefore, the system cannot be used for these types of proteins. Second, many iminobiotinyl derivatives have affinities for biotin too low to be useful.

Another approach to develop a reversible biotin affinity column is through the use of antibodies to biotin which bind biotin with a dissociation constant of approximately 10^{-9} *M* [1]. However, most antibodies have a molecular mass at least twice that of avidin, and only contain two binding sites per molecule. Therefore, the capacity of a column which uses immobilized antibodies for affinity chromatography of biotinylated proteins is generally much less than a similar column which employs avidin. In addition, the Fc portions of antibodies consist of oligosaccharide residues that may be responsible for non-specific binding. Moreover, some macrophages and lymphocytes recognize the Fc portion of the antibody and bind to the antibody. Although the lower dissociation constant (10^{-9}) allows more efficient removal of the antibody, it comes at the expense of less efficient and less selective capture of biotinylated species during sample application to the column [1]. Other biotin-binding proteins have been discovered which exhibit dissociation constants from 10^{-7} to 10^{-12}. The use of these proteins in affinity chromatography is currently being explored [1].

Based on previous research with chromatography of amino acids [8], we have shown that immobilized Pt(II) has a very high affinity and selectivity for methionine. This behavior differs sharply from amino acid chromatography using immobilized transition metal ions normally used in immobilized metal affinity chromatography (IMAC) [9]. Because the Pt(II)–methionine interaction is primarily due to the thioether functional group on methionine and follows Pearson's hard–soft acid base theory [10], we theorized that immobilized Pt(II) could be used to bind biotin since it also exhibits a thioether functional group. Use of metal ions for biotin binding is advantageous due to lower cost, ease in maintaining column sterility as well as column regeneration [9], and the potential for higher packing densities and minimization of non-specific protein–protein interactions. However, metal ions could introduce electrostatic interactions that could induce non-specific binding or alter protein binding kinetics as well as unwanted binding due to electrostatic attractions unless care is taken to minimize these effects through the use of buffer salts.

Although IMAC with Cu(II) has been used to separate biotinylated proteins and nucleic acids,

complexation with avidin, not biotin, resulted in retention of the conjugate on the column [11]. In a separate study, up to 15 m*M* biotin was tested as an eluent for immobilized photosystem proteins I and II sorbed to immobilized Cu(II). No significant elution of the protein was noted, indicating that biotin could not effectively compete with the protein for Cu(II) binding sites [12] again suggesting that copper ions do not coordinate strongly to biotin.

However, we have shown through amino acid chromatography with both immobilized Pt(II) and Ag(I), and by analogy, that soft metal ions have a high specificity for molecules containing thioether functional groups. Moreover, since methionine residues are usually found in the interior of proteins due to their hydrophobic nature, biotin present on the protein surface would likely be the sole driving force for biotinylated protein binding. We thus decided to test conditions where biotin conjugated BSA (BSA-Biotin) would bind to a column containing immobilized Pt(II) while BSA would not. In this way, immobilized Pt(II) would be rigorously tested for its suitability as a substitute for (strept)avidin in biotin affinity columns. Conditions under which BSA-Biotin can be eluted from the column without loss of Pt(II) were also briefly explored in the course of this work.

2. Experimental

2.1. Chemicals

Bio-Gel P200 polyacrylamide gel (Bio-Rad Laboratories, Richmond, CA, USA) extra fine, 100–200 mesh (wet) M_r 200 000 exclusion limit. Albumin, bovine (Sigma Chemical, St. Louis, MO, USA) fraction V, 99%, globulin free, prepared by cold alcohol precipitation. Albumin, bovine-biotin labeled. 95% protein (Sigma) balanced with citrate buffer salts, prepared from a companion lot of the BSA described above, which was processed at the same time as BSA and contains 10.6 mol biotin/mol BSA . Glutaraldehyde (Aldrich Chemical, Milwaukee, WI, USA) 25 wt.% in water. K_2PtCl_4, $PtCl_4^{2-}$ or Pt(II) potassium tetrachloroplatinate(II) 98% (Aldrich) was used for immobilization. Protein Assay Kit (P65656) (Sigma) for quantitative microdetermination of total protein. Thiourea (J.T. Baker Chemical, Phillipsburg, NJ, USA) used in gel activation was reagent grade.

2.2. Equipment

A Pharmacia Augmented FPLC system (Pharmacia, Uppsala, Sweden) was used for all chromatography experiments described here. A DU-70 Spectrophotometer (Beckman Instruments, Fullerton, CA, USA) was used for determination of total protein concentration via the Lowry Microprotein Assay Kit. A Varian Model 1100 (Varian, USA) was used in order to determine the amount of platinum immobilized on the activated gel.

2.3. Determination of total protein

Total protein concentrations were determined using Peterson's modification of the micro-Lowry method [13,14] using a Protein Assay Kit purchased from Sigma. Assays were performed by following the kit instructions exactly as specified for protein determination with protein precipitation. Essentially, the procedure required dilution of the sample with distilled water, followed by addition of trichloroacetic acid and sodium deoxycholate to precipitate the protein. After centrifuging each sample, the supernatant was decanted and blotted way from the protein pellet. The pellet was redissolved using the Lowry reagent solution, to which was added Folin and Ciocolteu's phenol reagent. After a sufficient incubation period, the absorbance was read at 750 nm. Standards with known BSA concentrations were prepared and analyzed identically along with the samples and used to construct a calibration curve.

2.4. Determination of Pt(II) concentration in solution by atomic absorption

All platinum analyses were carried out using an atomic absorption spectrometer. A Varian

Model 1100 was used for all measurements using an air–acetylene flame. The lamp current, slot width, and detection wavelength were 10 mA, 0.2 nm and 265.9 nm, respectively. All Pt(II) standard solutions were prepared fresh from K_2PtCl_4 in distilled water, unless otherwise indicated. In some cases, a small amount of nitric acid was added to each sample and standard prior to analysis. Fresh standards were analyzed to generate a calibration curve prior to sample analysis.

Pt(II) was sorbed to the resin by gentle shaking at room temperature for several hours. After sorption, the resin was allowed to settle and an aliquot of the supernatant was removed and analyzed directly by atomic absorption. The Pt(II) concentration in the supernatant was read from a calibration curve relating absorbance to Pt(II) concentration. The amount of Pt(II) sorbed to the resin was determined indirectly from decrease in Pt(II) concentration in the supernatant after sorption. In some cases, a small amount of HNO_3 was added to the sample and controls prior to analysis to improve the stability of the aqueous Pt(II).

2.5. Preparation of biogel polyacrylamide resins with immobilized Pt(II)

Biogel P200–Glut–Thio resin was prepared by Kim [15] as follows: First, 25% glutaraldehyde was polymerized at 70°C for 36 h in a heated water bath. Then 50 ml of the polymerized glutaraldehyde solution was added to 50 ml of D.I. water, and 1.85 g of Biogel P200 resin and shaken gently at 50°C for 24 h. Resin swelling and glutaraldehyde activation were allowed to proceed simultaneously. Upon completion of glutaraldehyde activation, the resin was washed batchwise 5 times with 70 ml of distilled water.

Thiourea activation was accomplished by adding 40 ml of a 1.0 *M* thiourea solution to 50 ml of the glutaraldehyde activated resin. The resin slurry was shaken gently for 24 h at 50°C. After completion of the thiourea sorption step, the resin was washed 20 times batchwise with 70 ml of distilled water, followed by column washing at 1.0 ml/min with 720 ml of distilled water. Each batchwise wash was accomplished by decanting the supernatant, adding the specified amount of distilled water, gently shaking the resin for several seconds to suspend it in the fresh water, then allowing the resin to settle for one h.

The Biogel P200–Glut–Thio–Pt(II) resin was prepared by activation of BP200–Glut–Thio described above with Pt(II). A 16.0-ml volume of 0.0126 *M* K_2PtCl_4 solution was added to 20.0 ml of Biogel P200–Glut–Thio resin and rotated gently for 1.2 h. The resin was allowed to settle for approximately 1 h, and the volume after sorption was determined to be 24 ml. The resin was then column washed at 0.15 ml/min with 700 ml of distilled water. The 700 ml of rinse solution was evaporated down to 26.6 ml, and then analyzed by atomic absorption to determine the concentration of Pt(II) in the rinse. The Pt(II) loading was determined to be 0.008 mmol Pt(II) per ml of wet resin.

2.6. Column liquid chromatography: effects of mobile phase composition

A glass column (5.45 × 0.5 cm) packed to a final bed volume of 1.1 ml was used at room temperature for all experiments. Mobile phase buffers were all prepared at a concentration of 0.05 *M* at pH 2.5, 4.8, and 7.0 using sodium phosphate (in NaH_2PO_4–H_3PO_4 form), sodium acetate, and sodium phosphate, respectively. NaCl was used to set the chloride concentration in the imidazole-free mobile phases. When both chloride ion and imidazole were present in the mobile phase buffer, the buffer was prepared by adding concentrated hydrochloric acid and imidazole solid to distilled water first. Then sodium hydroxide and the buffer salt were added to adjust the pH to the desired value. Individual stock solutions of BSA and BSA-Biotin were prepared by weighing each protein into a separate vial and diluting to a final concentration of $1.49 \cdot 10^{-4}$ *M* using a dissolution buffer. The stock solution was further diluted by a factor of 15 to a final concentration of $1.0 \cdot 10^{-5}$ *M* using the mobile phase prior to column application. The protein dissolution buffer consisted of 0.05 *M* sodium citrate–0.145 *M* NaCl, pH 7.0. BSA-

Biotin from the manufacturer had approximately 5% citrate salts. No citrate was present in the lyophilized BSA reagent. As citrate is known to chelate strongly to metal ions, excess citrate was added to the dissolution buffer in order to equalize any effect of citrate on the elution of each protein. Due to the small size of the citrate molecule, it was eluted after the protein.

For all experiments described below, protein applications to the column were performed pairwise sequentially, with BSA applied individually to the column first immediately followed by BSA-Biotin.

In order to investigate the variation in retention with mobile phase flow rate, a glass column (5.3 × 0.5 cm) was packed with 1.0 ml of Biogel P200–Glut–Thio–Pt(II) resin loaded with 0.008 mmol Pt(II)/ml wet resin and connected to the FPLC system. The same column and packing were used for all runs which used the Pt(II) activated resin. All control runs (no immobilized Pt(II)) were also performed using the same freshly packed Biogel P200–Glut–Thio resin (1.2 ml bed volume). Each column was washed with 10 bed volumes of a 0.05 *M* sodium acetate mobile phase (pH 4.8) prior to the initial injection of protein.

Each sample application to the column consisted of a 0.02-ml injection of protein. Three flow rates were studied in the following order: 0.05, 0.1, and 0.2 ml/min. BSA was always applied to the column first, followed by BSA-Biotin. Three pairs of BSA/BSA-Biotin injections (6 total) were applied initially to the column at 0.1 ml/min to test the stability of the column. Thereafter, a single injection of BSA was followed by a single injection of BSA-Biotin at each of the other two flow rates. Detection was accomplished at 280 nm and 0.02 AUFS. The column was equilibrated with at least 2 bed volumes of mobile phase prior to each injection.

The effect of pH, chloride concentration, and imidazole concentration on BSA and BSA-Biotin binding to Biogel P200–Glut–Thio–Pt(II) was studied in three experimental series, each performed using a separate column. In the first series, the effect of pH was studied. A glass column (5.6 × 0.5 cm) was packed with 1.1 ml of Biogel P200–Glut–Thio–Pt(II) resin loaded with 0.008 mmol Pt(II)/ml wet resin. The same column and packing were used for all runs in this series. Injections of BSA and BSA-Biotin were made sequentially at pH 7, 4.8 and 2.5. Sodium phosphate (0.05 *M*) was used to prepare buffers at pH 2.5 and 7, and sodium acetate (0.05 *M*) for pH 4.8.

Each protein application to the column consisted of a 0.02-ml injection of $1.0 \cdot 10^{-5}$ *M* BSA followed by an individual injection of BSA-Biotin at each pH. The flow rate was fixed at 0.1 ml/min. Detection was accomplished at 280 nm with 0.02 AUFS. At least 5 column volumes of mobile phase were used to equilibrate the column at each pH before making injections. The resin was equilibrated with at least 2 bed volumes of mobile phase prior to each injection.

In the second series, both the pH and concentration of sodium chloride were varied. A glass column (3.1 × 0.5 cm) was packed with 0.61 ml of Biogel P200–Glut–Thio–Pt(II) resin loaded with 0.008 mmol Pt(II)/ml wet resin. The same column and packing were used for all runs in this series. All experiments were carried out at 0.1 ml/min with detection at 280 nm/0.02 AUFS. Table 1 shows (in order) the mobile phases used with this column. The column was equilibrated with approximately 10 bed volumes prior to initial sample application for a given mobile phase. Thereafter, the column was washed with at least 2 bed volumes between sample applications. BSA and BSA-Biotin were individually applied to the column for each mobile phase. Injections consisted of 0.02 ml of $1.0 \cdot 10^{-5}$ *M* protein.

In the third series, chloride and imidazole concentrations were varied together. A glass column (2.7 × 0.5 cm) was packed with 0.53 ml of Biogel P200–Glut–Thio–Pt(II) resin loaded with 0.008 mmol Pt(II)/ml wet resin. The same column and packing were used for all runs in this series. All experiments were carried out using a 0.05 *M* sodium acetate mobile phase at pH 4.8. The imidazole concentration was fixed at the same value in the mobile phase as the chloride concentration for all experiments. For each mobile phase with a specific imidazole/chloride

Table 1
Mobile phases used to study the effects of pH and added salt on BSA and BSA-biotin retention

Mobile phase (in order used)	Sodium chloride, *M*	pH	Buffer, 0.05 *M*
1	0.1	7.0	Sodium phosphate
2	0.1	4.8	Sodium acetate
3	0.1	2.5	Sodium phosphate
4	0	7.0	Sodium phosphate
5	0	4.8	Sodium acetate
6	0	2.5	Sodium phosphate
7	1	7.0	Sodium phosphate
8	1	4.8	Sodium acetate

concentration, a single injection of BSA was followed by a single injection of BSA-Biotin. Mobile phases containing 1.0, 0.1, 0.01, and 0 *M* imidazole/chloride were each used in order from high to low imidazole/chloride concentration as indicated. For each mobile phase containing imidazole, a control run was performed by applying the protein-free dilution buffer (diluted by same factor in mobile phase as the protein samples) to the column. The "control" chromatographic response curve was subtracted from the sample curve for each mobile phase prior to plotting and integration, which reduced the impact of a secondary negative peak observed at $(V_e)/(V_L) = 1$. The secondary peak resulted from dilution of imidazole in the mobile phase by the dilution buffer. Subtraction of the control curve for BSA did not completely eliminate the negative peak, especially at high imidazole concentrations [16].

Approximately 10 bed volumes were used to equilibrate the column prior to making the initial protein injection using each mobile phase. When the mobile phase was devoid of imidazole/chloride, over 20 bed volumes were used to equilibrate in order to aid removal of any imidazole retained on the column from previous runs.

Each protein application to the column consisted of a 0.02-ml injection of $1.0 \cdot 10^{-5}$ *M* BSA or BSA-Biotin. The flow rate was fixed at 0.1 ml/min. Detection was accomplished at 280 nm with 0.02 AUFS. The resin was equilibrated with at least 2 bed volumes of mobile phase prior to each injection.

2.7. Column liquid chromatography: binding and elution with imidazole

A glass column (5.45 × 0.5 cm) was packed once to a final bed volume of 1.1 ml with Biogel P200–Glut–Thio–Pt(II) resin and used for all runs discussed in this section. Prior to the initial application of protein, the column was equilibrated by washing with 10 bed volumes of 0.05 *M* sodium acetate, pH 4.8.

Two trials were performed using the same column. Each trial consisted of application of a BSA-Biotin sample using 0.05 *M* sodium acetate, pH 4.8 (application buffer), followed by elution with 1.0 *M* imidazole–HCl, pH 7 (elution buffer), and restoration using 0.05 *M* sodium acetate (pH 4.8). The first trial consisted of application of 0.15 ml of $1.0 \cdot 10^{-5}$ *M* BSA-Biotin into the column. The flow rate was 0.05 ml/min, and 2.2 bed volumes of the application buffer were passed through the column after injection. Detection was made at 280 nm, 0.05 AUFS. Fractions measuring 1 ml were collected as soon as the BSA-Biotin peak appeared. Immediately after eluting the initial peak representing unbound protein, the elution buffer was used to recover bound protein from the column. A total of 3.2 bed volumes of this buffer were passed through the column, followed by 28 bed volumes of 0.05 *M* sodium acetate (pH 4.8) to restore the column.

The second trial consisted of an identical BSA-Biotin application and subsequent imidazole elution repeated using the restored column.

Essentially the same procedure just described was used, except that only 1.5 bed volumes of the application buffer were passed through the column after protein injection.

The amount of BSA-Biotin eluted from the column was determined by analysis of fractions using the Protein Assay Kit. Sample absorbance values were observed to drift (increase) significantly. In order to minimize the effect of absorbance drift on concentration measurement, absorbance values were measured twice for each sample according to the following procedure: The first absorbance value for each sample was obtained by reading samples sequentially. The second absorbance value for each sample was obtained by immediately reading samples in the reverse order, and the two absorbance values for each sample were averaged. This procedure greatly reduced the effect of absorbance drift.

Because the column was initially equilibrated with sodium acetate, the first fraction obtained during imidazole/HCl elution contained both imidazole and acetate buffer components. In order to estimate the relative concentration of both buffers in this fraction, the imidazole breakthrough curve was integrated over the time period during which the first fraction was collected [16].

3. Discussion

Under mobile conditions where BSA and BSA-Biotin bind to the column there is no change in peak retention volume or shape, but the peak area decreases in proportion to the amount bound. This behavior can be modeled using the following differential equation:

$$\epsilon \mathrm{d}V_t \frac{\partial C_m}{\partial t} + F\mathrm{d}C_m + \epsilon \mathrm{d}Vt_o C_m = 0 \qquad (1)$$

where the term $\epsilon \mathrm{d}V_t K_o C_m$ represents irreversible removal of protein from the mobile phase. Using the following initial and boundary conditions:

$$C_m(0,z) = 0 \qquad C_m(t,0) = C_{m_o}\delta(t)$$

Eq. 1 is solved to obtain:

$$\frac{C_m}{C_{m_o}} = \delta\left(t - \frac{z}{u}\right) \exp\left(\frac{-K_o z}{u}\right) \qquad (2)$$

If quasi-equilibrium is assumed, the rate of solute removal from the mobile phase (N_m) can be assumed to equal the rate of transport through the film (N_f). Furthermore, the rate at which material binds to the gel surface (N_r) is assumed to equal the rate at which material enters the pore through the film. Therefore, the following relations hold [17]:

$$N_m = N_f = N_r$$

$$N_f = k_f(C_m - C_p)$$

$$N_r = k_r$$

$$N_m = K_o C_m$$

$$\frac{1}{K_o} = \frac{1}{k_f} + \frac{1}{k_r} \qquad (3)$$

C_s is assumed to be zero due to the large excess of Pt(II) binding sites on the resin. K_o can then be viewed as an overall mass transfer coefficient for solute removal from the mobile phase.

The functionality of k_f can be elucidated using the correlation of Wilson and Geankoplis [18]:

$$k_f = Au^{1/3} \qquad (4)$$

for $0.0016 < Re < 55$ and $165 < Sc < 70\,600$, where

$$A = 1.09\left(\frac{d_p}{\epsilon D}\right)^{2/3}$$

If k_r is assumed to be constant, then the derivative of K_o with respect to the interstitial velocity can be calculated as:

$$\frac{\partial K_o}{\partial u} = \frac{A}{3u^{2/3}\left[\frac{Au^{1/3}}{k_r} + 1\right]} \qquad (5)$$

The Schmidt number was calculated to be 16 000 for the protein chromatography experiments assuming a diffusivity of $6.1 \cdot 10^{-7}$ cm^2/s for BSA [19]. The Reynolds number was calculated to be 0.006 and 0.024 respectively for 0.05 and 0.2 ml/min of aqueous solution flow through a 0.5 cm I.D. column. These values suggest that

Table 2
Application of BSA and BSA-biotin to Biogel P200–Glut–Thio–Pt(II) at pH 4.8 with various imidazole/chloride concentrations in the mobile phase [16]

Imidazole or Chloride, *M*	Protein	V_r/V_L	% Bound	K_o
1.0	BSA	0.58	0 ± 7	0
	BSA-biotin	0.60	7 ± 6	0.015 ± 0.013
0.1	BSA	0.58	0 ± 7	0.001 ± 0.013
	BSA-biotin	0.60	16 ± 6	0.033 ± 0.013
0.01	BSA	0.55	4 ± 6	0.008 ± 0.013
	BSA-biotin	0.60	18 ± 6	0.039 ± 0.013
0	BSA	0.51	0 ± 7	0
	BSA-Biotin	0.53	42 ± 4	0.107 ± 0.013

the correlation of Wilson and Geankoplis is suitable to predict the film mass transfer coefficient, k_f.

Results obtained by chromatography of BSA and BSA-Biotin are summarized in Figs. 1–8 and Tables 2 and 3. The data have been normalized by plotting K_o, the overall mass transfer coefficient, so that data taken on columns of different lengths can be compared. Increasing values of K_o translate to increased protein binding to the column. For a 5.3 × 0.5 cm column operated at 0.1 ml/min, 20% and 80% binding to the column corresponds to K_o values of 0.045 and 0.323 min^{-1}, respectively.

BSA-Biotin bound significantly to Biogel P200–Glut–Thio–Pt(II) using a 0.05 *M* sodium phosphate mobile phase at pH 4.8, and binding increased with decreasing flow rate (Table 3).

Table 3
Application of BSA and BSA-Biotin to Biogel P200–Glut–Thio and Biogel P200–Glut–Thio–Pt(II) resins

Flow rate (cm/min)	Packing (%)	Protein (%)	V_r/V_L	Bound (%)	Est. error	K_o (min^{-1})	Est. error
0.2	Biogel P200–Glut–Thio	BSA(2)	0.40	0	±6.7	0.000	±0.012
		BSA(2)-Biotin	0.42	0	±6.7	0.000	±0.012
	Biogel P200–Glut–Thio–Pt(II)	BSA(2)	0.39	0	±6.7	0.001	±0.013
		BSA(2)-Biotin	0.39	40	±4.0	0.103	±0.013
0.1	Biogel P200–Glut–Thio	BSA(2)	0.42	1	±6.6	0.001	±0.006
		BSA(2)-Biotin	0.45	0	±6.7	0.001	±0.006
	Biogel P200–Glut–Thio–Pt(II)	BSA(2)	0.43	40	±4.0	0.051	±0.007
	(First pair of injections)	BSA(2)-Biotin	0.41	82	±1.2	0.172	±0.007
	Biogel P200–Glut–Thio–Pt(II)	BSA(2)	0.42	0	±6.7	0.001	±0.007
	(Second pair of injections)	BSA(2)-Biotin	0.42	62	±2.6	0.096	±0.007
	Biogel P200–Glut–Thio–Pt(II)	BSA(2)	0.41	0	±6.8	0.001	±0.007
	(Third pair of injections)	BSA(2)-Biotin	0.40	58	±2.8	0.087	±0.007
0.05	Biogel P200–Glut–Thio	BSA(2)	0.44	0	±6.7	0.000	±0.003
		BSA(2)-Biotin	0.47	0	±6.7	0.000	±0.003
	Biogel P200–Glut–Thio–Pt(II)	BSA(2)	0.43	4	±6.4	0.002	±0.003
		BSA(2)-Biotin	0.41	73	±1.8	0.065	±0.003

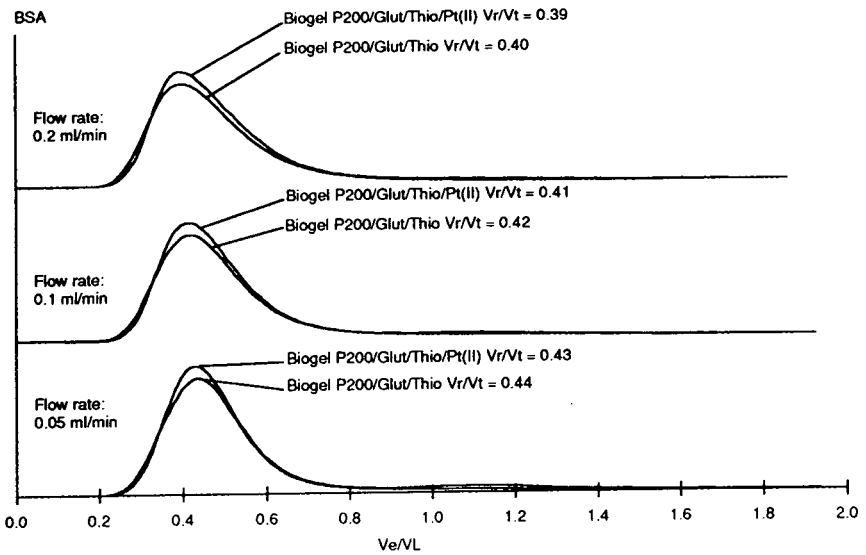

Fig. 1. Effect of flow rate on BSA binding to Biogel P200–Glut–Thio–Pt(II) and Biogel P200–Glut–Thio resins at pH 4.8.

However, as shown in Table 3, no BSA binding occurred to the gel containing immobilized Pt(II) at any of the three flow rates studied once the column was conditioned. Column conditioning can be accomplished either by addition of NaCl or by injecting BSA. BSA-Biotin binding to the resin appeared to be very strong, but exhibited slow kinetics. Approximately the same $(V_r)/(V_t)$ value was determined for BSA and BSA-Biotin at each flow rate on the activated gel, even when 73% of the BSA-Biotin was bound by the column (Figs. 1 and 2).

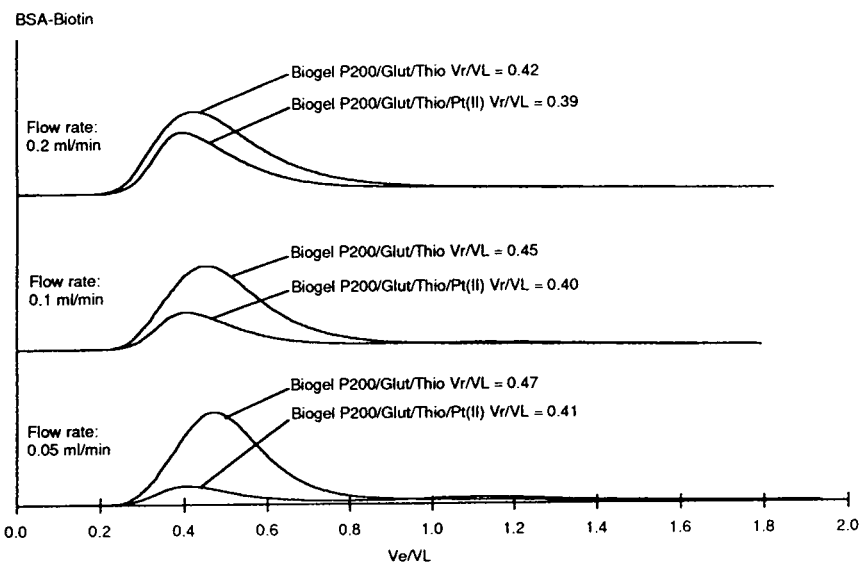

Fig. 2. Effect of flow rate on BSA-Biotin binding to Biogel P200–Glut–Thio and Biogel P200–Glut–Thio–Pt(II) resins at pH 4.8.

Gel permeation chromatography capacity is usually independent of flow rate [20,21]. Molecules fill their permeation volumes rapidly while traversing the column [22,23]. In many cases, local equilibrium can be assumed between protein molecules inside and outside the pores [24]. Published data suggest that for high-pressure size exclusion chromatography, retention volumes of solutes ranging from M_r 411 000 to M_r 41 are essentially independent of flow rate for bead sizes from 10 to 42 mm, and flow rates from 0.1 to 12.5 ml/min [25]. Although the hydrated Biogel P200 beads (90–180 mm) used in the BSA and BSA-Biotin chromatography experiments are considerably larger than the beads used in the experiment just described, the very slow flow rates probably ensured complete filling of the permeation volume by the proteins.

Rate theory has been applied to size exclusion chromatography in which pore diffusion and mobile phase lateral diffusion were included, but axial diffusion neglected [26]. Numerical solution of the governing differential equations showed gaussian chromatographic response peaks for near-equilibrium distribution of the solute into a porous stationary phase [26]. Furthermore, when flow rates were increased to create a condition of non-equilibrium distribution of solute into the stationary phase, response peaks were broader and significantly skewed in the direction of lower retention volume, suggesting that dispersion of SEC peaks is rate limited [26].

For the chromatograms shown in Figs. 1 and 2, there is no evidence of increased skewness or broadening of either BSA-Biotin or BSA peaks relative to each other or with increasing flow rate. In light of these observations, it appears that slow affinity binding of the BSA-Biotin to the immobilized Pt(II) causes a reduction in peak area, without changing the retention volume. Eq. (1) given above incorporates irreversible protein removal from the mobile phase proportional to the mobile phase protein concentration, and neglects diffusional limitations within the column. The analytical solution to this equation clearly predicts reduced peak areas with no change in retention volume for the protein chromatographic response peaks.

Binding of the BSA-Biotin to the resin probably requires proper orientation of the protein, and the actual binding of the biotin moiety to Pt(II) may itself exhibit slow kinetics. Furthermore, a protein molecule may bind to the column at several different points because each BSA molecule contains several biotinyl, imidazoyl and/or other moieties which may have an affinity for Pt(II). These factors together suggest that the interaction of BSA-Biotin with immobilized Pt(II) is slow, and strongest binding is achieved when multiple biotin moieties on a BSA-biotin conjugate molecule interacts on a 1:1 basis with Pt(II) ions on the resin.

If transport of protein to the bead surface was primarily limited by reaction at the bead surface, K_o would not be expected to depend on flow rate. However, Fig. 3 clearly shows that K_o decreases with decreasing flow rate, which is consistent with limited transport through a film surrounding each gel bead. If pore diffusional limitations were significant, K_o would be expected to increase with decreasing flow rate. If values of A and k_r are chosen to minimize the sum of squared deviations for K_o when calculated according to Eq. (1) above after substitution for k_f using Eq. (3), convergence to specific values of A and k_r does not result, and the sum

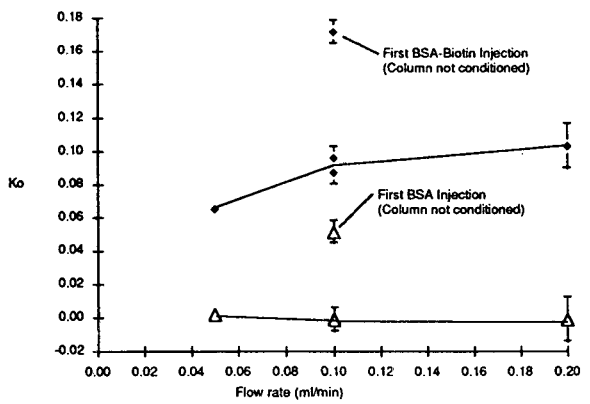

Fig. 3. Effect of previous column treatment and flow rate on BSA and BSA-Biotin binding at pH 4.8 (no added salt). Resin, Biogel P200–Glut–Thio–Pt(II); bed volume, 1.0 ml; mobile phase, 0.05 M sodium acetate; detection at 280 nm, AU 0.02. Injection, 0.02 ml of $1.0 \cdot 10^{-5}$ M BSA (△) or BSA-Biotin (◆).

of squares decreases as k_r is increased for optimal values of A. This behavior suggests that film transport is entirely responsible for mass transport limitations. However, such an interpretation is not consistent with the column conditioning data observed earlier, where the amount of protein bound for each successive BSA-Biotin application decreased. Furthermore, partial exclusion of the protein from the gel pores due to film limitations should result in skewed peaks and/or retention volume differences for protein applications to the Biogel P200–Glut–Thio gel compared to identical applications to Biogel P200–Glut–Thio–Pt(II), which has a high negative surface charge density. Retention volumes and chromatographic response peak shapes were nearly identical for BSA application to Biogel P200–Glut–Thio and Biogel P200–Glut–Thio–Pt(II).

If Eq. (3) is rewritten as

$$K_o = \text{Constant} + \frac{1}{\frac{1}{k_f} + \frac{1}{k_r}}$$

then the slope $(\partial K_o)/(\partial u)$ can be calculated at each flow rate using the experimental data [fitted to a function of the form $K_o = k_1 + k_2 \ln (u)$] and compared with the value of $(\partial K_o)/(\partial u)$ obtained from Eq. 5. In this case, more realistic values for A and k_r can now be determined as 0.43 and 0.33 respectively, suggesting that the mass transfer resistances for film transport and sorption are approximately of the same order of magnitude. In this case, film transport limitations can be used to rationalize the decrease in K_o observed with decreasing flow rate. Differences in k_r can be used to rationalize differences in K_o observed for BSA versus BSA-Biotin binding at a specified flow rate and differences in binding when different mobile phases are used, as well as to explain different binding behavior of the Biogel P200–Glut–Thio–Pt(II) resin compared to the Biogel P200–Glut–Thio resin.

For total permeation, a $(V_r)/(V_L)$ value for the packed column of approximately 1.1 was measured using imidazole and a conservative $(V_r)/(V_L)$ value for total exclusion was estimated to be 0.1. Typically, $(V_r)/(V_L)$ values of 0.5 were obtained for BSA and BSA-Biotin applications to Biogel P200–Glut–Thio–Pt(II). A linear relationship between molecular weight and $(V_r)/(V_L)$ for M_r 10 000 to 200 000 (as specified by the manufacturer for the native gel) was used to estimate the molecular weight of BSA as 120 000. Since BSA is known to have a molecular weight of approximately 70 000, the retention data suggest that BSA applied to Biogel P200–Glut–Thio or Biogel P200–Glut–Thio–Pt(II) is only able to permeate 50% of the internal gel volume normally permeated when the protein is applied to unactivated Biogel P200 gel. Activation of the gel using polymerized glutaraldehyde and thiourea probably result in a reduction in the accessible volume of the gel.

Table 4 shows the mobile phases used with each column. As indicated in Figs. 4 and 5, protein injections were made at pH 4.8 on all of the individually packed columns A, B, C, and D. Column C initially showed significantly higher BSA and BSA-Biotin binding values the first time these proteins were injected at 0.1 ml/min, but stabilized at lower values for subsequent injections. For Column A, single BSA and BSA-Biotin injections were made at pH 7 prior to BSA injection at pH 4.8. In this case, operating the column at pH 7 appeared to attenuate the capacity of the column for BSA and BSA-Biotin at pH 4.8 compared to initial injections of BSA and BSA-Biotin injections into Column C. The first injection of BSA into Column B resulted in approximately the same binding as observed for Column A. Single injections of BSA and BSA-Biotin into Column B were made using each of the following mobile phases prior to BSA injection at pH 4.8 (no NaCl): pH 7, 4.8 and 2.5 (all with 0.1 M NaCl) and pH 7 (no salt). The injections made using the aforementioned mobile phases should have resulted in conditioning of the gel. However, at pH 4.8 (no salt), high BSA binding was observed similar to that observed for Column A. In this case, it is possible that the low pH or the high concentration of chloride ions served to regenerate the column or restructure the resin such that high BSA binding could be obtained. As a result, the resin would

Table 4
Description of various columns and mobile phases used to obtain data shown in Figs. 4–6

Column	Bed volume (ml)	Flow rate (ml/min)	Buffers (in order used)
A	1.1	0.1	0.05 *M* sodium phosphate pH 7.0 0.05 *M* sodium acetate pH 4.8 0.05 *M* sodium phosphate pH 2.5
B	0.61	0.1	0.05 *M* sodium phosphate, 0.1 *M* NaCl pH 7.0 0.05 *M* sodium acetate, 0.1 *M* NaCl pH 4.8 0.05 *M* sodium phosphate, 0.1 *M* NaCl pH 2.5 0.05 *M* sodium phosphate pH 7.0 0.05 *M* sodium phosphate pH 4.8 0.05 *M* sodium phosphate pH 2.5 0.05 *M* sodium phosphate, 1.0 *M* NaCl pH 7.0 0.05 *M* sodium phosphate, 1.0 *M* NaCl pH 4.8
C	1.0	0.1	0.05 *M* sodium phosphate pH 4.8
D	0.53	0.1	0.05 *M* sodium phosphate, 1.0 *M* Cl^-, 1.0 *M* imidazole, pH 4.8 0.05 *M* sodium phosphate, 1.0 *M* Cl^-, 1.0 *M* imidazole, pH 4.8 0.05 *M* sodium phosphate, 0.1 *M* Cl^-, 0.1 *M* imidazole, pH 4.8 0.05 *M* sodium phosphate, 0.01 *M* Cl^-, 0.01 *M* imidazole, pH 4.8

All mobile phase buffers were prepared at 0.05 *M* concentration. UV detection at 280 nm with 0.02 AUFS. Each column was packed with Biogel P200–Glut–Thio–Pt(II) loaded with 0.008 mmol Pt(II)/ml wet gel.

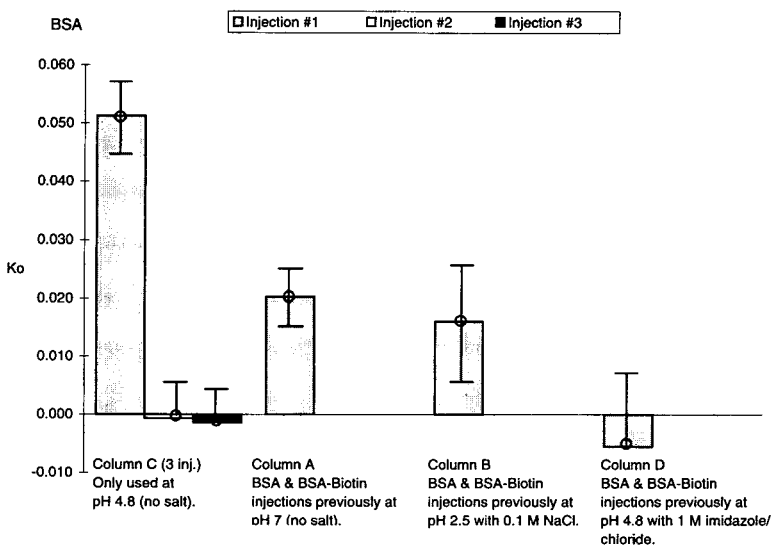

Fig. 4. Effect of previous column treatment on BSA binding at pH 4.8 (no added salt). Flow rate 0.1 ml/min; other experimental conditions as in Fig. 3.

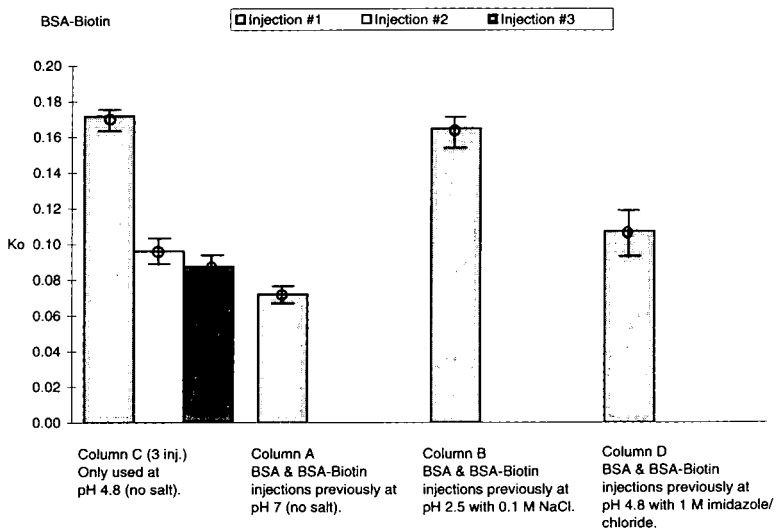

Fig. 5. Effect of previous column treatment on BSA-Biotin binding at pH 4.8 (no added salt). Experimental conditions as in Fig. 3.

behave as if it were not conditioned. BSA binding on column D was significantly reduced compared to columns A, B and C. Single BSA and BSA-Biotin injections were made into column D at pH 4.8 using imidazole/chloride concentrations of 1.0, 0.1 and 0.01 respectively, prior to making the injection of BSA at pH 4.8 with no salt or imidazole. Furthermore, some residual imidazole may not have completely washed from the strongest binding sites of this column. Neutralization of these sites would have the same effect as conditioning the column. BSA-Biotin binding at pH 4.8 can be analyzed in the same manner as for BSA described above, and the same trends were noted with regard to column conditioning and attenuation of binding at pH 7.0.

As shown in Figs. 6 and 7, BSA and BSA-Biotin binding generally increased with decreasing pH within the limits of experimental error. This result suggests that the gel surface carries a fixed negative charge. The isoelectric point for BSA is approximately 4.8. Therefore at pH 7.0, BSA and BSA-Biotin are negatively charged, and repulsion between the protein and the surface probably prevents the close distances required for binding of the biotin moiety of BSA-

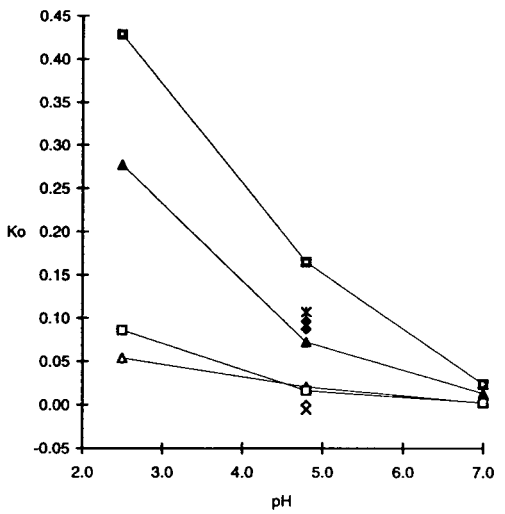

Fig. 6. Effect of pH on BSA and BSA-Biotin binding to Biogel P200–Glut–Thio–Pt(II) resin (no salt). Mobile phase, 0.05 *M* sodium phosphate (pH 2.5, 7.0)–0.05 *M* sodium acetate (pH 4.8); flow rate 0.1 ml/min; detection at 280 nm, AU 0.02. Injection, 0.02 ml of $1.0 \cdot 10^{-5}$ *M* BSA or BSA-Biotin. Symbols: ▲ = BSA-Biotin column A; ■ = BSA-Biotin column B; ◆ = BSA-Biotin column C (after conditioning); * = BSA-Biotin column D; △ = BSA column A; □ = BSA column B; ◇ = BSA column C (after conditioning); × = BSA column D

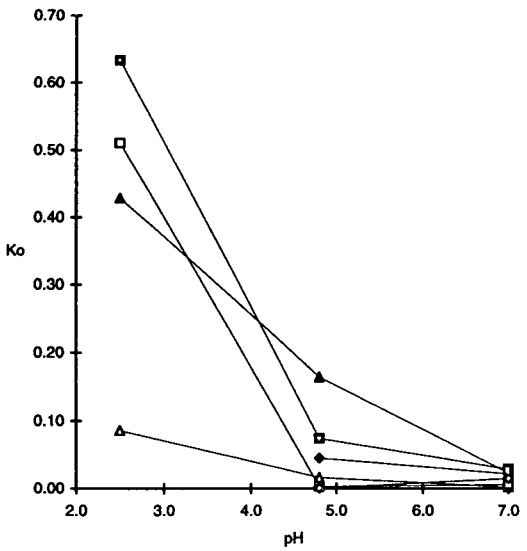

Fig. 7. Effect of pH and chloride concentration on BSA and BSA-Biotin binding to Biogel P200–Glut–Thio–Pt(II) resin. Experimental conditions as in Fig. 6. Symbols: ▲ = BSA-Biotin 0.0 *M* Cl^-; ■ = BSA-Biotin 0.1 *M* Cl^-; ◆ = BSA-Biotin 1.0 *M* Cl^-; △ = BSA 0.0 *M* Cl^-; □ = BSA 0.1 *M* Cl^-; ◇ = BSA 1.0 *M* Cl^-.

Biotin binding to immobilized Pt(II). At pH 2.5, BSA and BSA-Biotin are positively charged, and an ionic attraction exists which draws both proteins to the gel surface and may even cause partial unfolding of the protein. Unfolding may expose additional amino acid side chains which could coordination to Pt(II). Furthermore, the ionic attraction may cause reorientation of the protein relative to the gel surface. The net result is a loss of selectivity for BSA-Biotin and increased binding of both biotinylated and non-biotinylated proteins. Although it is surprising that BSA does not ion exchange on Biogel P200–Glut–Thio–Pt(II) at pH 7.0, this result is consistent with amino acid chromatography on Biogel P2–Glut–Thio–Pt(II) and Biogel P2–Glut–Thio–Ag(I) [15] where ion exchange was not seen to be a major factor, and may result because of competition by counterions in the mobile phase buffer [16].

Clearly, best column performance is expected when the mobile phase pH equals the protein isoelectric point, and experimentally, the best selectivity for BSA-Biotin was observed at pH 4.8, the isoelectric point of BSA. As biotinylation involves the side chain amino group of lysine in the formation of an amide bond, a lower isoelectric point would be expected for BSA-Biotin than for BSA, which has been confirmed by showing that BSA-Biotin precipitates from solution when the pH is lowered below pH 4.0, and remains dissolved at pH 4.8. Therefore, BSA-Biotin would be expected to have a decreased affinity for the Biogel P200–Glut–Thio–Pt(II) gel at pH 4.8 compared to BSA because it would carry a more negative charge. The fact the BSA-Biotin binding is higher than BSA binding at pH 4.8 indicates that effects other than ionic interactions are responsible for BSA-Biotin selectivity, such as coordination of the thioether sulfur of the biotin moiety to Pt(II).

Addition of salt to the mobile phase resulted in less protein binding at pH 4.8 and 7.0, and more binding at pH 2.5. The effect of salt appeared to be quite complex. Salt may affect the conformation of the protein, compete for ionic binding sites on the gel, and/or effect the electrical double layer that exists on the surface of the gel.

Over 90% of BSA-Biotin was bound to the resin at pH 2.5 for all mobile phases studied. Curiously, a tremendous increase in BSA binding was observed at pH 2.5 when 0.1 *M* sodium chloride was added to the mobile phase, causing BSA and BSA-Biotin binding to be nearly equal. At sodium chloride concentrations significantly above 0.1 *M*, BSA-Biotin precipitated from the acetate mobile phase at pH 2.5. Therefore, increased binding of BSA and BSA-Biotin with increasing salt concentration at pH 2.5 may result because chloride ions decrease the solubility of these proteins. Sodium chloride at 0.1 *M* concentration eliminates BSA binding to the resin within experimental error at pH 4.8. Under these conditions, a significant amount of BSA-Biotin was bound to the resin while no BSA was bound to the resin. Interestingly, use of 0.1 *M*

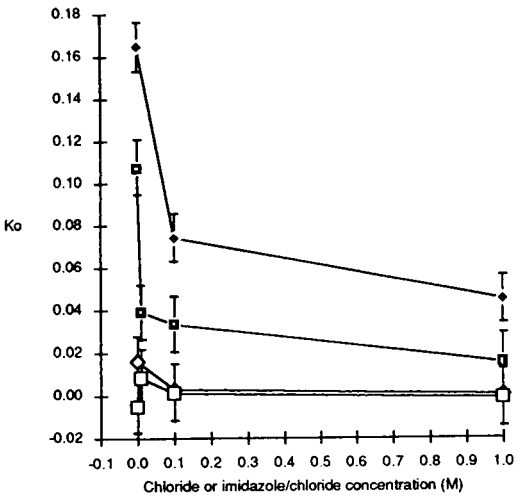

Fig. 8. Effect of imidazole/chloride concentration on BSA and BSA-Biotin binding to Biogel P200–Glut–Thio–Pt(II) resin at pH 4.8. Experimental conditions as in Fig. 6. Symbols: ◆ = BSA-Biotin, chloride; ◘ = BSA-Biotin, imidazole/chloride; ◇ = BSA, chloride; □ = BSA, imidazole/chloride.

sodium chloride gave the same result as shown in Fig. 4 for column conditioning, yet no conditioning was performed.

Fig. 8 shows the effects of simultaneously changing mobile phase imidazole/chloride concentrations on the binding of BSA and BSA-Biotin to Column D. For all runs, BSA binding was less than 5%, and slightly less than observed for column B. The effect of imidazole was more pronounced for BSA-Biotin binding, resulting in approximately half the BSA-Biotin binding at each imidazole/chloride concentration on Column D compared to the corresponding chloride concentrations on Column B. Imidazole probably competes with the protein for Pt(II) binding sites on the gel surface.

3.1. Binding and elution of BSA and BSA-Biotin

BSA-Biotin was applied to the gel using a sodium phosphate buffer at pH 4.8. Elution was accomplished using a 1.0 *M* imidazole–HCl buffer at pH 7.0, resulting in 60% of the bound BSA-Biotin being recovered. After extensive washing of the same column with the sodium phosphate buffer at pH 4.8, BSA-Biotin was applied again, followed by imidazole elution. A brief summary of these results is given in Table 5. Because the amount of BSA-Biotin recovered during imidazole elution for Trial no. 2 was greater than that recovered the first time the column was used (73% versus 60%), it is possible that some uneluted BSA-Biotin from Trial no. 1 may have been eluted along with the BSA-Biotin recovered during the elution step for Trial no. 2.

The fraction of the initial application of BSA-Biotin bound to the column was slightly greater for the second injection than for the first injection. This increase can be rationalized as experimental error. In an earlier experiment (Fig. 5), subsequent application of BSA-Biotin at pH 4.8 resulted in less protein binding for the second injection. This "conditioning" effect was not seen in the experiment reported here because the loss of sample due to conditioning would be much smaller than the experimental error for such a large sample injection.

Table 5
Application of BSA-Biotin to Biogel P200–Glut–Thio–Pt(II) and subsequent elution with 1.0 *M* imidazole at pH 7.0

	Trial no. 1	Trial no. 2
Percentage of initial BSA-Biotin application bound to column	37 ± 3	38 ± 3
Percentage of bound BSA-Biotin eluted with imidazole	60 ± 6	73 ± 7

4. Conclusions

Binding of BSA-Biotin to Biogel P200 containing immobilized platinum ions is best conducted at pH 4.8, and greater BSA-Biotin binding is obtained with the column described in this paper at lower flow rates. In order to achieve binding of BSA-Biotin without concomitant binding of BSA, the column required use of an application buffer with >0.1 *M* NaCl or preconditioning with an injection of BSA in order to remove the sites with high charge densities. BSA and BSA-Biotin binding generally increased with decreasing pH due to the fixed negative charge of the gel surface carrying. The immobilized Pt(II) column binds BSA-Biotin and no unconjugated BSA at pH 4.8, which is the isoelectric point of BSA. Addition of salt to the mobile phase resulted in less protein binding at pH 4.8 and 7.0, and more binding at pH 2.5. The effect of salt appeared to be quite complex. Salt may affect the conformation of the protein, compete for ionic binding sites on the gel, and/or affect the electrical double layer that exists on the surface of the gel. Elution of BSA-Biotin was accomplished using a 1.0 *M* imidazole–HCl buffer at pH 7.0, whereby 60% of the bound BSA-Biotin was recovered.

Binding of BSA-Biotin to Biogel P200 containing immobilized platinum ions appeared to exhibit slow kinetics. Film transport partially limits protein binding to the activated gel. Therefore, steps taken to increase the film transport coefficient could increase column performance. Increasing the superficial velocity, as well as disrupting the flow pattern through the packed bed would be desirable. Furthermore, nonspherical packings would be preferable to the spherical gel used in these experiments. In addition, proteins with large diffusivities would be expected to transport faster through the film, and exhibit higher binding to the column.

Acknowledgments

The authors would like to thank the National Science Foundation (BCS-9009301) for support for this work. One of the authors (D.M.) would also like to thank Genencor International (South San Francisco, CA, USA) and the ARCS Foundation for providing support in order to complete this work.

Symbols

A_c	Cross sectional area of chromatography column (cm^2)
AUFS	Absorption Unit Full Scale
B	Fraction of initial sample application that bound to the column, which equals $1-E$
C_m	Bulk concentration of solute in the mobile phase (mmol/ml)
C_p	Solute concentration within the pores of the gel (mmol/ml)
C_s	Concentration of sorbed solute on the gel (mmol/ml)
D	Diffusivity (cm^2/s)
d_p	Diameter of particle (cm)
E	Fraction of the initial sample application that was eluted from column, which equals $1-B$
F	Flow rate (ml/min)
k'	Capacity factor for a retained species applied to the gel, calculated as $(t_r - t_L)/(t_L)$ or $(V_r - V_L)/V_L$)
k_b	Binding constant defined as q/c
k_d	Distribution coefficient defined as the concentration of ligand bound to the immobilized metal ions divided by the concentration of free ligand in solution
k_f	Mass transfer coefficient representing transport through a stagnant film surrounding each gel bead (min^{-1})
K_o	Overall mass transfer coefficient (min^{-1})
k_r	Constant of proportionality for a first order reaction representing complexation of a ligand to the an immobilized metal ion at the gel surface (min^{-1})
L	Column length (cm)
q	Amount of material sorbed to column (mmol/ml hydrated solid volume)
Re	Reynolds number

Sc Schmidt number

t_L Measured value of t_r for a small molecule that totally permeates the gel, but does not interact with the gel (i.e., moves with the solvent front), in min

t_o Measured value of t_r for a species that is totally excluded from gel pores, and does not interact with the gel (min)

t_r Time at which the maximum point is reached for a chromatographic response peak (min)

t'_r $(t_r - t_L)/(t_L)$

u Superficial velocity defined as $(F)/(\epsilon A_c)$ (cm/min)

V_e Volume of eluent applied to the column (ml)

V_i Intraparticle pore volume in a packed column (ml)

V_L Total hydrated volume of the gel available for permeation by a liquid, equal to $V_i + V_o$, (ml)

V_o Interparticle void volume in a packed column (ml)

V_r Volume of eluent applied to the column at which the maximum point is reached for a chromatographic response peak (ml)

V_s Volume of solid packing within the column, equal to $V_t - V_L$ (ml)

V_t Total volume of the packed bed, including void and solid packing volumes (ml)

z Distance measured from the inlet port of the column (cm)

ϵ Void fraction of the column, equal to $(V_L)/(V_t)$

ν Kinematic viscosity (cm^2/s)

References

[1] M. Wilchek and E.A. Bayer (Editors), *Avidin-biotin Technology*, Academic Press, San Diego, CA, 1990.

[2] E.A. Bayer and M. Wilchek, *Methods Biochem. Anal.*, 26 (1980) 1–45.

[3] M. Wilchek and E.A. Bayer, *Anal. Biochem.*, 171 (1988) 1–32.

[4] M. Wilchek and E.A. Bayer, *Trends Biochem. Sci.*, 3 (1989) 408.

[5] E.P. Diamandis and T.K. Christopoulos, *Clin. Chem.*, 37 (1991) 625.

[6] E.A. Bayer and M. Wilchek, *J. Chromatogr.*, 510 (1990) 3.

[7] K. Hoffman, G. Titus, J.A. Montibeller and F.M. Finn, *Biochemistry*, 21 (1982) 978.

[8] D.H. Kim, A.A. García, D. R. Miles and R. Makam, *Reactive Polymers*, in press.

[9] J. Porath, *Protein Expression Purif.*, 3 (1992) 263.

[10] R.G. Pearson, *J. Am. Chem. Soc.*, 85 (1963) 3533.

[11] B. Rigas, A.A. Welcher, D.C. Ward and S.M. Weissman, *Proc. Natl. Acad. Sci. USA*, 83 (1986) 9591.

[12] S. Ritter, J. Komenda, E. Setlikova, I. Setlik and W. Welte, *J. Chromatogr.*, 625 (1992) 21.

[13] G.L. Peterson, *Anal. Biochem.*, 83 (1977) 346.

[14] O.H. Lowry, N.J. Rosebrough, A.L. Farr and R.J. Randall, *J. Biol. Chem.*, 193 (1951) 265.

[15] D.H. Kim, *PhD Thesis*, Arizona State University, Tempe, AZ, 1994.

[16] D.R. Miles, *PhD Thesis*, Arizona State University, Tempe, AZ, 1994.

[17] A.L. Hines and R.N. Maddox, *Mass Transfer: Fundamentals and Applications*, Prentice Hall, Englewood Cliffs, NJ, 1985, pp. 151–159.

[18] E.J. Wilson and C.J. Geankoplis, *Ind. Eng. Chem. Fundam.*, 5 (1966) 9.

[19] C. Lentner (Editor), *Geigy Scientific Tables*, Vol. 3, Ciba-Geigy, Basle, 1984, p. 136.

[20] W.W. Yau, C.P. Malone and H.L. Suchan, *Sep. Sci.*, 5 (1970) 259.

[21] W.W. Yau, J.J. Kirkland and D.D. Bly, *Modern Size-Exclusion Liquid Chromatography: Practice of Gel Permeation and Gel Filtration Chromatography*, John Wiley and Sons, New York, 1979, p. 29.

[22] W.W. Yau, H.L. Suchan and C.P. Malone, *J. Polym. Sci. Part A-2*, 6 (1968) 1349.

[23] J.J. Hermans, *J. Polym. Sci. Part A-2*, 6 (1968) 1217.

[24] W.W. Yau, J.J. Kirkland and D.D. Bly, *Modern Size-Exclusion Liquid Chromatography: Practice of Gel Permeation and Gel Filtration Chromatography*, John Wiley and Sons, New York, 1979, p. 28.

[25] J.N. Little, J.L. Waters, K.J. Bombaugh and W.J. Pauplis, *J. Polym. Sci. Part A-2*, 7 (1969) 1775.

[26] A.C. Ouano and J.A. Barker, *Sep. Sci.*, 8 (1973) 673.

ELSEVIER

Journal of Chromatography A, 702 (1995) 191–196

JOURNAL OF CHROMATOGRAPHY A

Ligand efficiency in axial and radial flow immunoaffinity chromatography of factor IX

J. Tharakan*, M. Belizaire

Department of Chemical Engineering, Howard University, 2300 6th Street, NW, Washington, DC 20059, USA

Abstract

Radial flow (RF) columns are attractive for process chromatography primarily because larger throughputs and lower pressure drops are achievable in such columns. Large scale immunoaffinity processes using soft resins can benefit most from this configuration. In this study, we compared immobilized ligand efficiency in axial flow (AF) and RF columns using monoclonal antibody against factor IX as the immobilized ligand and a coagulation factor IX complex as the source material. We examined the effects of flow-rate, total protein loading, feed antigen concentration and direction of flow (centrifugal or centripetal for RF, and downward or upward for AF) on immobilized antibody capacity (measured as mg antigen bound per mg antibody). Our results corroborate earlier work, and suggest that none of the factors, in the ranges examined, significantly altered the efficiency of the monoclonal antibody (MAb) in binding factor IX. We also investigated the efficiency of the immobilized antibody upon reuse and found that, over twenty cycles, there was no significant decrease in antibody efficiency. Our results demonstrated that efficiencies obtainable in AF columns can be achieved in RF columns with the same bed thickness, suggesting that radial dispersion, mass transfer and intraparticular diffusion may not have a significant influence on immunoaffinity chromatography efficiency in RF and AF columns.

1. Introduction

Protein isolation and purification from complex mixtures is becoming increasingly important to the advancement of the biotechnological industry. Immunoaffinity chromatography (IAC) is a specific, reversible purification method utilizing antibodies directed against the protein of choice [1]. IAC has only recently been applied on a large scale using conventional axial flow (AF) chromatography columns [2], and problems documented before [3] include high pressure drops leading to low throughputs and gel compression. Scaling-up from bench to production exacerbates these problems.

A potential solution for AF chromatography problems resides with radial flow (RF) chromatographic column configurations, due to the shorter bed depth [3]. Radial flow was originally developed to handle large gas flow-rates through packed beds with minimal pressure drop [4]. Analytical work has been done on the fluid mechanics [5,6] and the chemical kinetics and dynamics of heterogeneous catalysis in such systems [7]. Analysis and experimentation with RF reactors has been extended to reverse osmosis systems [8,9], as well as hollow fiber cell culture bioreactors [10,11]. CUNO [12] and Sepragen [3] manufacture chromatography sys-

* Corresponding author.

0021-9673/95/$09.50 © 1995 Elsevier Science B.V. All rights reserved
SSDI 0021-9673(94)01141-9

tems in an RF configuration. Planques et al. [13] used RF membrane affinity chromatography to purify plasminogen with greater than 85% recovery and a 110-fold increase in the specific activity. Other separations of biologicals have also been reported [14].

In the AF column, the cross-sectional area normal to flow is constant; in the RF column, the area normal to flow is variable, increasing for centrifugal flow and decreasing for centripetal flow. This results in a linear velocity that is decelerating (centrifugal flow) or accelerating (centripetal flow). The implications of this is that mass transfer coefficients and radial dispersion cannot be taken as constant [15] in the flow direction. The RF configuration provides a larger flow area and a shorter flow path that permits larger volumetric flow-rates and shorter step times [15] in liquid chromatographic separations.

We have demonstrated [16] lower process times and trans-chromatographic bed pressures for RF compared to AF. In this paper, we compare an AF and RF column of the same total volume (50 ml) and bed height (AF: 2.8 cm; RF: 3.0 cm) using immunoaffinity purification of factor IX (FIX) [17,18] as the experimental system. The effect of changing feed flow-rates, feed antigen concentration and flow direction on antibody efficiency is reported.

2. Materials and methods

2.1. Antibody and resin

The antibody was monoclonal, produced at the American Red Cross (ARC; [19]) and coupled to Sepharose CL2B (Pharmacia, Piscataway, NJ, USA) via CNBr activation. This affinity resin was generously donated by the ARC.

2.2. Starting material

Feed for all the immunoaffinity purification experiments was coagulation FIX, lot 29061202, supplied by the ARC, which is an FIX complex containing 10% (w/w) FIX [20].

2.3. Columns

The AF column was a 4.8 cm diameter glass column (Kontes Glass, Vineland, NJ, USA) that was silanized before use. The column was packed to a depth of 2.8 cm, yielding a total AF column volume of 50 ml. The RF column was purchased from Sepragen (San Leandro, CA, USA) and had a volume of 50 ml. The RF column was packed according to the manufacturer's instructions to a final volume of 50 ml with the affinity resin. Bed depth in the RF column was 3.0 cm.

2.4. Other equipment

Pumping of mobile phase buffers was provided by a Masterflex digital unified drive pump (Cole Parmer, Chicago, IL, USA). Protein flow through from columns was monitored using a Gilson 112 UV–Vis detector (Gilson Medical Electronics, Middleton, WI, USA) and a hard copy of chromatographic output was provided from a Kipp and Zonen BD40 (Delft, Netherlands) single-channel chart recorder. Final absorbance of pooled fractions was measured on a Spectronic 1001+ UV–Vis spectrophotometer (Milton Roy, Downington, PA, USA).

2.5. Chromatography protocol

Columns were first equilibrated with five column volumes (CVs) of equilibration buffer, 10 m*M* magnesium chloride, 100 m*M* sodium chloride, 20 m*M* phosphate, pH 7.0. The starting material, lyophilized coagulation FIX, was reconstituted with distilled water and brought to a final magnesium chloride concentration of 40 m*M*. Feed was then loaded onto the column and then the column was washed with 10 m*M* magnesium chloride, 1 *M* sodium chloride, 20 m*M* phosphate, pH 7.0 buffer until the effluent absorbance reached baseline. FIX was eluted using 20 m*M* sodium citrate, 110 m*M* sodium chloride, pH 6.8. The column was regenerated with 200 m*M* sodium citrate, 2 *M* sodium chloride, pH 7.0 buffer. Column effluent was collected as pools for each step, i.e. load pool,

unadsorbed (unbound material), wash pool, elution pool and regeneration pool and then assayed for total protein. Elution pools were periodically checked using a Gilson HPLC system with a TSK-3000 size-exclusion column for purity, always resulting in a single peak.

2.6. Flow direction variation

RF Column

Feed was pumped into the inner annulus for centrifugal flow or into the outer annular space for centripetal flow. In order to minimize compression during operation, the column was packed under higher than normal operational pressure. After packing, the operation of the column mirrored the AF column's operation in terms of feed, wash and elution.

AF Column

Feed was pumped into the axial flow column, either in a downward flow configuration or in an upward flow configuration.

2.7. Protein assay

Total protein was determined from the absorbance of the sample at 280 nm. The extinction coefficient was assumed to be 1.4. Samples with absorbances greater than 1.0 on direct reading were diluted to bring the absorbance into the range $0.0 < A_{280} < 1.0$.

2.8. Flow-rate variation

Flow-rate in both the AF and RF column experimental sets was varied. Flow-rate ranges for each set of experiments with the different columns ranged from 0.3 to 15 ml/min.

2.9. Feed concentration variation

Concentration of FIX in the feed stream was decreased by increasing the amount of distilled water used to reconstitute the coagulation FIX from the lyophilized vial. Three different reconstitution volumes were used, 5, 10 and 15 ml, resulting in protein concentrations of 6.9, 3.45 and 1.7 mg/ml, respectively.

3. Results and discussion

To evaluate affinity column performance, we compared the efficiency of the antibody, defined as the mass of antigen that is bound per unit mass of immobilized antibody. In order to calculate a *theoretical* maximum capacity for the immobilized antibody, we make the assumption that *if* an antibody is immobilized at the Fc portion, it will be fully active and capable of binding two antigen molecules. Naturally, CNBr activation of Sepharose is not suitable for immobilization through the Fc region; carbohydrate moiety coupling will provide a better condition for Fc immobilization [21,22]. However, for the purpose of our column antibody efficiency comparison, such a *theoretical* maximum provides a basis, and with FIX as the antigen (molecular mass ca. 50 000) a single immobilized completely active antibody (molecular mass ca. 150 000) would theoretically be able to bind two FIX molecules. On a mass basis, this theoretical capacity would be approximately 0.66 mg FIX/mg of antibody [18,23]. With this as a criterion, it is possible to evaluate the bulk performance of immobilized antibody in a particular process by estimating the mass of antigen captured per unit mass of immobilized antibody. This is possible if the amount of immobilized antibody is known and if the total amount of antigen bound is calculated from the difference between the mass of antigen loaded and the mass of antigen that passed through the affinity column in the unadsorbed pool, and also by calculating the amount of FIX protein that is recovered in the elution and regeneration steps of the process.

In our work, we report the effect of varying parameters (feed flow-rate and antigen concentration) and flow direction (centripetal/centrifugal RF or upward/downward AF) on the capacity of the antibody.

In Fig. 1, the results of varying the flow-rate in AF and RF columns is shown. Fig. 1a compares

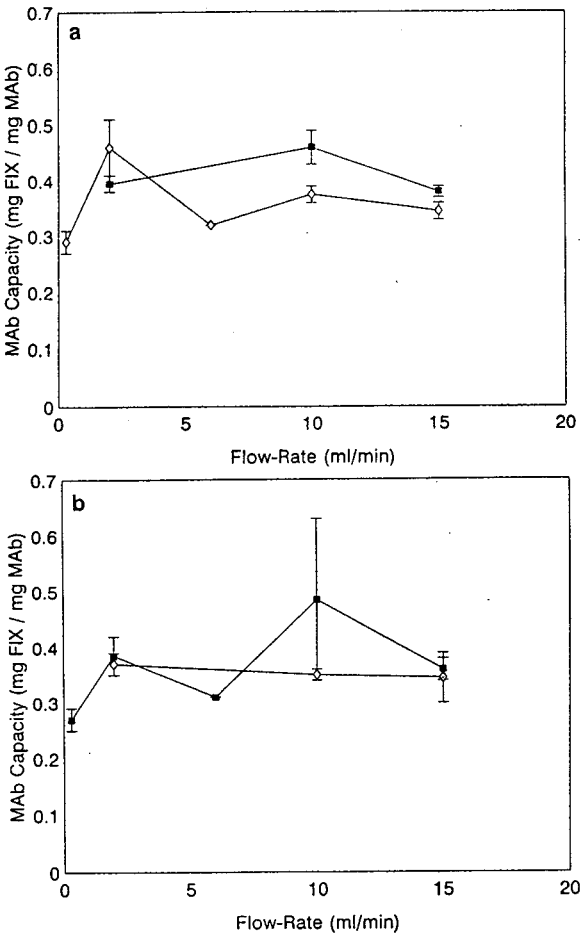

Fig. 1. Effect of flow-rate on antibody capacity. (a) Centrifugal radial flow (■) and downward axial flow (◇); (b) centripetal radial flow (■) and upward axial flow (◇). Data are reported as the mean ligand efficiency obtained for each flow-rate ± 1 S.D.

the antibody capacity between centrifugal RF and the equivalent downward AF. As the flow-rate increases, there is no statistically significant increase or decrease in antibody capacity for either of the flow configurations. These data are in agreement with our previous work [18] which showed no dependence of antibody capacity on flow-rate in an AF chromatography system. The ranges of flow-rate examined were similar. In Fig. 1b, antibody capacity as a function of flow-rate is shown for the case of both flow configurations with reversed flow, i.e. centripetal for the RF case and upward flow for the AF situation. Once again, we see that there is no statistical difference in antibody capacity for increasing flow-rate.

Fig. 2 shows the effect of increasing feed protein concentration on the capacity of antibody. The data are presented in a similar manner as in Fig. 1. Thus, we see centrifugal RF and downward AF in Fig. 2a, and in Fig. 2b the results for the reversed flow direction, centripetal RF and upward AF, are shown. The data in Fig. 2 suggests that there is no significant dependence of antibody capacity on feed protein concentration. The data in Fig. 2a do show a slight increase in the antibody capacity for the

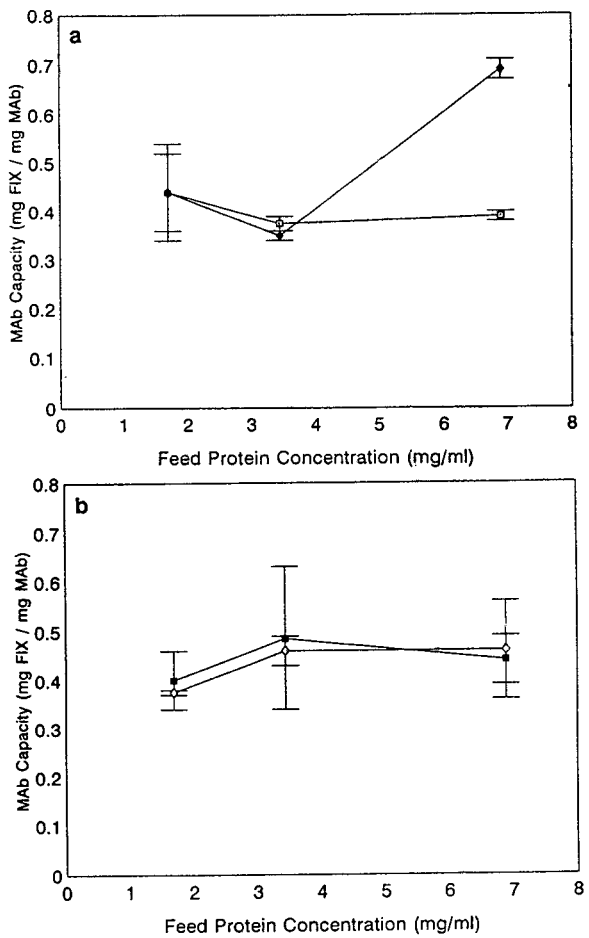

Fig. 2. Effect of feed protein concentration on antibody capacity. (a) Centrifugal radial flow (□) and downward axial flow (◆); (b) centripetal radial flow (■) and upward axial flow (◇). Data are reported as in Fig. 2.

centrifugal radial configuration. There is a slight increase for the axial configuration as well, although not as large as the RF data. Neither of the increases appear to be statistically significant, and it appears that over the ranges of inlet protein concentration studied, the antibody efficiency remained similar in both AF and RF.

We have suggested with earlier work [23] that a strong dependence on feed protein concentration and flow-rate would indicate that diffusional resistances for antigen binding to antibody would be high. In the absence of these strong dependences, as this and our previous data have shown, it is likely that diffusional resistance to antigen binding is low. We have previously argued [23], using the work of Carleysmith et al. [24], that the reason for this might lie in the depth to which antibody is immobilized. If antibody is only immobilized on a thin outer skin —say 10% of the radial co-ordinate, or about 8 μm— of the resin bead, it is unlikely that antigen will encounter diffusional resistances. This inference is supported by the data for the effect of flow-rate on antibody capacity. If diffusion was a significant resistance to antigen penetration, and hence antibody capacity, decreasing the flow-rate, or increasing the antigen feed concentration, would increase antibody capacity, a result not borne out by our data.

Gu et al. [15] have theoretically investigated RF chromatography and their results show that models for RF and AF columns become the same when radial dispersion and intraparticular diffusion are neglected and when the mass transfer coefficients are treated as constants. They also showed that under these conditions, centrifugal and centripetal flow differences disappeared. This and our experimental results suggest that, for IAC under our experimental conditions, radial dispersion, mass transfer and intraparticular diffusion may be neglected if the affinity ligand is only immobilized on a thin outer skin of the chromatography resin bead matrix.

Currently in our laboratory, we are staining and sectioning resin beads that have had antibody immobilized on them. The anticipated data should show the depth of penetration of antibody into the resin bead as a function of immobilization time, chemistry, bead porosity and other parameters. Preliminary data suggest that the penetration depth of the antibody into an activated Sepharose resin, when using CNBr-activated Sepharose as the affinity support, is of the order of 10% of the bead radius [25]. In addition to studies on the distribution of antibody, investigations of the distribution of antigen are also being initiated. Results from these investigations should shed light on the distribution and movement of ligand and ligate within an affinity support matrix, and the impact these have on the efficiency of the ligand.

Future efforts on the comparison of AF and RF chromatography will include studies on scaled versions of industrial columns. Since the bed heights of industrial-process RF and AF columns are very different, experiments are planned which will investigate columns of similar volume with different bed heights. Finally, the efficiency of ligand immobilized on newer, more structurally stable resins should be investigated as these resins may enable higher throughputs in immunoaffinity AF chromatography configurations.

4. Conclusions

A better understanding of RF IAC will facilitate its incorporation into the bioprocess industry. The data presented in this study show that antibody capacities equivalent to those of a conventional AF column are obtainable in an RF configuration. These results suggest that radial dispersion, mass transfer and intraparticular diffusion may not have a significant impact on IAC.

Acknowledgements

The authors thank the American Red Cross for the monoclonal antibody, immunoaffinity resin and factor IX complex source material. This research was conducted under the Howard University Faculty Research Support Grant program.

References

[1] A.H. Chase, *Chem. Eng. Sci.*, 39 (1984) 1099.
[2] D.B. Clark, W.N. Drohan, S.I. Miekka and A. J. Katz, *Ann. Clin. Lab. Sci.*, 19 (1989) 196.
[3] V. Saxena, K. Subramaniam, S. Saxena and M. Dunn, *Biopharm*, 3 (1989) 46.
[4] K. Johansen, *Chem. Eng. World*, 5 (1970) 8.
[5] V.S. Genkin, V.V. Dil'man and S.P. Sergeev, *Int. Chem. Eng.*, 13 (1973) 24.
[6] P.R. Ponzi and L.A. Kaye, *AIChE J.*, 25 (1979) 100.
[7] H.C. Chang and J.M. Calo, *ACS Symp. Ser.*, 168 (1981) 305.
[8] W.N. Gill and B.N. Bansal, *AIChE J.*, 19 (1973) 823.
[9] M. Soltanieh and W.N. Gill, *Desalination*, 49 (1984) 57.
[10] J. Tharakan and P.C. Chau, *Biotech. Bioeng.*, 28 (1986) 329.
[11] J. Tharakan and P.C. Chau, *Biotech. Bioeng.*, 29 (1987) 1064.
[12] R.M. Mandara, S. Roy and K.C. Hou, *Bio/Technology*, 5 (1987) 928.
[13] Y. Planques, H. Pora and F.D. Menozzi, *J. Chromatogr.*, 539 (1991) 531.
[14] D. McCormick, *Bio/Technology*, 6 (1988) 158.
[15] T. Gu, G.-J. Tsai and G.T. Tsao, in A. Fiechter (Editor), *Advances in Biochemical Engineering/Biotechnology*, Vol. 49, Springer, Berlin, 1993.
[16] J.P. Tharakan, C. Orthner, B. Kolen, A.M. Ralston, D. Gee, D. Clark and W. Drohan, presented at *International Chemical Congress of Pacific Basin Societies, Honolulu, HI, December 1989.*
[17] W.H. Velander, C.L. Orthner, J.P. Tharakan, R.D. Madurawe, A.H. Ralston, D.K. Strickland and W.N. Drohan, *Biotechnol. Prog.*, 5 (1989) 119.
[18] J. Tharakan, D. Strickland, W. Burgess, W.N. Drohan and D.Clark, *Vox Sang.*, 58 (1990) 21.
[19] H.-L. Wang, J. Steiner, F. Battey and D. Strickland, *Fed. Proc.*, 46 (1987) 2119.
[20] D. Menache, H.E. Behre, C.L. Orthner, H. Nunez, H.D. Anderson, D.C. Triantaphyllopoulos and D. P. Kosow, *Blood*, 64 (1984) 1220.
[21] D.J. O'Shannessy, *J. Chromatogr.*, 510 (1990) 13.
[22] G. Fleminger, *Appl. Biochem. Biotech.*, 23 (1990) 123.
[23] J.P. Tharakan, D.B. Clark and W.N. Drohan, *J. Chromatogr.*, 522 (1990) 153.
[24] S.W. Carleysmith, M.B.L. Eames and M.D. Lilly, *Biotech. Bioeng.*, 22 (1980)957.
[25] V. Ayers, *M.S. Thesis*, Howard University, Washington, DC, December 1993.

ELSEVIER

Journal of Chromatography A, 702 (1995) 197–206

JOURNAL OF CHROMATOGRAPHY A

Separation of peptide derivatives by pH-zone-refining counter-current chromatography

Ying Ma, Yoichiro Ito*

Laboratory of Biophysical Chemistry, National Heart, Lung, and Blood Institute, National Institutes of Health, Bethesda, MD 20892, USA

Abstract

pH-Zone-refining counter-current chromatography was applied to the preparative separation of oligopeptide derivatives containing up to three amino acids. Both acidic benzyloxycarbonyl peptides and basic peptides–β-naphthylamide were successfully separated with two-phase solvent systems composed of methyl *tert.*-butyl ether, 1-butanol, acetonitrile and water using a set of suitable retainer and eluent reagents for each group. The preparative ability of the method was demonstrated in the separation of multigram quantities of analyte with a standard separation column with a total capacity of 325 ml. The effects of important factors such as polarity of the two-phase solvent system, concentrations of the eluent base and the retainer acid were discussed.

1. Introduction

pH-Zone-refining counter-current chromatography (CCC) is a recently developed preparative method which provides important advantages over the conventional CCC method including an over 10-fold increase in sample loading capacity, high concentration of fractions, and concentration of minor impurities. The method uses a retainer acid (or base) in the stationary phase to retain the analytes in the column and an eluent base (or acid) to elute the analytes according to their pK_a values and hydrophobicities [1–15]. It produces a succession of highly concentrated rectangular peaks with minimum overlap similar to those observed in displacement chromatography [16]. The method has been successfully applied to the separation of a variety of compounds including acidic [1,4–7,11] and basic [12] amino acid derivatives, many hydroxyxanthene dyes [2–4,8–10], alkaloids from natural sources [13], geometrical [14], structural [15] and optical [17] isomers from synthetic products, chiral compounds, etc.

In this paper, pH-zone-refining CCC is applied to the separation of peptide derivatives. In order to reduce the complexity of their zwitterionic nature and to enhance the pH effects on their partition coefficient, a set of peptides with protected terminal amino or carboxylic groups was selected. A series of experiments demonstrated the effects of factors such as sample size, polarity of the solvent system, concentration of the retainer acid and eluent base on the separation.

* Corresponding author.

0021-9673/95/$09.50 © 1995 Elsevier Science B.V. All rights reserved
SSDI 0021-9673(94)00852-3

2. Experimental

2.1. Apparatus

A commercial model (Ito Multilayer Coil Separator/Extractor; P.C. Inc., Potomac, MD, USA) of the high-speed CCC centrifuge was used throughout the present studies. The detailed design of the apparatus was given elsewhere [18]. The apparatus holds a multilayer coil separation column and a counterweight symmetrically at a distance of 10 cm from the central axis of the centrifuge. The column holder is equipped with a plastic planetary gear which is engaged to an identical stationary sun gear mounted around the central axis of the apparatus. This gear arrangement produces the desired planetary motion to the column holder, i.e., rotation about its own axis and revolution around the centrifuge axis in the same direction at the same rate. This planetary motion also prevents the flow tubes from twisting during revolution, thus permitting the elution of the mobile phase through the column without the use of rotary seals.

The separation column consists of a single piece of 160 m × 1.6 mm I.D. polytetrafluoroethylene (PTFE) tubing (Zeus Industrial Products, Raritan, NJ, USA) wound around the column holder hub with 16 layers and 325 ml capacity. Each terminal of the column was connected to a flow tube (0.85 mm I.D. PTFE) (Zeus Industrial Products) by the aid of a set of tube connectors (Upchurch Scientific, Oak Harbor, WA, USA) which were rigidly mounted on the holder flange. A narrow-bore PTFE tube (5 m × 0.3 mm I.D.) (Zeus Industrial Products) was placed at the outlet of the column to stabilize the effluent flow, thus reducing noise level in recording the elution curves.

The speed of the apparatus was regulated with a speed controller (Bodine Electric, North Chicago, IL, USA).

2.2. Reagents

Acetonitrile, methanol, trifluoroacetic acid (TFA) and triethylamine (TEA) were glass-distilled chromatographic grade (Baxter Healthcare, Muskegon, MI, USA). Methyl *tert.*-butyl ether and 1-butanol were also HPLC grade while aqueous ammonia, hydrochloric acid and acetic acid were reagent grade (all from Fisher Scientific, Fair Lawn, NJ, USA). Peptide derivatives used in the present studies include (Z = benzyloxycarbonyl): Z–Gly–Asp, Z–Gly–Glu, Z–Gly–Ala, Z–Gly–Val, Z–Gly–Phe, Z–Gly–Leu, Z–Gly–Gly–Gly, Z–Gly–Gly–Val, Z–Gly–Gly–Phe, Z–Gly–Gly–Leu (Novabiochem, La Jolla, CA, USA), Z–Gly–Gly, Z–Ala–Ala, Z–Leu–Ala (Bachem California, Torrance, CA, USA), Z–Ala–Gly–Gly, Z–Gly–Gly–Ala, Z–Gly–Leu–Gly, H–Gly–Gly–βNA (βNA = β-naphthylamide), H–Ala–Ala–βNA, H–Gly–Trp–βNA (Bachem Bioscience, Philadelphia, PA, USA)

2.3. Preparation of solvent phases and sample solutions

The solvent pairs used for CCC separations were prepared as follows: desired volumes of methyl *tert.*-butyl ether, acetonitrile, 1-butanol and distilled water were thoroughly equilibrated in a separatory funnel at room temperature and the two phases were separated. TFA (5.4–21.6 m*M*) or TEA (5 m*M*) was added to the upper organic phase which was then used as the stationary phase. The mobile phase was prepared by adding aqueous ammonia (2.7–11 m*M*) or HCl (5 m*M*) to the lower aqueous phase.

Sample solutions were made by dissolving a set of peptide derivatives in 10–50 ml of the solvent usually consisting of about equal volumes of each phase. Each solution was sonicated for several minutes before injection into the column.

2.4. Separation procedure

In each separation, the column was first entirely filled with the organic stationary phase containing TFA or TEA. Then the sample solution

was injected through the sample port and the aqueous mobile phase was eluted through the column in the head-to-tail elution mode at a flow-rate of 3.0 ml/min (metering pump from Rainin, Emaryville, CA, USA) while the apparatus was rotated. The revolution speed was initially set at 600 rpm which was increased to 800 rpm after 20 min of elution. This minimized the carryover of the stationary phase after the mobile phase front emerged from the column. The effluent from the column was continuously monitored by absorbance at 206 nm (Uvicord S; LKB, Bromma/Stockholm, Sweden) and collected at 3.3 ml/tube (Ultrorac fraction collector, LKB). After all peaks were eluted, the centrifuge was stopped and the column contents were collected into a graduated cylinder by connecting the inlet of the column to a nitrogen line at 80 p.s.i. (1 p.s.i. = 6894.76 Pa). The retention of the stationary phase relative to the total column capacity was computed from the volume of the stationary phase collected from the column.

2.5. Continuous UV monitoring

As previously described [12], the elution curve produced by the continuous UV monitoring with an LKB Uvicord S needs further explanation: this monitor uses an interference filter (206 nm) which passes some amount of light in a broad range extending to the visual region. This particular feature helps us monitor the elution curves obtained by pH-zone-refining CCC in that highly concentrated peaks can be recorded at the lower portion of the chart while impurities which absorb different wavelengths can be detected above the main plateau as sharp peaks at the peak boundaries. Consequently, the chromatogram obtained by this monitor shows transmittance as a logarithmic scale, especially near the summit of the peak. Actual absorbance values at the highest portion of the peak (obtained with a Zeiss PM6 spectrophotometer at 206 nm) after diluting the fraction with methanol, were calculated to be about 200 units and obviously could not be directly detected with an ordinary UV monitor. For this reason, we do not indicate absorbance values in the chromatogram.

2.6. Analysis of CCC fractions

The pH value of each fraction was manually determined with a portable pH meter (Accumet portable laboratory; Fisher Scientific, Pittsburgh, PA, USA).

The peptide derivatives were identified by their partition coefficients (K_{std}) in the standard two-phase system composed of *n*-hexane–ethyl acetate–methanol–0.1 *M* NaOH (1:1:1:1, v/v). An aliquot of each fraction (usually 1 ml) was delivered into a test tube and dried under vacuum (Speed Vac concentrator; Savant, Hicksville, NJ, USA). Then, 2 ml of the standard solvent system (1 ml of each phase) were added to each tube and the contents vigorously shaken to equilibrate the solute. An aliquot of each phase (usually 100–200 μl) was diluted with 2 ml of methanol and the absorbance determined at 260 nm. The standard partition coefficient values (K_{std}) were obtained by solute concentration in the upper phase divided by that of the lower phase. The peak fractions were also analyzed by TLC (silica gel 60 F_{254}; EM Separations, Gibbstown, NJ, USA) with a chloroform–methanol–32% acetic acid (16:4:1, v/v) system and detection at 254 nm.

3. Results and discussion

Fig. 1 shows a typical chromatogram of Z-dipeptides obtained by the present method. The separation was performed with the solvent system methyl *tert.*-butyl ether–acetonitrile–water (2:2:3, v/v) in which 16 m*M* TFA (retainer acid) was added to the organic stationary phase and 5.5 m*M* ammonia (eluent base) to the aqueous mobile phase. A set of 8 different Z-dipeptides each in 100 mg amount was eluted as a broad rectangular peak. TLC analysis and partition

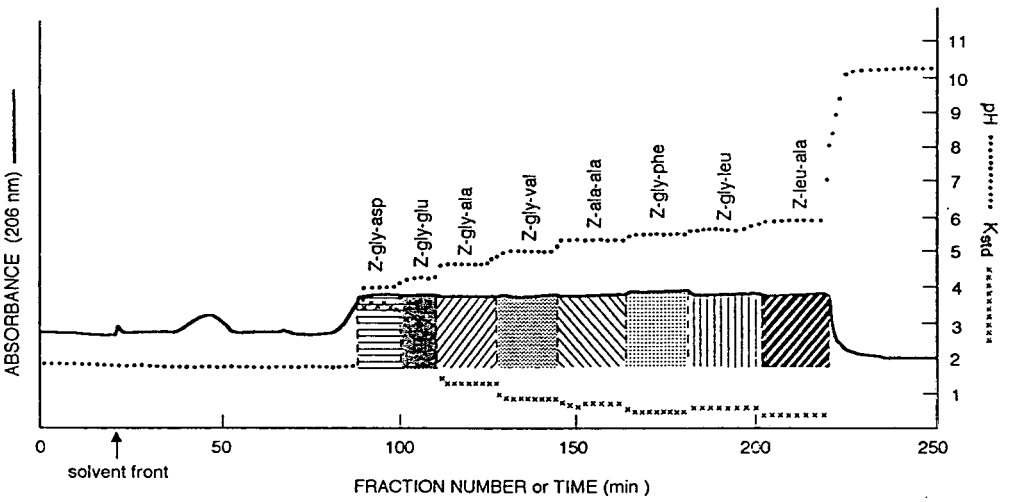

Fig. 1. Separation of eight Z-dipeptides by pH-zone-refining CCC. Experimental conditions: apparatus: multilayer coil high-speed CCC centrifuge with a semipreparative column of 1.6 mm I.D. and 325 ml capacity; solvent system: methyl *tert.*-butyl ether–acetonitrile–water (2:2:3, v/v), 16 m*M* TFA in organic stationary phase (pH 1.83) and 5.5 m*M* NH_3 in aqueous mobile phase (pH 10.62); samples: eight Z-dipeptides as indicated in the chromatogram, each 100 mg dissolved in 50 ml solvent (25 ml each phase); flow-rate: 3.3 ml/min in the head-to-tail elution mode; revolution: 800 rpm (600 rpm until 66 ml of mobile phase were eluted); stationary phase retention: 65.1% of the total column capacity.

coefficient measurements of each fraction revealed that each component was separated as a rectangular peak with minimum overlap as illustrated in the chromatogram. Sharp peak boundaries drawn in the chromatogram each contained no more than several milliliters of the mixing zone. The pH of the collected fractions formed a successive series of plateaus running in an upward staircase fashion (dotted line), each plateau corresponding to the specific analyte zone. These results indicate that the eight peptide derivatives with similar structures were efficiently separated.

Fig. 2 is a similar chromatogram of five Z-tripeptides in which only the terminal amino acid is different. The separation was performed with a more hydrophilic solvent system composed of methyl *tert.*-butyl ether–1-butanol–acetonitrile–water (2:2:1:5, v/v), where the organic stationary phase contained TFA (retainer acid) at 16 m*M* and the aqueous mobile phase contained ammonia (eluent base) at 2.7 m*M*. Again, each analyte was separated as a rectangular peak forming its own pH plateau as indicated by the dotted line in the diagram. TLC and partition coefficient analyses revealed that each pH plateau corresponds to the Z-tripeptide shown and that they elute in order of increasing hydrophobicity. As in the separation of Z-dipeptides (Fig. 1), each boundary between the neighboring peaks contained several milliliters of the mixing zone.

The present method also can be applied to the separation of basic analytes. Fig. 3 shows a typical separation of three free-amino-terminal naphthylamides (βNA-dipeptides) using a solvent system methyl *tert.*-butyl ether–acetonitrile–water (2:2:3, v/v). The separation of these basic peptides was achieved by adding TEA (retainer base) to the organic stationary phase and eluting with an aqueous mobile phase containing HCl (eluent acid) at 5 m*M*. The TLC analyses of the eluted fractions indicated that the βNA derivatives of three dipeptides were well resolved yielding three to seven pure fractions vs. one overlapping fraction and eluted in in-

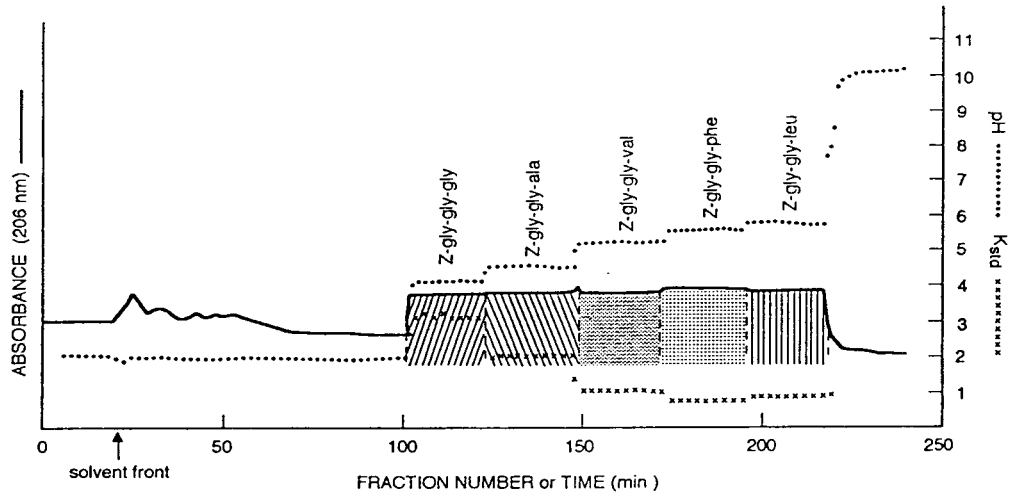

Fig. 2. Separation of five Z-tripeptides by pH-zone-refining CCC. Experimental conditions: apparatus: multilayer coil high-speed CCC centrifuge with a semipreparative column of 1.6 mm I.D. and 325 ml capacity; solvent system: methyl *tert.*-butyl ether–*n*-butanol–acetonitrile–water (2:2:1:5, v/v), 16 m*M* TFA in organic stationary phase (pH 2.00), 2.7 m*M* NH_3 in aqueous mobile phase (pH 10.35); samples: five Z-tripeptides as indicated in the chromatogram, each 100 mg dissolved in 50 ml of solvent (25 ml each phase); flow-rate: 3.3 ml/min in the head-to-tail elution mode; revolution: 800 rpm (600 rpm until 66 ml of mobile phase were eluted); stationary phase retention: 59.4% of the total column capacity.

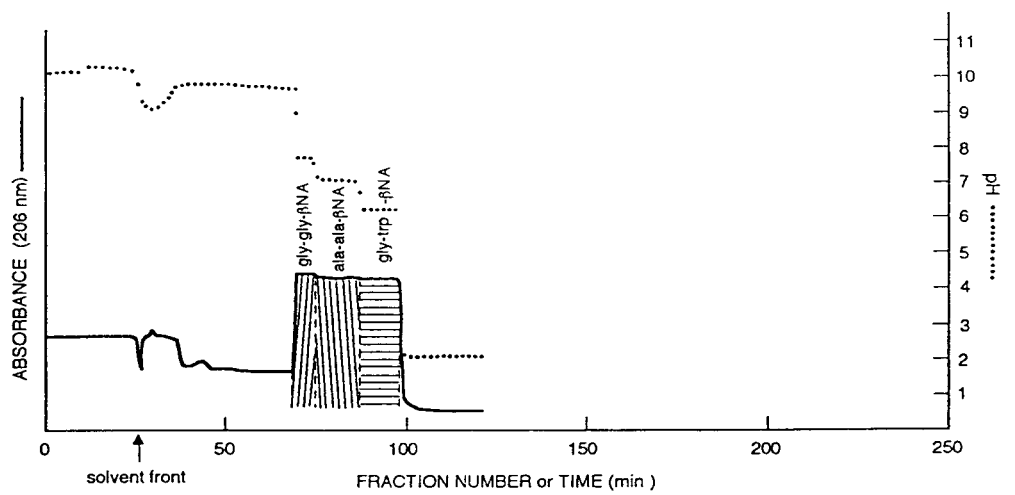

Fig. 3. Separation of three dipeptide βNA derivatives by the present method. Experimental conditions: apparatus: multilayer coil high-speed CCC centrifuge with a semipreparative column of 1.6 mm I.D. and 325 ml capacity; solvent system: methyl *tert.*-butyl ether–acetonitrile–water (2:2:3, v/v), 5 m*M* TEA in the organic stationary phase (pH 10.18) and 5 m*M* HCl in aqueous mobile phase (pH 2.08); samples: three dipeptide βNA derivatives as indicated in the chromatogram, each 100 mg dissolved in 30 ml solvent (15 ml each phase); flow-rate: 3.3 ml/min in the head-to-tail elution mode; revolution: 800 rpm (600 rpm until 66 ml of mobile phase were eluted); stationary phase retention: 67.0% of the total column capacity.

creasing order of their hydrophobicities. The percentage overlap will be reduced as the sample size is increased. As indicated by the dotted line in the chromatogram, pH plateaus display a downward staircase pattern, each corresponding to the respective analyte.

The preparative capability of the present method was demonstrated by a multigram separation of Z-dipeptides. Fig. 4 shows a chromatogram obtained from 3 g of a sample mixture containing Z–Gly–Gly, Z–Gly–Ala and Z–Gly–Leu each in 1 g. All components were resolved and eluted as highly concentrated successive rectangular peaks in 4.5 h. Impurities present in the sample solution were mostly accumulated at the boundaries of the third peak. A sharp boundary between the first and second peaks consisted of no more than several milliliters of the mixing zone while the boundary between the second and third peaks contained about 20 ml of the mixing zone including a sharp impurity peak. The above finding suggests that an increase in sample size nearly proportionally increases the width of the zone plateau while sharp peak boundaries are maintained, thus providing an even higher percentage yield of pure compound.

In the present method, the minimum width of the mixing zone is determined mainly by the partition efficiency of the column regardless of the applied sample size within a reasonable limit. Consequently, the percentage yield of pure fractions is improved by increasing the sample size as shown above. The method also provides a high recovery rate of the analyte since the separation column contains no solid support matrix which would cause adsorptive sample loss and deactivation.

In pH-zone-refining CCC, the concentration of the analyte in the eluted fractions is determined by and becomes close to the concentration of the eluent base (counterion) in the mobile phase, regardless of the initial analyte concentration in the sample solution [5,6]. Thus, the system is capable of concentrating the analytes from a dilute sample solution. In practice the sample loading capacity of the present system is limited by the solubility of the analytes in the organic stationary phase. When the concentration of the analyte in the stationary phase exceeds the solubility limit, solid precipitates are formed in the column leading to a detrimental loss of the stationary phase and finally plugging the tubing.

We found that the choice of solvent system has a great effect on the separation. Among the

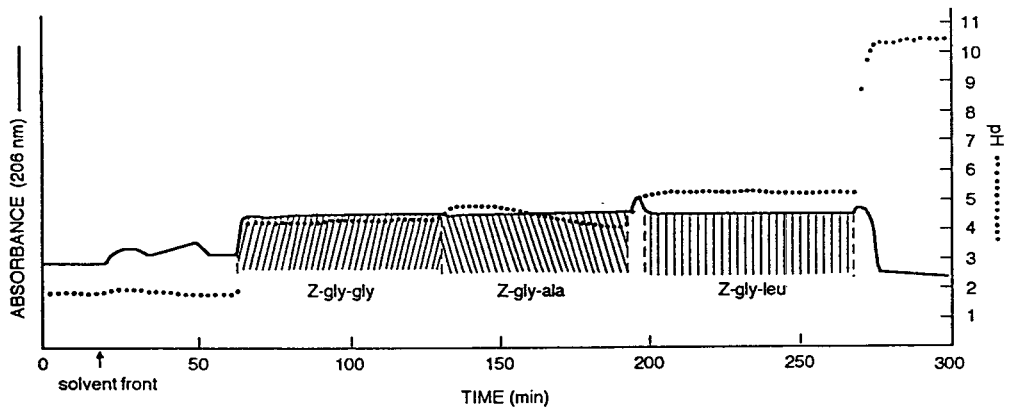

Fig. 4. Preparative-scale separation of Z-peptides by pH-zone-refining CCC. Experimental conditions: apparatus: multilayer coil high-speed CCC centrifuge with a semipreparative column of 1.6 mm I.D. and 325 ml capacity; solvent system: methyl *tert.*-butyl ether–acetonitrile–water (2:2:3, v/v), 16 m*M* TFA in organic stationary phase (pH 2.00), 5.5 m*M* NH_3 in aqueous mobile phase (pH 10.62); samples: three Z-dipeptides as indicated in the chromatogram, each 1000 mg dissolved in 100 ml of solvent (50 ml each phase); flow-rate: 3.3 ml/min in the head-to-tail elution mode; revolution: 800 rpm (600 rpm until 66 ml of mobile phase were eluted); stationary phase retention: 59.4% of the total column capacity.

Z-dipeptides studied, Z-Gly–Phe and Z–Gly–Leu were incompletely resolved in a hydrophobic binary solvent system methyl *tert.*-butyl ether–water. In this solvent system, the separation performed under optimum conditions using 21 m*M* TFA in the organic stationary phase and 2.5 m*M* ammonia in the aqueous mobile phase resulted in more than 60% overlap between the two peaks as shown in Fig. 5A. When a slightly more hydrophilic solvent system composed of methyl *tert.*-butyl ether–acetonitrile–water (4:1:5, v/v) was applied under otherwise identical experimental conditions, the mixing zone between the second and third peaks was reduced to 30% (Fig. 5B). Further improvement in the resolution between these two peaks was achieved by using a still more polar solvent system composed of methyl *tert.*-butyl ether–1-butanol–acetonitrile–water (2:2:1:5, v/v) as shown in Fig. 5C where the mixing zone between these two peaks was no more than several milliliters.

The choice of solvent system requires consideration of the hydrophobicity of the analytes to be separated. A decrease of hydrophobicity of the solvent system usually improves the resolution of the polar analytes. In related studies, we have found it necessary to use several different solvent systems to cover a relatively broad range of hydrophobicity. For example, a binary solvent system composed of methyl *tert.*-butyl ether and water was successfully used for the separation of amino acid derivatives such as dinitrophenyl amino acids [5,11] and amino acid benzyl esters [12]; a more hydrophilic ternary solvent system methyl *tert.*-butyl ether–acetonitrile–water (2:2:3, v/v) for the separation of Z-dipeptides (Fig. 1); and the polar quaternary solvent system methyl *tert.*-butyl ether–1-butanol–acetonitrile–water (2:2:1:5, v/v) for the separation of hydrophilic Z-tripeptides (Fig. 2).

As reported elsewhere [5], the pH of the equilibrated analyte zone (pH_z) in the present method is expressed using pK_a and both intrinsic (δ_s) and apparent (K_s) partition coefficients of the analyte according to the following equation:

$$pH_z = pK_{a\text{-}s} + \log [(\delta_s/K_s) - 1] \quad (1)$$

where the intrinsic partition coefficient (δ_s) represents the relationship between the hydrophobicity of the analyte and that of the two-phase solvent system used for separation. It appears that the difference in pH_z between the analytes may play an important role in determining the degree of peak resolution. In fact, the polar solvent system (Fig. 5C) gives a substantial difference in pH between the second and the third zones.

A set of four similar Z-tripeptides (Fig. 6) were chosen to investigate the effect of eluent base concentration in the two-phase solvent system methyl *tert.*-butyl ether–1-butanol–acetonitrile–water (2:2:1:5, v/v) where TFA (retainer acid) was added to the organic stationary phase at 16 m*M*. In the first experiment using ammonia (eluent base) at 2.7 m*M* in the aqueous mobile phase, the isomeric Z–Ala–Gly–Gly and Z–Gly–Gly–Ala peaks overlapped more than 33% (Fig. 6A). When the concentration of ammonia was increased to 5.5 m*M* under otherwise identical conditions, the resolution of the two peaks was slightly improved to about 25% overlap (Fig. 6B). Finally, when the concentration of the eluent base was further increased to 11 m*M*, complete resolution of the four Z-tripeptides was obtained. However, this approach must be used cautiously since an excessively high concentration of the eluent base in the mobile phase may precipitate analytes in the column leading to carryover of stationary phase and loss of peak resolution.

The concentration of the retainer acid also affects the resolution of the analytes. In our studies the separation of Z–Gly–Phe and Z–Gly–Leu was substantially improved by increasing the concentration of TFA (retainer acid) from 5.4 to 21.6 m*M* in the organic stationary phase while keeping the concentration of ammonia (eluent base) constant at 2.7 m*M* in the aqueous mobile phase. Increased concentration of the retainer acid does not significantly affect the concentration of analyte in the mobile phase but raises its concentration in the stationary phase. The improved peak resolution described above may be caused by the combined effects of a longer retention time and a shortened band width in the column. The overall results of the

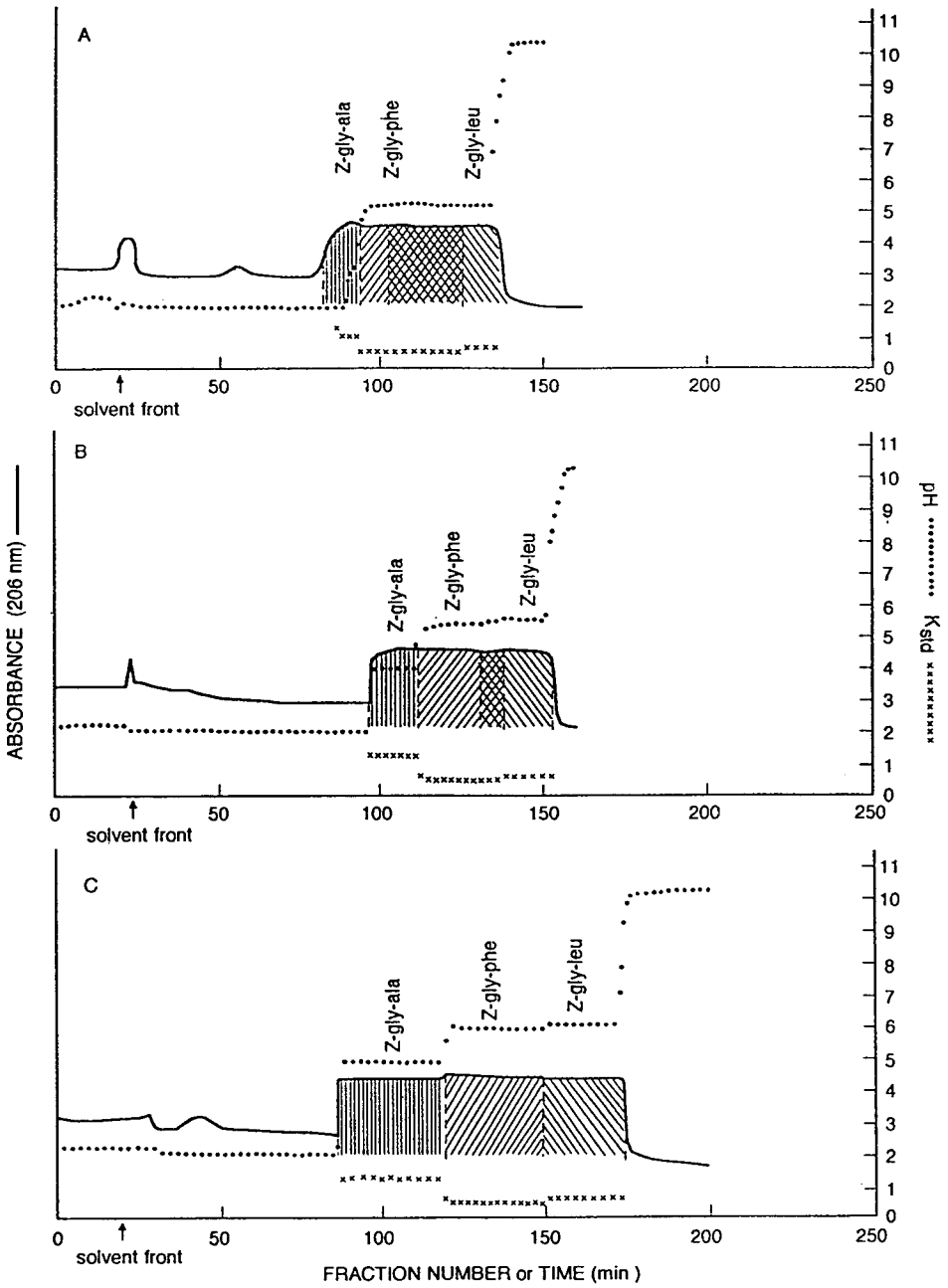

Fig. 5. Effects of hydrophobicity of solvent system on the separation of Z-dipeptides: Experimental conditions: apparatus: multilayer coil high-speed CCC centrifuge with a semipreparative column of 1.6 mm I.D. and 325 ml capacity; solvent system: (A) methyl *tert.*-butyl ether–water; (B) methyl *tert.*-butyl ether–acetonitrile–water (4:1:5, v/v); and (C) methyl *tert.*-butyl ether–*n*-butanol–acetonitrile–water (2:2:1:5), 21 m*M* TFA in organic stationary phase and 2.7 m*M* NH_3 in aqueous mobile phase; samples: three Z-dipeptides as indicated in the chromatogram, each 100 mg dissolved in 6 ml of each phase; flow-rate: 3.3 ml/min in the head-to-tail elution mode; revolution: 800 rpm (600 rpm until 66 ml of mobile phase were eluted); stationary phase retention: (A) 73.6%, (B) 71.8% and (C) 57.3% of the total column capacity.

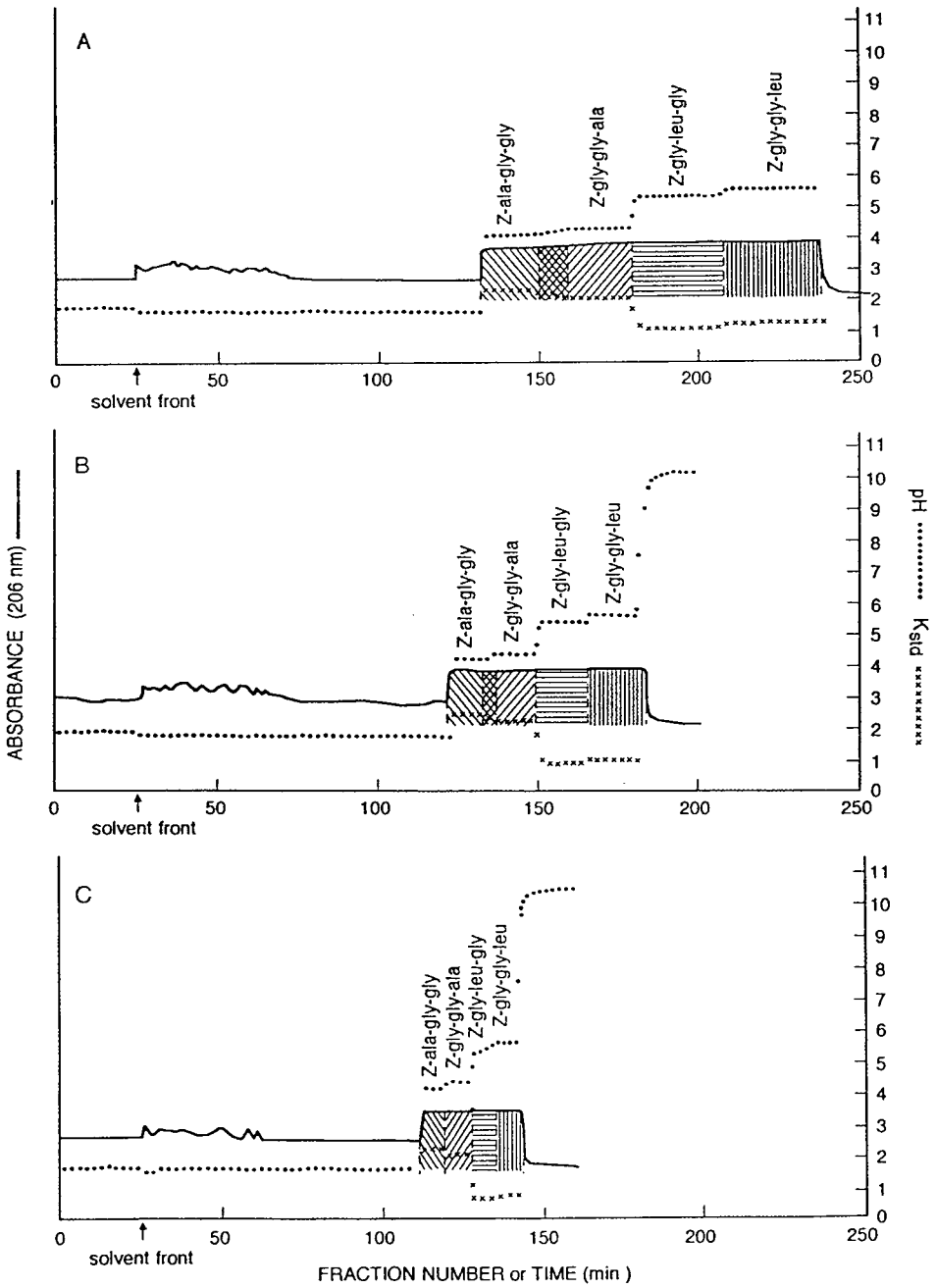

Fig. 6. Effects of eluent base concentration on the separation of Z-tripeptides by pH-zone-refining CCC. Experimental conditions: apparatus: multilayer coil high-speed CCC centrifuge with a semipreparative column of 1.6 mm I.D. and 325 ml capacity; solvent system: methyl *tert.*-butyl ether–*n*-butanol–acetonitrile–water (2:2:1:5, v/v), 32 m*M* TFA in organic stationary phase (pH 2.00), (A) 2.7 m*M* NH_3 (pH 10.27); (B) 5.5 m*M* NH_3 (pH 10.48); and (C) 11 m*M* NH_3 (pH 10.64) in aqueous mobile phase; samples: four Z-tripeptides as indicated in the chromatogram, each 100 mg dissolved in 40 ml solvent (20 ml of each phase); flow-rate: 3.3 ml/min in the head-to-tail elution mode; revolution: 800 rpm (600 rpm until 66 ml of mobile phase were eluted); stationary phase retention: (A) 59.8%; (B) 56.2%; and (C) 56.9% of the total column capacity.

present studies indicate that pH-zone-refining CCC is useful for the separation of oligopeptide derivatives containing either acid or basic groups. The two-phase solvent systems composed of methyl *tert.*-butyl ether–1-butanol–acetonitrile–water at various volume ratios are universally used for separations of analytes in a broad range of hydrophobicities. In all separations, TFA (retainer acid) and ammonia (eluent base) are used for acidic peptides and triethylamine (retainer base) and HCl (eluent acid) for basic peptides. We are currently examining extension of the method to derivatives of longer peptides.

Acknowledgement

We would like to thank Dr. Henry M. Fales for helpful discussions and critical reading of the manuscript.

References

[1] Y. Ito, K. Shinomiya, H.M. Fales, A. Weisz and A.L. Scher, presented at the *1993 Pittsburgh Conference and Exposition on Analytical Chemistry and Applied Spectroscopy, Atlanta, GA, 8–12 March, 1993*, abstract 054P.

[2] A. Weisz, K. Shinomiya and Y. Ito, presented at the *1993 Pittsburgh Conference and Exposition on Analytical Chemistry and Applied Spectroscopy, Atlanta, GA, 8–12 March, 1993*, abstract 865.

[3] A. Weisz, A.L. Scher, D. Andrzejewski, and Y. Ito, presented at the *10th International Symposium on Preparative Chromatography, Arlington, VA, 14–16 June, 1993.*

[4] A. Weisz, A.L. Scher, K. Shinomiya, H.M. Fales and Y. Ito, *J. Am. Chem. Soc.*, 116 (1994) 704.

[5] Y. Ito, K. Shinomiya, H.M. Fales, A. Weisz and A.L. Scher, presented at the *Countercurrent Chromatography Symposium, ACS National Meeting, Chicago, IL, 22–27 August, 1993*; *Countercurrent Chromatography (ACS Monographs)*, American Chemical Society, Washington, DC, submitted for publication.

[6] A.L. Scher, A. Weisz and Y. Ito, presented at the *Countercurrent Chromatography Symposium, ACS National Meeting, Chicago, IL, 22–27 August, 1993, Countercurrent Chromatography (ACS Monographs)*, American Chemical Society, Washington, DC, submitted for publication.

[7] Y. Ito, in Y. Ito and W.D. Conway (Editors), *High-Speed Countercurrent Chromatography*, Wiley Interscience, in press.

[8] A. Weisz, in Y. Ito and W.D. Conway (Editors), *High-Speed Countercurrent Chromatography*, Wiley Interscience, in press.

[9] A. Weisz, D. Andrzejewski and Y. Ito, *J. Chromatogr. A*, 678 (1994) 77.

[10] A. Weisz, D. Andrzejewski, R.J. Highet and Y. Ito, *J. Chromatogr. A*, 658 (1994) 505.

[11] Y. Ito and Y. Ma, *J. Chromatogr. A*, 672 (1994) 101.

[12] Y. Ma and Y. Ito, *J. Chromatogr. A.*, 678 (1994) 233.

[13] Y. Ma, Y. Ito, E. Sokolosky and H.M. Fales, *J. Chromatogr. A*, 685 (1994) 259.

[14] C. Denekamp, A. Mandelbaum, A. Weisz and Y. Ito, *J. Chromatogr. A*, 685 (1994) 253.

[15] Y. Ma, Y. Ito, D. Torok and H. Ziffer, *J. Liq. Chromatogr.*, 17 (16) (1994) 3507.

[16] Cs. Horváth, A. Nahum and J.H. Frenz, *J. Chromatogr.*, 218 (1981) 365.

[17] Y. Ma and Y. Ito, unpublished results.

[18] Y. Ito, in N.B. Mandava and Y. Ito (Editors), *Countercurrent Chromatography: Theory and Practice*, Marcel Dekker, New York, 1988, pp. 79–442.

ELSEVIER

Journal of Chromatography A, 702 (1995) 207–214

JOURNAL OF CHROMATOGRAPHY A

Separation and purification of peptides by high-speed counter-current chromatography

Martha Knight[a], Mirela O. Fagarasan[a], Kazuyuki Takahashi[a], Aicha Z. Geblaoui[a], Ying Ma[b], Yoichiro Ito[b,*]

[a]*Peptide Technologies Corporation, 8401 Helgerman Court, Gaithersburg, MD 20877, USA*

[b]*Laboratory of Biophysical Chemistry, National Heart, Lung, and Blood Institute, National Institutes of Health, Bethesda, MD 20892, USA*

Abstract

Preparative separations of peptides have been accomplished using high-speed counter-current chromatography. This has been made possible by the use of a particular solvent system that does not exhibit solvent carryover at high speed flow and centrifugation conditions. The solvent system composed of *tert.*-butyl methyl ether, *n*-butanol, acetonitrile and aqueous trifluoroacetic acid which can be adjusted in volume ratios and percent acid is employed in two instruments for counter-current chromatography. The cross-axis coil planet centrifuge was used for separation of various dipeptides. Superior resolution was obtained with the multi-layer coil planet centrifuge in the separation of six dipeptides and in the preparative purification of two synthetic peptides.

1. Introduction

Counter-current chromatography (CCC) [1] is a method of separation whereby substances are separated by partitioning between two liquid phases. In the coil planet centrifuge (CPC) this process takes place in open coiled tubing. Since there is no solid support, certain complications such as sample loss due to adsorption or deactivation on a solid phase are avoided. High-speed CCC, carried out in the multi-layer CPC, provides high partition efficiency and has been widely used for the separation of natural products and synthetic organic compounds [2]. Applying high-speed CCC to polar compounds, however, has been limited mainly due to less stationary phase retention of viscous polar solvent systems leading to less resolution. Consequently, peptide separations have been performed mostly on the horizontal flow-through CPC [3] which produces more reliable retention of the stationary phase but yields less efficient separations.

Recently this difficulty was overcome by the use of less viscous polar solvent systems composed of *tert.*-butyl methyl ether, *n*-butanol, acetonitrile and aqueous trifluoroacetic acid (TFA) at various volume ratios. The use of acetonitrile and aqueous TFA with another organic solvent has been introduced in a previous experiment [4]. The present paper describes the preparative separation by high-speed CCC of various peptides with the above two-phase sol-

* Corresponding author.

0021-9673/95/$09.50 © 1995 Elsevier Science B.V. All rights reserved
SSDI 0021-9673(94)01158-3

vent systems using two types of coil planet centrifuges.

2. Experimental

2.1. CCC instruments

The following two different types of coil planet centrifuges were employed: a prototype of the cross-axis coil planet centrifuge (cross-axis CPC) and a commercial model of the type-J multi-layer coil planet centrifuge (multi-layer CPC). The design of these instruments have been described previously [2,5].

The cross-axis CPC (Fig. 1A) used in the present study, recently fabricated at the National Institutes of Health, is especially configured for the use of the viscous aqueous polymer phase systems for separating proteins [5]. This instrument is distinct from the other CPCs in that the rotating tubing coil revolves perpendicularly to the centrifuge axis (Fig. 1B), whereas the tubing coil in the other CPCs rotate parallel to the centrifuge axis. There are two multi-layer coils that are interconnected and opposite each other.

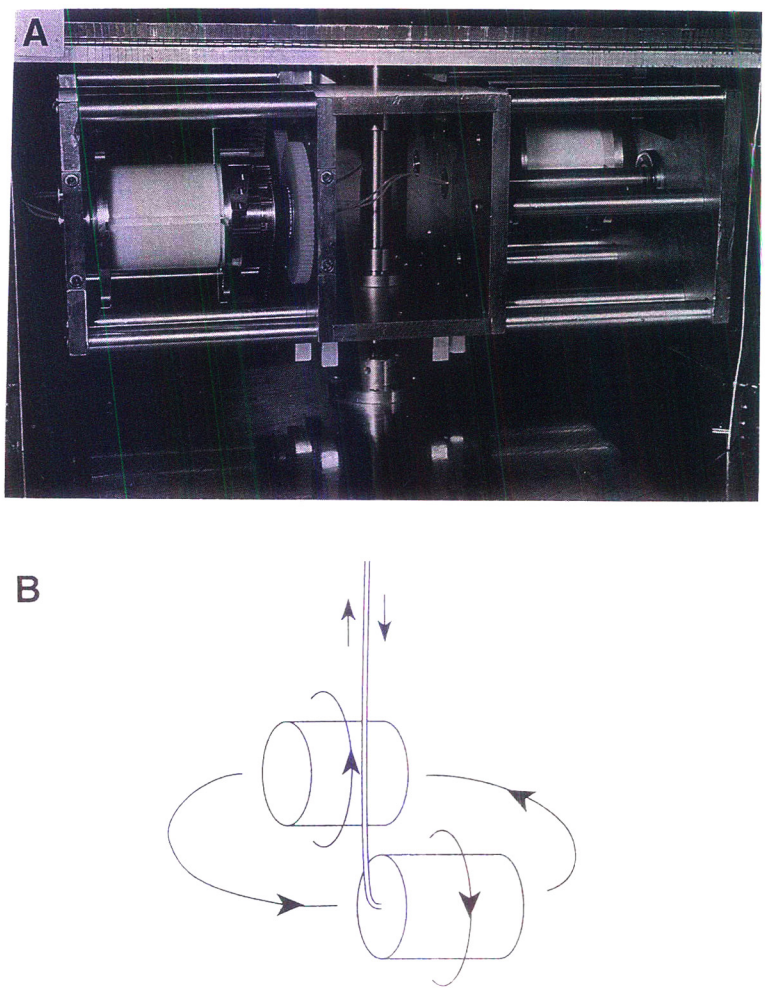

Fig. 1. The cross-axis coil planet centrifuge; photograph (A) and diagram of flow tubing, column-coil and motion (B).

These rotate on an axis perpendicular to the central centrifuge axis. In one revolution around the central axis, these rotate about their own axis one time. The coiled tubing column can be mounted either in the center or off-center on the frame. In the central position, the column is subjected to a strong radial centrifugal force across the diameter of the column which provides stable retention of the stationary liquid phase in the column. In the off-center position, the column is subjected to an additional force field around the rotating holder axis to produce very high mixing of the two phases in the column. Each column is a left-handed coil of 2.6 mm I.D. polytetrafluoroethylene (PTFE) tubing (Zeus Industrial Products, Raritan, NJ, USA) prepared by winding the tubing in multiple layers. The two columns are connected with a flow tube (0.85 mm I.D. PTFE) with a total volume of 570 ml.

The multi-layer CPC (Fig. 2A) is a commercial model (Ito Multilayer Separator/Extractor, P.C. Inc., Potomac, MD, USA). There is one multilayer coil with an opposite counterweight, both at a distance of 10 cm from the central axis of the centrifuge. The planetary gear mounted on the holder axis is engaged to an identical sun gear rigidly mounted around the centrifuge axis. The gear arrangement produces a synchronous planetary motion of the holder: one rotation about its own axis during one revolution around the central axis of the centrifuge both in the same direction (Fig. 2B). The multi-layer coil is of 160 m × 1.6 mm I.D. PTFE tubing in 16 coiled layers on the holder hub for a total volume capacity of 330 ml.

Both planet centrifuges were equipped with a controller (Bodine Electric, Chicago, IL, USA) which regulates the revolution speed up to 1000 rpm.

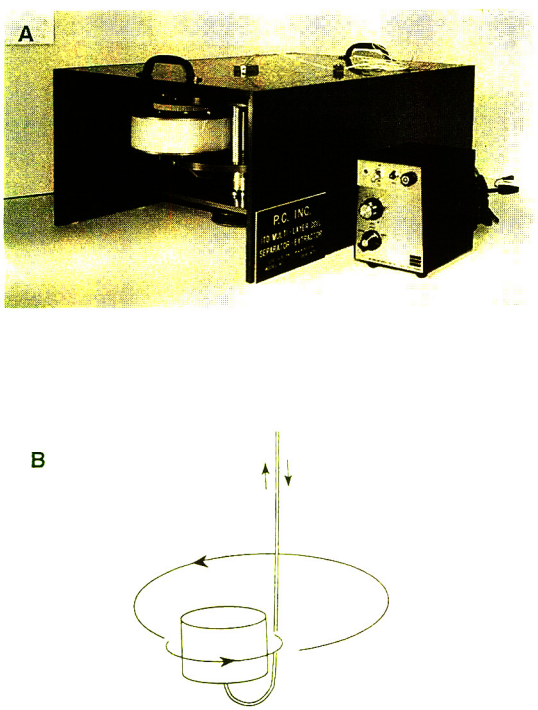

Fig. 2. The commercial model of multi-layer CPC: photograph (A) and diagram of flow tubing, column and motion (B).

2.2. Reagents

tert.-Butyl methyl ether, acetonitrile, *n*-butanol, methanol and TFA were glass-distilled chromatographic grade (Burdick & Jackson Lab., Muskegon, WI, USA). Water is distilled and passed through a Nanopure cartridge system (Barnstead, Boston, MA, USA).

Peptides were synthesized by automated solid-phase methods, coupling the fluorenylmethyloxycarbonyl-protected amino acids to the amino acyl hydroxybenzylalcohol resin [4,6]. The peptides were cleaved from the resin, and the protecting groups removed, by reaction with TFA. The peptides were extracted in a suitable solvent and lyophilized. The peptides were analyzed by HPLC and the amino acid composition determined.

2.3. Preparation of solvent systems and sample solutions

The suitable solvent system was selected by means of partition coefficient measurement. The present studies employed two-phase solvent systems composed of *tert.*-butyl methyl ether, *n*-butanol, acetonitrile and aqueous TFA where the partition coefficient values (K) were adjusted

to 0.5–1 for each sample mixture by changing the solvent volume ratios and/or the TFA concentration. The solvent system selected for the CCC separation was thoroughly equilibrated in a separatory funnel at room temperature and the phases separated.

The sample solution was prepared by dissolving a sample mixture in 4–20 ml (equal volumes of each phase) of the solvent system used for separation.

2.4. Separation procedure

The CCC separations were performed according to the standard technique as follows. The column was first completely filled with the organic stationary phase. Then the sample solution was injected into the coil and the aqueous mobile phase was pumped into the column at 2–5 ml/min while the apparatus was rotated at 700–800 rpm. The effluent from the outlet of the column was continuously monitored with a UV monitor (Uvicord S, LKB Instruments, Bromma/Stockholm, Sweden) and collected in 3–5-ml fractions in a fraction collector (Ultrorac, LKB Instruments). After the desired peaks were eluted, the apparatus was stopped and, by connecting the column inlet to a pressurized nitrogen line, the column contents were emptied into a graduated cylinder to measure the volume of the stationary phase retained in the column.

2.5. Analysis of CCC fractions

Contents of the peaks were analyzed by HPLC as previously described [6] on a S-5 C_{18} column (15 cm × 0.4 cm, 200 pores of 5-μm spherical silica; YMC, Wilmington, NC, USA) in 0.1% aq. phosphoric acid and gradients of acetonitrile at 0.8 ml/min in Waters analytical equipment (Waters, Milford, MA, USA) consisting of a U6K injector, Model 510 dual pumps. Model 481 UV detector and an SE120 chart recorder. The fractions determined to be pure were lyophilized.

3. Results and discussion

3.1. The cross-axis CPC experiments

Fig. 3 contains the chromatograms of three dipeptides separated in the cross-axis CPC in two column positions: the central position (A) and off-center position (B). Both separations were performed with a binary two-phase solvent system composed of *n*-butanol–water and eluting the aqueous phase at 5 ml/min under 700 rpm revolution. The sample solution contained 200

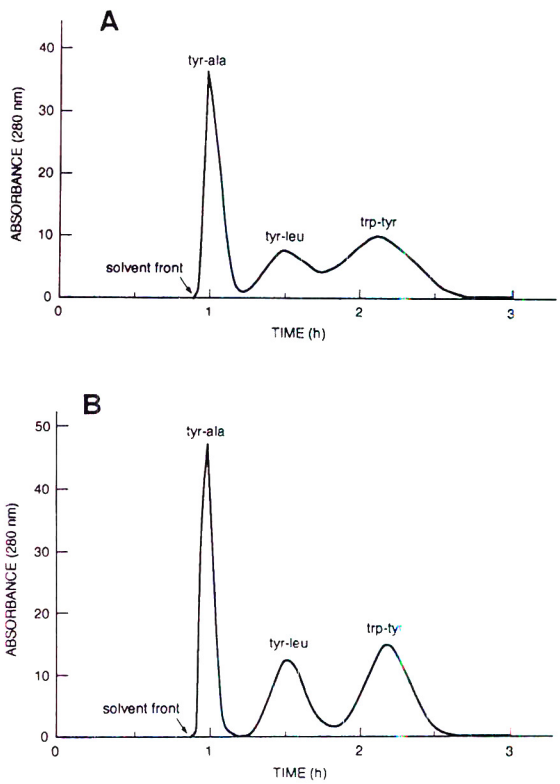

Fig. 3. Separation of 100–200 mg of three dipeptides in the cross-axis CPC in two column positions. (A) Central column position; (B) off-center column position. Experimental conditions are described in the text. Absorbance at 280 nm was determined manually of the fractions and total units are plotted per hour. The lower phase of *n*-butanol–water was used as the mobile phase at a flow-rate of 5 ml/min with a centrifugation at 700 rpm. Retention of stationary phase was 49.6% (A) and 60% (B).

mg each of Tyr–Ala, Tyr–Leu and 100 mg Trp–Tyr dissolved in 40 ml solvent (20 ml each phase). Presence of carried-over mobile phase droplets in the stationary phase produced too much noise in the on-line monitoring of the elution. Therefore, these chromatograms were drawn from the data obtained by manual absorbance measurements of the collected fractions. The results clearly indicated that the off-center position produces much higher peak resolution.

In Fig. 4 are shown similar chromatograms obtained from the separation of a set of 5 dipeptides (100 mg each) using the off-center column position. A two-phase solvent system composed of *tert.*-butyl methyl ether–acetonitrile–aq. TFA (2:2:3, v/v) was used by modifying the TFA concentration at 0.5% (v/v) (A) and 5% (v/v) (B). The separations were performed under the same experimental conditions used in the previous experiment. Higher TFA concentration increased the K value, hence the longer retention time of the analytes, resulting in better peak resolution. However, the first peaks (Tyr–Gly and Tyr–Ala) are only partially resolved.

The above results indicate that the present system is useful for separating several hundred milligrams of peptides with a fairly broad range of hydrophobicity from Tyr–Gly to Trp–Tyr.

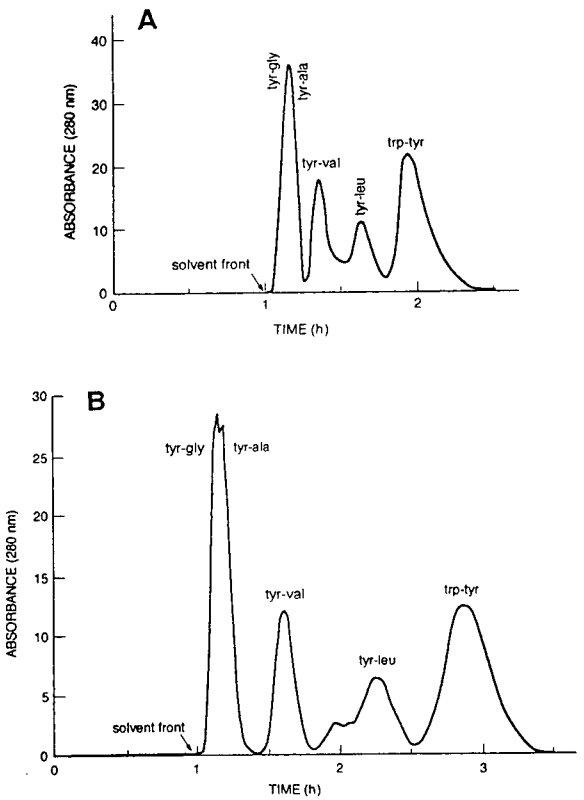

Fig. 4. Chromatogram of five dipeptides by the cross-axis CPC in off-center column position using the ternary solvent system composed of *tert.*-butyl methyl ether–acetonitrile–aq. TFA (2:2:3, v/v) with varying TFA concentrations. (A): 0.5% TFA; (B): 5% TFA. The lower aqueous phase was used as the mobile phase at a flow-rate of 5 ml/min at 700 rpm. Retention of stationary phase in this experiment was 60%.

3.2. Type-J multi-layer CPC experiments

The chromatograms of 50 mg each of 4 dipeptides (Fig. 5) run in the multi-layer CPC using the solvent system composed of *tert.*-butyl methyl ether–acetonitrile–5% aq. TFA (2:2:3,

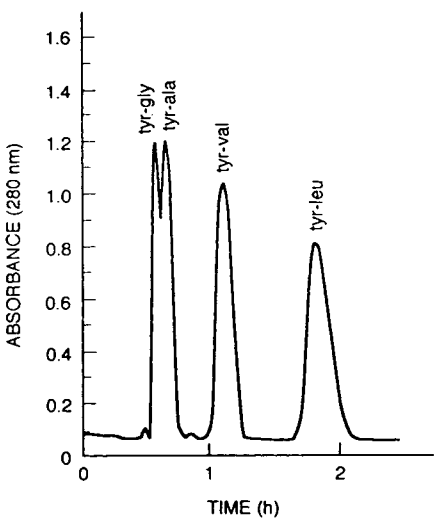

Fig. 5. CCC separation of four dipeptides in the multi-layer CPC. Sample size of each peptide was 50 mg. *tert.*-Butyl methyl ether–acetonitrile–5% aq. TFA (2:2:3, v/v) was the solvent system with the lower aqueous phase used as the mobile at a flow-rate of 3 ml/min at 800 rpm and retention of stationary phase was 68.5%.

v/v) are shown. The separation was performed at a flow-rate of 3 ml/min at 800 rpm. Because the present system provided a stable retention of the stationary phase, the on-line monitoring produced a noise-free elution curve.

The result shows that the resolution between the Tyr–Gly and Tyr–Ala peaks is much improved and the Tyr–Leu peak is eluted in about 2 h suggesting that the peak resolution may be further improved by increasing the polarity of the solvent system.

Fig. 6A is a chromatogram of 6 dipeptides (50 mg each) including peptides of similar composition but different sequence in the multi-layer CPC. The separations were performed with a more polar solvent system composed of *tert.*-butyl methyl ether–acetonitrile–1% aq. TFA (2:2:3, v/v) under otherwise identical experimental conditions as described in Fig. 5. The increased polarity of the solvent system further improved the peak resolution between the Tyr–Gly and Tyr–Ala but Tyr–Val and Val–Tyr are only partially resolved. Finally in Fig. 6B is illustrated a separation performed with a polar quaternary solvent system composed of *tert.*-butyl methyl ether–*n*-butanol–acetonitrile–1% aq. TFA (2:2:1:5, v/v). In this solvent system, all components are completely resolved and eluted in about 6 h. These results indicate that the multi-layer CPC has a high partition efficiency when used with polar solvent systems. The foregoing experiments showed that this instrument has higher resolution than the cross-axis CPC.

The present system was applied for purification of synthetic peptides using the above quaternary solvent system with various volume ratios adjusted to meet the polarity of the products. In Fig. 7 is shown a chromatogram of 50 mg of a synthetic undecapeptide using the solvent system *tert.*-butyl methyl ether–*n*-butanol–acetonitrile–1% aq. TFA (2:1:1:4, v/v). The major peak eluted in slightly over 1 h contained the purified peptide as shown in the analysis in Fig. 8. The yield after lyophilization was 16 mg.

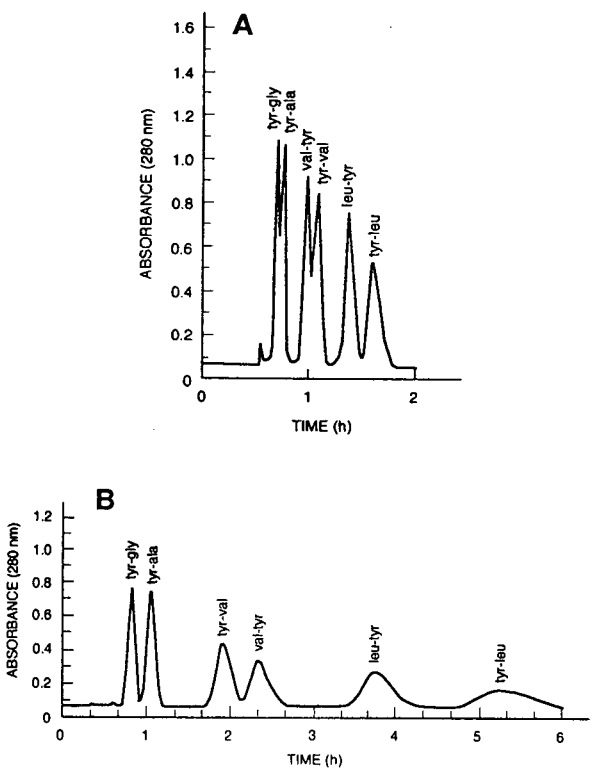

Fig. 6. Separation of 50 mg each of six dipeptides in the multi-layer CPC in two polar solvent systems: (A) *tert.*-butyl methyl ether–acetonitrile–1% aq. TFA (2:2:3) and (B) *tert.*-butyl methyl ether–*n*-butanol–acetonitrile–1% aq. TFA (2:2:1:5) under the same conditions as described in Fig. 5. Retention of stationary phase was 76.5% (A) and 73.4% (B).

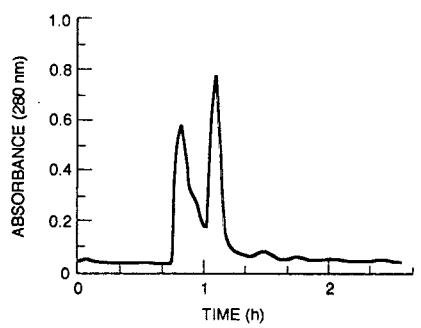

Fig. 7. CCC purification of 50 mg synthetic peptide (Cys.Asp.His.2Ile.Lys.2Arg.Thr.Trp.Tyr) in the multi-layer CPC using *tert.*-butyl methyl ether–*n*-butanol–acetonitrile–1% aq. TFA (2:1:1:4) with the lower phase mobile at a flow-rate of 2 ml/min and 800 rpm. Retention of stationary phase was 67.4%.

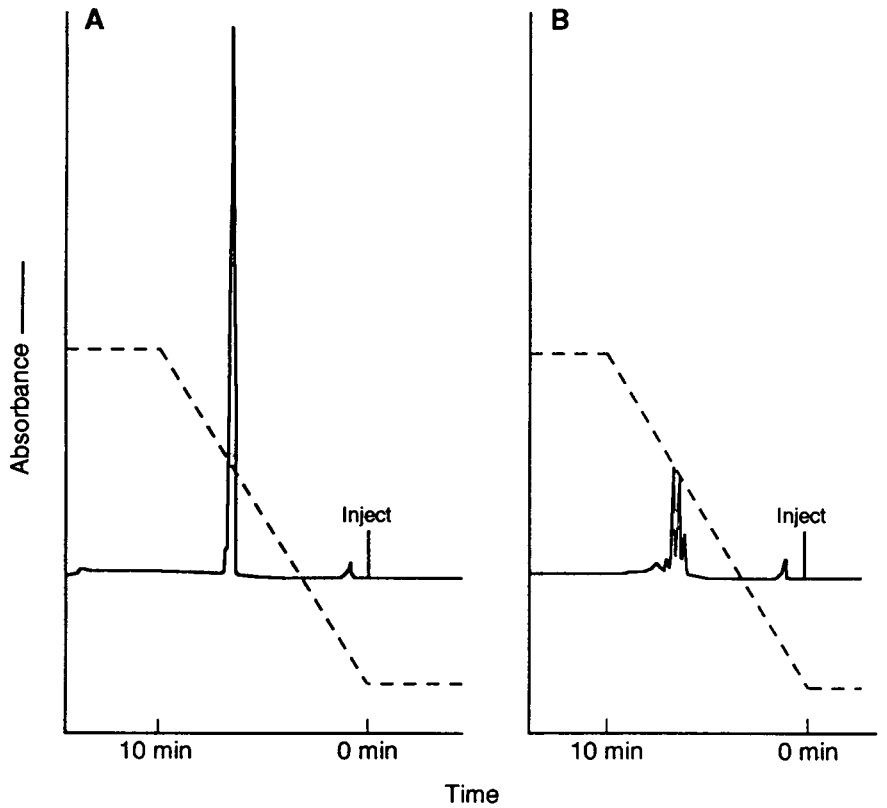

Fig. 8. HPLC analyses of peak fractions of the CCC of the peptide of Fig. 7. (A) Fraction 72, 5-μl injection, of the peak eluting at 1 h; (B) 5 μl of fraction 58 which is the peak after the solvent front (peak before 1 h). The HPLC column used is S-5 ODS 200 Å, 15 × 0.49 cm (YMC) with the solvent system A = 0.1% aq. phosphoric acid and B = 10% A in acetonitrile at a flow of 0.8 ml/min and a gradient of 5 to 40% B in 10 min. The detection is at 215 nm with 0.5 AUFS.

In Fig. 9 is shown a chromatogram of 50 mg of a synthetic 25-mer peptide using the same solvent components. Because of the higher charge of the peptide, the polarity of the solvent system was increased by modifying the volume ratios of the solvent system to 4:3:2:9. The peak at 2.5 h contained the separated peptide as shown in Fig. 10. The experiment using the solvent ratio of 2:1:1:4 eluted the major product near the solvent front while the solvent ratio of 2:2:1:5 retained the product over 4 h with an excessively long baseline (CCC chromatograms not shown). Analysis by HPLC (Fig. 10) of the 2:1:1:4 separation shows the material near the solvent front and the later-eluting purified peptide.

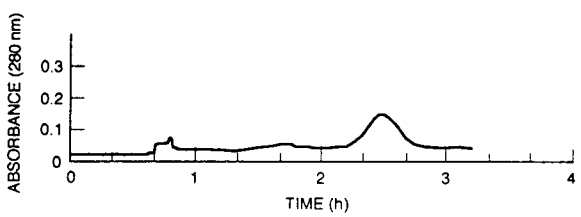

Fig. 9. (A) CCC purification of 50 mg of a 25-mer synthetic peptide [2Ala.Asp.8Glu.Phe.2Gly.Ile.Lys.2Leu.2Asn.Arg. Ser.Val.2Trp]under the same conditions as in Fig. 7 except that the volume ratios of the solvent system are 4:3:2:9. Retention of the stationary phase was 70.0%.

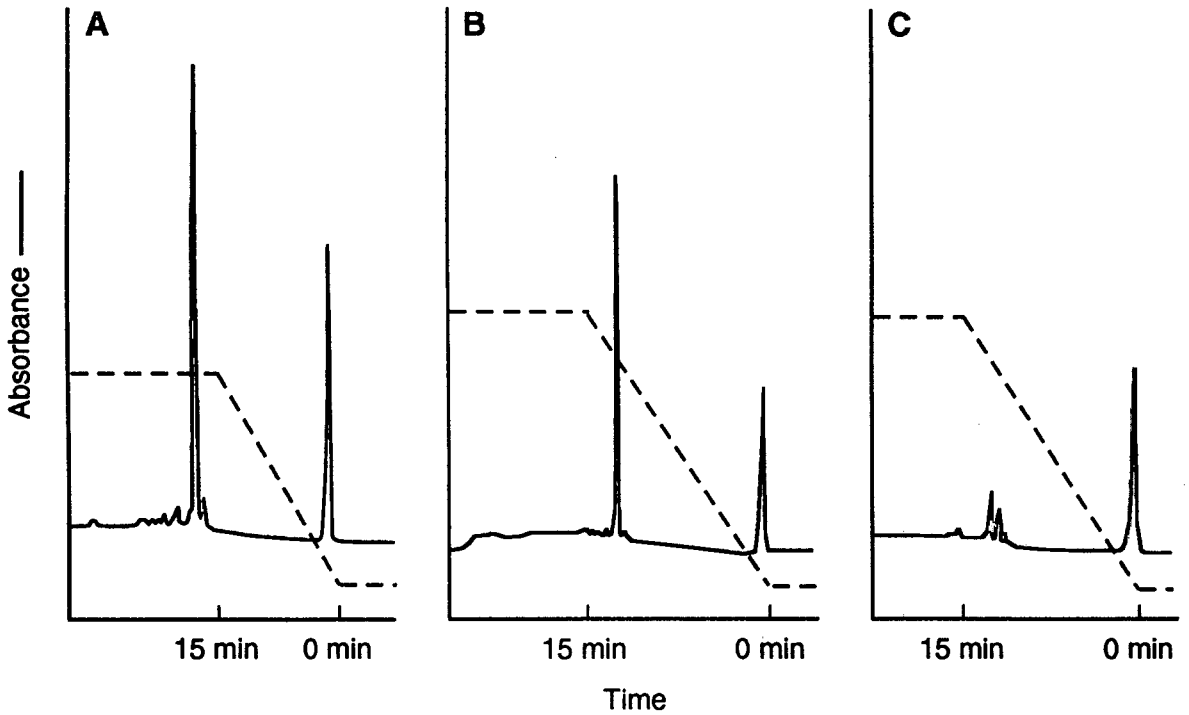

Fig. 10. HPLC analyses of CCC fractions. (A) Analysis of 50 μl of fraction 160, the peak at approximately 2.5 h. HPLC conditions are the same as Fig. 8. (B, C) Analyses of the CCC of the same peptide with a different solvent system as described in the text. The peptide was eluted closer to the solvent front and the HPLC analysis of the pure peptide peak is fraction 70 (B) and the material closer to the solvent front is the last chromatogram, fraction 54. The HPLC conditions are the same as in Fig. 8 except that the gradient is from 5 to 50% B in 15 min and sample injected was 25 μl.

4. Conclusions

The overall results of the present studies indicate potential utility of the two types of CPCs for the preparative purification of peptides.

(1) The cross-axis CPC has a large-scale preparative capability with a fair efficiency using the off-center column position.

(2) The type-J multi-layer CPC produces higher efficiencies for separations of up to 300 mg of peptides.

(3) The *tert.*-butyl methyl ether, *n*-butanol, acetonitrile and aq. TFA components can be adjusted for the optimal partition coefficient for most peptides. This solvent system makes it possible to use the multi-layer CPC at high-speed conditions for good efficiency in preparative peptide separation.

References

[1] Y. Ito, in N.B. Mandava and Y. Ito (Editors), *Countercurrent Chromatography: Theory and Practice*, Marcel Dekker, New York, 1988, pp. 79–442.
[2] Y. Ito, *CRC Crit. Rev. Anal. Chem.*, 17 (1986) 65.
[3] M. Knight, in N.B. Mandava and Y. Ito (Editors), *Countercurrent Chromatography: Theory and Practice*, Marcel Dekker, New York, 1988, pp. 583–616.
[4] M. Knight and K. Takahashi, *J. Liq. Chromatogr.*, 15 (1992) 2819.
[5] K. Shinomiya, J.-M. Menet, H.M. Fales and Y. Ito, *J. Chromatogr.*, 644 (1993) 215.
[6] M. Knight, S. Gluch, R. Meyer and R.S. Cooley, *J. Chromatogr.*, 484 (1989) 299.

ELSEVIER

Journal of Chromatography A, 702 (1995) 215–221

JOURNAL OF CHROMATOGRAPHY A

Preparative-scale liquid chromatographic separation of ω-3 fatty acids from fish oil sources

K. Hidajat, C.B. Ching, M.S. Rao*

Department of Chemical Engineering, National University of Singapore, 10 Kent Ridge Crescent, Singapore 0511, Singapore

Abstract

A preparative-scale chromatographic process for the enrichment and isolation of closely related compounds such as ω-3 fatty acids from fish oil supplements is described. An analytical-scale procedure was scaled up to a preparative level process to provide a simple, rapid, selective and sensitive method for the fractionation of these essential acids. The fish oil triglycerides were saponified into their free fatty acids. The polyunsaturated fatty acids were then enriched through urea crystallization. Subsequently, the individual ω-3 fatty acids were fractionated on a Waters PrepPak unit consisting of six cartridges (μBondapak phenyl silica) using an isocratic ternary mobile phase of acetonitrile–water–tetrahydrofuran (45:35:20, v/v/v). The separation was accomplished within 60 min without any recycling of the solutes. The fractions collected were further analysed by analytical liquid chromatography.

1. Introduction

The separation of biological compounds such as fatty acids from highly complex mixtures such as natural lipids is one of the key problems in current biochemical research. Further, isolation and purification on a preparative or process scale are also basic problems facing organizations attempting to translate the products of separation science from the laboratory to commercial viability. Therefore, for the commercial exploitation of high-value-added products such as ω-3 fatty acids, the acids must first be separated from their triglycerides and purified to a high degree for their effective end use.

ω-3 Fatty acids have many beneficial effects on human health from both therapeutic and nutritional points of view [1–5]. The main ω-3 fatty acids are eicosapentaenoic acid (EPA, C20:5 ω3) and docosahexaenoic acid (DHA, C22:6 ω3). These polyunsaturated fatty acids may be responsible for alleviating certain human health disorders related to heart and circulation problems, inflammation and cancer. They also play a dominant role in the visual, nervous and reproductive systems of the human body [6]. It was further reported recently that DHA afford some protection against Alzheimer's disease and stimulate mental growth in children [7]. The human body cannot produce large amounts of these acids to counter these problems, so external supplementation of these acids is necessary to achieve good health results.

The important natural sources of these acids are fish oils such as sardine, mackerel, cod and menhaden, which contain levels of about 20–30% [8]. Highly pure ω-3 fatty acids are very expensive and in demand in biochemical and biomedical research. Moreover, the separation of polyunsaturated fatty acids such as ω-3 acids

* Corresponding author.

0021-9673/95/$09.50 © 1995 Elsevier Science B.V. All rights reserved
SSDI 0021-9673(94)0881-7

from natural oils such as fish oils has been an important and basic research problem in fats and oil chemistry since 1945. Several traditional and modern separation methods have been developed since then to isolate and enrich these compounds. However, fish oils consists primarily of triacylglycerols, commonly called triglycerides, which are too complex and heterogeneous for individual components to be isolated efficiently with a single separation method. Therefore, most efforts have been directed towards isolating these acids or their derivatives such as methyl and ethyl esters at higher levels of purity without oxidation and isomerization through cost effective methodology. In the past two decades, several investigators have successfully accomplished modest separations of these acids at higher concentrations on analytical and preparative scales with the combination of one or two conventional and modern methods [9–15].

The main separation methods are crystallization, distillation, supercritical fluid extraction and chromatography. Some of these processes are recent and their application may not be feasible in industrial-scale processes [16]. Column liquid chromatography has become an important and often indispensable technique for analytical- and preparative-scale separations in a wide variety of fields, including fatty acid separations, during the last two decades owing to its speed of analysis, resolving power and relative ease of operation [17–21].

Reversed-phase high-performance liquid chromatography (RP-HPLC) is perhaps the most widely used technique in lipid analysis because of its versatility. The substantial literature dealing with its theory, instrumentation and application and also the ready availability of equipment prompted us to choose RP-HPLC as the main method in the separation of ω-3 fatty acids [22–25].

An analytical-scale chromatographic methodology in combination with a urea crystallization procedure was successfully developed in this laboratory for the separation and determination of ω-3 fatty acids [26,27]. The method consists of three main steps: (1) saponification of fish oil triglycerides into their free fatty acids, (2) enrichment of the polyunsaturated fatty acid content from the mixed acid concentrate by a urea crystallization procedure and (3) separation of the individual ω-3 fatty acids by RP-HPLC. A Waters μBondapak free fatty acid column with a ternary mobile phase of acetonitrile–tetrahydrofuran–water (45:20:35, v/v/v) was used. The fatty acids were isolated on the basis of carbon chain length and degree of unsaturation. The salient feature in this procedure was the achievement of rapid separations of these compounds through π–π interactions between fatty acids and the packing material. However, complete baseline separations of the individual acids were not accomplished owing to the short hydrocarbon chain length of the packing material.

This paper describes the development of a preparative-scale production method based on the above analytical procedure for the isolation of high-purity EPA and DHA concentrates. Six RCM PrepPak cartridges packed with the same μBondapak phenyl packing material were employed. The cartridges were connected in series with a cartridge holder. The preparative column was 85 times larger than the analytical column previously used. The other conditions were similar to those in the analytical-scale method. The oxidation of these acids was prevented by adding a small amount (0.005% w/v) of the antioxidant, butylated hydroxyanisole (BHA).

2. Experimental

2.1. Chemicals, reagents and fish oils

Fatty acid standards were obtained from Sigma (St. Louis, MO, USA). The mobile phase solvents acetonitrile and tetrahydrofuran were purchased from Fisher (Fair Lawn, NJ, USA). Water was deionized with an SA-105 Elgastat Spectrum unit (Elga) and filtered using a 0.45-μm filter. The mobile phase was prepared by mixing appropriate volumes of acetonitrile (ACN), tetrahydrofuran (THF) and water and then degassed in a B-1200 E3 ultrasonic bath (Brandon, Danbury, CT, USA).

Chemicals and the solvents such as potassium hydroxide, urea, anhydrous magnesium sul-

phate, hexane and ethanol, used in saponification and urea crystallization, were obtained from Merck and Fisher. The solvents were nitrogen degassed prior to use. Butylated hydroxyanisole was procured from Sigma.

The fish oils sardine oil (refined but not deodorized) and sanomega oil were provided by NOF (Tokyo, Japan) and the cod liver oil was supplied by Pronova Biocare (Sandefjord, Norway).

2.2. Equipment

A schematic diagram of experimental set up is shown in Fig. 1. An M-45 isocratic pump (Waters, Milford, MA, USA) was connected to a manually operated injection valve (Valco, Houston, TX, USA) which was fitted with a 2-ml sample loop. By turning the valve, the eluent pushed the sample in the loop into the column. The column effluent was monitored with a Waters R-401 differential refractive index detector. The detector signal was amplified using a laboratory-made voltage amplifier. It was then converted into digital form by a personal computer equipped with an analog-to-digital interface card (Flytech Technology, Taiwan) with a 12-bit operation. The digitized data were stored and processed by a program written in GWBASIC. The column temperature was controlled by circulating water from a thermostated bath (Braun) through a water-jacket. An RCM PrePak 25 mm × 10 cm cartridge (Waters) packed with 10-μm μBondapak phenyl packing material (pore size 125 Å) was employed. The mobile phase flow-rate was ca. 10 ml min^{-1}. Chromatograms for the injection of 2-ml samples of fish oil concentrates after urea adduction were recorded on chart paper with an R02 electronic chart recorder (Rikadenki, Tokyo, Japan) and digitally on a Phillips PC-3200. The chromatograms were subsequently analysed on a μBondapak free fatty acid analysis column (Waters).

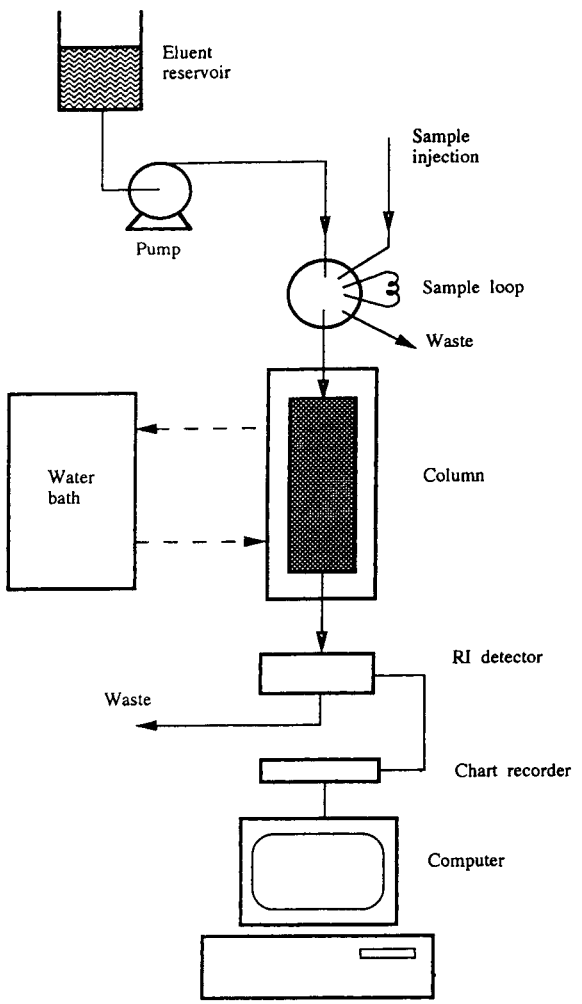

Fig. 1. Schematic diagram of chromatographic set-up.

2.3. Saponification

Saponification hydrolyses the triglycerides into their free fatty acids. The procedure reported by Ratnayake et al. [28] was employed with a few modifications. Fish oil (40 g) was saponified by refluxing with a mixture of KOH (9.2 g), water (17.6 ml) and absolute ethanol (52.8 ml) for 1 h in a nitrogen atmosphere. The saponified mixture was diluted with water (100 ml) and unsaponifiable matter was extracted thoroughly with 3 × 100 ml of hexane and discarded. The aqueous phase was then neutralized with 12.0–12.5 ml of dilute HCl (pH 4–5) and subsequently free fatty acids were extracted with 3 × 100 ml of hexane. The hexane extract was dried over anhydrous magnesium sulphate. The solids in the resulting slurry were removed with a Buchner funnel under suction, then the remaining solvent

was evaporated to dryness by using a rotary evaporator and the free fatty acids were recovered. The average yield of the mixed fatty acids for the three different fish oils in these experiments was 85%, which is comparable to that reported by Ratnayake et al. [28].

2.4. Urea crystallization

The free fatty acids (34 g) obtained from above saponification method and urea (102 g) were mixed with 180 ml of absolute ethanol. The mixture was heated with constant stirring until a clear, homogenweous solution formed. The solution was cooled to room temperature and subsequently crystallized at 4°C for 24 h. After the solution had thawed, the urea crystals (urea complex fraction) were separated from the liquid (non-urea complex fraction) with a Buchner funnel under suction. The non-urea complex fraction was diluted with an equal amount of water and acidified with dilute HCl to pH 4–5. The liberated fatty acids were extracted with 3×100 ml of hexane. The hexane layer was dried over anhydrous magnesium sulphate and subsequently hexane was evaporated to yield 8.0–8.5 g of polyunsaturated fatty acid concentrate. The resulting fatty acid concentrate was kept under a blanket of nitrogen and 0.005% (w/v) of BHA was added. The polyunsaturated fatty acid yields in these experiments were 20–21% of crude fish oils. These yields agree with those reported in the literature [25].

2.5. Chromatographic analysis

A 2.5-g amount of polyunsaturated fatty acid concentrate was dissolved in 5 ml of mobile phase and injected into the column through a 2-ml sample loop. The resulting response curves for each acid were integrated numerically in order to obtain first moments by using the following equation:

$$\mu = \frac{\int_0^\infty ct\,dt}{\int_0^\infty c\,dt}$$

The mean retention times were calculated by subtracting the dead times (t_0) from the first moments. The capacity factors (k') of the fatty acids were obtained from the mean retention times by using the equation

$$k' = \frac{t_R - t_0}{t_0}$$

The capacity factors obtained at various flow-rates are given in Table 1. It can be seen that the capacity factors not only are independent of flow-rates but are within the range 2.0–5.0, indicating economic viability of large-scale separation [29].

3. Results and discussion

Perfect baseline separations of EPA and DHA derived from three different fish oils were accomplished within 60 min. The chromatograms are shown in Figs. 2–4. The other minor peaks have not been identified. The elution sequence of these two ω-3 fatty acids was similar to that in analytical-scale separations [26]. However, baseline separations of the acids were not achieved in analytical chromatography, which indicates that the column size parameters such as diameter and length also play a role in the

Table 1
Capacity factors (k') of ω-3 fatty acids at various mobile phase flow-rates

ω-3 Fatty acid	k'		
	5.0 ml/min	7.5 ml/min	9.9 ml/min
Eicosapentaenoic aicd (C20:5 ω3)	3.35	3.87	3.96
Docosahexaenoic acid (C22:6 ω3)	4.24	4.39	4.83

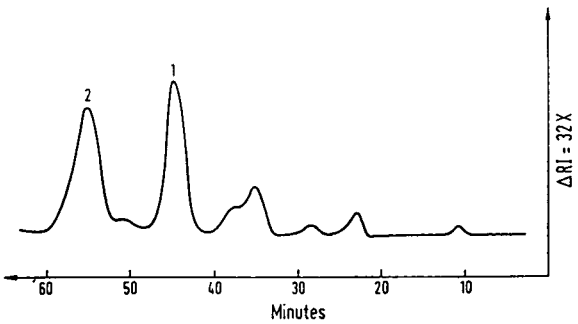

Fig. 2. Preparative chromatograms of ω-3 fatty acids from sardine oil. Stationary phase, RCM PrePak 25 × 10 cartridges packed with μBondapak phenyl-bonded silica; mobile phase, ACN–THF–H_2O (45:20:35, v/v/v) at a flow-rate of 9.9 ml/min; detection, refractive index at ambient temperature (24°C) and attenuation ×32; chart speed, 10 cm/h. Peaks: 1 = EPA; 2 = DHA.

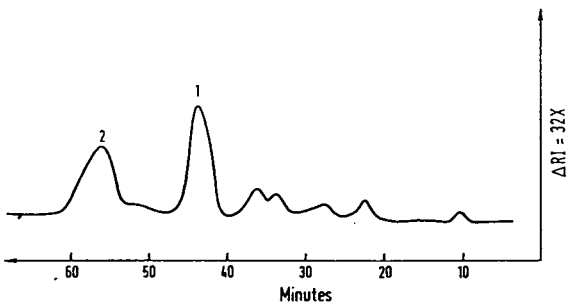

Fig. 3. Preparative chromatograms of ω-3 fatty acids derived from sanomega oil. Conditions and peak identification as in Fig. 2.

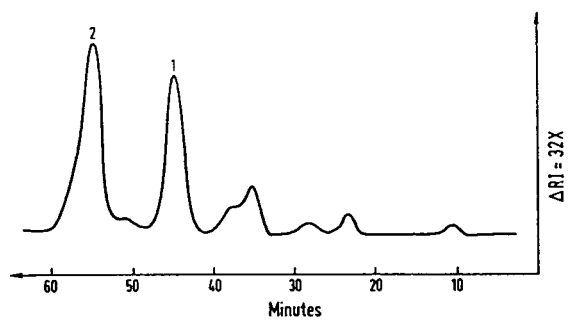

Fig. 4. Preparative chromatograms of ω-3 fatty acids derived from cod liver oil. Conditions and peak identification as in Fig. 2.

achievement of adequate separations of these components in addition to the chain length, saturation and position of the double bonds of the fatty acids [26,27,30,31].

Twenty fractions of preparative column effluents were collected at different points on the chromatograms of ω-3 fatty acids derived from Sanomega oil and analysed with the free fatty acid column. The integrated areas of the chromatograms thus obtained were used to calculate the percentages of these acids present in the fractions, as summarized in Table 2. The highest concentrations of EPA and DHA were 96.7% and 92.4%, respectively.

Interfering saturated and monounsaturated fatty acids such as palmitic acid (C16:0), stearic acid (C18:0) and oleic acid (C18:1 ω9) were successfully removed by the urea crystallization method. It was evident from Bengen's discovery that urea occludes straight-chain compounds such as long-chain saturated and monounsaturated fatty acids in a hexagonal structure and excludes methylene-interrupted polyunsaturated fatty acids due to the irregularities in their

Table 2
Compositions of ω-3 fatty acids in collected fractions determined by analytical chromatography

Fraction no.	EPA (C20:5 ω3) (%)	DHA (C22:6 ω3) (%)
1	62.4	
2	76.9	
3	88.2	
4	89.9	
5	96.7	
6	90.3	
7	84.8	
8	50.1	
9	20.4	
10	4.5	
11		34.9
12		53.5
13		78.2
14		86.6
15		92.4
16		90.1
17		81.7
18		40.1
19		12.4
20		1.4

Table 3
Composition of ω-3 fatty acids obtained at various ratios of urea to fatty acids and a crystallization temperature of 4°C

ω-3 Fatty acid	Urea: fatty acid ratio		
	2:1	3:1	4:1
EPA (C20:5 ω3) (%)	69	81	79
DNA (C22:6 ω3) (%)	52	74	71

molecules caused by the bends at each double bond [32]. It was observed that the extent of crystallization varies with the concentration ratio of urea and fatty acids and also with the temperature of crystallization, as shown in Tables 3 and 4. These tables also show that the higher concentration of ω-3 fatty acids was achieved when the urea concentration was three times higher than that of the fatty acids. The optimum temperature of crystallization was found to be 4°C. These results agree with previously reported results [33]. It was also found that saponification and urea crystallizations are simple chemical operations that can be performed under mild conditions in which no isomerization or degradation of the fatty acids occurs. Further, as oxidized products do not form urea adducts, the peroxidation of these highly unsaturated ω-3 fatty acids could be avoided during the extraction of free acids from fish oil triglycerides [34].

4. Conclusions

A simple, rapid and cost-effective preparative-scale chromatographic method was developed for the separation of gram-scale amounts of highly pure ω-3 fatty acids. These acids were eluted on the basis of their equivalent chain length (ECL), a parameter introduced by Miwa et al. [35] to determine the relative retention times of the fatty acids and their derivatives in gas and liquid chromatography. The ECL values for these acids are calculated by using the equation ECL = $N - 2n_{C=C}$, where N is the number of carbon atoms and $n_{C=C}$ is the number of double bonds present in the fatty acids. The ECL value for both EPA (C20:5 ω3) and DHA (C22:6 ω3) is 10. Such fatty acids having the same ECL values are termed as critical pairs and their separation was reported to be difficult in the past. However, the present methodology clearly demonstrates the enrichment and isolation of these high-value-added similar products within 60 min through urea crystallization folowed by RP-HPLC. Moreover, improvements are now under investigation such as converting the batch-scale operation to a continuous counter-current mode and total optimization of the process.

Table 4
Composition of ω-3 fatty acids obtained at various crystallization temperatures and a urea to fatty acid ratio of 3:1

ω-3 Fatty acid	0°C	4°C	10°C
EPA (C20:5 ω3) (%)	69	81	85
DNA (C22:6 ω3) (%)	80	74	64

References

[1] J. Dyerberg and H.O. Bang, *Lancet*, ii (1979) 433.
[2] H.M. Sinclair, *Postgrad. Med. J.*, 56 (1980) 579.
[3] J.M. Kremer, J. Bigauotette, A.V. Michalek, M.A. Timchalk, L. Linnger, R.I. Rynes, C. Huck, J., Zieminski and L.E. Bartholomew, *Lancet*, i (1985) 184.
[4] R. Virage, P. Bouilly and D. Fryman, *Lancet*, i (1985) 181.
[5] J.E. Kinsella, *Seafoods and Fish Oils in Human Health and Disease*, Marcel Dekker, New York, 1987.
[6] W. Yongmanitchai and O.P. Ward, *Process Biochem.*, 24 (1989) 117.
[7] Jpn. Chem. Week, November 4, 1993.
[8] J.E. Bonnet, V.D. Sidwell and E.G. Zook, *Fish. Rev.*, 36 (1974) 8.
[9] R.G. Ackman, P.J. Ke and P.M. Jangaard, *J. Am. Oil. Chem. Soc.*, 50 (1973) 1.
[10] N. Haagsma, C.M. van Gent, J.B. Lutten, R.W. de Jong and E.J. van Doorn, *J. Am. Oil Chem. Soc.*, 59 (1982) 117.
[11] M. Fujita and M. Makuta, *US Pat.*, 4 377 526 (1983).
[12] W. Murayama, Y. Kosuge, N. Nakaya, K. Nunogaki, J. Cazes and H. Nunogaki, *J. Liq. Chromatogr.*, 11 (1988) 283.
[13] R.G. Ackman, in E.G. Perkins (Editor), *Analysis of Fats, Oils and Lipoproteins*, AOCS, Illinois, 1991, p. 270.
[14] W.O. Eisenbach, *Ber. Bunsenges. Phys. Chem.*, 88 (1984) 882.
[15] V.J. Krukonis, *ACS Symp. Ser.*, 366 (1988) 26.

[16] E.H. Gruger, Jr., presented at the *11th Annual Conference, Pacific Fisheries Technologists, Gearhart, OR, 27–30 March 1960.*
[17] M.I. Aveldano, M. VanRollins and L.A. Horrocks, *J. Lipid Res.*, 24 (1983) 275.
[18] H.C. Jordi, *J. Liq. Chromatogr.*, 1 (1978) 215.
[19] A.G. Bailie, Jr., T.D. Wilson, R.K. O'Brien, J.M. Beebe, O.J.D. Stuart, E.J. Melilie and D.W. Hill, *J. Chromatogr. Sci.*, 20 (1982) 406.
[20] H. Traitler, H.J. Wielle and A. Studer, *J. Am. Oil. Chem. Soc.*, 65 (1988) 755.
[21] T. Rezanka and M. Podojil, *J. Chromatogr.*, 346 (1985) 453.
[22] J.M. Beebe, *Ph.D. Thesis*, University of Rhode Island, Kingston, RI, 1987.
[23] S. Tokiwa, A. Kanazawa and S. Teshima, *Bull. Jpn. Soc. Sci. Fish.*, 47 (1981) 675.
[24] M. Perrut, *LC·GC*, 6 (1988) 914.
[25] H.J. Wille, H. Traitler and M. Kelly, *Rev. Fr. Corps Gras*, 34 (1987) 69.
[26] M.S. Rao, C.B. Ching and K. Hidajat, *Ind.Eng. Chem. Res.*, submitted for publication.
[27] M.S. Rao, C.B. Ching and K. Hidjat, *Chromatogr. Sci.*, submitted for publication.
[28] W.M.N. Ratnayake, B. Olsson, D. Matthews and R.G. Ackman, *Fat Sci. Technol.*, 10 (1988) 381.
[29] L.R. Snyder and J.J. Kirkland, *Introduction to Modern Liquid Chromatography*, J. Wiley, New York, 1974.
[30] C.B. Ching, K. Hidajat and M.S. Rao, *J. Liq. Chromatogr.*, 16 (1993) 527.
[31] C.B. Ching, K. Hidajat and M.S. Rao, *Chromatographia*, 35 (1993) 399.
[32] F. Bengen, *Ger. Pat.*, 869 070, 1953.
[33] T. Miyakawa and H. Nomizu, *Abura Kagaku*, 9 (1960) 415.
[34] F.D. Gunstone, J. Mclaughlan, C.M. Scrimgeour and A.P. Watson, *J. Sci. Food Agric.*, 27 (1976) 675.
[35] T.K. Miwa, K.L. Kikolajezak, F.R. Earle and I.A. Wolff, *Anal. Chem.*, 32 (1960) 1739.

ELSEVIER

Journal of Chromatography A, 702 (1995) 223–231

JOURNAL OF CHROMATOGRAPHY A

Separation of enantiomers of 1*a*,2,7,7*a*-tetrahydro-3-methoxynaphtha-(2,3*b*)-oxirane by liquid chromatography: laboratory-scale elution chromatography and modelling of simulated moving bed

A.E. Rodrigues*, Z.P. Lu, J.M. Loureiro, L.S. Pais

Laboratory of Separation and Reaction Engineering, School of Engineering, University of Porto, 4099 Porto Codex, Portugal

Abstract

The separation of enantiomers of 1*a*,2,7,7*a*-tetrahydro-3-methoxynaphtha-(2,3*b*)-oxirane (Sandoz epoxide) on cellulose triacetate HPLC columns was investigated on the laboratory scale. The performance of the columns was calculated by HEPT measurements and the slopes of the adsorption equilibrium isotherms and effective diffusivities were calculated from elution chromatographic experiments. Multi-component adsorption equilibrium isotherms were calculated from single isotherms by using the ideal adsorbed solution (IAS) model. Simulation of continuous chromatographic separation of the racemic mixture of Sandoz epoxide in a simulated moving bed was carried out and the effect of mass transfer coefficient on process performance was analysed.

1. Introduction

The need for the separation of enantiomers for pharmaceutical applications is increasing as regulatory aspects become more stringent. The separation of enantiomers by HPLC is an active field of research. Many chromatographic packings have been developed and, according to Sheldon [1], can be classified into (a) chiral ligand-exchange phases, (b) affinity phases, (c) helical polymer phases, e.g., cellulose derivatives, (d) cavity phases, e.g., cyclodextrin, and (e) Pirkle-type phases, e.g., amino acid derivatives immobilized on silica by either ionic or covalent attachment.

In many instances these are difficult separations and therefore continuous chromatography should be considered. In the chemical engineering field the concept of the simulated moving bed (SMB) has been known since 1961 when the first patent by Broughton [2] appeared. Many processes are in industrial operations, e.g., Parex for the separation of *p*-xylene and Sarex for the separation of fructose and glucose in the high fructose corn syrup (HFCS) industry.

The application in the pharamceutical and fine chemistry industries is in its infancy, however. It is worth mentioning the development of simulated moving bed units for such applications made by Separex in cooperation with IFP on the pilot and industrial scales.

The operation of SMB units is not as simple as elution, frontal or displacement chromatography. Therefore, understanding how the system reacts to changes in operating parameters is of crucial importance. Modelling and simulation

* Corresponding author.

0021-9673/95/$09.50 © 1995 Elsevier Science B.V. All rights reserved
SSDI 0021-9673(94)01037-4

studies are of importance before running the system. This requires a knowledge of some basic information on equilibrium and kinetic parameters.

The test system to be studied here is the separation of enantiomers of 1*a*,2,7,7*a*-tetrahydro-3-methoxynaphtha-(2,3*b*)-oxirane (Sandoz expoxide; Sandoz, Basle, Switzerland):

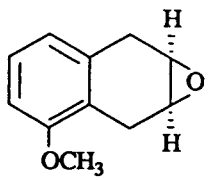

The objectives of this work were (i) to obtain equilibrium and kinetic parameters from elution chromatographic experiments; (ii) to predict multi-component equilibrium from single isotherms; and (iii) to provide a tool for understanding SMB operation.

2. Experimental and results

2.1 Equipment and chemicals

The laboratory-scale HPLC system (Gilson, Villiers le Bel, France) includes three piston pumps (Model 305 master pump and two Model 306 slave pumps with 10 WTI piston pump heads), a Model 117 UV detector with a standard 5 mm path length flow cell, a Model 811C dynamic mixer, a Model 805 manometric module, a Model 202 fraction collector and a IBM PC 386 computer; the system is completely automated.

Two columns of cellulose triacetate (TCA; Merck, Darmstadt, Germany) as stationary phase were used: column A, laboratory packed, 25 cm × 0.46 cm I.D., particle diameter 15–25 μm; column B, Merck 25 cm × 1 cm I.D., particle diameter 10 μm. Column A was prepared from TCA according to the activation procedure described by Dingenen et al. [3]. In fact, active centres of the adsorbent become accessible only after it has been submitted to swelling in boiling methanol. Therefore, 100 g of TCA in 500 ml of methanol were boiled at 80°C under reflux for 30 min. This suspension was allowed to cool at ambient temperature and then decanted in order to eliminate the fines, which would lead to high pressure drops in the column. An HPLC column slurry packer with axial compression to 200 bar was used to pack column A.

The columns used in the simulated moving bed pilot plant were wider (I.D. 2.6 cm, length ca. 9 cm). They were packed according to the procedure described by Nicoud [4].

The mobile phase used was methanol (LiChrosolv; Merck). All runs were carried out at 25°C. The total concentration of the sample (racemic mixture) was 0.25 g/l. The outlet concentration was determined by UV detection at 220 nm; the flow-rates used were in the range 0.1–2 ml/min.

2.2. Elution chromatography

Several elution chromatographic runs were carried out in order to assess the influence of the operating parameters on the column behaviour, namely the effect of flow-rate and particle diameter.

The effect of flow-rate on the separation of enantiomers is shown in Fig. 1 for column A at flow-rates 0.9, 0.5 and 0.1 ml/min. Similar results for column B are shown in Fig. 2 for flow-rates of 2, 0.7 and 0.3 ml/min. As the particle diameter is smaller and the column has a larger cross-sectional area, complete separation of the peaks is achieved even at a flow-rate of 2 ml/min.

2.3. Column performance

The column performance can be characterized by its height equivalent to a theoretical plate (HEPT), which can be calculated from the mean μ_1 and variance σ^2 of a chromatographic peak as $\mathrm{HETP} = \sigma^2 L/\mu_1^2$. The Van Deemter plot, i.e., HETP versus superficial velocity u_0, was calculated from experiments with column A at various flow-rates with the pure (+)-isomer previously separated in the same column from a racemic mixture at 1 g/l; for column B we directly used

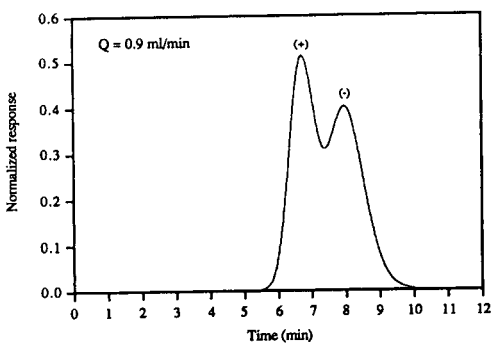

(a)

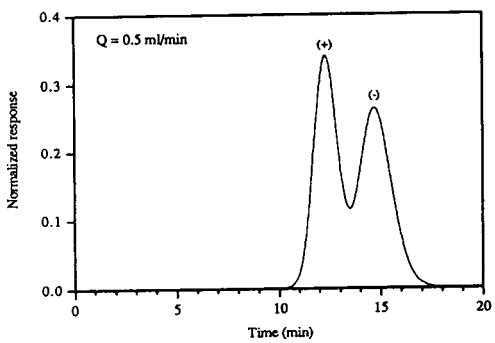

(b)

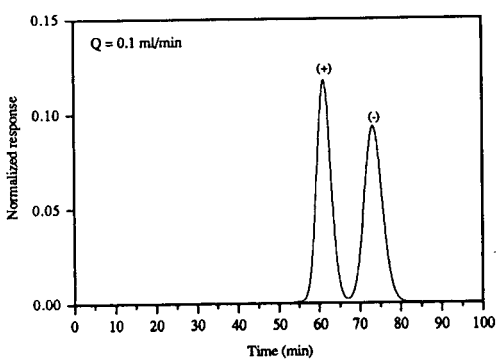

(c)

Fig. 1. Effect of flow-rate on enantiomer separation with column A (25 cm × 0.46 cm I.D.) packed with TCA particles of d_p = 15–25 μm.

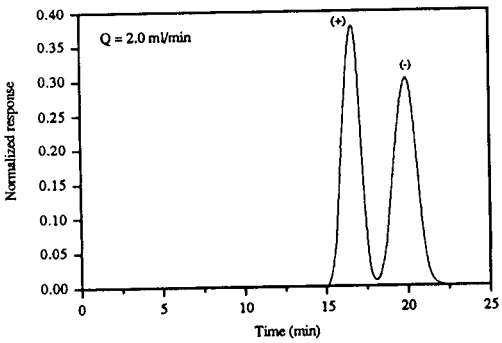

(a)

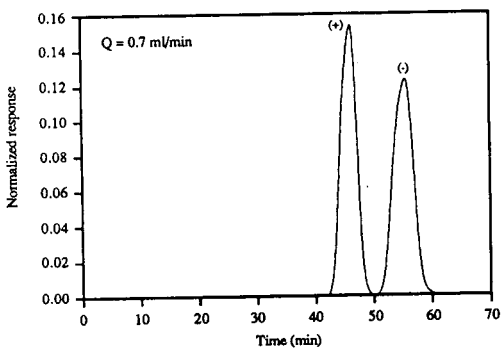

(b)

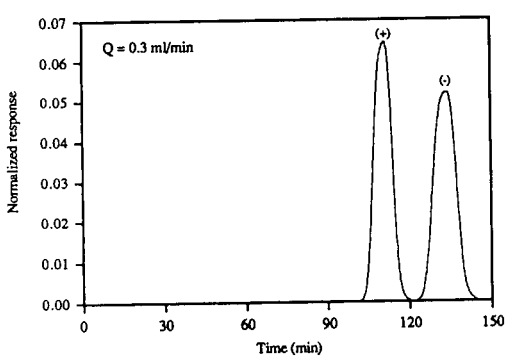

(c)

Fig. 2. Effect of flow-rate on enantiomer separation with column B (25 cm × 1 cm I.D.) packed with TCA particles of d_p = 10 μm.

the experiments in Fig. 2 as the peaks were already well separated.

Fig. 3 shows the experimental results obtained for the (+)-isomer in column A.

Van Deemter plots, i.e., HEPT vs. u_0 for columns A and B are shown in Fig. 4. The performance of a Merck column packed with 15–25-μm particles with a similar structure to the 10-μm particles would be represented by a line located above the curves shown.

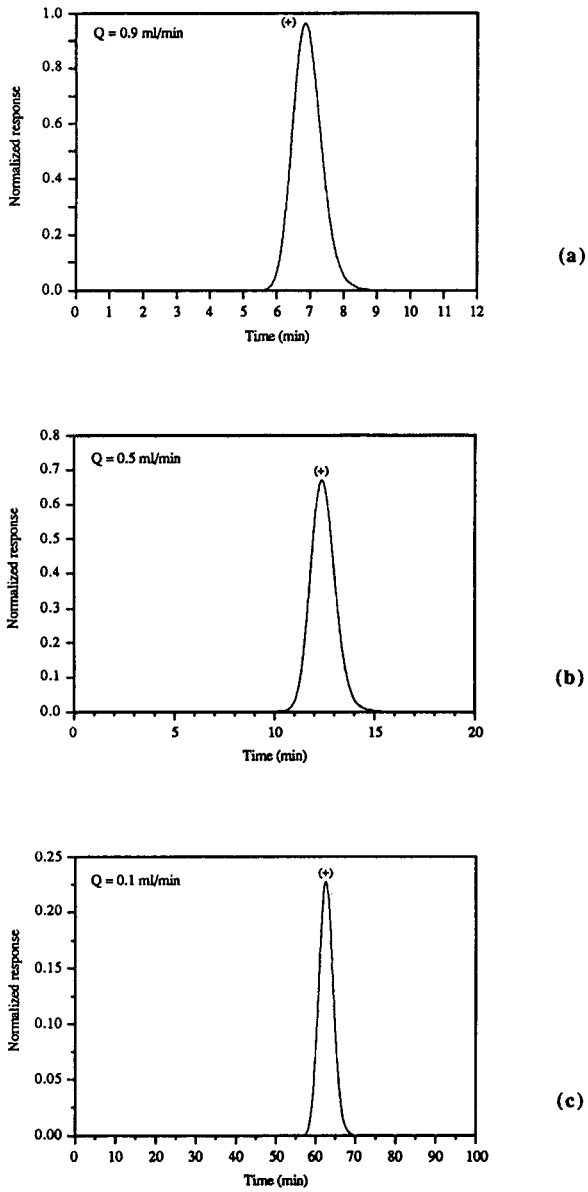

Fig. 3. Effect of flow-rate on the shape of the chromatographic peak of the (+)-isomer with column A.

2.4. Modelling and simulation of elution chromatography

The mathematical model of elution chromatography presented here is based on the following assumptions: homogeneous particle with spherical geometry where mass transport occurs only by diffusion and plug flow with axial dispersion of the outer fluid phase; species i are linearly adsorbed in the particle, i.e., the adsorption equilibrium isotherm relating the adsorbed concentration q_i^* with the bulk fluid phase concentration c_i of species i is $q_i^* = mc_i$. Model equations are then as follows.

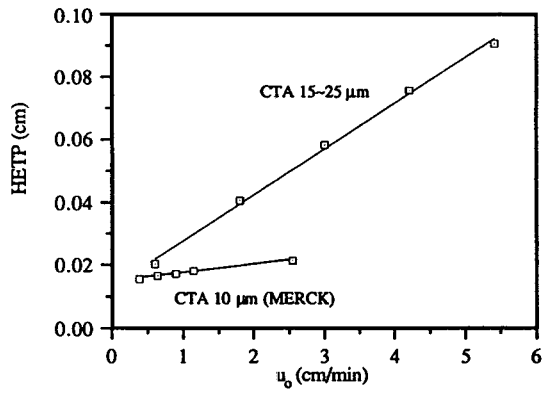

Fig. 4. Van Deemter plots (HETP vs. bed superficial velocity) for both columns.

(a) Mass balance inside particle:

$$\frac{\partial^2 q_i}{\partial \rho^2} + \frac{2}{\rho} \cdot \frac{\partial q_i}{\partial \rho} = \alpha \cdot \frac{\partial q_i}{\partial \theta} \tag{1}$$

with boundary and initial conditions

$$\rho = 0 \qquad \frac{\partial q_i}{\partial \rho} = 0 \qquad \forall \theta \tag{1a}$$

$$\rho = 1 \qquad q_i = q_i^* \qquad \forall \theta \tag{1b}$$

$$\theta = 0 \qquad q_i = 0 \qquad \forall \rho \tag{1c}$$

(b) Adsorption equilibrium isotherm at the liquid–particle interface:

$$q_i^* = mc_i \tag{2}$$

(c) Mass balance in a bed volume element:

$$\frac{1}{Pe} \cdot \frac{\partial^2 c_i}{\partial x^2} - \frac{\partial c_i}{\partial x} - \left(\frac{\partial c_i}{\partial \theta} + \frac{1-\varepsilon}{\varepsilon} \cdot \frac{\partial \langle q_i \rangle}{\partial \theta} \right) = 0 \tag{3}$$

with boundary and initial conditions

$$x = 0 \qquad c_i = M\,\delta(\theta) \qquad \forall\theta \tag{3a}$$

$$x \to \infty \qquad c_i \text{ limited} \qquad \forall\theta$$

$$\text{(open to diffusion boundary)} \tag{3b}$$

$$\theta = 0 \qquad c_i = 0 \qquad \forall x \tag{3c}$$

In these equations $x = z/L$ is the reduced axial coordinate, $\rho = r/R_p$ is the reduced particle coordinate, $\theta = t/\tau$ is time reduced by the space time $\tau = \varepsilon L/u_0$, ε is the bed porosity, c_i is the concentration in the bulk fluid phase, q_i is the adsorbed concentration in the particle, q_i^* is the adsorbed concentration in equilibrium with c_i, $\langle q_i \rangle$ is the average adsorbed particle concentration and M is the area of the pulse injected into the column. The model parameters are as follows:

$Pe = \dfrac{u_0 L}{\varepsilon D_{ax}}$ Peclet number, ratio of bulk convective and diffusive fluxes;

$\alpha = \dfrac{\tau_d}{\tau}$ ratio of diffusion time constant and space time;

space time;

$k' = \dfrac{1-\varepsilon}{\varepsilon} \cdot m$ adsorption capacity factor;

where $\tau_d = R_p^2/\mathscr{D}_h$ is the time constant for intraparticle diffusion.

2.5. Transfer function of the fixed bed

The transfer function $G(s)$ of the fixed bed is obtained by solving the resulting system of PDEs with Laplace transformation, i.e.,

$$G(s) = \exp\left\{\frac{Pe}{2} \cdot \left[1 - \sqrt{1 + \frac{4N(s)}{Pe}}\right]\right\} \tag{4}$$

where

$$N(s) = s[1 + k'M(s)] \tag{5}$$

and

$$M(s) = \frac{3}{\sqrt{\alpha s}} \cdot \left(\frac{1}{\tanh\sqrt{\alpha s}} - \frac{1}{\alpha s}\right) \tag{6}$$

2.6. Moments of the impulse response

The moments of the impulse response are obtained from the Van der Laan relationship:

$$\mu_n = (-1)^n \left.\frac{\partial^n G(s)}{\partial s^n}\right|_{s=0} \tag{7}$$

and so

$$\mu_1 = 1 + k' \tag{7a}$$

$$\mu_2 = \frac{2}{15} \cdot k'\alpha + \left(1 + \frac{2}{Pe}\right) \cdot (1 + k')^2 \tag{7b}$$

The mean of the peak is located at a time equal to $\mu_1\tau$. The variance $\sigma^2 = \mu_2 - \mu_1^2$ measures the contribution of all dispersive phenomena and is given by

$$\sigma^2 = \frac{2}{Pe}(1 + k')^2 + \frac{2}{15} \cdot k'\alpha \tag{7c}$$

The HETP is

$$\text{HETP} = \frac{\sigma^2 L}{\mu_1^2} = \frac{2L}{Pe} + \frac{2}{15} \cdot \frac{k'\alpha L}{(1 + k')^2} \tag{8}$$

or as a function of the superficial velocity u_0

$$\text{HETP} = \frac{2\varepsilon D_{ax}}{u_0} + \frac{2}{15} \cdot \frac{k'}{\varepsilon} \frac{\tau_d}{(1 + k')^2} \cdot u_0 \tag{8a}$$

2.7. Analysing results

Experimental results with the (+)-isomer in columns A and B are summarized in Tables 1 and 2, respectively.

From Table 1 we obtain the slope of the adsorption equilibrium isotherm of the (+)-iso-

Table 1
Elution chromatography: experimental results with column A (laboratory packed)

Q (ml/min)	$\tau\mu_{1,exp}$ (min)	$\tau^2\sigma^2_{,exp}$ (min^2)	m_{exp}
0.9	6.93	0.17	1.83
0.7	8.89	0.24	1.83
0.5	12.46	0.36	1.83
0.3	20.73	0.70	1.83
0.1	62.77	3.19	1.85

$\varepsilon = 0.4$; column volume = 4.15 ml.

Table 2
Elution chromatography: experimental results with column B (Merck)

Q (ml/min)	$\tau\mu_{1,exp}$ (min)	$\tau^2\sigma^2_{,exp}$ (min^2)	m_{exp}
2.0	16.59	0.24	2.15
0.9	35.72	0.92	2.06
0.7	45.90	1.45	2.06
0.5	64.38	2.73	2.06
0.3	110.65	7.58	2.15

$\varepsilon = 0.4$; column volume = 19.63 ml.

mer in the linear region $m = 1.83$, in agreement with that reported by Nicoud and co-workers [5,6]. From Table 2 the average value of $m = 2.10$ from column B is around 15% higher than that obtained in column A.

Simulations of experiments in column A with the (+)-isomer alone were carried out by using fast Fourier transformation to invert the transfer function $G(s)$, Eq. 4. In these simulations we used $m(+) = 1.83$ and the molecular diffusivity $\mathcal{D}_m = 5 \cdot 10^{-6}$ cm^2/s of the (+)-isomer estimated with the Wilke–Chang correlation, where the ligand molar volume was calculated by Schroeder's method [7]. With the above value of $\mathcal{D}_m$ the Peclet number Pe was calculated by the following correlation with $\gamma_1 = 20$ and $\gamma_2 = 0.5$:

$$\frac{1}{Pe} = \frac{\varepsilon\gamma_1\mathcal{D}_m}{u_0 L} + \varepsilon\gamma_2 \cdot \frac{d_p}{L} \qquad (9)$$

Simulation and experimental results are compared in Fig. 5 using for all runs $\tau_d = 0.2525$ min or $\mathcal{D}_h = 6.6 \cdot 10^{-8}$ cm^2/s. The mean deviation in variance between the theoretical and experimental values is around 24%.

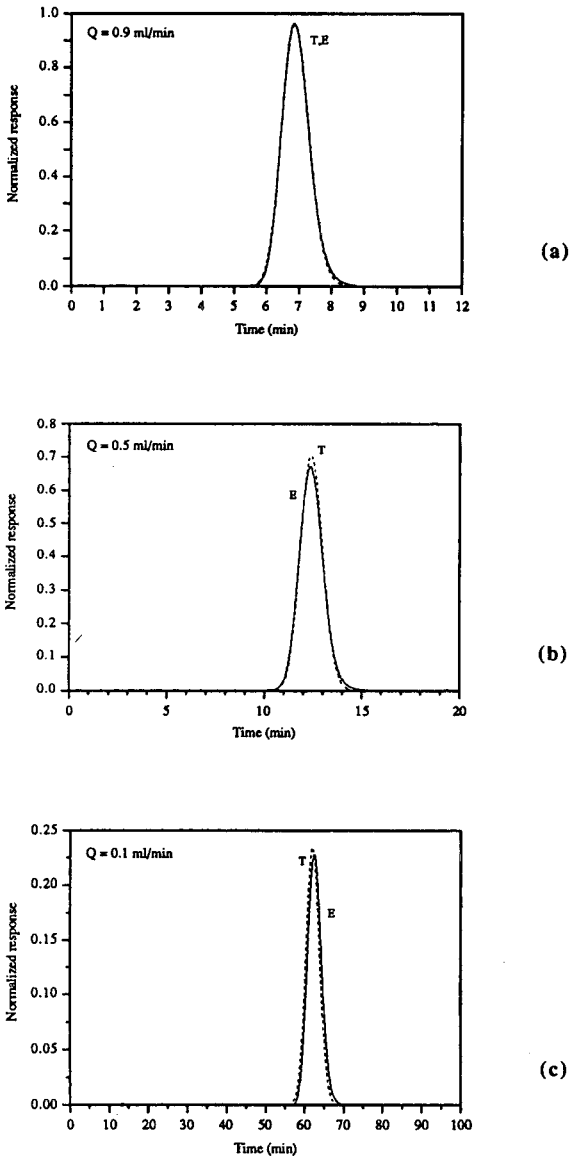

Fig. 5. Comparison between experimental (solid lines) and model (dashed lines) results for elution chromatography of the (+)-isomer with column A.

2.8. Continuous chromatography in a simulated moving bed

The SMB technology was applied to the separation of optical isomers by Negawa and Shoji [8]. The pilot-scale simulated moving bed (Licosep 12/26 [9,10]) is shown schematically in Fig. 6. It consists of twelve columns of 10×2.6 cm I.D.; the locations of the feed, extract and raffinate streams move clockwise. The rotation period is an important parameter for the operation of the SMB. The package developed for the SMB [11] considers a plug-dispersive model for bulk fluid phase flow and a linear intraparticle driving force (LDF) model for the particle equations, containing one parameter k (mass

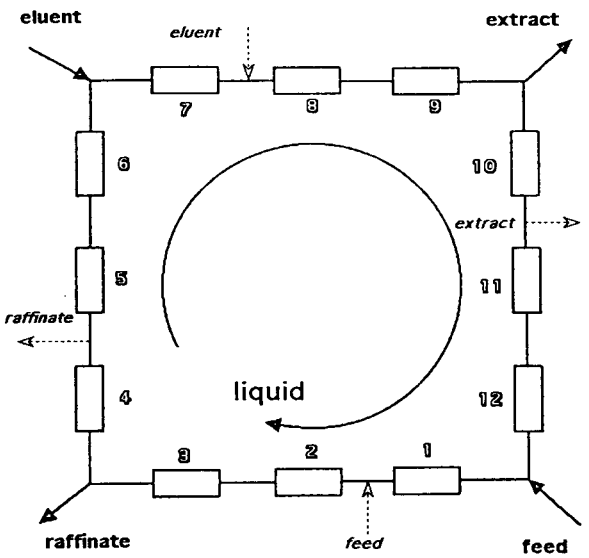

Fig. 6. Schematic representation of the Licosep simulated moving bed unit.

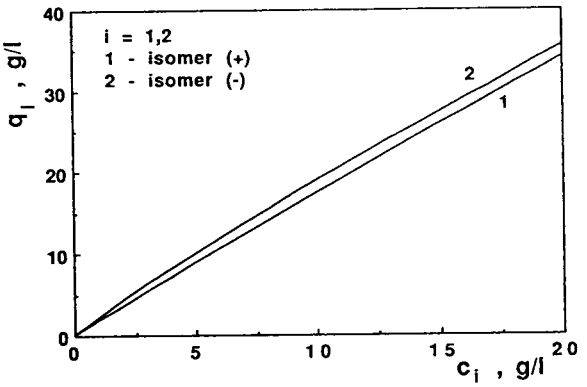

Fig. 7. Single-component adsorption equilibrium isotherms.

transfer coefficient). At this level approximations for "homogeneous" and "pore diffusion" equations can be included. For linear systems they are just linked by $1 + \xi_p$, where ξ_p is the particle capacity factor.

For packings containing large pores where intraparticle convection occurs the LDF still holds provided we consider the augmented mass transfer coefficient $\tilde{k} = k/f(\lambda)$, where [12]

$$f(\lambda) = \frac{3}{\lambda}\left(\frac{1}{\tanh \lambda} - \frac{1}{\lambda}\right)$$

and $\lambda = v_0 R_p / 3De$ is the intraparticle Peclet number.

The multi-component adsorption equilibrium isotherm was calculated from the single isotherms shown in Fig. 7 by using the ideal adsorbed solution (IAS) model [13,14], which leads to the results shown in Fig. 8.

Single adsorption isotherms of isomers on TCA are given by a linear + Langmuir equation:

$$q_i^0 = mc_i^0 + \frac{Qb_i c_i^0}{1 + b_i c_i^0} \qquad (10)$$

where the superscript zero refers to single-component adsorption, Q is the maximum langmuirian adsorbed concentration, equal for both isomers, and b_i are the respective Langmuir adsorption constants.

The prediction of multi-component equilib-

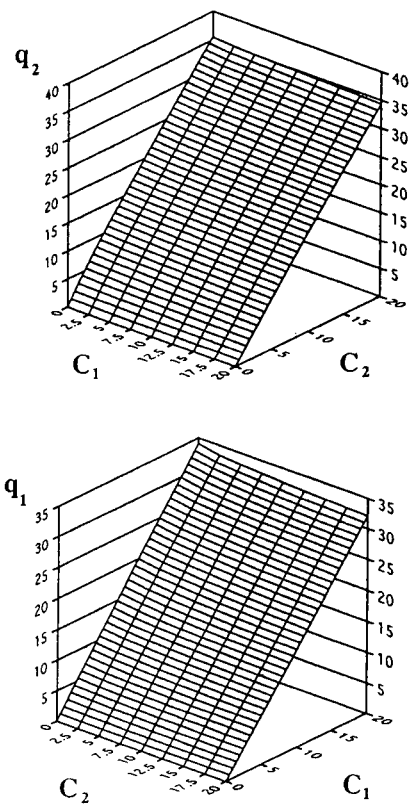

Fig. 8. Multi-component adsorption equilibrium isotherms for both enantiomers predicted by the IAS model.

rium with the IAS model involves iterative calculation with the following system of equations:

$$c_i = c_i^0(\pi_i, T)z_i \tag{11}$$

$$q_i^* = \frac{z_i}{\sum_{i=1}^{N} z_i/q_i^0} \tag{12}$$

$$\pi_i = \frac{\mathcal{R}T}{\sigma}\int_0^{c_i^0} \frac{q_i^0}{c_i^0}\,dc_i^0 \tag{13}$$

$$\sum_{i=1}^{N} z_i = 1 \tag{14}$$

In these equations, q_i^* is the adsorbed concentration of enantiomer i in equilibrium with c_i in the mixture, and q_i^0 and c_i^0, related by Eq. 10, are the respective concentrations in a corresponding (same modified spreading pressure) single-component system, z_i is the surface coverage mole fraction of component i, π_i is the spreading pressure of isomer i on the surface, σ is the surface area per unit weight of adsorbent, T is the absolute temperature and $\mathcal{R}$ is the perfect gas constant.

Simulated results for the SMB for the set of parameters shown in Table 3 are presented in Fig. 9. These results show the effect of the mass transfer coefficient k in the process performance. It is clearly seen that purity of the isomers recovered in the extract and raffinate streams increases with k. Therefore, in packings where intraparticle convection is important we expect a better performance for a given system operating under given conditions.

Table 3
Values of the parameters used in simulations of the SMB

Eluent flow-rate (ml/min)	4.53
Raffinate flow-rate (ml/min)	2.05
Extract flow-rate (ml/min)	4.00
Feed (ml/min)	1.52
Recycle flow-rate (ml/min)	20.35
Rotation period (s)	260
Feed concentrations of A and B (g/l)	5
Mass transfer coefficient k (s^{-1})	0.05–0.2

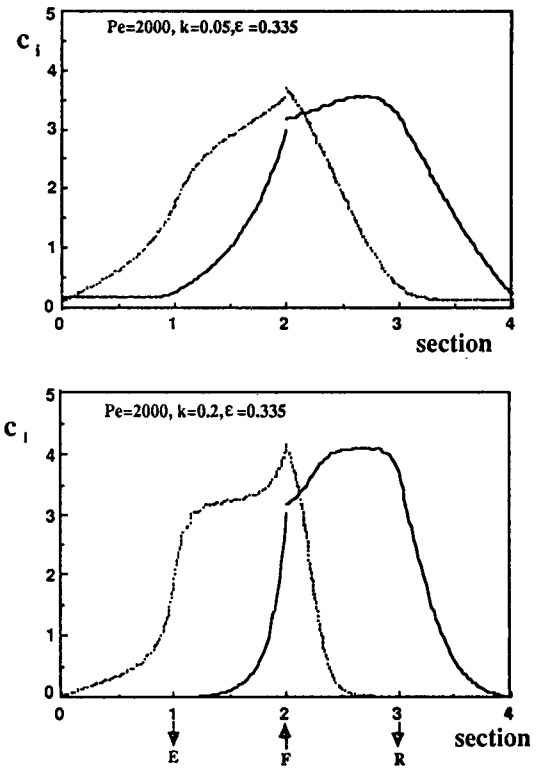

Fig. 9. Effect of the mass transfer coefficient k on the cyclic steady-state concentration profiles in an SMB unit.

3. Conclusions

We have considered the methodology for characterization of packings used in the chromatographic separation of optical isomers. Equilibrium and kinetic parameters (effective diffusivity) were obtained from laboratory elution chromatographic experiments.

From single-component adsorption equilibrium isotherms, multi-component equilibrium data were calculated based on the ideal adsorbed solution (IAS) model.

A model of the simulated moving bed (SMB) allowed the understanding of its operation; the effect of the mass transfer coefficient k on the performance of the system was studied; it has been shown that with increasing k (reducing intraparticle resistances), the performance improves.

Acknowledgements

The European Community under the BRITE-EURAM Programme (Contract no. BRE2-CT92-0337) is thanked for financial support and the staff of Separex for helpful discussions.

Symbols

c_i	fluid phase concentration of component i
c_i^0	fluid phase concentration of component i in a single-component system
d_p	particle diameter
D_{ax}	axial dispersion coefficient
D_e	effective diffusivity
$\mathscr{D}_h$	intraparticle diffusivity
$\mathscr{D}_m$	molecular diffusivity
k	mass transfer coefficient
$\tilde{k}$	augmented (by intraparticle convection) mass transfer coefficient
k'	column adsorption capacity factor
L	column length
m	slope of the linear adsorption isotherm
M	area of the injected pulse
Pe	bed Peclet number
q_i	adsorbed (solid-phase) concentration of component i
q_i^0	adsorbed concentration of species i in equilibrium with c_i^0 in a single-component system
q_i^*	adsorbed concentration of species i in equilibrium with c_i
$\langle q_i \rangle$	average adsorbed concentration of species i
r	particle coordinate
$\mathscr{R}$	perfect gas constant
R_p	particle radius
T	absolute temperature
u_0	bed superficial velocity
v_0	intraparticle superficial velocity
x	reduced axial coordinate in column
z	axial coordinate in column
z_i	surface coverage mole fraction of component i

Greek symbols

α	ratio of diffusion time constant and space time
$\delta(\theta)$	Dirac delta function
ε	bed porosity
γ_1, γ_2	parameters in the correlation for Pe
λ	intraparticle Peclet number
μ_n	moment of order n of the impulse response
π_i	spreading pressure of component i on the adsorbent surface
θ	time reduced by space time
ρ	reduced particle coordinate
σ	surface area per unit mass of adsorbent
σ^2	variance of the chromatographic peak
τ	space time
τ_d	diffusion time constant
ξ_p	particle capacity factor

References

[1] R. Sheldon, *Chirotechnology*, Marcel Dekker, New York, 1983.
[2] D. Broughton, *US Pat.*, 2 985 589 (1961).
[3] J. Dingenen, I. Somers, F. Pavwels and A. Van Loon, in M. Perrut (Editor), *Proceedings of the 9th International Symposium on Preparative and Industrial Chromatography*, Société Française de Chimie, Paris, 1992.
[4] R.M. Nicoud, *LC·GC Int.*, 6 (1993) 636–637.
[5] R.M. Nicoud, G. Fuchs, E. Küsters, R. Reuille and E. Schmid, presented at the *3rd International Symposium on Chiral Discrimination*, Tübingen, 5–8 October, 1992.
[6] G. Fuchs, R.M. Nicoud and M. Bailly, in M. Perrut (Editor), *Proceedings of the 9th International Symposium on Preparative and Industrial Chromatography*, Société Française de Chimie, Paris, 1992.
[7] R.C. Reid, J.M. Prausnitz and B.E. Poling, *The Properties of Gases and Liquids*, McGraw-Hill, New York, 4th ed., 1987.
[8] M. Negawa and F. Shoji, *J. Chromatogr.*, 590 (1992) 113–117.
[9] R.M. Nicoud, *LC·GC Int.*, 5 (1992) 43–47.
[10] B. Balannec and G. Hottier, in G. Ganetsos and P. Barker (Editors), *Preparative and Production Scale Chromatography*, Marcel Dekker, New York, 1992.
[11] A.E. Rodrigues, Z.P. Lu, J.M. Loureiro and L.S. Pais, in preparation.
[12] A.E. Rodrigues, B. Ahn and A. Zoulalian, *AIChE J.*, 28 (1982) 541.
[13] A. Myers and J. Prausnitz, *AIChE J.*, 11 (1965) 121.
[14] D. Frey and A.E. Rodrigues, *AIChE J.*, 40 (1994) 182.

ELSEVIER

Journal of Chromatography A, 702 (1995) 233–241

JOURNAL OF CHROMATOGRAPHY A

Preparative separation of taxol in normal- and reversed-phase operations

Dauh-Rurng Wu*, Klaus Lohse, Hellen C. Greenblatt

BTR Separations, Concord Plaza, Quillen Building, 3411 Silverside Road, Wilmington, DE 19810, USA

Abstract

A method is described that separates taxane compounds from crude extracts under either reversed- or normal-phase conditions using a Zorbax-based bonded material, "SW-Taxane". A crude plant extract of *Taxus canadensis* and five standard taxane compounds were separated. The method provides high selectivity and recoveries of compounds from a taxol extract in the isocratic mode. Under normal-phase conditions, the packing material has shown significantly greater selectivity of taxol-related compounds than bare silica and most other commercially available silica-based bonded materials. Reversed-phase separations on the column, are also superior compared to typical C_8 separations. In addition, a loading study demonstrates that this phase has a high taxol saturation capacity due to its large surface area.

1. Introduction

Taxol has gained increased significance as a chemotherapeutic drug in the fight against cancer and is in great demand. Taxol may be isolated from plant extracts such as bark and regenerable parts of yews such as *Taxus brevifolia* [1,2] or *Taxus canadensis*. Plant tissue cultures [3,4], and partial or complete synthesis [5], are also being explored as alternative sources of these potential drugs with increased yields.

Chromatographic methods have been developed to detect and isolate taxanes from the above sources on analytical and semi-preparative basis [6–11]. Frequently, they use reversed-phase C_{18} and other bonded phases in gradient elution modes. These procedures suffer from insufficient selectivity among closely eluting taxanes. Additionally, the low solubility of taxanes in aqueous solutions often results in increased column back-pressure, caused by precipitation of products in the crude sample.

In order to purify a large quantity of various compounds, preparative high-performance liquid chromatography (HPLC) is usually operated under the mass-overload condition. A considerable amount of literature on preparative HPLC in elution has been published by Knox and Pyper [12], Snyder and co-workers [13–18], as well as Guiochon and co-workers [19–25] in the past years. These studies have suggested that the rate of production of a purified product (i.e. throughput) in preparative HPLC can be significantly enhanced under the overload condition. Maximization of throughput can be achieved by optimizing separation conditions [26], column variables [27] and sample sizes [19,28]. It is also shown that the saturation capacities of solutes

* Corresponding author.

0021-9673/95/$09.50 © 1995 Elsevier Science B.V. All rights reserved
SSDI 0021-9673(95)00012-7

and their isotherms have an important influence on throughput in the preparative HPLC [29,30].

In this paper, we report a method for preparative purification of taxol using either normal- or reversed-phase systems in isocratic elution. In normal phase, a preparative separation of taxol under the overload condition was conducted where high alcohol concentrations were used to increase sample solubility. Loading studies were conducted to determine the saturation capacity of taxol using this method and column.

2. Experimental

2.1. Materials

Columns (25 × 0.46 cm) packed with Impaq 1010C8 (100 Å, 10 μm, C_8), 1010Si (100 Å, 10 μm, bare silica), and Zorbax "SW-Taxane" (60 Å, 10-μm silica particles, bonded with a proprietary phase) were from BTR Separations (Wilmington, DE, USA). Alkyl phenyl (60 Å, 10 μm) and pentafluorophenyl (PFP, 60 Å, 10 μm) columns (25 × 0.46 cm) were purchased from ES Industries (Berlin, NJ, USA). Taxol was obtained from Sigma (St. Louis, MO, USA). 10-Deacetylbaccatin III (10DAB), baccatin III (BIII), and 7-*epi*-taxol were from Hauser Chemical Research (Boulder, CO, USA). Hexane, ethanol, isopropanol and methanol were from EM Science (Gibbstown, NJ, USA). Heptane was from Fisher Scientific (Malvern, PA, USA). The series 410 LC pump, LC-95 UV–Vis detector, and Nelson 2700 chromatography software were purchased from Perkin-Elmer (Cupertino, CA, USA). A 7125 injector from Rheodyne (Cotati, CA, USA) was used for sample injection. We thank Biolyse (Port Daniel, Canada) for *T. canadensis* crude plant extract, which was prepared by methanol extraction and further by dichloromethane–water extraction as described in [31].

2.2. Methods

The dimensions of all the columns were 25 × 0.46 cm; no guard columns were used in this work. Unless stated otherwise, column effluents were monitored at a 227 nm wavelength; mobile phase flow-rate was 1 ml/min, and the columns were maintained at ambient temperature.

2.3. Comparison between SW-Taxane and other bonded phases

A 2–3-μl sample of 0.2–0.3 mg/ml per compound was injected into each column for comparison experiments. Separations of 10DAB, BIII, cephalomannine, taxol and 7-*epi*-taxol on Zorbax SW-Taxane, alkyl phenyl and PFP columns were conducted in normal phase at a flow-rate of 0.5 ml/min. For the Zorbax SW-Taxane, alkyl phenyl and PFP columns, the mobile phases were heptane–ethanol (50:50), heptane–ethanol (96:4) and heptane–ethanol (93:7), respectively. Separation of these five taxane standards on this medium was also carried out in the reversed-phase mode utilizing a methanol–water (60:40) mobile phase.

Separations of cephalomannine and taxol on Zorbax SW-Taxane were compared with C_8 in reversed phase, and with bare silica in normal phase. In reversed phase, the mobile phase was methanol–water (65:35). In normal phase, the mobile phase was heptane–isopropanol (60:40) for the Zorbax SW-Taxane column, and hexane–ethanol (90:10) for the bare silica column.

2.4. Purification of a crude plant extract of T. canadensis

Separations of crude plant extract on Zorbax SW-Taxane were carried out in both reversed and normal phases. In reversed phase, a 2-μl sample of 10 mg/ml (20 μg) was injected onto the column and the mobile phase was methanol–water (60:40). In normal phase, 12.5 mg of crude plant extract dissolved in 1 ml of mobile phase was loaded onto the column. In this preparative separation, the mobile phase was heptane–ethanol (75:25), with a flow-rate of 0.7 ml/min. The effluent was monitored at a wavelength of 260 nm. The fractions were collected every 30 s during the time interval 32–40.5 min. These

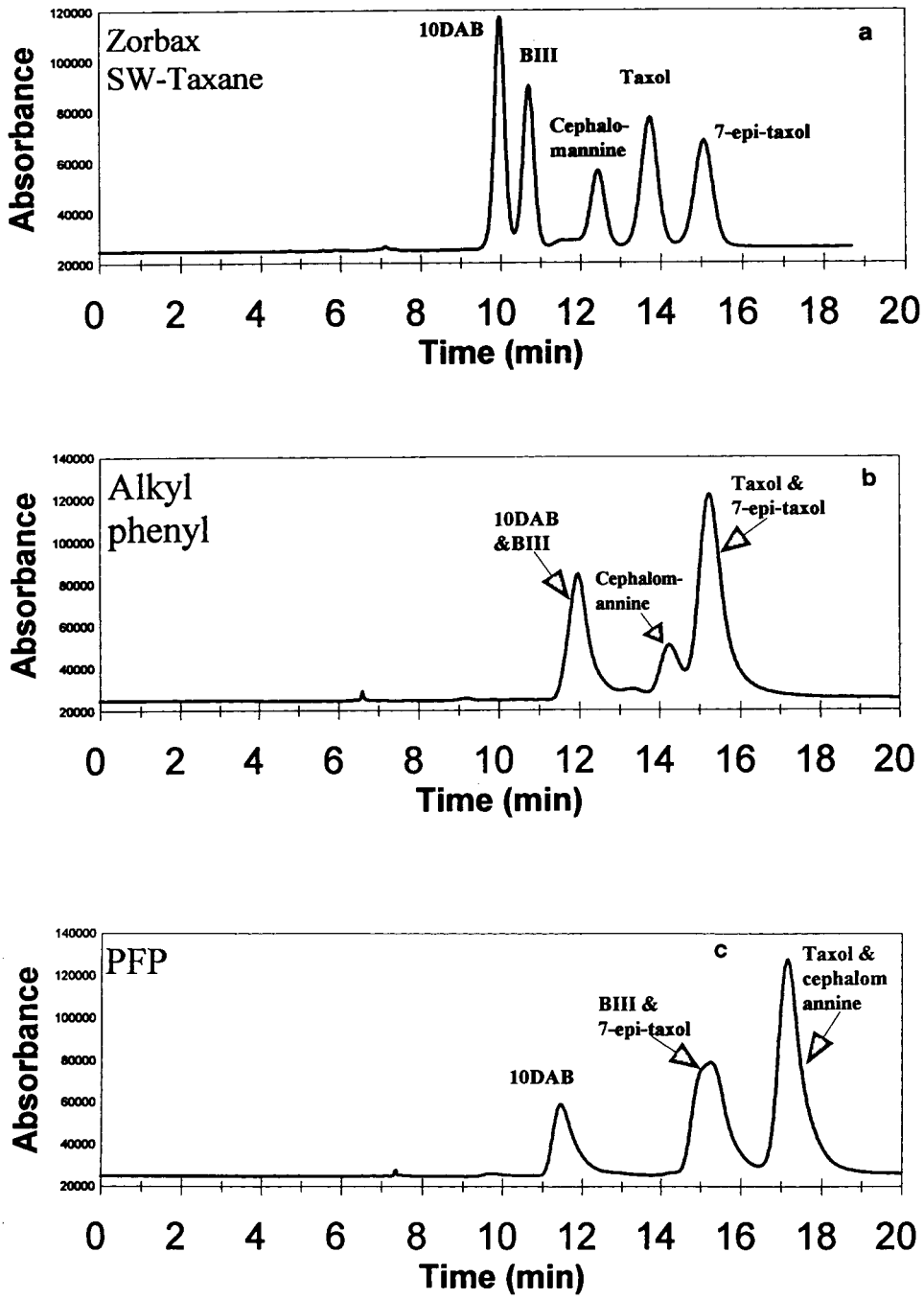

Fig. 1. Separation of a mixture of five standard taxanes containing 10DAB, BIII, cephalomannine, taxol and 7-*epi*-taxol in normal phase using (a) Zorbax SW- Taxane, mobile phase heptane–ethanol (50:50); (b) alkyl phenyl, mobile phase heptane–ethanol (96:4); (c) PFP, mobile phase heptane–ethanol (93:7). Column dimensions: 25 × 0.46 cm; sample concentration: 0.2–0.3 mg/ml per compound; sample volume: 2–3 μl; flow-rate: 0.5 ml/min; wavelength: 227 nm.

fractions were analyzed by re-injection into the column under reversed-phase conditions.

2.5. Column capacity study

Solutions of taxol and BIII were prepared at two concentrations (0.5 and 25 mg/ml for each compound). The mixtures were injected onto a column packed with Zorbax SW-Taxane at sample loadings of each compound from 2.5 μg to 1 mg and monitored at a wavelength of 270 nm. In normal phase, the mobile phase was heptane–ethanol (50:50). In reversed phase the mobile phase was methanol–water (70:30). The saturation capacity of taxol was calculated by [32,33]:

$$W_s = (3/8) \cdot [N_0 N/(N_0 - N)] \cdot [k_0'/(1 + k_0')]^2 W_x$$

where W_x, W_s, N_0, N and k_0' are sample load, saturation capacity, column efficiency at analytical loading, column efficiency at the sample load, and capacity factor at analytical loading, respectively.

3. Results and discussion

3.1. Comparison between SW-Taxane and other bonded phases

Fig. 1 presents separations of five standard taxanes on SW-Taxane, alkyl phenyl and PFP columns in normal phase. The method using the SW-Taxane column demonstrates a baseline resolution at high alcohol (i.e., ethanol) concentrations. In preparative taxol purification, high alcohol concentration is necessary to increase the solubility of the taxol components and to enhance the throughput of the process. Additionally, use of high alcohol concentrations decreases the likelihood of precipitation which often results in increased back-pressures and shortened column lifetime. All three columns performed equally well under reversed-phase conditions. Results of separations on Zorbax SW-Taxane phase are shown in Fig. 2. In addition, separation of cephalomannine and taxol on SW-Taxane was compared with that on bare silica and C_8. The Zorbax SW-Taxane results in a better

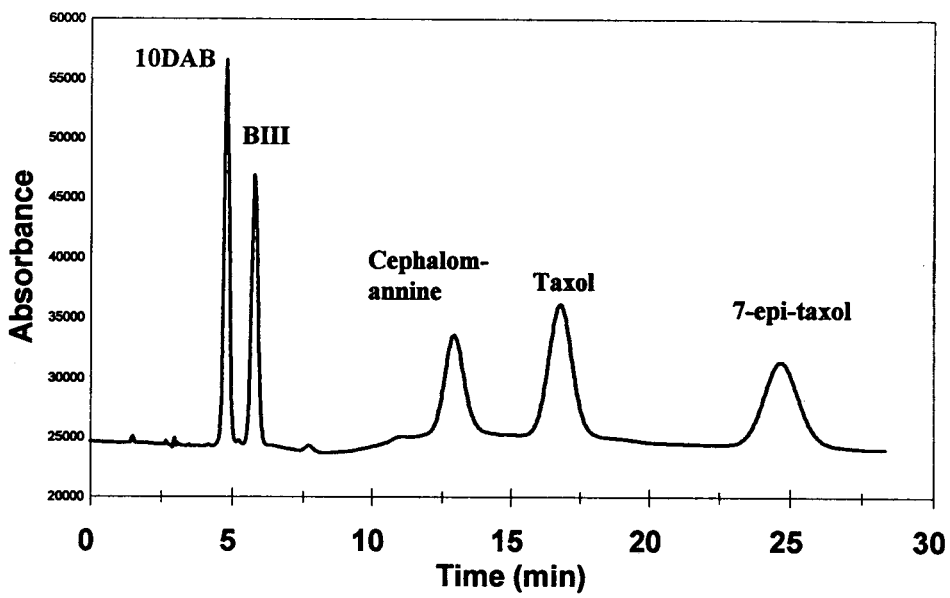

Fig. 2. Separation of a mixture of five standard taxanes containing 10DAB, BIII, cephalomannine, taxol and 7-*epi*-taxol in reversed phase using Zorbax SW-Taxane. Mobile phase: methanol–water (60:40); flow-rate: 1 ml/min. Other conditions as in Fig. 1.

resolution between cephalomannine and taxol than bare silica in normal phase (Fig. 3), and C_8 in reversed phase (figure not shown).

3.2. Purification of a crude plant extract of T. canadensis

Separation of taxol from crude extract of *T. canadensis* in reversed phase is especially useful for those interested in analytical studies (Fig. 4). However, for preparative purification, the normal-phase mode has definite advantages over reversed phase. Some of these are: use of solvents with low viscosity, high flow-rate (i.e., throughput), and simpler recovery of the products. Fig. 5 shows a normal-phase, preparative taxol purification loading 12.5 mg of crude extract of *T. canadensis* on a SW-Taxane column.

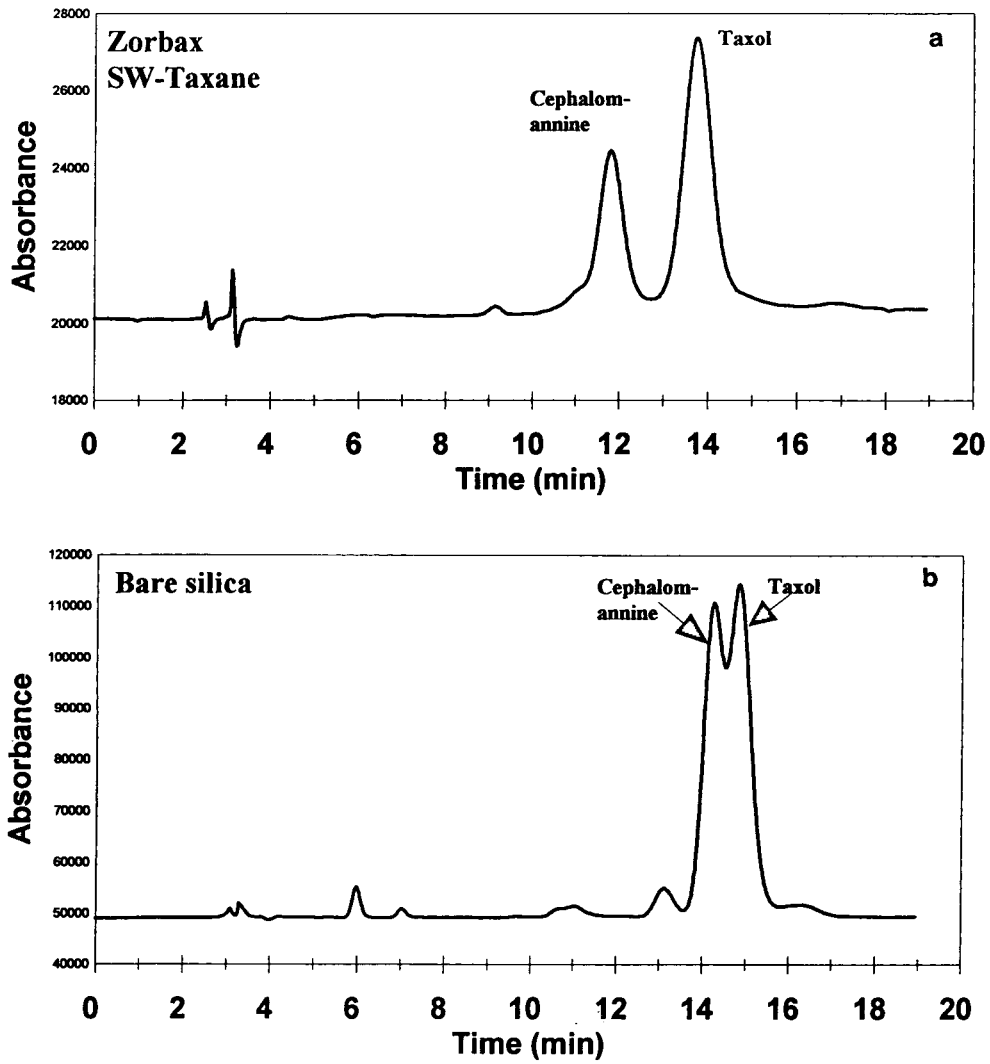

Fig. 3. Comparison of separation of cephalomannine and taxol in normal phase using (a) Zorbax SW-Taxane (mobile phase heptane–isopropanol, 60:40), and (b) bare silica (mobile phase hexane–ethanol, 90:10). Flow-rate: 1 ml/min. Other conditions as in Fig. 1.

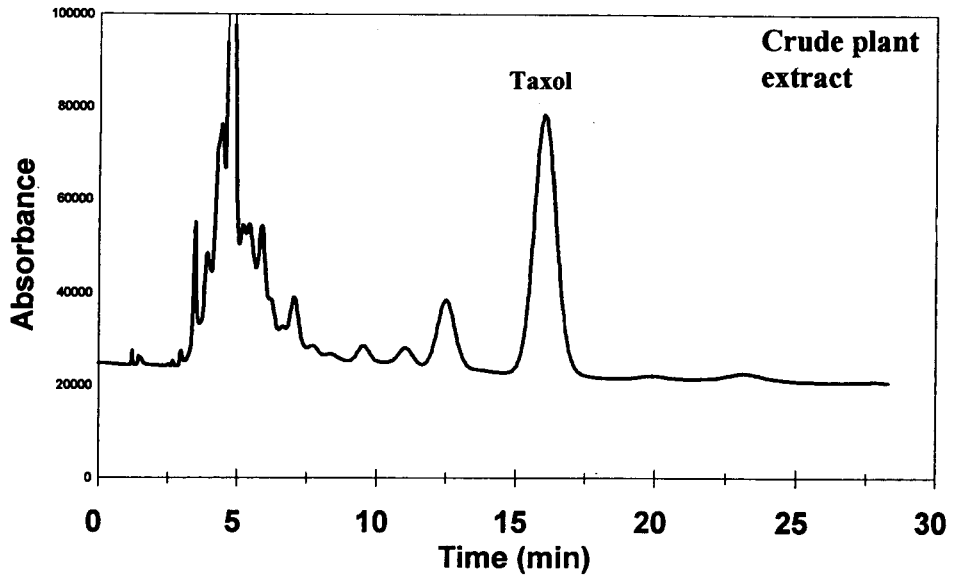

Fig. 4. Separation of taxol from crude plant extract of *T. canadensis* in reversed phase using Zorbax SW-Taxane. Mobile phase: methanol–water (60:40); flow-rate: 1 ml/min; sample concentration: 10 mg/ml. Other conditions given in the Experimental section.

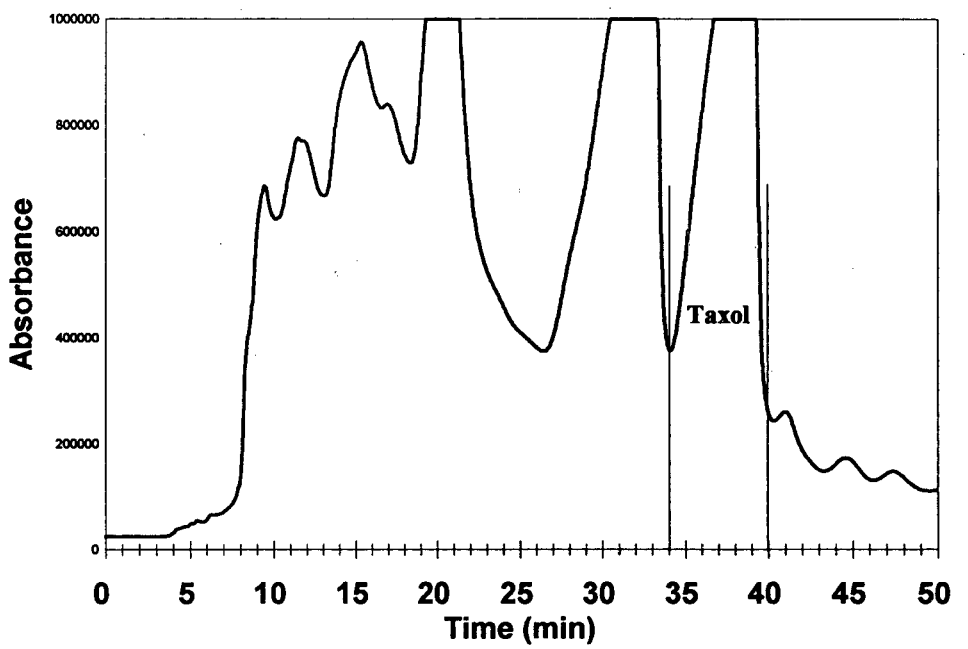

Fig. 5. Preparative separation of taxol from crude plant extract of *T. canadensis* in normal phase using Zorbax SW-Taxane. Mobile phase: heptane–ethanol (75:25); sample concentration: 12.5 mg/ml; sample volume: 1 ml; flow-rate: 0.7 ml/min; wavelength: 260 nm. Other conditions given in the Experimental section.

The rear part of the taxol peak is steeper than the front part, which indicates taxol follows non-Langmuir isotherms (e.g., S-shape). The taxol fractions were collected and analyzed (Fig. 6). These pooled taxol fractions (from 34 to 40.5 min) having a purity of about 98% (due to trace amounts of 7-*epi*-taxol), are free of cephalomannine. The recovery of taxol is greater than 90%. Practically speaking, a two-step process may be more practical for purification of crude extracts: partial purification by C_8 or bare silica, and then final polishing step using the methods outlined above.

3.3. Column capacity study

Saturation capacity (W_s) is the maximum mass of solute that can be taken up by the stationary phase when all the active sites of the absorbent surface are covered by a monolayer of solute molecules (Langmuir adsorption). The value of W_s, increasing with the higher surface area of the stationary phase, can be obtained either from isotherm data or from elution profiles under overload conditions [32,33]. Actual values of W_s per unit surface area can vary widely from 0.02 to 0.6 mg/m^2 for small molecules [29-30,34]. For adsorption in a flat configuration, the value of W_s per unit surface area is estimated to be 0.3 to 0.4 mg/m^2 [29,30]. Fig. 7 shows separation of taxol and BIII in normal phase at sample loadings ranging from 2.5 μg to 1 mg of each compound. The capacity factors (k') and plate counts for analytical and overload conditions are calculated. Based on the formula in the experimental section, the saturation capacities of taxol and BIII are 323 and 350 mg, respectively. With the total surface area of 977 m^2 in the column (2.9 g of packing material with 336 m^2/g), saturation capacities of taxol and BIII per unit surface area are 0.33 and 0.36 mg/m^2, respectively, which are in good agreement with the literature data cited above. The high level of saturation capacity achievable, is due to the large surface area of Zorbax 60 Å. This characteristic is desired in preparative purification in order to obtain a high throughput. Taxol saturation capacity in the reversed phase is calculated to be 295 mg (following the same procedure as in the normal phase), corresponding to 0.3 mg/m^2.

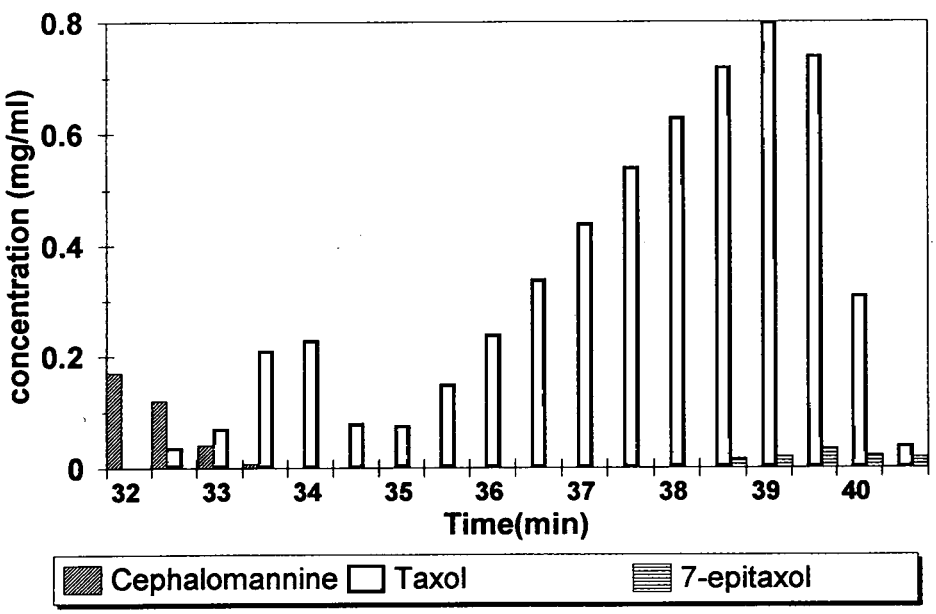

Fig. 6. Analysis of chromatogram of the taxol fractions collected from run represented in Fig. 5.

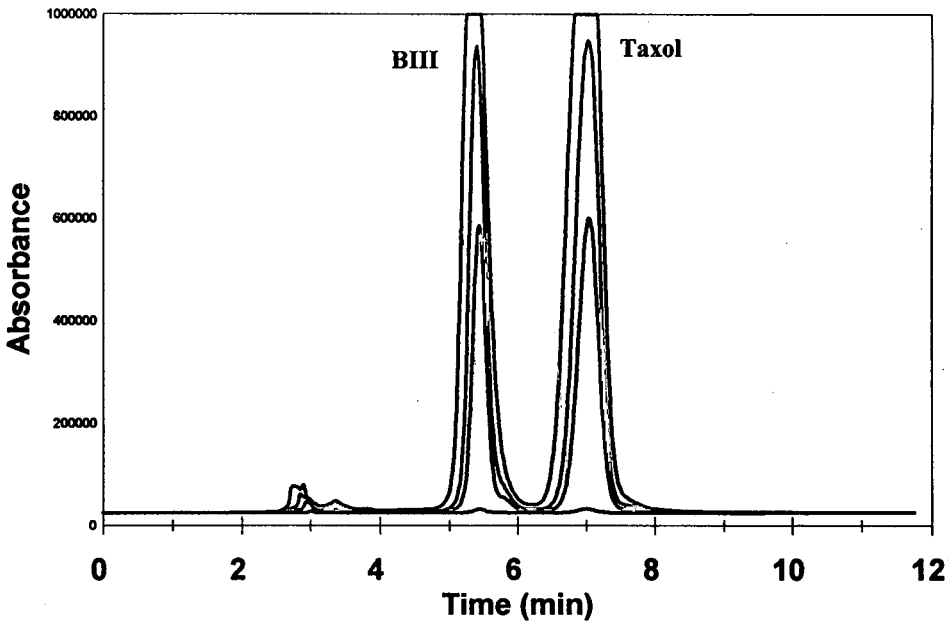

Fig. 7. Elution of a mixture of BIII and taxol at sample loadings of 2.5 μg to 1 mg of each compound in normal phase using Zorbax SW-Taxane. Mobile phase: heptane–ethanol (50:50); flow-rate: 1 ml/min; wavelength: 270 nm. Other conditions given in the Experimental section.

4. Conclusions

A method has been developed for preparative separation and purification of taxane compounds from crude extract using the Zorbax SW-Taxane in isocratic elution. Rapid separation with high selectivity is assured in either reversed or normal phase. The process works well at high alcohol concentrations. The increased solubility of the taxane compounds at high alcohol concentrations leads to a greater throughput. Zorbax SW-Taxane offers a large surface area and therefore a high taxol saturation capacity.

References

[1] S.D. Harvey, J.A. Campbell, R.G. Kelsey and N.C. Vance, *J. Chromatogr.*, 587 (1991) 300.
[2] N. Vidensk, P. Lim, A. Campbell and C. Carlson, *J. Nat. Prod.*, 53 (1990) 1609.
[3] D.M. Gibson, A.A. Christen and R.E.B. Ketchum, *Plant Physiol.*, 96S (1991) 96.
[4] A.A. Christen, J. Bland and D.M. Gibson, *Proc. Am. Ass. Cancer Res.*, 30 (1989) 566.
[5] R.A. Holton, *J. Am. Chem. Soc.*, 106 (1984) 5731.
[6] J.H. Cardellina, *J. Liq. Chromatogr.*, 14 (1991) 659.
[7] R.E.B. Ketchum and D.M. Gibson, *J. Liq. Chromatogr.*, 16 (1993) 2519.
[8] S.L. Richheimer, D.M. Tinnermeier and D.W. Timmons, *Anal. Chem.*, 64 (1992) 2323.
[9] S.O.K. Auriola, A.-M. Lepisto and T. Naaranlahti, *J. Chromatogr.*, 594 (1992) 153.
[10] K.M. Witherup, S.A. Look, M.W. Stasko, T.G. McCloud, H.J. Issaq and G.M. Muschik, *J. Liq. Chromatogr.*, 12 (1989) 2117.
[11] K.M. Witherup, S.A. Look, M.W. Stasko, T.J. Ghiorzi, G.M. Muschik and G.M. Cragg, *J. Nat. Prod.*, 53 (1990) 1249.
[12] J.H. Knox and H.M. Pyper, *J. Chromatogr.*, 363 (1986) 1.
[13] J.E. Eble, R.L. Grob, P.E. Antle and L.R. Snyder, *J. Chromatogr.*, 384 (1987) 25.
[14] J.E. Eble, R.L. Grob, P.E. Antle and L.R. Snyder, *J. Chromatogr.*, 405 (1987) 1.
[15] J.E. Eble, R.L. Grob, P.E. Antle, G.B. Cox and L.R. Snyder, *J. Chromatogr.*, 405 (1987) 31.
[16] G.B. Cox, L.R. Snyder and J.W. Dolan, *J. Chromatogr.*, 484 (1989) 409.
[17] L.R. Snyder, J.W. Dolan, D.C. Lommen and G.B. Cox, *J. Chromatogr.*, 484 (1989) 425.

[18] L.R. Snyder, J.W. Dolan and G.B. Cox, *J. Chromatogr.*, 484 (1989) 437.
[19] S. Ghodbane and G. Guiochon, *J. Chromatogr.*, 452 (1988) 209.
[20] S. Golshan-Shirazi and G. Guiochon, *J. Chromatogr.*, 461 (1989) 1.
[21] S. Golshan-Shirazi and G. Guiochon, *Anal. Chem.*, 61 (1989) 1276.
[22] S. Golshan-Shirazi and G. Guiochon, *Anal. Chem.*, 61 (1989) 1368.
[23] B. Lin, Z. Ma, S. Golshan-Shirazi and G. Guiochon, *J. Chromatogr.*, 500 (1990) 185.
[24] S. Golshan-Shirazi and G. Guiochon, *J. Chromatogr.*, 517 (1990) 229.
[25] S. Golshan-Shirazi and G. Guiochon, *J. Chromatogr. A*, 658 (1994) 149.
[26] L.R. Snyder, J.W. Dolan and G.B. Cox, *J. Chromatogr.*, 483 (1989) 63.
[27] L.R. Snyder and G.B. Cox, *J. Chromatogr.*, 483 (1989) 85.
[28] S. Ghodbane and G. Guiochon, *J. Chromatogr.*, 450 (1988) 27.
[29] J.E. Eble, R.L. Grob, P.E. Antle and L.R. Snyder, *J. Chromatogr.*, 384 (1987) 45.
[30] G.B. Cox and L.R. Snyder, *J. Chromatogr.*, 483 (1989) 95.
[31] P.K.S. Blay, P. Thibault, N. Thiberge, B. Kiecken, A. Lebrun and C. Mercure, *Rapid Commun. Mass Spectrom.*, 7 (1993) 626.
[32] L.R. Snyder, J. Dolan, P.E. Antle and G.B. Cox, *Chromatographia*, 24 (1987) 82.
[33] G.B. Cox, *Industrial Chromatography News*, No. 3, Prochrom, Champigneulles, 1991, p. 5.
[34] J. Jacobson, J. Frenz and Cs. Horváth, *J. Chromatogr.*, 316 (1984) 53.

ELSEVIER

Journal of Chromatography A, 702 (1995) 243–250

JOURNAL OF CHROMATOGRAPHY A

All-metal collection system for preparative-scale gas chromatography Purification of low-boiling-point compounds

Thomas J. Buckley[a,*], Keith A. Gillis[b]

[a]*Chemical Kinetics and Thermodynamics Division, Chemical Science and Technology Laboratory, National Institute of Standards and Technology, Gaithersburg, MD 20899, USA*

[b]*Thermophysics Division, Chemical Science and Technology Laboratory, National Institute of Standards and Technology, Gaithersburg, MD 20899, USA*

Abstract

We describe a purification system based on a commercial preparative-scale gas chromatograph with a custom-designed condenser, collector, and fraction handling system. In our fraction collector design, all the wetted surfaces were either 316 stainless-steel or nickel. The collectors and the integrated gas-handling manifold were designed to be used down to liquid nitrogen temperature and up to 7 MPa of pressure to accommodate low-boiling-point compounds, such as refrigerants. The design, operation, and performance of this apparatus are presented.

1. Introduction

Inconsistent or irreproducible measurements of thermophysical and chemical properties are often due to impure samples. The effects of impurities in fluids can greatly exceed imperfections in instrumentation. Along with the continued need for better measurement techniques and for better analytical instrumentation, there exists a growing need for methods of preparing ultra-pure samples. This is especially true for low-boiling-point liquids that require special handling and for liquids that form azeotropes with other production by-products, since distillation techniques are impractical in these cases.

The speed-of-sound in a gas and the vapor pressure and viscosity of liquids are examples of thermophysical properties that are sensitive to the presence of certain impurities. When highly accurate measurements of these properties are desired, the purity of the sample must be high enough that either the uncertainty due to the impurities is below the sensitivity of the technique used, or that the perturbation due to impurities is accurately calculable. It is often the case that an impurity level of 0.1%, typical of many commercially available compounds, is sufficient to dominate the uncertainty of a measurement. Even if these impurities are identified and their concentrations measured (itself a time-consuming and expensive task), the properties of the impurities may not be known with sufficient accuracy to correct the measurements.

As an example, consider that commercially available pentafluoroethane (CF_3CHF_2; designated in the refrigeration industry as R125) contains a mole fraction of 0.15% chloropentafluoroethane (designated R115). The presence

* Corresponding author.

0021-9673/95/$09.50 © 1995 Elsevier Science B.V. All rights reserved
SSDI 0021-9673(94)01140-0

of this impurity lowers the speed of sound from pure R125 by 0.02%. If not accounted for, this impurity would increase the ideal-gas heat capacity deduced from speed-of-sound data by 0.4%. This impurity-related error would be an order of magnitude larger than the errors in "routine" speed-of-sound measurements [1].

R125 has a normal boiling point of −49°C, a vapor pressure of 1445 kPa (210 p.s.i.a.) at 27°C, and it forms an azeotrope with R115 near the composition mentioned above. These properties of R125 preclude the use of glass apparatus for handling it and conventional distillation techniques for purifying it.

Minor impurities can also have a major impact in the field of chemical kinetics. The reaction rate of an impurity with a free radical, such as OH, can exceed that of the pure chemical species by orders of magnitude. A 100 ppm impurity which reacts 1000 times faster than the main component leads to a 10% error in the measured reaction rate. Methyl chloroform, CH_3CCl_3, is an important compound that is used as a standard for the lifetime of chlorofluorocarbons in the atmosphere [2,3]. In the troposphere CH_3CCl_3 is attacked by OH, then further oxidized and eventually washed out before it reaches the stratosphere where it would deplete ozone. A common impurity in methyl chloroform is the alkene CH_2CCl_2 which reacts nearly 1000 times faster with OH. Careful attention must be paid to this and other trace impurities in the tested samples to exploit the 10% uncertainty in the current state-of-the-art kinetic measurements.

When sample purity is critical, materials compatibility becomes an important issue. PTFE tape, elastomer O-rings, and greases for joint seals are examples of common laboratory materials that must be avoided. Since many compounds are hygroscopic, contamination may also occur if the sample comes in contact with air and/or water.

Preparative-scale gas chromatography (prep-GC) is a well-known [4,5] separation method, with which high-purity ($>99.9\%$) compounds may be isolated from a mixture of substances that are otherwise difficult to separate [6]. For a comprehensive discussion of the design and performance of prep-GC systems, the reader is directed to the work by Conder and Purnell [7–10]. However, prep-GC techniques are not routinely used with low-boiling-point compounds [11] such as alternative refrigerants. Most commercial prep-GC systems have fraction collectors made of glass, which severely limit the working pressure range. In addition to pressure limitations, glass systems require elastomer and/or greased joints (which can contaminate the purified sample) to ensure proper seals.

In this paper, we describe a purification system based on a commercial prep-GC system with a custom-designed condenser, collector, and fraction handling system. The special design of this system is meant to address the problems mentioned in the paragraphs above. In our design, all the wetted surfaces are either 316 stainless steel or nickel. The system was designed to operate down to liquid nitrogen temperature and up to 7 MPa pressure. A cryopumping technique used to transfer a purified sample to an all-metal storage vessel is also described.

2. Experimental

2.1. Gas chromatograph

Our prep-GC system was based on a Model PSGC-10/40 automated instrument made by Varex[1] (Burtonsville, MD, USA). The complete system as used in our laboratory is diagrammed in Fig. 1. The manufacturer provided the computer, printer, interface, GC control unit, oven assembly, part of the sample inlet system, and a custom-made fraction collection system built to our specifications. The GC control unit regulated the carrier gas flow-rate, oven and vaporizer temperatures, sample injection, and fraction collection. The control unit also monitored the

[1] Mention of manufacturers and brand names is to provide a complete description of the apparatus and does not imply endorsement by the National Institute of Standards and Technology or that the items are the best available for their purpose.

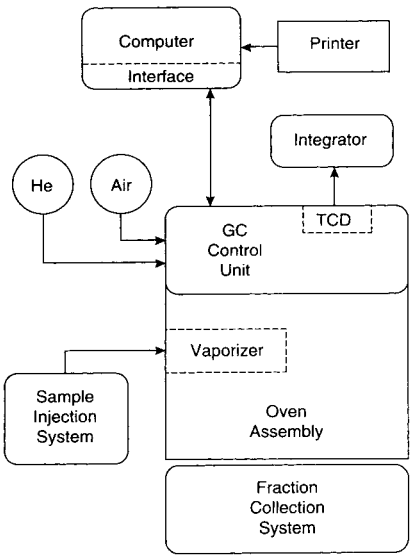

Fig. 1. Block diagram of the preparative-scale GC system used in our separations.

system for alarm conditions and would place the instrument in a safe configuration in case of a failure such as loss of carrier gas flow. A thermal conductivity detection (TCD) system monitored the evolution of gas through the column. An integrator (Hewlett-Packard Model HP3390A, Rockville, MD, USA) was used to record the TCD output and to integrate peaks. Helium (99% assay) was used as the carrier gas while compressed air was used to operate the pneumatic valves.

The prep-GC unit was capable of either manual control from the GC control unit front panel or of automatic control by the computer. The sample injector, fraction collection valves, and oven and vaporizer temperatures were computer controlled for unattended repetitive separations. Software developed by Varex provided for keyboard entry and hard disk storage/retrieval of the process control parameters and runs under MS-DOS (Microsoft, Redmond, VA, USA).

2.2. Sample inlet system

The system provided for both manual and automatic sample injection into the vaporizer. Samples could be manually injected through the injection port septum with a syringe. This technique was sometimes used to find an optimum injection size or to check sample purity during development of a separation protocol.

Samples that were liquids at room temperature were pumped into the vaporizer by an Eldex (Eldex Labs., Napa, CA, USA) precision metering pump. The liquid injection system is shown in Fig. 2. Samples that were sensitive to air were placed in a sealed container and pressurized with an inert atmosphere such as nitrogen or helium. The desired amount of liquid injected into the vaporizer was determined by the pump rate and the injection time. In the automatic mode, the duty cycle for the metering pump was controlled by the computer according to a schedule defined by the user. The pump could also be operated manually. The small-bore capillary tube, used to connect the pump to the vaporizer, added very little dead volume to the injection system; thus, it did not cause significant broadening of the chromatographic peaks. This method did not work for one of our liquid hydrofluorocarbon samples which boiled near room temperature, because the liquid boiled in the pump. Instead, this sample was heated in a bath and injected into the vaporizer as a gas.

Liquefied samples which are normally gases at ambient temperature and pressure were metered through a pneumatic actuated valve. Fig. 3 shows a diagram of the gas injection system. A sample that has a low vapor pressure near room temperature had to be heated until its vapor pressure was well above the column pressure. Then, the difference between the vapor pressure and the column pressure would drive the sample

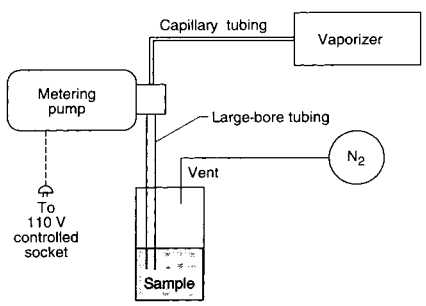

Fig. 2. Liquid sample injection system; schematic diagram.

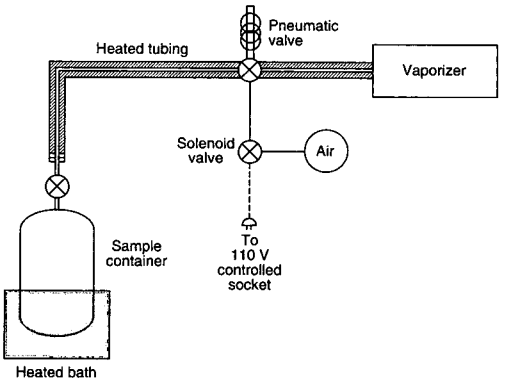

Fig. 3. Gas sample injection system; schematic diagram.

into the vaporizer when the pneumatic valve was opened. The tubing connecting the valve to the sample container and the vaporizer was heated above the bath temperature to prevent condensation in the tube. The preset duty cycle of the valve and the constant vapor pressure of the liquid in the storage container ensured that a reproducible amount of sample was injected. As long as there was liquid in the storage container, the vapor pressure regulated the amount of sample that was forced into the vaporizer.

2.3. Sample collection system

The fraction collection assembly was composed of six sample collection vessels, shown in Fig. 4, which could be selected manually or under computer control. Each port was a modular design consisting of a condenser, valves, and a collection trap. The sections were fastened together with zero clearance, face seal metal gasket connectors (VacuSeal; Parker Hannifin, Huntsville, AL, USA or VCR; Cajon, Macedonia, OH, USA). The prep-GC unit allowed easy access to the sample collection system for modifications. All wetted surfaces of the assembly were made from stainless steel or other non-corrosive metals. There were no elastomer O-rings, grease, or PTFE seals in the collectors or in the valves that were wetted by the sample. The condenser unit was thermostated by a flowing heat transfer fluid, such as tap water or antifreeze solution, from a circulating bath. The

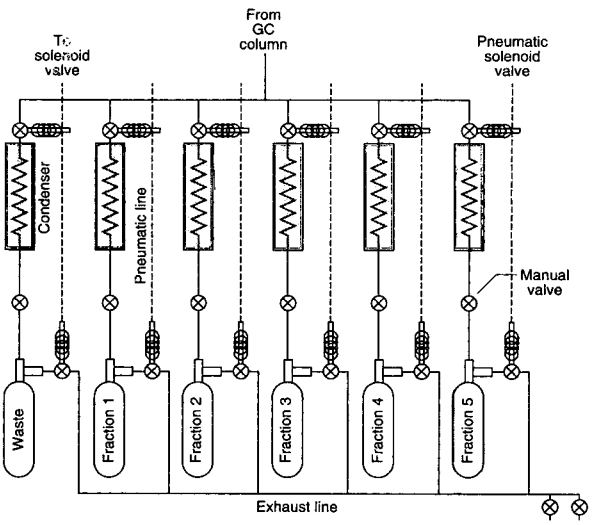

Fig. 4. Schematic diagram of the six fraction collection modules connected as a unit.

all-metal collection trap could be used down to liquid nitrogen temperature and up to 7 MPa pressure.

A normally closed pneumatic valve was located before each condenser and another was located after each fraction collection vessel. Each pair of valves operated in unison to divert the carrier/sample stream through the selected vessel and to prevent contamination from the exhaust line into the chilled collectors. Only one of the fraction collection modules was open at any given time. When desired fractions were not present, the designated waste module was open. The manual valve located between each condenser and its collection module was closed to isolate the fraction collection vessel from the condenser during cryo-transfer procedures.

Fig. 5 shows a cross-section of a fraction collection vessel. The vessel design was similar to a liquid nitrogen trap with a tube extending about a third of the way down the collection vessel. The tube was curved towards the side to allow the carrier gas and sample fraction to impinge on the liquid nitrogen-cooled wall. This configuration was used to improve collection efficiency by capturing aerosols which might otherwise be swept away with the carrier gas. The neck of the collection vessel was heated to

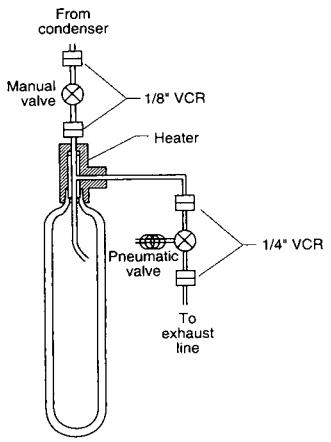

Fig. 5. Cross-sectional view of the fraction collection vessel and associated hardware. 1″ = 1 in. = 2.54 cm.

about 60°C with an electrical heater tape to prevent the incoming sample from freezing there and blocking the flow of carrier gas.

2.4. GC operation sequence

The major components of the carrier gas system are shown in Fig. 6. The sample was injected through the septum or the automatic injection port into the vaporizer where it was vaporized and mixed with pre-heated carrier gas. The carrier/sample mixture then passed through the chromatographic column where separation of the sample into its components took place.

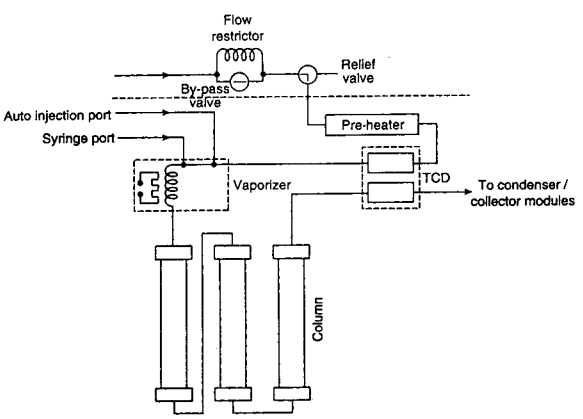

Fig. 6. Schematic diagram of the prep-GC carrier gas flow system (by permission of Varex).

Separated fractions passed through the TCD system and finally through the selected condenser/collection module. Samples were injected into the vaporizer under low carrier gas flow conditions by opening a by-pass valve to force the carrier gas through a flow restrictor. A relief valve was then momentarily opened to rapidly decrease the pressure in the vaporizer just before injection of gas sample. After the injection period, the by-pass valve was closed and the carrier gas flow was returned to its normal level. This procedure concentrated the sample at the head of the column.

TCD was used to monitor the degree of peak separation during the development of a separation process. When the system was performing repeated injections under computer control, TCD was turned off, and all events (injection, fraction selection, cycle completion) were based on time alone. The system conditions and the sample injections were very reproducible from cycle to cycle.

2.5. Sample transfer

Samples were transferred from the collection vessels to the sample storage containers by cryopumping. Fig. 7 shows the components used

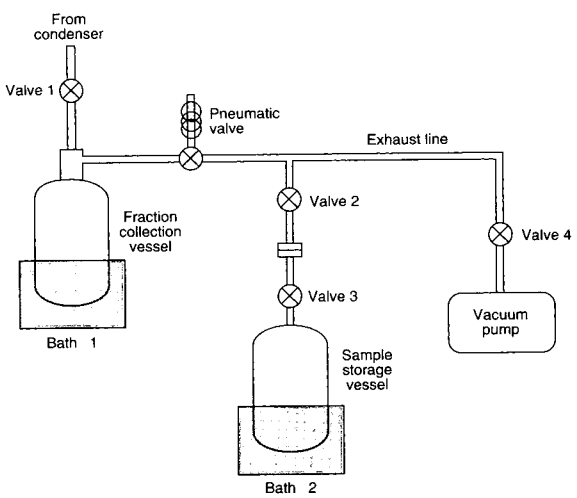

Fig. 7. Schematic diagram of the fraction collection plumbing used during cryopumping procedures. Irrelevant parts of the apparatus have been omitted for clarity.

during cryo-transfer procedures after a separation was completed. First, bath 1 was filled with liquid nitrogen, then the fraction collection vessel containing the frozen sample was isolated from the condenser by closing the manual valve 1. Next, the carrier and residual gases were pumped away through the pneumatic valve and valves 2, 3 and 4 with the attached mechanical vacuum pump. For the final step, valve 4 to the vacuum pump was closed. Bath 2 was then filled with liquid nitrogen, and bath 1 was emptied. The difference between the vapor pressures of the sample in the collection vessel and in the storage vessel drove a mass flow of the sample, and as the collection vessel was warmed this flow was toward the storage vessel. The warming rate and the temperature of the collection vessel were determined by observing the boil-off of the liquid nitrogen in bath 2 as the sample condensed in the storage vessel. The fraction collection vessel was slowly heated with a warm heat gun (or by filling bath 1 with warm tap water) until a steady, smooth boiling was achieved. When the nitrogen stopped boiling, the transfer was complete. Manual valves 2 and 3 were closed, and the purified sample was removed. The entire sample transfer procedure took approximately 10 min.

The sample storage vessels were designed to keep the purified material clean. They were single-ended, stainless-steel cylinders with a welded bellows cut-off valve leading to a high-vacuum fitting that was used to connect the vessel to other apparatuses. All joints were heliarc welded, and the container was tested under vacuum for leaks. The only opening to the purified sample was through manual valve 3.

3. Results

The performance of our prep-GC system is illustrated by the purification of pentafluoroethane. GC analysis before and after purification was performed using an analytical chromatograph with an automatic gas injector valve, a 60–80 mesh Carbopack B/5% Fluorcol

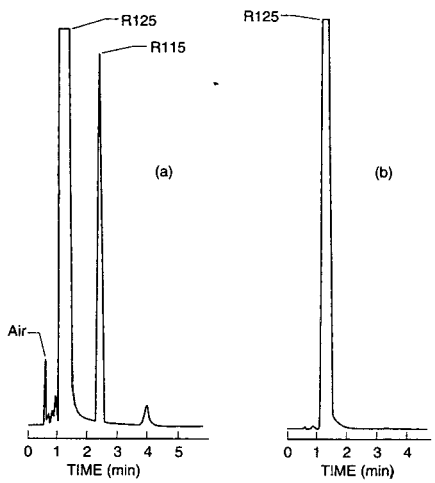

Fig. 8. Analytical chromatograms of the (a) as-received and (b) purified samples.

(Supelco, Bellefonte, PA, USA) packed column, 3 m × 3 mm O.D., and a TCD system. The temperature of the column was kept isothermal at 45°C. The carrier was helium gas at a nominal flow-rate of 50 ml/min. A chromatogram of the as-received sample of pentafluoroethane, R125, is shown in Fig. 8a. The peak areas from the analysis are given in Table 1. The chromatograph was calibrated using a gravimetrically prepared mixture of R125 and R115. The results showed that the sample contained 0.0015 ± 0.00007 mole fraction R115.

Table 1
GC analysis of as-received pentafluoroethane

Retention time (min)	Fraction area (%) (± 0.005)	Compound
0.64	0.030	Air
0.76	0.002	Unknown
0.89	0.005	Unknown
0.97	0.006	Unknown
1.10	99.697	Pentafluoroethane (R125)
2.42	0.241	Chloropentafluoroethane (R115)
3.98	0.019	Unknown

The as-received sample of R125 was processed through the preparative system using the gas injection system (Fig. 3). The same packing material used for the analytical work, namely 60–80 mesh Carbopack B/5% Fluorcol, was packed into a 2 m × 1 cm I.D. column and installed into the prep-GC system. The column temperature was isothermal at 45°C, while the vaporizer and detector were maintained at 60°C. The carrier gas was helium with a flow-rate of 400 ml/min. The helium carrier gas was easily removed from the purified sample by repeated freeze–pump–thaw cycles. The fraction collection vessel was immersed in a liquid nitrogen bath. The neck of the fraction collection vessel was heated to prevent freezing of the sample in the small-bore inlet tube, as discussed previously. The coiled condensers were not required for this separation and the jacket bath contained only air.

During each cycle, the automatic valves were programmed to divert the process stream to the collection cold trap just after the start of the R125 peak. Shortly before the end of this peak, the valves sealed off the collection trap and returned the stream to the normal pattern. Each cycle took 6 min to complete. After 17 cycles, a total of 7.65 g of R125 had been collected for a process rate of 4.5 g/h. The collected mass represented an estimated 80–90% of the injected sample. The purified R125 was then transferred to a sample storage vessel for analysis, using the cryopumping technique described earlier.

A chromatogram of the purified R125 is shown in Fig. 8b and the peak analysis is given in Table 2. The conditions for this analysis were identical to the analysis of the as-received sample. Within the resolution of the instrument, all of the main impurities had been successfully removed.

Table 2
GC analysis of purified pentafluoroethane

Retention time (min)	Fraction area (%) (± 0.005)	Compound
0.92	0.007	Unknown
1.19	99.993	Pentafluoroethane (R125)

4. Discussion

Safety issues were a concern in the design of this system. Many hydrofluorocarbons are stored as liquified gases with very high vapor pressures at room temperature. The all-metal system described here was capable of containing the purified sample in case of system failure and loss of liquid nitrogen in the fraction collection bath. Cryogenic fluids in the baths could be maintained overnight by a liquid nitrogen level control system. The worst-case scenario expected would be the thawing of the purified sample and the opening of the pneumatic valve by the high vapor pressure followed by loss of the purified sample. The pneumatic valves were normally closed by spring tension and opened by compressed air and were susceptible to being forced open by high sample pressure. In the event of a power failure, the oven and vaporizer temperature controllers would be disabled, the pneumatic valves to the collectors would close, and the carrier stream would be diverted through the normally open valve to the waste module. Normal operation could not resume until the system was manually reset.

The sample collection system was cleaned before use by heating and flowing carrier gas through it or evacuating it with a vacuum pump. We did not find any contamination problems with the purified fractions associated with the use of research-grade helium as a carrier gas. In the event that such contamination occurs, liquid nitrogen-cooled molecular sieve traps would be used to clean the carrier gas. The design of the fraction collection and storage vessels allowed the purified samples to be transferred to our experiments without ever being exposed to air or other unwanted materials.

We have described a new all-metal collection system for a preparative gas chromatograph that will operate down to liquid nitrogen temperature

and pressures up to 7 MPa. The performance of the system was demonstrated through the purification of a pentafluoroethane–chloropentafluoroethane (99.85:0.15) mixture to achieve 99.99% pentafluoroethane at a rate of 4.5 g/h.

Acknowledgement

The authors would like to thank Mr. Dana Defibaugh for his help in the analysis and purification of the pentafluoroethane.

References

[1] M.R. Moldover, J.B. Mehl and M. Greenspan, *J. Acoust. Soc. Am.*, 79 (1986) 253.
[2] B.J. Finlayson-Pitts, M.J. Ezell, T.M. Jayaweere, H.N. Berko and C.C. Lai, *Geophys. Res. Lett.*, 19 (1992) 1371.
[3] R.K. Talukdar, A. Mellouki, A. Schmoltner, T. Watson, S. Montzka and A.R. Ravishankara, *Science*, 257 (1992) 227.
[4] J.J. Kirkland, in V.J. Coates, H.J. Noebels and I.S. Fagerson (Editors), *Gas Chromatography —Proceedings of the 1st International Symposium on Gas Chromatography*, Academic Press, New York, 1958, Ch. 21.
[5] M. Verzele, in J. Krugers (Editor), *Instrumentation in Gas Chromatography*, Centrex Publishing, Eindhoven, 1968, Ch. 9; see also pp. 153–155.
[6] J.R. Conder and N.A. Fruitwala, *Chem. Eng. Sci.*, 36 (1981) 509.
[7] J.R. Conder, *J. Chromatogr.*, 256 (1983) 381.
[8] J.R. Conder and J.H. Purnell, *Chem. Eng. Progr., Symp. Ser.*, 65 (1969) 1.
[9] J.R. Conder and J.H. Purnell, *Chem. Eng. Sci.*, 25 (1970) 353.
[10] J.R. Conder, *Chromatographia*, 8 (1975) 60.
[11] C.H. Cheh, *J. Chromatogr. A*, 658 (1994) 283.

ELSEVIER

Journal of Chromatography A, 702 (1995) 251–257

JOURNAL OF CHROMATOGRAPHY A

Preparative gas chromatographic separation of the enantiomers of methyl 2-chloropropionate using a cyclodextrin-based stationary phase

Daniel U. Staerk, Aroonsiri Shitangkoon, Gyula Vigh*

Department of Chemistry, Texas A & M University, College Station, TX 77843-3255, USA

Abstract

The enantiomers of methyl 2-chloropropionate, a volatile synthetic precursor, have been separated by preparative-scale gas chromatography using a 1 m × 22.5 mm I.D. column, packed with 20% (w/w) trichloroacetyl β-cyclodextrin-coated 60–80-mesh Chromosorb A. The preparative column was installed in a custom-designed preparative gas chromatograph and operated in the isothermal mode. An effluent-sampling interface valve, located between the exit of the preparative column and the fraction collector took 10- μl samples of the effluent gas every 20 s and sent the samples onto a short, efficient analytical capillary column to provide on-line enantiomeric analysis of the eluting bands. This near-real-time knowledge of the enantiomer composition of the effluent gas leads to aggressive, yet safe, fraction pooling schemes and permits the precise calculation of product purity, recovery and production rate. Results for the preparative separation of racemic as well as enantiomerically enriched (95% enantiomeric excess) feedstock are presented in this paper.

1. Introduction

In three previous papers [1–3] we have described the design, construction and use of a first-generation custom-designed preparative gas chromatograph which combines the preparative-scale separation of enantiomers with integrated on-line analysis of the enantiomeric composition of the effluent from the preparative column. We have demonstrated that the system could provide sub-g/day-scale separation of the enantiomers of volatile anesthetics, enflurane and isoflurane, using a 1 m × 10 mm I.D. column packed with Chromosorb A, coated with 20% (w/w) trifluoroacetyl γ-cyclodextrin as chiral stationary phase. The objective of the present paper is to demonstrate that with a slight modification of the injector system and the injection sequence, the separation efficacy of the integrated preparative/analytical system can be preserved even when the diameter of the preparative column is doubled to 22.5 mm, offering production rates as high as 5 to 10 g/day using a chiral stationary phase, trichloroacetyl β-cyclodextrin.

The methyl ester of α-chloropropionic acid (MCP) was used as test compound in these studies. α-Chloropropionic acid esters are chiral synthons which can be used, among others, in the synthesis of enantiomerically pure herbicides, such as the (*R*)-α-phenoxypropionic acid esters [4]. While MCP is commercially available in enantiomerically enriched form (95.7% enantiomeric excess), higher-purity material is not readily available. MCP is quite suitable as a test

* Corresponding author.

0021-9673/95/$09.50 © 1995 Elsevier Science B.V. All rights reserved
SSDI 0021-9673(94)01035-8

compound for scale-up studies in chiral preparative gas chromatography, because a selectivity factor of 1.5 can be achieved for its enantiomers with an accompanying k_2' of 150 using the relatively inexpensive chiral stationary phase, trichloroacetyl β-cyclodextrin [5].

2. Experimental

The custom-designed preparative gas chromatographic system has been described in detail in Ref. [3]. Briefly, it was built from a modified Model 439 gas chromatograph (Chrompack, Middelburg, Netherlands), equipped with a septumless split/splitless injector with a modified, heated Series 7000 (Rheodyne, Cotati, CA, USA) switching valve-based vaporization loop, a flame ionization detection (FID) system, and a Model 4270 integrator (Varian, Walnut Creek, CA, USA) for data acquisition, a modified Model FE thermostatted circulating oil-bath system (Science Electronics, Dayton, OH, USA), modified HP 5982 MS interface heated transfer lines (Hewlett-Packard, Avondale, PA, USA), a modified, heated Series 7000 (Rheodyne) switching valve-based effluent sampling interface, a modified variable-split injector (Tracor, Houston, TX, USA) and a custom-made analytical capillary column installed in an HP 5890 Series II gas chromatograph (Hewlett-Packard), a septumless split/splitless injector, a FID system, and a ChemStation data collection/analysis system.

The preparative-scale GC separations were completed on 1.0 m × 22.5 mm I.D. stainless-steel preparative columns, which were packed as described in Ref. [3] with 60–80 mesh (approximately 175–250 μm) Chromosorb A (Alltech, Deerfield, IL, USA), coated with 20% (w/w) trichloroacetyl β-cyclodextrin (AMP-5). AMP-5 was synthesized by refluxing partially pentylated β-cyclodextrin in a mixture of 1,4-dioxane and trichloroacetyl anhydride, as described and characterized in Ref. [5]. The preparative column, which contained 44 g of AMP-5, was operated isothermally at 60°C and yielded a selectivity factor of 1.5 and an accompanying k_2' of 150 for MCP.

The effluent of the preparative column was analyzed on-line for enantiomeric purity using a 5.5 m × 0.15 mm I.D. fused-silica capillary column, statically coated [6] with a 0.15-μm thick film of AMP-5. Hydrogen was used as carrier gas at a linear velocity of 50 cm/s (methane was used as unretained compound). The capillary column was operated isothermally at 60°C.

MCP was obtained in racemic form as well as enantiomerically enriched form (lot No. 11401LZ, factory analyzed 95.7% ee) from Aldrich (Milwaukee, WI, USA), and used without further purification.

3. Results and discussion

3.1. Equipment modification

In order to accommodate the larger sample loads expected with the use of the 22.5 mm I.D. preparative column, the injector [2] has been modified by extending the original injector of the Chrompack Model 439 gas chromatograph with an expansion vessel constructed from a 1 m × 5.3 mm I.D. stainless-steel tube. The enlarged injector is connected between ports 2 and 3 of the Rheodyne Series 7000 heated valve. Ports 5 and 6 of the valve are connected by a short section of a 0.75 mm I.D. stainless-steel capillary. The carrier gas source is connected to port 1, the preparative column to port 4. In the load cycle, the valve routes the carrier gas through ports 1, 6, 5 and 4 to the preparative column, while the liquid sample, up to 1.5 ml in volume, is injected into the closed loop formed by ports 2 and 3, and the extended injector. After a brief evaporation time, the valve is turned routing the carrier gas through ports 1 and 2, the extended injector and ports 3 and 4 to the preparative column. The carrier gas is allowed to flush the sample onto the column only for a predetermined period of time: as soon as the vapor phase concentration begins to decrease at the exit of the expansion vessel, the valve is switched back to the load position providing a square-wave like injection plug devoid of a dilute tail. Though this solution ensures sharp boundaries for the injected sample

plugs, it results in incomplete sample transfer. Therefore, the analytical part of the system has to be calibrated through the analytical injector, the appropriate response factors must be determined and used to calculate the amount of material actually introduced into the preparative column.

The 1 m × 22.5 mm I.D. preparative column was packed with 60–80 mesh Chromosorb A, coated with 20% (w/w) AMP-5, as described in Refs. [2] and [3]. The Van Deemter curves of the column were determined at 60°C with hydrogen as carrier gas and 0.5 μl samples of racemic MCP as probe. At the optimum linear velocity of 4 cm/s, the column could provide 825 theoretical plates, at 8 cm/s linear velocity (with an inlet pressure of 70 p.s.i.; 1 p.s.i. = 6894.76 Pa), this decreased to 600 theoretical plates.

3.2. Column load studies and on-line effluent analysis

The preparative column was loaded with several samples of racemic MCP and the preparative detector traces (envelope chromatograms) were recorded as shown in Fig. 1. The touching-band condition develops at 37 mg load; a clear shoulder for the second enantiomer is observable up to the 206-mg load, the envelope chromatograms show only a single, distorted peak between the 425- and 1070-mg loads. In all cases, the envelope chromatograms indicate that the sample leaves the preparative column in 35 min.

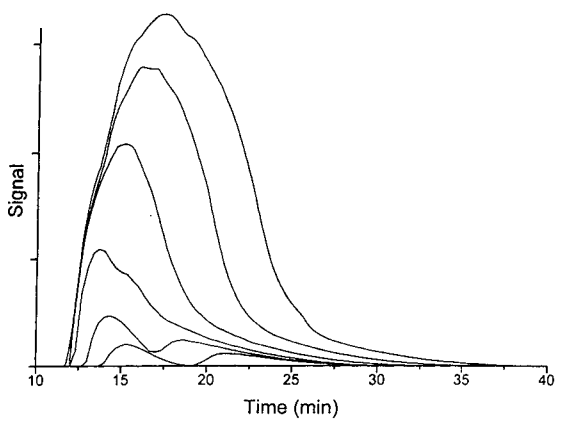

Fig. 1. Preparative FID traces (envelope chromatograms) for racemic MCP samples of increasing size. Column: 1 m × 22.5 mm I.D.; temperature: 60° C, isothermal; carrier gas: hydrogen at 8 cm/s linear velocity. Sample loads: 37, 87, 206, 425, 728 and 1070 mg, respectively, increasing as peak height.

In order to realize on-line enantiomeric analysis of the effluent gas of the preparative column, the cycle time of the analytical system must first be determined. As the worst case, a new, 10-μl effluent gas fraction can be injected by the interface into the analytical column as soon as the analytical FID signal returns to the baseline following the elution of the more retained enantiomer. However, as described in Ref. [3], the sampling frequency can be increased if the duration of the analytical chromatogram is an integer number multiple of the cycle time. The cycle time is made up from the duration of the pressure pulse that is caused by the turning of the interface valve to the inject position and back to the refill position, the duration of the flat baseline section before the peak of the less retained enantiomer, the duration of the first peak, the duration of the second peak (both determined at the highest effluent concentration expected during the preparative separation), and the duration of the flat baseline section after the peak of the more retained enantiomer necessary for reliable peak area determination. In this study the actual separation time on the analytical capillary column is 40 s, while the cycle time is 20 s. The detector trace is very clean, and can be easily integrated to yield the enantiomeric composition of the effluent gas of the preparative column. This results in 70 to 80 enantiomeric composition data points during the course of an average preparative separation. As an example, the analytical FID trace is shown in Fig. 2 as a function of time during the preparative-scale separation of a 206-mg MCP sample. The corresponding envelope chromatogram is shown in Fig. 1: it is the last one where the shoulder caused by the second enantiomer is still discernable.

The reproducibility of the entire integrated preparative/analytical system is indicated by the analytical FID trace of a 2-h segment of a production campaign shown in Fig. 3: three

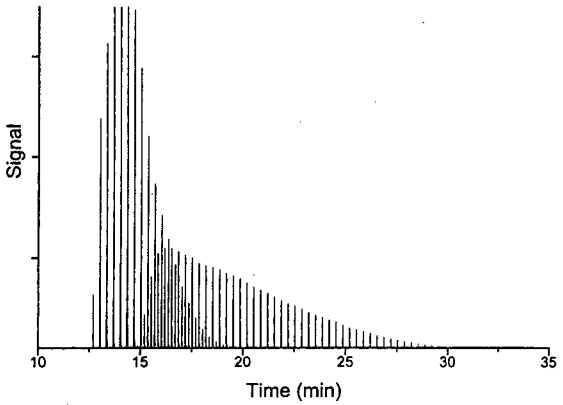

Fig. 2. Example of an on-line enantiomeric fraction analysis. Sample: 206 mg racemic MCP. Preparative column and conditions as in Fig. 1. Sampling volume: 10 μl, sampling cycling time: 20 s. Light peaks: (*R*)-(+)-MCP, dark peaks: (*S*)-(−)-MCP.

preparative cycles can be completed in slightly over 2 h. Since the MCP feedstock contains three slightly retained contaminants, amounting to about 5% of the sample, the preparative cycles cannot be nested as with the isoflurane and enflurane samples [2,3]. This lowers the daily production rates and indicates the importance of the chemical purity of the feedstock.

3.3. Preparative results

Using the on-line enantiomer analysis data of the effluent (an example of which is shown in Fig. 2 for the 206-mg load) and the appropriate response factors of the analytical system established by direct calibration, the enantiomeric purity vs. production and enantiomeric purity vs. recovery curves can be calculated, as shown, for example, in Fig. 4 for the 206-mg injection. The left-hand inset in Fig. 4 shows the envelope chromatogram, the right-hand inset shows the reconstructed chromatogram of the enantiomers. It can be seen that for a 206-mg injection of the racemic mixture, about 70 mg of the less re-

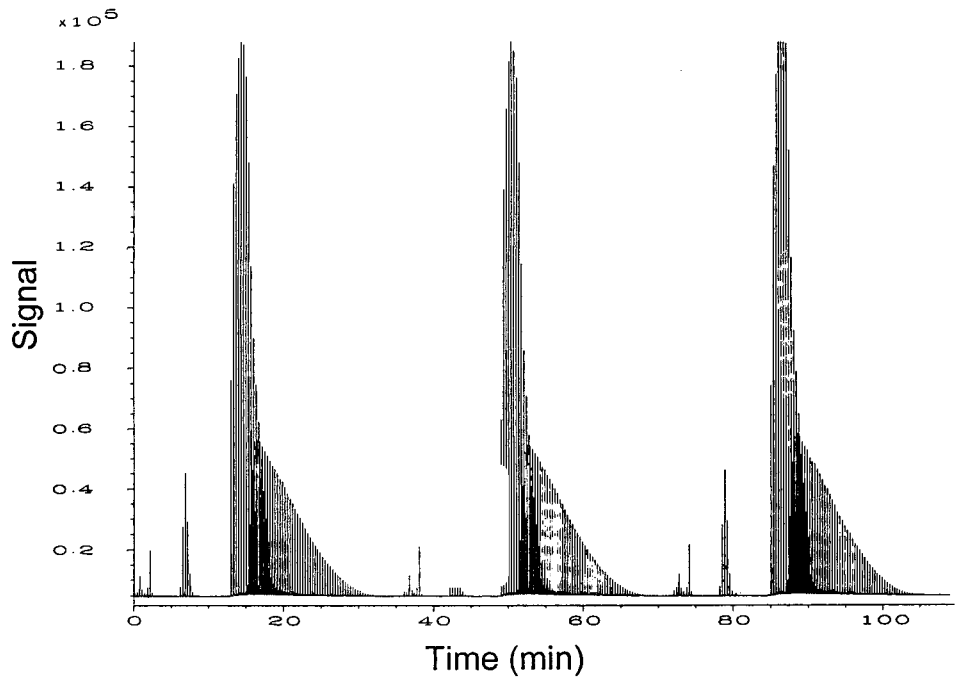

Fig. 3. Stability and reproducibility of the preparative GC system: a 2-h segment of the analytical FID trace during a single day's production campaign (206 mg racemic MCP injections, 35-min preparative cycle time, 20-s interface valve cycling time). Other conditions as in Fig. 2.

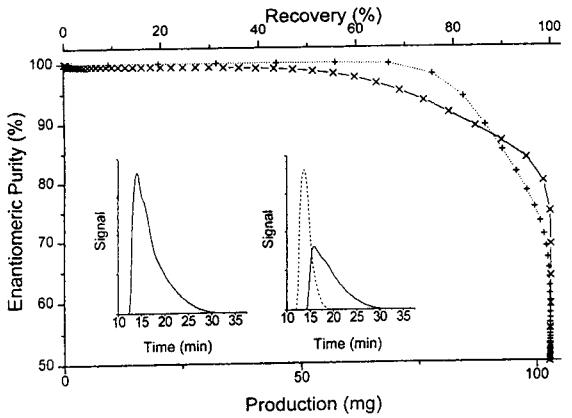

Fig. 4. Enantiomeric purity as function of production and % recovery for a 206-mg injection calculated from the on-line enantiomeric fraction analysis. Insets: preparative envelope chromatogram at left, reconstructed chromatogram of the enantiomers at right. Conditions as in Fig. 2. Symbols: + (dotted line) = less retained enantiomer; × (solid line) = more retained enantiomer.

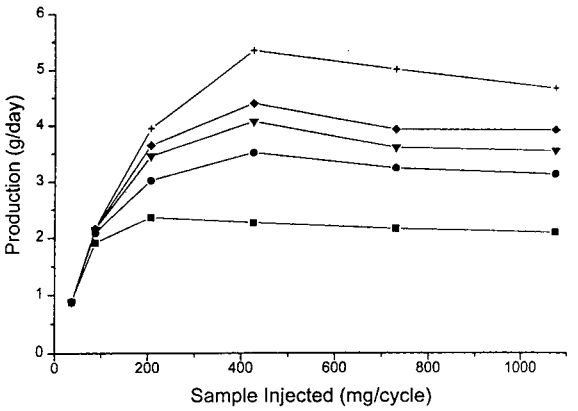

Fig. 5. Production for the less retained MCP enantiomer as a function of the injected sample amount at various levels of product purity. Feedstock: racemic MCP. Conditions as in Fig. 2. Symbols: + = 80%; ◆ = 90%; ▼ = 95%; O = 99%; □ = 100% purity.

tained enantiomer leaves the column at a purity higher than 99.99%. However, only about 2 mg of the more retained enantiomer are available at such a high enantiomeric purity. A small relaxation of the enantiomeric purity requirement leads to negligible increase in production for the less retained enantiomer, but significant increase for the more retained enantiomer.

Knowing that each run takes 35 min, one can calculate the daily production rates (g/day) for various enantiomeric purities as a function of the injected load in each cycle. The results are shown in Fig. 5 for the less retained enantiomer and Fig. 6 for the more retained enantiomer. If the less retained enantiomer is to be produced at greater than 99.99% purity, the maximum injection size must be about 206 mg. This leads to about 2.2 g/day of pure product. Larger injections slightly decrease the daily production at this purity level. If the purity requirement is relaxed to 99%, the daily production rate increases by about 50% (to 3.3 g/day) as the injection size is increased to 425 mg. Larger injections again result in slightly lower production rates. The amount of 425 mg remains the desirable injection size even when the product purity is relaxed successively to 95, 90 and eventually, 80%. At the 95% purity level (which is of interest, because it is close to that of the commercially available, enantiomerically "pure" material), the production rate is about 4 g/day. Even a drastic reduction of the target purity to 80% does not increase the production rate above 5.5 g/day.

The situation is different for the more retained enantiomer (Fig. 6). At greater than 99.99%

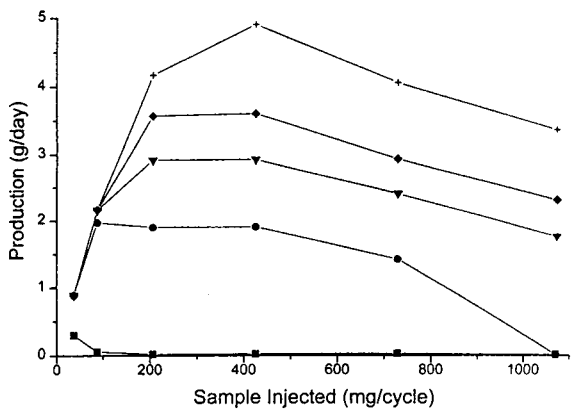

Fig. 6. Production for the more retained MCP enantiomer as a function of the injected sample amount at various levels of product purity. Feedstock: racemic MCP. Conditions as in Fig. 2. Symbols: + = 80%; ◆ = 90%; ▼ = 95%; O = 99%; □ = 100% purity.

purity, only 0.3 g/day can be produced, and only when the injection size is just below the "touching-band" load. When the purity requirement is relaxed to 99%, there is a dramatic increase in the production rate to 2 g/day. This is only a third less than the maximum production rate for the less retained enantiomer, and can be realized by injections as small as 80 mg. Quite fortunately, production rate remains flat (decreases only slightly) at this product purity as the injection size is increased to 425 mg. This means that one can achieve maximum production rate both for the less retained enantiomer and the more retained enantiomer at the same injection size (425 mg), without sacrificing either product purity or production rate.

It was instructive to see what happens when the racemic feedstock is replaced with an enantiomerically enriched feedstock (95.7% ee for the less retained enantiomer). The analytical FID trace at 420 mg load obtained with this feedstock is shown in Fig. 7, and the daily production rate vs. injected amount curves for greater than 99.99% purity and 99% purity in Fig. 8. There is no significant accumulation of the more retained enantiomer at the tail-end of the less retained enantiomer (Fig. 7); instead the

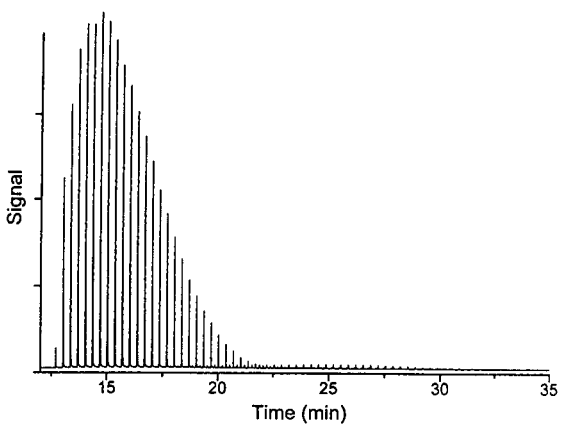

Fig. 7. Example of an on-line enantiomeric fraction analysis. Sample: 420 mg enantiomerically enriched (*R*)-(+) (95.7% ee) MCP. Preparative column and conditions as in Fig. 1; analytical column and conditions as in Fig. 2. Sampling volume: 10 μl, sampling cycling time: 20 s. Light peaks: (*R*)-(+)-MCP, dark peaks: (*S*)-(−)-MCP.

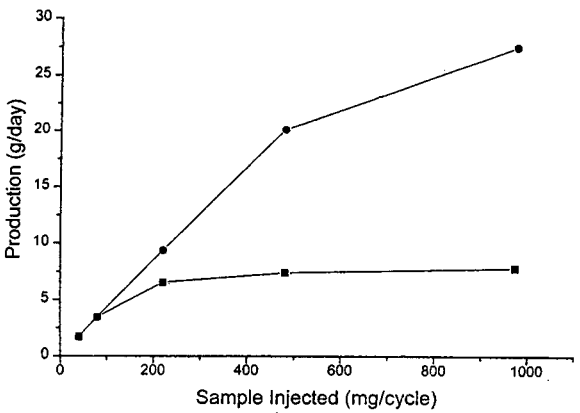

Fig. 8. Production for the less retained MCP enantiomer as a function of the injected sample amount at various levels of product purity. Feedstock: enantiomerically enriched (*R*)-(+)-MCP (95.7% ee). Conditions as in Fig. 7. Symbols: ○ = 99% purity; □ = 100% purity.

concentration of the second enantiomer remains rather constant during the last third of the peak of the first enantiomer. It can be seen in Fig. 8, that about 7 g/day of the less retained enantiomer can be produced at greater than 99.99% purity, a three-fold increase compared to what could be obtained with the racemic feedstock. At this level of enantiomeric purity, the production rate remains flat as the injection size is increased. However, when the purity requirement is relaxed to 99%, the production rate becomes as high as about 30 g/day, and the production rate maximum is not achieved even at 970 mg injection, the highest tested in this work.

4. Conclusions

The previously described integrated preparative/analytical GC system has been modified to accommodate columns as large as 1 m × 22.5 mm I.D. A liquid chiral stationary phase, AMP-5 could be successfully coated onto the 60–80 mesh Chromosorb A support and packed into 1 m × 22.5 mm I.D. columns yielding 825 theoretical plates at the optimum point of the Van Deemter curve. Operated isothermally at 60°C, the column resulted in $\alpha = 1.5$ and $k_2' = 150$ values for the enantiomers of the methyl ester of

α-chloropropionic acid. A 5.5-m long capillary column, coated with a 0.15-μm thick film of the same stationary phase permitted the on-line enantiomeric analysis of the effluent of the preparative column with a cycle time of 20 s, resulting in accurate effluent purity vs. production rate curves and production rate vs. injected sample size curves. It also leads to aggressive, yet safe, production regimes yielding 1 to 5 g/day production rates, depending on the level of required purity, with a racemic feedstock, and 7 to 30 g/day production rates (for 100 and 99% purity, respectively) with an enantiomerically enriched feedstock. Further work is underway in our laboratory to extend the system for the production of other enantiomers of value or interest.

Acknowledgements

Partial financial support by the National Science Foundation (CH-8919151), the US Department of Education (grant No. 415004), the Advanced Research Program of the Texas Coordination Board of Higher Education (project No. 010366-016), and a College of Science, Texas A & M University Research Enhancement Grant is gratefully acknowledged. The authors are indebted to the American Maize Products Corp. (Hammond, IN, USA) for the donation of the β-cyclodextrin samples.

References

[1] A. Shitangkoon, D.U. Staerk and Gy. Vigh, *J. Chromatogr. A*, 657 (1993) 387.
[2] D.U. Staerk, A. Shitangkoon and Gy. Vigh, *J. Chromatogr. A*, 663 (1994) 79.
[3] D.U. Staerk, A. Shitangkoon and Gy. Vigh, *J. Chromatogr. A*, 677 (1994) 133.
[4] R.A. Sheldon, *Chirotechnology*, Marcel Dekker, New York, 1993, p. 347.
[5] A. Shitangkoon and Gy. Vigh, *J. High Resolut. Chromatogr.*, 17 (1994) 727.
[6] K. Grob, *Making and Manipulating Capillary Columns for Gas Chromatography*, Hüthig, Heidelberg, 1986, p. 156.

Author Index

PUBLICATION SCHEDULE FOR THE 1995 SUBSCRIPTION

Journal of Chromatography A and *Journal of Chromatography B: Biomedical Applications*

MONTH	1994	J	F	M	A	M[a]	J	
Journal of Chromatography A	Vols. 683–688	689/1 689/2 690/1 690/2	691/1 + 2 692/1 + 2 693/1 693/2	694/1 694/2 695/1 695/2	696/1 696/2 697/1 + 2 698/1 + 2	699/1 + 2 700/1 + 2 702/1 + 2 703/1 + 2	704/1 704/2 705/1 705/2	The publication schedule for further issues will be published later.
Bibliography Section				713/1			713/2	
Journal of Chromatography B: Biomedical Applications		663/1 663/2	664/1 664/2	665/1 665/2	666/1 666/2	667/1 667/2	668/1 668/2	

[a] Vol. 701 (Cumulative Indexes Vols. 652–700) expected in October.

INFORMATION FOR AUTHORS

(Detailed *Instructions to Authors* were published in *J. Chromatogr. A*, Vol. 657, pp. 463–469. A free reprint can be obtained by application to the publisher, Elsevier Science B.V., P.O. Box 330, 1000 AH Amsterdam, Netherlands.)

Types of Contributions. The following types of papers are published: Regular research papers (full-length papers), Review articles, Short Communications and Discussions. Short Communications are usually descriptions of short investigations, or they can report minor technical improvements of previously published procedures; they reflect the same quality of research as full-length papers, but should preferably not exceed five printed pages. Discussions (one or two pages) should explain, amplify, correct or otherwise comment substantively upon an article recently published in the journal. For Review articles, see inside front cover under Submission of Papers.

Submission. Every paper must be accompanied by a letter from the senior author, stating that he/she is submitting the paper for publication in the *Journal of Chromatography A* or *B*.

Manuscripts. Manuscripts should be typed in **double spacing** on consecutively numbered pages of uniform size. The manuscript should be preceded by a sheet of manuscript paper carrying the title of the paper and the name and full postal address of the person to whom the proofs are to be sent. As a rule, papers should be divided into sections, headed by a caption (*e.g.*, Abstract, Introduction, Experimental, Results, Discussion, etc.). All illustrations, photographs, tables, etc., should be on separate sheets.

Abstract. All articles should have an abstract of 50–100 words which clearly and briefly indicates what is new, different and significant. No references should be given.

Introduction. Every paper must have a concise introduction mentioning what has been done before on the topic described, and indicating clearly what is new in the paper now submitted.

Experimental conditions should preferably be given on a *separate* sheet, headed "Conditions". These conditions will, if appropriate, be printed in a block, directly following the heading "Experimental".

Illustrations. The figures should be submitted in a form suitable for reproduction, drawn in Indian ink on drawing or tracing paper. Each illustration should have a caption, all the *captions* being typed (with double spacing) together on a *separate sheet*. If structures are given in the text, the original drawings should be provided. Coloured illustrations are reproduced at the author's expense, the cost being determined by the number of pages and by the number of colours needed. The written permission of the author and publisher must be obtained for the use of any figure already published. Its source must be indicated in the legend.

References. References should be numbered in the order in which they are cited in the text, and listed in numerical sequence on a separate sheet at the end of the article. Please check a recent issue for the layout of the reference list. Abbreviations for the titles of journals should follow the system used by *Chemical Abstracts*. Articles not yet published should be given as "in press" (journal should be specified), "submitted for publication" (journal should be specified), "in preparation" or "personal communication".

Vols. 1–651 of the *Journal of Chromatography*; *Journal of Chromatography, Biomedical Applications* and *Journal of Chromatography, Symposium Volumes* should be cited as *J. Chromatogr.* From Vol. 652 on, *Journal of Chromatography A* (incl. Symposium Volumes) should be cited as *J. Chromatogr. A* and *Journal of Chromatography B: Biomedical Applications* as *J. Chromatogr. B*.

Dispatch. Before sending the manuscript to the Editor please check that the envelope contains four copies of the paper complete with references, captions and figures. One of the sets of figures must be the originals suitable for direct reproduction. Please also ensure that permission to publish has been obtained from your institute.

Proofs. One set of proofs will be sent to the author to be carefully checked for printer's errors. Corrections must be restricted to instances in which the proof is at variance with the manuscript.

Reprints. Fifty reprints will be supplied free of charge. Additional reprints can be ordered by the authors. An order form containing price quotations will be sent to the authors together with the proofs of their article.

Advertisements. The Editors of the journal accept no responsibility for the contents of the advertisements. Advertisement rates are available on request. Advertising orders and enquiries can be sent to the Advertising Manager, Elsevier Science B.V., Advertising Department, P.O. Box 211, 1000 AE Amsterdam, Netherlands; Tel: 31 (20) 485 3796; Fax: 31 (20) 485 3810. Courier shipments to street address: Molenwerf 1, 1014 AG Amsterdam, Netherlands. *UK*: T.G. Scott & Son Ltd., Tim Blake, Portland House, 21 Narborough Road, Cosby, Leics. LE9 5TA, UK; Tel: (0116) 2750 521/2753 333; Fax: (0116) 2750 522. *USA and Canada*: Weston Media Associates, Daniel S. Lipner, P.O. Box 1110, Greens Farms, CT 06436-1110, USA; Tel: (203) 261 2500; Fax: (203) 261 0101.

Chiral HPLC Column

Application Guide for Chiral HPLC Column Selection

SECOND EDITION!

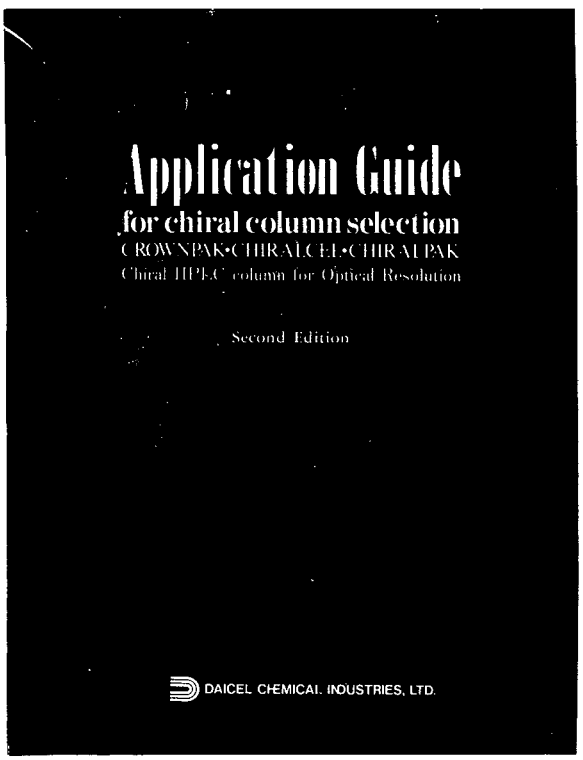

FREE OF CHARGE

The 112-page green book contains chromatographic resolutions of over 350 chiral separations, cross-indexed by chemical compound class, structure, and the type of chiral column respectively. This book also lists chromatographic data together with analytical conditions and structural information. A quick reference guide for column selection from a wide range of DAICEL chiral HPLC columns is included.

To request this book, please let us know by fax or mail.

DAICEL CHEMICAL INDUSTRIES, LTD.

AMERICA

CHIRAL TECHNOLOGIES, INC.

730 Springdale Drive, P.O. Box 564
Exton, PA 19341
Phone: 800-624-4725
Facsimile: 610-594-2325

EUROPE

DAICEL (EUROPA) GmbH

Oststr. 22
D-40211 Düsseldorf, Germany
Phone: +49-211-369848
Facsimile: +49-211-364429

ASIA/OCEANIA

DAICEL CHEMICAL INDUSTRIES, LTD.
CHIRAL CHEMICALS NDD
8-1, Kasumigaseki 3-chome,
Chiyoda-ku, Tokyo 100, JAPAN
Phone: +81-3-3507-3151
Facsimile: +81-3-3507-3193

484 a

5-170.38
- 5 O.A. 2538